SOCIETÀ ITALIANA DI FISICA

ATTI DI CONFERENZE

VOLUME 33

La Scienza della Fusione Fredda

Atti della seconda conferenza annuale sulla fusione fredda

a cura di T. Bressani, E. Del Giudice e G. Preparata
Como, 29 Giugno - 4 Luglio 1991

Centro di Cultura Scientifica «A. Volta», Villa Olmo

Società Italiana di Fisica
Bologna - Italia

ITALIAN PHYSICAL SOCIETY

CONFERENCE PROCEEDINGS

VOLUME 33

The Science of Cold Fusion

Proceedings of the II Annual Conference on Cold Fusion

edited by T. Bressani, E. Del Giudice and G. Preparata
Como, 29 June - 4 July 1991

«A. Volta» Centre for Scientific Culture, Villa Olmo

Italian Physical Society
Bologna - Italy

Technical Editing by Carmen Vasini

ISBN 88-7794-045-X

Printed in Italy

INTERNATIONAL ADVISORY COMMITTEE

J.O'M Bockris (U.S.A.)
T. Bressani (Italy) (co-chairman)
M. Fleischmann (U.K.)
H. Ikegami (Japan)
X.Z. Li (China)
M. McKubre (U.S.A.)
H. Menlove (U.S.A.)
S. Pons (U.S.A.)
G. Preparata (Italy) (co-chairman)
C. Sanchez Lopez (Spain)
J. Santucci (U.S.A.)
F. Scaramuzzi (Italy)
M. Srinivasan (India)
A. Takahashi (Japan)
F. Will (U.S.A.)

LOCAL ORGANIZING COMMITTEE

G. Casati (Milano)
E. Del Giudice (Milano)
F. De Marco (Frascati)
D. Gozzi (Roma)
F. Iazzi (Torino)
A. Zecchina (Torino)

SPONSORING AGENCIES

- Ansaldo Componenti S.p.a.	- Genova	(Italy)
- Centro Italiano Studi ed Esperienze	- Milano	(Italy)
- Consiglio Nazionale delle Ricerche	- Italy	
- Electric Power Research Institut	- Palo Alto	(U.S.A.)
- Ente Nazionale Energie Alternative	- Italy	
- Istituto Nazionale di Fisica Nucleare	- Italy	
- Regione Lombardia	- Italy	
- Technova Inc.	- Tokio	(Japan)
- Universita' degli Studi di Milano	- Italy	
- Universita' degli Studi di Torino	- Italy	

CONTENTS

INVITED PAPERS
==========

SUMMARIES
=========

APPENDIX
========

EDITORS' FOREWORD

The idea to keep open a fundamental channel of scientific information for people interested in Cold Fusion, came to us while visiting the now defunct National Cold Fusion Institute (N.C.F.I.), in Salt Lake City (Utah) in the Fall of 1990.

For those, like ourselves, who wished to keep the Cold Fusion file open those were very hard times. We were in the middle of a press (and otherwise) attack on the occasion of a scientific review of the N.C.F.I., that was alleged to have been deviously avoided by the two scientists, Martin Fleischmann and Stanley Pons, that made it all happen.

Naturally things went differently from what announced and reported in the press; the review was basically positive, the scientific interest of Cold Fusion was established, but the world, scientific and otherwise, seemed to take no notice and continued in the deep rooted conviction that Cold Fusion, like many other pretended scientific discoveries, permanently belonged to the Museum of Errors.

In organizing the II Annual Conference on Cold Fusion, after the first held in Salt Lake City at the end of March 1990, our main concern and effort has been to keep this event within the strict confines of a scientific meeting. As the more than 200 participants have had the opportunity to witness, the meeting has proceeded with a rather stern and exhausting program for 5 full days, undisturbed, uninterfered by the press or any other external source of perturbation. The discussion has never touched the political aspects (even though some of them are rather interesting), but it has always been focussed on the really burning issues, both experimental and theoretical. For us it has been a most rewarding experience, and we have evidence that such has been the general feeling. And in view of this we have thought it appropriate to give these Proceedings a

title: "The Science of Cold Fusion", which emphasizes what has been the main characteristic of the Conference.

Getting to the contents of the Proceedings, we have decided that the book should give a faithful image of what went on in the 5 days of the Conference. Thus we submitted the papers received to a refereeing process which was kept at a rather lenient level, mitigated by some "Editorial Notes", where some of the basic objections of the Referees were reported, with the aim to correctly represent the points where the disagreement among the interested scientists is more acute.

Following the structure of the Conference, we have organized the book in three main points: one containing the Contributed papers, the second the Invited papers, while the third comprises two summaries, one by Heinz Gerischer and the other by Martin Fleischmann, that actually was not delivered at the Conference, but we thought it worthwhile to include in these Proceedings. Finally in an Appendix, due to its importance in the light of nasty allegations that were made in the press in the last year, we have included the full Report that Wilford Hansen, one of the speakers that most stirred the Conference audience, recently presented to the Utah State Council on Energy/Fusion.

Finally we should like to thank most warmly the Members of the International Advisory Committee who have given their precious advice on the program of the Conference with solicitude and intelligence.

The Local Organizing Committee also performed in an impeccable way, and we take this occasion to gratefully acknowledge their work. We have highly appreciated the very effective collaboration of the "A. Volta" Centre for Scientific Culture in whose premises the Conference took place. The Secretariat carried out its tasks in a very effective and dedicated manner: for this we thank Miss F. De Zan, Miss F. Gandino, Mrs. C. Nuncibello and Miss P. Pistochini.

The Conference could not have taken place without the generous and enthusiastic support of our sponsors; for this we thank them all most deeply.

Tullio Bressani

Emilio Del Giudice

Giuliano Preparata

CONTRIBUTED PAPERS

Conference Proceedings Vol. 33
«The Science of Cold Fusion»
T. Bressani, E. Del Giudice and G. Preparata (Eds.)
SIF, Bologna 1991

ANALYSIS OF TRITIUM AND HEAT EXCESS IN ELECTROCHEMICAL CELLS WITH Pd CATHODES

L. Bertalot, L. Bettinali, F. De Marco, V. Violante
Associazione EURATOM-ENEA sulla Fusione, Centro Ricerche Energia Frascati, C.P. 65 -00044 Frascati, Rome, Italy

P. De Logu, T. Dikonimos Makris, A. La Barbera
ENEA, Dipartimento INN-PCM, Centro Ricerche Energia Casaccia, Rome, Italy

INTRODUCTION

The origin of the excess heat [1,2] developed during the electrolysis of heavy water in "Cold Fusion" cells is up to now open to question. The necessary presence of deuterium suggests that fusion reactions can be partially or totally responsible for the generation of excess heat.

Experience has shown neutron emission to be sporadic and very weak; on the other hand tritium was found in small but detectable amounts [3,4]. Moreover if tritium accumulates in the solution it can be comfortably measured postmortem.

Two experimental campaigns were performed:

The first one in Frascati having as main objective the detection of tritium excess. Particular care was exerted to avoid any tritium and hydrogen contamination.

The second one at the Texas A & M University in the framework of a scientific collaboration, having as objective the excess of heat and tritium measurement.

EXPERIMENTAL

Electrochemical cells

Two type of cells were used.

The first one was used in Frascati for nine tests (named C1 to C9) and is shown in Fig.1a. The vessel is made of glass and the lid of teflon. The lid is screwed on the top of the cell. The connector for the Pd cathode is a nickel tube containing a thermocouple to detect the cathode head temperature. The tube is insulated from the solution by means of a glass tube sealed with araldite. Different anodes and dimensions were used. Some details are reported in Table I.

The second type of cells was used at TAMU for three experiments (named C10 to C12) and it is shown in Fig 1b. It was made of stainless steel with a teflon lid. The lid is screwed on the top of the cell and it has two connectors and a valve to permit a free gas evolution. The connector for the Pd wire is a Pt wire spot welded and insulated from the solution by using a teflon tape wrapped around it.

All the Pd cathodes were annealed under vacuum before use. In the Frascati experiments they were treated at 1000 °C for 10 h. In the calorimetric tests the cathodes were treated at 950 °C for 1 h. In every case the Pd cathodes were washed in ethanol, rinsed in water and in heavy water just before the cell assembling. Pd wires from Engelhard 99.95% were used for the cells C1 to C4, from Johnson & Matthey 99.9997% for the cells C5 to C9 and from Alpha Product 99.997% for the cells C10 to C12. Platinum and Nickel from Carlo Erba 99.5% were used as anodes for the cells C1 to C9 and platinum from Alpha Product 99.9995% for the cells C10 to C12. Heavy water from Fluorochem Limited 99.9% atomic in deuterium for the cells C1 to C9 and from Aldrich with 99.8% atomic in deuterium for the cells C10 to C12 was used. Both had similar activity of about 185 dpm/ml. Lithium from Carlo Erba 99.9% for the cells C1 to C9 and from Aldrich 99.9% for the cells C10 to C12 was used. Deionized water for the cell C11 and Sodium deuteroxide from MSD Isotopic 99.8% atomic in deuterium for the cell C12 were used.

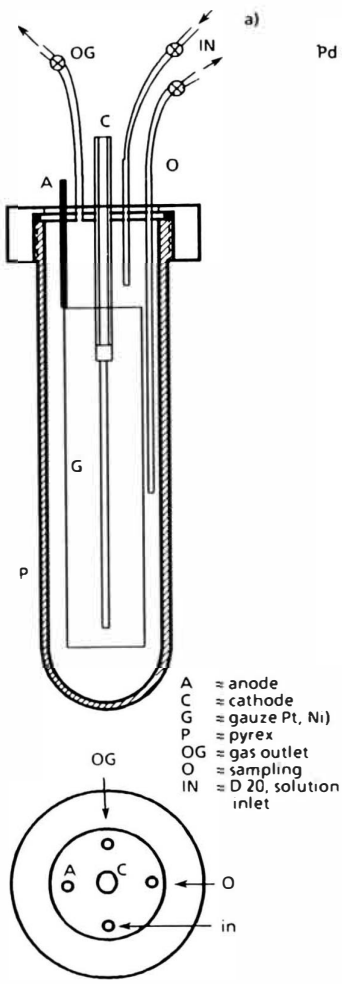

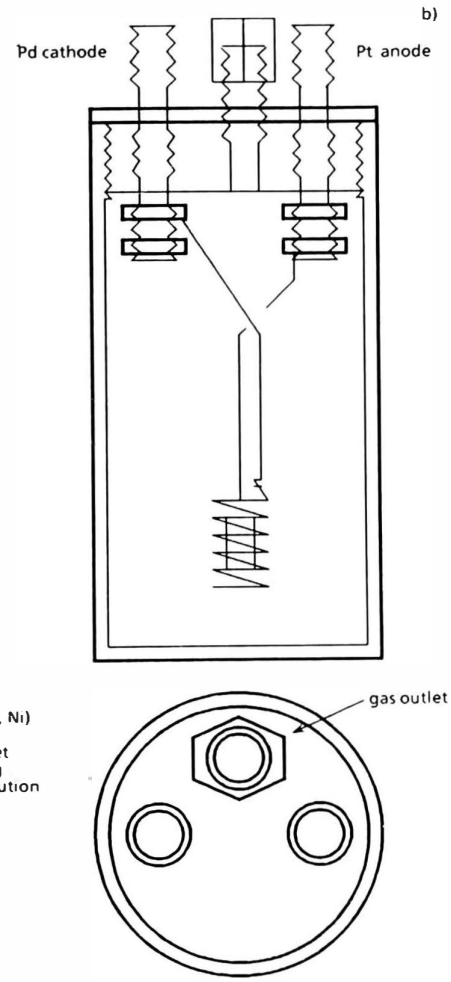

Fig. 1a - Frascati cell **Fig. 1b - TAMU cell**

Diagnostics

The neutron detection equipment consists of three ^3He neutron counters and a BF_3 counter, all embedded in polyethylene. One of the ^3He detectors is used to monitor the noise/background signal. The overall efficiency of the counters are in the order of 5 10^{-5}-10^{-4} cts/n. The minimum detectable neutron emission rate is 30 n/s at the source. No significant neutron emission rate above the minimum detectable rate has been observed in all the experiments.

The tritium measurements, within $\pm 3\%$ error, have been carried out by means of a BETA counter 2560 XL Packard, having a 33% efficiency for tritium. The background level was 4 CPM. The tritium measurements have been performed by taking into account the radiation energy spectrum emitted by the liquid scintillator.

Chemical and microstructural characterization of the cathodes was performed by using an high resolution scanning Auger spectrometer Perkin Elmer model 600.

Calorimetry

A commercial available 4 cells Hart Scientific Model 8244 heat conduction calorimeter was used to measure the heat output from the electrochemical cells. It was possible to operate with 4 cells at the same time in a power range up to 2 W

Table I - Synopsis of the Cells.

Cells	Anodes	Cathodes Pd wire (mm)	Current density (mA/cm^2)	Time (day)
C1	Pt[a]	1×37[d]	100-700	46
C2	Ni[a]	0.5×82[d]	100-700	36
C3	Ni[a]	as C2[d]	100-700	34
C4	Ni[a]	as C2[d]	100-1200	33
C5	Ni[a]	tube = 6.3[e] ×82×0.15	100	16
C6	Pt[b]	as C5[e]	60	84
C7	Pt[b]	as C2[e]	100-650	66
C8	Pt[b]	as C2[e]	100-650	82
C9	Pt[b]	as C2[e]	100-650	82
C10	Pt[c]	0.5×10[f]	500-950	62
C11	Pt[c]	as C10[f]	600-800	60
C12	Pt[c]	as C10[f]	600	48

[a] Gauze and [b] Coil from Carlo Erba. [c] Coil and [f] from Alpha Product. [d] from Engelhard [e] from Johnson and Matthey

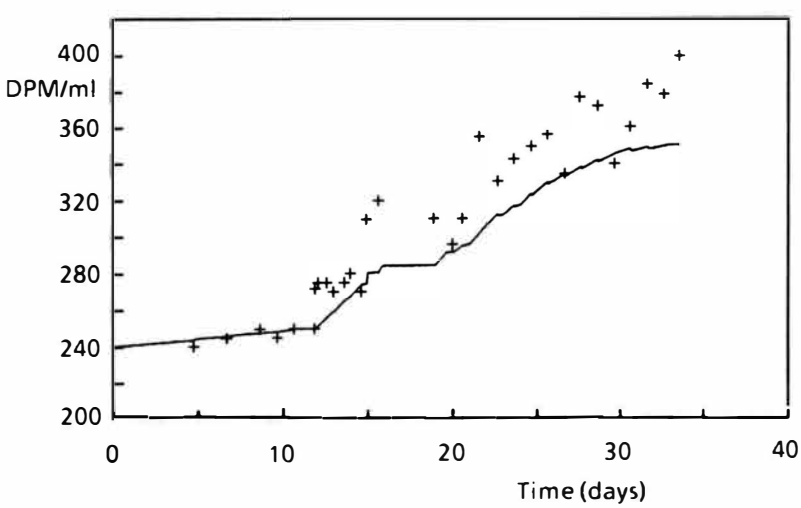

Fig.2 - Tritium enrichment vs time in C3

per cell. The calorimeter is based on the Seebeck effect. A potential proportional to a difference of temperature is generated. Such a potential is then directly proportional to the heat flow coming from the cell. . All the four cells have a twin cell. The system is mounted in a large aluminum block that is submerged in a

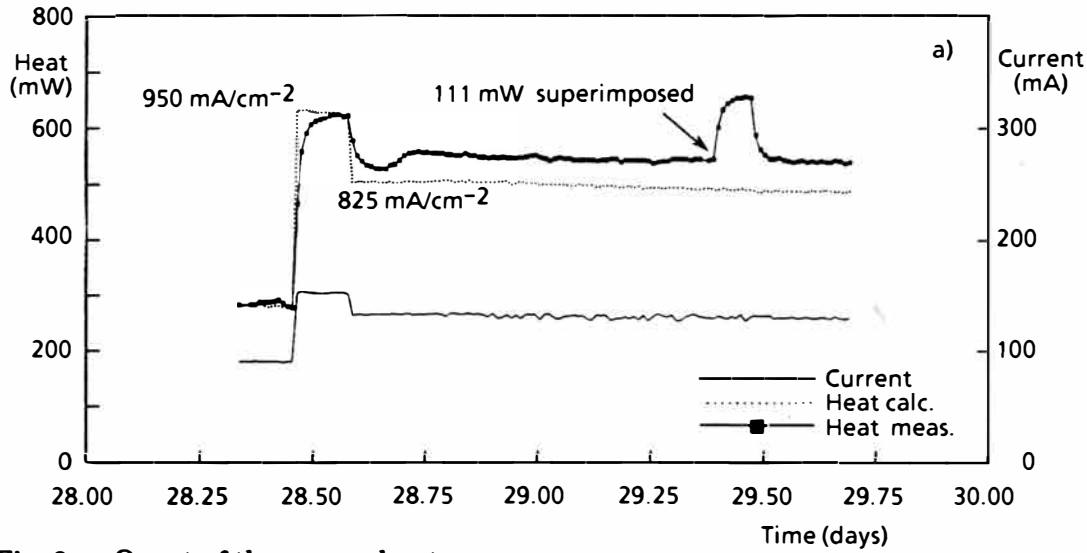

Fig. 3a - Onset of the excess heat

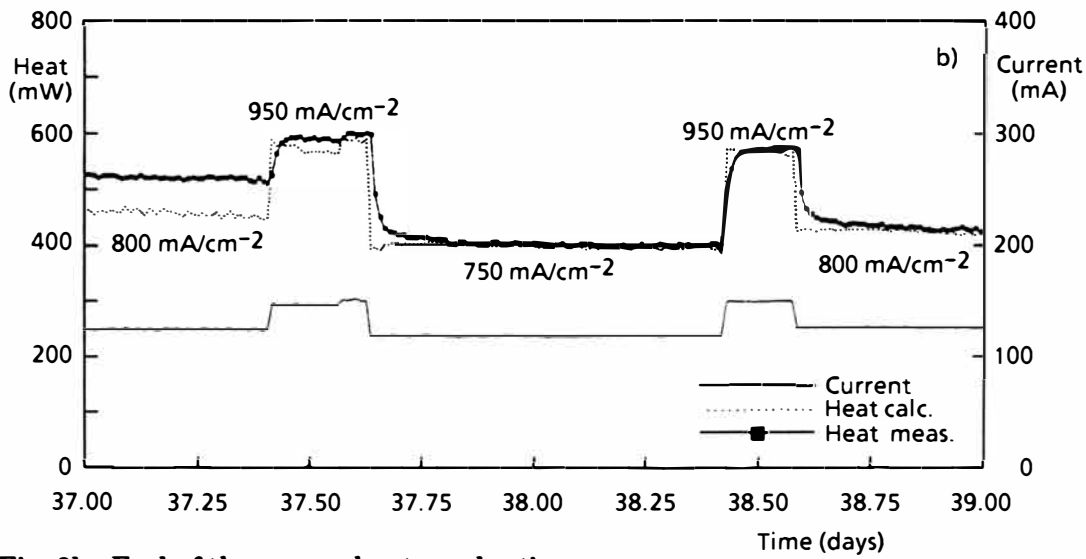

Fig. 3b - End of the excess heat production

constant temperature water bath. When a temperature change occurs in the working cell, a potential is generated and registered. The twin cell design has the advantage of canceling external thermic effect. The signals of the twin cells are connected in a differential way. This connection results in a long-term stability and reproducibility of the base line. The system can easily be calibrated by means of internal resistors and 5 mW is the maximum error estimated.

RESULTS AND DISCUSSION

Tritium measurement

The tritium measurement relative to the cell C3 is shown in Fig. 2. The continuous line shows the isotopic tritium enrichment by assuming 2 as separation factor. The content of tritium in all the experiments is in agreement

with the expected isotopic enrichment even if the behaviour of the single cells is different on a day to day basis. In two of them sharp, short ($\leq$ 12h) increases occurred a few times, that can be fitted with a separation factor larger than 5.

Heat Measurement

One cell out of three gave an excess of heat (cell C10). In Fig.3a and 3b two diagrams relative to heat versus time are shown. The cell was first operated for about 23 days by imposing different current densities and applying current pulses up to 1.4 A/cm^2 (for a maximum time of 30 min). During the following five days the cell was maintained at 600 mA/cm^2. Then the current density was enhanced up to 950 mA/cm^2 for three hours (i.e. the relaxation time of the calorimeter) and then decreased at 850 mA/cm^2. After three hours an excess of heat generation rate of about 50 mW was detected.

To verify if the system were working well 111 mW were superimposed by means of the internal resistor and after three hours exactly 111 mW more were measured (see Fig. 3a). The excess of heat generation rate lasted about 10 days, at that moment the current density was again increased up to 950 mA/cm^2 for a time and then decreased at 750 mA/cm^2: the excess of heat generation rate disappeared (see Fig. 3b). During the 10 days such an excess ranged between 50 and 80 mW, that means 12-20% of the power input. The total energy produced was about 57 kJ ($>$200 MJ/molPd). During the last three days of excess of heat generation rate, the gas evolution was several times measured by means of a flow meter to verify if any recombination took place. The result was 100% $\pm$ 5% of the expected flow rate. To produce an excess of heat of about 50-80 mW a recombination of 25-40% should be considered, which is rather far from the gas evolution measured.

Auger analysis

Semiquantitative Auger analysis performed on cathodes has shown a thick scale of about 200-300 Å mainly constituted of Oxygen, Iron and Calcium and lesser quantity of Copper, Platinum, Silicon and Carbon. Similar contaminants have been found on cathodes used at TAMU and at Frascati.

CONCLUSIONS

- Nine cells were set up in Frascati aimed to detect tritium as the indicator for D-D fusion trying to avoid contaminations.
- No tritium above the electrochemical isotopic enrichment was found.
- Three cells were set up at Appleby's laboratory at TAMU inside a commercial calorimeter.
- One cell gave an excess power ranging between 12 and 20% (25-40 W/cm^3) for about 10 days producing about 57 kJ.
- Post mortem Auger analysis on cathodes revealed similar contaminants.

REFERENCES

1) M.Fleischmann, S.Pons, M.W Anderson, L.J.Li, and M. Hawkins, J.Electr. Anal.Chem. **287** (1990) 293.
2) J.Appleby, Y.J.Kim, C.R.Martin, O.J.Murphy and S.Srinivasan, "Proc. Workshop Cold Fusion Phenomena" Santa Fe, New Mexico, May 22-25 1989.
3) J.O'M.Bockris, G.H.Lin, N.J.C.Packham, Fusion Tech. **18** (1990) 11.
4) E.Storms, "Review of Experimental Observation about the Cold Fusion Effect". To be published in Fusion Techn.

Conference Proceedings Vol. 33
«The Science of Cold Fusion»
T. Bressani, E. Del Giudice and G. Preparata (Eds.)
SIF, Bologna 1991

PRODUCT ANALYSIS FROM D_2O ELECTROLYSIS WITH PALLADIUM AND TITANIUM CATHODES

E. Brillas*, G. Sardin*, J.Casado, X.Doménech and J.Sánchez
Departament de Quimica Universitat Autónoma Barcelona.
Bellaterra (Barcelona) Spain.
*Departament de Quimica Física. Universitat de Barcelona.

ABSTRACT

The possible generation of tririum in the electrolyte and the incorporation of species such as tririum, lithium and platinum to cathodes during the electrolysis of 0.1M LiOD solutions with Pd and Ti cathodes and Pt anodes at low and high current densities have been studied by means of different techniques.

INTRODUCTION

During D_2O electrolysis, large amounts of deuterium are absorbed by Pd and Ti cathodes to yield the respective Pd+D and Ti+D phases. However, less is known about other species either incorporated or possibly generated in cathodes. In this way, Chêne and Brass [1] reported a small tritium production into Pd during the electrolysis of 0.1M LiOD in open cells at high current densities. Several authors[2,3] have proposed a slow diffusion of Li^+ ions into the bulk of Pd.

In this communication, we present results of a study on the electrolysis products of 0.1M LiOD solutions with Pd and Ti cathodes or produced in them, such as tritium, lithium and platinum, as well as to investigate the tritium enrichment of the electrolyte.

EXPERIMENTAL

0.1M LiOD solutions were prepared by addition of Li metal to 99.95% D_2O and 0.1 M LiOH solutions by adding LiOH to bidistilled light water. All chemicals were of analytical grade. A 0.1M LiOD solution with a tritium content 3 times higher than that of pure D_2O was prepared by addition of standarized tritium labelled water, supplied by Amersham.

Pd and Pt sheets of 99.9% purity (SEMP) with respective dimensions of 0.1cmx1.5cm and 0.25mm x 1.5cm x 3cm, and 1.4 cm diameter x 3cm Ti rods of 99.9% purity (Inagasa), were employed as cathodes in the electrolyses at low current density. In the experiments at high current density, Pd and electrolytic Ti (99.9% purity) sheet cathodes of 0.1cm x 0.5 cm were used.

D_2O electrolyses were carried out either at a low current density of 5 mA cm^{-2} for periods up to 30 days or at high current densities of 100 and 300 mA cm^{-2} for 15 to 16 days. Experiments were conducted in thermostatted cylindrical glass cells containing 20 ml of electrolyte. The cathodes were placed in the center of cells, being surrounded by spiral anodes (Pt) of 4 cm diameter x 4cm height. The volume of the electrolyte was maintained constant by addition of controlled amounts of solution after sampling for tritium analysis. The temperature was always kept constant at 25 °C. Gases evolved during electrolyses were vented through a glass rod placed in the top of the cells.

Tritium especific activity on samples of the electrolyte was determined using a Wallac Quantulus 1220 liquid scintillation. A 1 ml aliquot was periodically withdrawn from the cell and thoroughly mixed with 9 ml of a high efficiency water soluble scintillation cocktail(Optiphase Hisafe 3,LKB). Samples were left to stabilize in the chamber for at least 24h and counted for a 60 min period. The tritium efficiency of the system was found to be 0.38. No chemiluminiscence nor significant quenching was observed in any of the samples.

The products accumulated near to the surface of cathodes used in D_2O and H_2O electrolysis experiments were analy-

sed from SIMS spectra obtained with an Atomika A-DIDA 3000 secondary ion microscope, using O_2^+ with 6kV energy as primary ion beam. A Jeol JSM 840 scanning electron microscope (SEM) with 20kV accelerating voltage was used to determine the depth of the O_2^+ attack by SIMS. The overall Li and Pt contents for Pd and Ti sheets of 0.25 cm^2 area and for Ti rods of 0.5 cm height, before and after electrolysis, were respectively obtained with a Varian 875 atomic absorption spectroscope and a Jobin Yvon JY38VHR inductively coupled argon plasma spectroscope, after solving the metals with HCl acid.

RESULTS AND DISCUSSION

A mean tritium specific activity of 0.077 ± 0.008Bq ml^{-1} was obtained for all H_2O solutions before and during their electrolyses with Pd, Ti and Pt cathodes at 5 mA cm^{-2}. The mean tritium specific activity, a_o, for the two 0.1M LiOD solutions studied was of 280 ± 5 and 817 ± 12(after addition of tritium) Bq ml^{-1}. In all D_2O electrolyses carried out with Pd, Ti and Pt cathodes, at low and high current densities, a gradual increase of the tritium specific activity of the electrolyte at constant volume, $a_{i,v}$, was always found. The increase in this parameter with time for all cathodes was explained from the expected tritium enrichment in open cell, according to the equation[4]

$$a_{i,v}/a_o = 1/S\left\{1-(1-S)\exp\left[-Srt/N\right]\right\}$$

where S denotes the observed tritium-deuterium separation factor of the cathode, r the rate of electrolysis, t the electrolysis time and N the number of deuterium atoms in the solution Using this equation, S values of 0.4 to 0.6 for Pd and Ti and 0.55 to 0.75 for Pt were obtained from experimental data.

Several Pd and Ti cathodes previously charged either at low or at high current densities were thorougly rinsed with bidistilled water and further introduced in cells containing 20 ml of 0.1 M LiOH, which were then run at 100 mA cm^{-2} for 24h. After this, all species (D and T) previously contained in cathodes were completely displaced by hydrogen and trans-

ferred to the electrolyte, as confirmed by SIMS. Electrolytes proceeding from Ti cells did not show any increase in tritium activity, as expected if this species is not accumulated into Ti during D_2O electrolysis. Electrolytes of Pd cells, however showed increases of 40 to 60 Bq in tritium activity, indicating the presence of small amount of T into Pd cathodes.

From comparison with blank determinations, it can be established that small quantities of Li are incorporated into both Pd and Ti cathodes after prolonged electrolyses. The Li accumulated in Ti cathodes is higher than the accumulated in Pd cathodes. Also small amounts of Pt from anode are electrodeposited on both Pd and Ti cathodes.

SIMS depth profiles in the form intensity (counts s^{-1}) vs. sputter time (proportional to the depth) were simultaneously recorded for the positive and negative secondary ions generated until a m/e ratio of 7 from the O_2^+ attack on Pd and Ti cathodes. Positive and negative secondary ions with m/e ratio of 1 (H^+ and H^-) were always detected. Positive m/e=6 and 7 ions (Li isotopes 6 and 7) were also recorded. High increases of ca. 20 and 500 times in intensity with respect to that of virgin electrodes were found for spectra of Li^+ ions recorded for Pd and Ti cathodes, respectively. This indicates that a preferential accumulation of Li near to the electrode surface takes place in electrolyses of both D_2O and H_2O. All cathodes used in D_2O electrolysis showed SIMS spectra for positive and negative secondary ions with m/e values of 2, which can be ascribed to D^+ and D^- ions.

Inspection of the data obtained from SIMS analysis confirms that tritium is not accumulated into Ti. All Pd cathodes after D_2O electrolysis showed positive ions with m/e values of 3, 4 and 5. Since T is absorbed by Pd and H_2^+ and H_3^+ ions are detected for Pd cathodes saturated with hydrogen, T^+ and DH^+ ions can be ascribed to m/e=3, TH^+, D_2^+ and DH_2^+ ions to m/e=4 and TD^+, D_2H^+ and TH_2^+ ions to m/e=5.

Pd and Ti cathodes previously charged with deuterium and further electrolysed in 0.1M LiOH solutions at 100 mA cm^{-2} for 24h showed the same SIMS spectra obtained for cathodes only used in H_2O electrolysis, as expected if all species pre-

viously contained in them are displaced by hydrogen and transferred to the electrolyte.

ACKNOWLEDGEMENTS

The authors wish to thank to DGICYT (Ministerio de Educación y Ciencia, Spain) for financial support (grant APC-28/89).

REFERENCES

1)J. Chêne and A.M. Brass, J.Electroanal.Chem.,280, 199(1990).
2)J.W. Schultze, U. Konig, A. Hochfeld, C. Van Calker and W. Kies, Electrochim. Acta, 34, 1289(1989).
3)F. Dalard, M. Ulmann, J. Augustynsky and P. Selvam, J.Electroanal.Chem., 270, 445(1989).
4)D.E. Williams et al., Nature, 342, 375(1989).

«The Science of Cold Fusion»
T. Bressani, E. Del Giudice and G. Preparata (Eds.)
SIF, Bologna 1991

SOLID STATE AND ELECTROCHEMICAL PHENOMENA RELATED TO COLD FUSION IN TITANIUM

B. Escarpizo, F.Fernández, J. Sevilla, F. Cuevas and C. Sánchez

Dept. Física Aplicada C-IV, U.A.M., Cantoblanco, 28049 Madrid, Spain

I.Introduction

Attempts to reproduce cold fusion results/experiments follow, at least, two possible directions:

a) Improvements of characteristics (efficiency and so on) of detectors and reductions of background signals and noises.

b) Better knowledge of the system (electrolytic cell) i.e. of the cathode material and of the electrolysis itself.

We have been running several electrolytic experiments along all the past year (results will be reported elsewhere) and investigating on some electrochemical and solid state phenomena which could be related to the lack of reproducibility of cold fusion experiments. In this communication we will deal with one of them: the role played by the polycristalline grains during the charging of Ti cathodes with Deuterium by electrolytic means.

I. Distribution of Deuterium in Titanium cathodes

It has been pointed out by several authors that a heavy deuteration of the cathode is necessary if cold fusion is to be produced. Unfortunately we have concluded that high Deuterium concentrations in the bulk of Ti cathodes are hardly obtained in current and regular electrolytic

experiments. This conclusion is, in fact, suggested in experiments by Brauer et al. (1) who determined the Hydrogen profile in Ti pieces electrolytically loaded. The profile shows a plateau of thickness ~0.25 μm, where Hydrogen concentration is about 62 atoms per cent (TiH_x $x \simeq 2$), followed by a rapid decrease of the Hydrogen content up to thicknesses of about 0.7 μm where one finds only metallic Ti. This type of profile clearly suggests the existence of a barrier which prevents a full propagation of the Hydrogen atoms. If no barrier is present in the cathodes, and by considering that Hydrogen goes into Ti by electrolytic pressure and then diffuses into its volume, the calculated Hydrogen profile shows that Hydrogen concentration continuously decreases from a value of x=2 at the surface to x=0 at a thickness as large as 4 μm, seven times larger than the one found in the real experiment.

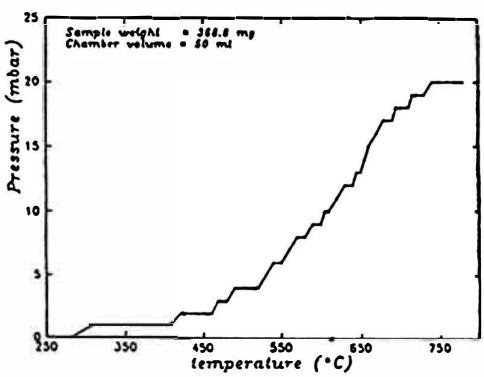

Fig.1. Accumulated pressure versus heating temperature during thermal desorption of Deuterium from one of the Ti cathodes used in electrolytic cold fusion experiments.

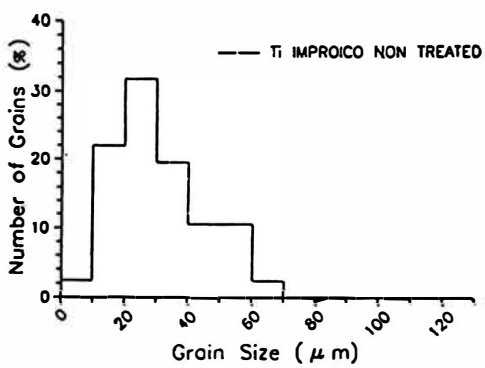

Fig.2. Distribution of grain size in commercial Ti plates. Number of grains is plotted against its size.

We have tested this point of view with all the Ti cathodes used through about twenty electrolytic cold fusion experiments. By using Thermal Desorption (TD) of the absorbed Deuterium and by applying Differential Scanning Calorimetry (DSC) to the same cathodes, we have concluded (2) that full deuteration of the cathodes is only produced in a layer close to the surface of thickness between 5-10 μm. Results of Thermal Desorption of one

of our samples are shown in Fig.1, where the Deuterium accumulated pressure is plotted against the sample temperature during its heating up to ~800^{0}C where the Hydrogen pressure reaches a plateau. Same results have been obtained with all the others samples used in our electrolytic experiments.

The electrolyte was in ten experiments acid and in three of them basic and the electrolysis charge in Ah ranged from about 290 Ah to 2080 Ah. All the results confirm that deuteration of our Ti cathodes takes place in a layer of thickness between 5-20 μm with Deuterium concentrations ranging between x=1 and x=2. Some authors apply X-ray diffraction to confirm that they have produced TiD_2. But this is a misleading tool because it gives only information on the structure of a layer equal to the penetration of the X-rays. In fact, some of our cathodes have been examined by XRD and Deuterium concentrations between x=1.5 to x=1.8 have been obtained, in agreement with the former conclusion because the penetration depth of the CuKα X-ray line is smaller than ~10 μm.

III. Role played by polycristalline grains

By using Optical and Electron Microscope Microphotographs we have determined the grain size of the different Ti cathodes used in our experiments before doing electrolysis. Results are shown in Fig.2 where the number of grains (in %) is shown against its size in μm. Although there is a grain size distribution between ~5 μm and ~70 μm, the peak of the distribution is for all the plates in grain sizes of 20-30 μm. This predominant grain size corresponds quite well to the thickness of the deuterated layer of the cathode we have found by other techniques. We therefore may draw the following picture of the deuteration process of commercial Ti used as cathode in electrolytic cold fusion experiments. Deuterium diffusion is limited by the grain boundaries of the polycristalline pieces which act as barriers for the Deuterium propagation. Therefore, the first layer of grains appears with high Deuterium concentration, often close to x=2, and the rest of the cathode with practically no Deuterium.

The proposed deuteration process of Ti has been further confirmed in the case of Ti cathodes electrolyzed in basic electrolytes. Microphotographs from the SEM show the existence of wide cracks between grains after prolonged electrolysis. These cracks appear as a consequence of the

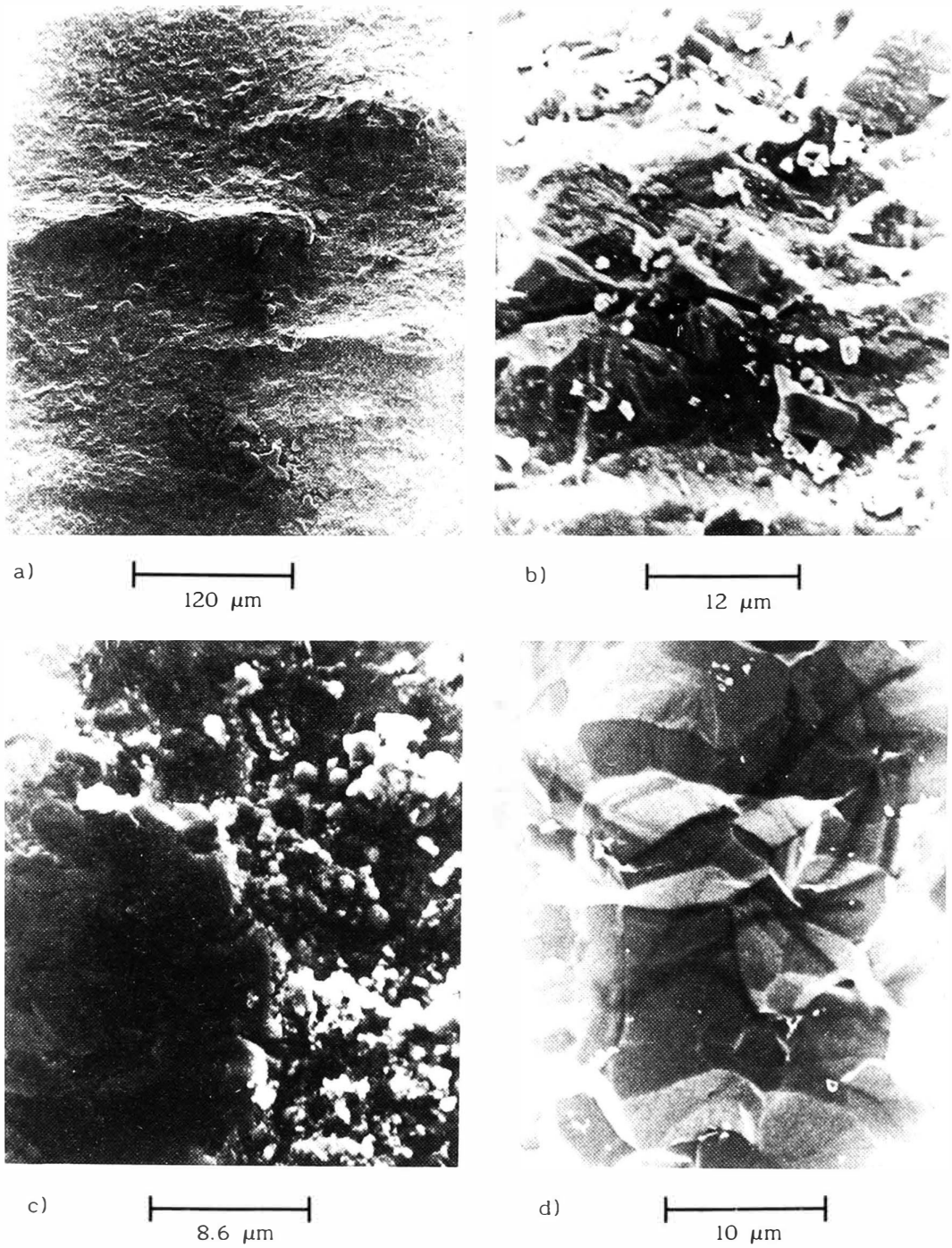

Fig.3. Scanning Electron Microscope photographs of: a) Surface of a Ti where elevations due to grain dilatations can be seen. b) A crack appearing on the top of "mountains" like the one in a) is shown. c) Surface of a Ti cathode where part of the grains have already dropped. d) Facets of clean Ti grains appearing after the first layer of deuterated grains released from the cathode.

dilatation of the grains induced by Deuterium absorption. Grains press one against each other forming elevations like mountains (photo a) of Fig.3) and on the crests of those mountains, where the grain boundary is, a crack appears (photo b)). Once the cracks are large enough, the grain releases from the cathode and drops to the bottom of the cell. This is shown in photograph c) where some grains have been already released. Finally, when a high enough number of grains have dropped from the cathode, a new and clean surface of it has to be deuterated, as can be seen in photograph d), where the facets of clean grains of the Ti cathode are visible. A qualitative picture of this mechanism is shown in Fig.4. This mechanism seems to be no operative in cathodes deuterated in acid electrolytes. At least, the morphology of the cathode surface after the experiments is very different. It resembles a spongy surface with many cavities and a large effective area.

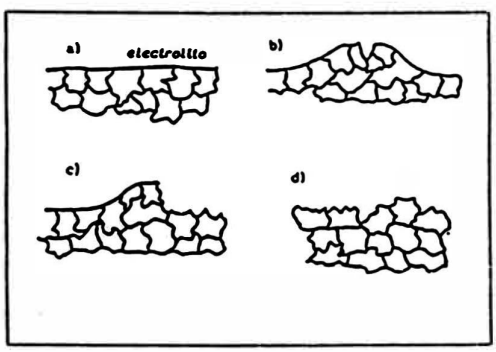

Fig.4. A qualitative picture of in the deuteration mechanism of a polycristalline Ti cathode.

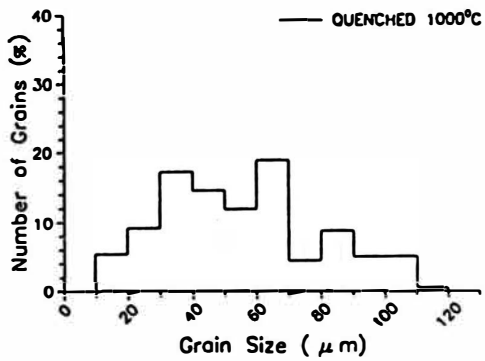

Fig.5. Distribution of grain size in quenched commercial Ti (to be compared with Fig.2).

The reason why the grain boundaries act as a barrier for Deuterium diffusion seems to be the gettering effect of Oxygen, Nitrogen, etc. atoms adsorbed there. Many authors anneal their samples in vacuum before the experiment in order to eliminate the gases adsorbed on the surface of the boundaries. However, the success of this pretreatment is not guaranteed at least a mass spectrometer be connected to the annealing camera to measure the desorbed gases.

We are trying in our experiments another approach to increase the deuterated volume of our Ti cathodes: to enlarge the grains by a thermal quenching. Some results are shown in Fig.5. Some samples quenched in water from different furnace temperatures show grain size distributions whose

peak increases with the furnace temperature. In fact, samples quenched from 10^3 ^{0}C are formed by grains with volumes 30 times larger than those of the untreated samples what means that the deuterated volume will be 3 times larger. In these cases and, if the surface cathode has been conveniently cleaned, the grains must be fully deuterated in a matter of hours with conventional current densities.

IV.Conclusions

We therefore can conclude from the content of this communication that:

Deuteration of Ti cathodes in electrolytic cold fusion experiments seems to take place in only the first grain layer. Grain boundaries seem to be barriers for the propagation of Deuterium in the next grain layer.

Differences in behavior are found between the hydrides formed in acid and basic electrolytes. In basic media, used by most of the authors, the deuterated grains release from the cathode and a new and clean surface of Ti appears periodically.

V.References

(1) E.Brauer, R.Gruner and F.Rauch, Ber. Bunsenges. Phys. Chem., 87, 341-345, (1983)

(2) J.Sevilla, B.Escarpizo, F.J.Fernandez and C.Sanchez, Fus. Tech., 19, 188, (1991)

Conference Proceedings Vol. 33
«The Science of Cold Fusion»
T. Bressani, E. Del Giudice and G. Preparata (Eds.)
SIF, Bologna 1991

MULTICELL EXPERIMENTS FOR SEARCHING TIME-RELATED EVENTS IN COLD FUSION

D. Gozzi, P.L. Cignini[+] and M. Tomellini*

Dipartimento di Chimica, Università "La Sapienza"
P.le Aldo Moro 5, 00185 - Roma, Italy

S. Frullani, F. Garibaldi, F. Ghio, M. Jodice and G.M. Urciuoli

Laboratorio di Fisica, Istituto Superiore di Sanità and sezione INFN-Sanità
V.le Regina Margherita 299, 00161 Roma, Italy

Abstract

A new ten-electrochemical cell experiment has been carried out in order to confirm the previous results and try to understand the key role of some experimental parameters in triggering the cold fusion events. The experiment was designed to detect: a) excess heat; b) loading factor by *in situ* measurement of the cathode displacement; c) nuclear products: neutrons, tritium in the electrolytic solution and in the recombined heavy water, γ-ray; d) effect of the palladium electrode preparation. To measure the excess heat, a calibration curve of the input power *vs* temperature of the LiOD + D_2O solution was obtained for cells equal in shape, materials and operating in the same experimental condition in which the experiment was actually performed. The unique difference was on the cathode. The cathode used in the calibration measurements was made of palladium rod gold-plated by electrochemical deposition. Neutron detector is a ^{3}He proportional counter, the same used in the previous experiments, but the data acquisition is now implemented by a fast pulse-shape storage and off-line discrimination for a very accurate counting. The findings of the experiment, lasted about 50 days, are: *i*) dependent on the type of the cathode, specific excess power values up to 96 W/cm^3 was found; *ii*) specific excess power showed linear dependence from the current density with a threshold at around 150 mA/cm^2; *iii*) the cathode swelling was dependent from the type of the cathode and in the case of rods it increased with the current density; *iv*) no evidence of nuclear products statistically significant was detected.

[+]CNR- Centro di Termodinamica Chimica alle Alte Temperature, c/o Dipartimento di Chimica, Università "La Sapienza", Roma
*Dipartimento di Scienze e Tecnologie Chimiche, Universita' di Roma II "Tor Vergata", 00100 Roma

In this paper the texts of the separate communications given by S. Frullani and D. Gozzi at the 2nd Annual Conference on Cold Fusion are jointly reported.

1. Introduction

The aim of the present paper is to report recent results obtained in a new ten-electrochemical cell experiment carried out in order to confirm the previous results (1-2) and try to understand the key role of some experimental parameters, if any, in triggering the *cold fusion* events.

Our approach to the *cold fusion* experimentation was and still is to search time-correlation among independent measured parameters, both to give a stronger evidence that we are not dealing with instrumental artifacts and to obtain useful information on the related mechanisms. Due to a permanent skepticism of a part of the scientific community, we believe useful that the people still working on this field must continue to show that a big amount of reliable experimental data give results which are not explained with conventional theoretical approaches and therefore we are concerned in a new frontier of the scientific knowledge.

The experiment was designed to detect: a) excess heat; b) loading factor by *in situ* measurement of the cathode displacement; c) nuclear products: neutrons, tritium in the electrolytic solution and in the recombined heavy water, γ-ray; d) effect of the palladium electrode preparation. The main difference between the present experiment and the previous one (2), is constituted by excess heat measurements, a more efficient neutron counting system based on the pulse shape discrimination and *in situ* measurement of the cathode swelling due to the absorption of the electrochemically generated deuterium.

2. Experimental

We shall only report those parts of the our experimental set-up and procedures which have been added with respect to the previous experiments which can be found in the literature (2). Just to facilitate the understanding, we can summarize the features of the experiment as follows:

- Ten equal cells connected in series operating in galvanostatic conditions;
- The only difference among them is in the preparation and/or shape and/or dimensions of the Pd cathode;
- All the cells are placed in a torus-shaped thermostated bath at (24.5 ± 0.1) °C. They are simmetrically located in the bath. Five K-type thermocouples are placed along the torus. Room temperature is kept constant at (20 ±1) °C;
- Before to fill the cells with the solution, a D_2 stream was maintained for some time;
- All the cells have a separate gas recombiner for tritium (T) monitoring in the gases;

- All the cells are provided with a device to maintain a constant level of solution by adding D_2O when consumed;
- Each cell is monitored for:
- Temperature of the cathode
- Temperature of the solution
- Voltage of the cell
- T in solution and in gas phase externally recombined
- Two cells out of ten have a displacement transducer to monitor the cathode swelling during D-loading;
- One ^3He proportional counter for neutron detection is placed in the centre of the torus and two γ-ray detectors (NaI and HPGe) are properly located around the bath.

2.1 Excess heat Measurements

Because our torus-shaped multicell apparatus is not a calorimeter, but it is an isothermal device, accurately thermostated, which allows to keep at constant temperature the external wall of each of the ten electrochemical cells, the variation cell to cell of the heat flux crossing each glass tube only depends from the temperature of the electrolyte solution since all the parameters influencing the heat transport (electrolytic solution and its volume, geometry of the cell and materials by which it is made of, exchange surface area, etc.) are equal for all the cells. Thus, at a fixed input power imposed to the cell, a stationary thermal gradient will be established between the inner solution and the thermostated bath. If the stationary values of the temperature of the electrolyte solution are reported as a function of the respective input power applied to the cell, we have a calibration curve which provides the excess heat data when well-defined deviations from it occur during the real experiment.

2.1.1 Calibration procedure

Few points are necessary to explain the procedure we adopted in making the calibration curves :

- Two cells (by dimensions, shape, materials, etc.) equal to those used in the experiment have been calibrated in the same experimental arrangement previously described;
- Two types of calibration for each cell were carried out both in LiOD + D_2O solution:
- Thermal (by an electric heater);
- Electrochemical (as in the experiment) by using gold plated Pd cathodes. Each electrode was carefully controlled by SEM microprobe mapping of Pd to be sure that Pd was not detected;
- In both the cases each stationary temperature of LiOD solution at fixed input power was kept as a point of the respective calibration curve;

- It can be shown that the stationary temperature at constant input power does not depend on the electrode mass. This can influence the time constant only. Thus, the calibration curve obtained is valid throughout our system.

The choice of this procedure was based on the fundamental concept that, in absence of processes other than the D_2O electrolysis, the two calibration curves must be found superimposed due to equality:

$$[|V| \times I]_h = [(|V|-V^\circ) \times I]_e , \qquad (1)$$

where $|V|$, I and V° are, respectively, the voltage at Joule heater or electrode leads, the current crossing the respective systems and the thermoneutral voltage given by $-\Delta H^\circ_f(D_2O,l)/2\mathcal{F}$ being $\Delta H^\circ_f(D_2O,l)$ and $\mathcal{F}$, respectively, the enthalpy of formation of liquid D_2O and the Faraday's constant. V° has been taken equal to 1.5367 V(3). The subscripts h and e stand for, respectively, by-heater and electrochemical calibrations. Furthermore, we used as blank for the calibrations heavy water solutions and Pd gold-plated cathodes because we believe that both these conditions allow to be closer to the real experimental situation. In fact, the use of light water solution instead of the heavy water solution as blank, though so widely adopted to guarantee the reliability of the cold fusion findings, is quite imprecise from the calorimetric point of view because heat capacity and thermal conductivity of the solution, enthalpy of vaporization of D_2O as well as thermal conductivity of H_2 and D_2 are all appreciably different. The gold-plating of Pd cathode avoids the process:

$$D_{ads} \rightarrow D_{bulk}\ (Pd) \qquad (2)$$

while the processes

$$D_{ads} + D_{ads} \rightarrow D_2(g)$$

and/or (3)

$$D_{ads} + D_2O + 2e(Au/Pd) \rightarrow 2\ OD^- + 1/2\ D_2(g)$$

remain the same as in the case of Pd only. The ads subscript stands for the chemisorbed status of the deuterium atom onto the cathode surface. Obviously, if the process 2 is completely forbidden, we can be sure that neither cold fusion phenomena nor chemical process occur.

Figure 1 shows some stationary steps used to build the calibration curves by making use of both an electric heater (Fig. 1A and 1B) and the electrolysis (Fig. 1C and 1D). Figures 1B and 1D display a portion corresponding to a single step of the respective A and C curves.

2.1.2 Electrodes and cells

Gold-plated Pd cathodes were prepared starting from Johnson & Mattey 6 mm diameter rod, cut in 25 mm long pieces, machined at one end for encasing the thermocouple and then accurately polished before the electrochemical plating. The gold layer thickness was

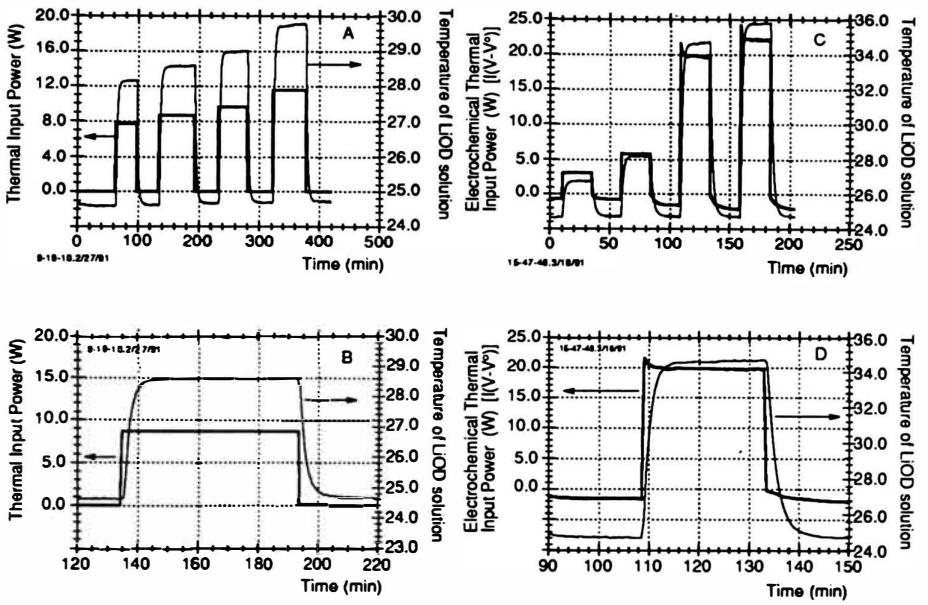

Figure 1. Typical trends of the temperature of the LiOD solution *vs* input power in the thermochemical and electrochemical calibration mode

about 4 μm. To improve the electrical contact also the shield of the all K-type thermocouples used in this experiment was gold plated. Since the shields are electrically insulated from the inner thermoelements, they also work as current leads for the cathodes. To obtain this, the shields were soldered on the top of each cathode. The space around the junction cathode/thermocouple were filled with epoxy resin and then covered by a piece of thermoplastic tube to avoid the direct contact with the alkaline solution. All the materials used were tested for long time to be inert in LiOD alkaline solutions.

Anode and cell geometry and dimensions were given elsewhere (2). Here it is just sufficient to mention the characteristic of the heater. This was a 50 W resistor obtained by winding Kantal wire on a capillary alumina tube. The whole diameter was 3.2 mm. It was placed in a NMR-type test tube filled with silicon oil and inserted in the proper hole of the cell teflon cap.

2.2 Furher details on the electrolytic cells

2.2.1 Cathode swelling measurement

Two cells out of ten were modified in the bottom part to allow the insertion of a LVDT (Linear Voltage Displacement Transducer) by Penny+Gilles, U.K. mod.1354. This kind of

transducers have an infinite resolution and the sensitivity is given better than 1 mV/μm practically depending on both the electronics of the d.c. power supply and voltmeter used for the readings. By our apparatuses, we can measure displacements greater than 0.1 μm and up to 5 mm in both the directions. The LVDT was placed in a teflon cylinder fitted to the bottom of the glass cell. To seal the LVDT from the alkaline solution and to allow the spring loaded probe to move free, a very thin plastic membrane was used. Due to the type of assembly, we can measure the electrode swelling only in the z-axis (major dimension) direction. The voltages were read by two of the 60 analogic input channels of the data logger and directly converted in μm according to the linear calibration curves previously found. LVDT data as well as the other ones coming from the entire apparatus are transferred through the data logger to a Macintosh II fx running on a home-made acquisition program written on LabVIEW 2.1 (National Instruments, Austin, TX).

2.2.2 Cathodes

The ten Pd cathodes used were prepared in different ways as reported in Table I below. The cathode and thermocouple assembly was done by the same procedure as reported in section 2.1.2.

TABLE I

#	Type	Treatment	Dimensions (mm)	Remark
1	rod	HVLHT	Ø 6x25	
2	powder sponge	pressed	5.3x4.3x25.7	300 MPa
3	rod	as received	Ø 6 x 25	LVDT
4	powder sponge	HVSS	5.2x4.4x25	LVDT
5	rod	as received	Ø 6 x 25	
6	rod	RFHQ	Ø 6 x 25	
7	amorphous lamina	as received	Ø 4.1x16	Teflon supported*
8	31 wires	CSD	Ø 0.5x22	Au welded one end
9	rod	RFHQ	Ø 3x22	
10	powder sponge	HVLS	4.7x3.9x23	

HVLHT = High Vacuum Long Heat Treatment (10 h at 1250°C and cooled at 6°C/h)
RFHQ = Radio Frequency Heated at 1350 °C for 10 min under Ar and Quenched in LN_2
HVSS = High Vacuum Short Sintering (5 min at 1250 °C)
CSD = Cold Screw Dislocated
HVLS = High Vacuum Long Sintering (10 h at 1250°C and cooled at 6°C/h)
*The Pd content was 32.35% in weight. The lamina thickness was 0.05 mm.
Amorphous lamina samples were supplied by Prof. P.H. Fang, Institute for Space Research, Boston College, MA

2.2.3 Electrolytic solution

It was a 0.2 M LiOD solution prepared in the usual way by using D_2O (Fluorochem Ltd., England) at 99.91 wt% in the isotopic content. The nominal T activity was 60 nCi/kg corresponding to 147 dpm/ml. In the first part of the experiment D_2O at higher T content (254 dpm/ml) was used.

The Li concentration in the electrolytic solution of each cell was systematically analysed during the experiment by plasma absorption spectroscopy. If the Li concentration was found less than the initial value, this was restored by a proper addition of a more concentrated LiOD solution. Li concentration generally decreases much more at high current densities due to the increased action of the evolving gases in carrying microbubbles of solution out of the cell and, as it will show in the results section, it decreases also because of the absorption by the Pd cathode.

2.3 Nuclear measurements

2.3.1 Neutron detection

With respect to the previous experiments (1-2), we improved our counting system by storing the analog signals from ^3He proportional counter and off-line discrimination based on the characteristic pulse shape produced by a thermalized neutron interacting with ^3He gas.

According to the scheme reported in Fig. 2, the logic signal from the neutron counter, through the look-at-me channel of the data logger, drew the computer to read the digitized pulse shape produced by the oscilloscope in 1024 byte string. The minimum interval of time between two acquired shapes was determined by the time resolution of the look-at-me channel which was 2 ms. Each stored shape was written together the event date in the format dd-mm-yy:hh-mm-ss.sss. The whole stored file of each run was constituted by an appended binary text file which can be segmented and converted in the voltage *vs* time original curves by a suitable home-made LabVIEW program.

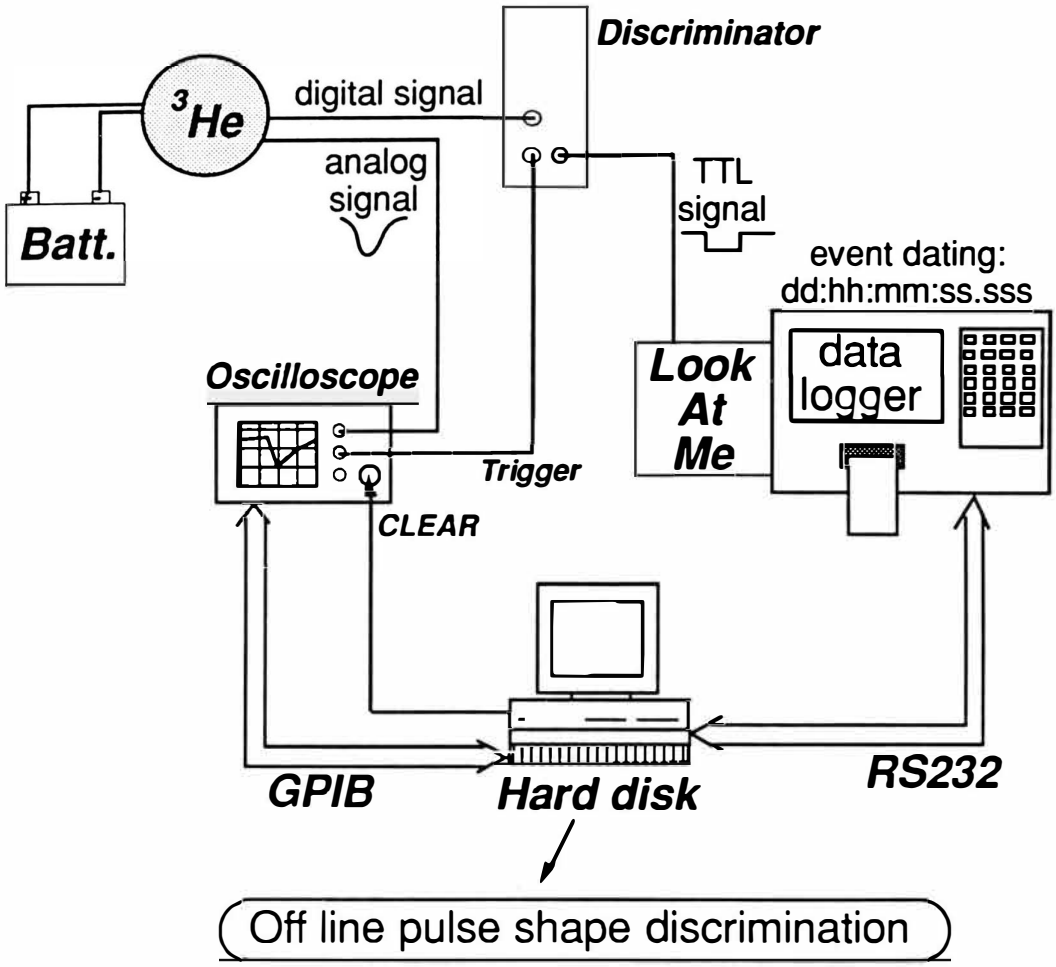

Figure 2. Scheme of the dated pulse shape acquisition from the ^{3}He neutron counter

The pulse shape associated to a thermalized neutron displays a negative voltage value without any positive component all along its length (see Fig 3A of ref.2) while a pulse produced by spurious electromagnetic signals picked-up by the counter shows both positive and negative values (see Fig. 3B of ref.2). Due to the characteristics of the signals, a suitable filter has been put in the off-line analysis. The program labels as neutrons only the events that go through the filter. Further check of the reliability of the adopted procedure was done. We calculated by integration of each filtered pulse the corresponding collected charge and, for each run, a spectrum was obtained (see Fig.3) which was always in agreement with the spectrum obtained by the calibration with an Am-Be source.

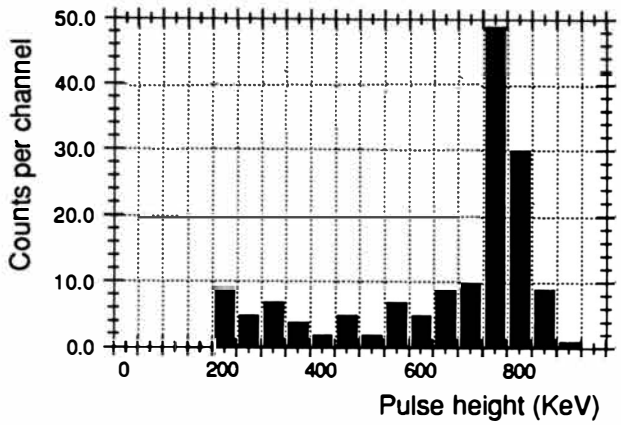

Figure 3. Pulse charge spectrum as given by the filtered *neutron signals* in a typical run. The peak value is at ≈ 765 keV as obtained when calibrating with Am-Be source

For each run the total counting and the counting rate were given only by filtered signals. The dating of the signals allowed to perform the counting choosing the proper time gate.

The signals which did not pass through the filter were stored in a separate file for further analyses. In fact, there are scattered evidences (2,4) that the electrochemical system itself could be source of electromagnetic signals. We are looking for some correlations, for instance, between the frequency of those spurious signals and applied current density.

2.3.2 Tritium measurements

The sampling for the tritium analysis both in the solution and in recombined gases was done at fixed values of the electrical charge passed through the cells. This is necessary to facilitate the control of the tritium mass balance. The external catalytic recombiner is constituted by porous Pt supported on alumina tube and heated at 400 °C. The D_2O recombined vapours are condensed on a water-cooled glass surface.

The tritium measurements were carried out by the procedure already reported (2).

2.3.3 γ measurements

Seven energy windows of the HPGe γ detector spectrum spanning between 350 keV and 2.8 MeV were monitored during the experiment. Lower energy windows were centered in the region where the emissions from the Pd nuclei levels occur due to the Coulomb excitation induced by 3.0 MeV protons generated in the d + d reaction. Energy window around 2.204 MeV was used to monitor the natural background due to ^{214}Bi. A window around 2.224 MeV was used to monitor the γ emitted in the radiative capture of neutron by proton.

Seven energy windows of the NaI γ detector spectrum spanning between 2.1 and 27.0 MeV were at the same time monitored. The lower energy window was again used to detect the radiative capture reaction, an energy window around 2.6 MeV was set to measure the natural background, an energy window around 23.8 MeV to monitor the d(d,γ) ^{4}He reaction.

3. RESULTS and DISCUSSION

3.1 Excess heat

3.1.1 Calibration curves

Figure 4 shows sequences of steady-states of the solution temperature when the heating occurred by the heater (h) or electrolysis (e) mode. The input power values, I_p, were calculated in both the cases according to the left and right side, respectively, of Eqn. 1. The calibrations were made at the same time on two identical cells containing, as shown before, gold-plated cathodes likely prepared in the same way. After each calibration the LiOD solution was analysed for the Li content and replaced in the cells by a fresh one having same volume and concentration. Figure 4 clearly shows that the calibration curve obtained in the electrolysis mode on cell #2 is quite anomalous with respect to the other calibrations which are satisfactorily represented by the best fitting line:

$$T_s = (25.3 \pm 0.1) + (0.477 \pm 0.002)\, I_p \qquad (4)$$

which was then assumed to evaluate the behaviour of all the cells during the ten-cells experiment.

To try for an explanation, at the end of the calibration measurements, we examined by SEM microprobe mapping the surfaces of both the cathodes to check the status of the gold layer. In the cathode of cell #2, we found two zones along the lateral surface of the cylinder clearly not covered by gold. The molar Li concentration, [Li], was found 0.184 and 0.075, respectively, for the cells labeled #1 and #2. If we compare these values with the initial value of 0.187 (equal for both the cells), changes are found in the Li concentration equal to -1.6% and -59.9%, respectively. Assuming that all the Li concentration change, Δ[Li] depends on the reduction and bulk-diffusion into the cathode, the final composition of the cathode has to be considered equal to $\Delta[Li]V_0M_{Pd}/1000W_c = 0.05$, i.e., $PdLi_{0.05}$, being V_0 = volume of LiOD solution = 35 ml, M_{Pd} = atomic weight of Pd and W_c = weight of the cathode of cell #2 = 8.55 g. Therefore, the decrease of [Li] is consistent both with the surface microprobe analysis and with the well-known fact that at high current densities, that is, high cathodic overvoltages, alkaline metals can be reduced in acqueous solution, even if, in an unstable state, except for in the case where a concurrent process does exist.

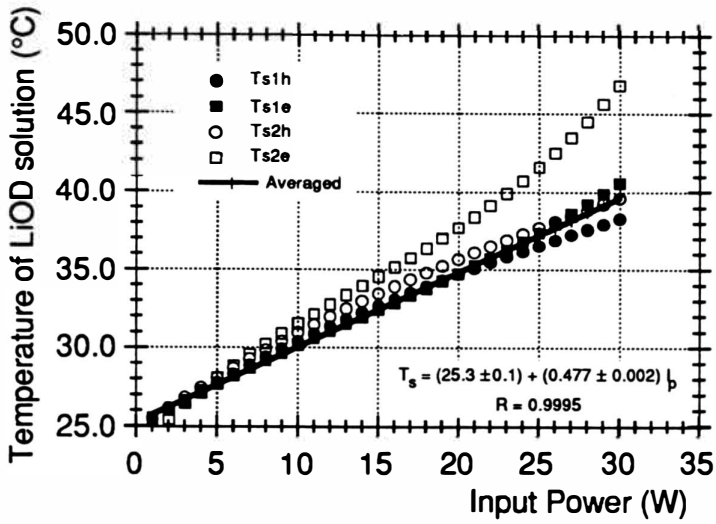

Figure 4. Thermal and electrochemical calibration curves obtained for two identical cells.The error bar length is comparable with the dimension of the points

By interstitial diffusion and a favourable chemical potential gradient, as in the case of hydrogen and its isotopes, Li penetrates into the Pd bulk producing solid solutions without going back into the aqueous solution because of the reaction with water. The difference observed in the case of cell #2 roughly means that the solution can be, for instance, heated at 40 °C by using an input power equal to ≈77% of that one necessary if the Pd cathode did not absorbe deuterium (cell #1). In terms of specific excess power, this means 10 W/cm^3 about if we consider all the volume of the cathode #2 subjected to deuterium absorption.

If we consider the right term of eqn.1, we realize that this is representative of a particular aspect of a more general treatment. In fact, only one electrochemical process was there considered (D_2O electrolysis) and no chemical process. In general, we would have to write the eqn. 1 in the form:

$$[|V| \times I]_h = [(|V| - \Sigma V_i^\circ) \times I]_e - \Sigma \Delta H_i^\circ v_i \qquad (5)$$

where the summations run over the all possible electrochemical and chemical processes. In eqn. 5, v_i is the reaction rate of the i-th chemical reaction which could be also current dependent. Obviously, if the input power axis of the calibration plot is recalculated by taking into account the right-side of eqn. 5, the slope of the curve can change and, in principle, the equality with the left-side term should be satisfied. All the tentatives made so far to lower, through eqn. 5, the slope of the electrochemical calibration curve of cell #2, plotted on Fig. 4, were unsuccessful. Work is still in progress to improve this calculation.

3.1.2 Ten-cell experiment

Concerning the experiment which started on May 6, 1991 and lasted 50 days approximately, we show on Figure 5 two quite different trends of the excess heat as recorded throughout the experiment.

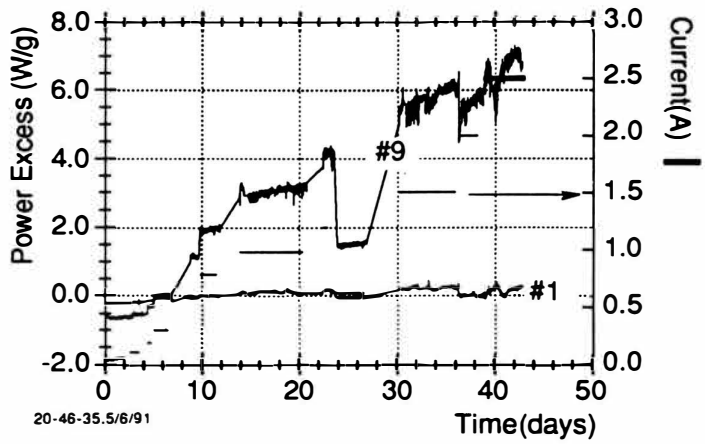

Figure 5. Specific heat power excess for cells #1 and #9 and applied current profile throughout the experiment

To compare correctly the excess heat data for all the electrodes, we used to normalize the excess heat power with respect to the cathode weight instead of its volume being this, for certain electrodes, difficult to measure due to their irregular shape. The applied current (all the cells are connected in series) is reported on the right ordinate of fig. 5. We can see that cell #1 does not show throughout the experiment appreciable excess heat values and they are not current dependent. A very different behaviour is shown by cell #9 where the excess heat has been found above any reasonable experimental error and the correlation with the current seems to be very close.

Figure 6 gives a bird-view, for all the cells, of the specific excess power results as function of the applied current density. We divided the curves of figure 6 in three categories chosen according to the preparation of the cathodes, as reported in Table I. We can focus our attention to some points emerging from inspection of fig. 6. These are:

- Except for cells #1, #3 and, for opposite reasons (see below), #8, all the cells show a threshold in the current density which is located around 100 mA/cm^2;
- While cell #1 and #3, as already mentioned, did not give any excess heat whichever was the current density, cell #8 started to produce excess heat at a lower current density value, below 50 mA/cm^2. This could be consistent with the fact that the whole cathodic surface area was not equal to the calculated value, given by $n\pi Ø(h + Ø/4)$, but, reasonably, it was less than that value because of the partial shielding of the innermost wires toward the

electrolytic solution, caused by the outermost wires. n, Ø and h are, respectively, the number of the wires, their diameter and length (see Table I). A similar reasoning could be done for cell #7 due to a

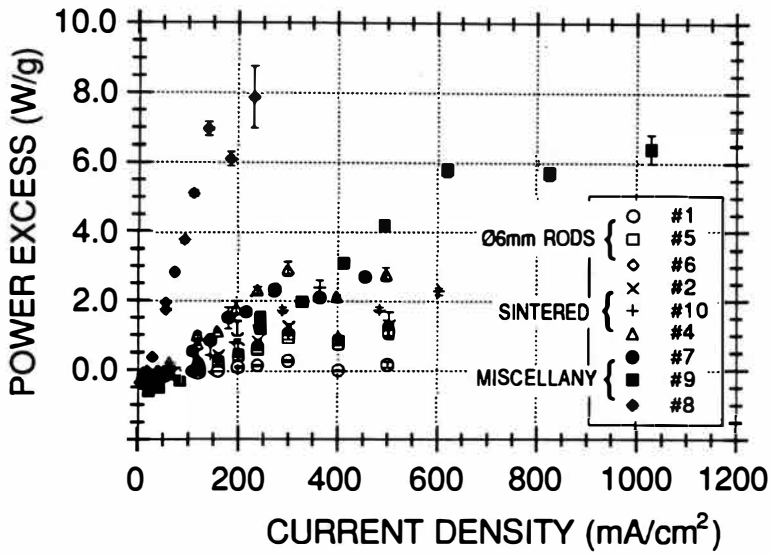

Figure 6. Trend of the specific excess power *vs* current density as found for the ten cells. Cell #3 has not be reported because its trend is very similar to cell #1 (see Table II)

possible not precise evaluation of the whole cathodic surface area;

- The cathodes, in categories *SINTERED* and *Ø 6mm RODS,* can be considered sufficiently comparable among them since at least the shape, dimensions and starting materials are in common for the cathodes belonging to the same category;
- By comparing the categories, it clearly appears that the cathodes made of 6 mm diameter rods show the lowest power excess but there is not a significant difference between as received and quenched cathodes ;
- On going from the cathode #1 to cathode #8, we pass from a practically undislocated material to highly dislocated one, whereas, in the *SINTERED* category, the concentration and distribution of dislocations probably remains unaffected by the type of preparation. In fact, it is reasonable that the cathodes maintain the same properties of the grains of the starting powder of the Pd sponge which is highly dislocated, as expected by itself nature;
- It is interesting to observe the very unlike behaviour between the two RFHQ cathodes (#6 and #9) which were different only by diameter. We believe that this has to be connected to the dynamics of the high compressive stress which is established in the rod in the direction from the surface toward the bulk when fast cooling occurs. Because the rate at which cooling proceeds into the bulk, all the other conditions fixed, depends on the diameter, the

magnitude of the compressive stress, which can dislocate the rod in an ordered way, becomes consequently a function of the diameter.

In Table II below it is reported the specific integral excess heat as calculated for all the cells.

TABLE II

Cell #	Category	Weight (g)	Specific Integral Excess heat (MJ/g)
1		8.2954	0.03
3	Ø6 mm RODS	8.3403	0.02
5		8.1150	1.5
6		8.5263	1.8
2		4.2158	2.0
10	SINTERED	3.5654	3.7
4		3.8545	4.8
7		3.3124	3.9
9	MISCELLANY	2.0283	9.5
8		1.6182	11.6

Figure 7 shows the comparison with the F.&P. (5) data and those of cell #8, for instance, concerning the specific power excess dependency from the current density.

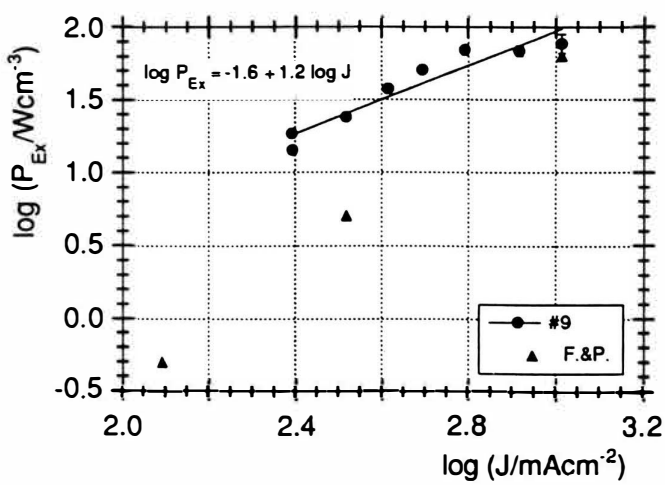

Figure 7. Specific power excess dependence on the current density compared with data in Ref. 5

Though our slope is less steep than the slope found by F.&P., it is important to observe that both the trends are linear and the difference in the slope and intercept can be reasonably attributed to the nature of the cathode.

3.2 Cathode swelling measurements

Before to show some preliminary results of cathode swelling measurements, performed in order to obtain *in situ* the loading factor [D/Pd], let us consider briefly some basic points related to this kind of measurements. According to the literature (6-7), in an unstrained Pd specimen, D_2 absorption produces a relative swelling, $\Delta V/V$, given by:

$$\Delta V/V = 3\ \Delta L/L = (0.20 \pm 0.01)[D/Pd] \qquad (6)$$

Due to the fcc structure of Pd, the swelling is an isotropic process producing the same relative elongation, $\Delta L/L$, along each of the x,y,z axis. Probably, only cathode #1 is in this quite-ideal situation due to the particular heat treatment that allowed it to loose all the internal stresses of the material reaching the state of internal thermodynamic equilibrium. In a cold-drawn rod having diameter Ø:

$$\Delta V/V = (\Delta x/x) + (\Delta y/y) + (\Delta z/z) \approx 2(\Delta Ø/Ø) + (\Delta z/z) \qquad (7)$$

due to the fact that there is a tensile strain along z-axis and compressive strain on the x,y plane. In this case, we cannot use the above relationship 6 for determining [D/Pd]. In a sintered specimen, eqn. 6 is still approximately satisfied but it is necessary to consider that the expected expansion, due to the deuterium absorption, occurs for a certain fraction, δ, in the free volume, V_p, of the pores. Thus, the eqn. 6 becomes:

$$(\Delta V - \delta V_p)/V = 3\ \Delta L_{meas}/L \qquad (8)$$

where $V_p = W_s(\rho_{Pd} - \rho_s)/\rho_s\rho_{Pd}$. W_s and ρ_s are, respectively, the weight and density of the sample s. In this case, the measured expansion, ΔL_{meas}, allows to measure δ by eqn. 8 through eqn . 6 as:

$$\delta = \{0.20\ [D/Pd] - 3\ \Delta L_{meas}/L\}[1/(1 - f)] \qquad (9)$$

if at least one [D/Pd] value is known and $f = \rho_s / \rho_{Pd}$.

In our experiment, we measure the expansion along the major axis of the cathode, that is, $\Delta L_{meas}/L$ (#4-sintered) and $\Delta z/z$ (#3-Ø6mm rod as received). In figure 8, we report the

recordings of the cathode swelling and the electrode temperature for the two cells equipped with the LVDT at the beginning of the experiment when, before to fill the cells with the electrolyte solution, a stream of $D_2(g)$ was allowed to circulate in the cells for conditioning the Pd cathodes. As it was already found (2,8), the response to the $D_2(g)$ exposure of the sintered cathode was completely different with respect to the rod and, as it will be shown, this difference will continue throughout the experiment.

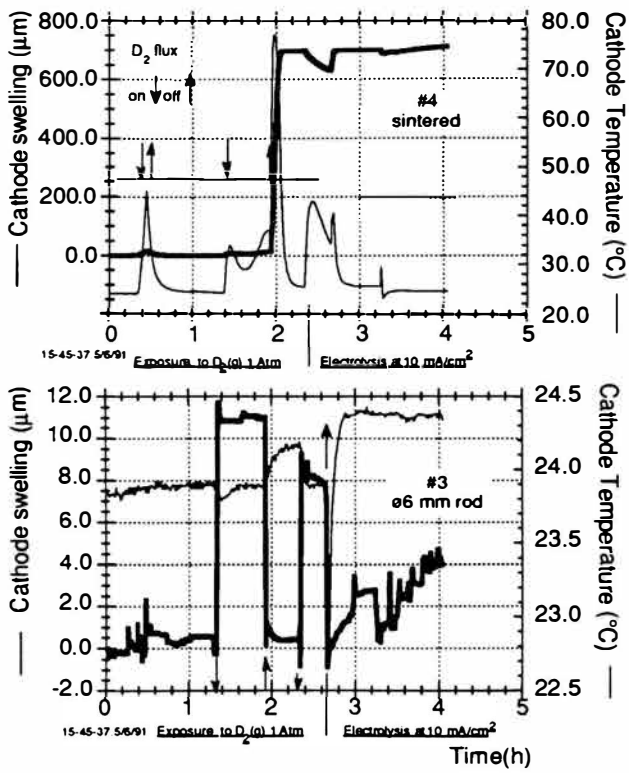

Figure 8. Behaviour of the cathodes monitored by the LVDTs when exposed both to D_2 stream, at atmospheric pressure, and D_2 electrochemically generated. Temperature of the cathodes is also shown

As shown in fig. 8, in the same experimental conditions, the swelling of the sintered cathode #4 was about 70 times greater than the swelling of the cathode #3. This could be easily explained by considering the respective porosity of the two materials which allows to the gas, in the case of the sintered cathode, to be in contact with a larger surface. Thermogravimetric measurements (9), carried out on sintered specimens, like #4, showed that at 101.3 kPa of $D_2(g)$ and at room temperature, the weight gain was such that an equilibrium [D/Pd] value of 0.67, as expected, was reached in a time interval of about 20 min which is comparable with that reported on fig. 8. Therefore, we can associate the $\Delta L_{meas}/L$ to [D/Pd] and, through eqn. 9, we can calculate $\delta = 0.114$. This means that at least 11% of the expected swelling does not

contribute to expand the cathode, provided that its density is assumed isotropic. Due to the unidirectional pressing applied in the preparation and subsequent short sintering, the density could be higher along the z-direction increasing f in the eqn. 9 and, accordingly, the value of δ. Previous calculations (8) made on the integration of the temperature *vs* time curve were and still are in satisfactory agreement with the heat expected to be produced by the exothermic reaction which yields [D/Pd] = 0.67 producing.

In fig. 8 the behaviour of the cathode just after the beginning of the electrolysis at 10 mA/cm^2 is also reported. The LVDT of cathode #4 did not detect any appreciable variation while cathode #3 LVDT showed a well-defined increasing trend which continued as shown in figure 9 below.

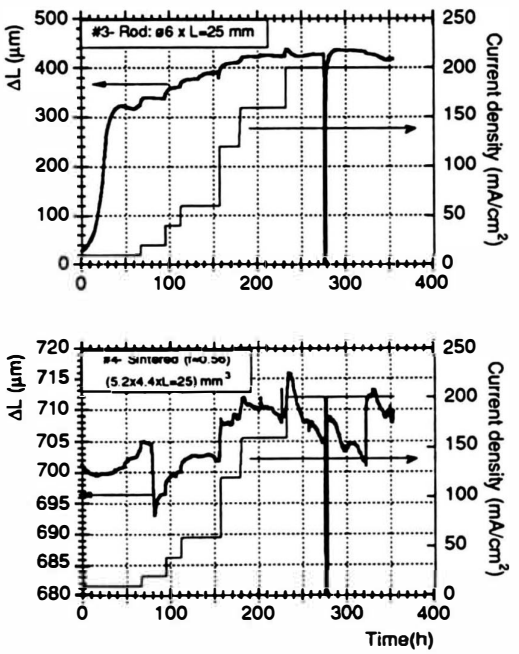

Figure 9. Behaviour of cathodes #3 and #4 observed in a long step-changing current density profile

If we take into account the different ΔL ordinates of the two plots above, we realize that the cathode #4 swelling was practically independent from the current density, maintaining quite constant the value which was reached during the exposure to $D_2(g)$ stream. For cathode #3, ΔL was found to be strictly current density dependent. We observed that to maintain a certain swelling value it was necessary to continue to increase the current density otherwise a contraction of the cathode occurred.

Though the dilatation measurements did not allow us to obtain an absolute value of [D/Pd], we believe the relative changes with respect to the current density are very interesting, when compared with the very low changes observed, simultaneously, on the sintered

cathode. In fact, these findings go in the direction of our precedent work (10), based on the assumption that [D/Pd] values out far from the thermodynamic equilibrium can be achieved if some structural and morphological conditions are present in the material. Particular structured domains, where the continuity of the chemical potential does exist, could be sites where high [D/Pd] values might be reached because of the effect of high local current densities on the low-ionic conductor PdD_x. This effect, as shown in literature (10), increases with the ionic transport number. To make this phenomenon macroscopically evident, it is necessary to have in the material a high concentration of large ionic-conductor domains satisfying particular structural arrangements able to set, locally, very high current densities. Due to the above considerations, we can only evaluate the lowest values of [D/Pd] for both the cathodes #3 and #4 which are, respectively, 0.26 (if eqn. 6 is calculated at the maximum measured value of ΔL, see Fig. 9) and 0.67. In this context, the respective excess heat data of Table II could be considered consistent.

3.3 Nuclear Measurements

3.3.1 Tritium measurements

As mentioned in the experimental section, we carried out systematically (roughly at fixed electrical charge passed through the ten-cell system) tritium measurements by 1 ml sampling both in each cell and in the respective catalytic recombinator. In figure 10, the trends

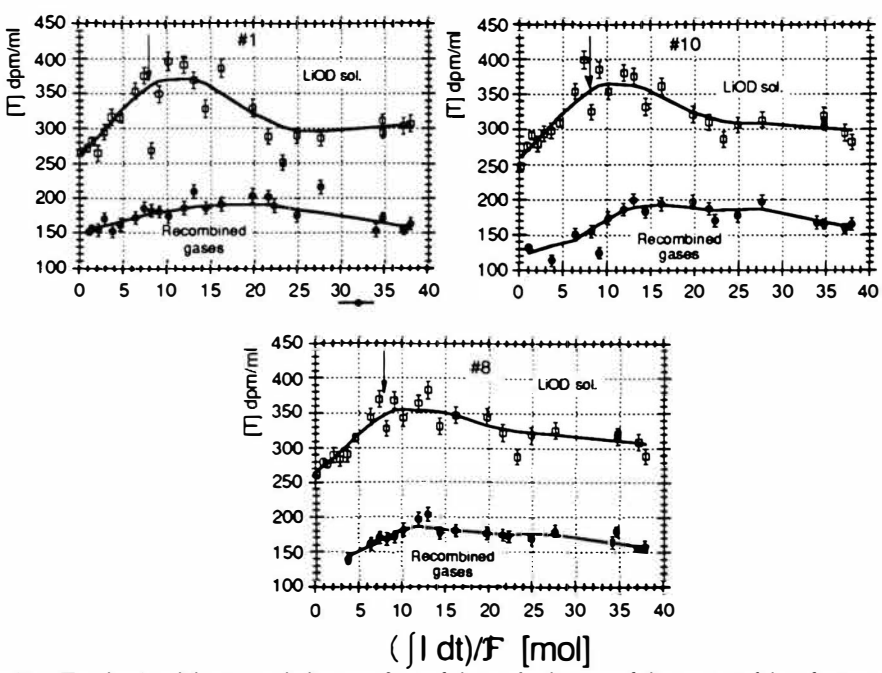

Figure 10. Typical tritium activity as found in solution and in recombined gases for three cells. Abscissa is quoted as ($\int I\,dt$)/$\mathcal{F}$ where $\mathcal{F}$ is the Faraday's constant. Arrows show the heavy water refilling from a new batch at lower T content

vs the integral charge passed both for tritium in solution and in recombined heavy water are given. The plots reported are considered typical and they refer to cells #1, #10 and #8, respectively, one for each category of cathodes. Detailed information on the procedure used to evaluate the tritium mass balance is reported elesewhere (2). Here it is sufficient to point out that the shape of the trends is due to the mixing, at the point marked by the arrow, of a new heavy water feed, at lower T content, $[T]^{\circ}_{\ell}$, with the solution at higher T content, $[T]^{\circ}_{h}$. In fact, the final T enrichment was always within the expected enrichments from $\approx 2[T]^{\circ}_{\ell}$ to $\approx 2[T]^{\circ}_{h}$, roughly. As a consequence of this, the trends for the recombined gases were influenced accordingly. However, no significant evidence of T excess was found throughout the experiment in any of the ten cells.

From data like those reported in fig. 10, it is possible to calculate the enrichment factor defined as the ratio, at a certain charge passed, between the tritium concentration in the solution and tritium concentration in the gas phase, i.e., $\alpha_E = [T]_{sol.}/[T]_{gas}$. The knowledge of this term is important to evaluate, after prolonged electrolysis, the final content of T, $[T]_f$, in a D_2O electrolytic solution having an initial concentration of tritium $[T]^{\circ}$. In fact, as it can be shown (11), $[T]_f \approx \alpha_E\,[T]^{\circ}$.

Figure 11 shows a typical trend of the enrichment factor for cell #9 throughout the experiment.

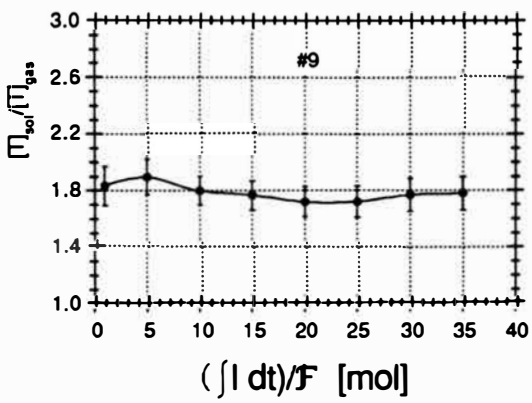

Figure 11. Typical trend of the enrichment factor. Here cell #9 is reported

It is important to observe that throughout this long experiment, α_E was found practically constant. Some authors reported (13) different results and explained the variations of the enrichment factor as due to co-deposition onto the cathode surface of impurities which change the nature of the electrode/electrolyte interface and, consequently, the relative rate of the charge transfer of the hydrogen isotopes.

The sensitivity of our measurements to detect an anomalous tritium content on the sample can be estimated to be of the order of 100 dpm/ml (effective value was 30 dpm/ml) that means a content of tritium of 10^9 atoms in one milliliter. By analysing the excess heat reported in table II, we can compute that all the cathodes, except to #1 and #3, have shown an integral excess heat of the order of 10 MJ. If this excess heat is to be attributed only to fusion reactions having tritium as final product, the number of reactions needed is of the order of 10^{19}. Even considering that the process lasted for all the length of the experiment (50 days) one would expect in the solution + gas phase a production of $\approx 10^{17}$ tritium atoms every day and, by taking into account the volume of the solution, 10^{15}-10^{16} atoms of tritium would have been in 1 ml solution sampled. This number is 10^6-10^7 higher than the level of sensitivity of our measurements and it is hard to think an artifact responsible for a negative result.

3.3.2. Neutron measurements

The frequency of neutron counting was analysed using variable time integration intervals. In figure 12 the frequency as counts per hour is reported for all the runs. No evidence of any neutron signal different from background was found.

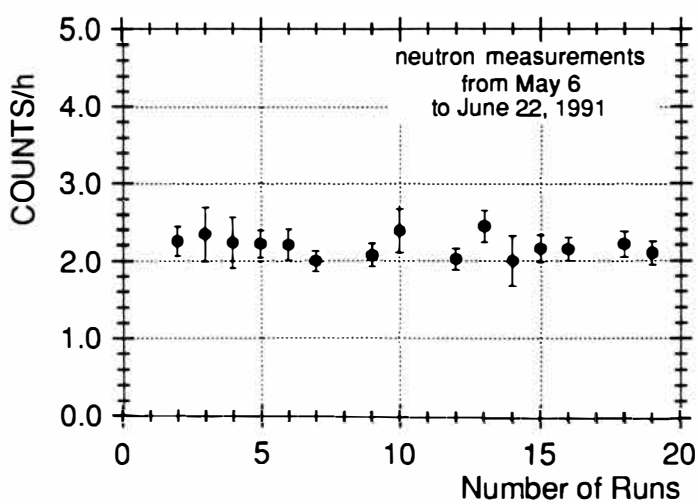

Figure 12. Average neutron counts per hour measured in all the acquisition runs

The analysis has been repeated for each run with several choices of time integration intervals (from 10 minutes to 1 hour) by comparing each of the obtained distributions with the relative Poisson distribution expected according to the measured count mean value. In figure 13 the result of this analysis is shown for one particular run which is representative of the results obtained in all the runs. The experimental data are shown as well as the expected

values. These are reported with an error bar indicating their possible variability when the mean value of the Poisson distribution is changed within the measured value of the standard deviation. In all the cases the mean value is compatible with the background value and the count distributions follow the statistics expected proving, in this way, the background nature of the neutrons detected.

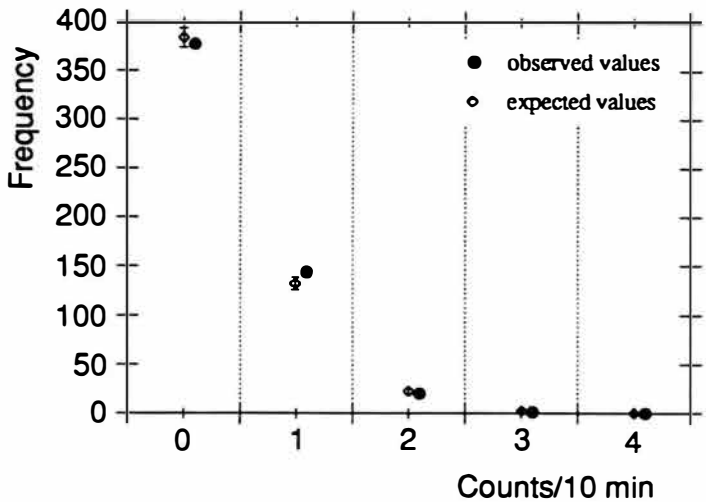

Figure 13. Frequency count of neutrons as observed in 542 intervals of ten minutes acquisitions and as expected in a Poisson distribution. The variability of the expected values obtained allowing the measured mean value to vary between $\mu-\sigma$ =0.32 and $\mu+\sigma$= 0.37 counts/10 min. is also reported.

Being one cell (#3) operated for a certain time with pulsed current, a special test has been made by analysing the time sequence of neutron counts with respect to the current value. No correlation has been found, being the count distributions during the $I=I_{Max}$ and I=0 time intervals described by the same Poisson distribution with an acceptable statistical significance.

According to the discussion at the end of the previous section 3.3.1 on the comparison between excess heat and nuclear products, a number of 10^{19} reactions is needed again to explain the heat found with the only fusion reaction having neutron and ^3He as final products.

Under the same assumptions already made and taking into account the efficiency of the neutron counter a counting rate greater than 10^{10} times the normal background would have been detected.

3.3.3 γ measurements

Gamma spectra from HPGe and NaI (Tl) counters, respectively, in the energy ranges of 0.30 - 2.83 MeV and 2.0 - 27.0 MeV, were sequentially acquired for living time intervals

of eight minutes. For each measurement the integral count of selected energy windows reported in tables III and IV were stored. For the spectra of both counters an energy window was reserved to monitor natural background, being the e channel of the Ge counter centered on the energy of a γ emitted by the ^{214}Bi (a daughter radioisotope of ^{238}U) and the b channel of the NaI counter centered on the energy of γ emitted by ^{208}Tl (a daughter radioisotope of ^{232}Th).

TABLE III

Ge detector

channel	window energy (keV)	motivation
a	349.9 - 450.7	*de-excitation of Pd isotopes*
b	475.9 - 561.7	*de-excitation of Pd isotopes*
c	986.9 - 1074.4	
d	2194.9 - 2211.5	*radiative capture*
e	2216.9 - 2230.8	*Bi-214 (natural background) (U-238 daughter)*
f	2605.6 - 2622.1	*Tl-208 (natural background) (Th-232 daughter*
g	2770.6 - 2825.7	

Table IV

NaI detector

channel	window energy (keV)	motivation
a	2124 - 2328.2	*radiative capture*
b	2455.1 - 2750.8	*Tl-208(natural background) (Th-232 daughter)*
c	18007.1 - 19992.5	
d	20013.6 - 21998.9	
e	22010.1 - 23998.4	$d + d \rightarrow {}^4He + \gamma(23.8\ MeV)$
f	24019.6 - 27004.6	

For each run the analysis of the measurements was made by checking the fluctuation of the ratio of the counts in a given channel against that of the background channel. In figures 14 and 15 we report an example of measurements with Ge and NaI counters, respectively. The

counting ratios fluctuate around the mean value. The upper dotted lines indicate the deviations from the mean of three times the maximum value of the error of the ratio on a single integration interval within the run. These levels can be considered as the threshold that indicates a statistically significant deviation. In all the measurements no significant deviation from background has been detected.

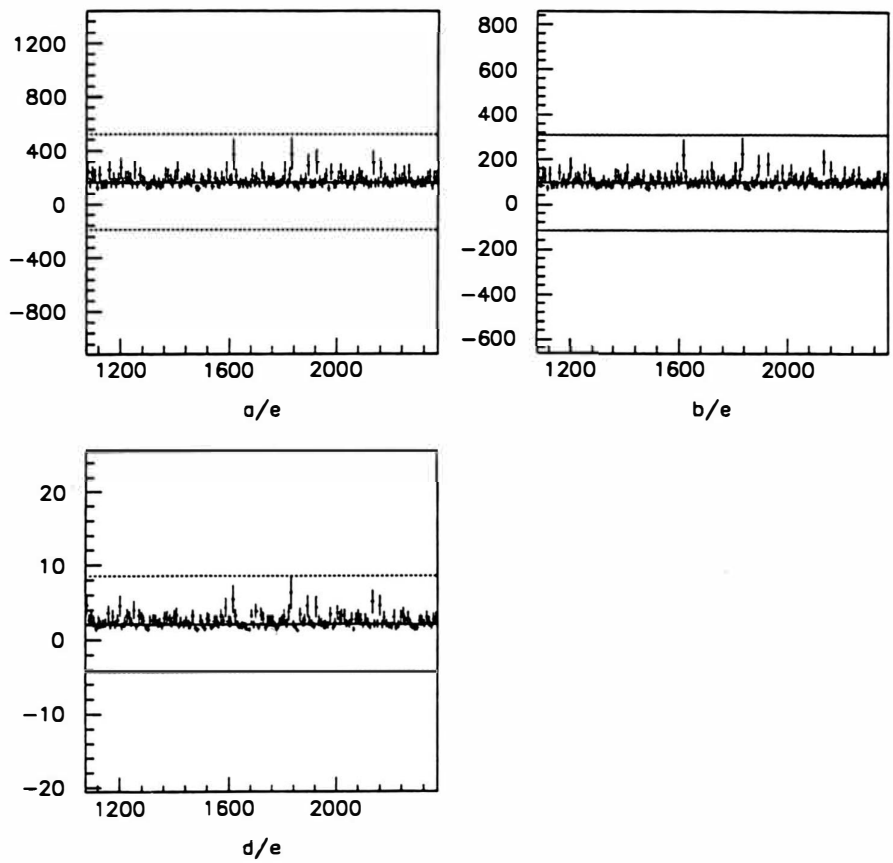

Figure 14. Ratio of the counts of different energy windows over natural background. Ge detector. *a, b, c, etc.* are the energy windows (see table III)

The sensitivity of the different channels to detect a possible fusion reaction is very different due to the several factors that affect the possibility to detect gammas of given energy coming from a fusion channel. Gammas of low energy 0.35 - 0.55 MeV are expected to be a signal of the reaction chain:

$$d+d \rightarrow {}^3H+p \ , \ p+Pd \rightarrow p+Pd^* \ , \ Pd^* \rightarrow \gamma+Pd$$

Taking into account the reaction yield and the counter efficiency the threshold sensitivity was about 10^{17} fusion reaction in ${}^3H+p$ channel in the time integration of eight minutes.

Photons coming from the radiative capture of neutrons by protons of materials containing hydrogen are expected in the energy window centered around 2.22 MeV.

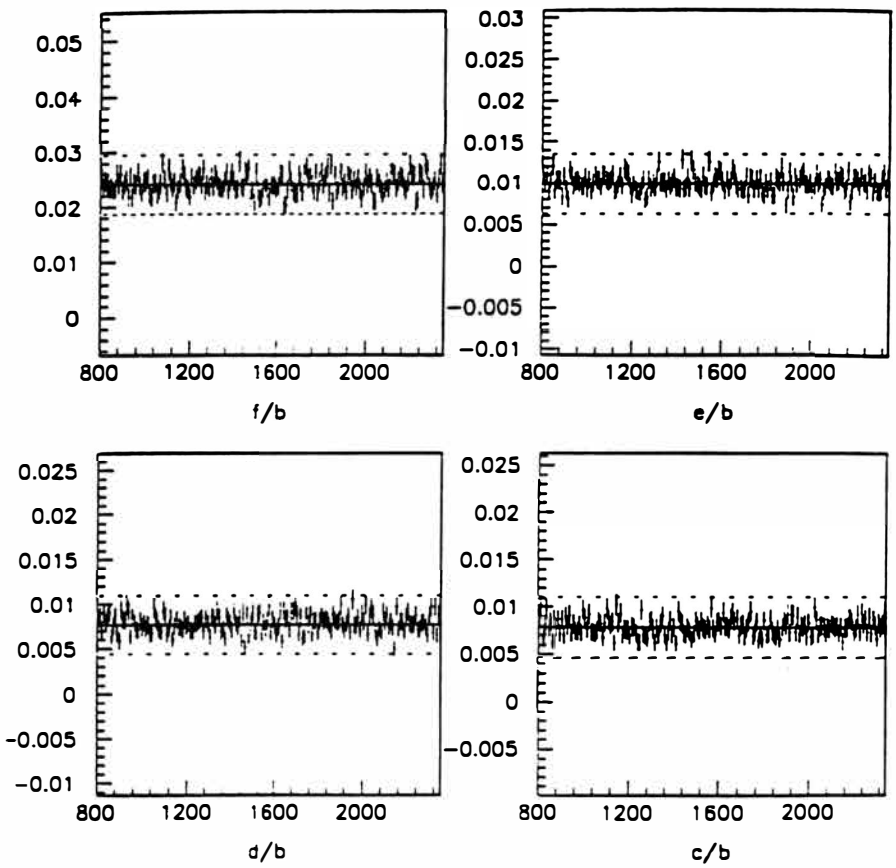

Figure 15. Ratio of the counts of different energy windows over natural background. NaI detector. *a, b, c, etc.* are the energy windows (see table IV)

This spectrum channel is a monitor of the reaction chain

$$d+d \rightarrow {}^3He+n \ , \ n+p \rightarrow d+\gamma$$

The threshold sensitivity both for Ge and NaI counters was about 10^6 fusion reactions in the ^3He+n channel in a time interval of eight minutes.

From the results shown in figure 6, by computing the power excess of different cathodes and taking into account the palladium mass, a maximum value of about 13 W is found. Considering fusion reactions in the two classical channels (p + T and n + ^3He) as

source of the power excess measured, a number of 10^{12} reactions per second are needed, that is $5x10^{14}$ if we consider that the phenomena lasted along all the eight minutes of the time interval integration. By comparing this value with the sensitivity threshold, we conclude that in the low energy window the sensitivity was not sufficient to detect the p + T channel through the γ measurements. On the contrary, in the windows selected to monitor the γ emitted by the radiative capture, the expected signal from n + ^{3}He reaction was 10^8 times higher than the sensitivity.

Gammas in the upper windows of the NaI spectrum would monitor the fusion channel

$$d+d \rightarrow {}^4He+\gamma\ (23.8\ MeV)$$

This reaction, on the contrary to the case in which the energy (and not only the momentum) is absorbed by the crystal lattice, does not release locally heat and should not give contribution to an observed excess heat generated in the cathode. The threshold sensitivity for this fusion channel was about 10^7 fusion reactions in the used integration time. To explain the heat excess measured in this experiment as generated by nuclear phenomena, a reaction not monitored by our instrumentation (for instance the ^{4}He production with the energy absorbed locally by the lattice) must be called.

4. Conclusions

The following conclusions can be drawn:

- Excess heat and cathode swelling were found strongly dependent from the preparation of the Pd cathodes;
- Sintered and bulk cathodes behave in different way with respect to the absorption of deuterium as shown by the displacement measurements. In the case of bulk cathode, the D/Pd ratio seems to be greatly influenced by the applied current density showing a real non-equilibrium condition. The sintered cathode absorbs deuterium without any correlation with the current density like in a state of thermodynamic equilibrium;
- The highest specific excess heat and power were found to be, respectively, 130 MJ/cm^3 and 96 W/cm^3;
- Specific power excess displays a linear dependence on the applied current density with a possible threshold effect according to the literature;
- From the double calibration procedure adopted (thermal and electrochemical) an intriguing evidence arises which is, by itself, the most important feature of the *cold fusion* nature to which a clear answer is still lacking;

- Though neutron, tritium and gamma measurements were taken throughout the experiment, no statistically significant evidence of release of these nuclear products was found;
- Evaluation of the sensitivity of the respective nuclear measurements gives confidence that if the energy were released through channels involving the generation of the monitored nuclear products they would be detected at a statistically significant level;
- To explain the heat excess measured in this experiment as generated by nuclear phenomena, a reaction not monitored by our instrumentation (for instance the ^4He production with the energy absorbed locally by the lattice) must be called;
- Also the findings here reported go into the direction of the scattered results still coming from *cold fusion* experiments which even more require a complete set of independent parameters to be controlled and nuclear products to be measured (^4He for instance) both to exclude the chemical nature of the heat generated and possible other sources of error.

5. Acknowledgements

Work was carried out with the financial support of the National Research Council (CNR), National Institute of Nuclear Physics (INFN-sezione Sanità) and Laboratory of Physics of the Istituto Superiore di Sanità, Roma.

The first author wish to thank Prof. E. Cardarelli and P. Porta of the Department of Chemistry of the Università "La Sapienza", Roma for their contribution in Plasma Absorption Spectroscopy analyses of lithium and XRD of palladium cathodes, respectively. He is also indebted with Dr. G.P. Bardi and D. Ferro both of the CNR-Centro di Termodinamica Chimica alle Alte Temperature for their support in making, respectively, TG measurements and SEM microprobe determinations.

The authors wish to thank Prof. G. Balducci for his assistance in preparing this manuscript.

6. References

1. D. Gozzi et al., Nuovo Cimento, **103A**, 143 (1990)
2. D. Gozzi et al., Fusion Technology, **21** (1992) in press; AIP Conference Proceedings **228**, *Anomalous Nuclear Effects in Deuterium/Solid Systems*, Provo, UT, October 22-24, 1990 (Eds. S. Jones, F. Scaramuzzi and D.Worledge), American Institute of Physics (New York) 1991, p. 481-493
3. J. Balej and J. Divisek, J.Electroanal.Chem., **278** (1989) 85
4. G.H. Lin, R.C. Kainthla, N.J.C. Packham and J. O'M. Bockris, J. Electroanal. Chem. **280**, 207 (1990)
5. M. Fleishmann and S. Pons, J.Electroanal.Chem., **287** (1990) 293
6. H. Peisl, in Hydrogen in Metals vol. I, ch.3, edited by G. Alefeld and J. Volkl , Springer-Verlag (1978)
7. F.A. Lewis, Palladium Hydrogen System, Ac. Press (1967)
8. D. Gozzi et al., unpublished results

9. G.P. Bardi and D. Gozzi, paper in preparation
10. M. Tomellini and D. Gozzi, J. Mat. Science Lett. **9**, 836 (1990)
11. S.K. Malhotra, M.S. Krishnan and H.K. Sadhukhan, "Material Balance of Tritium in Electrolysis of Heavy Water," P.K. Iyengar & M. Srinivasan (Eds.), BARC Studies on Cold Fusion (April-September 1989), Report BARC-1500 (1989)
12. D.E. Williams et al., Nature **342** (1989) 375; Conf. Proc. **24** of the Società Italiana di Fisica, Understanding Cold Fusion Phenomena, Varenna, September 15-16, 1989, (Eds. by R.A. Ricci, F. De Marco and E. Sindoni)

Conference Proceedings Vol. 33
«The Science of Cold Fusion»
T. Bressani, E. Del Giudice and G. Preparata (Eds.)
SIF, Bologna 1991

SOME RESULTS ON COLD FUSION RESEARCH

Zhou Hongyu, Wen Chenlin, Rong Yanin, Fan Guoying, Yan Hua,
Zhou Weidong, Wang Dachun, Hua Ming,
Liu Shuzhen and Han Zhuen
(Institute of Low Energy Nuclear Physics,
Beijing Normal University)

Wu Zhongda, Yu Runhu and Liu Zhenghao
(Chemical Department,
Beijing Normal University)

Ren Guoxiao
(Institute of High Energy Physics,
Chinese Academy of Sciences)

Abstract: Anomalous nuclear effects in Pd+Ti+D_2 system were investigated by means of a double liquid scintillator system. A recoil proton spectrum of 2.45 MeV neutrons was obtained from heavy water electrolysis experiment using Pd as cathode. Burst neutrons and random neutron emissions were observed in discharge experiments and temperature cycle experiments for Pd+Ti+D_2 system.

1. A double liquid scintillator system

Since Fleischmann and Pons announced that d-d fusion reactions in room temperature were found[1], some neutron physicists have being focused their attentions on searching 2.45 MeV neutrons produced by $D(d,n)^3He$ reactions[2-6]. Comparing with other neutron detectors, liquid scintillator have some clear advantages: a). it can give neutron energy spectrum. b). it has excellent neutron-gamma discrimination ability, and the results with higher effect to background ratio can be expected. c). it can give fast signal with nanosecond order, and can record burst neutron events.

We have used a bouble liquid scintillator system for detecting the neutrons in discharge experiments, electrolysis experiments and temperature cycle experiments. It was shown in Fig. 1. LSD1 and LSD2 are the same liquid scintillation detectors. Every detector both is used as a single detector to analyse and record incident neutron number with time-variation (RECORDER1 and RECORDER2) and energy spectrum (ADC1.1 and ADC2.1) and operates in coincidence mode to analyse and record neutron burst nember (RECORDER12) and burst neutron enrgy spectrum (ADC1.2 and ADC2.2). The background count rate from the anode signals,

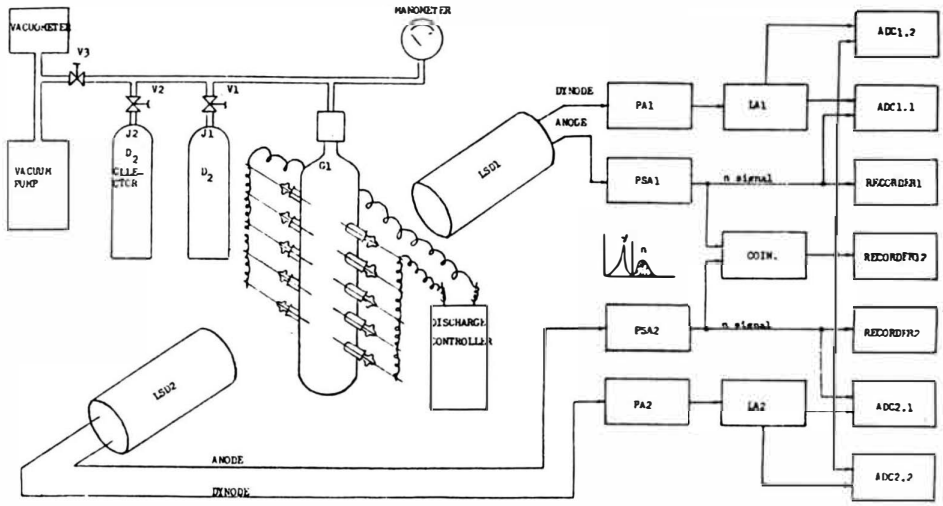

Fig. 1 The set-up and the double liquid scintillator measurement system used in the discharge activation experiment

which pass throuth the pulse shape analysis circuit, only is about 60 counts/hour. When the resolution time of the coincident circuit is 150 μs, the accidental coincident count rate is 0.001/hour, it is negligible. The efficiency of this system for 2.45 MeV neutrons is about 0.001. Maximum neutron count rate may reach 10^7 counts/sec. Some experiment results are following.

2. Results of discharge activation experiments

The set-up of discharge activation experiments are shown in Fig. 1. together with the double liquid scintillator system. The principle and set-up are similar to Nubuhiko Wada's[4]. G1 is a glass jar, it is about 500 ml in content and has 5 pairs of electrodes. The electrodes are the Pd-Ag tube of 2 mm diameter, wall thickness 0.1 mm, which is made from about 80% Pd and 20% Ag. J1 is used for storing high pressure D_2 gas. In the experiment D_2 gas of 0.9 atm. was filled into G1, and 6000-12000V voltage was applied to between the electrodes for 3-10 minutes for every discharge. Every run experiment lasted for 3-8 days, and discharge was repeated many times.

We have completed 40 runs of discharge activation experiments, in about 20 runs of which Clear anomalous neutron counts were observed. A result is shown in Fig. 3, in which only counts recorded by recorder1 (including random neutron counts and burst neutron counts) and coincident counts recorded by the recorder12 (neutron burst number)

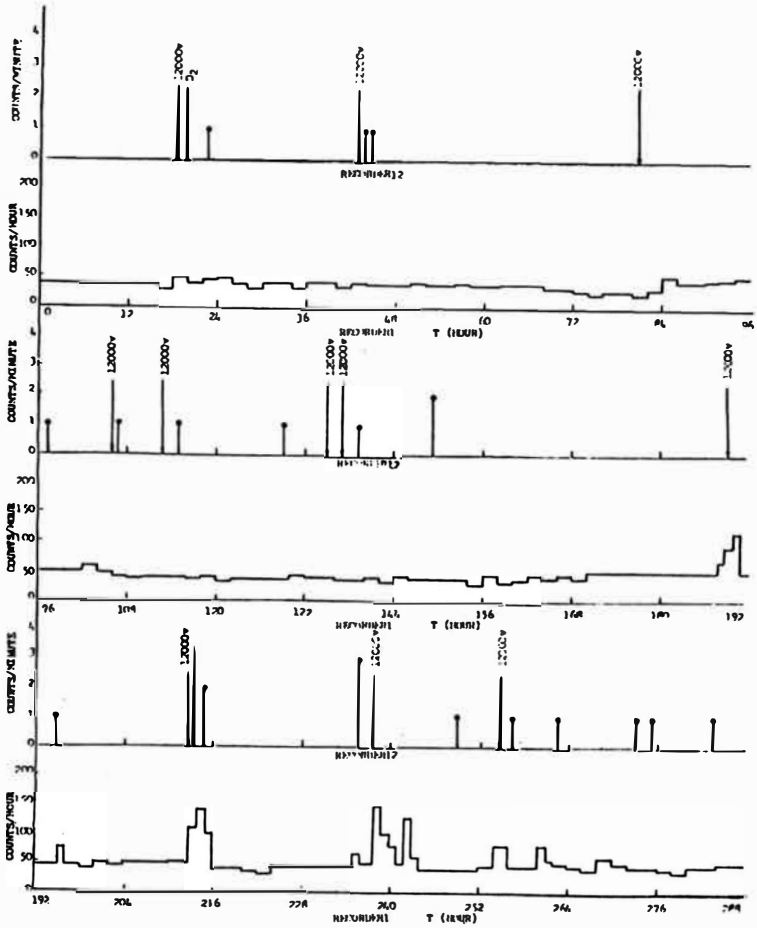

Fig. 2 Time-variation of count rate of the double liquid scintillator system in the discharge activation experiment

were shown. Clear anomalous neutron counts occur in the period of last four days, even seven neutron bursts occur in the period of one hour.

3. Results of electrolysis experiments

Our electrolysis experiment set-up was similar to Fleischmann's. The experiment was carried out in a glass jar, approximately 10 cm high x 10 cm diameter, held about 200 ml of 99.8 D_2O plus o.2% H_2O containing o.5 mol/L LiOD. A Pd tube of 10 cm long was used as cathode, a platinum wire as an anode. A DC power supplies of 0-30 volts provided electrolysis current of 100-150 ma.

After about 20 hours of beginning electrolysis neutron counts increased rapidly, and lasted for one hour. The maximum counting rate reach 447 n/minute. Luckily, before 20 minutes of producing high neutron counts integral background counts in the period of 20 hours were cleaned. 3142 counts were collected in the period of 70 minutes. The background

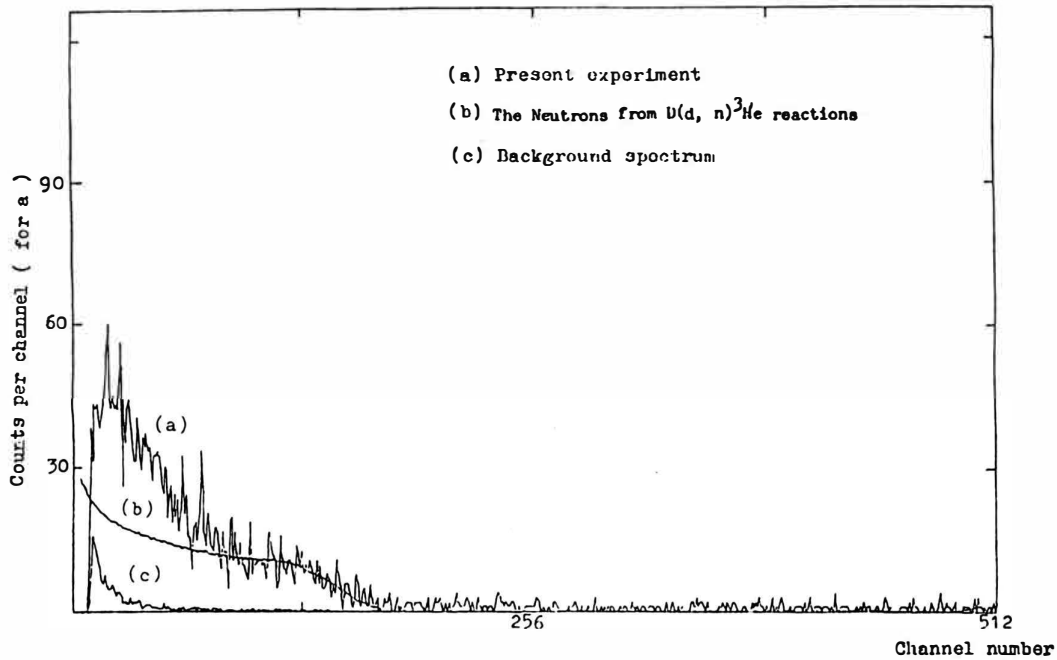

Fig. 3 A recoil proton spectrum measured by a liquid scintillator in the electrolysis experiment

counts only is about 70. Effect to background ratio reached 40:1. The recoil proton spctrum recorded by LSD1 is shown in Fig.3. This spectrum is basically coincident with the recoil proton spectrum caused by the neutrons from $D(d,n)^3He$ reactions, which were produced in 400 KV high voltage accelerator in Beijing normal University. This shows that $D(d,n)^3He$ reactions have occurred in the electrolytic cell.

4. Results of temperature cycle experiments

After having a steel jar S1 instead of the glass jar G1 in Fig. 1, Fig. 1 becomes the set-up used in temperature cycle experiments. When beginning experiment, a Pd sheet of thickness o.1mm and weight 0.1g. Ti chip of thickness 0.1mm and weight 50g and two CR-39 plastic sheets were put into S1 together. CR-39 was used for detecting energitic charged particles. S1 was sealed, evacuated and put into A Dewar filled with liquid nitrogen. In liquid nitrogen temperature S1 was filled with ten atm. of D_2 gas. Then the liquid nitrogen in the Dewar was evaporated in room temperature and S1 was warmed to room temperature. Then next temperature cycle was started. One run of temperature cycle experiment lasted for 6-12 days.

Fig. 4 shows a neutron measurement result. In the period of eighth temperature cycle 184 neutron bursts were recorded. It means that about 200000 reaction events occurred in the samples. Two CR-39 sheets recorded also charged particle signals in the same experiment.

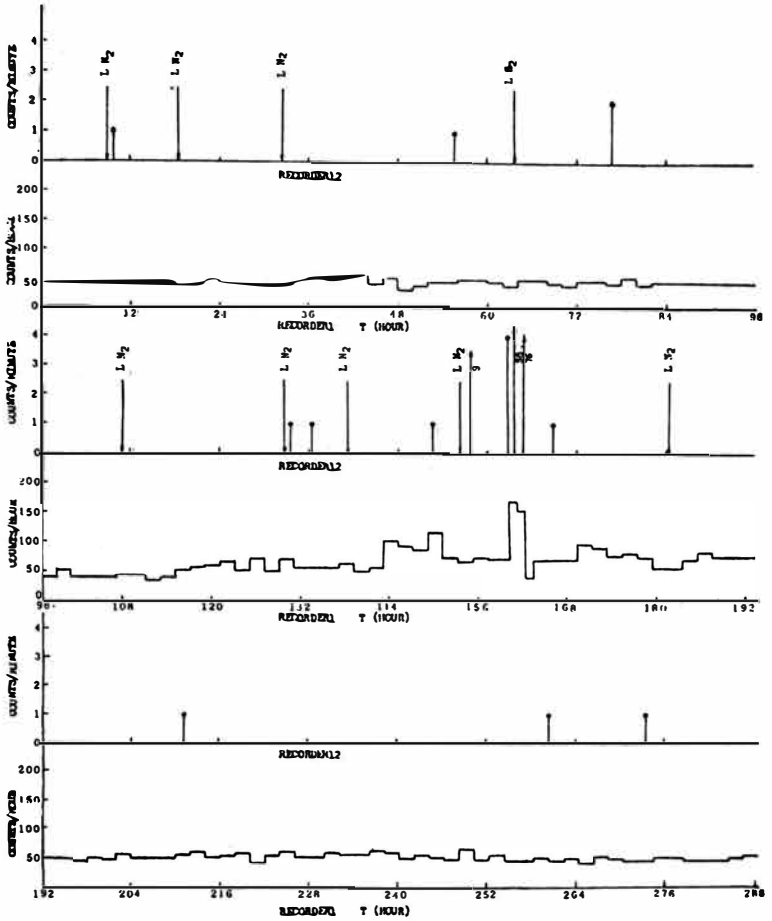

Fig. 4 Time-variation of count rate of the double liqu scintillator system in a temperature cycle experiment

Reference:

1) M. Fleischmann, S. Pons, J. Electroanal. Chem., 261, 301(1989)
2) S. E. Jones et al., Nature 338, 737(1989)
3) Nubuhiko Wada and Kunihide Nishizawa, Japanese Journal of Applied Physics, Vol. 28, No. 11, 2017(1989)
4) A. Takahasi et al., submitted to conference on anomalous effects in deuterium/solid systems (1990)
5) A. De Ninno et al., 'Evidence of Emission of Neutrons from a Titanium-Deuterium system', submitted to: Europphysics Letter (1989)
6) H. O. Meulove et al., 'Measurement of neutron emission from Ti and Pd in Pressurized D_2 gas and D_2O electrolysis cells', submitted to: Nature (1989)

EDITORIAL NOTE TO THE PAPER " SOME RESULTS ON COLD FUSION RESEARCH" BY Z. HONGYU ET AL.

The decision to publish these Proceedings as soon as possible did not allow any revision of the English presentation of the text originally submitted. This paper is particularly lacking in this respect, however due to the interest of the results presented we have decided to include it in the original form, asking the readers' forbearance.

Conference Proceedings Vol. 33
«The Science of Cold Fusion»
T. Bressani, E. Del Giudice and G. Preparata (Eds.)
SIF, Bologna 1991

Recent Progress on Cold Fusion Research Using Molten Salt Techniques

Bor Yann Liaw*, Peng-Long Tao*, and Bruce E. Liebert**

*Hawaii Natural Energy Institute
**Department of Mechanical Engineering
University of Hawaii at Manoa
2540 Dole Street, Holmes Hall 246
Honolulu, Hawaii 96822, U.S.A

A novel elevated-temperature molten salt technique has been demonstrated for generating high-level excess heat. More than 4 MJ mol^{-1} D_2 of excess heat, at least 600% over the input power, was measured in two incidents using a torched Pd anode and an Al alloy cathode in a eutectic LiCl-KCl mixture saturated with excess LiD above 350° C. No thermochemical explanation can account for this excess heat. Measurements on the hydrogen-based system showed the expected endothermic behavior.

The Pd samples were later examined for their morphology and for helium analysis. A porous microstructure of the samples was found. The electrolysis and deuteriding processes changed the morphology substantially. Enhancement of α-particles in the deuterided sample was detected, while the hydrided sample showed an opposite effect. The amount of the α-particles in the sample, however, was not commensurate with the measured excess heat.

Reproducibility of the experiments has been poor to date.

INTRODUCTION

The origin of excess heat found in the Pd-D electrolysis system at ambient temperatures, as reported by Fleischmann *et al.* [1], has not yet been conclusively identified. Despite the confusion over whether it was nuclear in nature, this phenomenon offered a potentially inexhaustible, clean, source of energy.

A novel molten salt approach [2], using a Pd | eutectic LiCl-KCl molten salt saturated with excess LiD | Al electrochemical cell, has recently been demonstrated

to generate excess heat above 350° C. This approach offers considerable merits, such as high-grade heat, faster rates, high efficiencies, and a strong reducing environment permitting use of less expensive materials for utility applications.

The high deuterium activity at high loading seems critical to reproducing excess heat, as suggested by Fleischmann *et al.* [1] and reported by others [3]. The molten salt approach can achieve high deuterium activities at a much lower loading at elevated temperatures, as depicted in the Pd-H phase diagram [4].

Using molten salt techniques to study metal-hydrogen reactions has been reported [5-8], and the principles were explicitly described by Deublein and Huggins [9]. Liaw *et al.* [10] employed a eutectic LiCl-KCl mixture saturated with excess LiH to study the thermodynamic and kinetic aspects of the Ti-H system. A similar approach using LiD to generate excess heat in the Pd-D system is the focus of this work. Due to the similar chemical properties between deuterium and hydrogen, we often describe the deuterium system with no distinction from its hydrogen analog in this context, except the anomaly in excess heat.

ELECTROCHEMICAL BEHAVIORS

Hydrogen-transparent metal surfaces can be prepared *in situ* using a eutectic LiCl-KCl molten salt saturated with LiH [9]. In Figure 1, the stability window of some base metals, such as Ti or V, is shown to explain their immunity to corrosion in the molten salt environment. The presence of excess alkali hydride imposes a very strongly reducing environment of extremely low oxygen and water activities, as Figure 2 shows. Thus, most metal oxides are unstable and can be readily removed from metal surfaces, facilitating deuterium reaction with metals in a controllable fashion in electrochemical cells.

Dissociation of the alkali hydride in the electrolyte results in an alkali cation and a hydride anion, which can be readily transported, exhibiting a conductivity

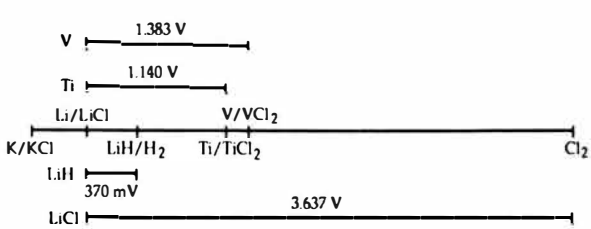

Figure 1. Immunity of Ti and V in the chloride melt at 700 K

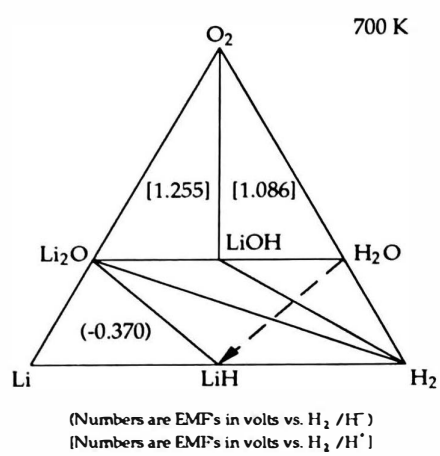

Figure 2. Ternary phase diagram of the Li-O-H system

typically of $10^{-1}\ \Omega^{-1}cm^{-1}$ [7]. Therefore, the excess heat effect can be tested using a cell, as described previously [2] (Figure 3). The cell half reactions are:

$$LiD = Li^+ + D^- \quad (1)$$

At the anode: $$Pd + x\,D^- = PdD_x + x\,e^- \quad (2)$$

At the cathode: $$Al + Li^+ + e^- = \text{"LiAl"} \quad (3)$$

which give the total cell reaction:

$$Pd + x\,Al + x\,LiD = PdD_x + x\ \text{"LiAl"} \quad (4)$$

with an endothermic reaction enthalpy, ΔH_r, approximately 3 kJ mol^{-1} at 700 K [11]. At this temperature, the palladium hydride and deuteride are above the α-β two-phase immiscibility regime [4]. The reaction of Li with Al in similar molten salts is very fast and the phase transformation proceeds at high rates [12-14].

The ΔG_f for LiH is -40.25 kJ mol^{-1} at 648 K (375° C) [15]. This corresponds to the reverse reaction of:

$$LiH = Li + 1/2\,H_2 \quad (5)$$

with an electrochemical stability window of 417.1 mV. A standard hydrogen reversible electrode (SHE) in the hydride electrolyte environment is thus 417.1 mV above a standard reversible lithium electrode (SLE). The "LiAl" | Al mixture has a constant potential, 308.4 mV above the SLE [13], over a wide composition range (Li=5.7-45.2 *at.%* [14]) at 375° C, and can be used as a reference electrode. The hydrogen evolution reaction therefore occurs at 108.7 mV above the reference electrode, which is the reversible cell potential for a PdH_x (at $a_H = 1$) | eutectic LiCl-KCl with excess LiH | "LiAl" | Al cell. The potential for the deuterium system should be slightly higher, as shown in Figure 4, where a cyclic voltammetry was performed on a Mo | $D_{2(g)}$ | eutectic LiCl-KCl with excess LiD | "LiAl" | Al cell.

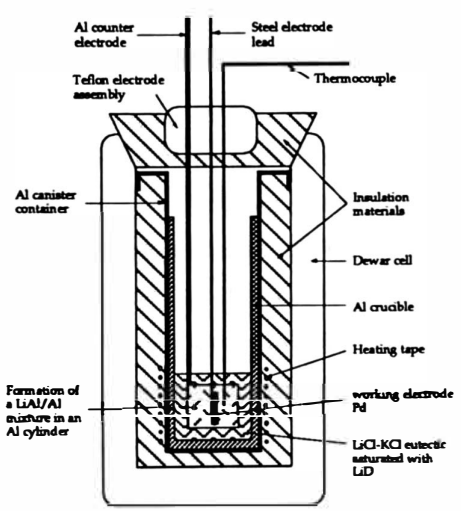

Figure 3. Schematic drawing of the molten salt cell

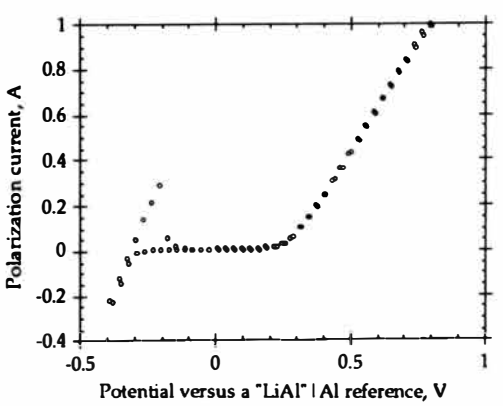

Figure 4. Polarization behavior of a Mo | $D_{2(g)}$ | eut. LiCl-KCl w/excess LiD | "LiAl" | Al cell at 375° C

EXPERIMENTAL ASPECTS

Experimental details regarding this experiment were described previously [2] and will not be elaborated here. Figure 5 shows some modifications of the recent cell design. This configuration allows on-line gas collection for quantitative analysis. Stainless steel dewar flasks show less degradation and are easier to handle than glass. Boron nitride can withstand the melt's reducing vapor and provide good electrical insulation. Inserted into the cathode holder were thermocouples to assure consistent readings without local hot spots. The use of steel crucibles avoids the shape changes found with Al crucibles. However, Li activity is less controllable and may cause excessive electronic leakage and reactions with anode or current leads.

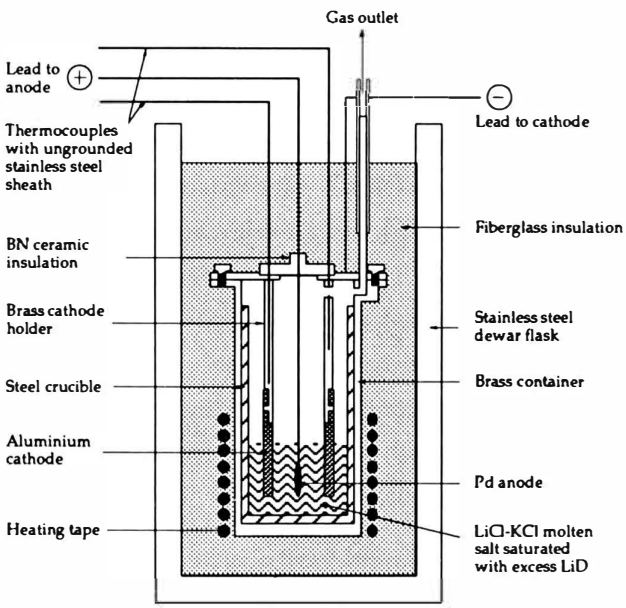

Figure 5. Schematic drawing of the new cell configuration

The heat balance of the cell was periodically monitored by thermocouples in an isoperibol-like calorimeter [2]. Calibration was conducted with an internal heater adapted from a standard Pt-resistance temperature detector from Omega Engineering, Inc., with its heating zone dimensions similar to the anode.

He analysis was performed by Rockwell International Corp. using a high-sensitivity mass spectrometer system that operates in the static mode and can measure as low as 10^{-11} atom fraction of ^{4}He and ^{3}He in solid metals.

RESULTS

Figure 6 shows the power excursions of a PdD_x | eutectic LiCl-KCl molten salt saturated with excess LiD | Al cell when subjected to high-current-density charging conditions. Significant excess power was measured above the input

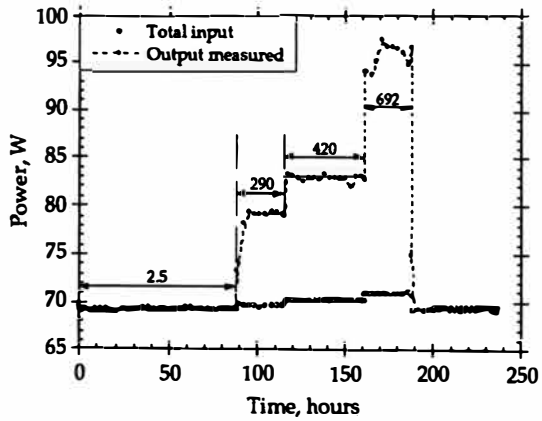

Figure 6. Power excursion during high current charging in a molten salt cell. Numbers are current densities in mA cm^{-2}.

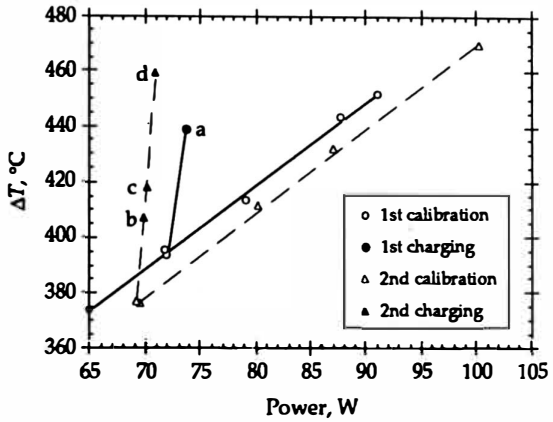

Figure 7. Calibration curves for two excess heat events. Current densities: a=606, b=290, c=420, and d=692 mA cm^{-2}.

power. Table 1 lists experimental variables and interpretations, in which excess heat is calculated under a pseudo-steady-state condition of a constant deuterium consumption rate. Figure 7 provides the calibration data for temperature-power conversion in Figure 6 and illustrates the marked power-temperature deviations in excess heat events. In this figure, other experimental data are also shown.

Integration of the difference between the two power curves in Figure 6 yields an excess energy of 5.02 MJ for this particular experiment, which was limited by the amount of LiD present in the melt. The charge applied to the cell during the charging period corresponded to 0.801 moles of D_2 gas. Thus, an excess heat of 6.26 MJ mol^{-1} D_2, or 1096 MJ mol^{-1} Pd, was obtained, similar to those shown in Table 1. In a particular case, where the charging current was 692 mA cm^{-2}, the resulting excess power gain was 1512%, in the range of 627 W cm^{-3} Pd.

Preliminary experiments based on LiH have been performed and no excess heat has been measured to date. A calorimetry result from the Pd-H system is shown in Figure 8, which agrees with thermochemical reactions, illustrating the correct response from the calorimetry technique.

The surface morphologies of the Pd samples are shown in Figures 9a and 9b.

Table 1. Experimental parameters and interpretation of data in excess heat events

Cell voltage V	Current desity mA cm^{-2}	Heater power W	Electrochem. power W	Total input W	Output measured W	Excess power W	Gain %	Excess heat MJ mol^{-1} D_2
3.230	606	71.91	1.94	73.85	86.76	12.91	665	- 4.15
2.188	290	69.25	0.63	69.88	79.24	9.36	1486	- 6.27
2.270	420	69.30	0.94	70.24	82.81	12.57	1337	- 5.83
2.453	692	69.25	1.68	70.93	96.34	25.41	1512	- 7.16

EDX results on the deuterided sample showed Fe and Zn contamination (Figure 10b) in contrast to the blank (Figure 10a).

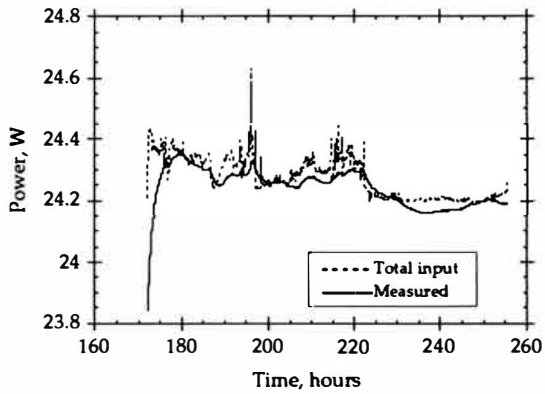

Figure 8. Calorimetric result from a controlled Pd-H system

The polarization of a Mo | eutectic LiCl-KCl molten salt with excess LiD | Al cell at 375° C (Figure 4) shows a reversible Li deposition reaction occurred at -300 mV and a deuterium gas evolution at ~200 mV versus a "LiAl" | Al reference.

Figures 11a and 11b show the ^{4}He analysis results for the deuteride and hydride systems, respectively. The enhancement of ^{4}He in all four deuteride specimens, in one case 12 σ, is shown above the background level. By contrast, the hydrogen specimens show a decrease in ^{4}He content after electrolysis, as severe cracking and embrittlement were observed in the hydride sample.

DISCUSSION

Thermochemical Aspects

Most thermodynamic data, such as enthalpies that represent heat associated with the reactions in the system, can be found in the literature (e.g., [15]). Table 2 lists possible chemical reactions and their corresponding enthalpies. All enthalpies are positive, indicating these reactions are endothermic in nature and should not contribute to any excess power or heat measured. This is verified by the work performed on the hydrogen system, as shown in Figure 8. Thus, the results from the deuterium system strongly suggest that the anomaly effect is non-chemical. The origin of the excess heat generation can only be attributed to a nuclear process or, perhaps, several processes that have yet to be identified.

Nuclear Evidence

The He analysis results indicate ^{4}He was enriched in the deuteride sample. An opposite effect was observed in the hydride sample. Bush *et al.* [17] recently

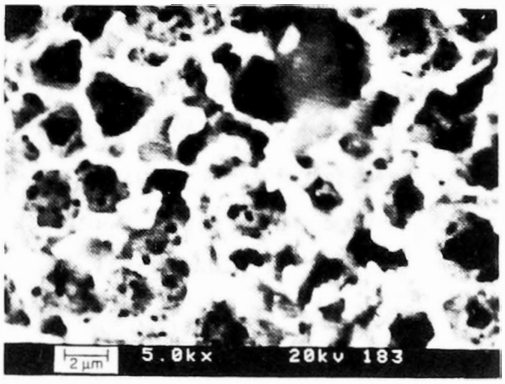

Figure 9a. SEM micrograph shows surface morphology of the as-prepared blank sample

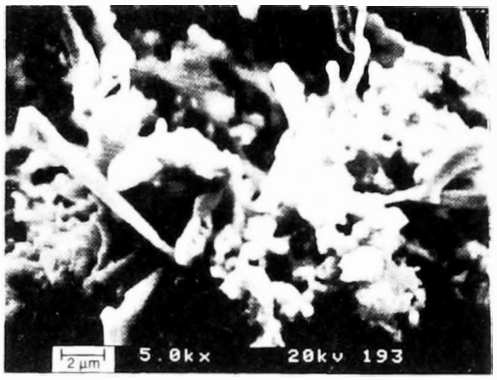

Figure 9b. SEM micrograph of the deuteride sample surface

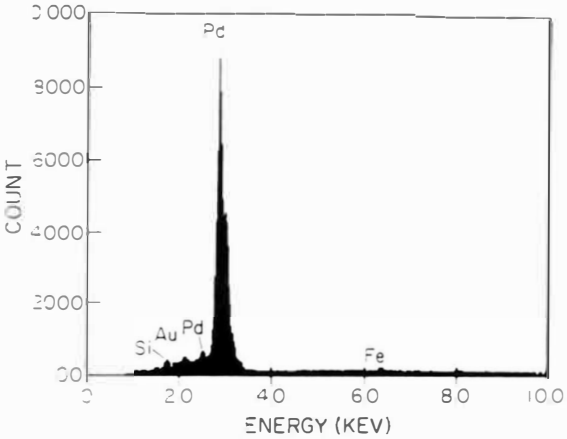

Figure 10a. EDX elemental analysis of the blank

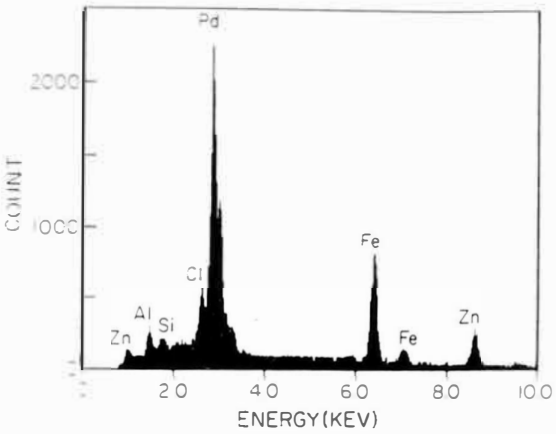

Figure 10b. EDX analysis of the deuteride sample

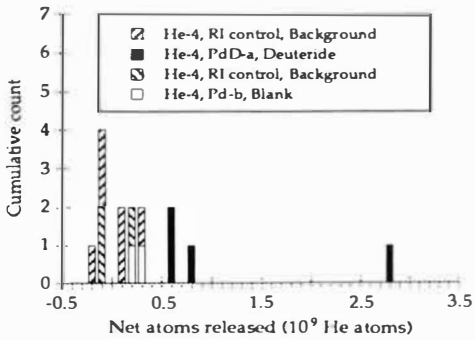

Figure 11a. ^{4}He analysis for the deuteride system. Four specimens all show signals above background level.

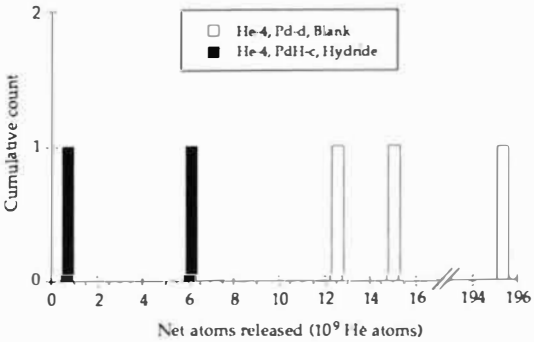

Figure 11b. ^{4}He analysis for the hydride system. Electrolysis reduced the ^{4}He content.

Table 2. Enthalpies of reaction in the Pd-H(D)/ molten salt systems

Reactions	ΔH_r, kJ mol^{-1} 298 K	700K
0.56 LiH + Pd + 0.56 Al = 0.56 "LiAl" + $PdH_{0.56}$ (hydride formation)	12.13	
0.56 LiD + Pd + 0.56 Al = 0.56 "LiAl" + $PdD_{0.56}$ (deuteride formation)	13.68	
δ LiH + PdH_x + δ Al = δ "LiAl" + $PdH_{x+\delta}$ (hydrogen dissolution)	23.05	2.13 (x=0.35) 29.74 (x=0.65)
LiH + Al = "LiAl" + 1/2 H_2 LiD + Al = "LiAl" + 1/2 D_2	41.66 41.95	41.45
2 LiCl + PdH + 2 Al = 2 "LiAl" + $PdCl_2$ + 1/2 H_2 2 LiCl + PdD + 2 Al = 2 "LiAl" + $PdCl_2$ + 1/2 D_2	556.55 555.17	

reported the detection of ^{4}He in the effluent gas from electrolysis cells producing excess heat. This evidence suggested a nuclear scenario with ^{4}He being the major product of the excess heat. The majority of ^{4}He was not retained in the electrode but escaped to the effluent gas, possibly through microcracks or pore channels. This suggests the ^{4}He was most likely produced near the surface region.

The mechanism of the ^{4}He production has yet to be identified. While a large amount of heat was expected to be released, energetic nuclear debris or secondary reaction products have not been detected to date, which is difficult to explain by the conventional theory. The d-d(^{4}He, γ) channel is less favorable than the (^{3}He, n) and (^{3}H, p) branches in conventional plasma fusion. No 23.8 MeV γ-ray has ever been reported, implying that ^{4}He production, if any, is untraditional. The to-be-released 23.8 MeV energy represents the difference between the excited ^{4}He* and ^{4}He ground state. An explanation of heat release through interactions with the lattice (phonons) or electrons seems to lack of a plausible theoretical justification.

Assuming the 23.8 MeV was released by a pair of deuterium to ^{4}He reaction, 6 MJ of excess heat combined from two experiments should result in 1.6×10^{18} ^{4}He atoms. The ^{4}He remaining in the electrode was estimated to be 2.9×10^{10} atoms, indicating that only 1.8×10^{-8} of the ^{4}He atoms produced by the reaction were retained in the electrode. Accordingly, the excess heat reaction consumed 1.6×10^{18} D_2 molecules. Compared to the total 1.036 moles, or 6.24×10^{23} D_2 molecules used, the excess heat episode occurred every 2.6×10^{-6} events – indeed a small fraction. However, the fusion rate, if the assumption is true, was 8×10^{-12} sec^{-1} d-d pair^{-1} – many orders of magnitude above that calculated by the conventional coulomb-barrier model.

Morphological Aspects

SEM micrographs show a large number of small pores and a grain structure on the as-prepared Pd surface (Figures 9a). These "ruffle-like" porous features were introduced by torch melting. The deuterided sample (Figures 9b) showed no evidence of any grain structure and a quite different texture on the surface.

The drastic morphology change by electrolysis is evidenced by "cauliflower-like" microstructures (Figure 9b). This new surface is still predominantly Pd, according to the EDX result (Figure 10b). We suspect the deuteriding process at high current density and potential had a parallel process that caused substantial Pd dissolution, possibly by chloriding as $PdCl_4^{2-}$, and co-deposited with D^- to the anode as a new Pd layer. Some needle-like Pd whiskers were identified by EDX, as shown in Figure 9b. The recent work of co-depositing Pd and D onto metal substrates, as demonstrated by Szpak *et al.* [17], suggests further investigation of this process in molten salts.

The Fe and Zn contaminants cannot be quantified by EDX (Figure 10b). The Fe contaminant likely came from the steel current collectors. The Zn contaminant was probably from the Al electrode (since 6061 Al alloys contain 0.25% Zn) or the brass container. The influence of these contaminants on the production of excess heat and morphology is not known. However, their presence and associated chemical reactions or the Pd co-deposition process cannot be the source of excess heat, because the amounts involved are far too small to be accounted for by the energy that was measured.

Reproducibility

Our present difficulties in reproducing the excess heat event stemmed from failures of the cell components due to uncontrolled high lithium activity and hydrogen embrittlement, improper Pd sample preparation that led to severe cracking and dissemination, uncontrollable chloriding corrosion behavior, and limited LiD solubility in the melt. Understanding the cell reactions at high current density and potential is the key to controlling reproducibility.

CONCLUSION

Employing molten salt electrochemical techniques, we found excess heat in the Pd-D system. In one case, a large amount of excess heat, 6.26 MJ mol^{-1} D_2, was measured. Evidence suggests that ^4He might be the prominent nuclear product. A Pd, D co-deposition process changed the anode morphology significantly. Reproducing excess heat was hampered by various uncontrollable parameters.

ACKNOWLEDGEMENTS

The financial support of the University of Hawaii, the Pacific International Center for High Technology Research, and Fusion Resources, Inc., is gratefully acknowledged. We are also indebted to Drs. S. E. Jones, N. J. Hoffman, B. M. Oliver, and D. H. Worledge for their assistance in this work.

REFERENCES

1. M. Fleischmann, S. Pons, and M. Hawkins, *J. Electroanal. Chem.* **261** (1989) 301 and its erratum in **263** (1989) 187.
2. B. Y. Liaw, P.-L. Tao, P. Turner, B. E. Liebert, *J. Electroanal. Chem.* (in press).
3. S. Pons, this Proceedings; M. C. H. McKubre, *et al.*, *ibid.*
4. P. L. Levine and K. E. Weale, *J. Chem. Soc. Faraday Trans.*, **56** (1960) 357.
5. C. M. Luedecke, G. Deublein, and R. A. Huggins, *J. Electrochem. Soc.*, **132** (1985) 52.
6. G. Deublein, B. Y. Liaw, and R. A. Huggins, *Solid State Ionics*, **28/30** (1988) 1078.
7. G. Deublein, B. Y. Liaw, and R. A. Huggins, *ibid* 1084.
8. G. Deublein, B. Y. Liaw, and R. A. Huggins, *ibid* 1660.
9. G. Deublein and R. A. Huggins, *J. Electrochem. Soc.*, **136** (1989) 2234.
10. B. Y. Liaw, G. Deublein, and R. A. Huggins, presented in the 6th Intern. Solid State Ionics Conference, Garmisch-Partenkirchen, Germany, Sept. 1987; paper submitted to *J. Less-Common Metals.*
11. The value is estimated from the hydrogen system in Table 2 at 298 K.
12. N. P. Yao, L. A. Herédy, and R. C. Saunders, *J. Electrochem. Soc.*, **118** (1971) 1039.
13. C. J. Wen, B. A. Boukamp, R. A. Huggins, and W. Weppner, *J. Electrochem. Soc.*, **126** (1979) 2258.
14. S.-W. Chen, C.-H. Jan, J.-C. Lin, and Y. A. Chang, *Metallurgical Trans. A*, **20A** (1989) 2247.
15. I. Barin, O. Knacke, and O. Kubaschewski, *Thermochemical Properties of Inorganic Substances*, Springer-Verlag, Berlin, 1973 and supplement 1977.
16. B. F. Bush, J. J. Lagowski, M. H. Miles, and G. S. Ostrom, *J. Electroanal. Chem.*, **304** (1991) 271.
17. S. Szpak, P. A. Mosier-Boss, and J. J. Smith, *J. Electroanal. Chem.*, **302** (1991) 255.

Conference Proceedings Vol. 33
«The Science of Cold Fusion»
T. Bressani, E. Del Giudice and G. Preparata (Eds.)
SIF, Bologna 1991

Tritium and neutron emission in conventional and contact glow discharge electrolyses of D_2O at Pd and Ti cathodes *

Giuliano Mengoli and Monica Fabrizio
Istituto di Polarografia ed Elettrochimica Preparativa del CNR, Corso Stati Uniti 4, 35020 Padova (Italy)
Claudio Manduchi, Giorgio Zannoni and Lucia Riccardi
Dipartimento di Fisica "G. Galilei", Università di Padova, Via Marzolo 8, 35131 Padova (Italy)
Antonio Buffa
Istituto Gas Ionizzati del CNR, Corso Stati Uniti 4, 35020 Padova (Italy)

We recently found that the level of ^3H in D_2O / 0.1 M LiOD solutions electrolyzed at Pd sheet cathodes increased, although sporadically (<20%), till a order of magnitude over background, we indeed used D_2O with very low background [1].

The surface of a Pd sheet cathode (1 x 1x 0.05 cm^3) which gave apparent generation of ^3H had developed localized swelling with deep pitting underneath; if this phenomenon was relating with ^3H, the latter was likely formed by means of a near-surface process, which might be easier to reproduce if electrodes of relatively larger dimensions are utilized.

The experimental design adopted for the four conventional electrolytic runs hereafter described was mostly in agreement with the above consideration.

We are also reporting on contact glow discharge electrolyses (CGDE) aimed at inducing critical conditions at/in the metal deuteride cathode.

Detection of nuclear particles

Tritium in both the electrolyte and D_2O from recombined gas was determined by counting the β-decay of solutions with LSC by the procedure and instrumentation already described <1>.

With respect to our previous conditions the β-energy windows of the spectrometer was reduced: although this compromise decreased the background fluctuations, efficiency fell from 40 to 11.5%.

A neutron spectrometer based on a NE 213 liquid scintillator was developed at the Dept. of Physics the University of Padova. The detector basically consists of 4500 cm^3 scintillator

* Work performed in collaboration with ENEA - Frascati

[1] G. Mengoli, M. Fabrizio, C. Manduchi, G. Zannoni, L. Riccardi, F. Veronesi, A. Buffa; J. Electroanal. Chem., 304 (1991) 279.

The upper end of the cylinder is sealed to a stainless steel container (internal ϕ = 10 cm, h = 12 cm) which composed the cavity for placing 1-2 electrolytic cells. The scintillator is seen by three XP 2020 photo-multipliers through optical contact with 3 windows at the bottom of the cylinder. Threefold coincidence is required with resolving time of less than 10 ns.

The usual technique of pulse shape discrimination was adopted to reduce γ-ray contamination: in one set of runs (normal electrolyses) a high energy threshold (1.7 MeV) was set to the proton recoil spectra and thus γ-ray contribution can be estimated at about 5%; conversely, in a subsequent set of runs (C.G.D.E.), the energy threshold was lowered to 0.75 MeV but a much more severe n / γ temporal discrimination was adopted.

With these arrangements the spectrometer was set at an effective n-efficiency in the range 0.3 - 0.35%, as determined by a weak ^{252}Cf source.

According to one acquisition line, the neutron frequency of pulses and the corresponding pulse amplitude distribution (proton recoil energy spectra) were stored in a Labview program in a Macintosh II PC linked to the detector by a Crate-Camac interface. Thus the computer at any given moment sampled a set of 100 pulses providing its neutron average frequency and pulse energy distribution.

The other parallel acquisition line was operated directly from the detector with a multichannel scaling analyzer with 6 or 2 s time steps for 16384 channels. In this way the proper frequency could be determined for each pulse with a temporal resolution of 1μs, as against 25 μs of the Labview system.

Conventional electrolyses

The electrolytic cells were assembled using centrifuge tubes having internal dimensions ϕ = 3.3 cm, h = 11 cm. The cathodes were: Ti rod (cells 1 and 2), ϕ = 1 cm, h = 3.5 cm, area = 10 cm^2 ; Pd sealed tube (cell 3), ϕ = 0.2 cm, h = 2.5 cm, thickness = 0.02 cm, area = 1.6 cm^2; Ti plate (cell 4) 3 x 2.5 x 0.1 cm^3. The anodes were: Ni coil (cells 1-3) spiral-wound around the cathode; Pt sheet (cell 4) 3 x 2 x 0.01 cm^3 facing the cathode.

Current till 1 A were supplied by an AMEL mod. 551 galvanostat; higher intensities were obtained by a dc constant voltage generator. The experiment of cell 1 was carried out using

D_2O with ^3H background = 88 ± 25 dpm ml^{-1}, whereas D_2O used for the other experiments had ^3H background = 260 ± 25 dpm ml^{-1}. During electrolyses the volume of solution was kept constant by periodical refilling; D_2 and O_2 gases were conveyed through the lid of the cell to a trap condensing D_2O vapour and taken to recombinate as D_2O (Pd catalyst).

1 Tritium results

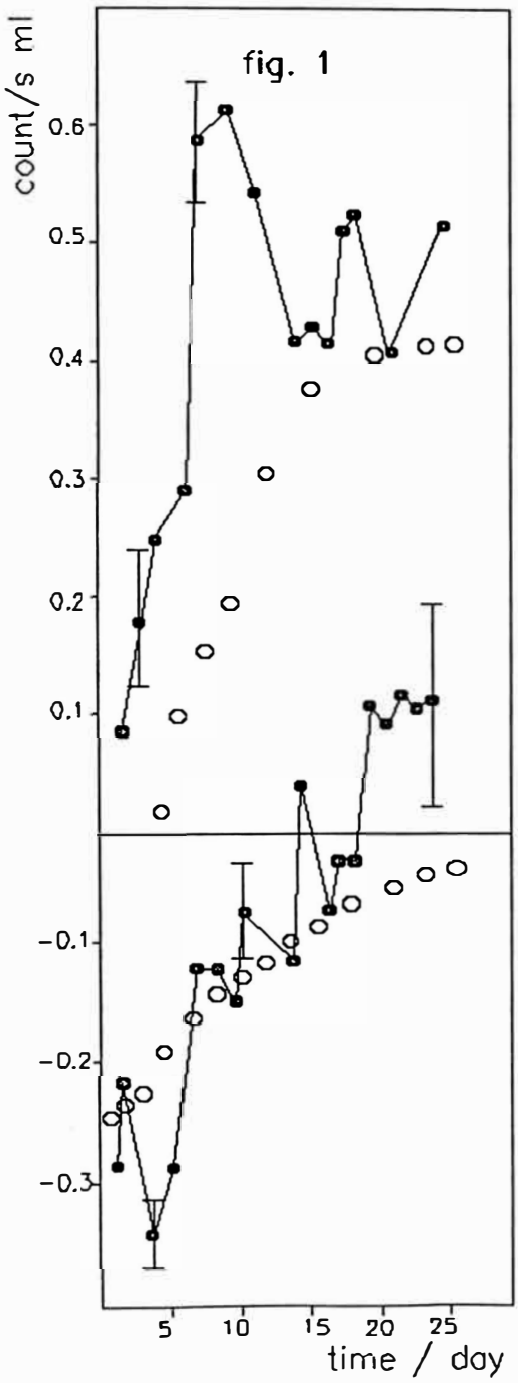

Cell 1 containing 45 ml of 5 M NaOD in D_2O was fed with i = 0.05-0.75 A cm^{-2} from 18/10/90 to 7/12/90. Systematic ^3H assays outlined that: no electrolytic separation between liquid and gas took place; ^3H tested in both phases was mostly above the background level. Although the excess in a single sample may be within statistical error (σ) limits, the general trend was definitely positive.

Cell 2 was running from 21/12/90 to 25/1/91 at about the same conditions of cell 1, but for D_2O which had higher ^3H content. Electrolytic ^3H separation did occur, as the liquid was here seen to be progressively enriched at the gas cost, but the overall ^3H balance was negative. The apparent loss of ^3H must be imputed to evaporation as a negligible D_2O / TDO separation is likely to occur in the vapour phase.

Cell 4, containing 40 ml of 1M Li_2SO_4, was running from 19/2/91 to 19/3/91. A sharp increase of ^3H level in the electrolyte did

occur after the first week; see figure 1 where experiment (full dots) is compared with theoretical prevision S = 2 (empty dots), the upper part refers to electrolyte, the lower to the gas. The major ^3H increase occurred within 1-2 days with i = 0.6 A; the subsequent decline was probably caused by the rise of the current to 1 A, whereby ^3H production apparently ceased and more frequent refillings of D_2O (at low ^3H) were necessary also to compensate significant evaporation loss. We note that figure 1 cannot be explained by any separation factor.

2 Neutron results

Neutron data were collected in continuous from November 90 to the end of March 91: periods during which the electrolytic cells were working inside the detector alternated with periods of blank determinations.

The background frequency corrected for the efficiency was above 100 neutron s^{-1} $\pm$ 15%. In these conditions, although the frequency during the electrolytic runs was something higher, any attempt of determining a net neutron flux based on subtraction of background measured in different periods can be questioned.

However statistical analysis of neutron frequency distribution as obtained from the multichannel scaler analyzer, revealed some significant differences between blank and experiments. Thus the rate of pulse frequency measured during a background period outlines about a Gauss curve; in other words, a Poisson distribution of the frequency can be predicted. Such distribution does not hold any longer for pulses recorded during the electrolytic runs. It appears that during electrolysis the background was overlapped by a phenomenon of higher frequency.

Contact glow discharge electrolysis

In conventional electrolysis performed with two electrodes of different sizes, conditions may be attained whereby the lines of current converging on the smaller electrode cause local vaporization of the solvent, creating a gas sheath around it. If the applied voltage is increased enough, normal electrolysis is then converted to contact glow discharge electrolysis: a bright steady discharge takes place between electrode and solution through ions forming in the

gaseous sheath.

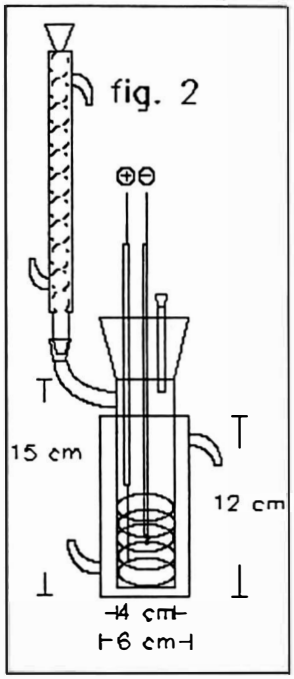

Our experimental design consisted of: one Pd rod cathode, ϕ = 0.1 cm h = 0.5 - 0.7 cm; one Pt coil anode, ϕ = 0.05 cm l = 20 cm, wound around the cathode at 1 cm distance; and 42 ml of $1.5 \cdot 10^{-2}$ M LiOD (or 10^{-2} M Li_2SO_4) solution. The gas exit of the cell was equipped with a cooler which refluxed vaporizing D_2O in the cell (figure 2).

The Pd electrode was generally charged for 2-3 days at 50-100 mA cm^{-2}, then potential current characteristics were varied to induce CGDE. The cell was operated inside the cavity of the n-spectrometer: particular care was taken to see the discharges did not induce electric noise in the detector. Oscillating currents, sparks and lightning are generated when trying to achieve the much more stable conditions of a steady-glow discharge.

To avoid possible electronic artefacts, we adopted the following:

- when setting up the right conditions, the electronics of the n-spectrometer were disconnected from the recorder. The operation required from a few to some tens of seconds before attaining a smooth discharge with 350 V applied and $\leq$0.1 A of current flow;
- an oscilloscope continuously monitored the signal and the occurrence of noise could be detected at any time;
- some control experiments were carried out in light water in the same CGDE conditions.

Results

Figure 3 shows how the pulse frequency increased remarkably over the background during the periods of CGDE (see the arrows). At this electrode the phenomenon could be reproduced over a few days, although with decreasing intensity, and eventually ceased. A maximum of 50 n s^{-1} excess over the background can be estimated.

Figure 4 shows histograms recorded under CGDE with two different electrodes for the same conditions but using light water. No increase over background frequency was observed.

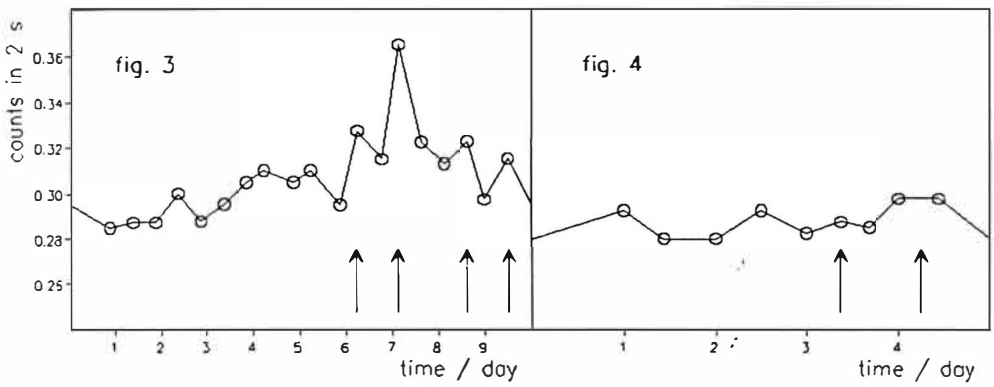

The results presented so far are preliminary and need to be studied further. We have programmed more conclusive experiments by using thicker electrodes, a dc generator of higher power, and careful shielding of the electronics.

We also note that, with CGDE, the most critical non-equilibrium conditions are created at/in the metal deuteride:

- many types of positive ions including deuterons and possibly charged D_2O clusters occur in the discharge;
- the temperature may reach the melting point of the metal.

Conference Proceedings Vol. 33
«The Science of Cold Fusion»
T. Bressani, E. Del Giudice and G. Preparata (Eds.)
SIF, Bologna 1991

NEUTRON EMISSION AND SURFACE OBSERVATION DURING A LONG-TERM EVOLUTION OF DEUTERIUM ON Pd IN 0.1 M LiOD

HIROO NUMATA, RYUZO TAKAGI AND IZUMI OHNO Tokyo Institute of Technology, 2-12-1 O-okayama, Meguro-ku Tokyo152 Japan
KAZUTAKA KAWAMURA Institute of Research and Development, Tokai University, 1117 Kitakaname, Hiratuka259-12 Japan
SHIRO HARUYAMA Tokyo National College of Technology, Kunugida, Hachioji, Tokyo153 Japan

ABSTRUCT

Long-term electrolysis for well annealed thick Pd rods (9.0 and 21.2 mm ø) in 0.1M LiOD have been performed to examine anormalous phenomena; neutron emission and heat bursts. The count rate of neutron (CRN) bunched for 3 h showed no significant increase at low current densities. High CRN appeared a few days later after the current increased to 102.4 mA/cm^2 and the temperature was raised to 50°C. In two experiments CRN and neutron energy spectrum of 2.45 MeV was reproduced.

Metallographic observation showed two faults, blisters, cross slips and holes on Pd surface and a raw of defects in a recrystallized grain. Microstructural changes of Pd electrode during long-term electrolysis is discussed.

INTRODUCTION

Fleischmann and Pons[1] and Jones et al.[2] recently reported the evidence of a nuclear fusion in condenced matter which undergoes unusual deuterium loading by means of electrolysis in heavy water system or deuterium gas equilibration and intense desorption induced by changing physical parameters i.e.temperature in a gas tight chamber[3-4]. Although many studies are aimed to duplicate the precausor's results, they did not obtain their purpose. A few reports, however claimed that low level neutron emission was observed with respect to 2.45 MeV energy spectrum[5-9] and only one group reported F&P type huge heat bursts[10]. An important aspect of these reports is that either neutron or heat bursts was observed sporadically, as such effect sustained for microseconds or several days. It is suggested that the characterization of materials is important to improve reproducibility of an experiment, consequently approach shortly the mechanism.

In our preliminary experiment[11],where an annealed Pd cathode (9 mm ø x 10 cm long) was used, high neutron count rate and neutron energy spectrum of 2.45 MeV were observed. Afterwards, the second experiment have been performed to test reproducibility using the same experimental set-up except twice in diameter of Pd electrode. During a long-term electrolysis initially no significant count rate of neutron was observed, while high count rate of neutron appeared for several hours or days after increasing current density and temperature.

In this study, the evidence of neutron emission is further discussed in connection with an electrode potential, temperature and metallographic observation during a long-term electrolysis.

EXPERIMENTAL

Electrolyte-0.1MLiOD-D_2O solution was prepared by addition of Li_2O(Wako pure chemicals:95 %) into D_2O(Merk:99.8 %, CEA:99.8 %, Isotec:99.9 %). The concentration of LiOD alkaline solution was substantially increased in the course of electrolysis since small amount of 0.1MLiOD was poured into the cell every day to replenish the exhausted one. During a long-term electrolysis incremental fills were made with pure heavy water to minimize the effect of electrolyte concentration on the eletrochemical system.

Electrolytic cell-The experimental cell(content is about 130 ml) was made out of transparent quartz, which has a water jacket. The temperature of circulating water in the jacket was controlled at 40 and 50°C by Coolnics(Komatsu-Yamato Co Ltd.). The upper part of the cell was plugged by a silicone rubber stopper where working, reference and counter electrodes and the assemblies (addition tube and the guides of thermocouples) were mounted. The electrode potential was refered to the potential of dynamic type (α+β) PdD reference electrode. The guide of the counter electrode was served as for gas outlet port. Once adjusting geometrical position of these electrodes, it was fixed to the cell and the gap was throughly sealed with a silicone rubber resin. The working electrode was a thick Pd rod (Nilaco Co Ltd. 99.95 %). Pd material was cast into a high purity alumina tube in a flow of Ar. The as-cast Pd rod was out gassed for 20 h in a 10^{-6} Torr vacuum at 800°C.

Ti rod (3 mm ø) gold plated was served as an electrical leading. It is screwed into the upper end of the Pd electrode as shown in Fig.1. The working electrode was set reasonably centrally in the cylindrical space circumscribed by the counter electrode (mixed oxides of Pd and Rh). Details of the electrode treatment before loading are shown in Table 1.

Microscopic observation after electrolysis-Surface appearance of a specimen was observed by an optical microscope and SEM (JOEL model T-330 20 kV). Microstructure observation inside the electrode was made by sectioning the rod with traverse and radial directions. The crosssectional area was polished using 6μ diamond paste. Then, it was lightly etched by dilute hydrochloric acid for optical microscopic observation.

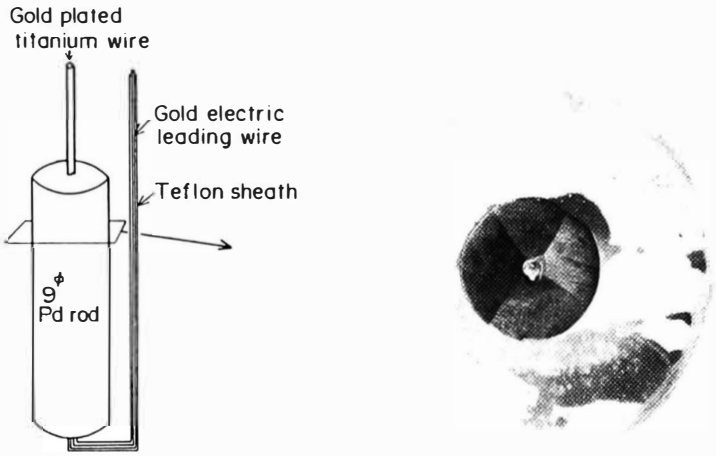

Fig.1 Schematic illustration of Pd electrode and optical micrograph of its crosssectional surface.

Table 1 Experimental conditions of Exp.1 and Exp.2; electrode dimention, pretreatment, current density.

Exp.1 ; Dimension of electrode $0.9^{\phi} \times 5.3^{\ell}$ cm Pd

Run No.	Current density mA cm-2	Pretreatments	Time/days
1st	0.05~40 40~500	Cast, 800°C annealing(10^{-6}Torr) acid treatment	Oct.16~Dec.20 1989
2nd	40	Polishing, acid treatment evacuation, Deuterium charge	Feb.16~Mar. 1 1990
3rd	40	Evacuation, polishing acid treatment	Mar. 1~Mar. 6
4th	40	Evacuation, polishing anodization	Mar.14

Exp.2 ; Dimension of electrode $2.1^{\phi} \times 3.2^{\ell}$ cm Pd

1st	0.05~ 102.4	Cast, 800°C annealing(10^{-6}Torr) Deuterium charge, acid treatment	Jul.20 1990 ~Feb. 1991

RESULTS AND DISCUSSIONS

We have performed two experiments (Exp.1 and Exp.2). In Exp.1 the Pd electrode was subjected to deuterium loading for two months, then the dilation of the electrode was ex-situ measured. The electrode was again pretreated (abrasion, degassing, D_2 loading and acid etching) before electrolysis and the above processes were repeated 4 times. The amount of adsorbed D_2 can be estimated by the variation of D_2 gas pressure. In Exp.2 deuterium loading had completed for 8 months without any interruption of electrolysis. The possibility of large neutron bursts has been examined in detail by monitoring the temperature and the overpotential (OP), so as to check a coincidental occurrence of neutron bursts and the increase of the temperature. Although the mechanism is still obscure, we used twice thicker Pd rod in Exp.2 considering Arata's suggestion[12].

OP and CRN of Exp.1

The galvanostatic cathodic current was applied on the Pd electrode, in which a current density was raised step by step from 0.05~102 mA/cm^2. The initial content of deuterium before electrolysis was estimated to be 0.36 in atomic ratio. At onset of a cathodic current the OP showed an irregular shift to noble direction, then it was reached at steady state value. At low current density it obeys the Tafel relation, which shows that the cathodic OP is a linear relation with the logarithm of a current density[13].

When the current density was increased to 40 mA/cm^2, significant count rate of neutron (CRN) above background was observed. However, this CRN did not last for a long time since it abruptly falled down to the background level somewhat later the current increase. This intermittent fluctuation of CRN was observed for several times ; 2nd~4th run followed by a current perturvation. This behavior of CRN was reproduced in Exp.2, as is shown below (see also Fig.5(c)). Menlove at al[3]. reported two different types of neutron emission from dueterium loaded Ti chips. It has become apparent that the bursts (200 μs) was occurred shortly during increasing temperature and the

intermittent weak neutron emission lasted for 12h after the temperature recovered. The latter intermittent CRN corresponds to our CRN fluctuation. On the other hands, large neutron bursts were not measured in Exp.1, which is sporadically appeared during intense desorption induced by discharge activation or temperature cycling. Interestingly the intermittent CRN (see also Fig.5 (c) and (d)) seems respond to the current on or temperature cycling, which suggests that cold fusion is induced by intense adsorption or desorption by electrochemical reaction or temperature cycling.

Energy spectrum during the period of high CRN in 1st run show the characteristic of 2.45 MeV neutron. We had carefully checked data with regards to the statistics, effect of cosmic ray, temperaure of the detector. The energytic neutron counted by an NE213 scintillator is believed to be strong evidence of d-d fusion reaction. Details on neutron measurement system and the results are given in the previous papers[7,11].

Now we must describe the results with attempting to distingush between the phenomena occurred by cold fusion and those of usual metal hydride system. It is obviously difficult to catch the evidence of d-d fusion except neutron data but comprehensive grasp of the experimental facts leads us understanding the phenomenon.

Dilation of Exp.1

A sample for microscopic observation was removed from the apex of the electrode after interruption of electrolysis and demantling the electrode from the cell. The diameter of the electrode was measured at three positions in height(top, middle and bottom as shown in Fig.2). Then, the electrode was carefully re-installed. Table 1 shows details of the procedures of each run. In Fig.2 the dilation of Pd electrode was plotted against the run number. For 1st run the dilation at bottom end shows the maximum 7 %, while those in the upper regions exhibited the lesser extent than that at bottom. During 2nd~4th run the values at these positions approached asymptotically to 7.8~8.3 %.

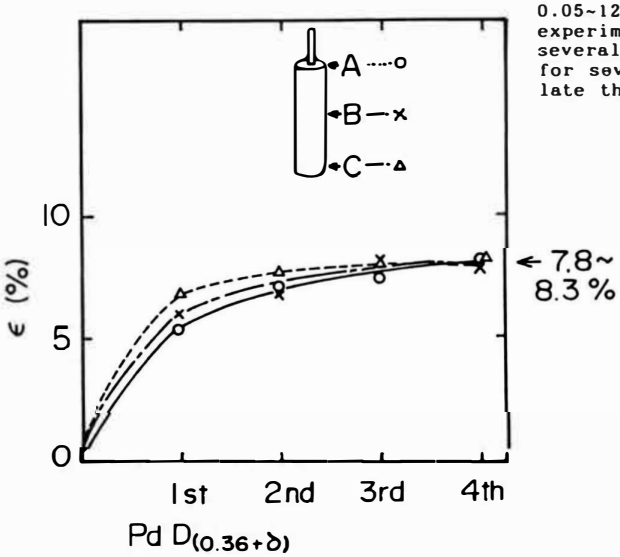

Fig.2 Radial dilation: ε % of post electrolysis Pd electrode at three positions (A, B and C) during 1st run.

It is noted that high CRN and energy spectrum of 2.45 MeV were appeared in the period of 1st run, where the most large dilatation occurred especially during 1st run. Although we have found no explanation about the relation between a neutron emission and large expansion of a material, it is helpful in understanding anormaly to inspect the inside in an aspect of metallography.

The microstructure obtained from the apex is shown in Fig.1 . In metallographic aspect the specimen as a whole is consisted of columnar crystals, which are gradually grown inside from a crucible wall during cooling. The picture of the specimen exhibits a peculiar grain structure, quadrified by two straight grain boundaries. Long prisms grow longitudinally along the electrode center. However, these results are unexpected, since temperatures of the electrode and that out side of the counter electrode showed no significant change corresponding to heat bursts. Hence, this is well acceptable, only when the small heat evolution in the interior lasts long time so as to promote abnormal grain growth. Coupland et al.[14] found the recrystalline grain near the areas of electrical connection. However, there has not been hitherto reported such kind of anomalous grain structure. This suggests that during emission of neutron, the heat evolution in the interior occurred slowly showing the symmetrical crystal structure. However, there is no experimental evidence that relates neutron emission to the increase of temperature assuming such huge heat bursts introduced by F&P.

OP and CRN of Exp.2

The experimental set-up and measurement system were the same as those of Exp.1, whereas twice thicker Pd electrode underwent a deuterium loading during a longer period was used. In spite that the electrode was subjected to high cathodic OP for a long time, the surface sustained the initial metallic gloss. The gloss of the electrode surface in Exp.2 was changed less than that in Exp.1, because the latter electrode had been treated with mechanical abrasion and chemical etching several times. Table 2 shows experimental results for the OP of the Pd electrode, which was deuterium charged galvanostatically. A current density was raised step by step 0.05~120.4 mA/cm^2, then two temperature cycle experiments: 50°C after cooling at 40°C for several hours and 50°C after cooling at 30°C for several hours, were performed to stimulate the transportation of adsorbed deuterium.

Temperature or Current Density Changed at	Current Density (mA/cm^2)	Palladium Overpotential (V)	Temperature of Circulating Water (°C)
1990			
July			
14	0.05	−0.92	40
19	0.10	−0.94	40
26	0.20	−0.99	40
August			
3	0.40	−1.02	40
10	0.80	−1.07 to −1.04[a]	40
17	1.60	−1.12 to −1.08[a]	40
24	3.20	−1.22 to −1.18[a]	40
September			
5	6.40	−1.31	40
10	12.8	−0.72 to −0.68[b]	40
19	25.6	−0.83 to −0.79, −1.44[c]	40
26	51.2	−1.00 to −0.97[b]	40
October			
17	102.4	−2.55	40
25	102.4	−2.44	50
November			
1	102.4	−2.44	50[d]
5	102.4	−2.44	50[d]
11	102.4	−2.44	50[d]
21	102.4	−2.44	50[e]

Table 2 Conditions of electrolysis; [a] Periodically changing, [b] Frequently changing, [c] See text, [d] After cooling at 40°C for several hours, [e] After cooling at 30°C for several hours.

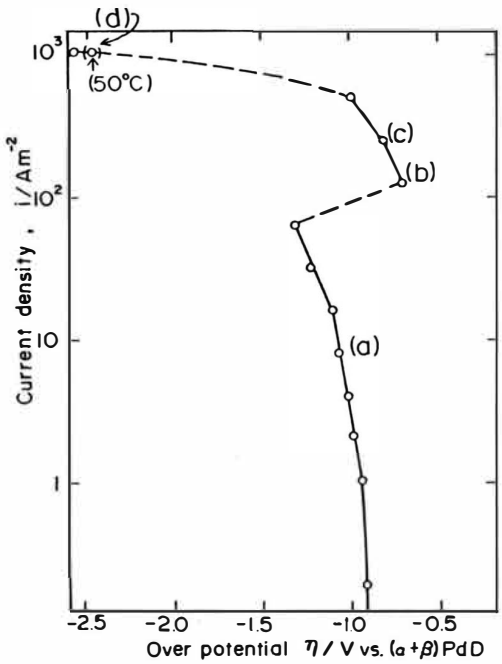

Fig.3 Current-potential curve for pre-loaded Pd in 0.1MLiOD at 40 and 50°C, each point shows a average value during long-term electrolysis, where (a)~(d) indicate the conditions in Table 2.

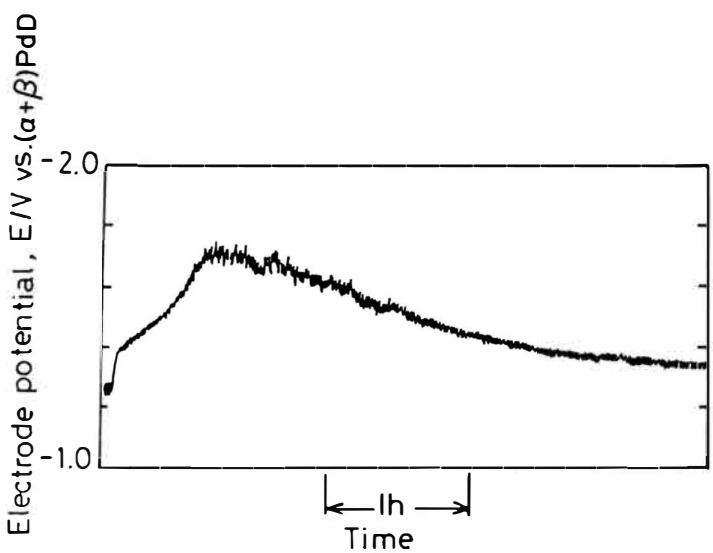

Fig.4 Strange behavior of the overpotential observed at a current density of 51.2 mA/cm^2.

In Fig.3 current-potential curve exhibits the Tafel line with the slope of 0.21 V/decade. The value of the slope is well consistent with that reported by Augustynski et al.[15]. At 102.4 mA/cm^2 the OP rises to almost -2.5 V; (d) in Fig.5, which is associated with poisoning of impurities of the electrolyte such as Zn and Pb or an underpotential deposition of Li^+.

Early state of electrolysis the OP changed periodically for 0.4 to 1.6 mA/cm^2. At 25.6 mA/cm^2 the OP drastically decreased from -1.31 to -0.7 V, then increased to -1.44 V 4 days later and then again decreased to -0.73 V 1day later. Afer then, the OP showed strange behavior, which is shown in Fig.4. Thus, when the current was increased to 25.6 mA/cm^2, the abrupt decrease of the OP ($\Delta\eta$ =0.6 V) was observed as is shown in the transition (a) to (b) in Fig.3. Mengoli et al. reported similar OP shift[16]. This kind of OP shift is far beyond the knowledge of ordinary electrochemical reactions. Hence, the other physical or chemical origin is asked for the strange behavior, which seems to be attributable to surface composition change or possibly heat effect by cold fusion. The latter case is not reasonable for our results because high CRN appeared over -2.55 V at 102.4 mA/cm^2 (refer Fig.5 (d)). This behavior may be explained in terms of an underpotential deposition of Li^+, which increases the OP due to change of surface condition of the cathode. There was no corresponding change of the OP to the high CRN, which may show that the cold fusion does not take place at the surface of the cathode[7].

The neutron measurement was interrupted three times during the long-term electrolysis because the printer brokedown. Since the multichannel analysers (MCAs) malfunctioned during the long time experiment, the foreground results was compared with that of low count rate which was assumed to be equivalent to the background. Figure 5 shows the count rate of neutron (CRN) bunched into 3 h intervals against time. Although during low count rate (Aug.5~Sep.5) no significant energy spectra of neutron was observed, there appeared a difference at 51.2 mA/cm^2. In Fig.5(c) gradual increase and decrease of CRN was appeared apparently coincident to increase of either current density or temperature. Thus, this CRN fluctuation was fairly reproduced in Exp.2. In Fig.5 (d) high CRN, which is three times higher values than that of background CRN bunched into 10 min. appeared a few days after changing the current density or the temperature of the circulating water. Appropriate three energy spectra were averaged during the periods of high CRN observed. The spectrum obtained by substracting the background spectrum (scaled counts per minute) is shown in Fig.6 , together with that of monochoromatic 2.45 MeV neutron (dotted line). The significant signal above the background strongly supports the occurrence of d-d fusion in Pd/D system.

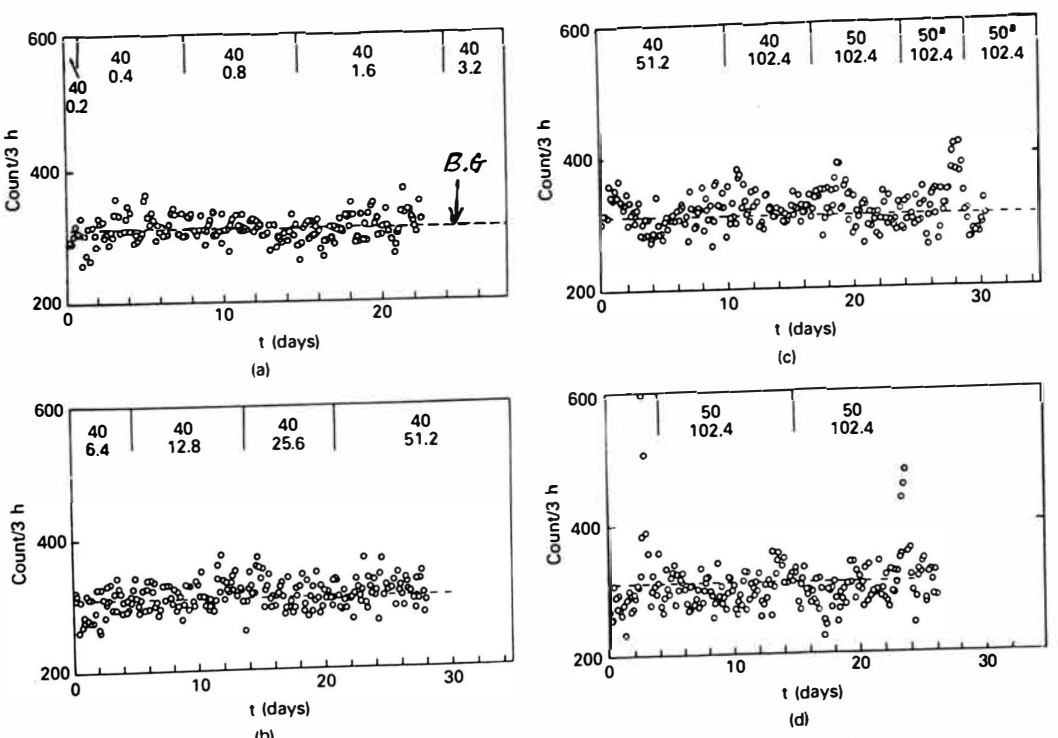

Fig.5 Time dependence of the neutron count rate for 3 h (a) August 2 to August 25, (b) Septenber 5 to October 3, (c) October 7 to November 7, and (d) November7 to December 3. Upper and lower numerical values in figures mean the temperature of the circulating water in degree Celsius and the current density in mA/cm^2, respectively.

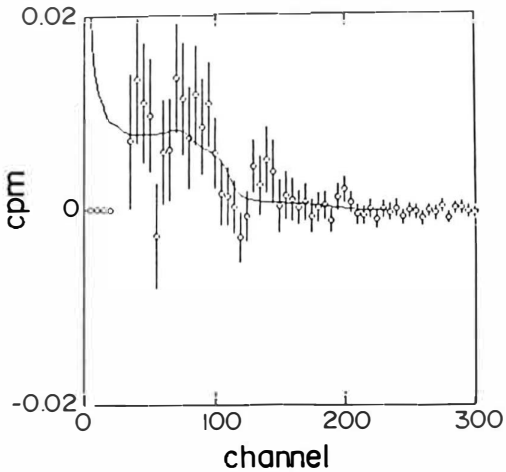

Fig.6 Difference in neutron energy spectrum.

Microscopic mechanism of dilation

Visual observation of the electrode surface is characterized by three different morphology, which is schematically drawn in Fig.7. We found no surface crack, but two faults (Fig.7 (c)), marked blisters (a) and blisters like a feather pattern to arrange each other in two arrays (b). These morphologies locate at 120° left turn and 120° and 150° right turns from the reference position: (b). Thus, there appeared two line imperfections; a long fault and a center line of the feather pattern all over the surface. It is verified that the traverse grain boundary on the crosssectional area of Pd electrode (Fig.12) thrusts out one side at the fault and the other side at the center of the feather. Without chemical etching SEM photographs show partly a plain terrace exposed (Fig.8) , partly covered by a gray overlayer along a long fault. Figure 9 shows another picture of the surface; a cross slip, which is attributable to a heavy local plastic deformation.

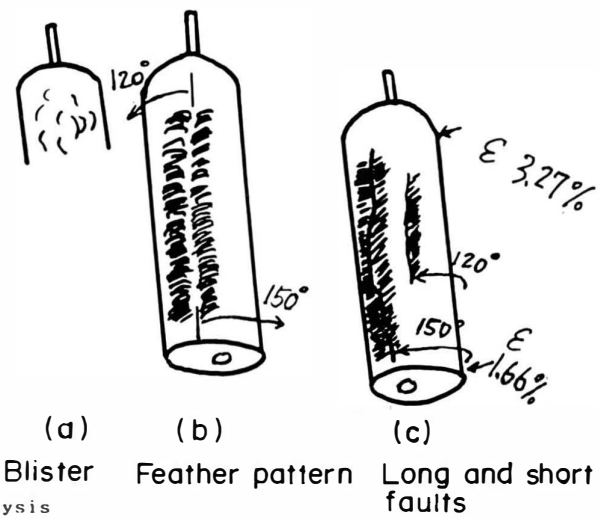

Fig.7 Surface appearance of post electrolysis Pd electrode showing (a) Blister, (b) Feather pattern, center line is reference position, and (c) Two, long and short faults.

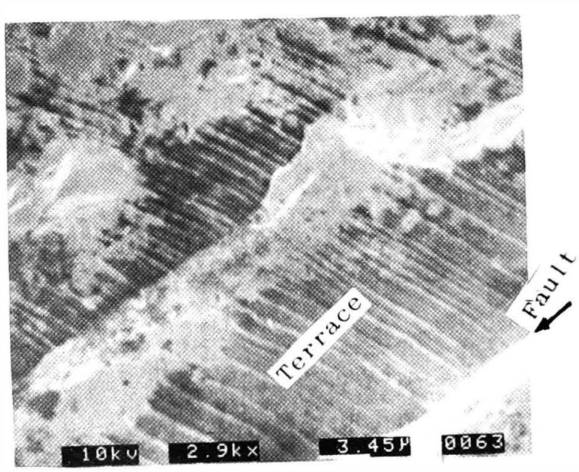

Fig.8 Scanning electron micrograph of Pd electrode surface showing exposed terrace along the long fault.

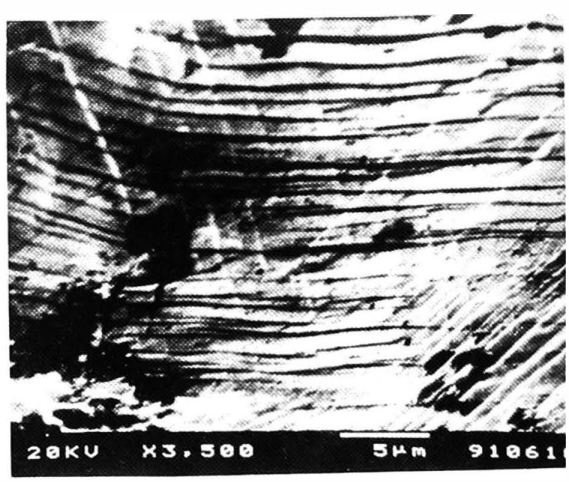

Fig.9 Scanning electron micrograph of Pd electrode surface showing cross slips by local plastic deformation.

On the other hands, the long fault gathers holes. The morphology of holes is shown in Fig.10 . The density of these holes decreased with increasing the distance from the fault line. Figure 11 shows the distribution profile of holes at three positiions (A 6.0, B 3.5, C 8.0 mm apart from the bottom side). Thus, it is considered that both morphologies; faults and holes are relevant. The microstructure of deuterium loaded Pd as a whole shows inhomogeneous structure, the core structure and a blanket as is illustrated in Fig.12 from optical microscopic observation. It consists of two big columnar grains in the interior and columnar grains with randam orientations near the surface. It seems that the latter grain structure was remained unchanged throughout the process, while the core was recrystallized resulting a grain growth. During a long term deuterization, the lattice of big two crystals expands different direction aligned in the figure, which cause a fault and/or a regular arrayed blister on a surface. Then, holes were formed around a fault, whereupon the deuterium gas including the reaction products of the inside gushed. It is useful to compare the formation process of a long fault and blisters with those found in a crater, fault and the behavior of mantle movement inside the earth. The earth evolves heat constantly. In the interior mantle behaves like the mis-oriented Pd grains . Its movement causes a fault and a crater on a crust where a volcano erupts gushing volcano gas, which is consistent with the process of the hole formation around the fault. Thus, several similarities are found between the behavior of deuterium loaded Pd electrode and geological features on the earth. Hence, we can support that the microstructure of Pd electrode is attributable to the heat evolution and plastic deformation in the interior.

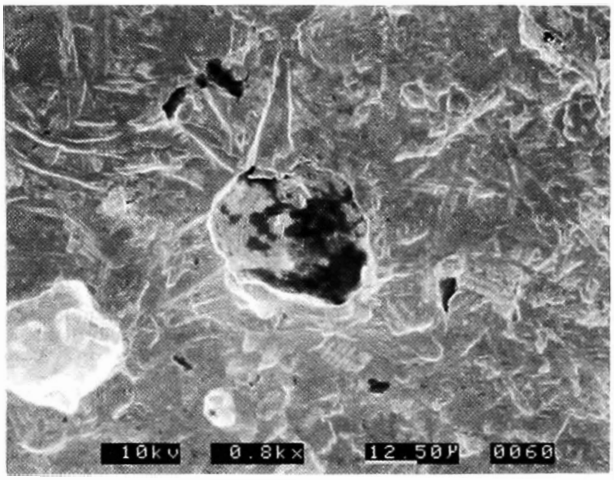

Fig.10 Scanning electron micrograph of Pd electrode surface showing the holes.

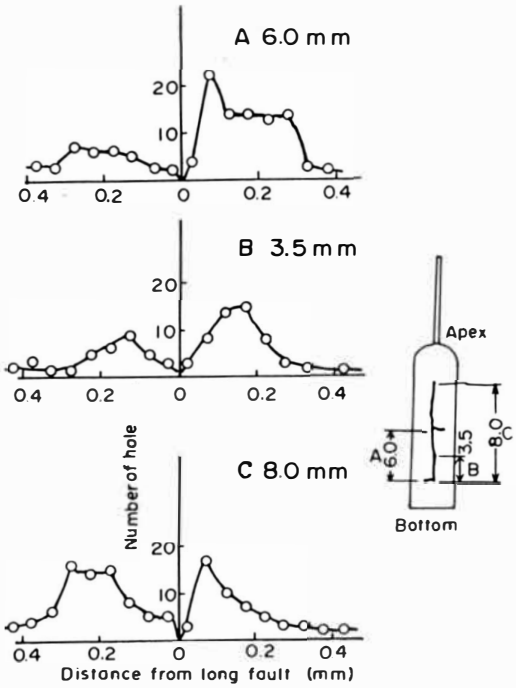

Fig.11 Distribution profile of the holes around the long fault.

Further, the microstructure of crosssectional area of post electrolysis Pd was carefully observed by SEM because it is verified that the neutron emission is not concerned with the surface conditions. As is shown in Fig.12, the interior was composed of two big crystals, one of which had a peculiar morphology; a row of defects. Figure 13 shows the morphology of the defect and their arrangement. Each defect is surrounded by differently colored layer, which seemed to be subjected to the change of physical conditions, i.e. temperature. The inner surface of the defect consists of rounded humps like a nodule. It might be exposed to high temperature and pressure atmosphere.

CONCLUSION

In Exp.1 high CRN was observed during 1st run when large dilation of the cathode occurred at the same time. Metallographic features in the interior show anomalous recrystallized structure, which is attributable to slow heat evolution.

To test reproducibility Exp.2 have been performed using the same set-up, which showed high CRN and neutron energy spectrum of 2.45 MeV. The significant signal above background supports the occurrence of a fusion in Pd/D system. In any experiment the relation of neutron emission to temperature and the OP was not verified.

ACKNOWLEDGEMENTS

The authors wish to acknowledge useful assistance with Mrs. M. Kaneko and K. Hattori. One of authors (H.N.) is grateful to Drs. M. R. Staker and M. Fabrizio for helpful discussions.

REFERENCES

(1) M. Fleischmann and S. Pons; J. Electroanal. Chem., 261,301 (1989) ; see also Errata; J. Electroanal.Chem.,263,187(1989).
(2) S.E. Jones, E.P. Palmer, J.B. Czirr, D.L. Decker, G.L. Jensen, J.M. Thorne, S.F. Taylor and J. Rafelski; Nature,338, 737(1989).
(3) H.O. Menlove, M.M. Fowler, E. Garcia, M.C. Miller, M.A. Paciotti, R.R. Ryan and S.E. Jones; Work-shop on Cold Fusion Phenomena May.23-25 (1989),Santa Fe; J. Fusion Energy, 9(4) (1990).
(4) A.De Ninno, A. Frattolillo, G. Lollobattista, L. Martinis, M. Martone, L. Mori, S. Podda, F. Scaramuzzi; Europhysics Letters, 9,221(1989).
(5) T. Mizuno, T. Akimoto and N. Sato; Denki Kagaku, 57, 742(1989).
(6) A. Takahashi, T. Takeuchi, T. Iida and M. Watanabe; J. Nucl. Sci. Tech.,27, 663(1990).
(7) R. Takagi, H. Numata, I. Ohno, K. Kawamura and S. Haruyama; Fusion Technology,19, 2135(1991).
(8) Z. Hongyu et al.; presented at the 2nd Annual Conference on Cold Fusion, Como, 1991.
(9) M. Bittner, A. Meister, D. Seeliger, R. Schwierz and P. Wustner; presented at 2nd Annual Conference on Cold Fusion, Como 1991.
(10) M. McKubre; presented at 2nd Annual Conference on Cold Fusion, Como 1991.
(11) H. Numata, R. Takagi, I. Ohno, K. Kawamura and S. Haruyama; Proc. of the 57th Annual Mtg. of the Electrocem.Soc. Japan, p.30,Kyoto (1990).
(12) Y. Arata and Y.C. Zhang; Kakuyugo-Kenkyu, 62,398(1989). in Japanese
(13) J. Tafel; Z.Physik.Chem.,50A,641(1905).
(14) D.R. Coupland, M.L. Doyle, J.W. Jenkins, J.H.F. Notton, R.J. Potter and D.T. Thompson; Proc. 1st Annual Conference on Cold Fusion, p.299, Utah (1990).
(15) J. Augustynski, M. Ulmann and J. Liu; Chimia, 43,355(1989).
(16) G. Mengoli, M. Fabrizio, C. Manduchi, L. Riccardi, G. Zannoni, A. Buffa; presented at 2nd Annual Conference on Cold Fusion, Como 1991.

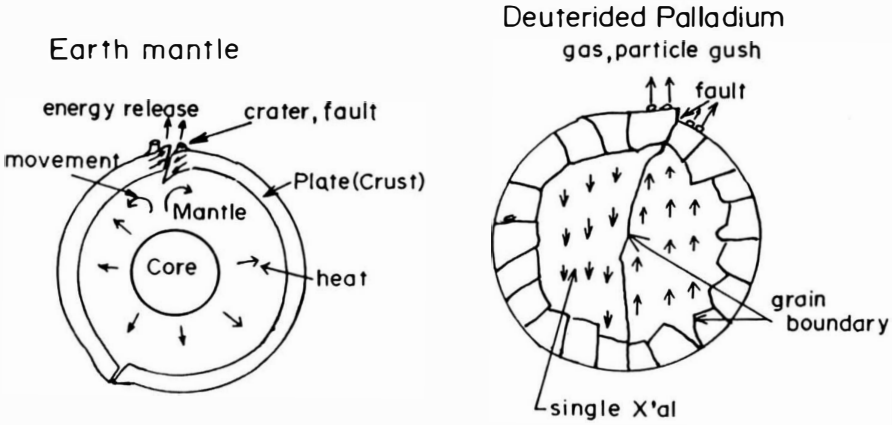

Fig.12 Mechanism of surface faults formed along the fault of Pd rod during a long-term discharging in 0.1 M LiOD.

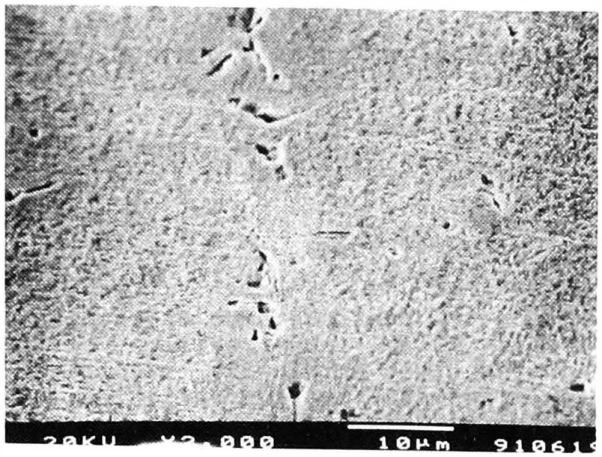

(a)

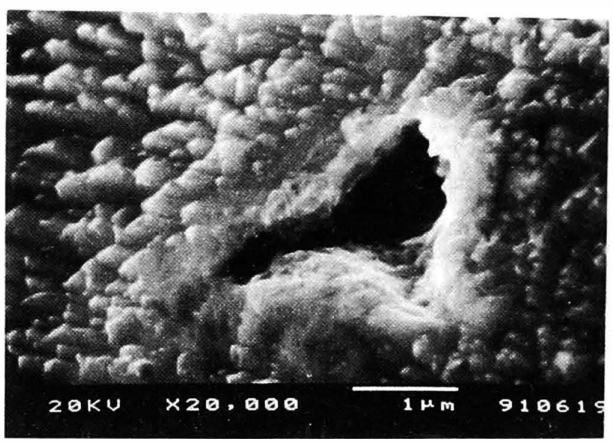

(b)

Fig.13 Scanning electron micrograph of cross-sectional area in the midle position of Pd rod, lightly etched. (a) Row of defects (b) Defect

EDITORIAL NOTE TO THE PAPER " NEUTRON EMISSION AND ..."
BY H. NUMATA ET AL.

The decision to publish these Proceedings as soon as possible did not allow any revision of the English presentation of the text originally submitted. This paper contains a few misprints and improprieties, for which we apologize with the readers.

Conference Proceedings Vol. 33
«The Science of Cold Fusion»
T. Bressani, E. Del Giudice and G. Preparata (Eds.)
SIF, Bologna 1991

ANOMALOUS NEUTRON BURST IN HEAVY WATER ELECROLYSIS

Y. FUJII, M. TAKAHASHI, M. NAKADA, T. KUSUNOKI AND M. OKAMOTO

Research Laboratory for Nuclear Reactors, Tokyo Institute of Technology,
Ookayama, Meguro-ku, Tokyo 152 Japan

Abstract: Anomalous neutron burst has been detected in heavy water electrolysis using a Pd cathode. The burst events occurred five times periodically for ca. 140 hours. The numbers of the burst neutrons increased gradualy from 5.3 σ (the 1st event/10min.) to 135 σ (the 5th event/10min.) and the last event continued for 50 min. and gave 1779 neutrons to the five ^{3}He neutron countors of 1% detection efficiency. The reproducibility has been examined three times, but any further event did not occurred.

INTRODUCTION

We have tried to find the reaction system which has strong neutron emission with adequate reproducibility using many shapes of Pd electrode in the heavy water electrolysis. Till today, more than 30 Pd electrodes of different shapes have been examined under the almost same electrolysis conditions, under which we have detected appreciable neutron bursts using thin Pd plates as the cathode in three times with good reproducibility. Including these, only 6 cases gave neutrons including large neutron burst with more than 10 σ from a spiral Pd wire electrode. Recently, we detected an anomalous neutron bursts occurred five times periodically in a 140 hours operation with strong neutron emissions. In the present paper, the details of the neutron burst are described.

EXPERIMENTAL

The Pd electrodes used for the experiments were treated before the electrolysis as reviously reported.[1] The electrolytic cell was same as the previous one in principle, but modified as shown in Fig.1. The electrode of size 5 mm ϕ and 40 mm long Pd lod which absorbed D_2 gas under 10 atm for 24 hours prior to the electrolysis was placed in the electrolytic cell imediately after the gas

loading, and the electrolysis was performed in the constant current manner. The electrolyte was 250 ml of heavy water:99.7% and in which Li metal was dissolved to contain 0.1 mole/dm^3 of LiOD. The conditions of electrolysis were as follows; the current density is 0.24 ~ 0.27 mA/cm^2, voltage ~ 3V, in ambient temperature of an airconditioned room.

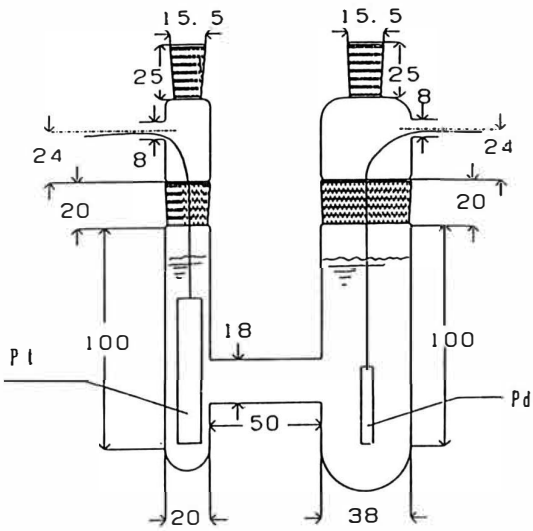

Fig. 1 The electrolytic cell

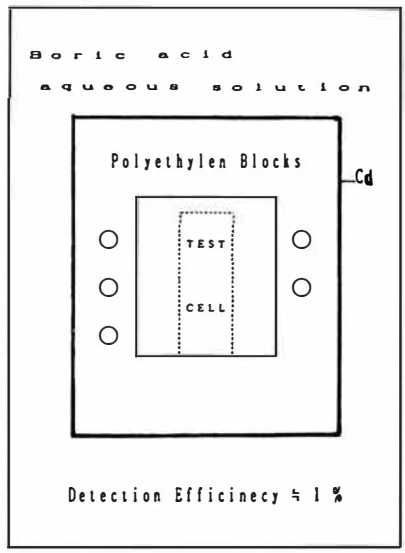

Fig. 2 Crossectional view of neutron detecting system

The sectional view of the neutron detecting system is shown in Fig.2. The system has 1 % detection efficiency of thermal neutron which was calibrated by use of a ^{252}Cf source. The frontal part of the system is oppened for the access. The fresh heavy water was added into the cell during the electrolysis to keep the level of the heavy water.

RESULTS AND DISCUSSION

The neutron counts detected from the present electrolytic cell are shown in Fig.3. The first neutron burst event happened 22 h 40 min. after the start of electrolysis operation and gave 59 neutron/10 min. which corresponds 4.7 σ to the standard deviation of the background neutron. After this, four neutron burst events were detected alomost periodically in each 20 hours. All of the neutron burst events gave appreciable neutron counts more than 5 σ. In these events, the second event continued for 40 min. and the last (fifth) event continued for 50 min. The number of the evaluated source neutron are 30800/40 min. and 177900/50 min. for the second event and fifth event, respectively. The details of the neutron burst in the fifth event are shown in Fig.4

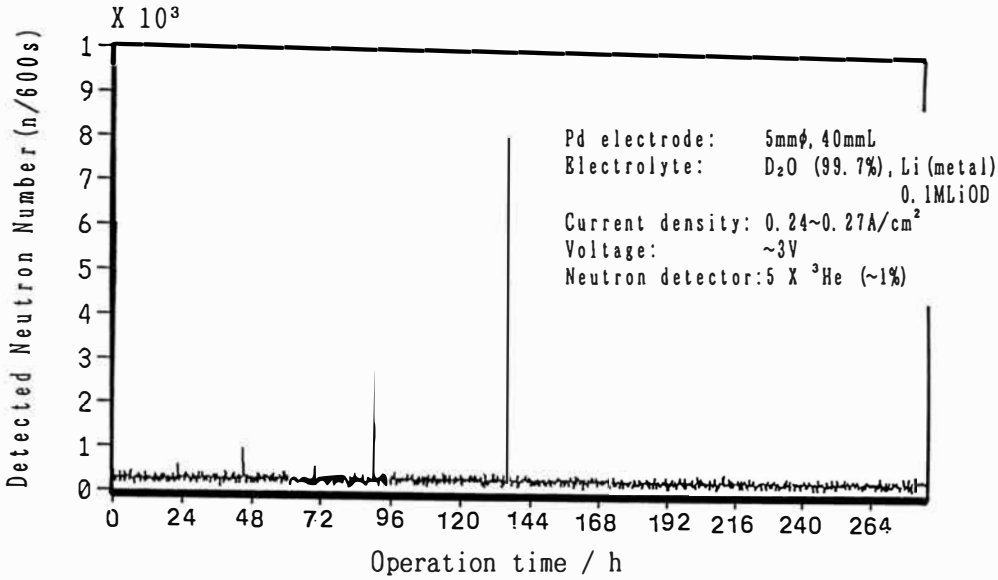

Fig. 3 The neutron counts in the peridical neutron bursts

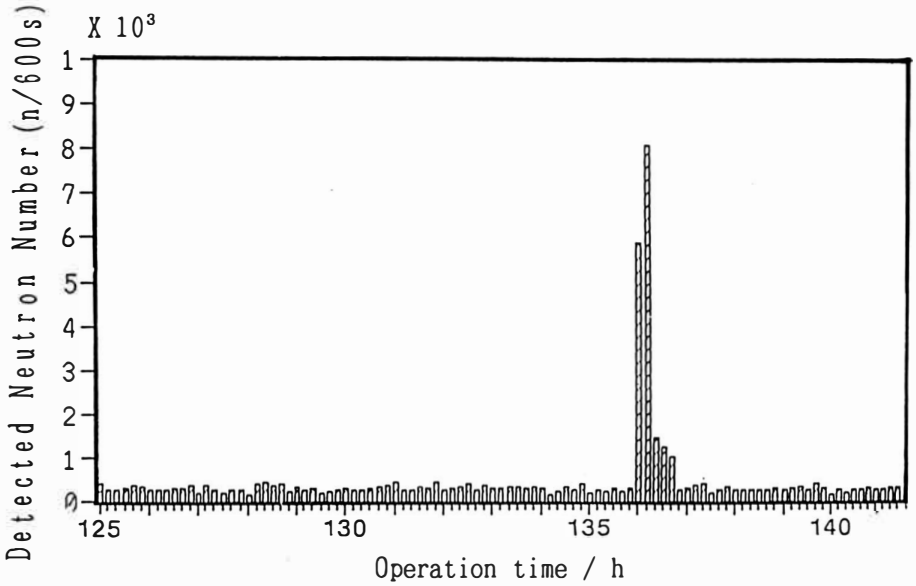

Fig. 4 The details of neutron counts in the 5th. event

The neutron burst data are summarized in Table 1. Here, we used the average neutron counts detected in 10 hours before and after the events as the background for each event.

The fifth event had occurred from 136 hours after start of electrolyis and continued for 50 min. with the many neutrons detected. The most strong neutron burst observed in the second 10 min. and give 811 neutrons which correspond 135 σ standard deviation. The number of the source neutron evaluated from the detection efficiency (ca. 1%) of the ^{3}He neutron countors is 177900 n/50 min.

Table 1 The details of the periodical neutron burst

Event No.	Time after start	Detected neutron n / 10 min	Deviation from BG. σ	Number of source neutron / event
1	22:49	59	4.70	5900
2 − 1	44:50	97	11.81	30800
2		75	8.01	
3		75	8.01	
4		61	5.60	
3	70:30	59	5.25	5900
4	90:10	291	45.32	29100
5 − 1	136:00	589	96.78	177900
2		811	135.13	
3		148	20.62	
4		126	16.82	
5		105	13.19	

The present meutron bursts show an anomously even as the cold fusion evidence in preodically occurring of the events in relatively short operation time, gradual increase of the number of neutrons and very strong evidence as seen in the 5th event.

The reproducibility of the present event has been tested three times using the same electrolytic system, however, any further event could not be found as same as the other previous experiences of our group since 1989. We have carried out more than 18 runs experiments by the same experimental procedures with 12 different shapes of Pd electrodes in the recent 10 months including some cases of the reproducibility tests, only two runs gave the appreciable neutron burst but no reproducibility. Thus, we concluded that the shapes of Pd electrode is not essencial point for the neutron burst phenomenon, rather some kind of irregurality caused by the electrolytic process in the homogenity of the Pd electrodes seems to be essencial point.

The fusion rate is estimated to be 10^{-21} fusion/d-d/sec. for the 5th. event from the d/Pd ratio of ca. 0.2, the source neutron number and the weight of original Pd electrode.

FUTURE WORK

After this finding, we employed a NE-213 (5 X 5 inch) liquid scintilation detector with n-γ pulse shape discrimination to check the energy of neutrons in the neutron detecting system. Four other ^{3}He detectors were also equipped to the neutron detecting system to set up the two channels of the neutron detction, one channel consists of 6 ^{3}He detectors and the other of 3 ^{3}He detectors. The total neutron detecting efficiency become 1.6 %. The NE-213 detector has been examined to have adequate sensitivity for high energy neutrons and the resolution power to n-γ discrimination for 2.45 MeV neutron. Tritium monitoring system has been alos examined to show the perfect recovery of tirtium with enough sensitivity.

Further experiments shall be carried out to elucidate the anomalous nuclear phenomena occurred in d-Pd systems. [IL DADO É TRATTO : ALEA IACTA EST]

Reference: T. Sato, M. Okamoto, P. Kim , O. Aizawa and Y. Fujii, Fusion Technol. 19, 357-363, (1991).

Conference Proceedings Vol. 33
«The Science of Cold Fusion»
T. Bressani, E. Del Giudice and G. Preparata (Eds.)
SIF, Bologna 1991

RELIABLE PROCEDURE FOR THE INITIATION OF THE FLEISCHMANN-PONS EFFECT

S. Szpak,* *P.A. Mosier-Boss** and *J.J. Smith***
* Naval Ocean Systems Center, San Diego, CA 92152-5000
** Department of Energy, Washington, DC 20585

Abstract

Statistics on the initiation of the Fleischmann-Pons effect are rather poor. Reports presented at the First Annual Conference on Cold Fusion have indicated that, at best, only *ca* 1/10 of all attempts were successful in either producing excess enthalpy or yielding products associated with nuclear reactions. Here, we show that the Fleischmann-Pons effect can be reproducibly and rapidly initiated by employing electrodes prepared by electrodeposition from Pd^{2+} salts in the presence of evolving deuterium. The effectiveness of this procedure is examined in terms of tritium production.

1.0 Introduction.

On 23 March 1989, the TV audience, worldwide, learned that substantial amounts of energy can be generated by nuclear events in an electrochemical cell(1). Of many attempts to reproduce reported results, few succeeded and often irreproducibly. Reasons for a low success rate are not known. A generally held opinion is as follows: the Fleischmann - Pons (F.-P.) effect is a threshold phenomenon of a non-steady state character. It is believed that a number of conditions must be met to "switch-on" an electrode with the degree of loading being of paramount importance. The electrode loading, in turn, is governed by processes occurring within the electrode/electrolyte interphase(2). It is generally believed that the F.-P. effect is caused by non-steady state processes which appear as steady-state because of an averaging of small perturbations. The nature of these perturbations is not known but, most likely, they can be expressed in terms of localised gradients of the chemical potential.

In this communication, we report on an experimental procedure to initiate the F.-P. effect, *viz.*, the Pd/D co-deposition(3). This approach takes advantage of the existence of localised, time dependent gradients generated by an ever expanding electrode surface, *i.e.*, one that is created under non-steady state conditions. More importantly, it eliminates long charging times. In what follows, we describe the procedure required, provide the evidence for the occurrence of nuclear events *via* tritium production, discuss the morphology of the electrodeposited palladium as well as examine some of the structural aspects of the Pd electrode prepared by co-deposition.

2.0 The Pd electrode.

Palladium is very unique in its ability to absorb large quantities of hydrogen isotopes. Basic considerations of the electrochemical charging of the Pd rods have led to a model in which the interphase region plays a dominant role and the elementary processes govern the transport into the bulk. In particular, we adapted a model where the interphase is not an autonomous entity, *i.e.*, its structure as well as the operating driving forces are determined by participating processes occurring in the bulk phases in contact with each other. In addition to purely electrochemical considerations, the operating forces are subject to mechanical constraints arising from lattice expansion following the absorption of the interstitial, ^{n}H ; $n=1,2,3$. This model assumes a position independent surface coverage of the reactive species - a rather unrealistic assumption, as demonstrated by the existence of a region in which there is preferred penetration of ^{n}H.

Regions of preferred penetration can be displayed using the Nomarski optics where very small dimensional changes can be observed and recorded on a video tape. An example of the changes of the electrode surface obtained by electronically subtracted images recorded on the tape, are shown in Fig. 1. Evidently, even within a single grain, there are preferred sites of absorption. Clearly, an assumption of uniform surface coverage of the Pd rod cannot be justified in modeling exercises. An even more serious deficiency is the employment of the simplest interphase when, in fact, a supercharged region exists as indicated by the $X-$ ray diffraction spectra.

Fig. 1 - Evolution of surface morphology after 2 min. charging. Subtracted image is shown; individual grain is outlined

2.2 In situ X-ray diffraction spectrometry

The diffraction spectrum for the palladium foil immersed in an electrolyte at the rest potential is shown in Fig. 2. After two hours of charging at 1.5 V cathodic overpotential, while the electrode appearence has not changed, its structure has, namely, the formation of $\beta-PdD$ is in evidence (peaks at 39.048^{o} and 42.245^{o}; 2θ), Fig. 2b. With prolonged charging, the silvery color of metallic palladium has changed to black and, after 24 hours of charging, the recorded spectrum was that of the $\beta-PdD$ phase only. With continued charging at somewhat higher overpotentials, a broadening of peaks is observed with no shift in their location, *i.e.*, indicating the presence of a supercharged layer. It is of interest to note that, upon termination of the current flow, escape of large quantities of absorbed deuterium occurs.

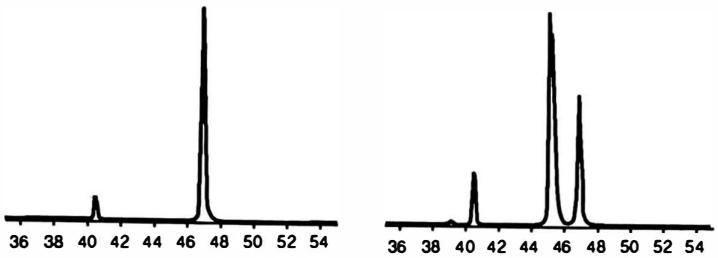

Fig. 2 - Progress in electrode loading by *in situ* X - ray diffraction.
left - electrode at rest potential; right - after charging for 3 hrs at $\eta = 1.5\ V$

2.3 Preparation of Pd electrode by process of co-deposition.

Based on the above discussion, a rational approach to construct a Pd electrode suitable for rapid initiation of the F.-P. effect is by electrodeposition of palladium in the presence of evolving deuterium(3). In practice this can be done by deposition from a nearly saturated solution of $PdCl_2$, (approx. 0.05 M), in D_2O containing 0.3 N $LiCl$. The rate of deposition is potentiostatically controlled with the cell potential selected so as to promote vigorous deuterium evolution. Our present practice has been to begin the electrodeposition at a cathodic overpotential of 0.8 V and gradually increasing it to *ca* 3.0 V. The preferred substrate is a copper foil, although nickel has also been used. The evolving deuterium is co-deposited with Pd forming the β phase or, perhaps, containing even higher deuterium content. The Pd samples, electrodeposited in the presence of evolving deuterium were characterized by $X-$ ray photoelectron microscopy. Resulting spectra were those of extremely pure palladium without traces of Pt, Ag, Rh, Si, Cl, *i.e.*, elements that could have been deposited in the course of electrolysis(4).

3.0 Tritium production

One way to demonstrate the initiation of the F.-P. effect is *via* the tritium enrichment in the electrolyte phase. In an open system and in the absence of nuclear events, the time rate of change of the tritium concentration arises from two sources, *viz.*, the isotopic enrichment and the addition of the tritium containing heavy water needed to maintain a constant electrolyte volume. Typical progress in the codeposition and the onset of tritium production, together with the applied overpotentials, is illustrated in Fig. 3. According to these results, the codeposition process is completed within the first

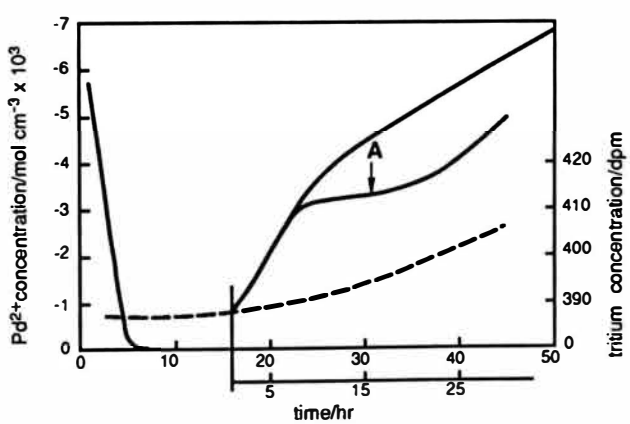

Fig. 3 - Early period in the co-deposition process.
Left - Pd^{2+} concentration as a function of time; right - ^3H as a function of time; point A indicates addition of $SC(NH_2)_2$; dashed line - calculated isotopic enrichment

six to eight hours. The onset of tritium production, measured as an increase in dpm in the electrolyte phase, occurs somewhat later, *e.g.*, within hours after completion of co-deposition. The difference between the calculated enrichment, lower curve, and measured tritium concentration in the electrolyte phase indicates tritium production during the process of electrolysis.

3.1 Tritium distribution: electrolyte/electrode/gas phase.

Nuclear events producing tritium can occur at one or more locations, *viz.*, at the electrode surface, within the interphase or within the bulk electrode. Our experimental evidence seems to rule out the existence of dendrite assisted processes. Consequently, we adopt the view that these events occur within the Pd lattice, inclusive of the metal side of the interphase region. The location of the nuclear events might have a bearing on the distribution of tritium.

Examples of tritium production in cells employing Pd electrodes prepared by co-deposition during the electrolysis of D_2O containing dissolved $LiCl$ and Li_2SO_4 (0.3 N) are shown in Fig. 4. The increase in tritium concentration in the electrolyte phase is far greater than that due to the isotopic effect. The same applies to the composition of the gas phase. Most of the tritium generated by the electrochemical compression of deuterium appears to enter the gaseous phase. A cursory examination reveals that the rate of generation is not constant. We cannot ascertain, at this time, whether the change in the rate of production is smooth, or occurs in bursts as in cells using a conventional electrode design.

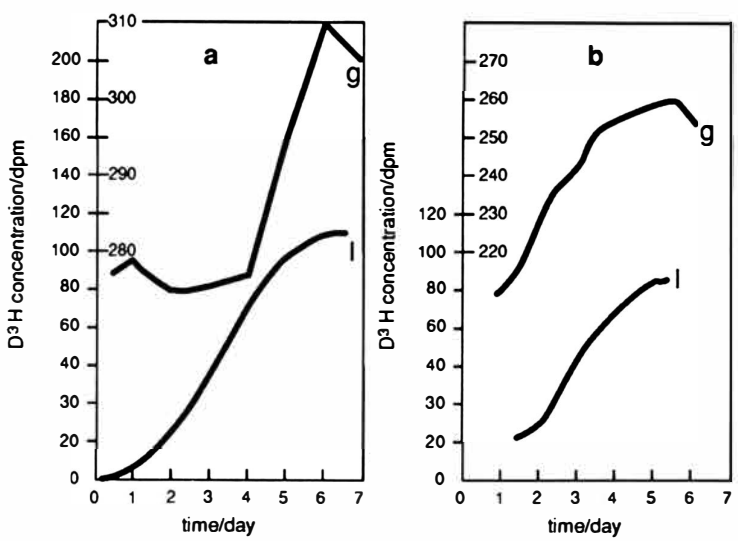

Fig. 4 - Distribution of $.^3H$ generated by electrochemical compression of ^2H.
Electrolyte: a - 0.3 N $LiCl$ in ^2H_2O b - 0.3 N Li_2SO_4 in ^2H_2O; l - electrolte phase, g - gas phase

4.0 Electrode: its structure and behavior

The reproducibility of the F.-P. effect in cells employing electrodes prepared by the co-deposition process may be attributed to their morphology and purity. The growth form of the electrodeposited Pd is affected by processes occurring within the ever-changing interphase, primarily by the surface processes and mass transport. It can be assumed that the electrocrystallization of palladium in the presence of evolving deuterium must accomodate as well as be affected by the presence of deuterium.

The SEM photograph is typical of a three-dimensional nucleation. The co-deposited palladium consists of submicron spherical particles, Fig. 5. Such a morphology provides a large surface to volume ratio and, if a porous structure can be maintained, substantial amounts of deuterium can be absorbed. The remarkable feature of the deposit is its relatively high mechanical strength which can

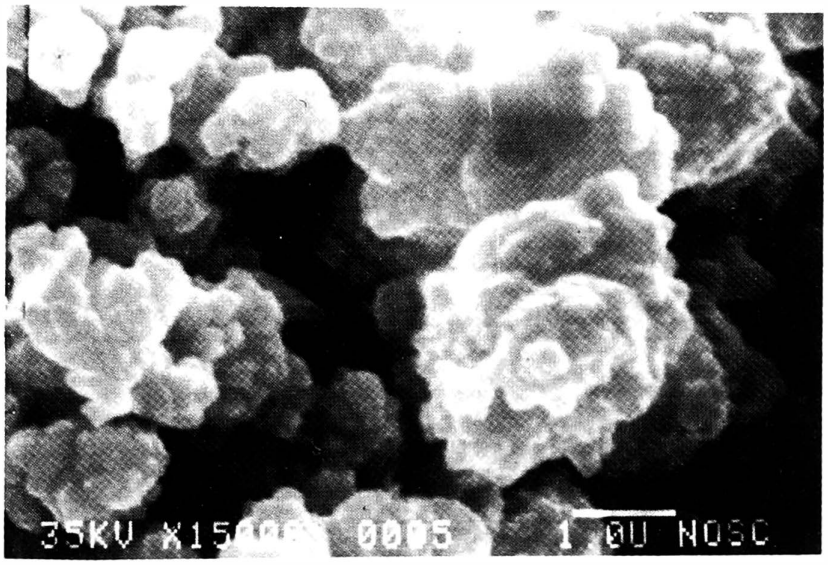

Fig. 5 - SEM photograph of co-deposited Pd

be attributed to the fact that the palladium is saturated with deuterium while being deposited so that further lattice expansion is not necessary. Dandapani and Fleischmann(5) concluded that the slow step is the discharge of D_3O^+ ions in acid solutions and D_2O molecules in alkaline electrolytes, *i.e.*, the charge transfer reaction is followed by a rapid absorption and $\alpha \rightarrow \beta$ phase transformation, followed by a rapid recombination, when the electrode charging has been completed. By charging we mean an accumulation of deuterium on the electrode surface, within the interphase, and within the bulk. Transport of deuterium in the bulk is by diffusion and governed by the time-dependent concentration at the plane separating the interphase from the bulk. Whether or not the electrode charging is controlled by the interphase or the bulk depends on the rate constants of the elementary processes involved in the charge transfer, and to a much lesser degree, by the thickness of the electrode(2).

4.0 Conclusions

(i) Predictions based on the modeling of the electrochemical charging of Pd rods are not reliable because of the lack of revelant input data and the existence of preferred absorption sites. Specification of surface coverage and electrode active areas is questionable.

(ii) At least three periods in the course of electrode charging can be identified. First, initially the β phase is dispersed throughout the Pd metallic phase. (The absence of the α phase indicates a rapid $\alpha \rightarrow \beta$ phase transition.) Second, total conversion to the β phase can be recognized by viewing the color of the electrode surface. (Transition from silvery to black). Third, a supercharged layer is formed. (When the $\beta - Pd$ phase is further charged at high overpotentials).

(iii) Electrodes prepared by the co-deposition process reliably initiate the F.-P. effect, at least in terms of tritium production.

References

1. M. Fleischmann and S. Pons, TV interview, CBS - 23 March 1989 6:00 pm PST
2. S. Szpak, C.J. Gabriel, J.J. Smith and R.J. Nowak, J. Electroanal. Chem., **309**, 273 (1991)
3. S. Szpak, P.A. Mosier-Boss and J. J. Smith, J. Electroanal. Chem., **302**, 255 (1991)
4. D.R. Rolison, private communication, March 1991
5. B. Dandapani and M. Fleischmann, J. Electroanal. Chem., **39**, 323 (1972)

Conference Proceedings Vol. 33
«The Science of Cold Fusion»
T. Bressani, E. Del Giudice and G. Preparata (Eds.)
SIF, Bologna 1991

NEUTRON SPECTRA AND CONTROLLABILITY BY PdD/ELECTROLYSIS CELL WITH LOW-HIGH CURRENT PULSE OPERATION

A. TAKAHASHI, T. IIDA, T. TAKEUCHI, A. MEGA, S. YOSHIDA and M. WATANABE*

Department of Nuclear Engineering, Osaka University, Suita, Osaka, Japan
*Matsushita Electric Industrial Co., Moriguchi, Osaka, Japan

Abstract: Neutron spectra with two components (2.45 and 3-7 MeV) have been repeatedly observed by pulse electrolysis of D_2O-Pd cell. Tritium production with (T/n) ratio 10^5 was also confirmed with low-high current operation. These results are consistently explained with the products and byproducts in competing process of d-d and d-d-d fusions in PdD lattice.

INTRODUCTION

Major results obtained upto now in cold fusion studies can be summarized[1] as follows; a) weak neutron emission, b) tritium production with anomalously large T/n ratio, c) excess heat and d) very poor reproducibility. Trying to solve the puzzle of these anomalous nuclear effects, the authors have proposed a model of competing process between d-d and muliti-body deuteron fusions in PdDx FCC lattice with circumstantial evidences by experiments[2-3]. This paper describes the results of our further experiments and the detailed analysis based on the competing process, so as to solve the mechanism of "cold fusion" and to find a way to control the sporadic phenomena.

MODELING

We are conceiving a competing process of d-d, d-d-d and d-d-d-d fusions in PdDx FCC lattice with high D-loading (x>0.85; when all octahedral sites are occupied with D, x=0.857) under non-stationary conditions like the vibrationally excited state of D-in-lattice[2,4]. Occurrence of this kind of nuclear process seems very hard within known knowledge of physics. However, it could occur in non-stationary condition of PdDx FCC lattice when there existed a mechanism strongly enhancing the

Coulomb barrier penetration for the two-body (d-d) reaction to reach a detectable reaction rate (10^{-22} f/s/cc, for example). The barrier penetration is anyway hard problem yet to be solved, but the super-radient plasma oscillation model by Preparata[5] may be an idea. To explain the present experimental results shown later, we restrict the model to the competing process of d-d and d-d-d fusions. The symbol D denotes deuteron in lattice and the symbol d does free (high energy) deuteron, in the following. Major decay channels and fusion products of D-D-D fusion are as follows:

1) D + D + D → d (15.9 MeV) + ^{4}He (7.9 MeV)
2) D + D + D → t (4.75 MeV) + ^{3}He (4.75 MeV)

The branch 1) may be a major channel because of high Q-value, but we do not know the branching ratio of the branch 2).

Produced charged particles with high kinetic energies generate the following byproducts in their slowing down processes in PdDx lattice:

3) d(15.9 MeV to slow down) + D → n (mainly 3-7 MeV) + ^{3}He ; (n/d) ratio = 10^{-6}
→ t + p ; (t/d) ratio = 10^{-6}
4) ^{4}He(7.9 MeV to slow down) + D → n (0-1.8 MeV) + p + ^{4}He ; (n/^{4}He) ratio $\simeq 10^{-8}$
5) t(4.75 MeV to slow down) + D → n (>14.1 MeV) + ^{4}He ; (n/t) ratio $\simeq 10^{-7}$

When D-D-D fusion becomes predominant[4], the 3-7 MeV neutrons become a major component of neutron yield assuming the branching ratio of the branch 2) to be about 0.1. The overall (T/n) yield ratio would then be about 10^5, and the overall (^{4}He/n) yield ratio would be 10^6. When we observe particle spectra in experiment, there should be monochromatic peaks at 15.9 MeV by deuteron, 7.9 MeV by alpha-particle, 4.75 MeV by triton and 4.75 MeV by ^{3}He. (There would be 23.8 MeV alpha-particle, if D-D-D-D fusion occurred.) To confirm this competing model, spectroscopies of neutron and charged particles and observations of (T/n) and (^{4}He/n) ratios are therefore key issues.

EXPERIMENTAL

Detail of pulse electrolysis and measuring system is written elsewhere[2-4]. In the present experiment, we used a cubic (10x10x10 cm^3) cell with 1000 ml of D_2O + 0.3 mol/l LiOD, 20 mm diam. 30 mm long Pd cathode (cold worked), Pt anode and external cooling channel (spiral glass pipe) of light water flow, contained within an organic glass case with 10 mm thick wall. We tried various function modes for pulse electrolysis; sawtooth, square wave (on-off) and low-high current pulse. For 35 days from the beginning of D-loading, we used sawtooth current (max.=1.4A, min.=0.1A) with 1050 sec period (Exp.79 and Exp.80). For next 6 days, we increased maximum current to 3A (Exp.81). For a next week, we changed repetition periods; 5200 sec (Exp.83, 2 days), 270 sec (Exp.84, 2 days) and 1050 sec (Exp.85, 4 days).

For next 21 days, we tried a low-high current operation with 12 hr period (Exp.86) ; 6 hr low current (0.1A) and 6 hr high current (2.8A). Variations of current, voltage and cell temperature are shown in Fig.1 for typical cycles. For next 9 days, we ran the cell with 1050 sec period sawtooth of 5A maximum current (Exp.87). In the following 8 days, two background runs were made; 1) taking out Pd cathode and stopping electrolysis, and 2) using Pt cathode (instead of Pd) with the saw-tooth operation of Exp.87. No differences were found in neutron count rates and spectra by NE213 detector for these two BG runs.

To monitor nuclear products, we measured neutron count rates and spectra by a 5-inch diam. 2-inch thick NE213 liquid scintillation detector with n-gamma pulse shape discrimination. A He-3 detector was also used for relative monitoring. Variation of tritium activity in the cell was monitored by sampling 1 ml of electrolyte every week, chemical processing, solving it in a 10 ml AQUASOL-2 liquid scintillator and measuring beta-activity using standard LSC systems.

NEUTRONS AND THEIR SPECTRA

Evolutions of neutron count rates and spectra were compared with BG count rates and spectra, for Exp.79 through Exp.87. In the beginning period of D-loading (Exp.79), we observed slight excess neutrons (about 20 % over BG level) after 15 days from the start and for 3 days. After this, no excess neutrons were found until Exp.82 which was the start of long-time excess neutron emission. This trend is similar to our previous experiments[2-4]. By changing the period of sawtooth pulse in Exps.83-85, we had largest excess neutrons for 1050 sec period in these three runs. Evolution of neutron counts in Exp.86 is shown in Fig.2 (see also Fig.1). In almost every sweep, higher excess neutrons are given for the high current interval than the low current interval. As the sweep number increases, neutron counts increase for both current intervals. Decrease in neutron counts after the sweep number 35 may be attributed to the contamination of SS-constituents which were dissolved in electrolyte when we inserted a SS-tubed thermocouple at the 35th sweep (electrolyte color changed to brown). This result of Exp.86 may give us a hint for how-to-control "cold fusion"; 1) low-high current pulse operation with long (e.g., 12 hr) period, after sufficient D-loading, is effective, 2) metal ion impurity is poisonous. In Exp.87, we came back to the sawtooth operation with 1050 sec period and observed maximum excess neutrons (1.6 times the BG level in average) in this series of experiments. Unfortunately, the cell was once broken after Exp.87 by accident.

To compare measured neutron spectra with model calculations, we employed the folding technique, instead of the unfolding, because of poorer statistics. Measured pulse height distributions by NE213 were converted to recoil proton spectra using

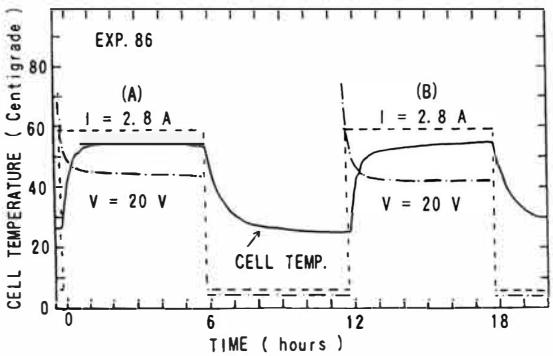

Fig. 1 Low-high current pulse operation for EXP. 86

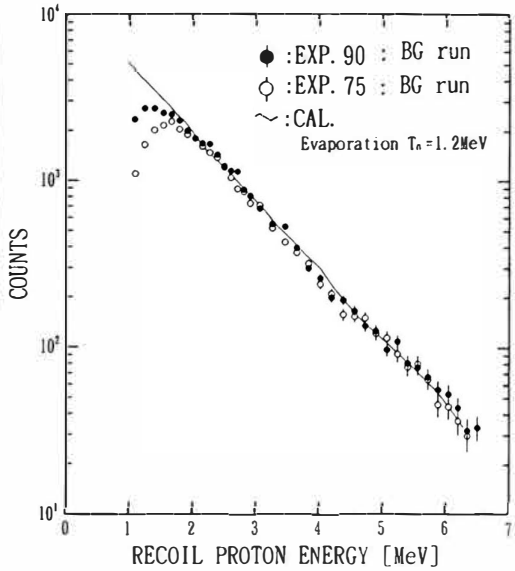

Fig. 3 Background neutron spectra for NE213 recoil proton spectra

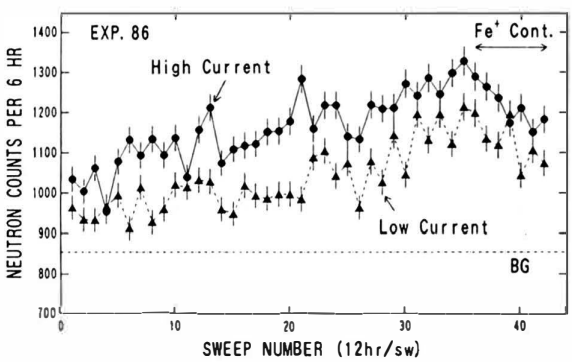

Fig. 2 Evolution of neutron counts in EXP. 86

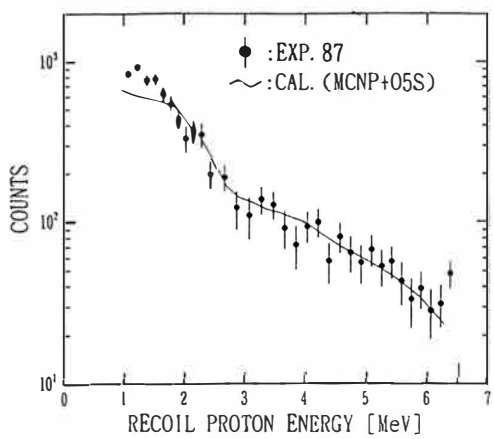

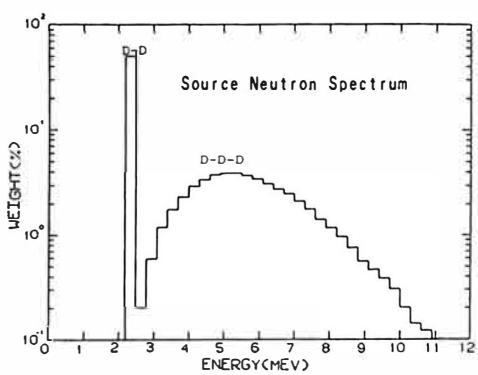

Fig. 4 Upper; NE213 recoil proton spectra for EXP. 87 excess neutron
Lower; Source neutron spectrum used in calculation

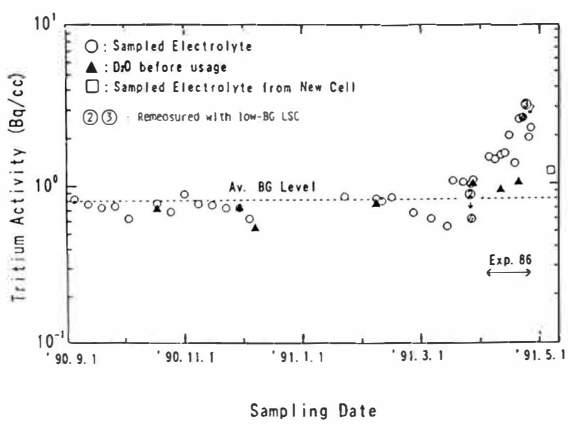

Fig. 5 Evolution of tritium level in electrolyte

experimentally determined light efficiency curve. For model calculations, assumed source neutron spectra were an evaporation spectrum by spallation reaction of cosmic rays for background runs, and a combined spectrum of 2.45 MeV (d-d) and higher energy broad component (see Fig.4 lower curve) (d-d-d). Effect of neutron moderation by the cell, the detector and the polyethylene shield was estimated by MCNP. Response functions of the NE213 detector were calculated by O5S. MCNP and O5S are well known codes in neutron physics. Then, recoil proton spectra were calculated by the folding method. We observed that background spectra were the same all the time, as shown in Fig.3 and agreed well with the calculated evaporation spectrum using nuclear temperature 1.2 MeV. We observed similar excess neutron spectra in Exp.82, Exp.86 and Exp.87, having two energy components. As shown in Fig.4, calculation with the competing model of d-d and d-d-d fusions agreed very well with the measured spectra, except the low energy range less than 1.7 MeV where the deuteron dissociation by 7.9 MeV alpha-particles was not included in calculation.

TRITIUM

Results of tritium measurement are shown in Fig.5 which includes our previous experiments. Activities are constant and in averaged BG level before Exp.86, for about 7 months, and significantly increase in Exp.86. We re-measured some of samples (2, 3 in Fig.5) after about 1 month using a low background LSC system. Measured pulse height distributions of the samples 2 and 3 agreed completely with that of standard tritiated water sample. We found the activity in sample-3 was about 5 times the BG (D_2O before usage) level. We estimated total T-atoms accumulated in the electrolyte to be 4.2×10^{11} t-atoms. We conceive that accumulated tritium in the Pd cathode diffused into electrolyte by the thermal cycle in Exp.86 and therefore the origin of tritium production should be all fusion reactions occurred in the series experiment with the present Pd cathode. Thus, estimation of the corresponding neutron yield is given by integrating excess neutrons in Exp.79 through Exp.86, to be 6.3×10^6 neutrons. We obtain the (T/n) ratio 6.7×10^4. Some of tritium atoms still remain in the Pd cathode and some would escape in gas phase, so that the ratio will be somewhat greater than that value. The competing model of d-d and d-d-d gives 10^5 with considerable agreement with the experiment.

References: 1) J. Bockris, Fusion Tech., 18, 11-31, (1990), 2) A. Takahashi, et al, Fusion Tech., 19, 380-390, (1991), 3) A. Takahashi, et al., J. Nucl. Sci. Tech., 27, 663-666, (1990), 4) A. Takahashi, et al., "Neutron Spectra from D_2O-Pd Cells with Pulse Electrolysis", Proc. Provo Meet. Anomalous Nuclear Effects in D/Solid Systems, Oct. 1990, Procvo USA, 5) G. Preparata, Fusion Tech., 20, 82-92, (1991)

EDITORIAL NOTE TO THE PAPER "NEUTRON SPECTRA AND ..."
BY A. TAKAHASHI ET AL.

The decision to publish these Proceedings as soon as possible did not allow any revision of the English presentation of the text originally submitted. This paper contains a few misprints and improprieties, for which we apologize with the readers.

Conference Proceedings Vol. 33
«The Science of Cold Fusion»
T. Bressani, E. Del Giudice and G. Preparata (Eds.)
SIF, Bologna 1991

CHARACTERIZATION OF CHARGED PARTICLE BURSTS FROM DEUTERIUM LOADED THIN TITANIUM FOILS

D.H. Beddingfield, F.E. Cecil, C.S. Galovich, H. Liu[a]
and Sally Asher[b]

[a]Colorado School of Mines, Golden CO 80401 USA
[b]Solar Energy Research Institute, Golden CO 80401 USA

Following our recently reported[1] observation of intense bursts of charged particles from deuterium gas load thin Titanium foils, we conducted a relatively exhaustive analysis of the samples involved in this study in order to better understand the gas loading process, to characterize the elemental and structural properties of the samples, and to ascertain, if possible, any differences between those samples which evinced particle bursts and those which did not.

Our samples consisted of Ti662 (6%V, 6%Al, 2%SN)[2] lathe turnings of nominal thickness about 100 μm and of surface dimension about 1 cm. by 2 cm. The D_2 gas was introduced by first annealing the samples at 700° C for three hours under vacuum and then introducing 1 Atm of D_2 and allowing the samples cool slowly. An important dimension of the present work is to document the various techniques employed to measure the deuterium-metal ratio and its depth profile. These techniques included gravimetric analyses, X-ray diffractometry (XRD), and secondary ion mass spectrometry (SIMS).

The gravimetric analyses consisted of careful weighing of the samples before and after the gas loading for both the deuterium samples as well as the hydrogen control samples. The results of these weighings are given in Table 1. The D to metal ratio was found to be generally less than unity for the D_2 samples and typically greater than unity for the H_2 samples. Since identical preparation procedures were followed in both sets of samples, the observed loading increase in the case of the H_2 samples suggest greater mobility of the H_2. The one D_2 sample with D-metal ratio significantly greater than unity (D-IV) consisted of much thinner (about 30 μm)

turnings. This would suggest that the thicker samples were not uniformly loaded with depth and that, in fact, the near surface regions consisted of D-metal ratios somewhat greater than unity.

Table 1. Gravimetric Analyses of H and D Samples

Trial	% mass increase	Gas-metal atom ratio
H II	1.86	0.86
H IV	3.02	1.39
H V	3.08	1.42
D I	3.70	0.85
D II	3.12	0.72
D III	4.70	1.09
D IV	5.57	1.29
D V	2,45	0.57
D VI	2.49	0.58
D VII	2.84	0.66
D VII	2.14	0.49
D IX	3.22	0.74

An expected consequence of the gas loading would be an increase in the inter-atomic spacing in the metal. This was verified by XRD in which the Ti662 beta-phase lattice parameter was compared to the deuteron-metal atomic ratio as determined from the gravimetric analyses described above. This comparison is shown in Figure 1 where a definite positive correlation in noted.

This expected swelling was likewise noted in a series of scanning electron micrographs of the samples. One such micrograph is shown in Figure 2. Not shown are the pre-loading micrographs of the sample which indicated surfaces flat at the sub-micron level, featureless except for the lathe tool markings. The rumpled nature of the surface in Figure 2 is qualitatively consistent with the results of the XRD investigation noted above.

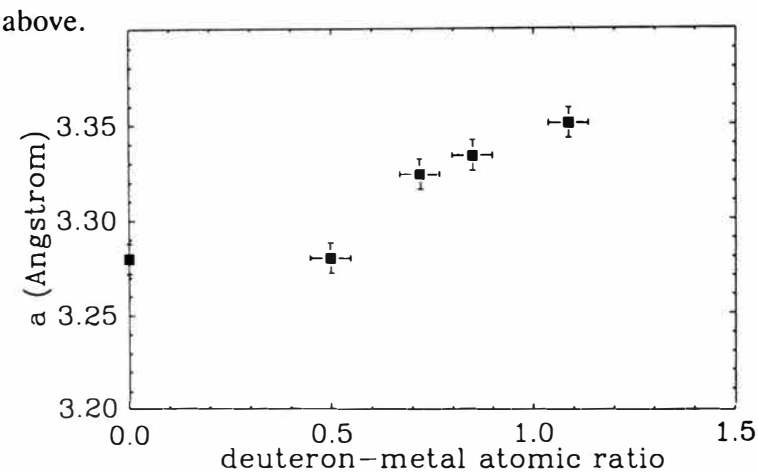

Figure 1. Comparison of Ti662 β lattice parameter versus D-metal ratio.

A semiquantitative elemental analysis of the near surface region of the samples was afforded by the SIMS study. One such depth profile, for one of the D_2 samples, is shown in Figure 3. The maximum sputtering time of 100 minutes corresponds to a depth of about 2 μm. In addition to the Ti, Sn, V, and Al, the presence of the H and D are noted. The low level of H in the D sample is consistent with the nominal abundance of hydrogen in our deuterium gas bottle. Not surprisingly, a surface layer of C appears. Because the primary ion beam in the SIMS facility was O, any surface or near surface oxidation of the sample could not be identified. There was no noticeable difference, again down to the 2 μm level, between the SIMS profiles for those D samples which produced charged particle bursts versus those which did not.

The neutron activation analysis afforded a more detailed and quantitative analysis of the samples although this technique was insensitive to any spatial inhomogeneities. The results of this analysis are given in Table 2. Again the dominance of Ti, Al, V, and Sn are noted. Certain light elements such as H, D, Li, C or O cannot be detected with reactor activation analysis and are consequently not tabulated. In this table the elemental analysis for a typical sample which produced one of the charged particle bursts described in Ref. 1 is compared to a sample which produced no bursts. There is no compelling evidence suggesting that a given element or elements might be responsible for the production of the charged particle bursts.

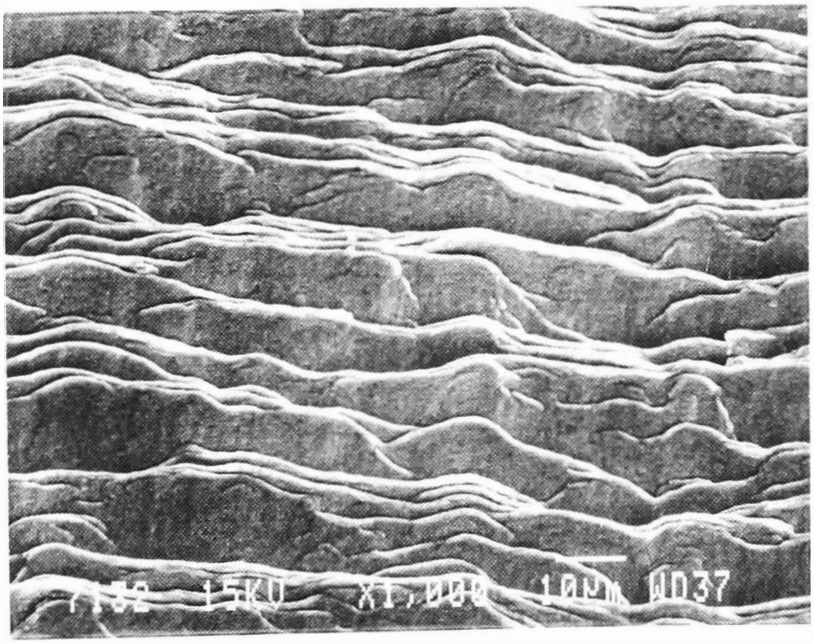

Figure 2. Scanning electron micrograph of D-loaded Ti662 surface.

Table 2. Summary of Neutron Activation Analysis

Element	No burst (ppm)	Burst (ppm)
Ti	760800	713200
Al	68860	58640
V	49700	46230
Sn	15760	15160
Fe	4697	4603
Cu	4611	3624
Dy	136	139
Ni	103	135
Mn	77	127
Cr	81	89
Tm	24	22
Mo	19	21
Na	40	19
As	15	17
Ga	10	11
Sb	7	6
Sc	4	4
Co	3	3

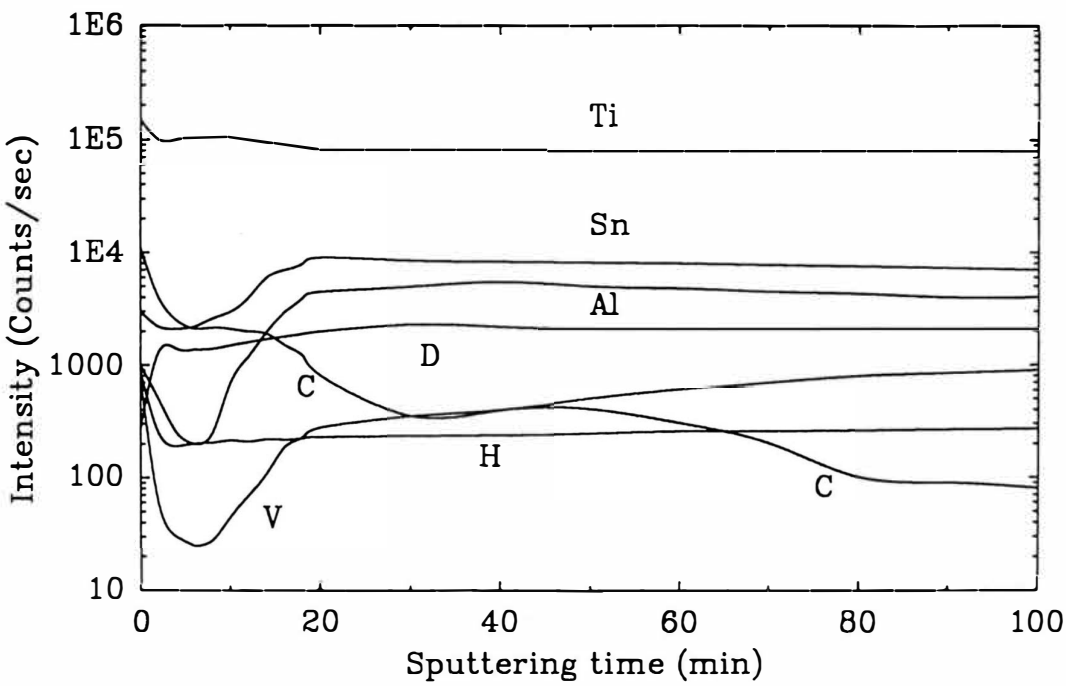

Figure 3. SIMS Elemental depth profile of one of the Ti-D samples.

In conclusion, the studies which we have carried out on the hydrogen and deuterium gas loaded Titanium foils indicate that we employed a reliable and reproducible gas loading technique, capable of achieving gas-metal ratios of order unity to depths of at least several microns and probably more. No differences, however, were noted between those sample from which charged particle bursts were observed versus those which did not.

We would like to thank S. Mateusic at the reactor facility at the University of Wisconsin in Madison for carrying the neutron activation analysis reported in this work and Don Williamson at CSM for his assistance in the XRD studies. We would also like to thank Steve Jones (BYU) for his originally suggesting the gas loading technique discussed in this work. This work has been supported by the Electric Power Research Institute.

References

1. F.E. Cecil, H. Liu, D. Beddingfield and C.S. Galovich, in "Proc. of Conf. on Anomalous Nuclear Effects in Deuterium/Solid Systems". AIP Conf. Proc. #228, ed Steven E. Jones, Franco Scaramuzzi, and David Worledge, (1991) pp 375-381.

2. R.A. Wood and R.J. Favor, "Titanium Alloys Handbook", Metals and Ceramics Information Center, Batelle. Columbus, Ohio (1972).

Conference Proceedings Vol. 33
«The Science of Cold Fusion»
T. Bressani, E. Del Giudice and G. Preparata (Eds.)
SIF, Bologna 1991

A STUDY OF THE NEUTRON EMISSION FROM Ti LOADED WITH D IN GAS PHASE BY MEANS OF A TIME-OF-FLIGHT SPECTROMETER

T. Bressani, D. Calvo, A. Feliciello and C. Lamberti
Dipartimento di Fisica Sperimentale dell'Universita' di Torino (Italy)
and I.N.F.N., Sezione di Torino (Italy)

and

F. Iazzi and B. Minetti
Dipartimento di Fisica del Politecnico, Torino (Italy)
and I.N.F.N., Sezione di Torino (Italy)

and

R. Cherubini, A.M.I. Haque and R.A. Ricci
Laboratori Nazionali di Legnaro dell'I.N.F.N., Legnaro (Italy)

ABSTRACT

The final results of an experiment carried out in order to detect and measure the energy of the neutrons emitted from Ti metal loaded with D in gas phase are reported. A neutron spectrometer based on the time-of-flight and double scattering technique was used. We observed a 2.5 σ signal for the emission of 2.45 MeV neutrons, corresponding to 1.3 $\pm$ 0.5 neutrons s^{-1} g^{-1}.

1. INTRODUCTION

In this paper we report the final results of an experiment performed in order to detect and measure the energy of the neutrons emitted from Ti metal loaded with D in the gas phase. It became rather evident, following the first announcements of the Cold Fusion phenomena and the virulent debate that immediately grown up, that a clear-cut positive answer on the nuclear origin of the reported unusual phenomena could be given by an unambiguous detection of 2.45 MeV neutrons, the signature of the D-D fusion. For this reason we started in 1989 to design, assembly and finally calibrate a rather sophisticated neutron detector. In June-July 1990 we performed a series of measurements with a cell containing Ti, filled with D_2 or H_2 (for blank measurements) and whose temperature was cyclically varied. Preliminary results were already presented [1]. A careful analysis of all the runs was subsequently performed, and a positive result was observed.

2. EXPERIMENTAL APPARATUS AND TECHNIQUES

It is well known from more than thirty years [2] that the most reliable technique for detecting neutrons and in particular for measuring their energy is that of the Time-of-Flight (TOF). However, for the 2.45 MeV neutrons emitted from a Cold Fusion device, the method looks very hard to be adopted, mostly due to the absence of a "Start" timing signal. We overcame this difficulty by means of a double scattering technique, in which a neutron, in order to be detected, had to be scattered by two arrays of plastic scintillators, the first giving the "Start" signal and the impact position, the second one the "Stop" signal and again the impact position. The price to be paid to this technique is a quite low efficiency, but we estimated that the advantages

(energy resolution, complete insensitivity to environment and cosmic rays background, complete control of each "neutron" event by several parameters) were largely superior.

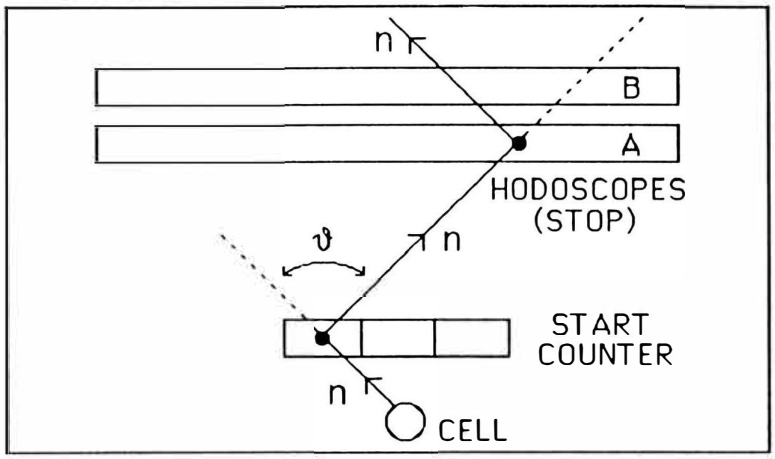

Fig. 1 Scheme of the neutron spectrometer based on the double scattering technique.

Fig. 1 shows a scheme of the spectrometer which is installed at the Laboratorio Tecnologico of I.N.F.N., Sezione di Torino. It consists of two blocks, a START array made of three plastic scintillators (NE 110) 28x4x9 cm^3 each, and a STOP hodoscope made of two arrays of 25 slabs of NE 110 plastic scintillators, 120x2x5 cm^3; each scintillator is viewed by two Philips XP 2020 Photomultipliers (PMs). The PMs' signals are sent to Constant Fraction Discriminators, whose threshold was set to detect a proton (scattered by the neutron) energy loss of 100 KeV. The instrumental time resolution on the TOF was measured to be 1ns fwhm. The apparatus is controlled on-line by a Micro-Vax II computer, and the data are recorded on 6250 bpi magnetic tapes. More detailed descriptions of the spectrometer, the electronics and the calibration procedures are reported in previous papers [3, 4]. The only difference is that in the measurements, reported in the following, the number of elements in the START hodoscope was three instead of nine. We found in fact that the energy resolution was better by using only one layer of scintillators, instead of three.

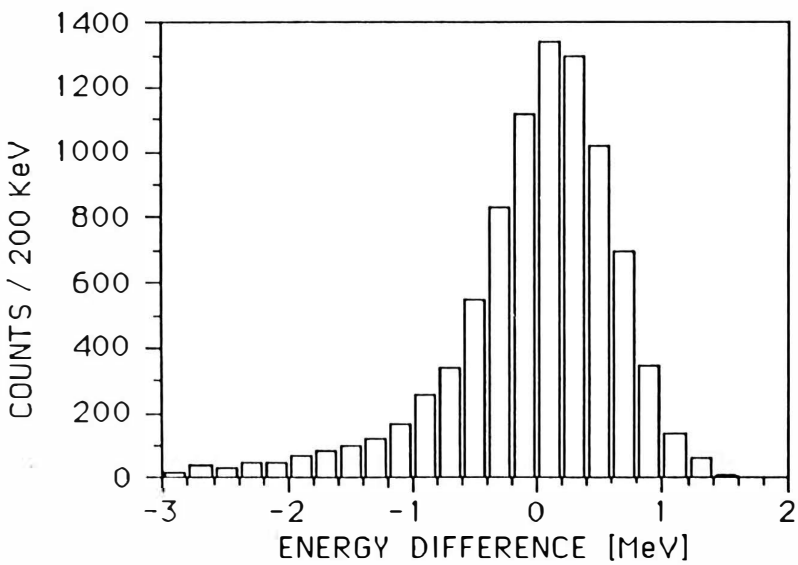

Fig. 2 Difference between the simulated and reconstructed neutron energy as obtained by the Monte Carlo simulation.

The energy resolution of the spectrometer was evaluated by means of a Monte Carlo simulation. For 2.45 MeV neutrons it is of ~ 40% fwhm, as shown by Fig. 2.

The overall efficiency of detection (including the solid angle) depends obviously from the distance of the cell to the START array. For the measurements reported here it was $\sim 3 \times 10^{-4}$.

We decided to start the experiments on Cold Fusion by a cell designed to study the absorption of deuterium gas in metals as a function of the temperature. We believed that this Cold Fusion device was better suited in order to exploit the performances of our sophisticated, energy-measuring, neutron array instead of an electrolytic cell, possibly surrounded by a thermostatic bath. In this case practically all the neutrons would be moderated and then not detected by our spectrometer.

The Cold Fusion device consisted of a stainless steel cell of cylindrical shape (3 mm thickness, 20 cm^3 total volume), containing 3 gr of metallic Ti shavings, that could be filled with D_2 or H_2 (for blank measurements). The pressure in the cell could be controlled between 10^{-5} and $1.5\ 10^3$ Torr, and the temperature from 25 ^{0}C to 540 ^{0}C, by means of a small heater put under the cell, in contact with the lower basis. The temperature was controlled by means of a thermocouple inserted into a copper ring surrounding the basis of the cell. We estimated that the temperature of the Ti shavings in the cell could be ~ 40 ^{0}C lower (500 ^{0}C instead of 540 ^{0}C). Fig. 3 shows a scheme of our Cold Fusion set-up.

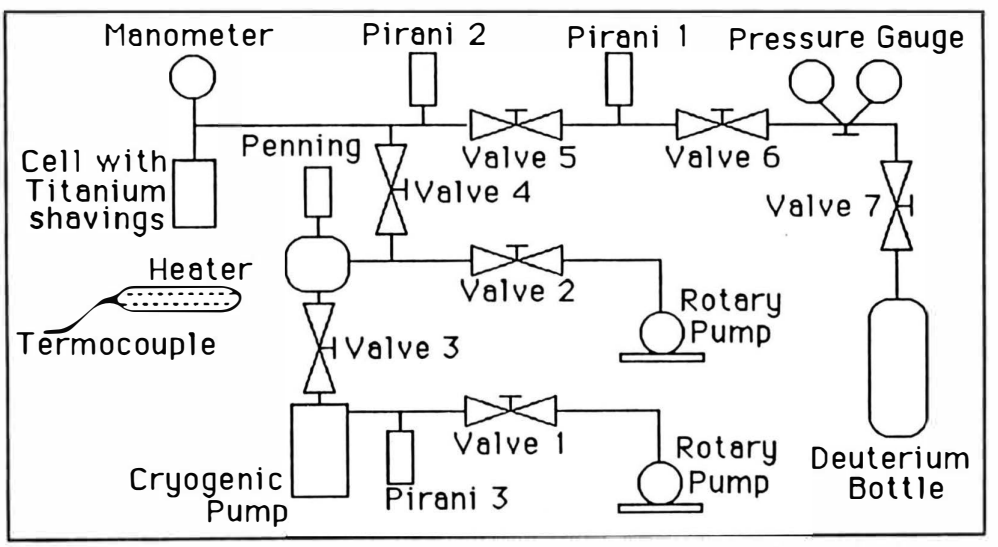

Fig. 3 Scheme of the vacuum system and of the gas loading circuit for the Cold Fusion set-up.

3. MEASUREMENTS AND ANALYSIS OF THE DATA

Before starting the runs, the cell was degased in vacuum for 24 hours at 540^0 C. Two sets of measurements have then been performed filling the cell with D_2 and H_2 respectively; each set consisted in a sequence of measurements with the cell heated and cooled alternatively. During the heating phase the heater was kept on for a period of ~ 2 hours (~ 1 hour in a temperature ramp up from ~ 25 ^{0}C up to ~ 540 ^{0}C and ~1 hour at steady temperature); during the cooling phase the heater was kept off for a period of ~ 22 hours (~ 4 hours in a temperature ramp-down from ~ 540 ^{0}C down to ~ 25 ^{0}C, ~ 18 hours at steady room temperature). In the cycle up, the Ti reached the conditions of complete degasing, while in the cycles down it was filled again by D_2 or H_2. The number of complete cycles was 9 with D_2 and 6 with H_2.

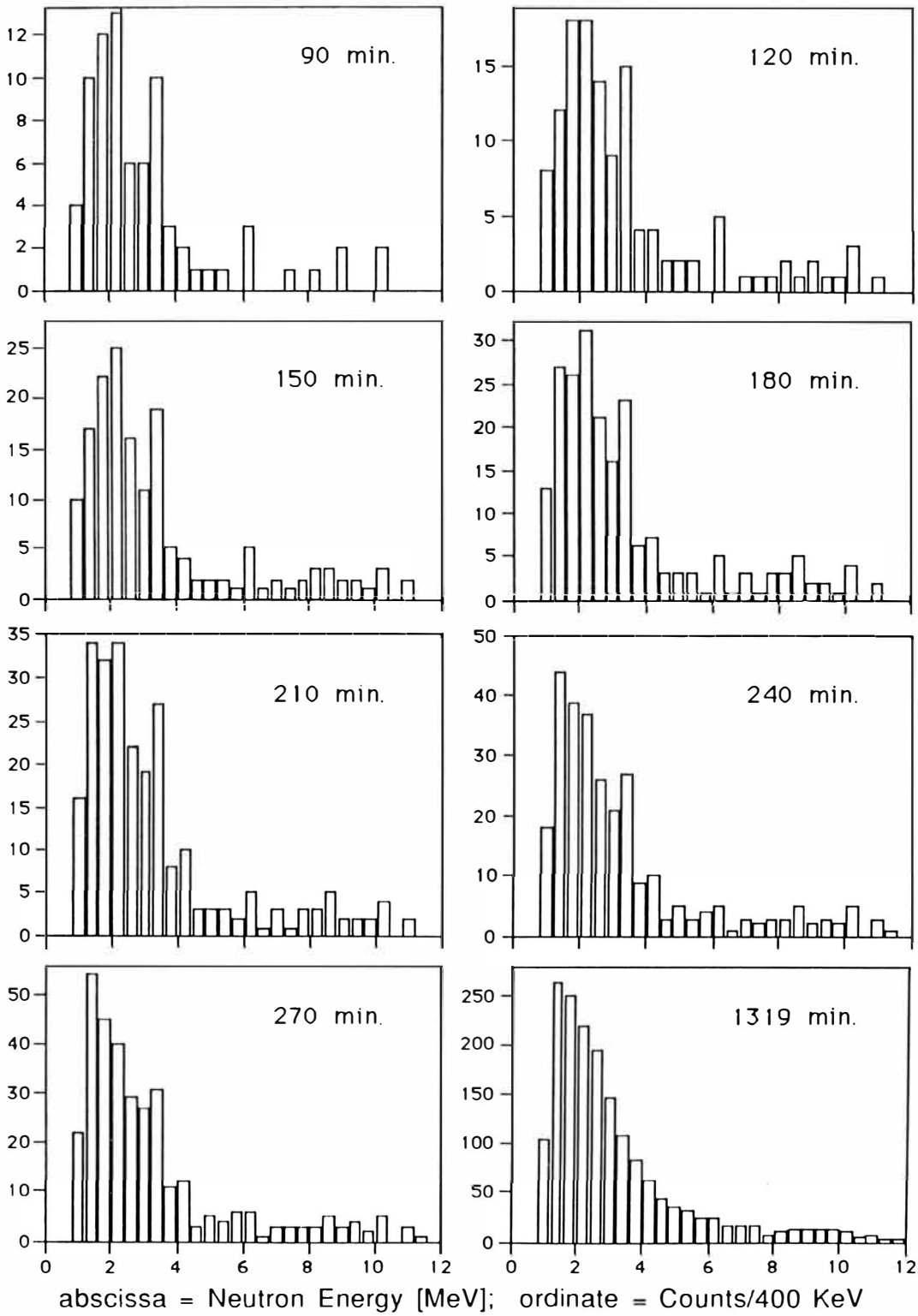

Fig. 4 Time sequence of the growing of the neutron energy spectra during a cooling down run, as observed in the on-line monitor.

During the cycles down with the D_2 filling we observed in the on-line monitors some abnormal behaviors of the neutron energy spectra, namely a small enhancement of the events around 2.45 MeV in the first hours. Fig. 4 shows the spectra of the detected neutrons at different times in a cycle down. No such enhancement was observed with the H_2 filling. At the end of the cycle down the enhancement is hardly visible in the spectrum, which closely resembles to that measured in a blank run (see Fig. 5).

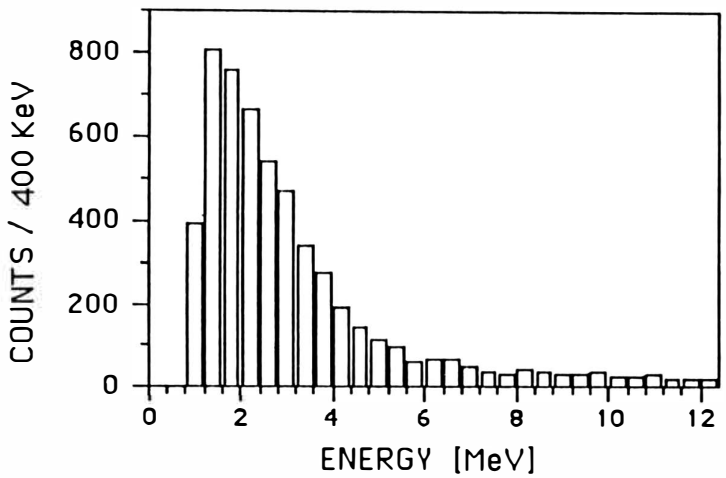

Fig. 5 "Neutron" energy spectra obtained in a blank run.

The first, obvious, trial to make more evident such an effect was that of subtracting the spectra obtained in all the runs with H_2, properly normalized to the total running times, from those obtained in all the runs with D_2. The resulting difference spectrum, was not completely satisfactory. Another approach, based on the normalization of the total number of events contained in the D_2 spectra to that contained in the H_2 spectrum, with the exception of those falling in the energy range from 2.0 to 2.8 MeV is shown in Fig. 6.

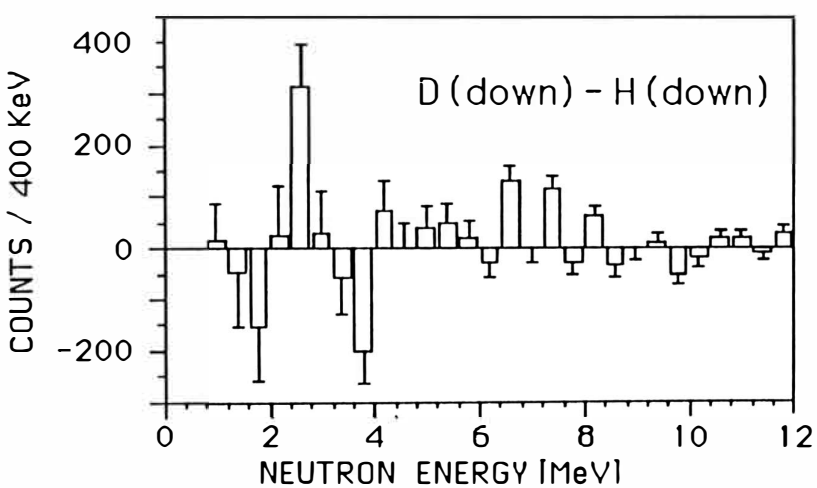

Fig. 6 Difference of the neutron energy spectrum measured in the runs D(down)and that measured in the runs H(down), normalized at the total number of events with the exception of those falling in the energy range from 2.0 to 2.8 MeV. The errors are the statistical ones.

A rather clear signal around 2.45 MeV was observed, but the overall behavior of the event distribution around the signal was not consistent with a statistical analysis, showing some systematic effect.

A careful inspection of the runs, in particular of the spectra and of the correlation plots showed the most likely reason of this unsatisfying behavior. The background in our "neutron energy" spectra (see Fig. 5) is not due to physical events (cosmic rays, natural radioactivity), but is totally instrumental, inherent to our technique. In order to detect with the maximum of efficiency the recoil protons scattered by the neutron in the first and second hodoscope, respectively, we kept in fact the threshold on each of the 26 photomultipliers of the detector at a very low value, close to the peak due to the single electron emission from the photocathode. We had then a certain amount of random coincidences, about 260/hour in the full spectrum, corresponding to ~ 20/hour reconstructed in the channels around 2.45 MeV. The shape of the background spectrum (no cell) is fully consistent with this hypothesis (see Fig. 5). On the other hand, the spectra corresponding to the D_2 and H_2 filling were taken at about 3 weeks of delay and the "average" room temperature was then different. As a result the photomultiplier's noise was different, slightly larger in the runs with the H_2 filling. Consequently the background spectra were slightly different too.

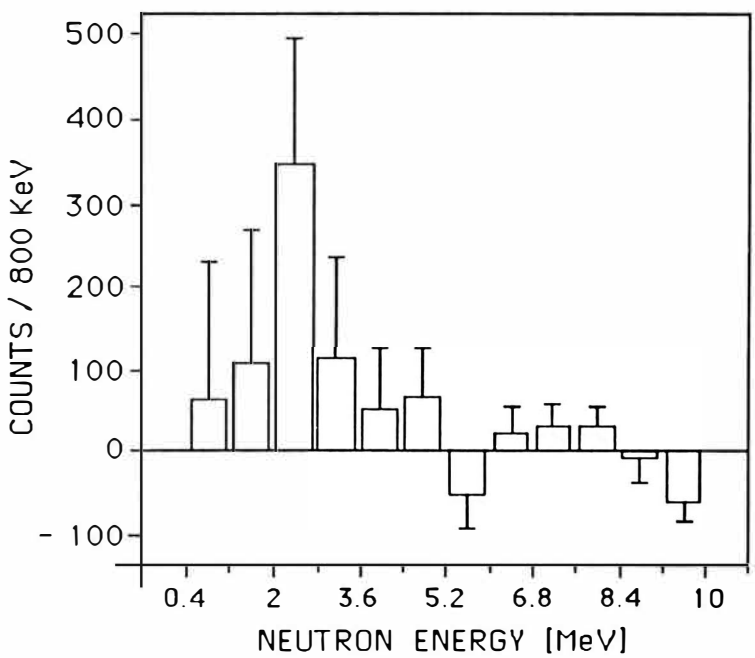

Fig. 7 Difference of the neutron energy spectrum measured in the runs D(down) and that measured in the runs D(up), normalized to the same time. The errors are the statistical ones.

A better, daily, control on the background was obtained by comparing directly the runs "down" with those "up" even if statistically quite different. Fig. 7 shows the spectrum obtained by subtracting the sum of the runs "up" normalized in time to the sum of the runs "down". A clear peak centered at ~ 2.45 MeV is visible with a satisfactory background subtraction around the peak. The resolution of the peak is fully compatible with that expected by a Monte Carlo simulation. The same procedure of subtraction, applied to the runs in which the cell was filled with H_2, gave a spectrum statistically compatible with zero everywhere.

4. DISCUSSION OF THE RESULTS AND CONCLUSIONS

The neutron emission measured in this experiment is 4.0 ± 1.5 n s^{-1}, corresponding to 1.3 ± 0.5 n s^{-1} g^{-1}. It must be noticed that this value has to be considered as a lower limit for these measurements, just due to our subtraction technique. In fact, if the neutron emission would be the same for the runs "up" and "down", we should observe a null effect. If some neutron emission would be present even in the runs "up", this should lower the neutron emission reported for the runs "down".

It appears that the neutron emission seems not concentrated in a few bursts of short duration, as reported by several authors [5, 6], but perhaps distributed along the runs. Attempts to correlate the neutron emission to particular temperature conditions were in fact unsuccessful.

A final remark is that, from the volume and pressure measurements, we estimated that the D/Ti ratio in this experiment was 0.32. On the other hand, this value is totally inconsistent with the Ti-H Phase Diagram [7]. In the range of temperatures and pressures scanned in this experiment we would expect in fact a D/Ti ratio of ~ 1.8. A possible explanation is that the surface condition of the Ti shavings was such to avoid a complete filling of Ti with D near the value expected from the Phase Diagram and that only a reduced portion of the sample could reach the equilibrium conditions expected from the Phase Diagram. Our results are also in qualitative agreement with those reported by Seeliger et al. [8], with a less sophisticated neutron detection device.

In conclusion we report a ~ 2.5 σ evidence for 2.45 MeV neutron emission following absorption of D_2 from a Ti sample. The main source of background was the photomultiplier's noise, which gave the main contribution to the experimental error. The experiments will be continued with a more carefully monitored cell, already built [9], and with electrolytic cells. Finally, a system for cooling the photomultiplier's photocathodes is under design. This would decrease the instrumental background by at least an order of magnitude.

We are indebted to Prof A. Zecchina for enlightening discussion on the Ti/D system and to Prof. G. Preparata for his continuous encouragement.

REFERENCES:

1) M. Agnello et al., in "Anomalous Nuclear Effects in Deuterium/Solid Systems", Provo (Utah) 22-24 Oct. 1990, AIP Conference Proceedings 228, edited by S.E. Jones, F. Scaramuzzi and D. Worledge, pag. 17 New York 1991

2) L. Cranberg and J.S. Lewin, Phys. Rev. 103, 343 (1956)

3) G.C. Bonazzola et al., in Proc. on "Understanding Cold Fusion Phenomena", Conf. Proc. Vol. 24 (ed. Ricci, E. Sindoni and F. De Marco), S.I.F., Bologna (1989), p.313

4) G.C. Bonazzola et al., Nucl. Instr. Meth. A299 (1990), 25

5) H.O. Menlove et al., Report LA-UR-89-1974

6) A. De Ninno et al., Europhys., Lett. 9, 221 (1989)

7) A.D. Mc Quillan and M.K. Mc Quillan "Titanium", Butterworths Scientific Publications, London (1956), p.211

8) D. Seeliger et al., published in Proc. 2nd Annual Conference on Cold Fusion (Como, 29 June-4 July 1991)

9) M. Agnello et al., published in Proc. 2nd Annual Conference on Cold Fusion (Como, 29 June-4 July 1991)

«The Science of Cold Fusion»
T. Bressani, E. Del Giudice and G. Preparata (Eds.)
SIF, Bologna 1991

SEARCH FOR NEUTRON EMISSION FROM DEUTERIDED HIGH TEMPERATURE SUPERCONDUCTORS IN A VERY LOW BACKGROUND ENVIRONMENT.

F.Celani,[1] A.Spallone,[1] L.Liberatori,[1] F.Croce,[2] L.Storelli,[3] S.Fortunati,[4] M.Tului,[4] N.Sparvieri.[5]

[1] INFN, Laboratori Nazionali Frascati, Via E.Fermi, 00044 Frascati (Italy).
[2] Department of Chemistry, Univ. "La Sapienza", Roma (Italy).
[3] Faculty of Engineering, Univ. "La Sapienza", Roma (Italy).
[4] CSM-ILVA (IRI), Via di Castel Romano 100, 00129 Roma (Italy).
[5] ALENIA (IRI), Research Dep., Via Tiburtina Km 12.400, 00131 Roma (Italy).

ABSTRACT

Following the experiments performed with deuterided High Temperature SuperConductors (HTSC) at underground Gran Sasso Laboratory, we have learnt the capacity to absorb Deuterium (D) by these materials and the role played by non-equilibrium conditions to get neutron burst emissions in the framework of Cold Fusion.

So far, some $Y_1Ba_2Cu_3O_{7-\delta}$ (YBCO) pellets and high pressure D_2 gas were enclosed in a stainless steal vessel and a charging-up procedure was performed. The vessel was put in a thermal neutrons field and some thermal cycles (300-> 77-> 300 K) were performed; moreover, for comparison, background and blank runs were performed. A specific acquisition system, able to detect multiple neutron signals in defined time-windows ("time-correlated events"), was set-up.

One thermal cycle run showed a large increase of time-correlated events in respect to the blanks; one other run, although with no relevant mean-value increase of events detected, showed, on the other hand, one interesting multiple neutron signal (triple); other similar runs produced no relevant values.

One-other kind of experiment, at constant temperature (300 K), characterized by a heavy D_2 gas refill, showed both some increase of time-correlated events and few 'triple' neutron signals.

MOTIVATIONS

According both to our opinions [1], mainly based on some similarities between the behaviour of H or D doped Pd and $Re_1Ba_2Cu_3O_7$ (RBCO) in the superconducting state, and to some theoretical suggestions and considerations [2,3], we found some interests in studying compounds of deuterated rare-earths. Moreover our first tests were independently confirmed by S.E.Jones at BYU [4] who operated with deuterided YBCO in thermal cycles and mechanical stresses.

There are several similarities between the behaviour of heavily hydrogenated Palladium [1] and heavily oxygenated $Re_1Ba_2Cu_3O_{(6.5+\delta)}$ compounds (Re is any trivalent rare-earth apart yttrium). Among these we note:

1) As indicated in an our previous paper [1] and experimentally found in [5], the absorption of H in RBCO occurs only if the RBCO is a superconductor material otherwise the H degrades the RBCO giving CuO, Cu_2O, Cu and BaO as final products.
2) The RBCO are superconducting only when Oxygen content is larger than 6.5. The critical temperature (Tc) depends steeply on Oxygen content (e.g. $Y_1Ba_2Cu_3O_7$ Tc=92 K, $Y_1Ba_2Cu_3O_{6.5}$ Tc~60 K).
3) The HTSC are easy to loose the Oxygen in excess of 6.5, i.e. these are intrinsically not stable.
4) It is possible to add H or D (nobody tried T) to superconductors even increasing Tc despite initial content of Oxygen (but at least larger the 6.5) [6].
5) There is no clear evidence for the usual isotopic effect.
6) Several authors found the rare property of inverse pressure coefficient in $Y_1Ba_2Cu_3O_{7-\delta}$.
7) By NMR measurements [7] has been found that H in $Y_1Ba_2Cu_3O_{(7-\delta)}H_{0.2}$ occupies sites in the Cu-O planes and that it diffuses or moves dynamically in the crystal above 170 K but below 150 K it is trapped. In other words, after cooling to 77 K, during warming up we might have a moving of trapped H. Similar effects can be expected with D at similar temperatures.
8) There exist a particular value of H doping that increases [6] the critical temperature. The particular value seems to depend on sample preparation and H loading procedure [8,9].

Moreover, we note that the HTSC have perovskite structure, the same structure of most abundant minerals of the Earth's lower mantle $(Mg,Fe)SiO_3$; the pressure of the core-mantle boundary is as large as $1.4*10^6$ Bar [10]. Then, we can suppose that a proper perovskite

structure can be efficient like the "Mother-Earth-Soup" used by S.E.Jones [11] to search for geological-like Nuclear Fusions.

In other words, among the large unusual properties of HTSC there is their ability to absorb a large amount of hydrogen [6,7,12,13,14]. The possible sites, where the H or D are located, can be identified by Mossbauer spectroscopy as recently suggested by E.Kuzmann et al. [15,16].

Most of these properties have induced us to use high quality HTSC like YBCO in a gaseous system, instead of "standard" Ti or Pd, to research for Cold Fusion anomalous phenomena.

APPARATUS AND ACQUISITION SYSTEM

The apparatus is shown in (fig. 1). It consists of two ^{3}He tubes surrounded by paraffin and lead bricks to detect neutrons and a lead well where a weak (2200 n/s of ~4 Mev and 1500 γ/s of 4.43 MeV) Am-Be neutron source is located; the source is covered by 8 cm of water, in a plastic container, in order to moderate the neutrons. We put 6 YBCO pellets (disk shaped: diameter ~19 mm, thickness 4-6 mm, density 5.5-5.9 g/cm^3, total weight ~50 g) in a PTFE coil (about 1 mH) enclosed in a cylindric stainless-steal vessel for high pressure gas.

The acquisition system (fig. 1) was based on digital counter and analog acquisition by a fast digital scope (TEK 2430) of the signals coming from the ^{3}He detectors; moreover the independent detector's signals were acquired by a MCA. All neutron signals are independently counted by proper counters (scalers), some of these were gated. Each signal from the proper detector is charge-amplified, shaped (6-8 μs of duration) and discriminated. From the discriminator one output is straightforward counted by a scaler, a second output, throw a specific circuitry that inhibits any other signal arriving within 10 μs, is counted by an other scaler. These last signals are used to get the "time correlated events" as below detailed. Each single signal coming from any detector opens for a defined time window the gate to the proper scaler which counts all the other signals (except the first) arriving during this time window.

The counts in a time window come from the logic OR pulses of the 2 detectors. We used 3 different contiguous and separated time windows:

a) from 0 to 10 μs
b) from 10 to 110 μs
c) from 110 to 1110 μs

The time window in 10-110 μs was used as trigger to the digital scope in order to acquire and visualize the analog signals from both detectors (to check for the correct neutron signal shape). We consider the events in the time window b) the most significant events because the expected 2.45 MeV extra-neutrons, due to deuteron-deuteron reactions, have an expected thermalization time of the order of few tenth of μs in our experimental set-up.

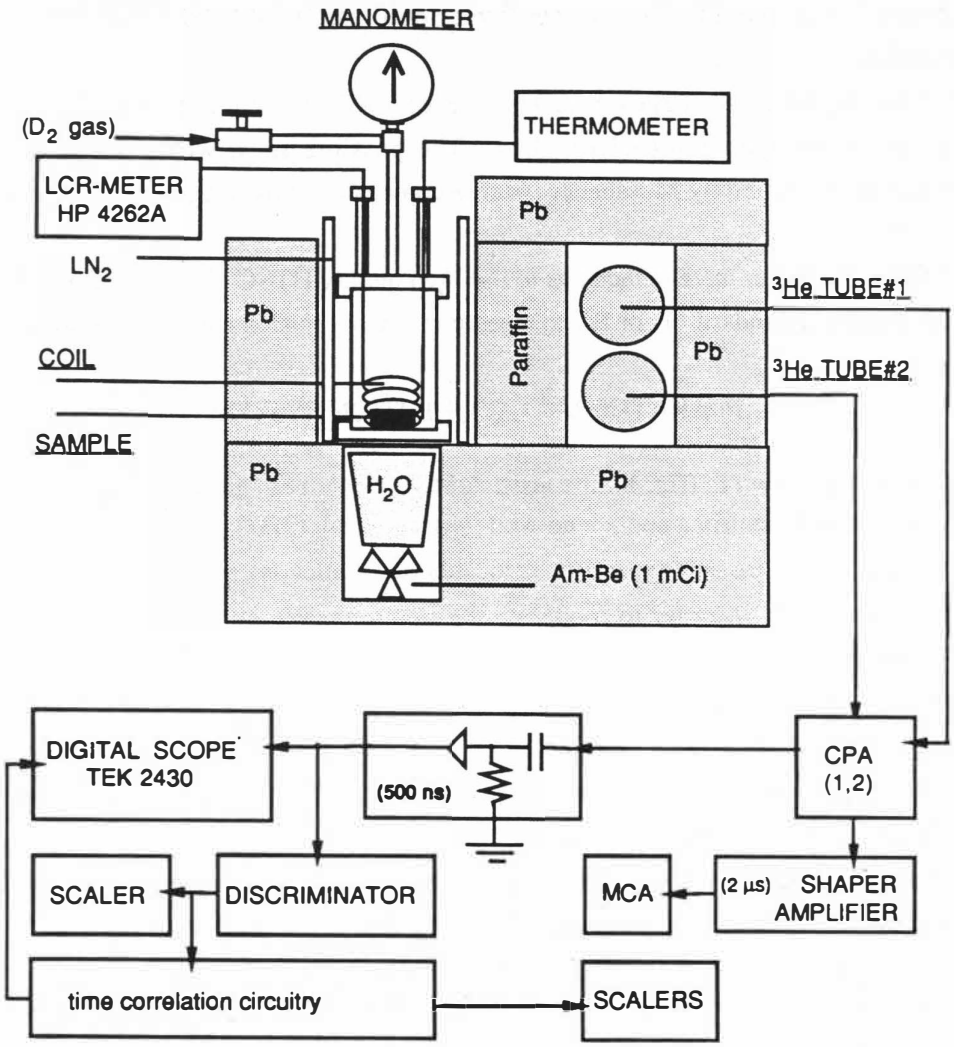

[Fig. 1] Experimental set-up. The total neutron detection efficiency, in respect to the Am-Be source, is 0.4%. The underground Laboratory neutron flux is about 10^{-6} n cm^{-2} s^{-1}. At the bottom of the figure is shown schematically the electronics set-up.

EXPERIMENTAL PROCEDURES AND MEASUREMENTS PERFORMED

The experimental procedure adopted to deuteride the superconductor material is summarized as following:

1) We put the superconductor inside the coil in the stainless steel vessel and we measured the inductance variation of the sample vs temperature (300-> 77-> 300 K) with a AC magnetic field of about 1 Gauss at 1 KHz.

2) We filled with deuterium gas the vessel at a typical pressure of 35 Bar at room temperature.
3) The vessel was warmed-up to about 370 K and hold at this temperature for about 1 hour, after the temperature was decreased to about 360 K and held for 3 hours.
4) We cooled, in few minutes, the vessel from 360 K to about 300 K.
5) We refilled the D_2 gas to the vessel up-to 36 Bar.
6) We started the neutron detection performing thermal cycles (300->77->300 K). In order to check for the D absorption, because the low accuracy of manometer, we measured at 77 K the inductance value due to the diamagnetism of the sample [1] and the value of superconducting transition temperature during the warming up.

We estimated a upper limit loading factor of 0.5 in D/YBCO ratio.

In this specific measurements we further investigated [1] the eventual neutron emission enhancement due to stimulation of the sample by a neutron source in order to detect time-correlated events; thermal cycles were performed during the stimulation in order to induce further non equilibrium states of the material.

We define the different kinds of measurements performed according to the following:

A - Background: measurement with neutron source but no vessel.

B - Blank: measurements with neutron source and vessel filled with HTSC samples in this sequence:

B1) no D2, T= 300 K
B2) D2 at 40 bar, T= 300 K
B3) D2 at 36 bar, T= 300 K after the deuteration procedure.

C - Thermal cycle: measurements after the deuteration procedure with n-source, vessel filled with D_2 at 36 Bar (300K) and thermal cycles (300->77->300 K) operations.

RESULTS

As shown in fig. 2, we made different tests, as above defined, performed in sequential independent runs. Typical Background (1,2,5,10) and Blank (3,4,6) runs ranged from 0.5 to 10 hours of acquisition time, while the Thermal cycle (7,8,9,11) runs ranged from 0.5 to 1 hours. As it results from fig. 2, no significant statistic differences come out from Background and Blank runs (we adopt Gauss statistic for errors calculation).

The Thermal cycle runs showed different cases: the runs 8 and 11 had no significant statistic differences in respect to Blank runs while the runs 7,9 presented different peculiarities. In the run 7, although we did not record large excess counts, anyway we recorded, on the digital scope (fig. 3), one "three neutron signal" (triple event). This triple event, recorded from both detectors, occurred in the 10->110 μs time window during a superconductive temperature transition. By statistic considerations, we expect such event is

occurring once in about 80 hours and we have to consider that all Thermal cycle runs lasted only about 2.4 hours.

We like to note that one other triple event occurred in further thermal cycles performed (3 cycles 150->77->150 K performed in 30 min of measurement).

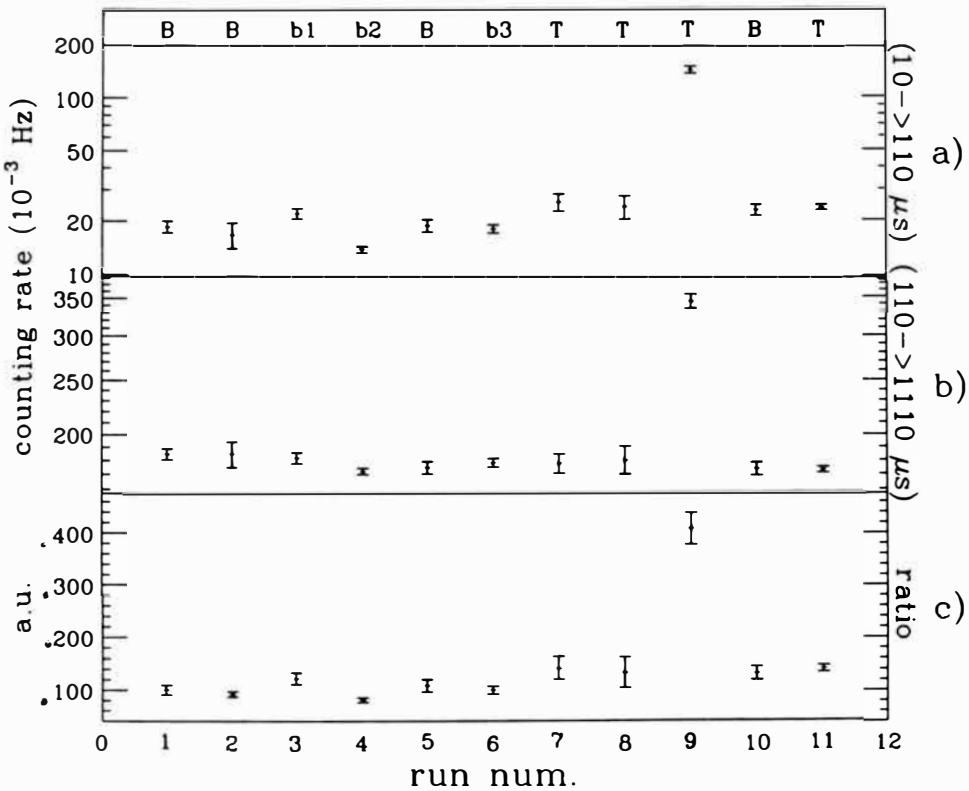

[Fig. 2] Time correlated events vs run type. Run type symbols:
B = Background;
b (1,2,3) = Blanks in three different conditions;
T = Thermal cycles.

[.a)] counting rate (Log) in time window 10->110 μs

[.b)] counting rate (Log) in time window 110->1110 μs

[.c)] ratio (Lin) between a) and b) counting rates.

In the run 9, a large excess of time-correlated events occurred, over 7 times larger in respect to the blank and corresponding to over 30 standard deviations. Most of them were observed at the scope and they look like 2 neutrons in 10->110 μs; no spurious signals were observed. This excess was recorded, with different relative intensity, as in 10->110 μs as in 110-> 1110 μs time windows (fig. 2.a,b).

In fig. 2.c we put in evidence that in the run 9 the ratio between 10-110 μs time-window and 110-1110 μs time-window is about 4 times larger than the Blank runs. This can be consistent with several neutron bursts (separated in time much more than 1 ms) having burst

intrinsic time duration << 110 μs. We recall that the expected thermalization time of 2.45 MeV neutrons lies in the 10-110 μs time-window.

It is quite improbable that some persistent disturbances can reproduce this kind of behaviour.

In an other test performed at room temperature (one month later, at about 20 Bar D_2 gas pressure) we increased the pressure to 42 Bar and after about 10 hours we put the vessel into the source well. The measurement, starting a few second later, gave immediately a large excess in 0-110 μs time correlated events (fig. 4) for few minutes. Moreover, we observed at the scope at least 3 "triple events" (similar to fig. 4) occurring in a time window of 200 μs during the excess counts.

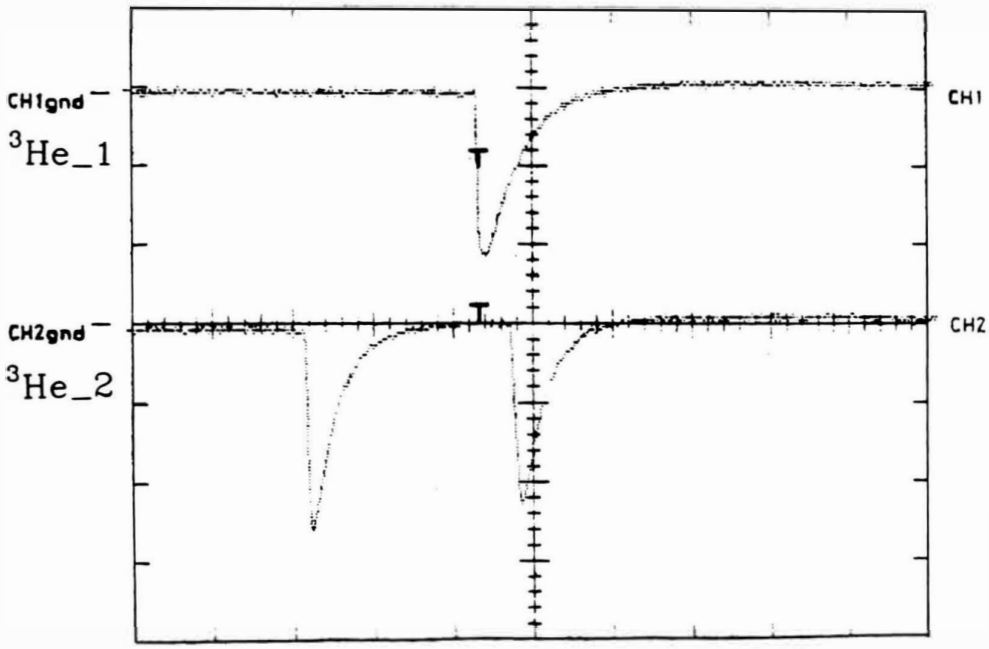

[Fig. 3] The triple event occurred in run 7 of fig.2.and acquired by digital scope. X-scale = 20 μs/div, Y-scale = 100 mV/div. The event occurred in correspondence of superconducting transition temperature, around 95 K.

CONCLUSIONS

Taking in account that HTSC materials (only "high quality" and perovskite structure) as YBCO are able to absorb Deuterium, without destroying the crystalline structure, we put deuterated YBCO pellets in a neutron radiation field and we operated thermal cycles. In this double non-equilibrium condition we looked for a neutron rate enhancement selecting "time-correlated" events, burst-like.

In one thermal cycle we recorded a large increase, in respect to blank runs, of these events. Not all thermal cycle runs gave excess counts results although in some of them we visualized multiple neutrons (triple event) in a very short time-window. These multiple events were sporadic (typically during the superconductive temperature transition), although the probability that these events were simulated by the background was quite low.

In an other particular test, after a D_2 gas refilling at room temperature, we measured an increase of "time-correlated" events and we recorded some triple neutron events lasting to some minutes.

We have to conclude that HTSC materials can be used with a lot of interest in the Cold Fusion experiments and that non-equilibrium conditions are required to stimulate eventual neutron bursts. A full reproducibility of the phenomena detected until now is not under complete control.

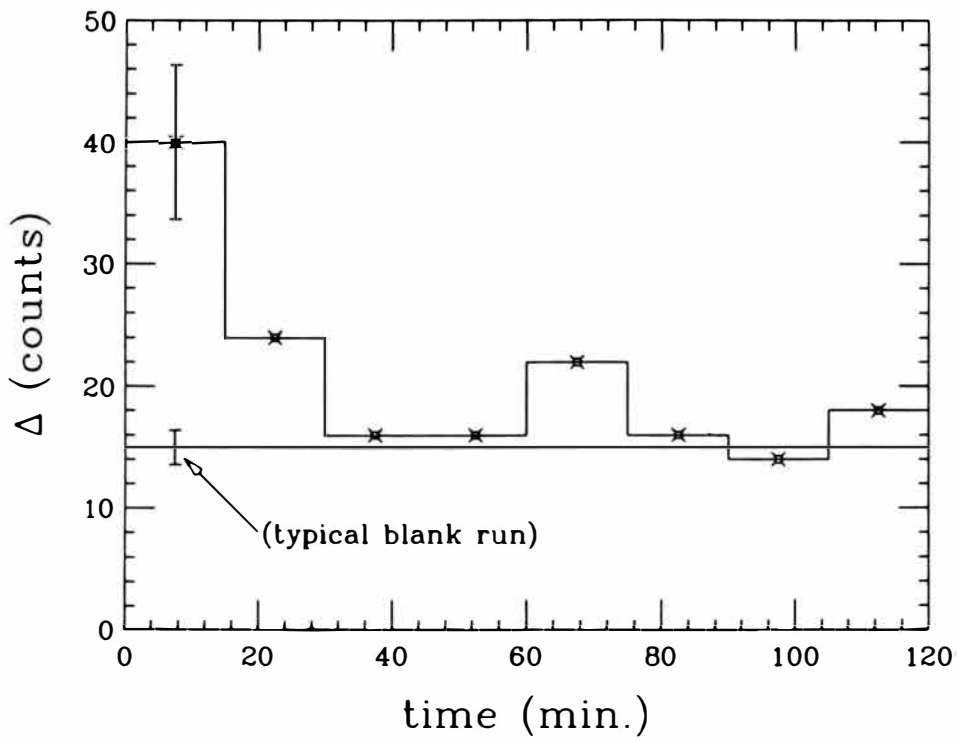

[Fig. 4] Time correlated events occurred after long time D_2 low pressure loading and 10 hours high pressure refilling. The abscissa indicates the time elapsed from the initial irradiation. Several triple events were observed during this measurement.

ACKNOWLEDGEMENTS

We are indebted to Dr F.Ferrarotto and M.Corradi (Rome Un., Physics Dep.) for the time they spent with us during the experiment installation and data taking at G.Sasso Laboratory; moreover we thank Prof. B.Stella (Rome Un.) for his criticism on data interpretation.

We are grate for invaluable and skillful cooperation and technical assistance to F.Basti (INFN,Roma) and M.Giardoni (INFN,LNF).

We would like to thank prof. S.E.Jones (B.Y.U. Provo), prof. G.Preparata (Milan Un.) and prof. G.Bologna (Turin Un.) for their stimulating discussion, criticism and suggestion on nuclear aspects.

A special thank to prof. S.Pace (Salerno Un.) for stimulating discussions on superconducting materials.

This work is supported by grants from INFN and Italian Council of Research (CNR), "Comitato Nazionale per le Ricerche Tecnologiche e le Innovazioni".

REFERENCES

[1] F.Celani et al.
S.E.Jones, F.Scaramuzzi, D.H.Worledge eds. "Anomalous Nuclear Effects in Deuterium/Solid System" AIP Conference Proceeding 228 pg. 62 (1991).
[2] M.Rabinowitz, Modern Physics Letters B Vol. 4, No. 4 pg. 223 (1990).
[3] G.Dattoli et al. preprint ENEA RT/89.49 Jul 6, (1989), Italy.
To be published by "Il Nuovo Cimento" (1991).
[4] S.E.Jones et al.
S.E.Jones, F.Scaramuzzi, D.H.Worledge eds. "Anomalous Nuclear Effects in Deuterium/Solid System" AIP Conference Proceeding 228 pg.206 (1991).
[5] M.V.Abrashev, L.N.Bozukov and M.N.Iliev. Physica C 178, 317 (1991).
[6] J.J.Reilly et al., Phys. Rev. B 36, 5694 (1987).
[7] H.Niki et al., Solid State Comm., vol.69, 547 (1989).
[8] H.Hemmes et al. Phys. Rev. B 39, 4110 (1989).
[9] T.Takabatake et al., Physica C 162-164, 9865 (1989).
[10] E.Knittle and R.Jeanloz, Science vol. 251, pag. 1438, (1991).
[11] S.E.Jones et al. Nature 338, 737 (1989).
[12] C.Y.Yang et al., Phys. Rev. B 36, 8798 (1987).
[13] H.Fujii et al., Jpn. J. Appl. Phys. 27, L525 (1988).
[14] T.Kato et al., Jpn. J. Appl. Phys. 27, L564 (1988).
[15] E.Kuzmann et al.
S.E.Jones, F.Scaramuzzi, D.H.Worledge eds. "Anomalous Nuclear Effects in Deuterium/Solid System" AIP Conference Proceeding 228 pg.262 (1991).
[16] E.Kuzmann et al.
"MOSSBAUER SPECTROSCOPY CHARACTERIZATION OF SAMPLES FOR COLD FUSION EXPERIMENT" ACCF 2, June 29 - July 4, 1991 Como - Italy.
To be published as Conference Proceeding of "II Annual Conference of Cold Fusion" SIF, Bologna, (1991) Italy .

Conference Proceedings Vol. 33
«The Science of Cold Fusion»
T. Bressani, E. Del Giudice and G. Preparata (Eds.)
SIF, Bologna 1991

SEARCH FOR PRECURSOR AND CHARGED PARTICLES IN "COLD FUSION"

Da W. Mo, Yi S. Liu, Li Y. Zhou,
Shi Y. Dong, Ke L. Wang, Shi C. Wang①
Xing Z. Li

Tsinghua University, Beijing 100084, CHINA

I. Introduction

After two years the puzzle of nuclear phenomena in a metal lattice (cold fusion) is still with us. Excess heat [1], or anomalous neutron emission [2] was the goal being searched in most of the "cold fusion" experiments, however, we switched to search the precursor and the energetic charged particles in stead of excess heat or anomalous neutron emission. In fact, we started the electrolysis cell experiment early in April, 1989; the neutron bursts were detected by BF_3 detector, and the tritium was measured by liquid scintillation detector [3]. The sporadic nature of the signals and the difficulties in reproducing these signals forced us to look for a new approach in identifying this anomalous nuclear effect.

We suggested [4] that the energetic charged particles are necessary products for any anomalous nuclear effect, since after the reaction of any two charged nuclei there must be at least one charged product. In contrary, the neutron may not be the necessary product.

Besides, we believe that there must be some precursors before the anomalous nuclear effects. Once the precursor is identified, the difficulty in reproducing these sporadic signals would be reduced. We suggested that the electromagnetic radiation is a possible candidate for precursor, since the charged particles must change their states before the penetration of the coulomb barrier becomes feasible. The energy of this electromagnetic radiation has been estimated to be the order of keV; therefore, it is quite different from the electromagnetic radiation caused by fusion product, which is in the range of hard X ray or Gamma radiation. The

①Institute of High Energy Physics, Beijing 100039 CHINA

Frascati type experiment [5], led by Prof. Scaramuzzi, is particularly suitable for the detection of energetic charged particles and the low energy electromagnetic radiation, since there is no electrolyte to hinder the measurements. The plastic track detector (CR−39) and thermoluminescence detector (TLD) were proposed to detect the energetic charged particle and the low energy electromagnetic radiation [4]. The preliminary run of experiments showed positive results [6]; however, the abovementioned detectors are of integrated nature. It is desirable to measure the signals in real time sequence, then it would be more confident to identify the "precursor".

Au−Si surface barrier detector is suggested to do this real time measurement, because it is sensitive to both energetic charged particles and electromagnetic radiations, and it has comparable sensitivity as CR−39 does. In this note the preliminary results of measurement will be presented.

II. Experimental Arrangement

Fig.1 is a schematic diagram of the experiment system. The degassed palladium and titanium foils were sealed in a stainless steel vessel, facing the Au−Si surface barrier detector in a close−up way. This vessel was connected to a pressurized deuterium storage of 2 atm. Before this connection the vessel was pumped out by a mechanical pump for half an hour. After the connection the vessel was immersed in a liquid nitrogen dewar to let deuterium absorbed into palladium and titanium foils. When the system was cooled down and reached steady state, the valve was closed and the liquid nitrogen dewar was taken away. The system warmed up to room temperature, then this temperature cycle ran again.

Fig.2 shows the block diagram for electronic circuits, which was designed particularly for detection of both electromagnetic radiation and energetic charged particles, for detection of both single signal and the burst of signals. The low energy channels in the multiple channel analyzer (MCA) correspond to the electronic noise and the electromagnetic radiations. With careful setting of discriminator we could still detect part of the electromagnetic radiation in the vicinity of noisy background. The high energy channels in MCA could detect the single signal up to 12.5 MeV. If a burst of high energy charged particle came in a very shot period, the single channel analyzer (SCA) would definitely record it although the MCA might lose it.

Particular attention was paid to avoid any false signals due to the moisture near the cryostat system, and it was successful.

III. Results

Fig.3 shows the result of the measurement of background using MCA, we could not see any signals there except in the low energy channels (dotted line). Fig.4 is the result of calibration using a ^{239}Pu α−source ($E_\alpha = 5.1$ MeV). Fig.5 is

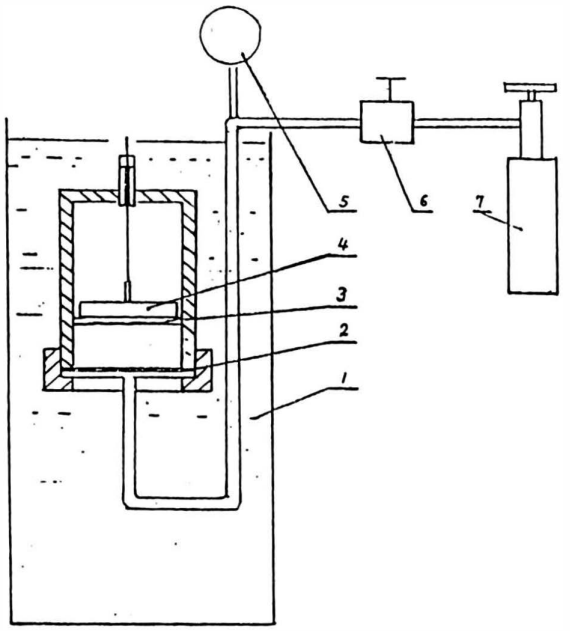

Fig.1 Schematic Diagram of Experiment System

1. LN_2 2. Sealing Spacer 3. Pd, Ti foils

4. Detector 5. Manometer 6. Valve 7. D_2

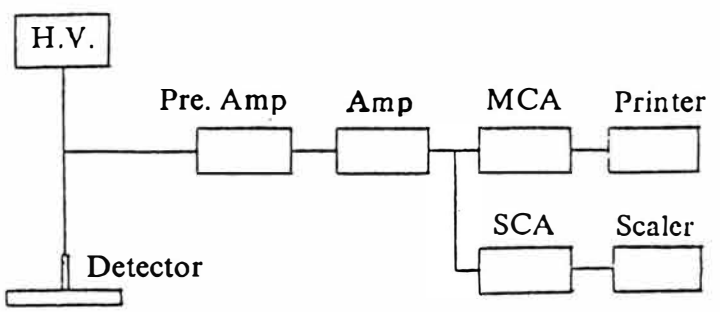

Fig.2 Block Diagram of Electronic Circuits

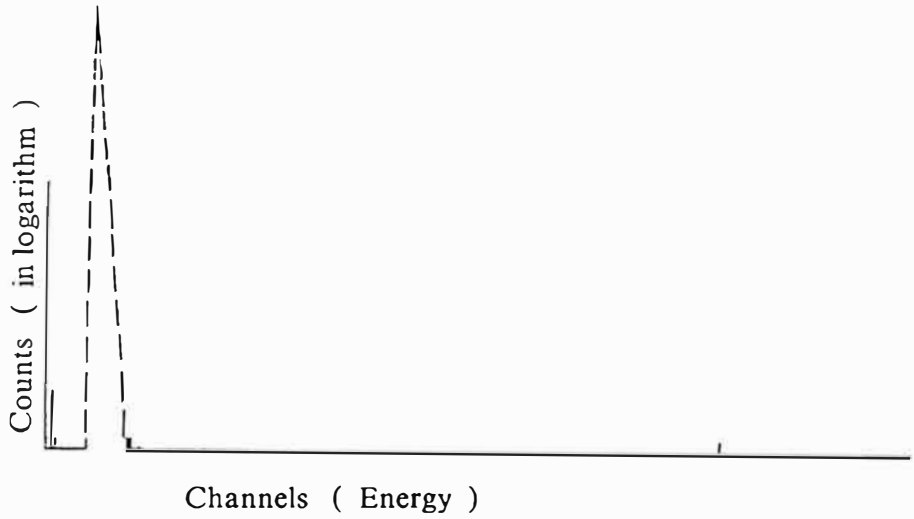

Fig.3 Background

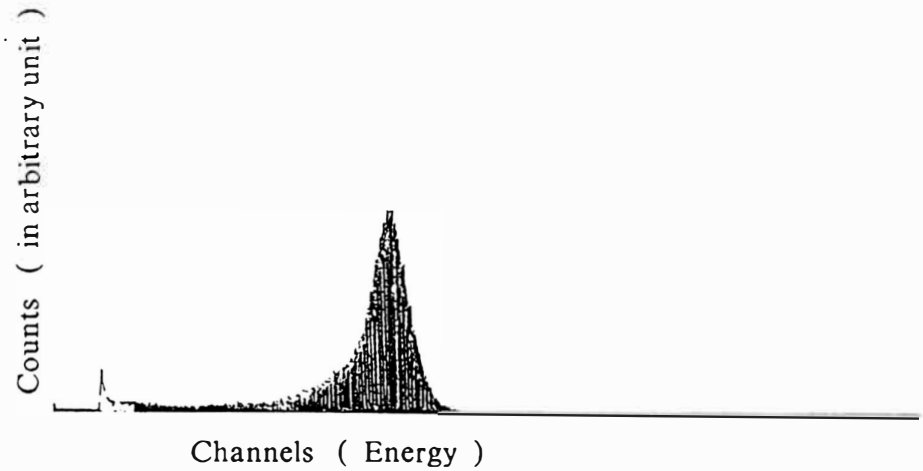

Fig.4 Curve for calibration (^{239}Pu 5.15 MeV α − source)

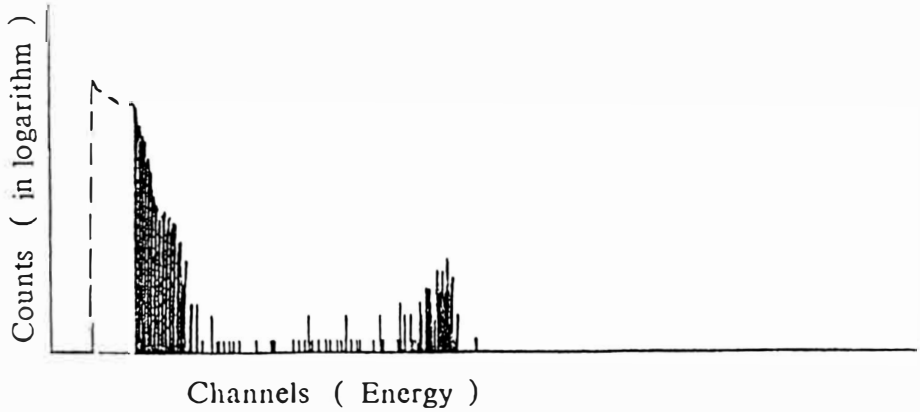

Fig.5 Signals in warming up period

the result for a typical run in the warming up period. The high energy peak corresponds to energy greater than 5 MeV, and the peak accumulated slowly in one hour. In contrast, the signals in the low energy channels, which is just above the electronic noise channel (dotted line), appeared in a very shot period (the rate is about hundred counts in one second). It might be caused by some electromagnetic radiations, since we reproduced similar signals in the similar channels by simply shinning visible light on the same Au–Si detector.

These phenomena were reproduced once and once again in the temperature cycles. Some times the single channel analyzer obtained more than 20–90 counts as well.

The titanium foil was from the titanium shaving, and the palladium foil was cut from the product of Johnson and Matthey Inc. (thickness 25μ). Both of them were friendly given by American scientist.

Ⅳ. Discussion

It is clear that the energy of charged particle has a peak above the 5 MeV. It does not fit with any conventional binary D–D reaction. Although the extraordinary branch, $D+D \rightarrow {}^{4}He+23.8$ MeV, might give more energy, we had to assume an anomalous branching ratio. It is suggestive to use dE / dx detector for identification of the charged particles.

If we assume that the low energy signals were caused by electromagnetic radiation, this was a good manifestation of precursor. We planned to use photo–electric diode for confirmation of this observation. Was there any mistake which might cause the fault signals? We were worried about this also. A good verification was that we did not detected any signals as before when the vessel sealing failed in one of the experiments.

Ⅴ. Acknowledgements

This work is supported by Natural Science Foundation of China and the contingent research funds from National Education Commission and Tsinghua University.

References

〔1〕 M. Fleischmann and S. Pons, J. Electroanalytical Chemistry and Interfacial Electrochemistry, Vol.261, 301 (1989).

〔2〕 S.E.Jones, et al., Nature 338, 737 (1989).

〔3〕 Cold Fusion Research Group, Institute of Nuclear Energy Technology, Tsinghua University, The Proceedings of the Symposium on Cold Fusion (Beijing, May 10–12, 1990).

〔4〕 Cold Fusion Research Group, Tsinghua University, Ibid.

〔5〕 De Ninno, et al., Europhysics Letters, Vol.9, 221 (1989).

〔6〕 X.Z.Li, et al., The Proceedings of Anomalous Nuclear Effects in Deuterium / Solid System (Provo, UT, 1990), Ed. S.E.Jones, F.Scaramuzzi, and D. Worledge (AIP, New York).

Conference Proceedings Vol. 33
«The Science of Cold Fusion»
T. Bressani, E. Del Giudice and G. Preparata (Eds.)
SIF, Bologna 1991

THE PRODUCTION OF NEUTRONS AND TRITIUM IN THE DEUTERIUM GAS-TITANIUM INTERACTION

A. De Ninno, F. Scaramuzzi
ENEA, Area Energia e Innovazione, Dip. Tecnologie di Punta, C.R.E. Frascati,
C.P. 65 - 00044 Frascati, Rome (Italy)

A. Frattolillo, S. Migliori
ENEA, Associazione EURATOM-ENEA sulla Fusione, C.R.E. Frascati,
C.P. 65 - 00044 Frascati, Rome (Italy)

F. Lanza
JRC Euratom, 21020 Ispra, Varese, (Italy)

S. Scaglione
ENEA, Area Energia e Innovazione, Dip. Tecnologie di Punta, C.R.E. Casaccia,
Via Anguillara, 301, S. Maria di Galeria, Rome, (Italy)

P. Zeppa
ENEA, Area Nucleare, Dip. Reattori Innovativi, C.R.E. Casaccia,
Via Anguillara, 301, S. Maria di Galeria, Rome, (Italy)

C. Pontorieri
ENEA student, Frascati

INTRODUCTION

The search for neutron emission due to the interaction between deuterium gas and titanium in non-equilibrium thermodynamic conditions was first proposed by the Frascati Group of ENEA, and preliminary results, obtained in April 1989, were published (1). The same results, enriched with new data, were presented at the Santa Fé Workshop on Cold Fusion Phenomena in May (2) and at the Workshop *Understanding Cold Fusion Phenomena*, held in Varenna in September 1989 (3). These data, as well as all the others in the field, were characterized by lack of reproducibility.

The first results were obtained by having titanium chips (produced with a lathe) to interact with deuterium gas at pressures up to 60 bars. The system was then cycled between liquid nitrogen temperature (77 K) and room temperature. The neutrons were detected, during warm-up, by a single BF3 moderated neutron detector, having a very low efficiency (in the order of 10^{-4}). The time structure of the neutron emission appeared to be in "bursts", by burst meaning the emission of many neutrons in a time comparable with the die-away time of the neutrons in the detector-moderator system

(typically a few tens of microseconds). We will refer to these first measurements as to the *first generation* measurements.

At the Santa Fé Meeting similar results were presented by a Los Alamos Group, led by H. Menlove [4], with two main improvements in the detection system. A much higher efficiency was obtained (up to 45%) by using many ^{3}He tubes in a cylindrical geometry, and a peculiar technique was used to analyse the time structure of the neutron emission. The latter can be shortly summarized (in a simplified way) as follows: when a neutron is detected by the system, it is added in a register called *totals*; at the same time, a time window (typically 128 μs) is opened, and the neutrons detected in this window are summed up in a register called *reals*. The *reals* detected give information about the neutrons emitted all together in a short time interval, i.e., the *bursts*. It can be easily shown that there is a simple relation between the number of *reals*, R, and the corresponding number of neutrons detected in the burst, n:

$$R = kn(n-1)/2$$

where k is an instrumental parameter of order 1.

In the Autumn of 1989, in the light of the many contradictory results presented at the Santa Fé Meeting, we faced the dilemma of whether to try to measure the energy of the neutrons, or to concentrate our efforts on the study of the time structure of the neutron emission, and possibly of the correlation between the neutron emission and the thermodynamic parameters of the system. The first route would have made impractical to study these two features. We decided to follow the second route, adopting the improvements to the instrumentation suggested by the Los Alamos Group. We ordered an *ad hoc* detector from Jomar [5], and in the meanwhile we were able to borrow a *standard* Jomar detector (normally used for nuclear safeguard activities), with 15 active ^{3}He tubes and an efficiency of about 15%. With this instrument we performed a series of experiments, still in the Frascati Laboratory (FL), in the period November 1989-February 1990. In addition, in collaboration with the Ispra Center of Euratom, we started to look for tritium in titanium samples that had been treated with deuterium. The positive and encouraging results obtained in both types of measurements (neutron and tritium) were presented at the *First Annual Conference on Cold Fusion* [6] in March 1990. We will refer to these measurements as to the *second generation* experiments.

In the Autumn 1990 we received our new detector. Furthermore we had become aware of the importance of reducing the neutron background in our measurements. Thus we had asked, and obtained, the hospitality of the INFN (Istituto Nazionale di Fisica Nucleare) in its underground laboratory under the Gran Sasso massif near

L'Aquila [Laboratorio Nazionale del Gran Sasso (LNGS)]. After the first calibrations at Frascati, we moved at LNGS in Autumn, and started our measurements towards the end of the year. Preliminary data about the system and its calibration, and about the neutron background at LNGS, were presented at the *Workshop on Anomalous Nuclear Effects in Deuterium-Solid Systems* (7), held in Provo, Utah, USA in October 1990. Here we are presenting the results of the first months of measurements performed with the new detector at LNGS, up to June 1991. We will refer to them as to the *third generation* experiments. We want to point out that the difficulties connected with the logistics of the experiment (LNGS is about 150 km from FL) had as a consequence a limited number of runs, meaning by runs the thermal cycles of deuterium gas-titanium samples. Furthermore the first three to four months were dedicated to the search for a reproducible pretreatment of the samples, trying also procedures suggested (at the Provo Meeting) by other groups, in particular by the Los Alamos Group (M. Paciotti) (8) and a Beijing group (Prof. Zhu) (9). All the data referring to these measurements will be reported here. We continued also the search for tritium in titanium-deuterium samples, with some positive results.

THE NEUTRON MEASUREMENTS

We refer to the communication presented at the Provo Meeting (7) for the details on the detector and its calibration, both at FL and at LNGS. Here we want only to remember that the detector is composed of an inner ring (IR) with 20 ^{3}He tubes (efficiency 27%) and an outer ring (OR) with 8 ^{3}He tubes, all the tubes being immersed in high density polyethylene; a veto counter (VC), permits to discard signals due to noise in the electric feed line. Another feature that we want to remember is the background of reals, which was about one per hour at FL, with values of R centred about 6; at LNGS, it was of one real, with R = 1, per week.

Table 1 shows the list of tests on 18 samples, starting November 1990 and ending June 1991. After trying the Zhu's and the Paciotti's methods for pretreating the samples, without positive results, a method devised by us was chosen and used starting February 1991. We used the titanium alloy called 662 (6% vanadium, 6% aluminium, 2% tin), worked at the lathe in long threads 50 μm thick and 1 mm large. During the lathe cutting a flow of pure ^{4}He gas was sent onto the contact point between the tool and the metal, in order to favour the cooling down of the thread with as low as possible oxidation. The sample ($\approx$120 g) was then put into the experimental cell, and heated under vacuum up to about 100 °C for a couple of hours, and then let under vacuum while cooling down. Next day the cell was brought to LNGS. Here it was charged with D_2 gas up to 20 bars, and then closed. The cell was then heated in an oven, while controlling pressure and temperature, until D_2 gas was

Table 1
Data on the tests performed on 18 samples,starting November 1990 till June 1991

Sample	Date	Pretreatment	Material	Absorption	Notes
C1	11/11	Frascati meth.	Ti		
C2	5/12	Zhu method	Ti		
C3	12/12	Zhu method	Ti		
C4	19/12	Zhu method	Ti		
C5	1/1	Zhu method	Ti		
C6	10/1	Paciotti meth.	Ti		
C7	17/1	Paciotti meth.	Ti		
C8	28/1	Frascati (new)	Ti662	none	
C10	21/2	Frascati (new)	Ti662	correct	burst
C12	3/3	Frascati (new)	Ti662	correct	burst
C13	14/3	Frascati (new)	Ti662	low P	
C14	19/3	Frascati (new)	Ti662	little	
C15	27/3	Frascati (new)	Ti662	too much	
C16	4/4	Frascati (new)	Ti662	little	
C18	2/5	Frascati (new)	Ti662	too much	
C19	6/5	Frascati (new)	Ti662	little	
C20	27/5	Frascati (new)	Ti662	correct	
C21	6/6	Frascati (new)	Ti662	correct	burst

- The pretreatment called *Frascati (new)* is the procedure described in this paper; for the Zhu method see Ref. (9), for the Paciotti method see Ref. (8); for sample C1 the procedure described in Ref. (1) was used.
- The date indicates the beginning of the run.
- The expressions *little*, *too much* and *correct* for the absorption are referred to the curves shown in Fig.1

absorbed, with a controlled rate of absorption, up to an average stoichiometric composition of the order of a few percent D atoms per Ti atom. Figure 1 shows the behaviour of a parameter indicating the absorption of deuterium as a function of time during this phase for samples C10, C12, C20 and C21, which were the only four for which the D_2-charging procedure was rather comparable. The parameter is the ratio between temperature (absolute) and pressure (in bars), normalized to the starting point. The steep part of the curves represents the absorption phase. When the desired

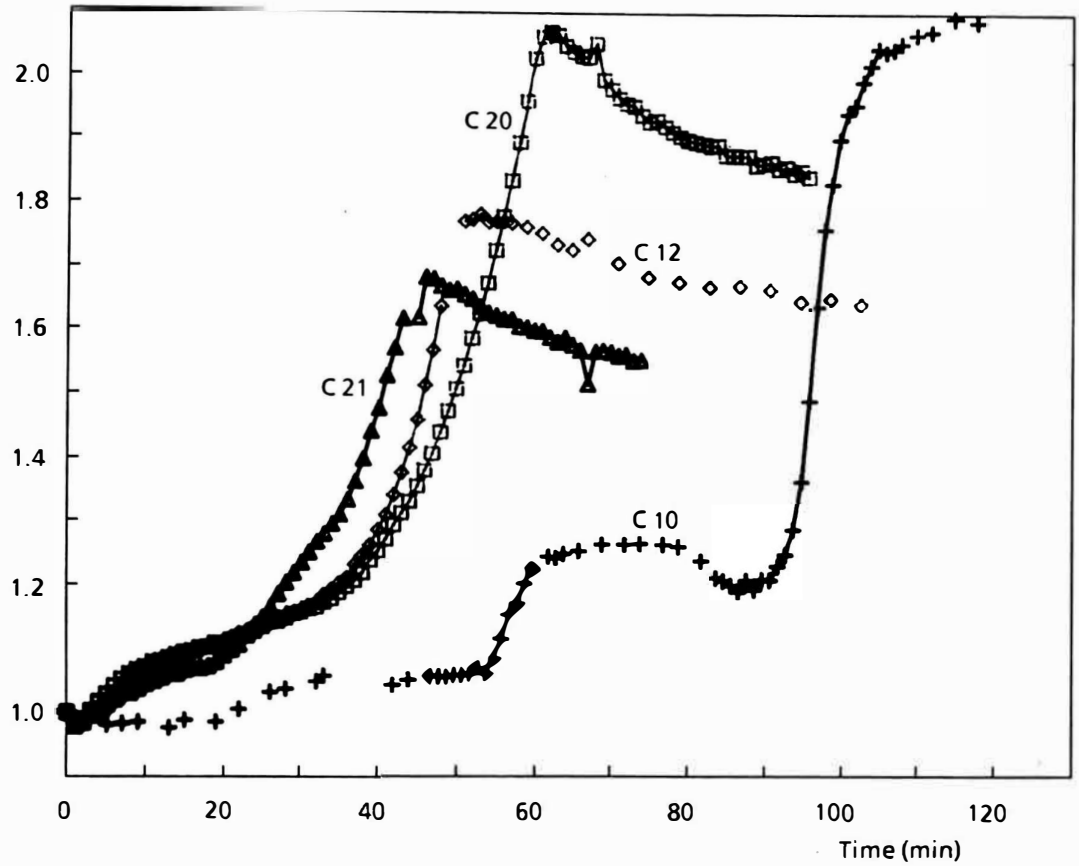

Fig. 1 The ratio between temperature (in K) and pressure (in bars), normalized to the starting point (room temperature, 20 bars), in the cell, as a function of time, during the D_2 absorption procedure. D_2 is absorbed during the steep part of the curves; then the sample is taken out of the oven, and the ratio decreases. Only samples C10, C12, C20 and C21, for which the absorbing procedure was similar, are considered.

amount of D_2 had been absorbed, the cell was taken out of the oven, and the parameter started to decrease. The maximum temperatures reached were between 180 and 300 °C. At this point the sample was let to cool down to room temperature; then more D_2 gas was added, bringing up the pressure typically to 30 bars, and the cell, closed, was immersed in liquid nitrogen, bringing it in a few minutes at 77 K. The last step was to put the cell immersed in a dewar full of liquid nitrogen in the sample well of the detector, leaving it alone for the next days, while the nitrogen evaporated and the sample's temperature increased; the neutron emission and the temperature were recorded. In order to reduce the dead time due to the transmission of data from the Jomar system to the memory of the computer, we decided to use a quite long measurement time interval, 1000 s. On Table 1 it is indicated that in three out of these four runs, and precisely for the samples C10, C12 and C21, a big burst was seen on the IR: the values of R are respectively 994, 2032 and 1134. The corresponding values of the totals were coherent with the equation quoted before; for

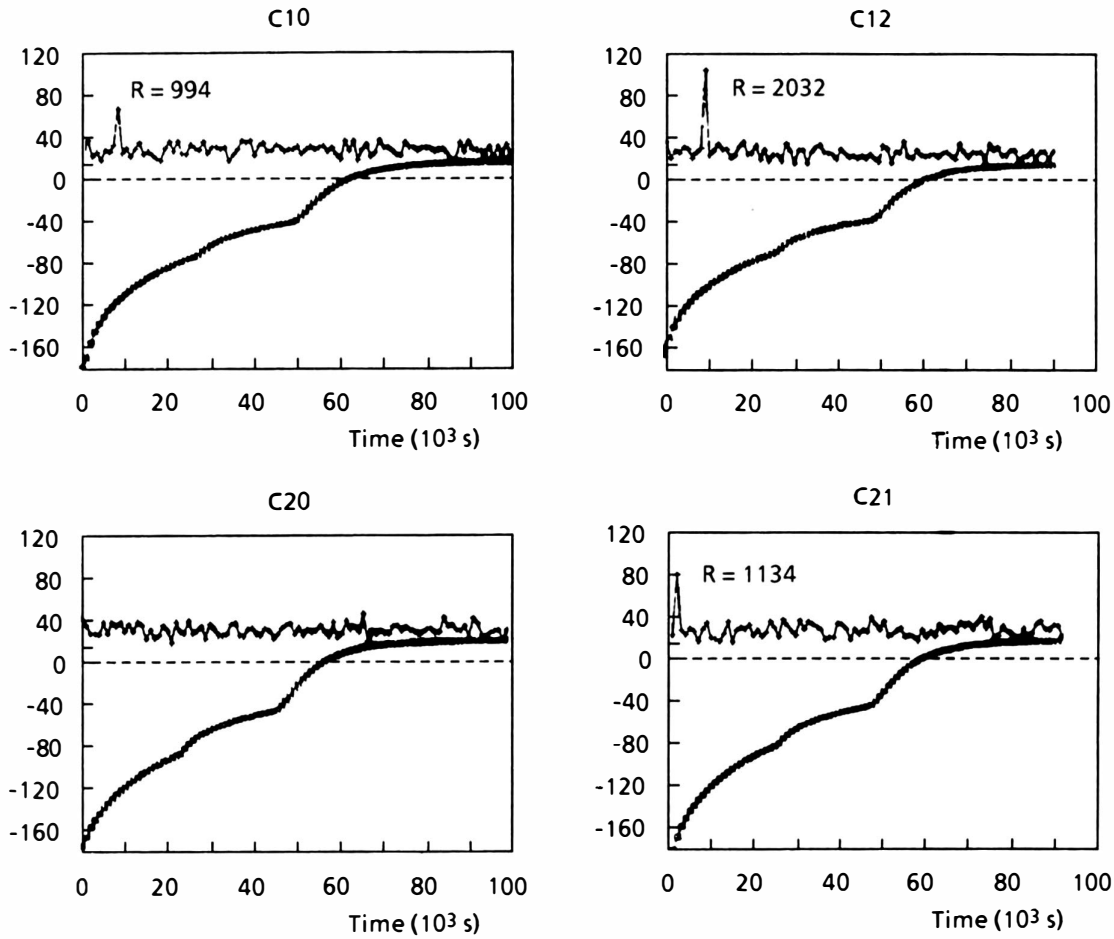

Fig. 2 **The time evolution of the neutron countings (upper curve) and of the cell temperature (in °C), during warm up. The counts reported are the *totals* recorded in each 1000 s time interval, for the samples quoted in Fig.1. For samples C10, C12 and C21 a burst could be detected, both on the *totals* and on the *reals*: the value of R is reported.**

sample C12 the value of 2032 could be better explained with two bursts of R ≈ 1000 taking place in the same time interval. The veto counter showed no anomalies in these measurement intervals, confirming thus that the bursts could not be attributed to electric disturbance in the electric feed line. The only incoherent feature is the absence of corresponding reals in the OR; taking for good the calibration performed with the ^{252}Cf source (see (7)), one should have expected a value of R in the order of 10, but the value measured in correspondence with the IR bursts was always zero. In Fig. 2 the time evolution of the neutron emission (totals) and of the temperature of the sample is shown. The values of the reals for the three bursts are written close to the *totals' bursts*. The two changes in slope of the temperature curves presumably represent the instant in which the cell is no more in contact with liquid nitrogen, and then the moment in which all liquid nitrogen is evaporated.

Concluding, we have presented an experiment performed in particularly clean conditions, both for the good quality of the detector and for the particularly low level of the neutron background (note that in the LNGS the ambient conditions are outstanding: temperature is constant at about 20 °C and humidity is quite low, less than 40%). We have found three events (bursts) in four runs which were characterized by quite similar procedures in preparing the sample. The bursts corresponded to about 200 source neutrons, but the absence of countings on the OR sets a doubt on this evidence. In order to explain it, one should imagine that the neutrons detected are of energy much lower than the 2.5 MeV expected from a D-D fusion reaction: in this case the calibration with ^{252}Cf would be no more valid. On the other side it is striking that the three bursts are characterized by very similar experimental features, such as:

- similar pretreatment of the sample
- similar temperature range of the event (-160 to -120 °C, while warming up)
- coherent relation between *totals* and *reals*
- negative signature of the VC, excluding electric noise.

Experiments on this line will continue, trying to optimize the pretreatment of the sample, and to increase the frequency of the runs.

Another improvement will consist in adding, in parallel to the Jomar shift-register, another system for collecting the countings, which will record each of them with its *date*, i.e., the indication of the absolute time of arrival of the detected neutron, with the accuracy of 0.5 μs (10). The comparison between the two registrations will permit a more thorough comprehension of the events (reals).

SEARCH FOR TRITIUM

The technique used to look for tritium absorbed in the titanium samples has been described elsewhere [11]. Here we will recall the main features. The titanium sample, on which deuterium, and presumably tritium, is absorbed, is put in an oven at 1000 °C under a flow of ^{4}He gas, so that all the hydrogen isotopes are desorbed. The flowing gas passes through a CuO catalyst at 400 °C, where the hydrogen isotopes are transformed in water vapours. Then it passes through two water scrubbers (containers with distilled water), set in series and kept at the temperature of 4 °C, where the vapours are condensed and mixed up with the water of the scrubbers. Part of the content of the scrubbers is then examined with a scintillation spectrometer, and the presence of tritium is detected.

Part of the samples of the third generation of experiments have been partially examined (not all the ≈120 g of titanium used for the neutron experiments have been subjected to the procedure described above). The amount of tritium contained

Table 2
The amount of tritium found in titanium samples C1-C13, expressed in Bq/g (becquerel per gram of deuterium desorbed from the sample). The amount of tritium contained in the original deuterium gas (9.3 Bq/g) has been subtracted. Only part of each sample has been subjected to this measurement. The error in the measurement is 0.5 Bq/g.

Sample	Amount of tritium
C2	1.9
C5	2.9
C7	2.3
C10	5.4
C13	2.6

originally in the D_2 gas was accurately measured, and, for the two bottles used in the measurements quoted, it was ≈ 9 Bq/g of deuterium. The results of the third generation measurements are reported in Table 2 (the value of the tritium contained originally in the gas has been subtracted). The values are not high, but the accuracy of the measurements is quite good; thus they can be considered meaningful.

OTHER EXPERIMENTS

The experiments described here, from the first to the third generation, show clearly the difficulty of defining accurately the parameters that characterize the material used and its treatment, including D_2 absorption. The need for a better characterized system is strongly felt. Thus, while still continuing the measurements described here, we decided to start a new line, inspired by the work of Zelensky, Rybalko et al. (12), i.e., the study of titanium thin layers on which deuterium has been implanted at low temperature (typically 77 °K), thus creating locally a very high concentration of deuterium, then heating up the sample, in order to create non-equilibrium conditions, while looking for the emission of neutrons and charged particles. We hope to perform this experiment at LNGS, where the very low neutron background should permit quite favourable experimental conditions for neutron detection. The main aim of such an experiment is to be able to obtain an experimental procedure with a much better reproducibility. Preliminary tests for this kind of experiment have been started.

ACKNOWLEDGEMENTS

We want to acknowledge the important contribution to the realization of the apparatus given by Mr. Luciano Mori. Messrs Giuseppe Lollobattista and Luciano Mori are deeply thanked for their skillful and enthusiastic participation to the measurement campaign at LNGS, in which they head to face the inconveniences of commuting between FL and LNGS.

REFERENCES

(1) A. De Ninno, A. Frattolillo, G. Lollobattista, L. Martinis, M. Martone, L. Mori, S. Podda, F. Scaramuzzi, Europhysics Letters, **9**, 221 (1989)

(2) Workshop on Cold Fusion Phenomena, Santa Fé, NM, USA, May 23-25, 1989

(3) A. De Ninno, A. Frattolillo, F. Scaramuzzi, Proceedings of the Workshop "Understanding Cold Fusion Phenomena", Varenna, Como, Italy, September 15-16, 1989; edited by R. Ricci, F. De Marco and E. Sindoni, The Italian Physical Society (SIF), p. 41 (1990)

(4) H. Menlove et al., Workshop on Cold Fusion Phenomena, Santa Fé, NM, USA, May 23-25, 1989, and Proceedings of the First Annual Conference on Cold Fusion, Salt Lake City, March 28-31, 1990, edited by the National Cold Fusion Institute, p. 250 (1990)

(5) Jomar Systems, 110 Eastgate Drive, Los Alamos, NM 87544, USA

(6) F. D'Amato, A. De Ninno, F. Lanza, C. Pontorieri, F. Scaramuzzi, P. Zeppa, Proceedings of the First Annual Conference on Cold Fusion, Salt Lake City, March 28-31, 1990, edited by the National Cold Fusion Institute, p. 170 (1990)

(7) A. De Ninno, C. Pontorieri, F. Scaramuzzi, P. Zeppa, Proceedings of the Conference on Anomalous Nuclear Effects in Deuterium/Solid Systems, Provo, UT, USA, October 1990, edited by AIP, pag. 122 (1991)

(8) M. Paciotti, presented at the Conference on Anomalous Nuclear Effects in Deuterium/Solid Systems, Provo, UT, USA, October 1990, unpublished

(9) Zhu Rongbao et al., presented at the Conference on Anomalous Nuclear Effects in Deuterium/Solid Systems, Provo, UT, USA, October 1990, unpublished

(10) F.V. Frazzoli, R. Renetti, P. Zeppa, private communication

(11) F. Lanza, C. Ronsecco, Technical Note I.90.08, Joint Research Centre, Ispra site, Italy

(12) V.F. Zelensky, V.F. Rybalko, A.N. Morozov, G.D. Tolstolutskaya, V.G. Kulish, S.V. Pistyak, L.S. Martinov, Report of the Physical-Technical Institute of the Ukrainian SSR Academy of Sciences, Kharkov, preprint KhFTI 89-61 (1989)

Conference Proceedings Vol. 33
«The Science of Cold Fusion»
T. Bressani, E. Del Giudice and G. Preparata (Eds.)
SIF, Bologna 1991

FUSION NEUTRON EMISSION INDUCED BY INJECTION OF DEUTERIUM INTO TITANNIUM TARGET IN A MIRROR PLASMA

S.Y.DUAN W.S.GUAN S.Q.CHENG J.ZHANG S.L.HAO B.GU J.Q.LI W.X.LIANG
G.Y.ZHANG S.X.PEI J.C.HUANG K.W.CHEN R.LIU X.R.LIU Ying LI

Southwestern Institute of Physics
P.O.Box 432, Chengdu, Sichuan 610041, P. R. China

ABSTRACT

A target, titannium sheet laden with deuterium, is immersed in the deuterium plasma confined in MM-2U magnetic mirror and it is biased at about -10 kv. The deuterium nuclei-deutrons are infused into the crystal structure of titannium target. After having implanted deuterium for several hours, random neutron emissions are observed and neutron bursts are measured by using two identical BF-3 neutron detectors No.1 and No.2 located at different positions and a neutron dosemeter.The neutron count rates are up to 100 times higher than the background count rate of 0.8 count/sec. It is corresponding to neutron flux of (2-8)E+5 neutron/sec. No gamma-ray counts beyond background are detected in our experiments. It is suggested that random neutron bursts may be from cold nuclear fusion reactions related to the propagation of microcracks of the metal lattice.

I INTRODUCTION

The "COLD FUSION" announced by professors Martin Fleischmann and Stanley Pons on March 23,1989 [1] evoked great excitement and stimulated many scientists to repeat their results. The cold fusion phenomenon has been demonstrated in collaborative experiments at Brigham Young University and at other laboratories. Current efforts focus on trying to understand and control (or repeat) this cold fusion phenomenon.

Just as pointed out by S.E.Jones[2], non-equilibrium states of the deuterium-metal (D-Ti or D-Pd) system are essential conditions for creating cold fusion reaction. As we know, electrolysis is one way to produce states which are far from equilibrium. The other ways, such as varying external parameters of a system, temperature, pressure and contact potential, etc. will also generate non--equilibrium states of a system. Implantation of deuterium ions into the metals is one of the effective methods for generating a non-equilibrium state. Based on this idea we started our experiments since April,1989. The recent results of fusion neutron emission induced by infusion of deuterium into a titannium target in a simple mirror machine MM-2U are presented here.

II EXPERIMENTAL APPARATUS AND ARRANGEMENT

MM-2U is simple mirror device, mirror ratio is 2:1, spacing between two mirrors is 0.8 M andcentral magnetic field strength is 500 G. After pumping to pressure of 1E-4 Pa the pure deuterium is poured into the device to ambient pressure of 5E-2 Pa. An electron beam with current of 6mA and energy of 1 kev is injected into the device along the axis.The deuterium plasma parameters obtained are : electron density Ne=5E+9 cm-3 and ion temperature Ti=1 ev.

A titannium plateof 2*4 cm+2 as a target is inserted into the deuterium plasma at the central plane of the device and is perpendicular to the magnetic field lines. A high negative voltage about 10-20 kv is exerted on the target to obtain the infusion of deuterium. As the target is at the negative potential, an ion sheath around it must be formed.The deuterium ions entered into the sheath will be accellerated to bombard the Ti-target and to be implanted into it at once (see Fig.1).

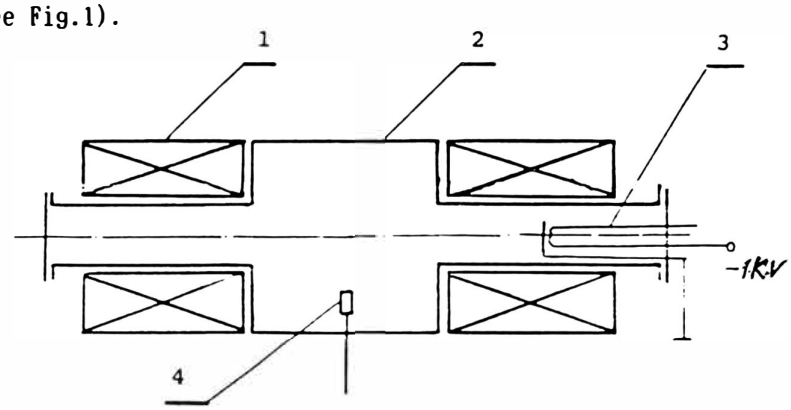

Fig.1 The diagram of the experimental device

1--coil 2--vacuum vessel

3--electron gun 4--Ti-target

We use two identical BF-3 neutron detectors No.1 and No.2 located at different positions and a neutron dosemeter to detect the fusion neutrons and a NaI(Tl) crystal scintillation counter to monitor the gamma--ray emission (see Fig.2). The detectors are calibrated by a Ra--Be neutron source and Cs-137 radiation source, respectively. The calibration curve is shown in Fig.3.

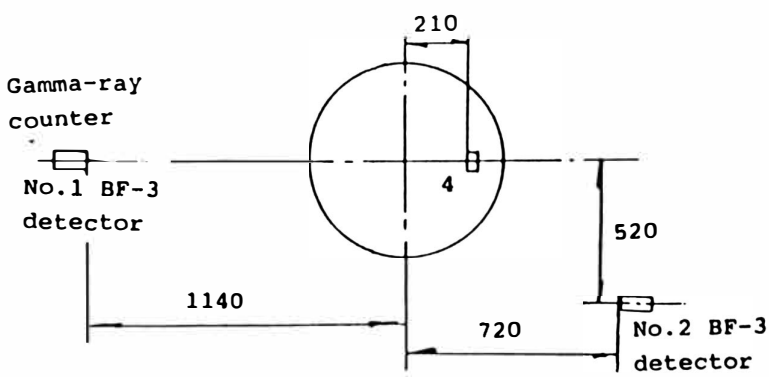

Fig.2 Arrangement of the detectors

III THE EXPERIMENTAL RESULTS

The experiments last for 30 days and some results obtained are as follows:

(1) The electron beam current is 3 mA, electron energy is 1 kev, negative voltage on the target is 8-10 kv. After having implanted deuterium for nine hours, the burst neutron emission is observed and lasts for 2-3 min.. The neutron count rate is corresponding to 9.5E+4 neutron/sec (see Fig.4-1).

(2) The implanting deuterium conditions are ditto. Three hours later, the burst neutron signal appears and its count rate is corresponding to 6.5E+5 neutron/sec. The duration of neutron emission is about 10 min. (see Fig.4-2).

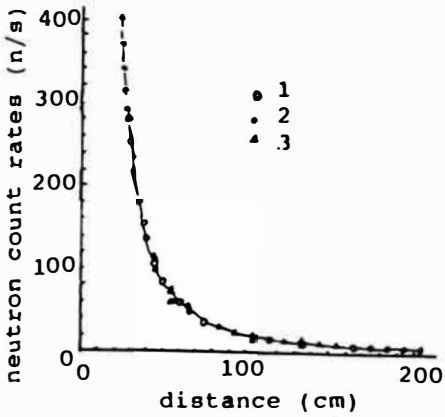

Fig.3 The calibration curve of BF-3 detectors
1--calculated value
2- and 3- show the count rates collected by No.1 and No.2 detectors, respectively.

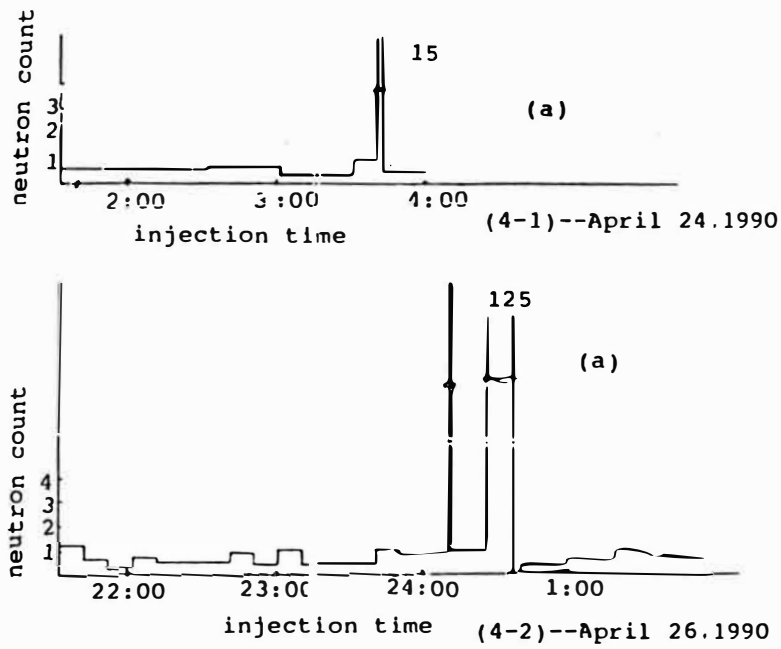

Fig.4 Variation of neutron count rates with the time of deuterium injection
The dashed line indicates the average background rates, it's about o.8 count/sec
(a) and (b) show the results measured by the No.1 and No.2 detectors, respectively.

(3) Implanting erium ions for three hours, the count rates of No.1 and

No.2 detectors are corresponding to 5E+5 and (1-5)E+5 neutron/sec, respectively. They are shown in Fig.4-3

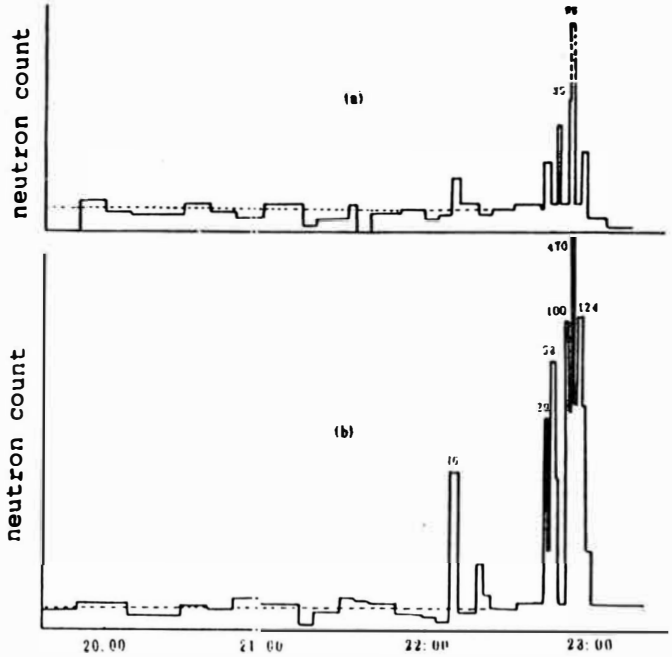

injection time (4-3)--April 29,1990

(4) After having implanted deuterium for three and a half hours, the BF-3 counters show the peaks of count.(See Fig.4-4). The No.1 and No.2 detector count

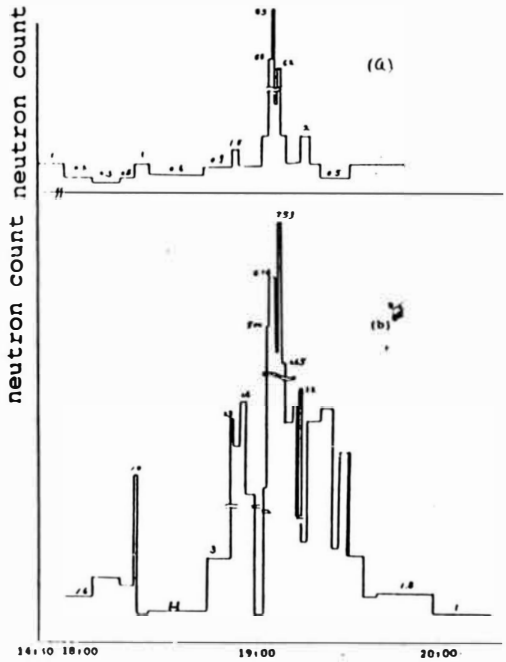

injection time (4-4)--April 30,1990

are corresponding to 5E+5 and 8E+5 neutron/sec. respectively.

(5) In above mentioned experiments, we have never detected gamma--ray count beyond background level.

During the experiments, we change parameters of electron beam, target voltage and ambient pressure etc. to observe the variation of neutron emission. As a result, the higher the parameters the more easily the neutron emission is induced. Once the neutron bursts, its count rate will be very high and then will come back to the background level immediately no matter whether the parameters of operation are still to be maintained at the original value.

IV DISCUSSION AND CONCLUSION

The neutron signals obtained in our observation are different from the neutron sighals obtained by beam--target intereactions.

The discussion is as follows:

When the high negative voltage is held at the target the backgroound count rate is 0.8 neutron/sec which is corresponding to (1-5)E+4 neutron/sec. But when the high negative voltage is removed from the target, the background count rate decreases to 0.5 neutron/sec. So we can consider the neutron count coming from beam-target reaction. The beam--target intereaction has certain relation between neutron signals and beam current and energy. In our measurements, the neutron bursts are uncertain in creating time and count rate. The neutron burst can only be observed after deuterium is injected for several hours,i.e. deuterium infused into the Ti-target is accumulated to a certain level. Thus a conclusion can be drawn that "fusion" can be induced only at the deuterium (or deutron) in the lattice reaches a certain level. Then the neutron emission characteristic of existance of nuclear fusion can be detected.

REFERENCE

[1] M. Fleischmann, S. Pons and M. Hawkins, J.Electronal.Chem., 261,P.301,(1989)

[2] S.E. Jones et.al., Nature, 338,P.737(1989)

Conference Proceedings Vol. 33
«The Science of Cold Fusion»
T. Bressani, E. Del Giudice and G. Preparata (Eds.)
SIF, Bologna 1991

ANOMALOUS NUCLEAR EFFECTS IN DEUTERIUM PALLADIUM SYSTEMS

JIN Shangxian, ZHANG Fuxiang, YAO Decheng and WU Bailu

Graduate School, Academia Sinica, Beijing 100039, PRC

ABSTRACT

Intense bursts of charged particles far larger than background have been reproducibly detected for the first time by using CR-39 solid state nuclear track detector during ether a high voltage discharge between deuterated palladium electrodes or a non-equilibrium out-diffusion of deuterons in palladium. No any anomalous effects were found in the control experiments of Pd-H system under the same experimental conditions. This indicates that some anomalous nuclear effects were definately produced in the Pd-D system under certain conditions.

Since Fleischman and Pons[1] and Jones et al[2] reported that nuclear fusion of deuterium occurred at room temperature in Pd or Ti cathodes during the electrolysis of heavy water(D_2O) much effort has been made to replicate or reinvestigate the possibility of cold fusion in solid matter[3].

Our calculation showed[4] that D-D fusion rate in the equilibrium Pd/D system at normal temperature will never reach the level that can be measured experimentally. It, however, is possible to produce a measurable nuclear fusion if some non-equilibrium processes were occurred in the Pd/D system spontaneously or externally.

1). One of the way to produce nonequilibrium process in Pd/D system is a high voltage discharge between deuterated Pd rods. It has been reported[5] that spontaneous neutron emissions were intermittently detected from activated Pd rods well soaked with deuterium gas by stimulasion of the Pd rods with a high voltage discharge. Here, we report a new evidence of anomalous nuclear effects in Pd/D system. A large number of nuclear tracks has been reproducibly detected for the first time by using CR-39 solid state track etch detector during the discharge experiments.

The schematic arrangement of the experimental system is shown in Fig. 1. The discharge tube is a glass tube of 35mm diameter and 400ml volume with a pair of Cu electrodes stems. The palladium(99.9%) rods of 2.5mm x 30mm were fixed to the Cu electrode stems. The purity of deuterium gas was 99.9%. The CR-39 track-etch detectors which were used to detect charged particles and neutrons were stuck to inner and outer wall of the glass tube. In order to activate the Pd rods, 5-10Kv,DC or AC,50Hz was applied between the electrodes in the vacuum of 10^{-4} torr. After the activation, the tube was filled with D_2 of 1 atm.

The activated Pd rods began to absorb the deuterium

gradually with time and the inner pressure of the tube decreased. A typical time variation of D_2 pressure in the discharge tube is shown in Fig.2. The pressure showed a few Plateau region at different pressures. No obvious charged particle or neutrons were detected during the absorption process.

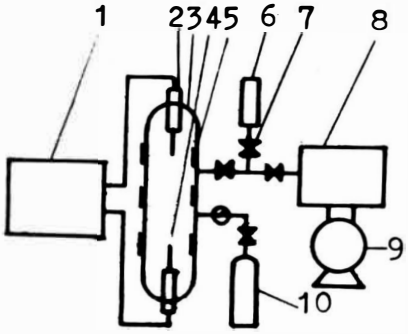

Fig.1. Schematic diagram of the experimental arrangement.
1-AC and DC high voltage supply,2-Cu stem,3-Glass tube,4-Pd rod,5-CR-39 6-Vacuum gage,7-Valves 8-Diffusion pump,9-Rotary pump,10-D_2 tank.

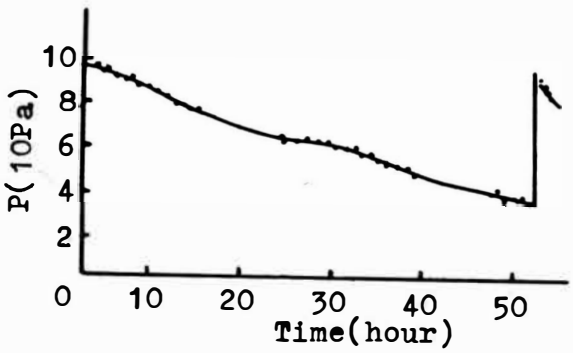

Fig.2.Time variation of D_2 pressure in the tube during the absorption process.

Stimulation of Pd rods with high voltage discharge was applied when the inner pressure of the tube was in the second plateau region after 2 to 3 days absorption. The CR-39 were then taken out and etched(6.8 mol NaOH + 4% alcohol 60°C)for 13 hours and observed in the microscope.

A photo of the nuclear tracks on the CR-39 stuck to inner wall of the tube in a typical discharge experiment is shown in Fig.3. The average number of the tracks on this CR

-39 is $\sim 2x10^3/cm^2$ and $>10^5/cm^2$ in the dense region. The nuumber density of the tracks on the CR-39 stuck to outer wall of the tube is $\sim 3x10^2/cm^2$, far less than one detected at the inner wall. This indicates that a large number of charged particles were produced during the discharge. In order to check the reproducibility, we conducted approximately 10 experiments with the same procedure and all showed similar results

The same experiments were performed with hydrogen gas instead of deuterium and no anomalous effects were observed . Also no any anomalous phenomina were found in the control experiments of D-Cu and D-Pd(no soaked with deuterium) systems.

Fig.3. Micrographs of the tracks of charged particles on the CR-39 in one of the typical discharge experiment of the Pd/D system.

2). The other way to induce non-equilibrium process in Pd/D system is a controlled out-diffusion of deuterons in palladium developed by Yamaguchi and Nishioka. They reported that[6] a gigantic neutron burst of $(1-2)x10^6/s$ had been detected from deuterated Pd plates with hetrostructures set in a vacuum chamber. We attempted to look for charged particle reaction products in the similar experiment and a large number of nuclear tracks have been reproducibly detected by using CR-39.

In our experiment, a 10nm layer of Mn and O was deposited on one of surface of a pure Pd film(10mm x 10mm,thi-

ckness=.09mm) and the film was loaded with D_2 gas(99.9%,10^5 Pa) for 24 to 48 hours. A 100nm thick of Au film eas then deposited on the other surface of the Pd film. A CR-39 detector was stuck to Mn-O film side and the sample was then placed in a stainless-steel chamber and evacuated to 10^{-3} Pa. After about two hours, the sample was taken out and etched. A photo of nuclear tracks on the CR-39 is shown in Fig.4. The average number density of the tracks is $\sim 3x10^3/$ $/cm^2$ and $> 5x10^5/cm^2$ in the dense region. No any anomalous effects were found in the control experiment of Pd-H system.

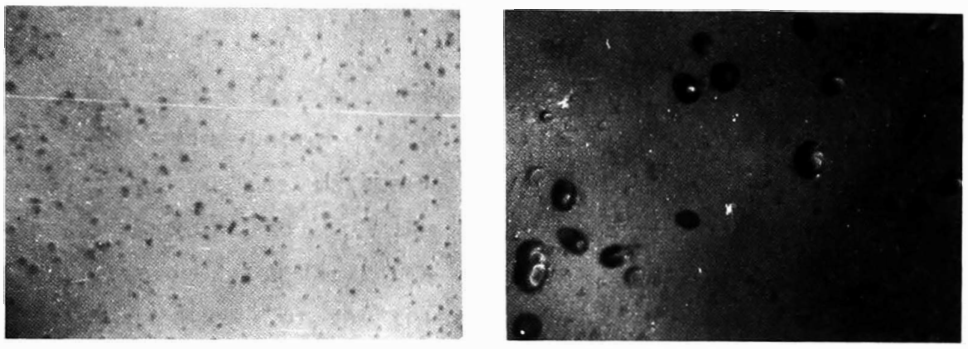

x100 x400

Fig.4. Micrographs of the tracks of charged particles on the CR-39 in one of the nonequilibrium out-diffusion experiment.

We coclude that some anomalous nuclear effects were definately occurred in the Pd/D systems during a high voltage discharge or a non-equilibrium out-diffusion processes.

REFERECES

1. M.Fleischman and S. Pons,J.Electroanal. Chem. 261(1989).
2. S.E. Jones et al, Nature 338(1989)737.
3. "Proc. of Anomalous Nuclear Effects in Deuterium/Solid Systems Conference",Brigham Young Univ.,Oct. 22-24,1990.
4. S.X.Jin et al,Science in China(Series A),34(1991).
5. N.Wada & K.Nishizawa,Jpn.J.Apl.Phys. 28(1989)L2017.
6. E.Yamaguchi & T.Nishioka,Jpn.J.Apl.Phys. 29(1990)L666.

Conference Proceedings Vol. 33
«The Science of Cold Fusion»
T. Bressani, E. Del Giudice and G. Preparata (Eds.)
SIF, Bologna 1991

Tritium production resulting from deuteration of different metals and alloys

F. Lanza, G. Bertolini, V. Vocino, E. Parnisari, C. Ronsecco

Commission of the European Communities, Institute od Advanced Materials, Ispra site, Ispra-21020, Italy

Abstract

Previous experiments have shown that tritium is produced in deuterated titanium. To define better the phenomenon a series of tests have been performed using various metals and alloys and different deuterating conditions. Sheets and shavings of titanium, zirconium, hafnium, tantalum, Zircaloy 2 and Ti-Zr 50% alloy have been tested.

A statistical analysis of the tritium production shows that significant differences are obtained varying the type of metal used. Using pure metals the tritium production increases with the increase of the atomic number of the metal. Moreover higher productions of tritium have been obtained using materials of technical purity as tantalum, Zircaloy 2 and Ti-Zr alloy.

1. Introduction

A possibility of obtaining a cold fusion phenomena was suggested by Scaramuzzi (1) which detected, during a low temperature treatment of gas deuterated titanium shavings, emission of neutrons in bursts of high intensity. A successive analysis performed on the deuterated titanium shavings (2) has allowed to detect in some cases a production of significant amounts of tritium. Also in a study conducted at BARC (3) tritium production has been detected after deuteration of titanium sheets and chips.

In fact it appears that (4) tritium production represents today the strongest evidence of cold fusion events even if reproducibility is always lacking. In order to try to understand the causes of non-reproducibility of the tests we have performed a systematic analysis

of tritium production varying the type of metals and the deuteration conditions.

Up to now tests have been performed only on palladium and titanium. Titanium belongs to the group IVb which comprises also zirconium and hafnium. All the three metals forms hydrides having the same crystallographic habit. In view of the similarity existing between these three metals it appears reasonable to extend the investigations also to zirconium and hafnium. Titanium and zirconium having a purity 99.99% has been used while hafnium has a purity of 97% containing also 2.7% of zirconium. In addition it was decided to test also tantalum which presents a large deuterium solubility (5) and do not form hydrides at temperatures higher than 42°C. The tantalum was of technical purity. Finally some tests on Ti-Zr 50 at.% alloy and on Zircaloy 2 were also performed.

A parameter which appears to be important is the deuterium stoichiometry. For the tests performed using heavy water electrolysis it is usually assumed that a high deuterium content is needed to obtain positive results. The influence of stoichiometry has been investigated on zirconium and tantalum in order to cover the case of deuterides formation and pure solubility.

Finally another parameters that will be taken into consideration is the isotopic enrichment of the deuterium gas.

2. Experimental

To verify if in an experiment tritium has been really produced it is necessary to analyse not only the deuterated metal samples but also the starting deuterium gas and possibly the residual gas which is present in the autoclave after the deuteration. A system has been set up which allows to determine the tritium content in the gas and in the deuterated metals (6).

The analysis of deuterium in the metals is performed degassing the hydrides at 1000°C for six hours in a flow of pure helium. The gas mixture is sent through a tube filled with CuO held at 420°C where the hydrogen species are oxidized to water vapor. The helium, acting as a carrier, transports the water vapor to a trap, cooled by liquid nitrogen. The collected water is then counted in a liquid scintillation spectrometer. The liquid scintillator used is the Tricarb 1400 produced by Packard Instrument Co. The cocktail Pico Fluor LLT, specific for

measurement of low levels of tritium in pure water, has been used. The counting efficiency has been obtained using a tritium standard. The analysis of the tritium contained in the deuterium gas is conducted in a similar way.

The tests were conducted using a selected deuterium having a mean tritium content of 9.5 Bq/g.

An attempt has been made to measure also the possible neutrons emission. The detection system was composed by 16 detectors 1 meter long filled with ^{3}He acting as proportional counters. The detectors were situated in six polyethylene slabs 10 cm thick which act as a neutrons moderators. Only the pulses corresponding to the peak around 764 Kev has been counted in order to minimize the influence of the electrical disturbances.

The six slabs are surrounding the deuteration furnace. In this configuration, using a ^{252}Cf source, the total efficiency measured is 13%.

The deuteration system consists of an autoclave which is connected to one side to a vacuum system and to the other to the deuterium gas bottle and to a calibrated gas reservoir. A tritium analysis on the deuterium collected in the gas reservoir was performed every deuteration in order to compare directly the tritium contained in the feed gas to that contained in the metal. For each type of metals or alloy a blank test using hydrogen was performed. The details of the deuteration procedure are given in ref. (7).

The influence of isotopic composition was examined performing some additional tests with a series of deuterium bottles, produced by C.I.L., having a deuterium enrichment of 99.8, 99.9 and 99.98%. Their tritium content was also around 10 Bq/g. Some tests were performed using deuterium-hydrogen mixture containing 5 and 10 vol.% of hydrogen.

3. Results and discussion

The blank tests performed using hydrogen to impregnate the different metals and alloys above mentioned did not show any tritium production. In the test performed using deuterium the amount of tritium produced was low and the scattering of the data rather high.

Of the different variables investigated the nature of the metal matrix seems to be predominant. A statistical analysis of the tritium produced in the different matrix has been performed. We will consider the tritium production indicative when it is higher than three times the

corresponding standard deviation (σ) and significant when it is higher than five times the σ . In table I are given, for the different metals, the number of tests which comply to these criteria together with the total number of tests.

A further analysis has been performed evaluating the mean value and the standard deviation of the tritium produced in all the tests performed using the same metal or alloy. In table II are shown the obtained values. On the same table is also given a significance factor corresponding to the ratio of the mean value to the standard deviation.

Observing the data of the two tables it appears that both comparisons give the same indications which is a signal that possible accidental errors do not play an important role.

TABLE I: Tests showing indicative and significant tritium production

Material	$T > 3\sigma$	$T > 5\sigma$	N° of tests
Titanium	2 (29%)	-	7
Zirconium	3 (27%)	1 (9%)	11
Hafnium	4 (44%)	1 (11%)	9
Tantalum	9 (75%)	4 (37%)	12
Ti-Zr 50 at%	11 (79%)	4 (29%)	14
Zircaloy 2	3 (100%)	1 (33%)	3

TABLE II: Tritium content: statistical evaluation

System	mean value Bq/g	sign. fact.	N° of tests
Titanium	0.26 + 0.161	1.61	7
Zirconium	0.55 + 0.125	4.40	11
Hafnium	0.72 + 0.147	4.90	9
Tantalum	2.13 + 0.154	13.83	12
Ti-Zr 50 at%	1.64 + 0.105	15.61	14
Zircaloy 2	1.78 + 0.263	6.77	3

The comparison between pure metals show that the tritium production increases with the increase of the atomic number. This is valid also for hafnium even if the metal used contained 2.7% of zirconium.

The materials of technical purity, tantalum and the two zirconium alloys, show a tritium production which is significantly higher than that obtained using pure metals. If we compare the tritium produced in our tests using pure titanium with those reported by Scaramuzzi (9) which uses a titanium alloy, the same effect appears. It has to be noted however that even for technical metal the data are largely scattered. It cannot be excluded that such a high scatter is due to the different distribution of impurities in the different metal sheets.

The samples treated with deuterium of high isotopic purity did not show a significant difference in the tritium production. On the contrary tests performed with 5 and 10% hydrogen-deuterium mixture showed no tritium production.

Stoichiometry did not appear to have any influence.

Neutron counts, during and after deuteration, did not show any difference in respect to background. Assuming that the possible neutron production is equal or lower than the standard deviation of the background and that tritium production arrives during deuteration we obtain a detection limit for the neutron to tritium ratio which is $3*10^{-6}$.

References

1. A. De Ninno, A. Frattolillo, G. Lollobattista, L. Martinis, M. Martone, L. Mori, S. Polda, F. Scaramuzzi: Europhysics Letters 9 (1989) 221-224
2. F. D'Amato, A. De Ninno, F. Scaramuzzi, P. Zeppa, C. Pontorieri, F. Lanza: First annual conference on cold fusion, Salt Lake City, Utah, March 1989
3. P.K. Iyengar: Fusion technology, 18 (Aug. 1990) p. 32
4. D.H. Worledge: First annual conference on cold fusion; Salt Lake City, Utah, March 1990
5. W.M. Muller, J.P. Blackledge, G.G. Libowitz; Metal hydrides; p. 599, Academic Press (1968)
6. F. Lanza, E. Parnisari, G. Ronsecco: EUR 13367 EN (1991)
7. F. Lanza: to be published as EUR report
8. T. Bressani, E. Del Giudice, G. Preparata: Proc. of the workshop Understanding cold fusion phenomena, Varenna, Italy, (Sept. 1989)
9. A. De Ninno, A. Frattolillo, F. Lanza, C. Pontorieri, F. Scaramuzzi, P. Zeppa: this conference

Conference Proceedings Vol. 33
«The Science of Cold Fusion»
T. Bressani, E. Del Giudice and G. Preparata (Eds.)
SIF, Bologna 1991

TIME-CORRELATED NEUTRON DETECTION FROM DEUTERIUM LOADED PALLADIUM

T.Tazima, K.Isii, and H.Ikegami.

National Institute For Fusion Science, Nagoya, 464-01, Japan

Abstract: Significant neutron bursts and good time-correlation between two independent neutron detection systems were observed in two kinds of experiments on cold fusion. One employed two palladium rods of 2 mm diameter and 5 cm length, deuterated under 1 atm for 30 days, and plasma discharge was applied as a trigger. The other was palladium shavings of 10 g deuterated under 11 atm for 40 days. The averaged background level was 5-6 counts/dwell time (100 s). In both cases, significant neutron emission of successive bursts of 13-60 counts/100 s were observed for several hours and repeated several times during 2-11 days in some cases.

INTRODUCTION

Since firstly reported on cold fusion[1,2], most of gas phase experiments employed titanium[3,4] and not much is reported on neutron emission due to the cold fusion from deuterium gas loaded palladium. In the case without any shielding of cosmic ray background, studies were made to generate large neutron bursts from deuterium gas loaded palladium.

It is widely believed that the reduction of neutron background levels is critical, however as shown in the present paper, one can observe large neutron bursts if a dwell time is properly chosen. In a too long case, those rare bursts are buried in the background level, which may lead to conclude lower background level. In a too short case, those bursts are decomposed into frequent one- or two- neutron events like random emission.

EXPERIMENTAL SET-UP

Figure 1 shows an experimental set-up. We tested two kinds of experiments. One(Exp.I) employed two palladium rods of 2 mm diameter and 3 cm length facing each other located in a glass chamber of 500 cc volume. The chamber was initially filled with deuterium gas of 1 atm

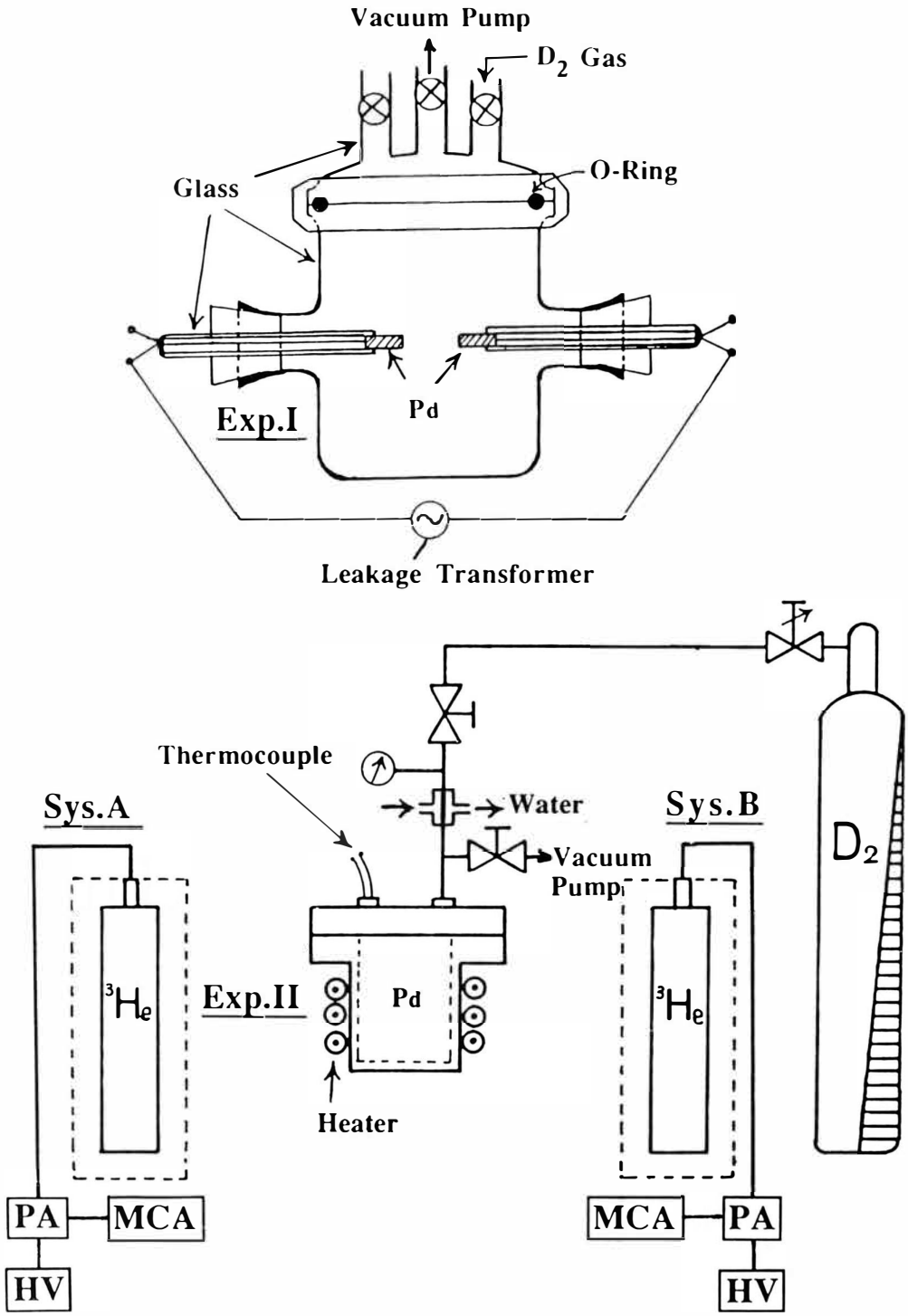

Fig.1 Experimental Set-up.

pressure which was reduced down to 0.54 atm after 30 days with absorption of deuterium into palladium. The estimated ratio of deuterium atoms to palladium atoms was 0.92. We applied AC plasma discharge two times for 5 min.(60 Hz, max.15 kV, max.20 mA) as a trigger for the cold fusion[5].

The other(Exp.II) employed palladium shavings of 10 g weight in a small ss chamber, of which thickness, width, and length were ≈0.3 mm , ≈1. 3 mm, and 3-6 cm, respectively. Deuterium gas of 11 atm pressure was mainly filled but many thermal cycles were tried to activate palladium surface for 40 days. The typical cycle after activation was as follows, i.e.

11 atm -> evacuation(≈10^{-2} Torr) -> 11 atm(max.40 °C up)
-> 5.7 atm after 2 hrs -> 11 atm -> 9.3 atm after 10 hrs
-> evacuation(≈10^{-2} Torr)

We thought above final evacuation was the trigger for the cold fusion.

In order to confirm that signals are originated from the deuterated palladium, two independent sets of neutron counter employing ^{3}He tubes, were located to check time-correlation between the bursts detected by these counters. We called these as Sys.A and Sys.B. The tube of Sys.A had 5 cm diameter, 40 cm length, and 8 atm pressure, and that of Sys.B had 2.5 cm diameter, 30 cm length, and 9.9 atm pressure. Both were housed in paraffin moderators. The respective distances from the center of the chamber were 25 cm and 22 cm, so that efficiencies were approximately 1 % and 0.5 % when calibrated by ^{252}Cf. The pulse height windows were set at best to eliminate spurious signals. The dwell time was 100 sec in most of the cases. The counts were recorded in each multi-channel analyzer.

EXPERIMENTAL RESULTS

Figure 2 shows neutron counts in Exp.I. No neutron burst had been observed during deuterium loading and discharge phase, but first group of neutron burst was observed 2 days after the discharge. Three groups of successive bursts appeared during 11 days after the discharge.

We can see good time-correlation between the neutron bursts detected by Sys.A and Sys.B. Since the ratio of signal levels of Sys.A to those of Sys.B corresponds to that of each efficiency, signal should be originated from deutrated palldium.

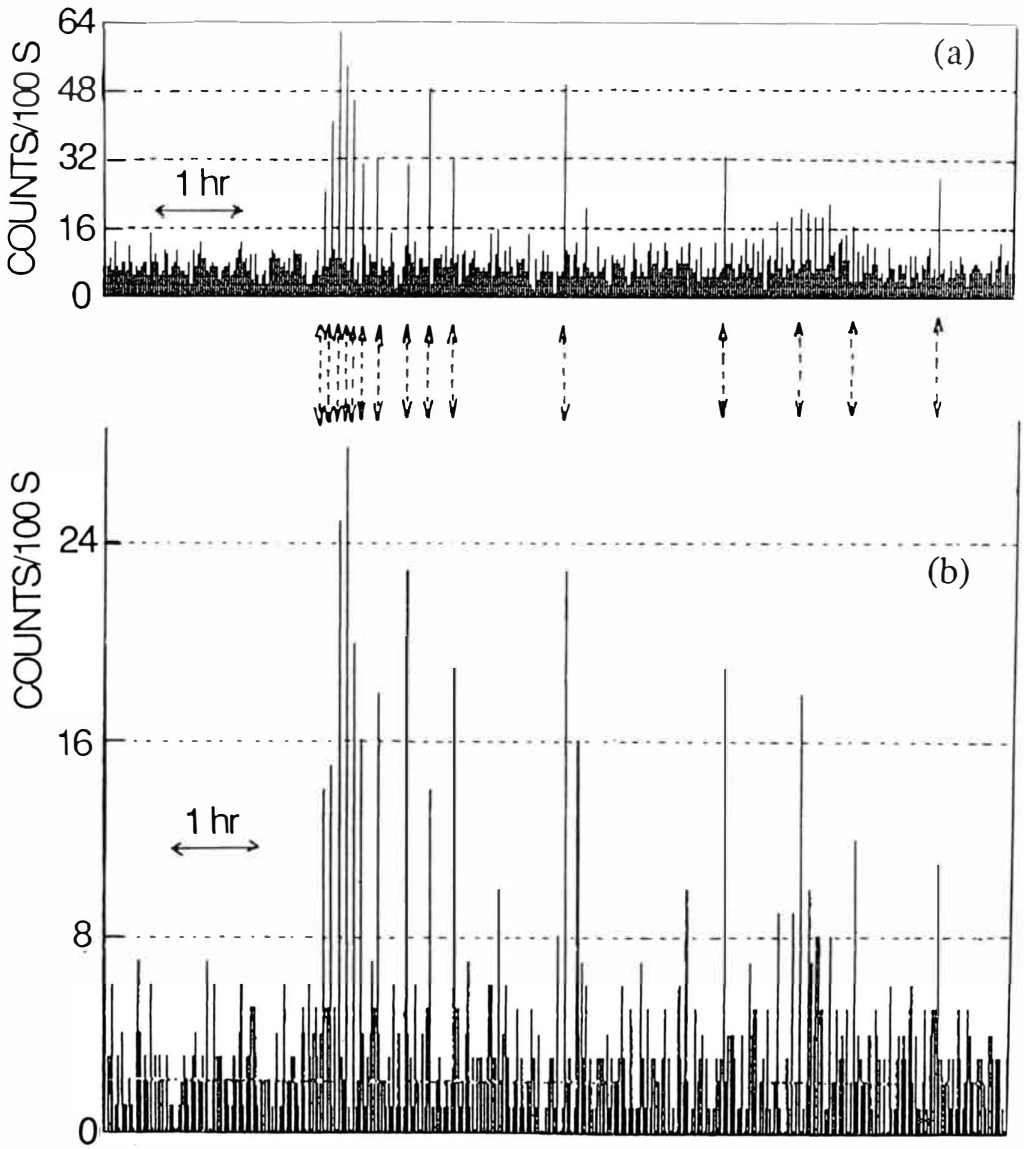

Fig.2 Neutron Bursts in Exp.I(6-8 Spt.1990) Measured with (a)Sys.A and (b)Sys.B

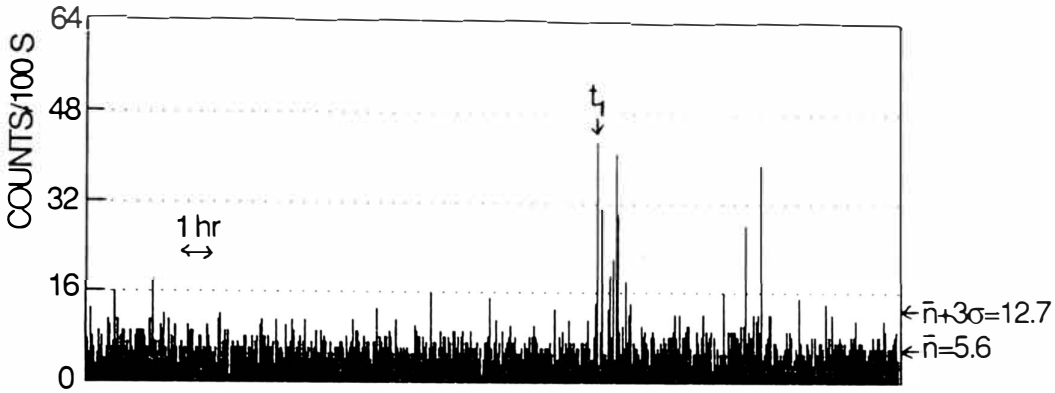

Fig.3(a) Neutron Bursts in Exp.II Measured with Sys.A(4-5 Feb.1991).

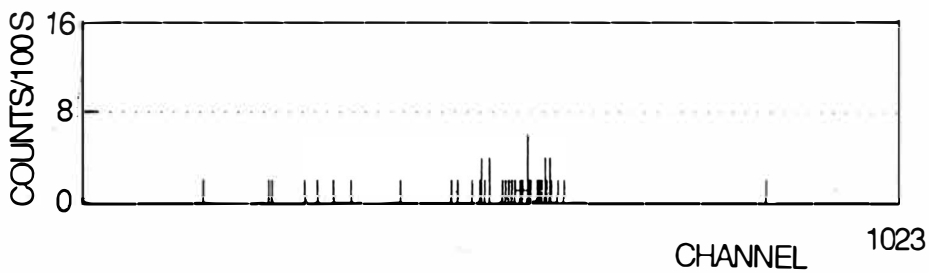

Fig.3(b) PHA at time t_1 in Fig.3(a).

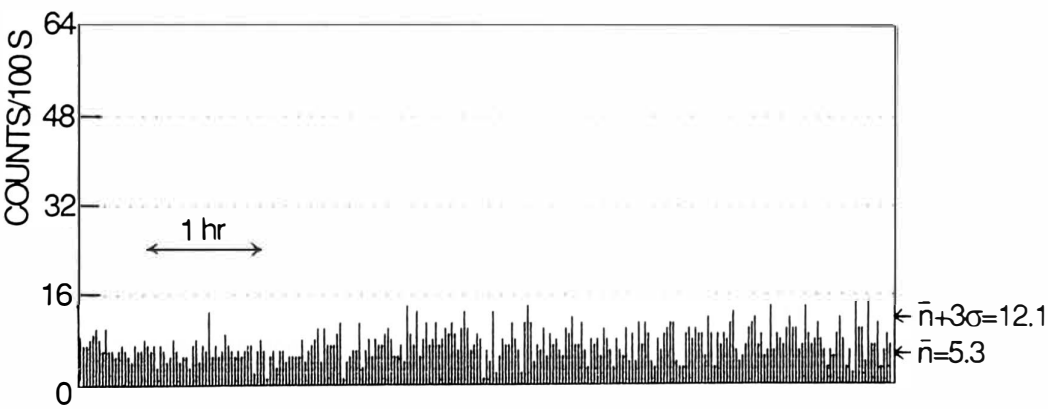

Fig.4 Background Signals Measured with Sys.A(7 Feb.1991).

In Exp.II first group of the neutron bursts appeared within one hour after evacuating started as shown in Figure 3(a). The neutron bursts of 24 channels had been observed among 2000 channels of MCS(i.e. 54 hours). The maximum count was 42 when an average count $\bar{n}$ was 5.6 and $\bar{n}+3\sigma$ =12.7.

Figure 3(b) shows a typical PHA at the time of the maximum count of MCS. Most of pulses was caused by neutrons thermalized in the paraffin moderators surrounding the ^{3}He tube.

Two days after the experiment, we checked the background level as shown in Fig.4. The average count $\bar{n}$ was 5.3 and $\bar{n}+3\sigma$ =12.1.

CONCLUSIONS

(1) Even in the case of no shielding to reduce the background of which level was 5-6 counts/100 s, large neutron bursts of 13-60 counts/100 s from deuterium gas loaded palladium were detected when the neutron detector of 1 % efficiency was employed.

(2) The neutron bursts were composed of many short time bursts, so that MCS spectrum will change drastically with the chosen dwell time.

(3) Although many groups of the bursts lasting for 2-11 days were observed, no burst had been observed during triggering (plasma discharge or evacuating) and gas loading phases.

(4) The neutron bursts were reasonably time-correlated between the two independent detection systems, so that it is hardly conceivable that those signals were originated from some spurious sources.

(5) Mechanism of the cold fusion and major parameters to produce neutron are still open question, but in our case high deuterium concentration might be needed, for example the ratio of deuterium atoms to palladium ones should be higher than 0.9, and cold-worked palladium might be essential to attain such high ratio.

REFERENCES

[1] M.Fleischmann and S.Pons; J.Electroanal.Chem.261(1989)301.
[2] S.E.Jones, et al.; Nature 338(1989)737.
[3] A.De Ninno et al.; Europhys.Lett.,9(1989)221.
[4] H.O.Menlove et al.; J.Fusion Energy 9,4(1990)495.
[5] N.Wada and K.Nishizawa; Jpn.J.Appl.Phys.28(1989)L2017.

Conference Proceedings Vol. 33
«The Science of Cold Fusion»
T. Bressani, E. Del Giudice and G. Preparata (Eds.)
SIF, Bologna 1991

SEARCH FOR BETTER MATERIAL FOR COLD FUSION EXPERIMENT USING CR–39 DETECTOR

Ke L. Wang, Xing Z. Li, Shi Y. Dong, Shi C. Wang①, Da W. Mo
Cheng M. Luo, Qin R. Lin, Xiao D. Wu, Wei Z. Li
Yong F. Zhu, Ping L. Zhou, Lee Chang

Tsinghua University, Beijing 100084, CHINA

I. Introduction

It was noticed that most of the "cold fusion" experiments were using palladium or titanium just based on the first set of experiments [1], [2]. However, based on our own experience [3] the results of experiments depend heavily on each material. Even if for the same material, it seems that the performances of the materials from different manufactories are different. For example, the palladium film from Russia produced the greatest density of energetic charged particle tracks.

It was also noticed that some surface processes might affect the performance as well. For example, the cleaning by aqua regia might introduce a deep layer of chlorine on the palladium surface and deteriorate the performance.

It is natural to raise two questions: whether there is any better material for the "cold fusion" experiment? whether there is any surface process which may enhance the effect of cold fusion phenomenon?

In our first set of experiments the plastic track detector (CR–39) was proved to be a good tool to make a scrutiny of the materials and surface processes. CR–39 is very sensitive and efficient, we need only a little sample (several square centimeters of foil with thickness of 20~ 30μ) for the test. Therefore, in a small pressurized vessel (volume of 10 cubic centimeters) we might put 10 samples in it. This makes the scrutiny quicker and guarantees the same condition for a batch of

①Institute of High Energy Physics, Beijing 100039, CHINA

materials; hence, the comparison between different materials and different surface processes is easier. More than 200 samples were tested in about 20 runs of Frascati–type [4] experiments.

II. Experimental Arrangement

As described in Ref.[3], CR–39 plastic track detector were combined with Frascati–type gas–loading experiment to detect the energetic charged particles, which were supposed to be the token of the anomalous nuclear effect (cold fusion phenomenon). Preetching of CR–39 was done to distinguish the background tracks which were produced between the time it was manufactured and the time it was used in experiment. The control run was done to discriminate the effects due to radioactive impurities in the samples (e.g. uranium 238, radon's daughter et al.), or due to air borne radon, or due to cosmic rays. Dozens of different materials were tested. Most of them were palladium and titanium from various sources. We tested titanium alloys (e.g. V6–Al6–Sn2), silver, zirconium, nickel, lanthanum, cerium, niobium, rhenium, ceramic and hydrogen–storage materials (e.g. $LaNi_5$, TiFe) also. The palladium were from Russia, USA, Northeast China and Southwest China. They were in the shape of tube, foil, wire, powder, sponge, chips turnings and vapour deposit film.

Many kinds of processing were used to induce any possible effect. For example, we tried (1) annealing under high vacuum (500℃–1500℃); (2) irradiation by laser beam; (3) irradiation by neutron source; (4) irradiation by protons, or helium using tandem accelerator; (5) mechanical cold work; (6) surface cleaning by hydrofluoric acid.

III. Primary Results

The Russian palladium foil imported in 1950's gave the highest yield of charged particles. In average it is higher than 1000 particles per cm^2 per day. The Ti–662 alloy was not as good as Russian palladium; its yield was about several hundred particles per cm^2 per day. However, Ti–662 alloy had high repetition rate. Other materials did not give evident signals distinct from background, which was less than 100 particles per cm^2 per day.

The highest yield from Russian palladium foil was more than 10^5 particles / cm^2. Table 1 gives the results of 11 runs of experiments using Russian palladium foils.

Fig.1 Tracks from Russian Palladium Foil

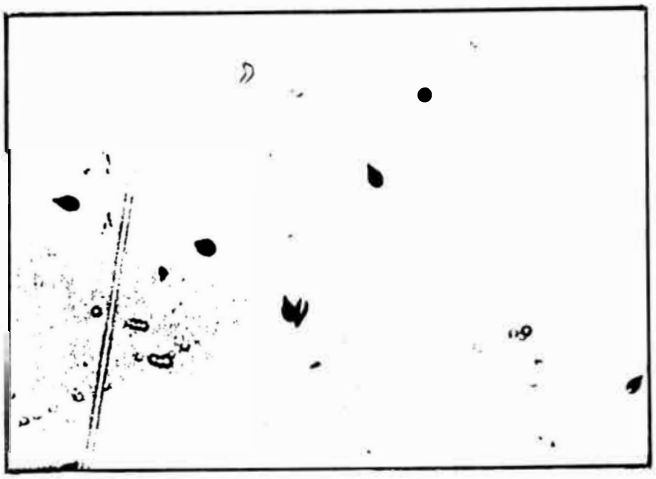

Fig.2 Tracks from Used Russian Palladium Foil

Fig.3 Tracks from American Palladium Foil

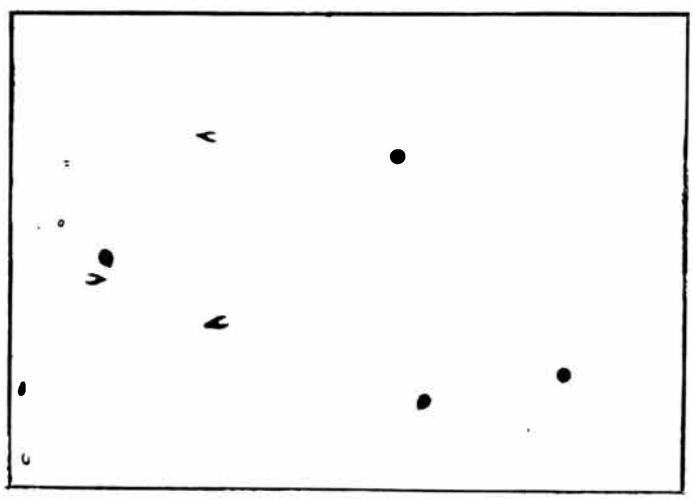

Fig.4 Tracks from Ti—662 Alloy Shaving

TABLE 1 Tracks in CR−39 (for Russian Palladium)

Run No.	Tracks (particles / cm^2)
1	10^5
2	1.1×10^3
3	1.6×10^5
4	10^4
5	3×10^3
6	100 (cleaned by aqua regia)
7	2×10^4
8	$> 10^3$
9	3.5×10^4(average)
10	2.7×10^4(average) ($2-4 \times 10^4$)
11	6.5×10^4(average) (Maximum 7.5×10^4)

The palladium foil from America (Johnson Matthey Inc.) produced similar charged particle density as that from Ti−662 alloy. The Chinese palladium wire gave a positive result of 2×10^3 particles / cm^2. The palladium foils from both Northeast China and Southwest China did not give any positive result.

The Russian palladium foil became worse after the first usage. It exhibited a decaying behavior. Fig.1 is a photo for CR−39 taken by microscope with a magnification of 150x. This CR−39 recorded the charged particles from the Russian palladium foil. Fig.2 is a similar photo, but the Russian palladium had experienced once in the previous D_2 gas−loading experiment. The density of charged particles reduced by an order of magnitude. Fig.3 is the similar photo for American palladium foil. Fig.4 is the photo for Ti−662 alloy foil. The contrast is very clear.

Using vapour deposit technique to plate the Russian palladium on another substrate did not give positive result. In fact we did not find any processing, which might enhance the positive result.

Ⅳ. Acknowledgements

This work is supported by Natural Science Foundation of China and the contingent research funds from the National Education Commission and Tsinghua University. Mr. Tang Lin's deep concern is gratefully acknowledged.

Reference

〔1〕 M.Fleischmann and S. Pons, J. Electroanalytical Chemistry and Interfacial Electrochemistry, Vol.261, 301 (1989).

〔2〕 S.E. Jones, et al., Nature, 338, 737 (1989).
〔3〕 X.Z.Li, et al., The Proceedings of Anomalous Nuclear Effects in Deuterium / Solid Systems (Provo, UT, 1990), Ed. S.E. Jones, F.Scaramuzzi, and D. Worledge (AIP, New York).
〔4〕 De Ninno, et al., Europhysics Letters, Vol.9, 221 (1989).

Conference Proceedings Vol. 33
«The Science of Cold Fusion»
T. Bressani, E. Del Giudice and G. Preparata (Eds.)
SIF, Bologna 1991

IDENTIFICATION OF THE ENERGETIC CHARGED PARTICLES IN GAS–LOADING EXPERIMENT OF "COLD FUSION" USING CR–39 PLASTIC TRACK DETECTOR

Shi C. Wang*, Tie S. Kang*
Ke L. Wang, Shi Y. Dong, Yu Y. Feng, Da W. Mo, Xing Z. Li

* Institute of High Energy Physics, Beijing, 100039, China
Tsinghua University, Beijing, 100084, China

I Introduction

Since observation of "cold fusion" was claimed in 1989, a great number of experiments have been done for verifying these claims [1–4]. Most of laboratories were not able to reproduce the observations and among the results of experiments there are obvious inconsistencies. It has been realized that even if the "cold fusion" happened, its signals would be quite weak. Thus for sake of confirming the presence of "cold fusion", it is desirable to use detection techniques which have high collecting power, low background and can stably work for long time. CR–39 plastic track detector is able to work in passive and time–integrated modes and has a number of unique merits in comparison with electronic detectors. In gas–loading experiment, if a piece of CR–39 film is clamped on the surface of a metal foil of Pd or Ti, charged particles emitted by deuterated metal can be collected by the CR–39 foil with 2π solid angle. The information on charge, energy, location and direction of the emitted particles can be determined from track parameters.

In the present work, CR–39 plastic films (Track Analysis Systems Inc. Bristol, United Kingdom) have been used for searching for charged particles from deuterized Pd and Ti foils. The effects of high pressure D_2 gas and low temperature on response of CR–39 have been studied and background levels of charged particles from several sources have been estimated. A procedure for identification of nuclear charge of particles has been developed and preliminary result of charge identification was given.

II The response of CR–39 to light charged–particles

The nuclear charge and incident kinetic energy can be determined for particles which come to rest in CR–39 by measuring two parameters, range and sensitivity (S). To identify a charged particle, one needs relating the two parameters to the charge Z and energy E of the particle. We define $S = V_t / V_g$, where V_t is etch rate along the track. V_g is general etch rate. By means of calibration with α particles at known energies, the relation between S and dE/dx for a given CR–39 film and etching conditions can be obtained. A ^{252}Cf source and an ^{241}Am source were used for the calibration, α particles from the sources were slowed by Al foils to following energies: 6.1, 5.5, 4.5, 3.5, 3.0 and 2.0 MeV. CR–39 films were irradiated in 10^{-2} torr. vacuum and 25℃ with the α particles. Then CR–39 films were etched in 6.8N NaOH solution at 70℃ for 5 hours. The diameters of α tracks and fission fragment tracks from a ^{252}Cf source were measured at magnification of 1500x. The sensitivity S for α particle registration is given by:

$$S = \frac{1 + (D_\alpha / D_F)^2}{1 - (D_\alpha / D_F)^2} \times \frac{1}{\cos\phi} \qquad (1)$$

where

ϕ is the incident zenith angle of α particles.

D_α is minor mouth diameter of the surface ellipse of α track.

D_F is the diameter of etch pit of vertically incident ^{252}Cf fission fragment.

The range of α particles in CR–39 were calculated by the range–energy relation, given by Benton and Henke [5] . The result of a calibration of CR–39 film under condition of room temperature and 10^{-2} torr vacuum was shown in Fig.1

In D_2 gas loading experiment CR–39 detector is put in a cell filled with high pressure D_2 gas and then subjected to temperature cycles from 25℃ to −196℃ . The response of CR–39 detector may change with the environment. To mimic experimental condition as closely as possible, CR–39 films were also calibrated in following environmental condition. D_2 gas was filled into the high pressure cell to a pressure of 15 bar and immersed the cell in liquid nitrogen for 1 hour to allow sufficient time to cool the cell, and then removed it from the liquid nitrogen to allow it to warm up to room temperature in several hours. The cooling and warming cycle was repeated twice a day for 4 days.

CR–39 films were divided into two groups: one group was irradiated with α particles first, then was subjected to loading D_2 gas and temperature cycle. The another group was at first subjected to loading D_2 gas and temperature cycle, then irradiated with α particles. The relationship between S–1 and R for these two groups are given in Fig.1.

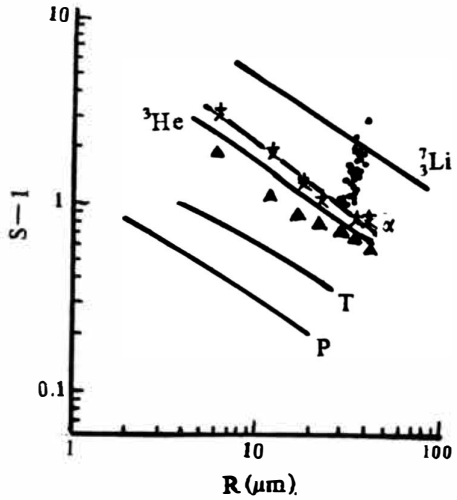

Fig.1 Response curves of CR−39 to α particles under three environmental conditions as well as the data of two runs of gas−loading experiment. The curves labelled "P", "T", "^{3}He" and "$^7_3$Li" were scaled from α particle curve.

▲ D_2 gas−loading and temperature cycle first, then α irradiation

× α irradiation first, then D_2 gas−loading and temperature cycle

\+ α irradiation in 25 ° and 10^{-2} torr vacuum.

• charged particles detected by CR−39 film on the surface of Pd or Ti foil.

The results show that for post−irradiation group the environmental condition of D_2 gas loading experiment has little effect on response of CR−39; in contrast, for pre−irradiation group, the environmental condition makes the S of CR−39 decreasing. Fortunately, the decrease of S is so small that identification of nuclear charge is still possible.

The restricted energy−loss model of track formation has been successfully used to describe etching behavior of charged particles in plastic track detectors. We used the expression in ref.6 to compute restricted energy loss (REL) for α particles used in this experiment. The relationship between S−1 and REL obtained with least−squares fit is

$$S - 1 = 1.36 \ \mathrm{REL}^{1.27} \tag{2}$$

Equation (2) can then be used to interpolate response for energies and for other light particles not specifically determined from our calibration. The predicted relations between S−1 and R for P, α, ^{3}He and $^7_3$Li were given in Fig.1. The results show that the calibration curves for Z = 1, 2 and 3 are wide apart separated. Thus it is possible to identify charge Z of light particles by measuring S and R in CR−39. The charge resolution depends on the error of measuring range R and sensitivity S.

III Estimation of background from several sources

Since signals of charged particles from deuterized Pd and Ti foil are very weak, it is important to know charged particle background. There are three types of charged particle backgrounds in CR−39, which are relevant to the present experiment. 1) α particle tracks emitted by nuclides such as ^{238}U and ^{232}Th series, present as impurities in CR−39 and Pd or Ti foils; 2) cosmic−ray spoliation tracks; 3) α−decay tracks due to airborne radon.

CR−39 film itself has accumulated background tracks from above−mentioned sources between the time it was made and the time it is used. A CR−39 film was etched in 6.8N NaOH solution at 70℃ for 8 hours. All tracks were counted. The density of tracks was found to be 114 tracks / cm^2. These kinds of background tracks can be reduced by preetching the CR−39 for 1 hour in 6.8N NaoH solution at 98℃ and by protecting the CR−39 film from airborne radon during the experiment.

Table1 Charged particle background measured by preetched CR−39 film

Place or material	The rate of production of background tracks(track / cm^2.day)
high pressure cell	5
open air in lab	6
Pd foil (30μm)	2
Pd foil (25μm)	1
Ti foil	1

By using preached CR−39 films, we have estimated the background levels in metal materials, high−pressure cell and laboratory environment. The results are given at Table 1. It is shown from Table 1 that, the background level from all possible sources should be less than about 20 tracks / cm^2day.

IV Identification of charged particle tracks from deuterized Pd and Ti foils

Pd or Ti foils and CR−39 film were stacked together in a sandwich−like structure and put in a stainless−steel cell attached to a source of D_2 gas. The cell was subjected to the same temperature cycle as above mentioned. Then, we etched the CR−39 films in 70℃ 6.8N NaOH solution in an interrupted way. After each etching process, we scanned CR−39 films at magnification of 150x to search for charged particle tracks and measured the track parameters at magnification of 1500x. For a track etched to the end of its range as in Fig.2, the quantities D_1, D_2 and R (and a knowledge of G) provide a pair of S and R [7] .

Etch pits of about 10^3 tracks / cm^2 density were found in 2 runs of 4 runs.

They are from a Pd foil and a Ti foil made in U.S.A. After etching for 8 hours we measured track parameters of 40 tracks. Their data of S and R are drawn in Fig.1. The data points locate between curves of Z = 2 and Z = 3.

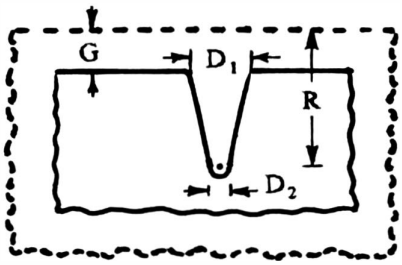

Fig.2 Etch pit of a normally incident particle of range R after removing a layer of thickness G. After a certain etch time, from the measurement of D_1 and D_2 and depth we calculate S and R.

V Discussion

The calibration using pre and past irradiation treatments of gas–loading experiments mimics the actual experimental condition only in some extents. In fact, the effect of environment takes place just during irradiation. So in order to identify charge Z more accurately, the response of CR–39 should be calibrated using α particle irradiation under the condition of high–pressure D_2 gas and temperature cycle.

Since a contamination of α particles occurs not very seldom, more experiments are under way to obtain more reliable results.

VI Acknowledgements

This research is supported by the Natural Science Foundation of China and the contingent research funds from the National Education Commission and Tsinghua University.

References

1. M.Fleischmann, S.Pons and M.Hawkins, J.Electroanal. Chem., 261, 301 (1989).
2. S.E.Jones et al., Nature (London), 338, 737 (1989).
3. P.B.Price, et al., Phys. Rev. Lett., 63, 1926 (1989).
4. R.Ilic′, et al., Nucl. Tracks Radiat. Meas. 17, 483 (1990).
5. E.V.Benton and R.P.Henke, Nucl. Instr. Meth. 67, 87 (1967).
6. G.Somogyi, et al., Nucl. Instr. Meth. 134, 129 (1976).
7. P.B.Price, Annu. Rev. Nucl. Part. Sci. 39, 19 (1989).

Conference Proceedings Vol. 33
«The Science of Cold Fusion»
T. Bressani, E. Del Giudice and G. Preparata (Eds.)
SIF, Bologna 1991

EVIDENCE OF NEUTRON EMISSION FROM A TITANIUM-DEUTERIUM SYSTEM

D.Seeliger, M.Bittner, A.Meister, R.Schwierz, T.Streil

Dresden University of Technology
Institute for Nuclear and Atomic Physics

INTRODUCTION

Recently, a considerable number of experimental investigations have been carried out in different laboratories to determine, whether a possible catalysis of deuterium-deuterium fusion processes in condensed matter takes place or not. In some papers evidence was found for a weak neutron production, similar as it was announced by Jones et al. [1] for the electrolysic of heavy water using Titanium cathodes. Some-what later the observation of neutron emission during the absorption of Deuterium gas in Titanium and other metals was announced, too [2,3].

The present paper describes experiments aimed at the replication of the results obtained in [2,3] for charging of Titanium with deuterons from the gas phase.

EXPERIMENT

The experimental arrangement was similar to that of De Ninno et al. [2]: In a sealed stainless steel vessel (length 75 mm, diameter 45 mm) 58 g of Titanium turnings are contained. The container can be evacuated by a vacuum pump and filled with definite portions of Deuterium gas through valves and pressure regulator. It can be heated up to about 400 degree Celsius by an electrical heater located outside of the vessel

and also cooled down to liquid Nitrogen temperature. Both the temperature and the gas pressure in the container can be measured during the experiment by means of sensors located inside of the vessel.

The neutron production is observed using the fast neutron spectrometer, described in the publications [4]. It consists of a NE 213 liquid scintillator (diameter 5 inch, height 1.5 inch) coupled to an XP2040 photomultiplier. The proton recoil signals are stored in 5 broad channel ranges ChR N1 .... N5 for getting an improved counting statistics of the very small effects. The channel ranges have the following proton recoil energy (PRE) bounds:

ChR N1:	threshold	. . .	0.85	MeV	PRE
ChR N2:	0.85 MeV	. . .	1.7	MeV	PRE
ChR N3:	1.7 MeV	. . .	2.95	MeV	PRE
ChR N4:	2.95 MeV	. . .	4.5	MeV	PRE
ChR N5:	4.5 MeV	. . .	6.0	MeV	PRE.

Signals from registration of single dd-neutrons are expected to occur in N2 and N3, the efficiency of registration of dd-neutrons is about 1.7% and 0.8% for the first and a second run, respectively.

The background can be determined before and after the effect measurements, but also in between of them, putting absorber materials between the vessel and the detector. In the present experiment all effect measurements were taken within equal 10 min. time-intervals.

The change of both temperature and pressure in the course of the first experimental run are shown on Fig. 1, together with the detector counting rates in the ChR's N2 ... N5. D_2-gas was added in small portions. Fig. 1 shows, that this Deuterium was absorbed by the Titanium turnings very fast and after every adding portions of gas the pressure falled down rapidly to an effective saturation pressure, which increases with increasing the total ammount of already absorbed Deuterium. The counting rates are shown in the lower part of Fig. 1. Of special interest are the counting rates in ChR's N2+N3.

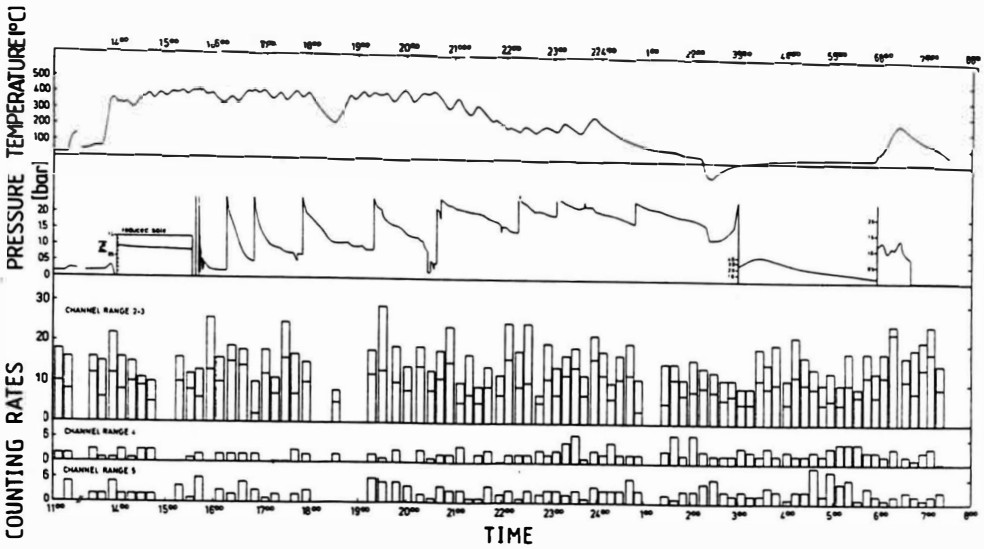

Fig. 1. Temperature, Pressure and Counting rates during the course of the first run.

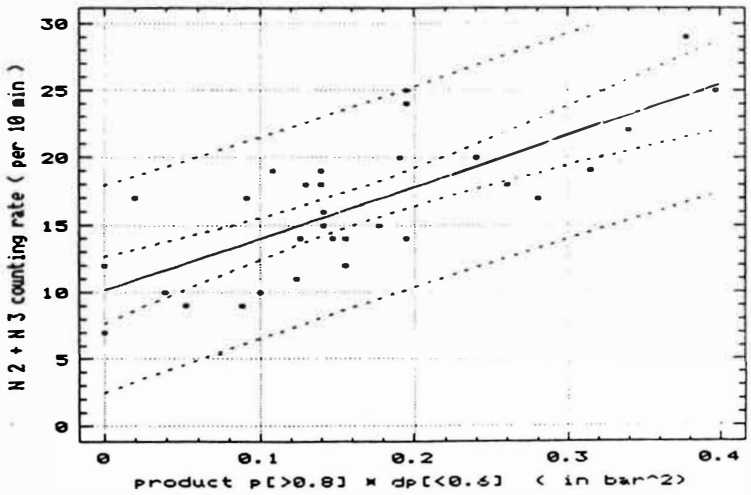

Fig. 2. Correlation analysis between the N2+N3 counting rates and the product p·dp.

We investigated, whether there is a correlation between the counting rate N2+N3 and the average gas pressure p, its decrease dp during the 10 min measuring interval or their product pdp. We found practically no correlation between the counting rate N2+N3 and the pressure p (correlation coefficient 0.018). The correlation with the pressure change dp is more pronounced (correlation coefficient 0.565). The most pronounced correlation appears between counting rates and the

product pdp. On Fig. 2 the corresponding analyses for restricted areas $p \geq 0.8$ bar and $0 \leq dp \leq 0.6$ bar are shown, giving a correlation coefficient of 0.742.

Both "effect" and "background" spectra are transformed in a counting rate difference versus proton recoil energy spectrum, averaged over 250 KeV PRE bins, see Fig. 3. The PRE spectrum obtained is in accordance with the expectation, that the origin of registrated difference counts could be signals from dd-neutrons having 2.45 MeV energy: The energy determined from the slope of the PRE can be estimated with $E_n = (2.65 \pm 0.25)$ MeV. There is also a weak, but statistically not significant indication for events with nearly the double dd-neutron energy.

In a second run using the same Titanium turnings but somewhat different geometry and procedures of changing both temperature and pressure the regression analysis of the measurements again shows, that there is no correlation of the counting rate with the pressure p (correlation coefficient -0.019) but a weak correlation with dp (correlation coefficient +0.239). The largest correlation coefficient is between the counting rate and pdp, however, it is only 0.363. This means, that correlations where less pronounced than it was observed for the first run.

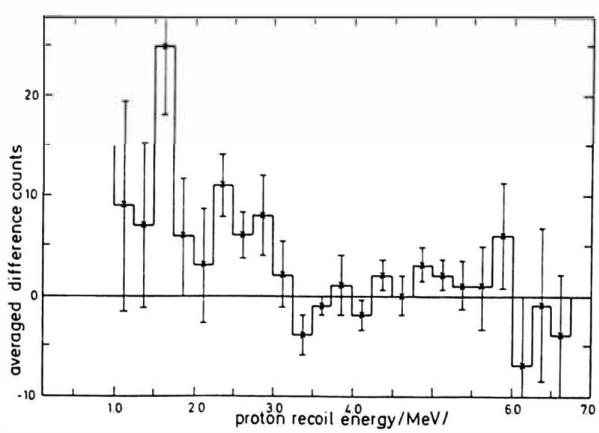

Fig. 3. Cummulative proton recoil spectrum after subtracting the background.

DISCUSSION AND CONCLUSIONS

In both experimental runs we have observed definite signs for a weak neutron production with a PRE spectrum, which corresponds to the assumption, that dd-neutrons have been detected. Following the paper of Jones et al. [1], the reaction rates should be expressed in terms of the fusion rate λ_{dd} per dd-pair and second. If we assume a full loading of the Titanium, corresponding to TiD_x with x = 2, the number of dd-pairs in the Titanium probe is equal to the number of Titanium atoms in it, which is equal to $7.28 \cdot 10^{23}$. The fusion rate obtained is $6.6 \cdot 10^{-25} s^{-1}$ or $2.67 \cdot 10^{-24} s^{-1}$, for the average and maximum effect, respectively.

However, we have seen, that there is no correlation between the reaction rate N_{dd} and the pressure p. This means that there is also no simple proportionality between N_{dd} and the number of deuterons absorbed in the sample! In opposite, the present experiment gives some indication, that the dd-reaction rate is gouverned by dp, that means by the particle flow into the metal per second. May be even more pronounced is the dependence on p·dp, that means to the product of already absorbed deuterons and the additional flow of particles through the surface. This would be qualitatively in accordance with a simple plasma model of dd-fusion processes in condensed matter, published recently [5]. However, direct quantitative application of this model in the present case is difficult, due-to the complicated surface-to-volume geometry of the titanium turnings.

REFERENCES

[1] S. E. Jones et al.,Nature 338 (1989) 737.

[2] A. De Ninno et al.,Europhys. Lett. 9 (1989) 221.

[3] H. O. Menlove et al., Report LA-UR-89-1974.

[4] M. Bittner et al., Fusion Technology 18 (1990) 120; Fusion Technology, July 1991, to be publ.

[5] D. Seeliger, A. Meister Fusion Technology, July 1991, to be publ.

Conference Proceedings Vol. 33
«The Science of Cold Fusion»
T. Bressani, E. Del Giudice and G. Preparata (Eds.)
SIF, Bologna 1991

OBSERVATION OF D-D FUSION NEUTRONS DURING DEGASSING OF DEUTERIUM LOADED PALLADIUM

M.Bittner, A.Meister, D.Seeliger, R.Schwierz, P.Wüstner

Dresden University of Technology
Institute for Nuclear and Atomic Physics

INTRODUCTION

Many experiments on charging palladium with deuterium, either electrolytically or by gas absorption, indicate a production of fast neutrons or other products of d-d fusion reactions accompanying the charging process under special, hitherto not fully understood conditions, see e. g. Ref. [1]. These results need further work towards experimental confirmation and understanding of underlying physical processes.

At the Dresden University of Technology after a first experiment confirming a very small neutron production during electrolytic charging of palladium cathodes with deuterium [2] further studies on the phenomenon of nuclear fusion in condensed matter are carried out, which systematically hint at a weak neutron production as a typical function of the period of charging [3].

The experiments described in this paper are designed to search for neutron events during the degassing of palladium samples charged with deuterium. Of special interest is the search for neutrons with an energy of 2.45 MeV, originated by the fusion reaction

$$d + d \longrightarrow n + {}^{3}He + 3.27\ MeV.$$

EXPERIMENT

In the present experiment two massive palladium samples are used, in which deuterium was stored. These samples are heated up on an electrical heating device in front of two neutron detectors. The measurements are carried out by short time runs of 10 minutes and alternating the sample under investigation between positions in front of both detectors. While with one detector the sample is observed, with the other detector the background counting rate for the empty position is registered. In this manner with two detectors the effect and the background counting rate are measured quasi-simultaneously for the whole period of the experiment.

For neutron detection and spectrometry two recoil proton detectors with 5-in.-diam.x1.5-in.-high NE-213 liquid scintillator coupled to XP 2040 photomultipliers are used. The pulse high spectra of these detectors are recorded by multichannel analysers. In some more detail the spectrometer is explained in a previous paper [3]. For an additional background reduction the experimental setup is surrounded by a shielding consisting of polyethylene and water of about 50 cm thickness.

The two cylindrical palladium samples Z6 (86.3 g) and Z8 (518.2 g) had been loaded cathodically with deuterium by heavy water electrolysis before the degassing experiment. The electrolyte was a solution of 1 M LiOD in heavy water enriched to 90 per cent in D_2O. The deuterium inventory in the samples is determined by weighing. From this follows an average ratio of D to Pd atoms of 0.74 ± 0.05 (Z6) and 0.80 ± 0.01 (Z8) after the electrochemical charging. Practically all deuterium leaved the samples during the degassing experiments.

The sample Z8 was degassed putting it on the already heated plate. The temperature measured after degassing on surface of the heating plate and on the top of sample Z8 was 375°C and 205°C, respectively. In a second experiment sample Z6 was degassed. But, this time starting at room temperature with switching on the heating device.

RESULTS

In Fig. 1 the counting rates during the periode of degassing sample Z8 are shown for two recoil proton energy intervals and both detectors. The hatched sections of the histograms indicate measurements with sample Z8 being in front of the detector, whereas the clear sections are counting rates for measurements with empty position in front of the detector. Both detectors indicate after starting the degassing in the energy range 1.9-3.3 MeV counting rates, which are significantly above the background . Later on, after the 13th run no difference between measurements with and without sample would be found. In the higher energy range 3.3-5.2 MeV no measurements indicate any difference between effect and background outside the statistical uncertainties. These results for sample Z8 give rise to the assumption, that neutrons occur within the sample for about 100 minutes after starting the degassing.

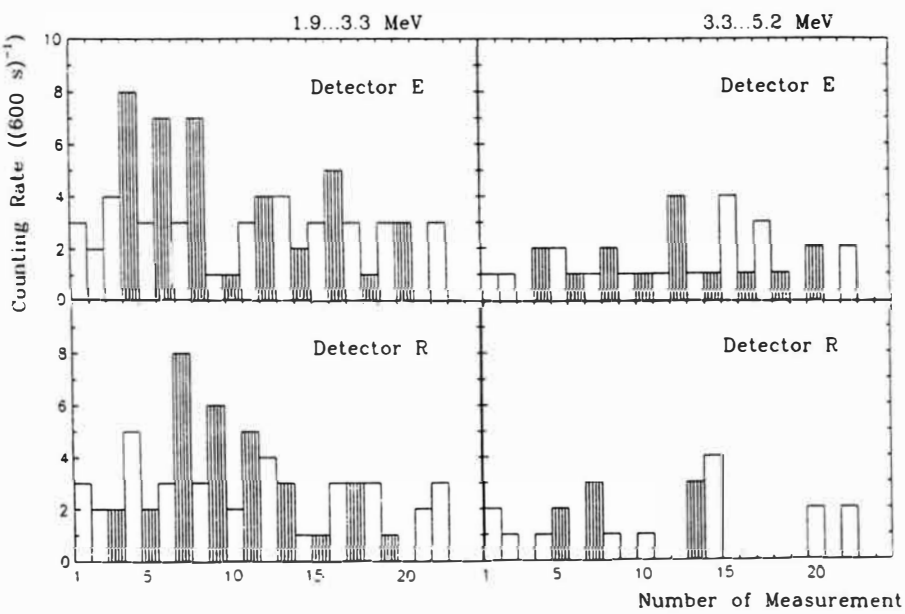

Fig. 1. Counting rates for the experiment with sample Z8 within the recoil proton energy intervals 1.9-3.3 MeV and 3.3-5.2 MeV from both detectors. The hatched sections of the histograms are measurements with sample, the clear sections without sample.

Fig. 2 shows the recoil proton spectrum within the time interval between the fourth and ninth measurement, when the counting rate difference for sample Z8 is at maximum. For the determination of the background all the other 38 measurements are used. For comparison in Fig. 2 also a recoil proton spectrum measured with good statistics for 2.48 MeV neutrons from the d-d reaction at a neutron generator is included. The agreement between both spectra is very well. From this can be concluded, that the energy of neutrons detected during degassing of sample Z8 is about 2.5 MeV. This confirms the assumption, that these neutrons are originated by d-d fusion.

The results for the sample Z6 are different from those of Z8. There are no results coming out of the background measurements. Both samples are distinguished mainly by their different masses, which is assumed to be the reason of the different behaviour observed.

For comparison the experimental data should be expressed in terms of nuclear reactions events per deuteron pair and second as done in many papers, following the deuteron pair fusion model from Ref. [4]. From measurements number 4 to 9 with sample Z8, when the effect is near to its maximum, this

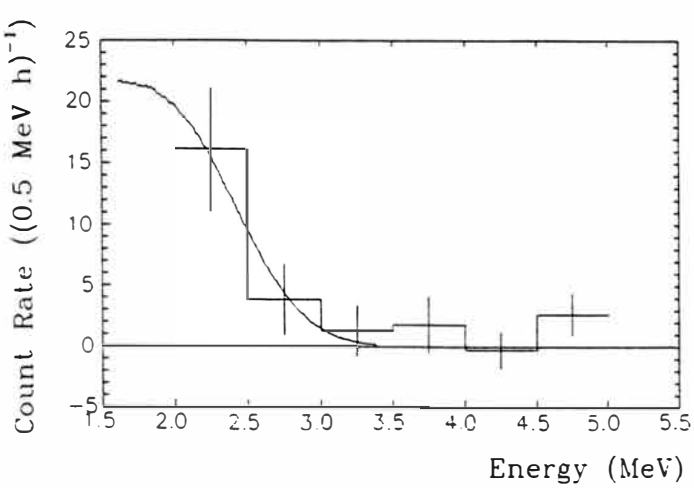

Fig. 2. Proton recoil spectrum during degassing of sample Z8 with 0.5 MeV energy bins and spectrum for 2.48 MeV neutrons from d-d reaction at a neutron generator (curve).

gives $\lambda_{d-d}=(3\pm1)\times10^{-25}$ per deuteron pair and second. This value is in the same order as our results from previous experiments on neutron production at electrochemically loading of palladium samples with deuterium [2,3,5]. As in our previous analysis a d-d neutron production becomes observable during non-equilibrium conditions only.

From measurements with Z6 an estimate of an upper limit for λ_{d-d} could be obtained. Starting from the 1σ-statistical error of one single short time run as an minimal observable effect, this yields $\lambda_{d-d} < 10^{-24}$ per deuteron pair and second. From this point of view, the results from Z8 and Z6 are not incompatible. A more detailled analysis of these experiments will be published elsewhere [6].

CONCLUSION

The present experiment with a 0.5 kg palladium sample shows a definite excess neutron counting rate for an period of about 1 h. This period is just the time interval during which the deuterium is expulsed from the massive palladium sample. The energy of detected neutrons is near to 2.5 MeV, as expected for d-d fusion neutrons. Therefore the conclusion is obvious, that these neutrons are caused by the d-d fusion reaction. The neutron excess counting rate, which is time dependent, corresponds in its maximum to a d-d reaction rate of $(3\pm1)\cdot10^{-25}$ per second and deuteron pair.

REFERENCES

[1] J.O'M. Bockris, G.H. Lin, and N.J.C. Packham, Fusion Technology **18**, 11 (1990).

[2] D. Seeliger et al.,Electrochim. Acta **34**, 991 (1989).

[3] M. Bittner et al., Fusion Technology **18**, 120 (1990); Fusion Technology, in print.

[4] S.E. Jones et al., Nature **338**, 737 (1989).

[5] D. Seeliger and A. Meister, Fusion Technology **19**, July (1991).

[6] M. Bittner et al, submitted to Fusion Technology

Conference Proceedings Vol. 33
«The Science of Cold Fusion»
T. Bressani, E. Del Giudice and G. Preparata (Eds.)
SIF, Bologna 1991

ENHANCEMENT OF FUSION RATE INDUCED BY THE COLLECTIVE ELECTRON EXCITATIONS

Marcello Baldo

INFN, Corso Italia 57 - 95129 Catania, Italy

After the claimed experimental evidence of deuteron cold fusion reported in the literature[1], a large amount of theoretical work has been done, either to support the possibility of this unexpected phenomenon, either to present arguments against it. The paper by Legget and Baym[2] appears of fundamental relevance to this respect. In that work a rigorous upper bound is given for the fusion rate of deuterons embedded in a crystal, which is too small to be compatible with the claimed experimental values. The upper bound is expressed mainly in terms of the chemical potential of neutral helium atoms and deuteron molecules with respect to a crystal of Palladium, or in general of the absorbing material. The smallness of this upper bound is a consequence of the small value of the chemical potential of neutral helium atoms. The latter has been taken to be close to zero, according to the experimental evidence. Thus the result appears unavoidable, and in agreement with this finding some authors have suggested unconventional phenomena to give support to the anomalous fusion rate. However, within the conventional solid state theory, there is still a possibility. One can in fact postulate that the interaction energy between helium atoms and the Pd crystal possesses a second minimum, separated from the till now observed one by a large potential barrier, and at lower energy. This minimum could be practically unreachable by the usual experiments with neutral helium atoms interacting with the crystal, because of the large potential barrier, but it could be easily reached along the rather different path followed by the deuteron–deuteron fusion process. In this contribution we explore this possibility in detail, by studying the interaction of a positive charge with the electrons of a crystal of Pd. The response function of an electron gas can be described in terms of its possible excitations. A positive charge of mass comparable with the mass of the deuteron can be considered as a fixed charge, since its recoil energy is negligible with respect to the energy of the electron excitations. Let us consider the coupling of the charge with one of the excitation mode. We schematize the latter with a simple bosonic branch of energy $\hbar\omega(q)$, with $q \leq q_c$. The cutoff q_c is of the order of $2\pi/a$, a being the average lattice spacing. Then the system is described by the hamiltonian

$$\mathcal{H} = \sum_q \hbar\omega(q) a_q^\dagger a_q + \sum_q v(q)(a_q^\dagger + a_q) \tag{1}$$

The *exact* ground state of the hamiltonian (1) is the product of coherent states $|\alpha_q>$, one for each mode q, with energy E

$$|\Psi_0> = \Pi_q |\alpha_q> \quad ; \quad \alpha_q = -v(q)/\hbar\omega(q) \tag{2}$$

$$E = -\sum_{q \leq q_c} \frac{v(q)^2}{\hbar\omega(q)} \tag{3}$$

The same result can be obtained by using perturbation theory for the charge particle energy, in the limit of large mass. The first non-vanishing contribution is the ***second order*** term, which gives $E = -\sum_{q \leq q_c} v(q)^2/q^2/2M + \hbar\omega(q)$.For $M \to \infty$ one regets the result of eq. (3). This also shows that the perturbation theory actually has zero radius of convergence, as one can verify directly by considering higher order terms of the energy expansion. It has to be noticed, however, that the second order wave function can be quite different from the exact one. A third way of getting the result of eq. (3) for the ground state energy is to use the expansion of the self-energy of a particle in the framework of the dielectric formulation of many-body theory. The dielectric function $\epsilon(q,\omega)$ of the system of bosons can be written

$$\epsilon^{-1}(q,\omega) = \frac{\omega^2(q)}{\omega^2 - \omega^2(q)} \tag{4}$$

The self-energy $\Sigma(q,\omega)$ of a particle moving in the system can be expanded in powers of the dielectric function. Again, to lowest order, one regets eq. (3), provided one regards $\Sigma(q,\omega)$ as the energy of the particle and take the limit $M \to \infty$ and consistently the unperturbed particle energy $E = 0$ (Raleigh-Schrödinger perturbation theory). This last formulation of the problem is quite useful, because it can be generalized to more realistic case, where the collective excitations are not schematized by simple bosons, but properly described within the many-body theory of the electron system. In this case the dielectric function of eq. (4) is substituted by more microscopic expressions. In view of the above discussion, however, it is likely that also in this microscopic formulation the perturbation expansion is divergent, and it is apparent that the best strategy to adopt is to calculate, also in this case, the energy to lowest order, since it should give a result rather close to the exact one. The main feature of the result of eq. (3) is the dependence of the energy on the square of the coupling $v(q)$. It follows that a particle of charge Q has an energy E proportional to Q^2, $E = \beta Q^2$, $\beta < 0$. Consequently two separated particles, each one of charge Q, have a total interaction energy $E_{1+1} = 2\beta Q^2$, which is a factor two smaller in absolute value with respect to the case they are close to each other to form essentially a single particle of charge $2Q$, $E_2 = 4\beta Q^2$. The decrease in energy is $E_2 - E_{1+1} = 2\beta Q^2$. Thus the coupling with the electron collective excitations produces an attractive potential between two charged particles. This is well known in the theory of charge screening in solids[3], but it has to be noticed that it is a more general phenomenon. For instance the phonon exchange, which produces the Cooper pairs in ordinary superconductors,

has a similar origin. For an electron system the dielectric function can be parametrize as

$$\epsilon^{-1}(q,\omega) = \sum_i \frac{S_i}{\omega^2 - \omega_i^2(q)} \tag{5}$$

where the strengths $\{S_i\}$, one for each mode i, are constrained to fulfil the $f-$sum rule (or "oscillator sum rule")

$$\int_0^{+\infty} d\omega \mathrm{Im}\left(\epsilon^{-1}(q,\omega)\right)\omega = \frac{\pi}{2}\sum_i S_i = \frac{2\pi^2 e^2 n}{m} \tag{6}$$

where n is the electron density and m the electron mass. For a purely collective excitation $S_i = \omega_i^2$. In general one can assume $S_i = s_i\omega^2$, with $0 \leq s_i \leq 1$, and the sum rule reads

$$\sum_i s_i\omega_i^2 = \frac{4\pi e^2 n}{m} = \omega_p^2 \tag{7}$$

Once the frequencies $\{\omega_i\}$ are given, this relationship constrains the possible values of the weights $\{s_i\}$, as it will be discussed later on. In general the momentum q of each excitation has a cut-off value, above which the excitation become overdamped. For simplicity one can assume the same cut-off q_c for all the excitations. According to eq. (3) the energy of a particle of charge Ze is given by

$$E_Z = -\frac{(Ze)^2}{\pi} q_c(\sum_i s_i) \tag{8}$$

and the corresponding gain in energy ΔE for "fusion" of two particles, each of charge Z, is twice this value (for $d-d$ fusion $Z=1$). From the constraint (7) one gets

$$\sum_i s_i = \omega_p^2/\overline{\omega}^2 \quad ; \quad \overline{\omega}^2 = \sum_i s_i\omega_i^2 / \sum_i s_i \tag{9}$$

It follows that the total strength $\sum_i s_i$ is larger if the average energy $\overline{\omega}$ of the electron excitations is smaller. This result has a simple physical interpretation : a smaller $\overline{\omega}$ implies a larger polarizability and thus a stronger interaction energy of a charged particle with the medium. If one assumes a dispertionless frequency ω_i, it is possible to get an analytical expression for the potential energy between two particles of charge Ze at a distance R, due to their coupling with the electron system. Following ref.[4] one gets

$$V(R) = -2\frac{(Ze)^2}{\pi} q_c(\sum_i s_i) I(q_c R) \quad ; \quad I(x) = \frac{1}{x}\int_0^x \frac{\sin(y)}{y} dy \tag{10}$$

Before discussing the implications of this result for the specific case of Pd, let us consider some possible criticisms to the validity of eqs. (10) First of all the dielectric function of eq. (5) does not display the zero at $\omega = 0$, $q \to 0$, which characterizes the dielectric function of a metal, the so called "complete screening". This is due to

the fact that eq. (5) does not include the single particle conduction band transitions, which are responsible for the static screening in a metal. Their inclusion should affect only a range of momenta around $q = 0$ of the static inverse dielectric function $\epsilon^{-1}(q,0)$ and the result (8) should be essentially unaffected. Another warning about the dielectric function of eq. (5) comes from the observation that, as a function of q and for $\omega = 0$, it is negative in the relevant momentum range. This fact could cast some doubts on its validity, since it could be in contrast with the stability condition of the crystal. For a deformable jellium model, in fact, negative values of $\epsilon^{-1}(q,0)$ indicate that the system is unstable to density fluctuations[5], which are not observed in transition metals. It has to be kept in mind however that the dominant contribution to the crystal stability is due to the Ewald energy[6], which originates from the non-jellium structure of the crystal. Eq. (5) has to be considered as an average of the dielectric function on orientation of the wave vector $\vec{q}$. The instability coming from the negative values of $\epsilon^{-1}(q,0)$ can be counter-balanced by the stabilization due to the Ewald static energy from the crystal structure. The experimental data on inelastic electron scattering on Pd of ref.[7] are reported in fig. 1, where the second derivative spectrum is shown as a function of the excitation energy.

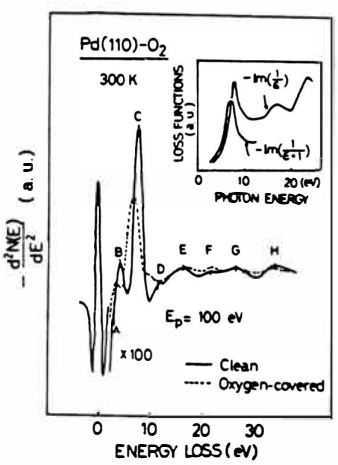

Fig. 1 *Electron energy loss spectrum (full line) from ref. 7.*

Several peaks are observed. Even if some of them could be simple atomic transitions, nevertheless they are associated with transitions in the *sd* valence band. According to ref.7 the two peaks at $\omega_1 = 7.5$ eV and $\omega_2 = 26.5$ eV correspond to plasmon excitations mainly of the s and *d* band respectively. Accordingly the broad peak observed at $\omega =$ 33.8 eV, quite close to $\omega_1 + \omega_2$, must be interpreted as due to the simultaneous (second order) electron excitation of both the *s* and *d* plasmons. Therefore the bump does not correspond to an independent excitation, and its energy has not to be included in the sum of eq. (7). The theoretical justification of the two independent plasma excitations of the *s* and *d* bands can be the smallness of the particle-hole matrix elements between the two bands, which involve different orbitals with a small overlap. Using the Pd electron density $n \approx 0.4\text{Å}^{-3}$, one gets $\sum_i s_i \omega_i^2 \approx 10^3$ eV^2, and, according to the preceeding discussion, eqs. (7) gives $\sum_i s_i \approx 6$. The corresponding $d - d$ potential of eqs. (10) is depicted in fig. 2. The value of $q_c = 2.2\text{Å}^{-1}$ has been assumed. In ref.[8] the branch at $\omega = 7.5eV$ has been observed up to q ≈ 1 Å^{-1} with essentially no

dispersion. No data on the other excitations are available in the literature.

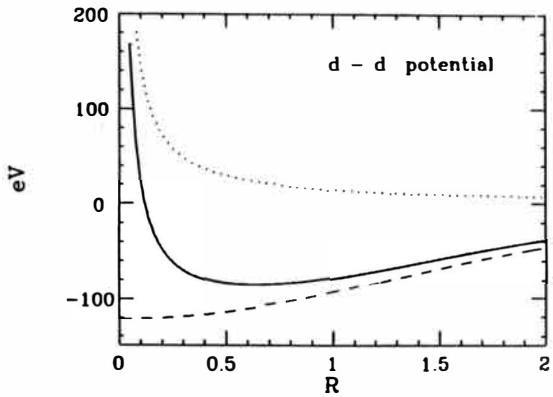

Fig. 2 *Interaction potential between two deuterons (full line). The dotted and dashed lines are the coulomb and electron contribution respectively. The distance R is in Å.*

The large interaction energy is a consequence of the large charge electron displacement around the positive charge. The latter can be calculated from the dielectric function of eq. (5) and is reported in fig. 3 as a function of the distance from the positive charge. The total polarization charge concentrated in the first large peak depends only on the strength $\sum_i s_i$, and it exceeds largely the positive charge in this case. In that sense one can speak of "overscreening" of the positive charge. The phenomenon is possible due to the collectivity of the excitations, which prevents the electron kinetic energy to increase too much as the electron charge is localized, since the collective excitations have a large "mass". It must be stressed that the above discussed correction of the dielectric function near $q = 0$ modifies the large distance behaviour of the polarization charge, and it is necessary in order to ensures that total displaced charge, obtained integrating up to infinity, is equal to the positive charge, according to a general property of the electron gas [9]. The fusion rate R can be calculated by considering a deuteron gas interacting through the potential of eqs. (10), following the same line of ref. 3. The result gives

$$\mathrm{R} \approx 1\mathrm{fusion}/sec./mole \tag{11}$$

The rate R is of course sensitive to q_c. The assumed value $q_c = 2.2\text{Å}^{-1}$ appears realistic. The "delocalized" configuration described here of a positive charge interacting with the electron collective excitations is quite different from the one corresponding to an atom–like configuration where the positive charge is surrounded by its electrons, essentially as in its free configuration. For helium the delocalized configuration is largely favourable in energy with respect to the atom–like one. However an helium atom inside the crystal cannot decay spontaneously to the delocalized configuration. Suppose in fact to polarize the helium atom to bring it to the decolized configuration. On one hand this requires some energy, and on the other hand the interaction, with the electron gas, of the so formed dipole produces a gain in energy, according to the above described model. Which one of the two energy changes actually dominates is determined by the curvature of the energy surface. The latter can be estimated as E_B/a^2, where E_B is the binding energy and a the size of the system. It turns out that for helium atom the curvature is much larger, because of its small size, despite the

smaller binding energy. This is the physical origin of the potential barrier between the two configurations.

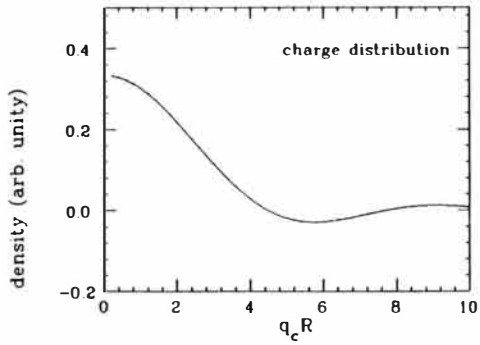

Fig. 3 *Electron charge displacement around a positive charge .*

The same reasoning can of course be followed for the deuteron (or hydrogen) atoms. In this case however the size of the atom is larger, and the two curvatures may be comparable. Thus, according to the model, the second minimum might be reachable under favourable conditions. The experimental observation of this second minimum for deuteron (or hydrogen) atoms would strongly support the model. In conclusion the model presented here explains a fusion rate of the order given by eq.(11). Furthermore it predicts the formation of deuteron–like molecules inside the crystal, sitting at the minimum of the potential of fig. 2. This implies additional heat production (for both hydrogen and deuteron atoms), whose rate, however, is determined by the approach to equilibrium (towards the bottom of the potential). A first attempt to describe the dynamics towards equilibrium was presented in ref.[10], but it requires further investigations.

[1] M.Fleischmann and S.Pons, J.Electroanal. Chem., **261**,301(1989) and **263**,187 (1989), S.E.Jones *et al., Nature*, **338**, 737(1989), and this conference.

[2] A.J.Legget and G.Baym, *Phys. Rev. Lett.*, **63**, 191 (1989).

[3] J.Callaway, *The Quantum Theory of the Solid State*, Academic Press 1974, p. 595–598.

[4] M.Baldo and R.Pucci, Proceeding of the Workshop *Understanding of cold fusion phenomena*, September 1989, R.A. Ricci, E.Sidoni and F.DeMauro Eds., Editrice Compositori (1990).

[5] D.Pines and P.Nozieres, *The Theory of Quantum Liquid*, Benjamin 1966, p. 208-209.

[6] N.W.Ashcroft and N.D.Mermin, *Solid State Physics*, Sounders College 1976, see also V.Heine and D.Weaire, *Solid State Physics* **24**, 249 (1970).

[7] M.Nishijima, M.Jo, Y.Kuwahara and M.Onchi, Solid State Comm., **58**,75,(1986).

[8] T.Bornemann, J.Eickmans and A.Otto, Solid State Comm., **65**, 381 (1988).

[9] See for instance A.F.Fetter and J.D.Walecka, *Quantum Theory of Many-Particle Systems*, McGraw–Hill 1971.

[10] M.Baldo, R.Pucci and P.F.Bortignon, Fusion Technol., **18**,347 (1990).

Conference Proceedings Vol. 33
«The Science of Cold Fusion»
T. Bressani, E. Del Giudice and G. Preparata (Eds.)
SIF, Bologna 1991

BINUCLEAR ATOMS AS FUSION PRECURSORS IN A HOT CLOUD

G.F. Cerofolini[1], R. Dierckx[2], A. Foglio Para [3] and G. Ottaviani[4]

[1] *Istituto Guido Donegani, EniChem, 20097 San Donato MI, Italy*
[2] *EEC Joint Research Center, 21020 Ispra VA, Italy*
[3] *Dipartimento di Ingegneria Nucleare, Politecnico di Milano, 20133 Milano MI, Italy*
[4] *Dipartimento di Fisica, Università di Modena, 41100 Modena MO, Italy*

ABSTRACT

Deuteron-deuteron fusions were claimed by a Brookhaven group to result from the impact on deuterated surfaces of clusters of 25 - 1350 D_2O molecules with energy up to 300 keV. The collective motion in the impact region is tentatively assumed to be responsible for these fusion events. The number of involved atoms is of the order of 10^4, with a mean energy of some electronvolts. The model is able to reproduce qualitatively the Brookhaven data according to an Arrhenius plot, with an activation energy $E^* \simeq 2\,E_0$, where E_0 is the hydrogen ionization energy. At this energy an activated precursor is postulated to be synthesized; it can tentatively be identified as the binuclear atom $(D^+ - D^+)2e^-$.

1. INTRODUCTION

A Brookhaven collaboration has recently presented surprising results concerning the detection of D - D fusion products in TiD targets following bombardment with $(D_2O)_n$ clusters $(25 < n < 1350)$ [1]. The evidence of fusion events was successively extended using perdeuteriopolyethylene $\leftarrow CD_2 - CD_2 \rightarrow_{n'}$ and $ZrD_{1.65}$ targets [2].

The experimental arrangement utilized in the first work [1], though apparently simple, was subjected to criticisms, since in-flight fragmentation or evaporation after mass separation or poor mass separation of the clusters may reproduce the observed fusion rate and its energy dependence [3]. Indeed, a single D^+ ion per cluster, accelerated at a few kiloelectronvolts, can reproduce the Brookhaven results without advocating any new phenomenon.

In order to identify a possible fragmentation of the cluster in light fragments, the use of a pulsed beam and the detection, by a coincidence technique, of the time of emission of the reaction products was proposed. The fragmentation of the cluster into light ionized fragments is indeed characterized by the arrival on the target of these fast fragments some microseconds before the cluster arrival [4]. A coincidence set-up in the microsecond range should detect these early events, if any, and attribute them to a trivial fragmentation process and not to a new, at the moment unexplained, phenomenon.

A cluster-impact experiment in the pulse mode with a repetition frequency in the hertz range was executed by another group [5]. No protons were revealed following the impact of 100 – 150 keV pure deuterium clusters, constituted by 200 - 300 D atoms, on $TiD_{1.7}$ and $\leftarrow CD_2 - CD_2 \rightarrow_{n'}$ targets. Though this part of the experiment does not confirm the Brookhaven results, the Brookhaven collaboration has very recently obtained positive results in the pulsed mode too [6].

Another possible source of experimental error in the Brookhaven set-up is due to deuterium atoms backstreaming from the target under cluster bombardment. Backstreamed atoms

could successively be ionized and accelerated in the column onto the target [7].

However, already in the reply to this criticism [8] and mostly in the second work [2], the Brookhaven group produced a lot of evidence which seems to exclude fragmentation or evaporation, poor mass separation, or backstreaming. In the following we assume the unrestricted validity of the Brookhaven results.

We note that artifacts, if any, are due to the presence in the beam of fast atoms and that in the fusion events originated by, say, 10 keV D^+ impinging onto the target, the energy of the protons emitted toward a detector placed at a scattering angle around 125° is about 70 keV less than the energy, 3.02 MeV, of protons emitted in fusions promoted by low energy deuterons. *This shift in the proton energy spectrum should easily be detected if the detector is properly placed and if its resolution in the experimental set-up is sufficient* — these considerations should be able to rule out, or to confirm the presence of, all hypothesized artifacts.

2. DISCUSSION OF BROOKHAVEN RESULTS

The Brookhaven results are particularly surprising if plotted as a function of the kinetic energy E_D of a deuterium atom in the cluster, $E_D = (M_D/nM_{D_2O})E \simeq 0.1E/n$, where E is the cluster energy and M_X is the mass of the molecule X. Indeed, the comparison of the data collected at constant E and variable n with the data taken at given n and variable E shows that the fusion yield per deuteron y is not a single-valued function of E_D, but depends also on cluster composition [9]; this fact is completely inconsistent with the view of fusions produced by independent collisions of $2n$ impinging deuterons.

In order to remove this contradiction, we are led to consider in greater detail the impact of the cluster on the target using a model which describes the collective motion of the atoms in terms of hot cloud formation. If the number of atoms in a cluster is high enough, the collisional cascades produced by single atoms superimpose and form a unique cascade so dense to be treated as a hot cloud; the duration Δt of this phenomenon and the number N of involved target atoms is much larger than the values estimated by Beuhler et al. [1], i.e. $\Delta t \approx 10^{-11}$ s vs 10^{-13} s, and $N \approx 10^4$ vs 10^3 [10,11]. A much larger number of deuterons can therefore interact for a much longer time Δt, however with a lower mean kinetic energy E_{kin} than assumed by Beuhler et al. If a phenomenon able to activate fusion at low energy exits indeed, it is plausible that the relevant parameter for the description of the phenomenon is no longer E_D, but the cloud temperature T, assumed to be related to E_{kin} by the usual formula $E_{kin} = \frac{3}{2}k_B T$, where k_B is the Boltzmann constant [12].

If we assume for the moment that only deuterium atoms are able to inject useful energy into the cloud, the average kinetic energy in the cascade is given by

$$E_{kin} = \eta(4/20)E/(2n+N), \tag{1}$$

where η is the fraction of the impinging energy which is not lost in electronic collision. Simulations carried out with the MARLOWE code give η in the range 0.6 – 0.8 (tentatively we assume $\eta = 0.7$) and suggest that most of the useful energy in the cascade is indeed injected by the deuterium atoms, owing to their identical mass with the target atoms [13]. By contrast, the oxygen imparts most of its energy to titanium, so that this energy deposition seems to be decoupled from the deuterium cloud energy. In a way, the particular choice of projectile and target of the Brookhaven group, though scarcely efficient in terms of deposition of useful energy, gives rise to a very simple situation to be modeled, in which only deuterium atoms or ions are involved. The small fraction ($\simeq 4/20$) of incoming energy useful to promote fusion events delineates a framework very different from the one presented by Echenique et

al. [14] in which the deposition to deuterium atoms in the target of the whole cluster energy is assumed, so that some high energy deuterons in the upper tail of the resulting energy distribution could promote fusion events according to conventional nuclear physics.

From eq. (1) E_{kin} can be considered independent of n only for $2n \ll N$. Since the data of Beuhler et al. are nearly constant from $n = 10^2$ to $n = 5 \times 10^2$, a first underestimate of N, $N \gg 10^3$, results. In order to take into account the data at variable E for fixed n, we note that an assigned value of N in eq. (1) combined with the variation with E which results from the experimental data allows the corresponding theoretical fusion yield $y(n, N; E)$ to be calculated. The value $N = 10^4$ fits adequately the experimental data and is in accordance with the results of molecular dynamics simulations [10] and with evidence from silicon amorphization [15].

While the two curves are able to describe in a satisfactory manner the data for high n, they cannot be extended in the low n region. In this region E_D is responsible for a projected range R_p of the deuterium atoms larger than the diameter L of the collisional cascade; this suggests that N should vary as

$$N = N_0(1 + R_p/L) = N_0(1 + \beta E/n) \tag{2}$$

where R_p/L has been assumed proportional to E/n through the coefficient β. The description of the cascade can be further refined taking into account the increase of the electronic energy loss at deuterium energy higher than 0.5 keV and the sparse collisional cascades formed by small clusters. These phenomena can in a first approximation be described with a reduced increase of E_{kin} for increasing E and decreasing n. The global effect is similar to the one described by eq. (2),

$$E_{kin} = \eta(4/20)E/[2n + N_0(1 + \alpha E/n)] \tag{3}$$

where α (which includes β) is now a parameter to be estimated by fitting the experimental data.

Using this formula, all the data may be reported in an Arrhenius plot [9]. The best fit of all data gives: $N_0 = (10 \pm 0.5)10^3$, $\alpha = 1.8 \times 10^{-2}$ keV^{-1}, and $E^*/\eta = (33 \pm 2.5)$ eV. Interestingly enough, the estimate $N_0 \simeq 10^4$ is in a satisfactory agreement with those of ref.s [10,11,15], thus underlining an intrinsic coherence in the developed picture.

Though the hot cloud model explains the behaviour of fusion rate vs T and therefore vs n and E, showing that with a good approximation this rate is a function of $E/[2n + N_0(1 + \alpha E/n)]$, however, it cannot explain the extremely high values obtained by the Brookhaven group. Indeed, taking $\eta = 0.6 - 0.8$, E^* results in the interval $20 - 26$ eV, i.e. a value too low to be associated with the overcoming of the internuclear Coulomb barrier. However, the fairly accurate description of all data obtained with the hot cloud model makes us confident in the search of a physical significance of E^*. In this respect it is interesting to note that the value of E^* is approximately twice the ionization energy E_0 of the deuterium atom, so that an atomic, rather than nuclear, phenomenon seems to drive the fusion events. We therefore assume that at the energy E^* a metastable precursor in a favorable situation to fuse is formed.

Further considerations must be taken into account for the development of the model. First of all, in the considered energy range the deuterium atoms move in the target in an atomic rather than in an ionic form, thus allowing, for an assigned kinetic energy, closer nucleus-nucleus encounter and hence higher fusion yield. This consideration is based on the formula of ref. [16] giving the effective charge on hydrogen and deuterium at various kinetic energies; for instance the effective charge is $0.18e$ at 2 keV and $0.13e$ at 1 keV (e is the

unitary charge). Secondly, the interaction potential of two deuterium atoms must take into account the screening effect of the orbiting electrons; we assume that screening is described by the Debye potential

$$U(r) = (e^2/r)\exp(-r/a) \tag{4}$$

where a is a screening length. Historically, potential (4) was used in the description of most of screening problems concerning the penetration of atomic particles through matter [17]; this description is accurate enough at separations of the order of the Bohr radius a_0. For hydrogen $a = a_0$, and for two interacting atoms with atomic numbers Z_1 and Z_2 the Firsov composition rule, $a = a_0/(Z_1^{1/2} + Z_2^{1/2})^{2/3}$, holds true [18]. This rule is routinely used in the calculation of the stopping powers and of the damage effects for practically all projectiles in solids [16].

In the description of the interaction of two deuterium atoms, large and small separations must be independently considered.

Large separation. For large D - D separation, only electrostatic effects are important and the random relative spin orientation is mute in the description of the system. The total energy of two separate repelling atoms is therefore:

$$E_{(D^+)e^-+(D^+)e^-}(r) = (e^2/r)\exp(-r/a) - 2E_0 \quad [E(\infty) = -2E_0] \tag{5}$$

Small separation. At kinetic energy higher than 27 eV the nuclei can approach at distances lower than $0.5\,a_0$, so that the D - D system can no longer be treated as formed by two moderately perturbed atoms. In a way, the nuclear separation admits a stationary electronic configuration resembling that of the helium atom so that the system can be regarded as a $(D^+D^+)2e^-$ binuclear heliumlike atom. Its total energy can be estimated by the formula

$$E_{(D^+D^+)2e^-}(r) = e^2/r - (E_1 + E_2 - 2E_0)\exp(-0.46r/a_0) - 2E_0 \tag{6}$$

where E_1 and E_2 are the first and the second ionization energies of the helium atom; the term $\exp(-0.46r/a_0)$, which spans from 1 to 0 for r ranging from 0 to ∞, is derived by a least square procedure from the curve which describes the electronic energy of the molecular ion H_2^+, for which an exact theory exists. It must also be noted that eq. (6) matches within 1 eV in the interval $0.4 - 0.7\,a_0$ the most accurate calculations available [19] for H_2.

In the paraheliumlike case (antiparallel spins), $E_1 = 24.58$ eV and $E_2 = 54.40$ eV; for the orthoheliumlike case $E_1 + E_2 = 59$ eV. These situations corresponds to the two stationary states of the system. Because of the random spin orientation, however, the state of the system is generally a non-stationary linear combination of orthohelium and parahelium states; correspondingly the electronic energy of the system will assume an intermediate, spin-dependent, value.

Calculating the total energy of the system by means of eq. (5) for $r > 0.6\,a_0$ and of eq. (6) for $r < 0.5\,a_0$, the energy of the system must have a minimum in the interval $0.4\,a_0 < r < 0.5\,a_0$ (the system is unstable with respect to dissociation in all its components for $r < 0.4\,a_0$) provided that the relative spin orientation is not too far from the antiparallel one, so that a metastable configuration must exists in this separation range. Hence, the D - D collision in a suitable energy range and with an appropriate impact parameter leads to a nuclear configuration for which the total energy has a relative minimum. If a third body is able to absorb a small fraction of the original kinetic energy, then the colliding deuterium atoms can be bound in a binuclear heliumlike atom. This metastable state can decay either by

dissociation or by fusion. The stability of the heliumlike configuration, the *metastable precursor*, is higher the higher the activation energy for its dissociation; to estimate this energy a knowledge of the spin orientation distribution and a detailed calculation around $r = 0.5\,a_0$ is necessary. In any case, in the most favourable conditions the binuclear atom allows much longer interaction times for the two deuterium nuclei than an ordinary collision, so that extraordinarily fusion rates are no more surprising.

A possible consequence of the existence of the metastable precursor concerns the suggestion to utilize coincidence techniques in the microsecond range as a signature of the arrival of the different projectiles. However, if the observed extraordinarily high fusion rates are indeed due the formation of a metastable precursor, the fusions are no more prompt and decay exponentially with time according to the mean life of the precursor. The most recent Brookhaven result with pulsed beam does not totally clarify this point.

General semiquantitative considerations based on the structure of the collisional cascade allow the identification of classes of projectiles and target materials to be used in order to enhance the hot cloud temperature and hence the fusion rate. The best choice is obtained by combining as light as possible targets with very heavy projectile not containing light atoms. Volatile heavy molecules allow the preparation of very simple sources, surely useful when they are maintained at high potential as it happens in ion implanters. These sources prevent from artifacts originating from in-flight fragmentation or evaporation of ionized deuterium fragments from the cluster; as far as the experimental set-up is concerned, an ion implanter with mass selection after ion acceleration also protects the experiment from in-flight fragmentation. An activity in this field is in its preliminary stage.

REFERENCES

[1] R.J. Beuhler, G. Friedlander and L. Friedman, Phys. Rev. Lett.**63**, 1292 (1989)

[2] R.J. Beuhler, Y.Y. Chu, G. Friedlander, L. Friedman and W. Kunnmann, J. Phys. Chem. **94**, 8494 (1990)

[3] C. Carraro, B.Q. Chen, S. Schramm and S.E. Koonin, Phys. Rev. A **42**, 1379 (1990)

[4] D.E. Alburger, J. Phys. Chem. **93**, 8494 (1990)

[5] M. Fallavier, J. Kemmler, R. Kirsch, J.C. Poizat, J. Remillieux and J.P. Thomas, Phys. Rev. Lett. **65**, 621 (1990)

[6] R.J. Beuhler, G. Friedlander and L. Friedman, Acc. Chem. Res. **24**, 198 (1991)

[7] F.E. Cecil and J.A. Mc Neil, Phys.Rev.Lett. **64**, 2210 (1990)

[8] R.J. Beuhler, G. Friedlander and L. Friedman, Phys. Rev. Lett. **64**, 2211 (1990)

[9] G.F. Cerofolini and A. Foglio Para, *Alternatives in low energy fusion?*, Workshop on *Exotic Atoms in Condensed Matter*, Erice, Italy (May 19 – 25,1990)

[10] T. Diaz de la Rubia, R.S. Averback, H. Hsieh and R. Benedek, J. Mater.Res. 4, 579 (1989)

[11] G.F. Cerofolini and L. Meda, Phys.Rev.B **36**, 5131 (1987)

[12] G.F. Cerofolini, N. Re and A. Foglio Para, *$(D^+ - D^+)2e^-$ binuclear atoms as activated precursors in cold and warm fusion*, in *Anomalous Nuclear Effects in Deuterium/Solid System*, an Int. Progress Review, Provo, UT (Oct. 22 – 24, 1990)

[13] G.F. Cerofolini, R. Dierckx, A. Foglio Para and G. Ottaviani, Nuovo Cimento D, in press

[14] P.M. Echenique, J.R. Manson and R.H. Ritchie, Phys. Rev. Lett. **64**, 1413 (1990)

[15] G.F. Cerofolini, L. Meda and C. Volpones, J. Appl. Phys. **63**, 4911 (1988)

[16] J.F. Ziegler and G.J. Iafrate, Radiat. Eff. **46**, 199 (1980)

[17] N. Bohr, Mat.Phys.Medd.Dan.Vid.Selsk No. 18,1 (1948).

[18] O.B. Firsov, Zh. Eksp. Teor. Fiz. **34**, 447 (1958); English translation: JETP **7**, 308 (1958)

[19] W. Kolos and L. Wolniewicz, J. Chem. Phys. **49**, 404 (1968)

Conference Proceedings Vol. 33
«The Science of Cold Fusion»
T. Bressani, E. Del Giudice and G. Preparata (Eds.)
SIF, Bologna 1991

AN EXPLANATION OF COLD FUSION AND COLD FUSION BY-PRODUCTS, BASED ON LATTICE INDUCED NUCLEAR CHEMISTRY

Scott R. Chubb and Talbot A. Chubb

Research Systems, Inc., 5023 N 38th St., Arlington, VA 22207, U.S.A.

In this paper, first we re-examine the assumptions associated with applying the fundamental "scientific paradigm"[1] of hot fusion to the problem of cold fusion and then explain how much of the cold fusion controversy can be reconciled once an alternative paradigm, based on solid state physics, is adopted. The new world-view that results from this different perspective is the basis of our "Lattice Induced Nuclear Chemistry" (LINC) theory[2] of cold fusion. We conclude the paper by summarizing some of the more important results of LINC. These include our predictions (prior to the experimental work by Bush et al[3]) that 1) it is to be expected that the primary cold fusion by-products in the electrolytic experiments involving Pd and D probably are heat and low-energy ^{4}He, 2) the ^{4}He should remain largely untrapped within the bulk electrode and be found primarily in the surface region and outgases, and 3) there is a need to satisfy a critical loading condition (of x~1 in PdD_x) in the electrolytic experiments.

The conventional paradigm of nuclear fusion is that two, clearly identifiable deuterium nuclei "collide" at a specific location and give off energy as a result of the ensuing decrement in mass. Three critical assumptions of this paradigm are: 1) the participants of the reaction are "particles" (of nuclear dimension), 2) the particles are readily identifiable, and 3) the reaction occurs at a specific (readily identifiable) location of nuclear size.

Preparata[4], in particular, has emphasized that as a result of these three assumptions most "normal" physicists consider nuclear processes in cold fusion to be impossible because of a single fundamental idea: "how is it possible to 'penetrate' the Coulomb barrier." He has also suggested that a second important idea must be reconciled: "how is it possible to evade Asymptotic Freedom," where Asymptotic Freedom refers to the notion that on the length scale associated with nuclear interactions, individual "particles" must behave as if they are free particles.

There is a third issue that "normal" physicists raise as an objection to cold fusion being the result of nuclear reactions: "the lack of discernible high-energy particle nuclear ash" that Jones[5] has recently suggested is important. The basis of this issue is that "normal" fusion reactions result when nuclear particles collide at a specific location. Then, if cold fusion is the result of "normal" fusion reactions, energetic by-products not only must be produced but released from the solid because the energy from nuclear reactions is so large that none of the known, "normal" electrostatic processes that occur within a solid is capable of "trapping" the energy inside the solid without violating energy or momentum conservation.

In our theory, we reconcile this final issue in a manner consistent with the way we reconcile all the issues: we simply replace the three initial assumptions of the fusion paradigm with a set of new assumptions. The new assumptions, in fact, arguably are more suitable at low temperature because they are based on the single, established "paradigm" of physics, "solid state physics", and the remaining laws of quantum mechanics.

As we explain elsewhere in this Proceedings[6], the reason that solid state physics allows us to reconcile the three "problems" of cold fusion is that through the solid state physics paradigm, to minimize the energy of the system, a solid may alter the corpuscular nature of the potentially reacting "particles" in important ways. As a consequence, 1) the locations of the participating "particles" need not be clearly defined, 2) each of the resulting nuclear reactions may occur at all periodically equivalent locations, and 3) only a small fraction of a particle need be found and reaction take place at an individual location. In other words, "just because a deuteron looks like a particle, and it acts like a particle in one place, it does not have to look like or act like a particle somewhere else; just because the energy from nuclear fusion is released entirely in

one place in one case, fusion energy does not have to be released all in one place in a different case; where the energy is released, and whether or not the deuterons behave like particles are both dictated by the known laws of solid state physics, quantum mechanics, and the requirement that the energy of the system be minimized."

As we have shown[2,7], consistent with the experimental conditions of cold fusion, this alternative paradigm provides a means of altering the spatial distribution and physical make-up of nucleons in a manner that completely invalidates the underlying premises associated with conventional Gamow theory, the very concept of a huge Coulombic barrier (that must be penetrated for fusion to occur) and the expectation that "conventional" fusion products are to be expected. Also, because the new world-view begins with the idealization of the solid state physics paradigm, the prerequisite boundary condition of the resulting description is that the system is periodic in the low temperature limit and system energy be minimized. Thus, the wave function of each reactive deuteron must solve the Schroedinger equation of a bound particle, interacting with a periodic, electrostatic potential. As a consequence, the wave function does not asymptotically approach the wave function of a free particle at short length scales, and asymptotic freedom "can be evaded" simply because it does not apply.

The starting point for understanding LINC is the idealization in which a macroscopically infinitesimal number of deuterons attempt to bond to a fully loaded, stoichiometric, periodic PdD host. A very important aspect of this problem is that it applies to PdD, where it is known that the loading is dominated by the bonding effects associated with hybridization of s-electrons from the injected deuterons with 5s and 4d states provided by the Pd. As a consequence, near x=1 in PdD_x, as has been shown in several ab initio electronic structure calculations[8,9], only a very small (~ 0.1 e), predominantly isotropically distributed (and s-like) electronic charge occupies the region in the vicinity where the deuteron cores bind to the solid. (For this reason, the D are only weakly bound to [and undergo large zero-point-motion fluctuations about] their equilibrium positions.)

In order to minimize energy with respect to further injection of D atoms beyond the value x=1, four important effects then may come into play. 1) Because system energy must be minimized with respect to changes in the electronic structure, in the limit in which only a macroscopically

infinitesimal number (~10^{-7} e/unit cell) of electrons are added (as a consequence of injecting additional deuterium atoms), the additional electronic charge will be distributed among the unoccupied 5s-like states immediately above the Fermi level, which are associated with electrons which are found predominantly (i.e., more than 90 percent of the time) in regions away from the locations where the D-nuclei preferentially bind in the stoichiometric (x=1) compound. 2) Because only an infinitesimal number of D atoms are added, again to minimize the electrostatic energy of the system, each additional D-nucleus "attempts" to bind to an octahedral site, where D-nuclei do bind in the limit that x=1. 3) As a consequence of the first two factors, each added D-nucleus behaves as if it is a D^+ ion that interacts with a time-independent, periodic potential over time scales that are short with respect to times associated with the disruptions of periodic order that result from interactions with phonons, finite-size effects, etc. 4) Then, because the potential is periodic, the deuterons, which effectively are ions, may occupy energy band states, <u>and,</u> provided the number of deuterons that are injected is sufficiently small ($< \sim 10^{-4} \times N_L$, where N_L is the total number of unit cells[7]), it becomes energetically favorable, as a means of minimizing strain energy, for them to do so.

The key points are that the additional deuterons will occupy energy band states near the limit x=1 as a means of minimizing energy, and they effectively behave like ions as a consequence of the <u>known</u> electronic structure of PdD. Because each ion occupies an energy band state, only a very small fraction ($1/N_L$) of each ion is located in each unit cell. Because each of these band state deuterons behaves like an ion, each of them is indistinguishable from the others. Then, they all must share a common, many-body wave function. The result of these effects is that small fractions of a deuteron may interact, without the prerequisite Coulombic tunnelling requirement[7]. Reaction occurs as a consequence of the implicit algebraic properities of the many-body wave function provided the zero-point-motion broadening of the deuteron wave function is sufficiently large.

Because only a small fraction of each excess deuteron is present at any site, only a small fraction of each reaction (and reaction energy), on the average, occurs at each site. Energy release occurs only through processes which preserve the quasi-equilibrium conditions which give rise

to the occupation of the initial state many-body, ion band state wave function. This requirement leads to a selection rule that final state by-products in the primary reaction channels be formed from integer numbers of proton-neutron pairs. (^3H and ^3He, protons and neutrons are explicitly excluded.) Also, high energy radiation is forbidden, and the dominant low temperature processes approximately preserve periodic order. As a consequence, at low temperature, in agreement with the experimental findings of Bush et al[3], LINC predicts that the dominant interactions involve the production of ^4He through occupation of ionic ^4He energy band states with subsequent energy release through coupling to phonons or coherent motion (in which the lattice moves as a whole), accompanied by the expulsion of "untrapped", low-energy ^4He (from ionic energy band states) into the surface and outgasing regions. Release of high energy alpha particles at isolated sites is allowed and is promoted by sudden disruption of crystalline order (which may occur, for example, when the electrolytic overpotential is suddenly reduced).

[1] T. S. Kuhn, *The Structure of Scientific Revolutions, Vol II*, 10, (Univ. of Chicago Press, Chicago, 1962).

[2] S. R. Chubb and T. A. Chubb, in *Anomalous Nuclear Effects in Deuterium/Solid Systems*, AIP Conference Proceedings 228, 691, (Amer. Inst. Phys. (New York), 1991).

[3] B. F. Bush, J. J. Lagowski, M. Miles and G. S. Ostrom, *J. Electroanal. Chem.* 304, 271, (1991). Also, talk presented by M. Miles during this meeting.

[4] G. A. Preparata, *Fusion Technology*, 20, 82, (1991).

[5] S. E. Jones, private communication (1991).

[6] T. A. Chubb and S. R. Chubb, "Cold Fusion and a Non-Corpuscular View of Matter," in this Proceedings.

[7] T. A. Chubb and S. R. Chubb , *Fusion Technology*, 20, 93, (1991).

[8] A. C. Switendick, in *Hydrogen in Metals I*, 101, (Springer, Berlin, 1978).

[9] D. A. Papaconstantopoulos, B. M. Klein, J. S. Faulkner, and L. L. Boyer, *Phys. Rev. B* 18, 2784 (1978).

EDITORIAL NOTE TO THE PAPER "AN EXPLANATION OF COLD FUSION..." BY S.R. CHUBB AND T.A. CHUBB

In spite of strong objections of the Referees, we publish this paper, for we wish that all attempts of explanation of a new phenomenon be brought to the attention of the readership, provided they are not trivially wrong or pointless.

The Referees' objection focus on the low credibility of an approach that tries to avoid the difficulties of the existence of a Coulomb barrier between deuterons, by assuming that deuterium is in fact spread out on a large region.

In quantum physics it is the probability amplitude, not the matter distribution, that is spread out. Thus the view presented is in fact in disagreement with quantum mechanics.

Conference Proceedings Vol. 33
«The Science of Cold Fusion»
T. Bressani, E. Del Giudice and G. Preparata (Eds.)
SIF, Bologna 1991

Coherent and Semi-Coherent Neutron Transfer Reactions

Peter L. Hagelstein

Research Laboratory of Electronics, Massachusetts Institute of Technology
Cambridge, Massachusetts 02139, USA

Abstract

The novel process of coherent neutron transfer in the presence of a lattice is proposed to be the basis of a number of anomalous phenomena which have recently been reported in investigations of the Pons-Fleischmann effect.

1. INTRODUCTION

We have examined mechanisms for the coherent neutron capture onto, and the coherent neutron removal, from nuclei in the presence of a lattice. Under fairly restrictive circumstances, it appears to be possible to satisfy both energy and momentum conservation requirements between the microscopic nuclear system and the macroscopic lattice such that coherent nuclear energy transfer to and from the lattice occurs.

This mechanism enables coherent neutron donor and acceptor reactions to occur, with deuterium as the optimum donor nucleus. Coherent reaction pathways leading to heat, tritium, and helium generation are proposed: Heat generation in Pons-Fleischmann cells would result from coherent neutron capture onto ^{6}Li in the lattice; tritium generation would result from coherent neutron capture onto deuterium; coherent neutron capture onto ^{7}Li would lead to ^{8}Li, which would beta decay to ^{8}Be, and ultimately alpha decay to form two ^{4}He nuclei.

Semi-coherent reactions, in which the neutron capture part of the reaction would yield energetic products, are also proposed to account for fast triton production and secondary fast neutron generation.

The present conference proceedings contains a very abreviated version of results and discussions that will appear elsewhere. For detailed references, extended discussions, further comments about notation, etc., the reader is referred to Ref. 1.

2. Coherent Neutron Capture in the Presence of a Lattice

The coherent transfer of a neutron to or from a nucleus in the presence of a lattice in our model is mediated by an electromagnetic transition as depicted in Figure 1. The initial state for coherent neutron removal would include a donor nucleus X and an initial lattice L_X; the final state would include a product nucleus Y, a Bragg state neutron, and a final state lattice L_Y. The transition between the initial state and final state is mediated through near-field $\mathbf{d}\cdot\mathbf{E}$ or $\mu\cdot\mathbf{B}$ hamiltonians, with the electric or magnetic fields being long wavelength macroscopic fields imposed externally, or in the case of electric fields, perhaps arising internally.

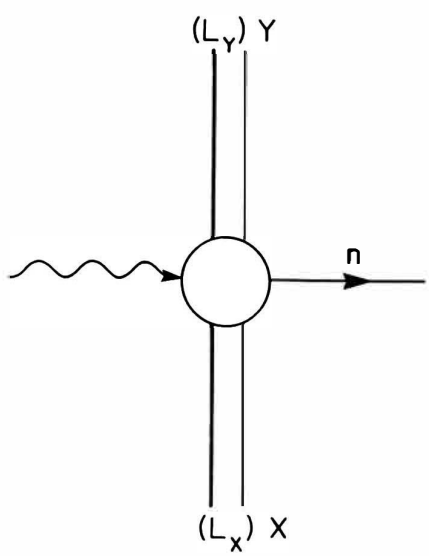

Figure 1. Feynmann-like diagram for a single coherent neutron transfer reaction.

The transition hamiltonian which corresponds to the magnetic version of this

process is described in second quantization through $\hat{H}_{-\mu\cdot\mathbf{B}}$, which is

$$\int d^3\mathbf{r}_1 \cdots \int d^3\mathbf{r}_N \left[\hat{\Psi}_Y^\dagger(\mathbf{r}_1,\cdots,\mathbf{r}_{N-1}) \wedge \hat{\Psi}_n^\dagger(\mathbf{r}_N)\right] \left[-\sum_j \mu_j \cdot \mathbf{B}(\mathbf{r}_j)\right] \hat{\Psi}_X(\mathbf{r}_1,\cdots,\mathbf{r}_N)$$
$$+ \int d^3\mathbf{r}_1 \cdots \int d^3\mathbf{r}_N \hat{\Psi}_X^\dagger(\mathbf{r}_1,\cdots,\mathbf{r}_N) \left[-\sum_j \mu_j \cdot \mathbf{B}(\mathbf{r}_j)\right] \left[\hat{\Psi}_Y(\mathbf{r}_1,\cdots,\mathbf{r}_{N-1}) \wedge \hat{\Psi}_n(\mathbf{r}_N)\right] \tag{2.1}$$

where the nucleon field operators are defined elsewhere[1]; for example

$$\hat{\Psi}_X(\mathbf{r}_1,\cdots,\mathbf{r}_N) = \sum_i \sum_{\alpha_X} \hat{b}_{X,\alpha_X}(i) \Phi_X^{\alpha_X}\left(\mathbf{r}_1 - \hat{\mathbf{R}}_i, \cdots, \mathbf{r}_N - \hat{\mathbf{R}}_i\right) \tag{2.2}$$

The center of mass position is determined as a function of the phonon mode amplitudes through $\hat{\mathbf{R}}_i = \mathbf{R}_i^o + \sum_m \hat{q}_m \mathbf{u}_m(i)$

Upon substituting in our expressions for the various operators which occur in the transition operator we obtain

$$\begin{aligned}\hat{H}_{-\mu\cdot\mathbf{B}} &= \sum_i \sum_{\alpha_n} \sum_{\alpha_X} \sum_{\alpha_Y} \sum_{\mathbf{k}} \hat{b}_{n,\alpha_n,\mathbf{k}}^\dagger \hat{b}_{Y,\alpha_Y}^\dagger(i) \hat{b}_{X,\alpha_X}(i) \left[-\mu_{Y,n,X}^{\alpha_Y,\alpha_n,\alpha_X}\left(\hat{\mathbf{R}}_i^{X_i}, \hat{\mathbf{R}}_i^{Y_i}\right) \cdot \mathbf{B}_i\right] \\ &+ \sum_i \sum_{\alpha_n} \sum_{\alpha_X} \sum_{\alpha_Y} \sum_{\mathbf{k}} \hat{b}_{X,\alpha_X}^\dagger(i) \hat{b}_{n,\alpha_n,\mathbf{k}} \hat{b}_{Y,\alpha_Y}(i) \left[-\mu_{X,Y,n}^{\alpha_X,\alpha_Y,\alpha_n}\left(\hat{\mathbf{R}}_i^{X_i}, \hat{\mathbf{R}}_i^{Y_i}\right) \cdot \mathbf{B}_i\right]\end{aligned}$$

where the first magnetic dipole operator appearing in this equation is defined by

$$\mu_{Y,n,X}^{\alpha_Y,\alpha_n,\alpha_X}\left(\hat{\mathbf{R}}_i^{X_i}, \hat{\mathbf{R}}_i^{Y_i}\right) = \int \cdots \int \left[\Phi_Y^*\left(\mathbf{r}_1 - \hat{\mathbf{R}}_i^{Y_i}, \cdots, \mathbf{r}_{N-1} - \hat{\mathbf{R}}_i^{Y_i}\right) \wedge \Phi_{n,\mathbf{k}}^*(\mathbf{r}_N)\right] \left[\sum_j \mu_j\right]$$
$$\Phi_X\left(\mathbf{r}_1 - \hat{\mathbf{R}}_i^{X_i}, \cdots, \mathbf{r}_N - \hat{\mathbf{R}}_i^{X_i}\right) d^3\mathbf{r}_1 \cdots d^3\mathbf{r}_N \tag{2.4}$$

Some brief discussion of the physical content of this model is in order; the model describes a transfer of a neutron from X whose center of mass is located "at" $\hat{\mathbf{R}}_i^{X_i}$, resulting in the product nucleus Y whose center of mass is located "at" $\hat{\mathbf{R}}_i^{Y_i}$. The positions of the initial and final state nuclei are determined by the degree of lattice excitation and by the lattice displacement vectors, both of which will differ between the initial and final states due to the neutron transfer. The spatial overlap integral given in equation (2.4) ensures that a transfer occurs only when the initial and final center of mass coincide to within fermis; no transfer occurs for large separation. Hence, the magnetic dipole operator is a highly nonlinear function of the lattice

phonon mode amplitudes; we have found an approximate Gaussian dependence on relative separation ($\mu \sim e^{-\frac{1}{2}B|\hat{\mathbf{R}}_i^X - \hat{\mathbf{R}}_i^Y|^2}$, with B on the order of fermi^{-2}) .

3. Energy and Momentum Transfer Between Nuclei and a Lattice

The fundamental theoretical dilemma that presents itself is: how can a large MeV nuclear energy quanta can be transferred to a lattice whose energy levels are quantized on the meV scale? Our initial efforts were focussed on transferring the energy one phonon quanta at a time; this approach, however, appears to be unproductive. The only alternative is to transfer the nuclear quanta in a single step, which requires a large nonperturbative nonlinearity on the part of the lattice in order to accept the energy.

We may view the neutron transfer process as involving a collision between a lattice and a nucleus; the hamiltonian for the lattice may be taken to be of the form

$$H = \sum_m \frac{p_m^2}{2M} + \sum_m \frac{1}{2} M\omega_m^2 q_m^2 + V(t) e^{-\frac{B}{2}\sum_{m,m'} D_{m,m'} q_m q_{m'}} \tag{3.1}$$

The lattice is composed of a large set of oscillators, each with mode amplitude q_m and momentum p_m. We may construct a large dimensional vector $\mathbf{q}$ from the individual mode amplitudes $\mathbf{q} = \sum_m \hat{i}_m q_m$ which would represent the position of the lattice in a N-dimensional space where N is the total number og phonon modes. The nucleus exists in 3-space, but since the center of mass position coordinates are functions of the phonon mode amplitudes, the nuclear scattering potential is mapped into the N-dimensional space as indicated in the above hamiltonian. As a result, the problem that we are interested in analyzing is basically of simple inelastic collisions in q-space between the lattice and nucleus.

We know from an analysis of kinematics in 3-D that energy and momentum must be separately conserved, and that the constraints imposed through conservation determine the essential features of the reaction. We would like to understand how energy and momentum conservation works in this case, especially since it is generally believed that the low energy phonon modes of the lattice cannot accept a nuclear energy quantum; the arguments against this ultimately have to do with whether energy and momentum can be conserved simultaneously.

We may formulate the problem simply: we require that

$$E_i + \Delta E_N = E_f \tag{3.2}$$

and

$$\mathbf{p}_i + \Delta\mathbf{p} = \mathbf{p}_f \tag{3.3}$$

be satisfied at the same time, where E_i and E_f are the total initial and final lattice energies, and where $\mathbf{p}_i$ and $\mathbf{p}_f$ are the total N-dimensional lattice momenta. The nuclear energy transfer is ΔE_N. The lattice may be thought of for the purposes of the present argument as a wave incident on a time-dependent perturbation localized around the origin in q-space; diffraction effects give rise to $\Delta\mathbf{p}$. We find that energy and momentum can be matched simultaneously since

$$\Delta E_N \approx \frac{|\Delta\mathbf{p}|^2}{2M} \approx \frac{\hbar^2 B}{2M} \tag{3.4}$$

by the uncertainty principle.

The diffraction of the lattice off of the localized nuclear potential in q-space is responsible for the momentum transfer, and we have argued here that this momentum transfer can be consistent with the large energy transfer since the phonon mode amplitudes must be localized to within fermis for a coherent neutron transfer reaction to take place. The effect is purely quantum mechanical, since it is diffractive, with no classical analog. The arguments given above can also give constraints on lattice size and total lattice energy required for transitions to occur: these constraints entail the requirement that many modes must be present so that the momentum transfer to each is small, and that sufficient energy be present in each mode so that in an endothermic reaction the energy is available for extraction. We shall discuss these issues further elsewhere.

References

1. P. L. Hagelstein, "Coherent and Semi-Coherent Neutron Transfer reactions. I-IV," submitted to *J. Fusion Tech.* (1991).

Conference Proceedings Vol. 33
«The Science of Cold Fusion»
T. Bressani, E. Del Giudice and G. Preparata (Eds.)
SIF, Bologna 1991

SUMMARY OF PROGRESS IN HYDRON PHYSICS

Frederick J. Mayer and John R. Reitz†

Mayer Applied Research Incorporated*

Abstract: Electromagnetic scattering resonances in the e^-p^+, e^-d^+, e^-t^+ systems produce short-lived, charge-neutral, particles called hydrons. These particles provide the screening of repulsive Coulomb forces so that nuclear reactions between a hydron nucleus and a reaction partner are possible. Hydron formation, reactions, and applications to anomalous nuclear observations in the laboratory and geophysics are summarized.

Introduction: Many researchers are now aware that, in recent years, there have been numerous experiments which appear to be associated with nuclear reactions, but in an energy regime so low as to make them, in effect, impossible. The so-called "cold fusion" observations are but one class of such seemingly impossible nuclear reactions. These experiments, and others such as "cluster impact fusion" and some quite anomalous geophysical observations of the earth, all point to new physical processes that allow nuclear reactions to be accessed by a mechanism other than by overcoming the Coulomb barrier by highly energetic particles.

We have suggested[1,2] that the new process is the creation of compact, unstable, hydrogenic particles that we have called *hydrons*. They are of three types: the π, the δ, and the τ, corresponding to the three hydrogen isotopes. We expect that hydrons and their reactions will play a role in the understanding of a number of astrophysical problems. These range from the geophysical modeling of the earth's interior to the "missing neutrino problem" in solar physics.

Hydron Formation: Hydrons are small, charge-neutral, unstable particles formed in resonant scattering of an electron and a hydrogen nucleus. An electron with just the right energy may be "captured" for a relatively long time

in a deep, attractive potential well, but because it is a scattering process, the electron is released after its natural lifetime or sooner if other forces, for example due to collisions, perturb the system to disassemble. We have suggested[2] that the potential providing the scattering resonance between the two particles is the magnetic dipole-dipole (MDD) interaction, going as $V_m = -2\mu_1\mu_2/r^3$. At large distances (≈ Å), the Coulomb potential, $V_c = -e^2/r$ dominates, whereas at very short distances (≈fm), the MDD potential dominates. We have made a simple square-well model of the scattering calculation to determine the well-depth and radius for the scattering resonances to exist. The radius of the charge-neutral object is estimated to be of the order $a_{12} \approx [(32/\pi)\mu_1\mu_2/(\hbar c)]^{1/2}$. For the e^-e^+ resonance, this gives $a_{ee} \approx [(8/\pi)r_e\lambda_c]^{1/2}$ = 53 fm. Spence[3] and Vary, from a quantum electrodynamics model, find $a_{ee} \approx$ 30 fm. In the π-hydron case, we find $a_{ep} \approx 2$ fm, whereas Benesh[4], Spence and Vary find a value of "a few fermis", adequate agreement given the simplicity of our model. Figure 1 shows the results from the square-well calculations including the V_m and V_c potentials for the e^-e^+ and e^-p^+ cases. δ- and τ-hydrons have comparably small sizes. Being neutral, the hydron penetrates close to the nucleus of a reaction partner, with quantum tunneling penetrating the "residual" barrier to allow nuclear reactions to proceed.

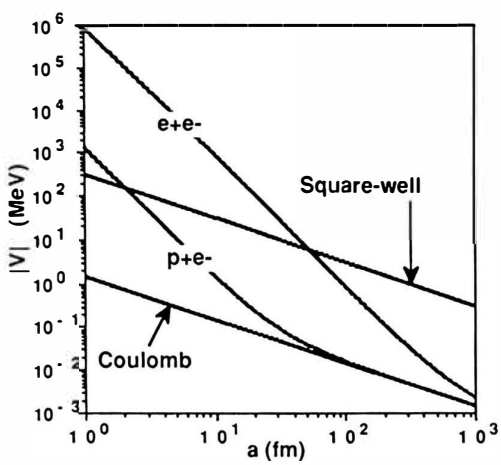

Figure. 1

Plot of the interaction potentials (evaluated at a/2) as a function of a, along with the square-well potential required for the first scattering resonance.

Nuclear Reaction Rates and Cluster Impact Fusion: Hydrons may participate in both fusion and resonant direct nuclear reactions[1] (RDNRs). In RDNRs, the hydron's electron may, due to it's close proximity, carry away some reaction energy. We have examined[2] cluster impact fusion data with hydron generation. The notation is specialized to the case of a δ-hydron reacting with a deuteron, but generalization of the formulae for the π- and τ-hydrons and reactions are straightforward. Averaging over a Maxwell-Boltzmann energy

distribution (at temperature T), the reaction rate for the "screened" δ-d rate is given by,

$$<\sigma v>_s = 1.5\times10^{-15}T^{-1/2}S(0)\,P \quad cm^3/s \qquad (1)$$

with S(0) in keV-barns, T in eV, and P is the "residual" Coulomb barrier factor. The usual "unscreened" d-d rate is given by,

$$<\sigma v>_u = 7.2\times10^{-19}\,\zeta^2 \exp(-\zeta)S(0) \quad cm^3/s \qquad (2)$$

with $\zeta = 197\,T^{-1/3}$. The total reaction rate (per cm^3) of a mixture of δ and d particles is then given by,

$$r = n_\delta n_d <\sigma v>_s + (n_d n_d/2)<\sigma v>_u \qquad (3)$$

where n_d is the deuteron number density. An example of the effect of the δ-hydrons upon the total d-d nuclear reaction rate is shown in Figure 2 where we have taken, P = 1 (complete screening), and S(0) = 55 keV-b. These curves show that substantial reaction rates are possible even with relatively small numbers of δ-hydrons.

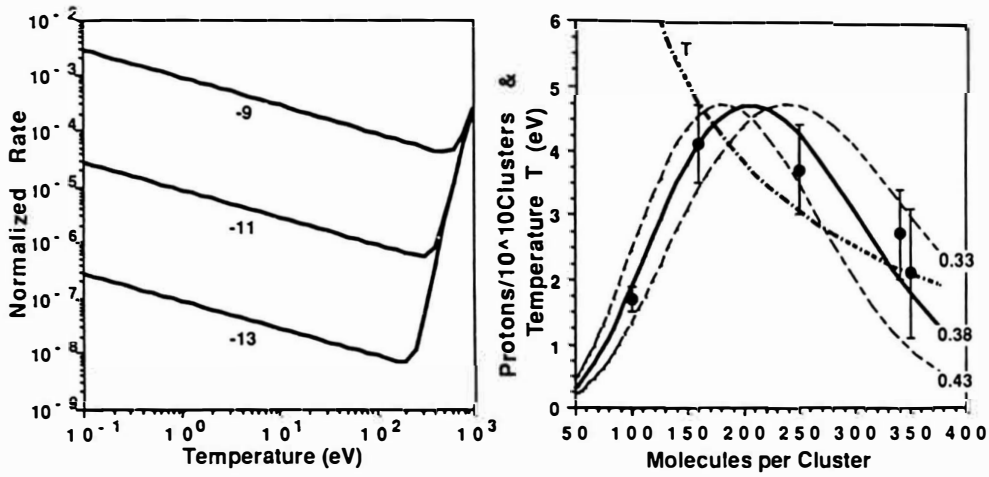

Figure 2 The normalized total reaction rate ($r10^{19}/n_d^2$) as a function of temperature. The parameter is $Log_{10}[n_\delta/n_d]$.

Figure 3 The proton yield data (points) produced in the experiments of BCFFK (with E_{cl} = 300 keV) vs. the number of water molecules in a cluster. The solid & dashed curves are the model results.

In our plasma model[2] for the "cluster impact fusion" experiments of Buehler, Chu, Friedlander, Friedman, and Kunnmann[5](BCFFK), the cluster kinetic energy is shared between the cluster neutrals, electrons, and ions and a larger amount of target material (≈ f times the cluster mass). The cluster kinetic energy deposited is then equated to the thermal energy given by,

$$E_{dep} = N_{cl}[(3/2)(3 + x_e)T + E_i + 9]\,f \qquad (4)$$

where N_{cl} is the number of heavy water molecules in the cluster (≈ 200), x_e is the number of electrons per heavy water molecule at the self-consistent electron

temperature T, E_i is the ionization energy supplied per D_2O molecule, and 9 eV for each dissociated D_2O molecule.

Figure 3 shows a plot of N_p (the proton yield) versus N_{cl} for three different values for the maximum electron thermal conduction (usually about 0.32) and where the lifetime τ_n has been adjusted for a "best fit". Also shown is the self-consistent temperature for the experiments. The "best fit" δ-hydron lifetime extracted from these data is 1.5×10^{-8} seconds.

Other Experiments: The most controversial of these has been the "excess" heat, tritium, and neutrons in "cold fusion" experiments. We have suggested[1] that production of δ- and τ-hydrons, in a metal lattice, may remove the conflicts between theory and experiments in deuterated metals. The new class of nuclear reactions (RDNRs) is a resonant analogue of the direct nuclear reactions in which a neutron is transfered (with positive Q) between a projectile and target nuclei. These resonant reactions are also analogous to low-energy, neutron absorption resonances. Both (d,t) and (t,d) reactions may be operable in cold fusion experiments, allowing for both tritium production and/or consumption but with little or no neutrons or high-energy gamma rays being released. There is some evidence in experiments[1] that RDNRs are responsible for the "excess" heat, tritium, and possibly MeV particle production.

In the experiment of Klyuev[6], et al, a crystal of LiD was fractured by a shock wave produced by the impact of a 0.2 km/s projectile, producing both ionization and dislodged deuterons. These conditions are favorable to the production of a small number of δ-hydrons which can react with deuterons, producing a small number of d-d neutrons.

Arzhannikov and Kezerashvili[7] report small, but statistically significant numbers of d-d neutrons were produced when LiD pellets were dropped into a test-tube of "heavy" water. In this case, some δ-hydrons could have been produced from the slight ionization in the chemical reaction, with the hydrons then producing d-d neutrons.

Implications for Astrophysics and Geophysics: Hydrons may play a role in astrophysical situations. One case is the heat generated in Jupiter, about twice as much as it receives from the sun. We have developed[8] a model calculation based upon hydron generation which may account for this "excess heat". Another well-known astrophysical paradox is that of the "missing" solar neutrinos. π-hydrons in the sun may allow the "burning" of protons in π-p reactions at much lower energy, thereby providing the same nuclear energy at a lower average temperature. With the sun's central temperature slightly lower,

many of the higher energy neutrinos expected from the "standard" solar model would be much reduced if not eliminated altogether[8].

The third example is that of the Earth's heat and helium flux. Jones[9] et al, have suggested that fusion reactions may be occuring inside the Earth given the observation that tritium is released from active volcanoes. Geologists believe that the radiogenic nuclides can account for only about five percent[10] of the heat flow out of the earth. Although mostly iron, the Earth's core contains lower density components including, perhaps, some hydrogen[11]. We consider the possibility of hydron-mediated fusion reactions as the source of the observed heat and helium fluxes[12]; the reactions are: $d(p,\gamma)He^3$, $d(d,p)t$, $d(d,n)He^3$, and $d(He^3,p)He^4$. The total nuclear power generated/cm^3 is obtained from the appropriate rate equations. We find the surface fluxes of He^3, He^4, and heat to be 1.6×10^5/sec-m^2, 2.4×10^{10}/sec-m^2, and 87 mW/m^2, respectively, in reasonable agreement with the measured values[13].

Discussion and Conclusions: The existence of relatively long-lived scattering resonance states in electron-hydrogen nuclei systems allows nuclear reactions in metals and plasmas with sufficiently high hydrogen densities and temperatures. Both fusion reactions and a new type of reaction, RDNRs, have been identified in various experiments. The RDNRs have a unique characteristic -- they do not release neutrons, potentially important for the development of these reactions in nuclear reactors.

* Mayer Applied Research Inc., 1417 Dicken Drive, Ann Arbor, MI 48103
† 2260 Chaucer, Ann Arbor, MI 48103

References:

(1) F. J. Mayer and J. R. Reitz, Fusion Technology 19, 552 (1991).
(2) F. J. Mayer and J. R. Reitz, to be published in Fusion Technology.
(3) J. R. Spence and J. P. Vary, Phys. Lett. B, 254, 1 (1991).
(4) C. J. Benesh, J. R. Spence, and J. P. Vary, BAPS 35, 1673 (1990).
(5) R. J. Buehler, Y. Y. Chu, G. Friedlander, L. Friedman, and W. Kunnmann, J. Phys. Chem. 94, 7667 (1990), and references therein.
(6) V. A. Klyuev, et al., Sov. Tech. Phys. Lett. 12, 551 (1986).
(7) A. V. Arzhannikov and G. Ya. Kezerashvili, "First Observation of Neutron Emission from Chemical Reactions", a preprint of the Institute of Nuclear Physics, 630090, Novosibirsk, USSR.
(8) F. J. Mayer, W. B. Fechner, and J. R. Reitz, unpublished.
(9) S. E. Jones, et al., preprint submitted to Nature (Mar. 23, 1989).
(10) E. R. Oxburgh and R. K. O'Nions, Science 237, 1583 (1987).
(11) D. L. Anderson, Physics Today, March 1989, pg. 38.
(12) F. J. Mayer and J. R. Reitz, to be published.
(13) R. K. O'Nions and E. R. Oxburgh, Nature 306, 429 (1983).

EDITORIAL NOTE TO THE PAPER "SUMMARY OF PROGRESS IN HYDRON PHYSICS" BY F.J. MAYER AND J.R. REITZ

Some grave flaws can be pointed out in the assumptions of this article. See the following contribution of Prof. Mc Neil, and Preparata's report.

Conference Proceedings Vol. 33
«The Science of Cold Fusion»
T. Bressani, E. Del Giudice and G. Preparata (Eds.)
SIF, Bologna 1991

RELATIVISTIC HYPERFINE INTERACTION AND THE SPENCE-VARY RESONANCE

J. A. McNeil

Department of Physics
Colorado School of Mines
Golden, Colorado 80302
USA

Introduction

Spence and Vary[1,2] have reported a resonance in calculations of positronium and hydrogen in the "axion" (0^-) channel. The energy and lifetime of the positronium resonances have led these authors to suggest this new state as an explanation for the anomalous e^+e^- peaks seen at GSI[3]. They and others[4] speculate that similar states in hydrogen may explain anomalous nuclear reactions reported in metal lattices at low temperatures ("cold fusion").

Spence and Vary calculate the Bethe-Salpeter four-leg amplitude using a Blankenbechler-Sugar reduction. They use single photon exchange in Coulomb gauge for the kernel of their equations. Their results seem to depend critically on the use of this gauge. Attempts by others[5] to reproduce their result in Feynman gauge have not been successful. The starting point in either calculation is gauge invariant so the reduction formalism must introduce spurious gauge dependence. Whether the results of Spence and Vary are spurious is not known at this time.

In an attempt to address this question in a qualitative yet gauge-invariant way, we have studied the two fermion system using the Breit equation. The wavefunctions explicitly obey current conservation so the Coulomb gauge terms can have no effect on the results. For the purposes of obtaining qualitative features of the affect of the hyperfine interaction at short distances we approximate the relative coordinate Breit equation by the equivalent Schrödinger-form equation for hydrogen ($m_1 \gg m_2$, for applications to positronium we use the reduced mass). We examine the hyperfine interaction in the axion channel and solve the equation in the energy range of interest ($0 \rightarrow 2$ MeV). We find the hyperfine interaction introduces an effective attractive interaction at very short distances ($\sim$10 fm for positronium), but find no evidence for a resonance in the energy range of interest.

Description of Calculation

The Breit equation assumes an additive hamiltonian in the space of the two interacting Dirac particles. This cannot be exact, but provides a reasonable and tractable model for examining qualitative relativistic features and provides quantitatively accurate results for weak interactions. The resulting equation separates into relative and center-of-mass coordinates[6]. The relative coordinate Breit equation with single photon exchange interaction is

$$[(\vec{\alpha}_1 - \vec{\alpha}_2)\cdot\vec{p} - \beta_1 m_1 - \beta_2 m_2 - \frac{e^2}{r}(1 - \vec{\alpha}_1\cdot\vec{\alpha}_2)]\Psi = E\Psi \tag{1}$$

We use Feynman gauge for the interaction but note that since the wavefunction explicitly obeys current conservation the calculation is independent of gauge. This equation can be solved in the

16x16 matrix product space using the Fermi-Yang[7] representation. For the purpose of qualitatively studying a possible resonance, it is sufficient to consider the hydrogen atom limit ($m_1 \gg m_2$). This allows one to reduce the Breit equation to an effective Schrödinger equation[8]:

$$\left(\frac{-\nabla^2}{2m} + V(r)\right)\psi(\vec{r}) = E\psi(\vec{r}). \tag{2}$$

where

$$\begin{aligned} V(\vec{r}) = & \frac{-E\,e^2}{m\;\;r} + \frac{l(l+1) - e^4}{2mr^2} \frac{1}{2m(E+m+\frac{e^2}{r})}\frac{e^2}{r^3}(r\frac{d}{dr} - 2\vec{s}\cdot\vec{L}) \\ & + \frac{e}{2m}\frac{2}{(E+m+\frac{e^2}{r})}\frac{e^2}{r^3}\mu\vec{I}\cdot(\frac{\vec{s}}{r} - \frac{\vec{r}\vec{s}\cdot\vec{r}}{r^3}) \\ & + \frac{e}{2m}2\mu\vec{I}\cdot(\frac{\vec{L}-\vec{s}}{r^3} + \frac{3\vec{r}\vec{s}\cdot\vec{r}}{r^5} - 4\pi\delta^3(\vec{r})) \\ & + \frac{e^2}{2m}\frac{\mu^2}{r^4}(I^2 - \vec{I}\cdot\hat{r}\vec{I}\cdot\hat{r}) \end{aligned} \tag{3}$$

and where $\vec{I}$ is the spin of the 'heavy' particle and μ is its magnetic moment. Equation (3) differs from the corresponding expression in Ref. (8) because no assumptions regarding the relative magnitudes of E and e^2/r have been made. This expression is appropriate for hydrogen and should provide qualitative results applied to positronium using a reduced mass.

For the axion resonance (0^-) the spin-dependent operators are diagonal in the $|[[s_1, l]j_1, I]J>$ representation.

$$2\vec{s}\cdot\vec{L} = (j_1(j_1+1) - l(l+1) - 3/4)|[[s_1, l]j_1, I]J> \tag{4}$$

$$\vec{I}\cdot\hat{r}\vec{s}\cdot\hat{r}|[[s_1, l]j_1, I]J> = \frac{J(J+1) - j_1(j_1+1) - 3/4}{8j_1(j_1+1)}|[[s_1, l]j_1, I]J> \tag{5}$$

$$\vec{I}\cdot\vec{s}|[[s_1, l]j_1, I]J> = \frac{j_1(j_1+1) - l(l+1) + 3/4}{2j_1(j_1+1)}\frac{J(J+1) - J_1(j_1+1) - 3/4}{2}|[[s_1, l]j_1, I]J> \tag{6}$$

The resulting effective potential for positronium is shown in Fig. 1. Note the four regions where the various terms in V dominate. For r greater than about one angstrom the familiar coulomb attraction dominates. Between about 10 fermis and 1 angstrom the centrifugal repulsion dominates. The hyperfine interaction dominates the effective interaction below about 10 fermis. In the axion channel for positronium the hyperfine interaction is attractive down to about 1 fermi below which the repulsive $1/r^4$ hyperfine term dominates. Note, especially, the large scale of the effective interaction at these short distances. For any hope of quantitative accuracy, one should include vacuum polarization effects. At short distances such corrections will be large on the scale of the electron rest mass, but still small on the scale of the main effective interaction term, and as such should not affect the qualitative features found by neglecting them.

The effective Schrödinger equation is solved numerically using Numerov with regular boundary conditions near the origin. To provide numerical stability over the enormous range of distance scales we use a dynamically rescaled (exponentially) grid spacing. These solutions may be matched onto asymptotic Coulomb wavefunctions and the hyperfine part of the phase shift extracted. We find that the relativistic hyperfine phase shift is small ($\sim$ .01 radians) and slowly varying over the range of energies near the reported resonance. In this range the attractive hyperfine interaction puts a node in the wavefunction at around 10 fermis (see Fig. 2). The phase shift is given approximately by this distance times the asymptotic wave number. The behavior of the wavefunction in the short distance region is quite stable in this energy range. In conclusion we have presented an approximate, but gauge invariant, calculation of the relativistic hyperfine phase shift. The calculation, while not quantitatively accurate, should reveal qualitative features such as scattering resonances. We find no evidence for a resonance in the energy range of that reported by Spence and Vary.

Acknowledgements

This work was supported in part by the United States National Science Foundation. The author thanks F. E. Cecil, C. J. Horowitz, and C. E. Price for helpful conversations.

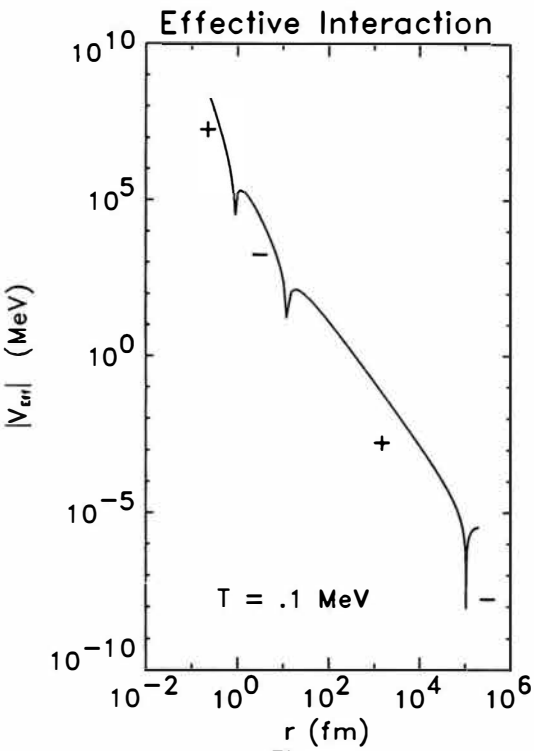

Figure 1

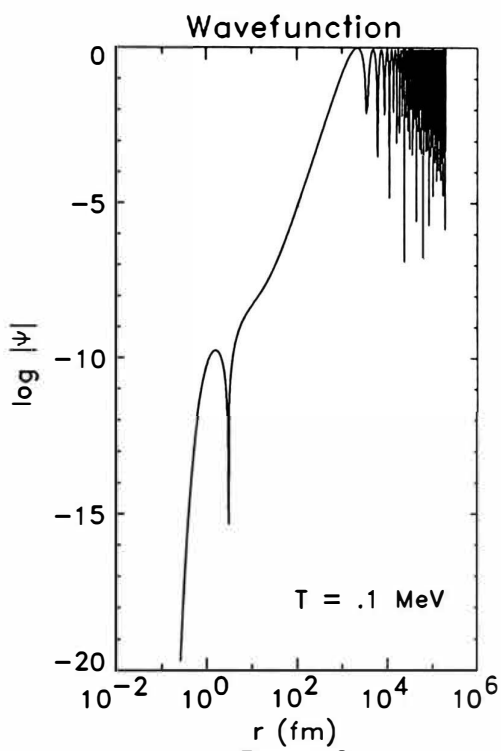

Figure 2

References

1. J. R. Spence and J. P. Vary, BAPS **35**, 1677 (1990).
2. C. J. Benesh, J. P. Vary, and J. R. Spence, BAPS **35**, 1673 (1990).
3. T. Cowan, et al., Phys. Rev. Lett. **56**, 444 (1986).
4. F. J. Mayer and J. R. Reitz, Fusion Tech. **19**, 552 (1991), see also F. Mayer in these proceedings.
5. C. J. Horowitz, private communication.
6. A. O. Barut and N. Unal, Fortsch. der Phys. **33**, 319 (1985).
7. E. Fermi and C. N. Yang, Phys. Rev. **76**, 1739 (1949).
8. M. Weissbluth, **Atoms and Molecules**, Academic Press, New York, 1978.

Conference Proceedings Vol. 33
«The Science of Cold Fusion»
T. Bressani, E. Del Giudice and G. Preparata (Eds.)
SIF, Bologna 1991

ANOMALOUS DEUTERON TO HYDROGEN RATIO IN OKLO SAMPLES AND THE POSSIBILITY OF DEUTERON DISINTEGRATION

M. Shaheen, M. Ragheb, and G. H. Miley
Fusion Studies Laboratory
University of Illinois at Urbana-Champaign
103 S. Goodwin Ave., Urbana, IL 61801 USA
(217) 333-3772

H. Hora and J. Kelly
The University of New South Wales
P. O. Box 1
Kensington, New South Wales, Australia 2033

Abstract

A hypothesis is presented to explain the anomalous D/H ratio observed in samples from the site of the naturally occurring fission reaction at Oklo. The experimentally observed D/H ratio of 127 ppm exceeds the naturally occurring value of 150 ppm. Further, using a multicomponent system consisting of hydrogen, deuterium, tritium and helium nuclei to model the Oklo reaction phenomenon and assuming a thermal fission process term, we calculate a D/H ratio of 445 ppm in the presence of the thermal neutron fluence attributed to Oklo. However, solving the same rate equations with a deuterium sink term to represent the hypothesis of deuteron disintegration, we find a deuteron disintegration constant of $7.47 \times 10^{-14} s^{-1}$ yields the observed D/H ratio. Indeed, deuteron disintegration would provide a neutron source (in addition to the fission neutrons) that could have driven the Oklo system as a subcritical (vs. a critical) reactor over the extended period attributed to it.

Introduction

The historic phenomenon where a naturally occurring fission chain-reaction took place is located at the Oklo mining site in Gabon, Africa.[1,2] Geological characteristics at Oklo allowed the formation of soluble uranium salts in water. Since fission products have been found in samples from the site, it was determined that a fission process had taken place in this ore. Based on the measured depletion of U^{235} and the concentrations of the fission products, the reaction is estimated to have lasted for a period between 600,000 to 3,500,000 years [3]. The fluence of neutrons required to account for these observations has been estimated by various investigators to be about 10^{21} n/cm^2[1-4].

The D/H Anomalogy

Samples from the Oklo site have been analyzed for water and hydrogen content by heating them to about 1200°C. The D/H ratio in natural water is close to 150 ppm. In contrast, when water from minerals at the Oklo site was analyzed, the D/H ratio was found to range around 127 ppm[5]. This discrepancy is even more serious when it is realized that, as we show later, for the neutron fluence estimated for Oklo, the D/H ratio should have increased to about 450 ppm because of neutron capture in hydrogen. To our knowledge this discrepancy, namely the low D/H ratio measured at Oklo, has not previously been discussed in the literature nor has any explanation been proposed prior to this.

Analysis

Figure 1a depicts a multicomponent system that describes the major isotopic transitions for elements (Hydrogen, Deuterium, Tritium and He-3) undergoing a neutron irradiation. Assuming that all of the He^3 produced escapes

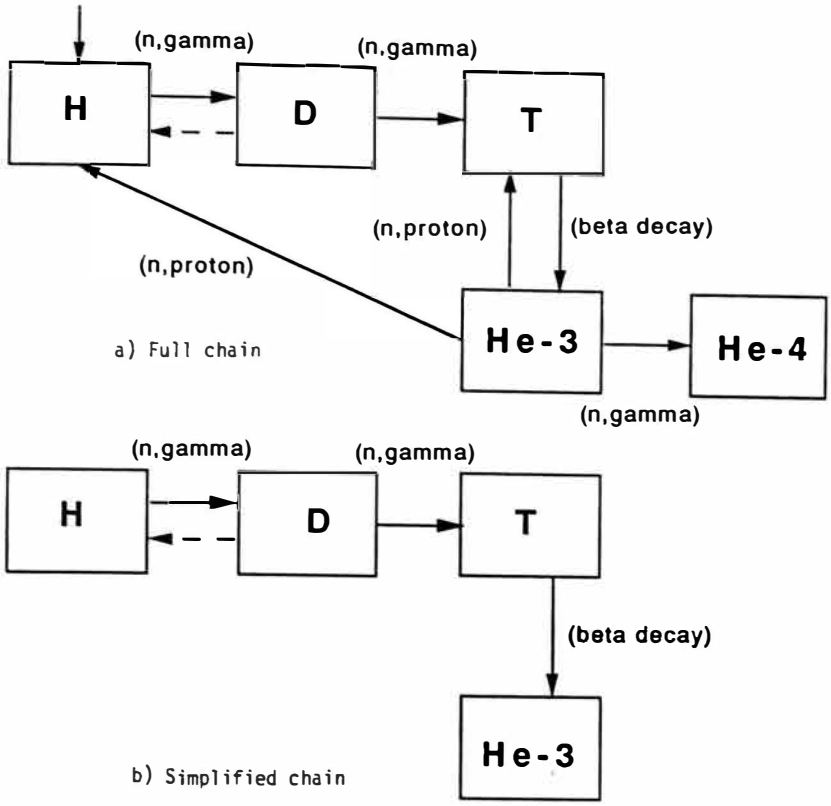

Figure 1. Multicomponent System Consisting of Hydrogen, Deuterium, Tritium, and Helium-3 and Isotopic Transitions of Elements in a Neutron Flux.

from the site so that it doesn't contribute further to the isotopic changes, the chain is simplified to the one shown in Fig. 1-b. (If He^3 did not escape from the reaction site, it could either undergo an (n,p) or an (n,γ) reaction). Then, in this multicomponent system, hydrogen can be produced from two sources: 1) the He^3 (n,p) reaction, and 2) postulated deuteron disintegration according to: ${}_1D^2 \rightarrow {}_0n^1 + {}_1H^1$. Deuterons are produced from neutron capture in hydrogen and are provided with two sinks: disintegration into hydrogen [6,7], and capture of a neutron with production of tritium. Tritium decays by β^- emission to He^3 with a half life of 12.3 years.

Because of the presence of water, we are justified to assume that the Oklo neutron energy spectrum was basically thermal with a Maxwellian shape at temperature T_o. Table I shows the thermal neutron cross sections for the various reactions in this chain.

The rate equations for the multicomponent system shown in Fig. 1, assuming a pure fission process but with the added hypothesis of deuteron disintegration (decay constant λ_D) into H + n, can be written as:

$$dH/dt = -\beta_H H + \beta_p He + \lambda_D D \quad (1)$$

$$dD/dt = \beta_H H - (\beta_D + \lambda_D) D \quad (2)$$

$$dT/dt = \beta_D D - \lambda_T T + \beta_p He \quad (3)$$

$$dHe/dt = \lambda_T T - \beta_p He \quad (4)$$

Here H, D, T, and He are the concentrations in atoms/cm^3 of hydrogen, deuterium, tritium, and helium-3, respectively.

We have defined:

$$\beta_H = \sigma_{\gamma H}\phi, \quad (s^{-1}) \quad (5a)$$

$$\beta_D = \sigma_{\lambda D}\phi, \quad (s^{-1}) \quad (5b)$$

$$\beta_p = \sigma_{pHe}\phi \quad (s^{-1}) \quad (5c)$$

where we made the approximation:

$$\sigma_{pHe} \simeq \sigma_{aHe} \quad (6)$$

Table I. Thermal Cross Sections for H, D, T, and He^3 Neutron Reactions

Reaction	Thermal Neutron Cross Section (Barns)
H (n,γ) D	0.333
D (n,γ) T	0.51×10^{-3}
T (n,γ) H^4	$< 6 \times 10^{-3}$
He^3 (n,p) T	5330
He^3 (n,γ) He^4	0.05

This assumption implies that absorption in He-3 mainly cause the (n,p) reaction which has a large cross-section value as shown in Table I.

As a first step, we are interested in the H and D concentrations without deuterium disintegration ($\lambda_D = 0$). Solving the corresponding set of coupled differential equations, we find the ratio R=D/H in this case is:

$$R = \{R_o + \frac{\sigma_{\gamma H}}{\sigma_{\gamma H} - \sigma_{\gamma D}}\} e^{(\sigma_{\gamma H} - \sigma_{\gamma D})\Phi} - \{\frac{\sigma_{\gamma H}}{\sigma_{\gamma H} - \sigma_{\gamma D}}\} \quad (7)$$

where the reference (starting) ratio is taken as the natural value, i.e., $R_o = D_o/H_o = 150$ ppm.

We note that R is function of the fluence only, since all other parameters are constants. Using the estimated value of the fluence for Oklo, $\Phi = 10^{21}$ n/cm^2, we find that R = 445 ppm. This then is the R ratio expected under the natural thermal reactor assumption without deuteron disintegration.

Figure 2 shows the variation of the ratio R = D/H as a function of the fluence. We notice that R remains as a constant (R_o) up to a value of the fluence $\Phi = 10^{20}$, after which it rises sharply with increasing fluence.

The fact that the D/H ratio observed in the Oklo samples (127 ppm) is reduced below the natural value R_o (150 ppm), when it should have risen to around 445 ppm as calculated above, is in direct contradiction with the expectations based on the natural reactor assumption alone. This anomaly is the focus of our study.

We next consider the case with postulated deuterium disintegration. This is a tempting assumption since, as seen from Table II, compared to other low-Z elements, deuterium has a uniquely low binding energy. Here we have assumed that the anomaly is due to a nuclear process since we are unaware of any chemical or other physical process

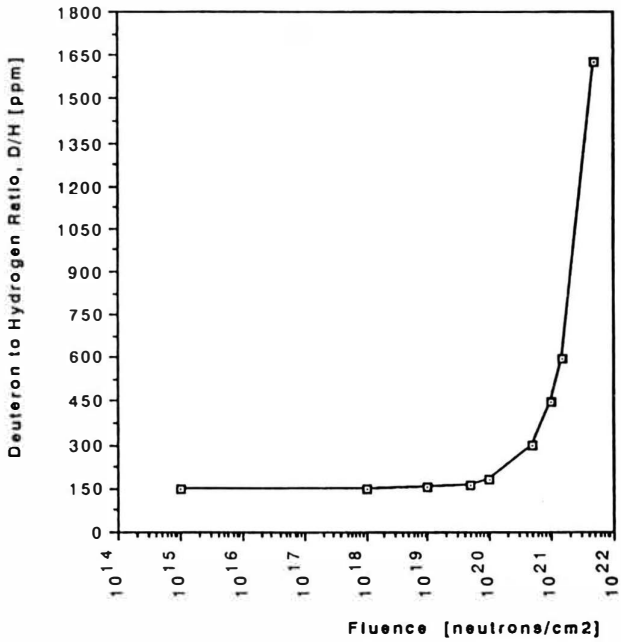

Figure 2. D/H Ratio for Different Fluences in Case of no Deuteron Disintegration ($\lambda_D = 0$).

Table II. Binding Energy (BE) of Typical Nuclides [5]

Nuclide	BE/A (MeV/nucleon)	BE (MeV)
D-2	1.12	2.23
T-3	2.83	8.48
He-3	2.57	7.72
He-4	7.08	28.30
Li-6	5.33	32.00
Li-7	5.60	39.20
Be-9	6.47	58.19
Average per nucleon	~ 8.50	--

which could have depleted the deuterium and/or enriched the hydrogen content of the ore mineral. Thus we propose that the deuterons have undergone a process involving disintegration. Then, regardless of the mechanism involved, the following reaction would have, in principle, taken place:

$$ {}_1D^2 \longrightarrow {}_1H^1 + {}_0n^1 \qquad (8) $$

For an Oklo reaction that has lasted for a time duration t_d, the final D/H ratio, R_k, is then given by:

$$ R_k = \frac{1}{\lambda_D} \left[\frac{(s_1 R_o + \beta_H)\, e^{s_1 t_d} - (s_2 R_o + \beta_H)\, e^{s_2 t_d}}{\frac{(s_1 R_o + \beta_H)}{(s_1 + \beta_H)}\, e^{s_1 t_d} - \frac{(s_2 R_o + \beta_H)}{(s_2 - \beta_H)}\, e^{s_2 t_d}} \right] \qquad (9a) $$

where both s_1 and s_2 are functions of λ_D, i.e.

$$ S_1, S_2 = 1/2 \left\{ -(\beta_H + \beta_D + \gamma_D) \pm [(\beta_H + \beta_D + \gamma_D)^2 - 4\beta_H \beta_D]^{1/2} \right\} \qquad (9b) $$

Results

We have calculated the value of the deuteron disintegration constant λ_D under the conditions of the Oklo phenomenon for three values of Φ around 10^{21}, namely: 0.5×10^{21}, 1.0×10^{21}, 1.5×10^{21}, and for different time durations in the range: 3×10^5-1.2×10^6 years. Although the variation of the estimated time duration is large, the value of λ_D calculated for the same fluence and limiting time periods is not very large. Similarly, for the same time duration, the variation of λ_D for fluence values of 0.5×10^{21} and 1.5×10^{21} is also not large. Thus, we adopt as a reference case values of $\Phi = 10^{21}$ and $t_d = 10^6$ years. In Fig. 3 we show the D/H ratio, R, for the range of λ_D values between 10^{-20} and 10^{-6} s^{-1} for the three fluence cases for $t_d = 10^6$ years.

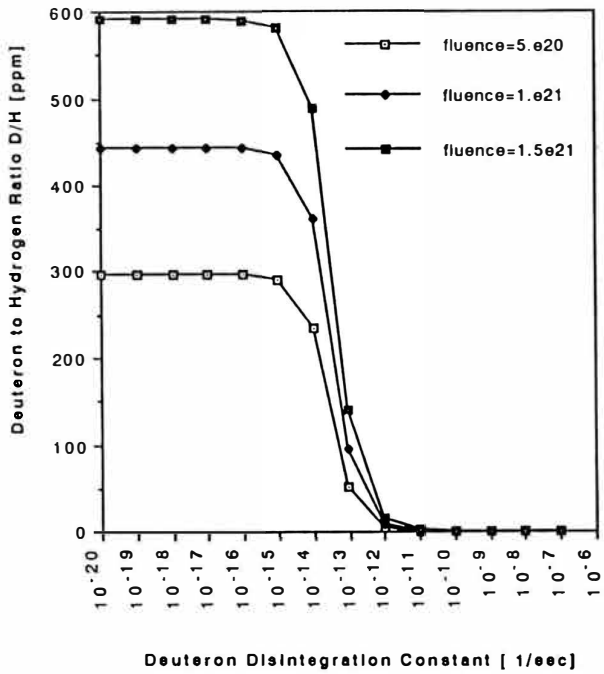

Figure 3. Deuteron to Hydrogen (D/H) Ratio Versus the Deuteron Disintegration Constant for Different Fluences.

One can compute λ_{Dk}, i.e., the value of λ_D that will lead to a D/H ratio $R=R_k=127.3$ (from the Oklo sample #310) for a reaction where the fluence Φ has lasted for time t_d. For the reference case, this turns out to be $7.47\times10^{-14}s^{-1}$.

COMMENTS ABOUT PROCESSES

Up to this point the results are independent of the specific deuteron disintegration process assumed. Now it is interesting to consider several possible processes and the consequences implied. We assume that deuteron disintegration is not a single particle reaction but rather a multiple particle interaction, i.e., unlike natural decay, the deuteron disintegrates under the unique system created by the collection of the deuteron itself and the surrounding atoms under the thermodynamic conditions present. Then the deuteron disintegration reaction may proceed in one of two ways. First, postulating a free neutron reaction, we have:

$$ {}_1D^2 + {}_ZN^A \text{ ----> } {}_1H^1 + {}_0n^1 + {}_ZN^A \quad . \tag{10} $$

Here the nucleus ${}_ZN^A$ acts as a catalyst for the deuteron disintegration process, and does not undergo any isotopic changes.

A second way for the reaction to proceed involves isotopic changes in the medium that involve a "neutron swapping" type reaction[6,7]. Then the deuteron gives up its neutron to the neighboring nucleus ${}_ZN^A$ according to:

$$ {}_1D^2 + {}_ZN^A \text{ ----> } {}_1H^1 + {}_ZN^{A+1} \quad . \tag{11} $$

An example of this kind of reaction for Oklo would be:

$$ {}_1D^2 + {}_1D^2 \text{ ----> } {}_1T^3 + {}_1H^1 \tag{12a} $$

$$ {}_1T^3 \text{ ----> } {}_{-1}e^o + {}_2He^3 \quad . \tag{12b} $$

Provided that the reaction time is long enough to allow for the complete decay of the tritium to helium-3, we can write the net reaction as:

$$ {}_1D^2 + {}_1D^2 \text{ ---> } {}_{-1}e^o + {}_1H^1 + {}_2He^3 \quad . \tag{13} $$

It is instructive to compare this result to the deuterium transformation driven by neutron capture:

$$ {}_1D^2 + {}_on^1 \text{ ---> } {}_1T^3 \tag{14a} $$

$$ {}_1T^3 \text{ ---> } {}_{-1}e^o + {}_2He^3 \quad . \tag{14b} $$

Again, if the reaction proceeds for a long enough time, then the net reaction is:

$$ {}_1D^2 + {}_on^1 \text{ ---> } {}_{-1}e^o + {}_2He^3 \quad . \tag{15} $$

Both reactions involve the depletion of deuterons with the production of tritium and He^3. However, the first reaction

involves the depletion of twice as many deuterons and also leads to the production of protons. If an experiment is performed in which the Oklo conditions are reproduced, the neutron swapping hypothesis could be tested based on reactions 12-13 vs. 14-15.

According to the preceding disintegration assumption, we can state, in general, that the rate of disintegration of deuterons is proportional to the product of the deuteron concentration and to the concentration of host atoms N, i.e.:

$$\lambda_D \; D \; \alpha \; D \; N \quad . \tag{16}$$

We further assume that the concentation of the host atom, corresponding to uranium in the Oklo case, is constant. This assumption is reasonable since the fractional uranium depletion in the estimated fluence will be only $\sim 10^{-3}$. Then denoting the proportionality constant in Eqn. 16 by μ_D, we obtain:

$$\lambda_D = \mu_D N \tag{17a}$$

or

$$\mu_D = \lambda_D / N \quad cm^3/s \quad . \tag{17b}$$

Note that μ_D has the same units as $\langle \sigma v \rangle$, the reaction parameter used in plasma physics and fusion studies.

If the reaction is a D-U disintegration reaction, i.e., deuterons disintegrating while present in the Uranium lattice, assuming that the mineral was in the form of UO_2, we find for the Oklo sample #310 data:

$$\mu_{DU} = \lambda_D / U = 2.24 \times 10^{-35} \; cm^3/s \tag{18}$$

where a U concentration of 3.33×10^{21} U atoms/cm^3 was used.

The above result is not valid for D-D disintegration, however, since then the term describing deuteron

disintegration rate should be λD^2. We have accounted for that situation in the numerical calculation scheme. Then the D-D disintegration constant needed to account for the D/H ratio R_k is found to be $\sim 10^{-31} cm^3/s$. Further, if the reaction involved was a D-D disintegration such that it can be described by the term $\lambda_D D$, then the reaction constant is $\sim 7.47 \times 10^{-14}$ [D disintegrations/D.sec] as noted earlier.

Tritium and Helium-3 Concentrations

As shown in Fig. 1, the Oklo reaction will lead to the production of T and He^3. To obtain their concentrations, the rate Equations 3 and 4 are solved with D(t) given by the solution of Equations 1 & 2. It is possible to obtain a solution in the case where the initial concentrations of T and He^3 are not zero. However, there is no reason to assume that T or He^3 existed in the ore initially, and hence we will not show the solution in that case. Interestingly, an examination of these equations shows that the concentrations of T and He^3 are proportional to the initial water content in the rock. For the typical case of $\Phi = 10^{21}$, $t_d=10^6$ so that $\lambda_D=7.47 \times 10^{-14}$ and the final concentrations in this case are $T(t_d) = 3.8 \times 10^7$ and $He(t_d)=3.78 \times 10^{11}$. The corresponding rate of He^3 production would be $He(t_d)/t_d=0.012$ He^3 atom/cm^3.s.

Uranium Anomaly

Earlier Vlasov[8] pointed out that the U^{238}/U^{235} ratio was anomalously low. This seems to imply that fast neutron fission of U^{238} occurred. Thus, Vlasov suggests that an annihilation explosion of an antimatter meteorite caused the formation of free fast neutrons[8]. He further estimates the yield of such an explosion to be from 3-5 neutrons per antinucleon annihilation depending on the conditions. However, if our deuterium disintegration hypothesis is employed under the assumption of neutron swapping, the postulate of an antimatter explosion is not necessary. This

can be understood by considering the various reactions that may have occurred. According to the proposed neutron swapping model, U^{238} can undergo the following reactions:

$$ {}_1D^2 + {}_{92}U^{238} \text{ ----> } F_1 + F_2 + {}_1H^1 + \nu\ {}_0n^1 \qquad (19) $$

or

$$ {}_1D^2 + {}_{92}U^{238} \text{ ----> } {}_1H^1 + {}_{92}U^{239} \qquad (20) $$

where F_1 and F_2 are fission products. The U^{239} decay chain eventually produces Pu^{239} which could undergo thermal fission. This process could possibly explain the low U^{238}/U^{235} ratio.

COMPARISON WITH EARTH CORE HYPOTHESIS

Jones et al.[9] have suggested that cold fusion takes place in the earth interior. Based on an estimated He^3 flow of $2x10^{19}$ He^3 atom/s out of the earth's mantle, and using a mantle water reservoir of $1.4x10^{24}$ g, they estimate a value for the cold fusion D-D fusion constant of 10^{-24} fusions/deuteron-s. The value which we calculated for a D-D disintegration reaction in the Oklo medium is $7.57x10^{-14}$ disintegrations/deuteron-sec, which is about ten orders of magnitude higher than the Jones, et al. value.

We can estimate, according to our hypothesis, the He^3 flow out of the earth's mantle. We have calculated that under the localized conditions of the Oklo deposit, the rate of He^3 escape out of the deposit is 0.012 He^3 at/cm^3.sec. If we assume that the same conditions that existed at Oklo prevail in the mantle of the earth, then we find a total He^3 flow out of the earth's mantle due to an Oklo-type reaction is ~ $1.7x10^{22}$ He^3 atm/sec. This is to be compared to the Jones, et al. value of $2x10^{19}$, keeping in mind that the conditions of the Oklo reaction may have been more favorable than the earth's mantle for the deuteron disintegration reaction.

Conclusion

The anomalously low D/H ratio found in samples from Oklo strongly suggest that a deuterium disintegration process occurred. If so, for Oklo conditions, the rate is shown to be about 7.5×10^{-14}D disintegrations/deuteron-sec. The exact mechanism involved is open to debate and study. We favor a neutron swapping type reaction which would be enabled by the unique Oklo conditions of thermodynamic parameters and D-U mixture. If so, this reaction could offer an alternate explanation to the anomalously low U^{238}/U^{235} ratio cited earlier by Vlasov. While the results show higher rates than those found by Jones, et al., for earth mantle reactions, the difference could be due to the specific conditions present at Oklo, e.g., the relatively high uranium concentration.

Acknowledgments

One of the authors (M. Shaheen) first called attention to the D/H anomaly during a special topic study. Partial support by Fusion Cells, Inc., Champaign, Illinois is gratefully acknowledged.

References

1. P. K. Kuroda, "The Origin of the Chemical Elements and the Oklo Phenomenon," Springer-Verlag, Berlin, Germany (1982).

2. M. Neuilly, et al., Comptes Rendus Acad. Sci., 275, D-1847 (1972).

3. R. Hagemann, et al., "Le Pheonomenon d'Oklo," Proc. IAEA Int. Symp. Oklo Pheonomenon, Libreville, Gabon, June 23-27, 1975, CONF-750461, International Atomic Energy Agency (1975).

4. M. Neuilly and R. Naudet, "Le Phenomenon d'Oko," Proc. IAEA Int. Symp. Oklo Phenomenon, Libreville, Gabon, June 23-17, 1975, CONF-750461, International Atomic Energy Agency (1975).

5. G. Baudin, et al., Comptes Rendus. Acad. Sci., 275, D-2291 (1972).

6. M. Ragheb and G. Miley, Fusion Technology, 16, 243-247 (1989).

7. M. Ragheb and G. H. Miley, Journal of Fusion Energy, Vol. 9, No. 4, 1990.

8. N. Vlasov, Soviet Atomic Energy, Vol. 34, No. 5, p. 395, 1973.

9. S. Jones, E. Palmer, J. Czirr, D. Decker, G. Jensen, J. Thorne, S. Taylor, and J. Rafelski, Nature, 338, 737 (1989).

Conference Proceedings Vol. 33
«The Science of Cold Fusion»
T. Bressani, E. Del Giudice and G. Preparata (Eds.)
SIF, Bologna 1991

THE CROSS SECTION FACTOR FOR THE REACTIONS $^2H(d,p)^3H$ + $^2H(d,n)^3He$ AT VERY LOW TEMPERATURE

A.Scalia, P.Figuera

Dipartimento di Fisica dell'Universita' di Catania
Corso Italia 57, I95129 Catania - Italy

1. The shadow model.

A determined value of the fusion cross section $\bar{\sigma}_f$ can be obtained by using the Rutherford differential cross section $\sigma_R(\vartheta)$, in fact for a fixed value of $\bar{\sigma}_f$ there exist a value ϑ_f of ϑ such that:

$$(1) \qquad \sigma_f = 2\pi \int_{\vartheta_f}^{\pi} \sigma_R(\vartheta) \sin(\vartheta)\, d\vartheta$$

Eq.(1) could be considered a merely numerical result, however this is not true if we assume that the subbarrier fusion process is the shadow of the elastic scattering[1], so that the particles which fuse are those which in the Rutherford scattering are detected in the shadow region. In fact, by assuming the "shadow" point of view there exist a value ϑ_f of the scattering angle ϑ such that the particles which fuse are those that in Rutherford scattering are detected in the angular range

$$(2) \qquad \vartheta_f \le \vartheta \le \pi$$

i.e. the "shadow" region, see fig.1, so that eq.(1) follows from the "shadow" assumption. Now we remind that in Rutherford scattering it is

$$(3) \qquad R_f = \eta/k \left(1 + 1/\sin(\vartheta_f/2) \right)$$

where R_f is the distance of closest approach of the Rutherford trajectory with $\vartheta = \vartheta_f$, η is the Coulomb parameter and k is the wave number. By using eq.(3), eq.(2) becomes:

$$(4) \qquad 2\eta/k \leq R \leq R_f$$

so that in the "shadow" approach the particles which fuse are those having a distance of closest approach R that satisfies inequality (4).

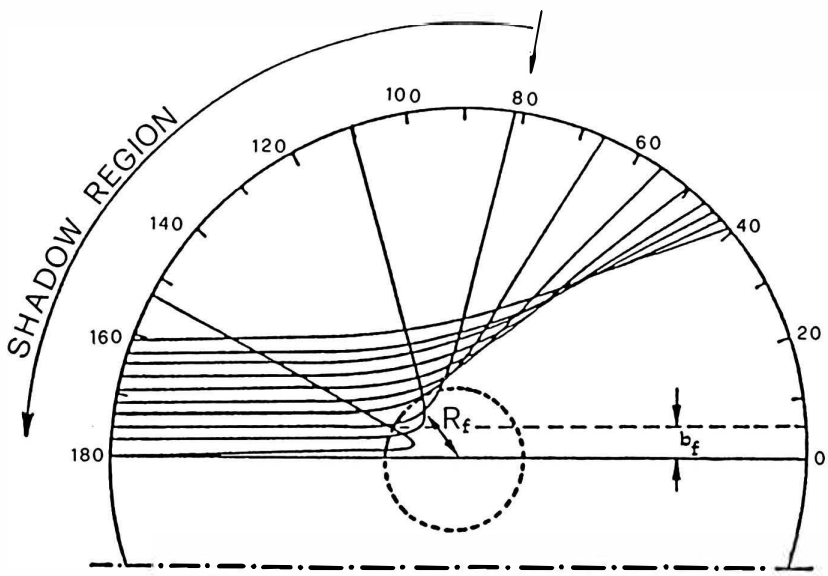

Fig.1 Rutherford trajectories for different values of the impact parameters. The dashed line shows the range of strong interaction.

By using eq.(3), eq.(1) can be rewritten as:

$$(5) \qquad \bar{\sigma}_f = \pi R_f^2 \left(1 - 2\eta/kR_f \right)$$

where R_f must be determined. From eq.(5) it follows that

$$(6) \qquad \frac{R_f}{2\eta/k} - 1 = -1/2 + 1/2 \left(1 + \frac{\bar{\sigma}_f \, k^2}{\pi \, \eta^2} \right)^{1/2}$$

and by putting in eq.(6) $\bar{\sigma}_f = \sigma_f^{ex}$, σ^{ex} being the experimental fusion cross section, we have:

$$(7) \qquad \frac{R_f^{ex}}{2\eta/k} - 1 = -1/2 + 1/2\left(1 + \frac{\sigma_f^{ex} k^2}{\pi\eta^2} \right)$$

Now we consider the function $y^{ex}(E)$ defined as follows:

$$(8) \qquad y^{ex}(E) = \ln\left\{ \ln\left[-\ln\left(\frac{R_f^{ex}}{2\pi/k} - 1 \right)\right]\right\}$$

and we remember that the energy of the Coulomb Barrier V_B can be obtained approximately by using the following expression:

$$(9) \qquad V_B = \frac{Z_1 Z_2 e^2}{1.07(A_1^{1/3} + A_2^{1/3}) + 2.72} \quad \text{MeV}$$

so that if we report $y^{ex}(E)$ versus $(V_B - E)$ we obtain that $y^{ex}(E)$ is a linear function of E[1,3]. In tables 1,2 some systems investigated in refs. 1 and 3 respectively, are reported. From the above arguments it follows that R_f can be rewritten as

$$(10) \qquad R_f = 2\eta/k \left\{ 1 + \exp\left[-\exp\left(\exp(y) \right) \right] \right\}$$

where

$$(11) \qquad y = (E_B - E)/E_S$$

and E_B and E_S are two parameters, expressed in MeV, to be determined. By using eq.(10), eq.(5) can be rewritten:

$$(12) \qquad \bar{\sigma}_f = \pi(2\eta/k)^2 \left[1 + G(y) \right] G(y)$$

where

$$(13) \qquad G(y) = \exp\left[-\exp\left(\exp(y) \right) \right]$$

and the parameters E_B and E_S can be determined by comparing the experimental values of fusion cross section with those obtained by using eqs.(11-13).

Now we remind that eqs.(11-13) are not able to reproduce the experimental values of fusion cross section for light systems at very low energy[4,5] so that we suggested[4,5] to modify eq.(12) as follows:

$$(14) \qquad \sigma_f = \bar{\sigma}_f \left[1 - g(y) \right] \left[1 - g_1(y) \right]$$

where

$$g(y) = \exp\left[- \left(\frac{d - y}{d - y_m} \right)^{\gamma_1} 2.789 \right]$$

$$(15) \qquad g_1(y) = \exp\left[- \left(\frac{d - y}{d - y_1} \right)^{\gamma_2} 2.789 \right]$$

$$d = E_B / E_S \quad , \quad y_m = (E_B - E_m)/E_S \quad , \quad y_1 = (E_B - E_1)/E_S$$

the values of E_B, E_S, E_m, E_1, γ_1, γ_2, can be determined by fitting the experimental data. The values of E_B, E_S, E_m, E_1, γ_1, γ_2 for the reactions $^2H(d,p)^3H$ + $^2H(d,n)^3He$ are reported in table 1.

Table 1

System $^2H + ^2H$					
E_B(MeV)	E_S(MeV)	E_m(MeV)	E_1(MeV)	γ_1	γ_2
0.18919	0.21250	0.00944	0.03660	4.48091	3.64950

A comparison between the experimental values of fusion cross section[7] and those obtained by using eqs.(11),(14),(15) for the above reactions is shown in fig.2.

2. The cross section factor[4-6].

The reaction rate r_{12} in a thermal equilibrium distribution is given by weighting the cross section by the Maxwell-Boltzmann velocity distribution

$$(16) \qquad r_{12} = n_1 n_2 \langle \sigma v \rangle / (1+\delta_{12})$$

with

$$(17) \qquad \langle \sigma v \rangle = \int_0^{\infty} \left[8/\pi \; M_{12} (KT)^3 \right]^{1/2} \sigma(E) \exp(-E/KT) \; E \; dE$$

where M_{12} is the reduced mass of particles 1 and 2 n_1 and n_2 are the number densities of particles 1 and 2, v is the relative velocity, E is the center of mass energy, K is the Boltzmann constant, and T is the temperature.

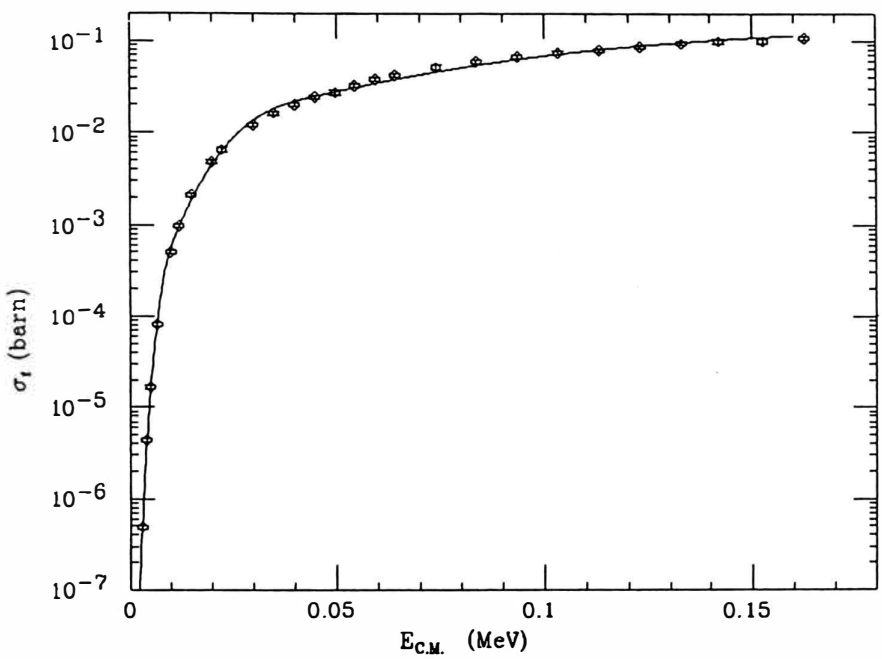

Fig.2 Comparison between the experimental values of fusion cross section[6] and those obtained by using eqs. (14) and (15)

For non resonant reactions the cross section $\sigma(E)$ is written usually[8]

$$\sigma(E) = S(E)/E \exp(-2\pi\eta)$$

with

$$2\pi\eta = 2\pi \frac{Z_1 Z_2 e^2}{\hbar v} = (E_G/E)^{1/2}$$

where E_G is the Gamow energy, η is the Coulomb parameter , Z_1 and Z_2 are the nuclear charges of the two particles, S(E) is the nuclear astrophysical factor. By assuming for the cross section $\sigma(E)$ the expression obtained in the framework of the "shadow" model, see eqs.(11),(14),(15), the cross section factor $\langle\sigma v\rangle$ can be rewritten

$$(18)\quad \langle\sigma v\rangle = \int_0^{\infty} \left[8/\pi\ M_{12}(KT)^3\right]^{1/2} \sigma_f(E)\ \exp(-E/KT)\ E\ dE = \int_{-\infty}^{d} M(T)\ I_3^T(y)\ dy$$

with

$$M(T) = \frac{(8\pi)^{1/2}\ (Z_1 Z_2 e^2)^2}{M_{12}^{1/2}\ (KT)^{3/2}}$$

and

$$I_3^T(y) = \left[1/(d-y)\right] G(y)\ \left[1 + G(y)\right]\ \exp\left[-\frac{E_B - yE_S}{KT}\right]\ \left[1-g(y)\right]\ \left[1-g_1(y)\right]$$

so that by using a numerical integration code we can obtain the values of $\langle\sigma v\rangle$ at different temperatures.

A comparison between the values of $N_A\langle\sigma v\rangle$ obtained by using our approach and those reported in the literature[9] is shown in table 2. N_A is the Avogadro's number.

Table 2

T(K)	System $^2H + ^2H$ $N_A\langle\sigma v\rangle^{(a)}$ ($cm^3 s^{-1} mol^{-1}$)	$N_A\langle\sigma v\rangle^{(b)}$ ($cm^3 s^{-1} mol^{-1}$)
$0.500\ 10^9$	$1.061\ 10^7$	$1.043\ 10^7$
$0.300\ 10^9$	$0.455\ 10^7$	$0.473\ 10^7$
$0.150\ 10^9$	$0.118\ 10^7$	$0.125\ 10^7$
$0.100\ 10^9$	$0.461\ 10^6$	$0.485\ 10^6$
$0.500\ 10^8$	$0.611\ 10^5$	$0.660\ 10^5$
$0.250\ 10^8$	$0.477\ 10^4$	$0.496\ 10^4$
$0.150\ 10^8$	$0.473\ 10^3$	$0.456\ 10^3$
$0.500\ 10^7$	$0.525\ 10^0$	$0.443\ 10^0$
$0.300\ 10^6$	$0.283\ 10^{-8}$	
$0.300\ 10^5$	$0.646\ 10^{-15}$	
$0.300\ 10^4$	$0.151\ 10^{-21}$	
$0.300\ 10^3$	$0.353\ 10^{-28}$	

a)present work results b)ref.(9) data

Acknowledgements

Thanks are due to Prof.R.Giordano for stimulating discussions.

References

1)A.Scalia, "The subbarrier fusion as the shadow of the elastic scattering";"The "shadow" model for the subbarrier fusion" to be pubblished in Il Nuovo Cimento A

2)A.Scalia, P.Figuera, "The "shadow" model for the subbarrier fusion applied to light system: determination of the reaction rate" submitted to Il Nuovo Cimento.

3)A.Scalia, Il Nuovo Cimento A98,571(1987)

4)A.Scalia, Il Nuovo Cimento A101,795,(1989) A102,953,1101,1105,(1989) A103,85,213,255,927,1177,(1990) A104,563(1991)

5)A.Scalia,R.Giordano,P.Figuera,S.Pirrone, Il Nuovo Cimento A103,465(1990)

6)A.Scalia,Journal of the Italian Astronomical Society, Vol.60,n°1,2(1989)

7)A.Krauss,H.W.Becker,H.P.Trautvetter,C.Rolfs, Nucl.Phys.A,465,150(1987)

8)D.D.Clayton,"principles of stellar evolution and nucleosynthesis" (McGraw-Hill, New York, 1968).

9)G.R.Caughlan,W.A.Fowler,M.J.Harris,B.A.Zimmerman, At. Data Nucl. Data Tables,32,197(1985)

EDITORIAL NOTE TO THE PAPER "THE CROSS SECTION FACTOR ..."
BY A. SCALIA AND P. FIGUERA

The authors assume that the fusion cross section is the shadow of the elastic scattering cross section. This assumption is plausible when energy is not small. At $E \approx 0$ the assumption becomes implausible, for the Rutherford formula cannot disagree with the Gamow barrier factor, which emerges from the solution of the problem of the quantum electro-static interaction between charged particles.

Conference Proceedings Vol. 33
«The Science of Cold Fusion»
T. Bressani, E. Del Giudice and G. Preparata (Eds.)
SIF, Bologna 1991

AN IMPROVED ZERO GRADIENT CALORIMETER FOR THE INVESTIGATION OF COLD FUSION PHENOMENA

Thomas F. Droege, Lee John Droege
2 S. 942 Thornecrest La. Batavia, IL 60510 USA

ABSTRACT

A second generation null balance calorimeter has been constructed for measuring anomalous heat in electrolytic cells. This calorimeter is similar in concept to an isothermal calorimeter except that it is operated with zero temperature differential. The calorimeter accuracy is 4 milliwatts when operated at a total power of 12 watts. Calibration is performed in situ by operating the cells under test reversed or at zero current.

APPARATUS

Introduction

The first version of this calorimeter was hurriedly assembled after the initial announcement of Fleischmann and Pons [1]. Work with this design suggested interesting phenomena which were just beyond its sensitivity and stability. After a years operation, experience has guided an improved design.

Calorimeter

Thermo Electric Devices (TED) (Melcor Corp., Trenton, NJ) are used as in the earlier design [2] to pump and measure heat flow. The new design is built from machined parts around a 2 liter stainless steel dewar, Figure 1. A puck shaped plug of aluminum fills the mouth of the dewar and is sealed to it with an "O" ring. The dewar is mounted over a copper plate with the gap between the puck and the plate filled with two sets of three TEDs arranged symmetrically to provide uniform heat distribution. A high power set is driven at constant current in the Peltier mode and pumps heat from the dewar. The second set, with fewer thermoelectric junctions, is operated in the Seebeck mode and measures the temperature difference between the puck and the plate. The plate is mounted through another set of six high power, 30 watt, TEDs to a water cooled base plate.

A spool shaped aluminum block with thick walls to evenly distribute the heat is bolted to the puck. The spool contains a cavity to hold the test cell. Several sets of heaters are contained in holes drilled in the spool wall. Milled slots in the puck allow the routing of wiring from the thermal stabilization entry pipe to terminal strips for connection to a cell.

The arrangement of the temperature servos has been improved over the earlier design. A high power, high speed servo amplifier uses the puck-plate seebeck devices as error

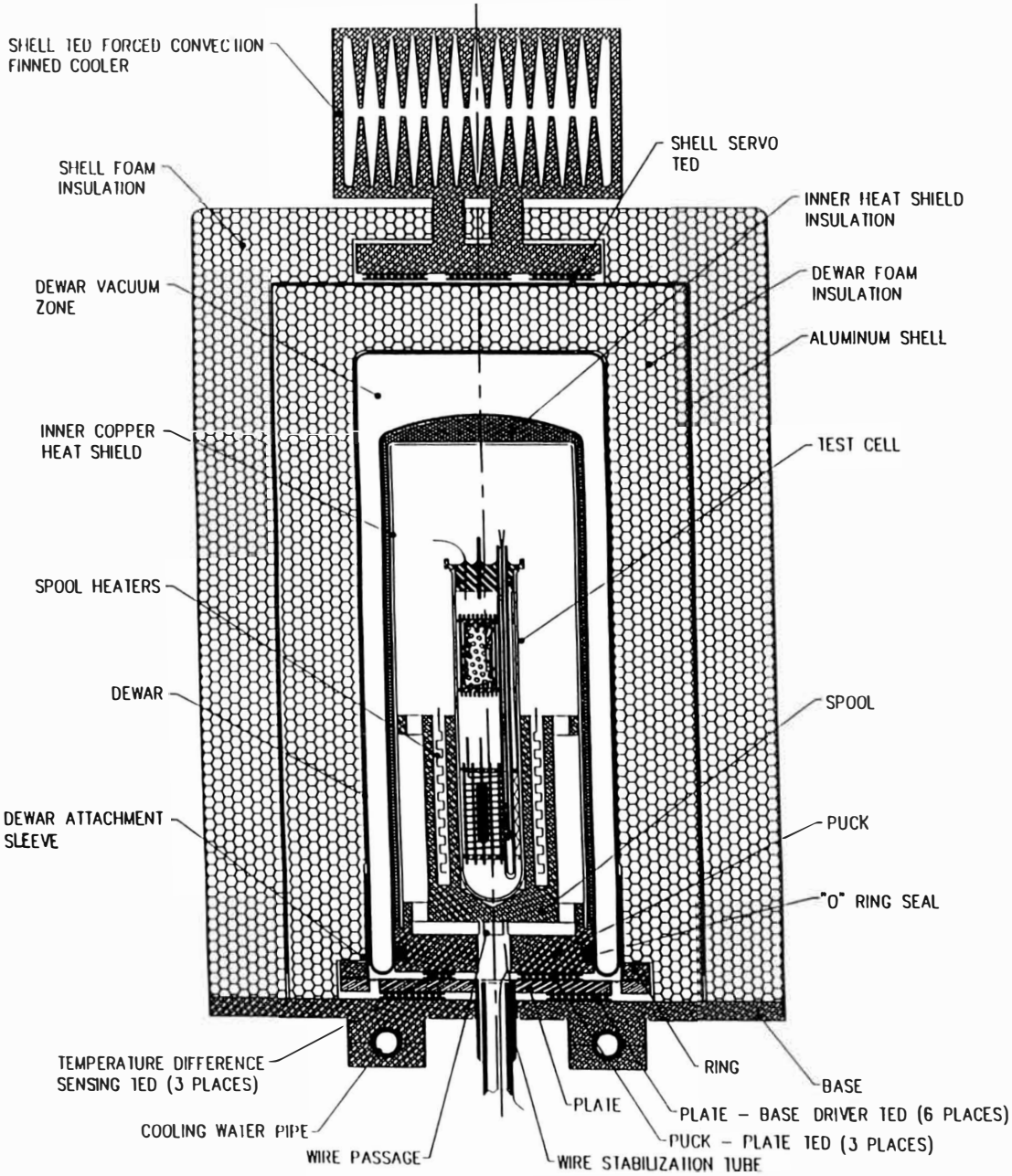

Figure 1. The new calorimeter. The mouth of a stainless steel dewar is filled with the aluminum puck. Two sets of thermoelectric devices (TED) couple the puck to the plate. One set pumps heat from the dewar to the plate. The second set measures the temperature difference between the puck and the plate. The plate makes thermal contact with the outside of the dewar. A high power set of six thermal electric devices uses the puck-plate sensor TEDs to hold the plate to the same temperature as the puck. This holds the inside and outside of the dewar to the same temperature. A copper heat shield inside the dewar reduces thermal gradients which cause radiation losses. A servo TED driven outer heat shell provides a second level of radiation loss protection. A heavy spool shaped aluminum block holds the test cell. Heaters in the spool balance the internal heat load to the refrigeration provided by the puck-plate TEDs. The heater power required to hold the dewar inside to the set temperature plus the measured cell power are balanced against the refrigerator calibration. Any difference is a measure of anomalous heat.

detectors and drives the plate-base TED's to hold the plate and connected outer wall of the dewar to the same temperature as the puck and inner wall. The purpose of this servo is to hold the outer wall of the dewar to the same temperature as the inside of the dewar without concern as to what the temperature might be. To the extent that this is done, there will be no heat lost from the dewar except that due to transient thermal gradients which cause radiation losses. To further reduce thermal gradients, the spool is connected to a heavy copper heat shield which is insulated from the inner wall of the dewar.

The plate cooling water is pumped through a 30 gallon garbage can which exhausts heat to the environment. This provides a large thermal mass so that the relatively fast plate-base servo can easily track changes.

A slower response servo is controlled by a temperature sensor mounted in the puck. This servo drives the spool heaters to hold the experiment to the desired temperature. If the experiment is set up so that the cell power is less than the refrigerator power, then the spool heaters will always require some power and control will be possible. The system fails if the cell power rises above the anticipated maximum value whence it is no longer possible to maintain a balance.

The outer wall of the dewar is insulated with foam, which is in turn covered by an aluminum shell heat shield. This shield is driven by another set of TEDs which are connected to an air cooled heat sink. A servo amplifier drives the TEDs to hold the shell heat shield at the same temperature as the inside of the dewar providing a second level reduction of radiation.

Electrical leads and gas tubes necessary for operating an experiment are brought out through a double walled copper pipe thermally connected to the plate, Figure 2. The arrangement provides good thermal contact between the leads and the pipe. By making this pipe relatively long, the leads will be brought to the uniform temperature of the experiment by the time that they reach the puck-plate interface. To the extent that both sides of the interface are at the same temperature, there will not be any heat transfer through the leads. In practice, the thermal conduction of the puck-plate TEDs is much greater than the lead conduction and so is the primary concern of the design.

Great care is taken to assure that the energy supplied to the inside of the dewar is accurately measured. All sensitive electronics is located in a temperature controlled case. The dewar is treated as a multi-terminal black box. Each lead is provided with a temperature controlled shunt. A separate potential lead measures the voltage as each lead transits the puck-plate (see Figure 2.) interface to assure that only the lead heat loss that occurs in the calorimeter is included in the energy balance.

Heat supplied to the dewar is determined by computing the algebraic sum of the volt-ampere product of the various leads. Because all leads contain a shunt, which is one more than needed, a consistency check requires that the currents add to zero.

Experiments are performed by installing a test cell in the spool, Figure 1. Any heat released by the cell will result in an unbalance in the heater servo since the puck will

attempt to become warmer than the set point. The servomechanism acts to prevent this by reducing the power applied to the spool heaters. Anomalous heat is indicated when the total power supplied to the cell and heaters is less than the heat removed by the refrigerator.

Access to the test space is provided by lifting off the dewar, the attached foam shells, and the convection cooler. This exposes the spool which can then be approached from all sides for experimental changes. Machined surfaces and bolts inserted from underneath allow clamping the plate to the ring to provide good heat transfer between the plate and the dewar outer wall. A milled groove in the plate reduces the effect of the temperature gradient through the plate.

Instrumentation

Closed loop control of the experiment is performed by analog techniques. A 16 bit high speed digital system collects data under the control of a 80286 based computer. An extended version of this paper contains some details relating to system accuracy.

CALIBRATION

For calibration it is first necessary to determine the refrigeration constant at the selected calorimeter power and temperature. A first level calibration can be made by setting a temperature and noting the power in the balancing heater. With a closed loop time constant of 13 minutes, the system settles to 0.01% in 2 hours. By integrating the difference between the balance power and the determined calorimeter constant over time, the energy drift of the calorimeter can be measured.

Figure 3 was made with a Pt-Pd cell in the calorimeter operating with the Pd electrode as the anode so as to not introduce anomalous heat. The 3.39 cm sq electrode was operated at 60 ma per sq cm. The refrigerator was operating at 8 watts. The maximum indicated drift rate of 50 joules in 5 hours during the first part of the run represents 3 mw. At ten hours and at each hour thereafter, an impulse was added through a second heater which was not included in the computed power balance. Pulses were 5, 10, 20, 40, and 80 joules. Since the computer does not know the pulses have been inserted, the heat is detected as a positive net energy balance. With heaters only, the calorimeter noise is 10 milliwatts rms. Operating cells are noisy, 15 milliwatts rms at 50 ma per sq cm and 40 mw rms at 500 ma per sq cm are typical measurements made with 1 sq cm cathodes. The impulse sensitivity is a function of the calorimeter time constant. We estimate that a practical sensitivity is close to 20 joules (1 sigma) at a high current operating point.

While standard calibration curves have been performed, we believe that a dynamic test is a better measure of the calorimeter under operating conditions. We have performed such tests both with and without an operating cell in the calorimeter. For this test, the calorimeter is operated with two heaters in the active volume. One is connected to the balance servo which works to hold the inside of the calorimeter at constant temperature. The second heater is driven by the computer from a random number generator so that the heat applied varies over a range, in the following case of one watt. This is an

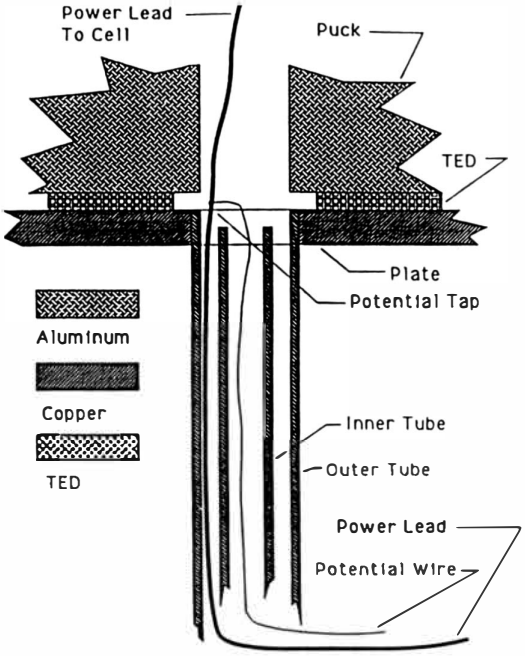

Figure 2. Lead entry detail. Power leads entering the dewar are pressed between two copper pipes so that they make good contact with the outer pipe. The outer pipe is in contact with the plate. This results in the power leads reaching the dewar temperature by the time they reach the puck-plate interface. The lead heat load is carried by the plate. Potential leads measure the power leads as they cross the puck-plate interface to insure that only the lead loss in the dewar is included in the energy balance.

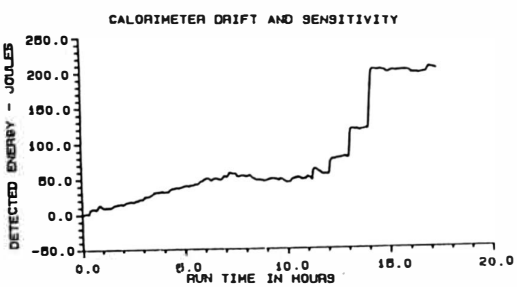

Figure 3. Calorimeter drift and sensitivity. The first ten hours show typical drift for the calorimeter operating at 8 watts total power. At hour 10 and at each hour following, calibration pulses of 5, 10, 20, 40, and 80 joules were inserted by a separate heater not in the computed energy balance.

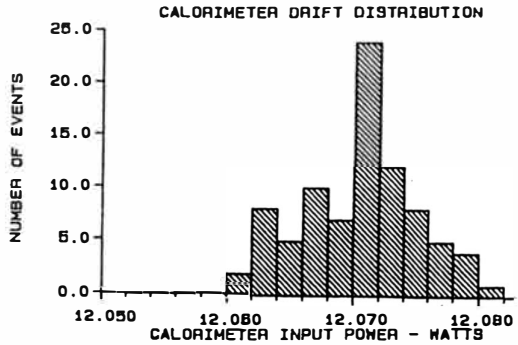

Figure 4. Calorimeter random drift test. In addition to the balance heater, the calorimeter is fitted with a heater driven by a random number generator. Every three hours the random value is changed. After two hours, the total power input is averaged over the third hour to determine a power value. The curve contains 86 three hour measurements, with a mean of 12.0784 watts and a sigma of 0.0044 watts.

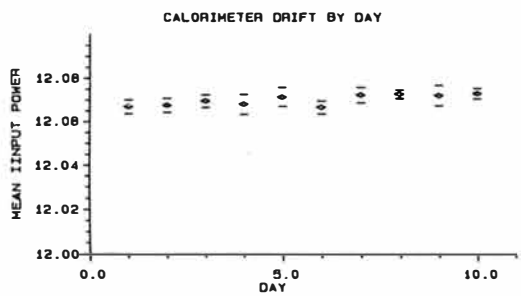

Figure 5. Calorimeter drift by day. The data of Figure 4. plotted by day. The error bars are one sigma..

optimistically high range for anticipated anomalous heat.

For the test of Figure 4, every three hours the random number generator selects a new heat value. After two hours, the two heater powers are averaged over the next hour to give a power value. A perfect calorimeter would always come to the same total power value. The distribution shown in Figure 4 represents 86 points or nearly 11 days of operation. The measured mean was 12.0785 watts with a sigma of .0044 watts. Figure 5 shows the mean and 1 sigma error by day over the 10 full days of the run. The daily variation is somewhat less (3 mw one sigma typical) than the error of Figure 4 and would be even less were it not for a curious periodic component which is under investigation.

DISCUSSION

Measurements indicate that heat removed from the dewar is a constant if the puck-plate Peltier TEDs are operated at constant current and constant temperature. With this design, both sides of the TEDs are held to the same temperature. We have not identified any aging effects, but have mechanically damaged the TEDs on several occasions requiring re-calibration.

The long time constants of these servo loops were a challenge. Because the conventional measurements are so lengthy with long time constants, we attempted a computer model. Because of the limitations of personal computer SPICE simulators, we were not able to generate a model which approached the real calorimeter. After a number of "seat of the pants" attempts gave rather poor results, a long run of random data was processed by the FFT to derive the transfer function. The resulting 13 micro-hertz corner frequency demonstrates the difficulty of generating a Bode plot by a conventional frequency scan.

CONCLUSIONS

We are able to detect a change of 4 milliwatts (1 sigma) from a 12 watt operating point for a passive experiment. An experimental cell generates noise and requires a broad range of operating point with time. This is a greater challenge for calibration. A definitive calibration over the calorimeter range has not yet been accomplished but preliminary data indicates an accuracy in the 10 milliwatt range.

ACKNOWLEDGEMENTS

We wish to thank E.C. Tibbals for preparing drawings and the presentation of this paper.

REFERENCES

[1] M. Fleischmann, S. Pons and M. Hawkins, "Electrochemically Induced Nuclear Fusion of Deuterium", J.Electroanal. Chem. 261 (1989) 301.

[2] L. J. Droege and T. F. Droege, "A Zero Gradient Calorimeter for the Measurement of Anomalous Heat from the Electrolysis of Deuterated Metals", Proc. of the First Annual Conference on Cold Fusion, Salt Lake City, Utah, 28-31 March 1990, p. 229.

Conference Proceedings Vol. 33
«The Science of Cold Fusion»
T. Bressani, E. Del Giudice and G. Preparata (Eds.)
SIF, Bologna 1991

IMPROVEMENT OF THE TOFUS APPARATUS

M. Agnello, F. Iazzi, B. Minetti
Dipartimento di Fisica del Politecnico, Torino(Italy)
and I.N.F.N., Sezione di Torino
and
E. Botta, T. Bressani, O. Brunasso, D. Calvo, D. Dattola,
P. Gianotti, C. Lamberti
Dipartimento di Fisica Sperimentale dell' Universita' di Torino (Italy)
and I.N.F.N., Sezione di Torino
and
A. Zecchina
Dipartimento di Chimica Fisica dell'Universita' di Torino (Italy)

ABSTRACT

The TOFUS experiment was started in order to detect 2.45 MeV neutrons emitted from a Ti/D system in the gas phase. Improvements in the electronics of the neutron detector, based on the double scattering technique, and in the performances of a new cell are described.

1. INTRODUCTION

The TOFUS detector was designed and realized at the beginning of the studies on the Cold Fusion phenomena in order to detect the 2.45 MeV neutrons from the reaction D+D -> ^{3}He+n which seemed to be the undoubtable signature of the nuclear origin of the phenomenon. The goal of the TOFUS experiment (performed at the I.N.F.N. Laboratories in Torino) was to measure the energy of each detected neutron, instead of counting their number in correlation with the time or/and with thermodynamic conditions of the D/metal system.

In the following we will describe the features of this detector together with its performances and the most recent improvements on the electronics and on the gas loading monitor system.

2. THE DOUBLE SCATTERING TECHNIQUE

The detector and its operating principle were already described elsewhere [1,2,3]: let us recall just the geometry of the set-up, consisting of a block (START) of three scintillators for detecting the first scattering of a neutron arriving from a cell put in front of it and two arrays A and B (STOP) for detecting the second scattering.[see fig.1 in ref.1] The scheme of the flux of information coming from the detector signals up to the neutron energy reconstruction algorithm and to the correlations with other kinematic variables is shown in fig.1.

The signals from the PM's at both ends of the scintillator slabs are sent to an equal number of TDC's and ADC's channels, through Constant Fraction Discriminators (CFD). These channels are read by the computer on-line acquisition system, buffered and stored into a mass memory unit (disk or magnetic tape). The computer is a MicroVax II, the acquisition system is the DAQP package developed at C.E.R.N. Data Division and the magnetic tape unit is a CYPHER-6500 bpi.

Together with the ADCs and the TDCs, a number of scalers is recorded: they count the number of logical operations (AND, OR, XOR) amongst signals, which have a

physical meaning. A Pattern Unit (P.U.) accounting for the multiplicity in the START array is recorded too.

From this information it is possible to evaluate the Time of Flight (TOF) between the START and the STOP and the impact points of the neutron in the START and in the STOP slabs. With the kinematical relations other physical quantities (n energy before and after the first scattering, the first scattering angle, the recoil proton energy ...) can be calculated. The neutron energy, as emitted from the Cold-Fusion cell, which is the relevant physical variable, is reconstructed with an incertitude due to the TOF error (±1 ns) and to the impact position approximation on both detectors. This uncertainty has a double origin: ±4.5 cm in the horizontal direction for the START slabs and ±1.0 cm in the vertical direction for the STOP slabs, due to the finite granularity of the scintillators and ±2.0 cm in the vertical direction for the START slabs and ±2.0 cm in the horizontal direction for the STOP slabs, due to instrumental precision.

The reconstructed energy distribution for a 2.45 MeV neutron [see fig.2 in ref.1] has a FWHM ≈1.1 MeV, as evaluated both from a Monte Carlo simulation and a calibration with the neutrons emitted from an Am-Be source in coincidence with the associated γ's. The overall efficiency of the detector, including the solid angle and the acceptance, has been measured as a function of the distance between the neutron source and the START by mean of the same Am-Be source and is reported in fig.2.

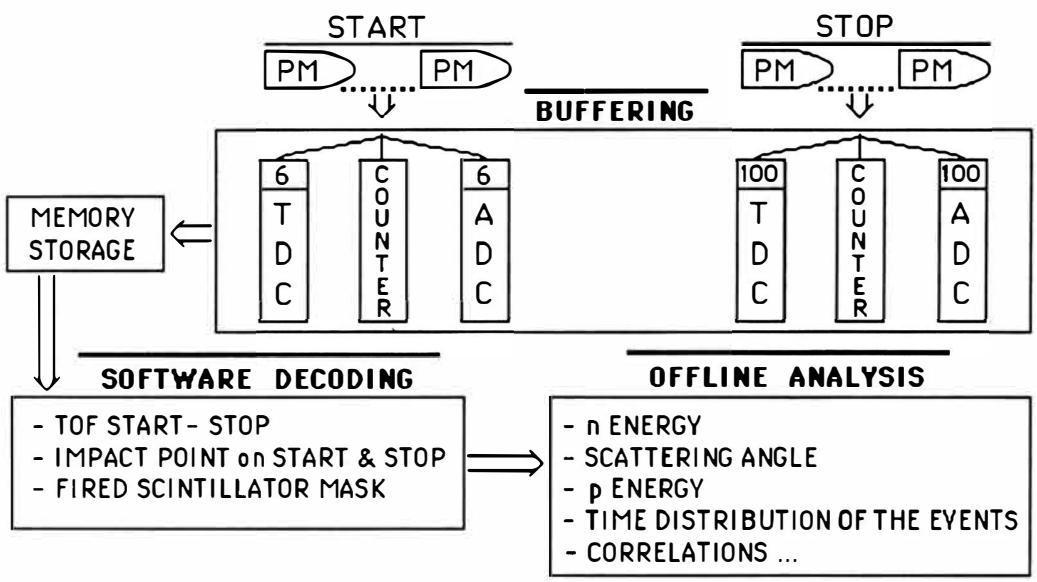

Fig.1 The TOFUS experiment information flow diagram.

3. THE TRIGGER OF THE DETECTOR

From the physical point of view a "good" event, i.e. a 2.45 MeV neutron emitted from a pointlike source in front of the detector, must satisfy the following requirements:

1) one and only one scintillator in the START array must be fired in coincidence with one and only one in the STOP (A.XOR.B): in this way events suffering multiple scattering are rejected and spurious events due to cosmic rays are minimized;

2) the time interval between the START and the STOP signals must be suitable to take into account the time spent by the neutron to travel from the START to the STOP arrays: this time is spread over 35 ns due to the different velocities of the fastest

neutrons which lose few KeV in the START and the slowest ones which lose ≈1 MeV at a scattering angle of ≈ 50°.

The hardware trigger is schematized in fig.3 : it is divided into two parts, the right one concerns the START signals while the left one concerns the STOP signals.

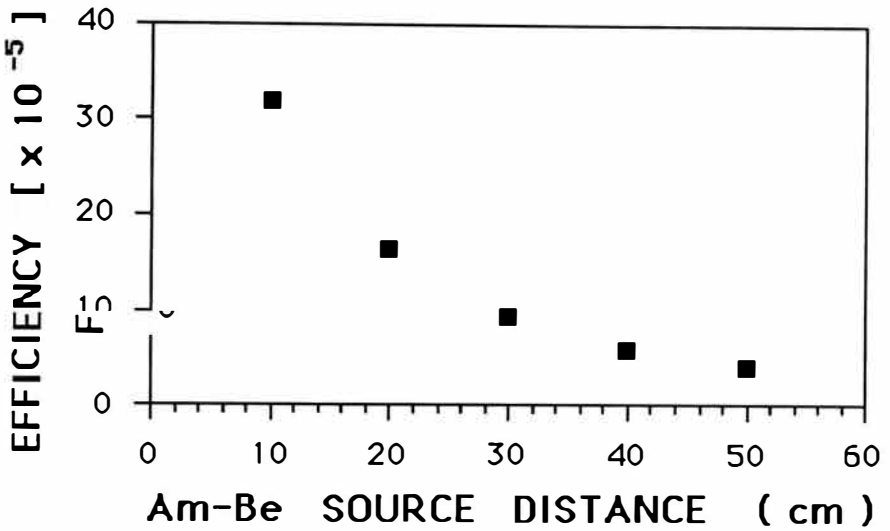

Fig.2 Detector efficiency versus Am-Be source distance.

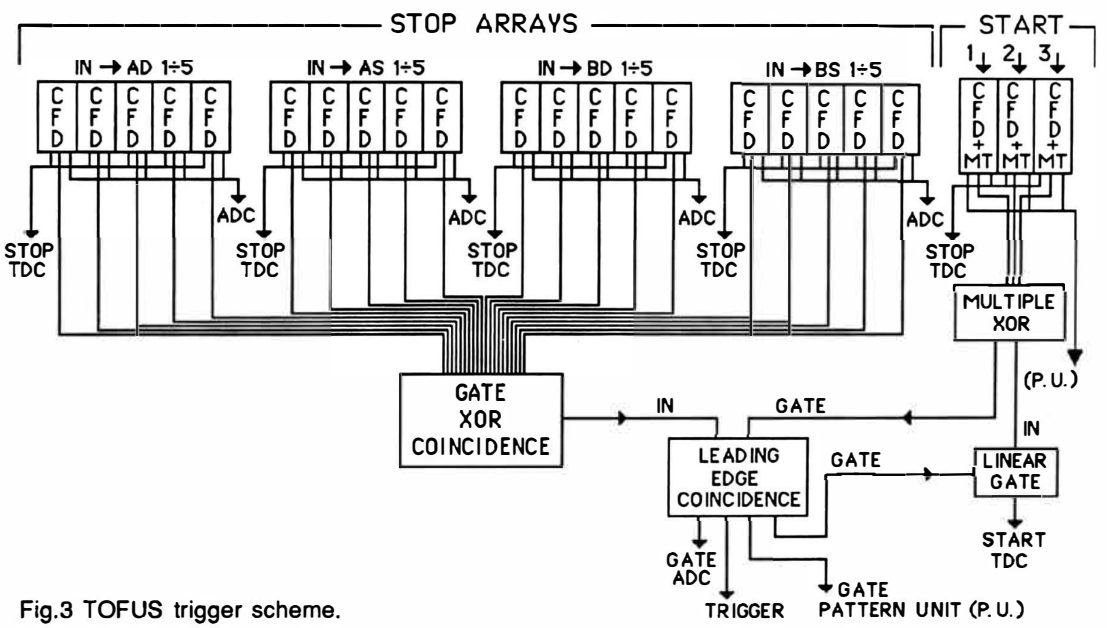

Fig.3 TOFUS trigger scheme.

The discriminated Mean Timer signals (CFD + MT) of each START slab are sent to a module which performs an exclusive OR amongst them (Multiple XOR): the output signal opens a 35 ns gate on a Leading Edge Coincidence. Looking at the left part of the figure, the signals from the five PM's for each side of the STOP arrays are sent, through CFD channels, to a GATE-XOR module which selects those events with a pattern of signals with one and only one fired PM at both sides of one and only one array, A or B. The output of this module is sent to the Leading Edge Coincidence, forming then the trigger.

Concerning the small amount of energy lost by the neutron inside the scintillators it must be noticed that the threshold of the PM's have been set at very low values: as a consequence a high amount of spurious signals due to the large electronic noise comes out from the PM's.

On the other hand the selective combination of logic AND and XOR in the trigger strongly reduces such a noise and a further reduction arises from the kinematical correlations in the software off-line analysis.

The last remark about the detector performances concerns the dead time for the whole event acquisition. The time for the formation of the signals (PM's) and for the electronic read-out (TDC, ADC, COUNTERS and P.U.) is less than 200 ns, while the time used by the computer for recording a triggered event is about 3.9 ms: this means that the maximum neutron rate that can be recorded is 250 hz, while neutron bursts for which the time interval between two detected neutrons is greater than 200 ns can be detected at the counting level (and then time correlated).

4. SPURIOUS BURSTS REJECTION

As an exemple of both the burst counting and the spurious rejection, the results of a particular data taking run, in which electronic troubles occurred, are illustrated.

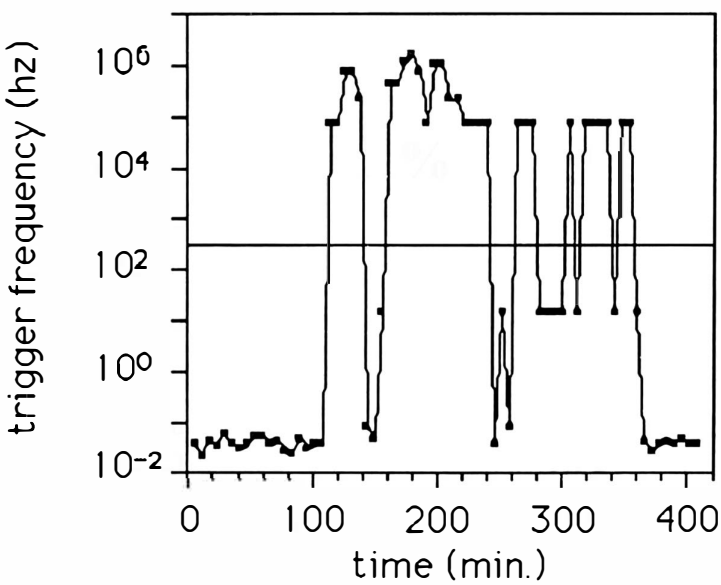

Fig. 4 Frequency of the hardware triggers versus time, in a data taking with bursts of spurious signals from electronic malfunctioning.

During a set of measurements (≈ 7 h) the overheating of a CAMAC-BUS produced a series of random spurious triggers in coincidence with the PM's usual noise. The trigger frequency increased up to values greater than the recording maximum frequency, 250 hz, as shown in fig. 4 as a function of the time. The straigth line at 250 hz separates the recorded and reconstructed events (lower half) from the only counted events (upper half): one can see that frequencies of the order of Mhz are detected at counting level.

As said before this run contained an anomalous amount of spurious events with average frequency ≈ 10 sec^{-1} at the trigger level: the capability of rejection of such spurious was fully satisfying, as demonstrated by the fact that the frequency of the accepted events after the kinematical reconstruction was ≈ 0.015 s^{-1} (≈ 0.006 s^{-1} in

the interesting range 1.5÷3 MeV), the same average value obtained in all the other analogous runs [4].

5. THE Ti/D CELL AND THE VACUUM SYSTEM

For the 1991 runs a new cell has been designed (see Fig. 5a) in order to improve the control of the thermodynamic variables of the Ti-D system (temperature, pressure and gas concentration). This cell, containing 20 g of high purity Ti sponge, is the core of a sophisticated vacuum circuit entirely made in UHV material (SS304L) and sketched in fig. 5b. The cell with its contents can be heated and degased (up to 10^{-6} Torr at 750 ^{o}C by means of a turbomolecular pump) or filled by D_2 or H_2 alternatively: the pressures inside the circuits are monitored by a Piezoresistive Transducer, a Cold Cathode Gauge, an Ionization Gauge Penning Tube and a Pirani Gauge and all the temperatures are measured by K-type thermocouples.

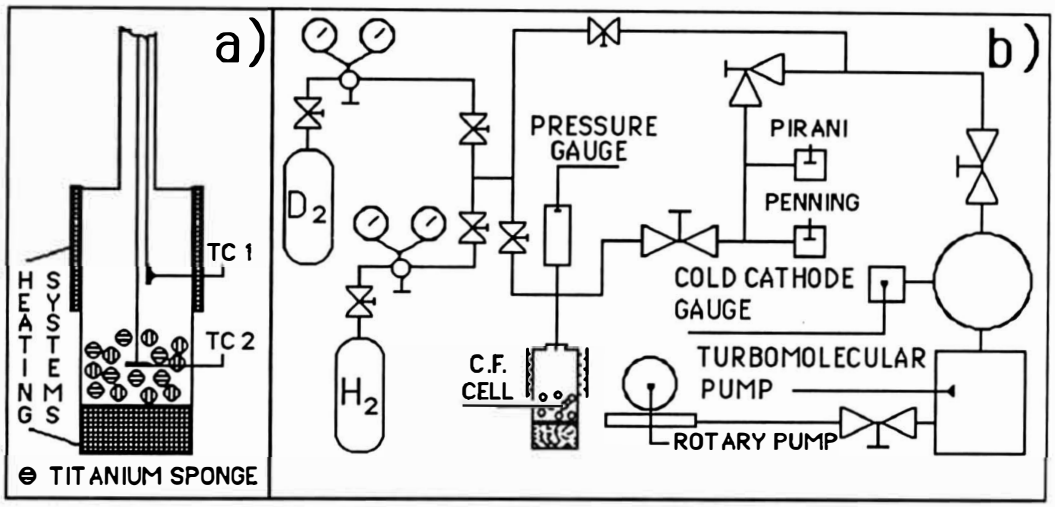

Fig.5 a) cell and b) vacuum system of the TOFUS experiment.

The typical phases of a cell cycle are: a) degasing of the Ti at 750 ^{o}C, b) filling of the cell with gas (D_2 or H_2), c) consecutive cycles of increasing (up to 540 ^{o}C) and decreasing (down to ≈ 28 ^{o}C) the Ti temperature. In the filling step a temperature rise of about 500 ^{o}C in few seconds was observed by TC2, in agreement with the exothermic formation of the hydride phase.

During these cycles the Ti temperature as a function of the time showed the caracteristic flat behavior in correspondance with the phase transition of the Ti/D system[5], as shown in Fig. 6.

6. CONCLUSIONS

The TOFUS apparatus has been improved in the electronic trigger components and in the cell handling system. Performances on the time resolution in the acquisition and the control of the cell thermodynamic conditions are better than 1990 runs.

Further improvements are planned in the next future: they are a granularity of the START scintillators, in order to increase the neutron energy resolution, and the cooling of the PM's, in order to lower the electronic noise.

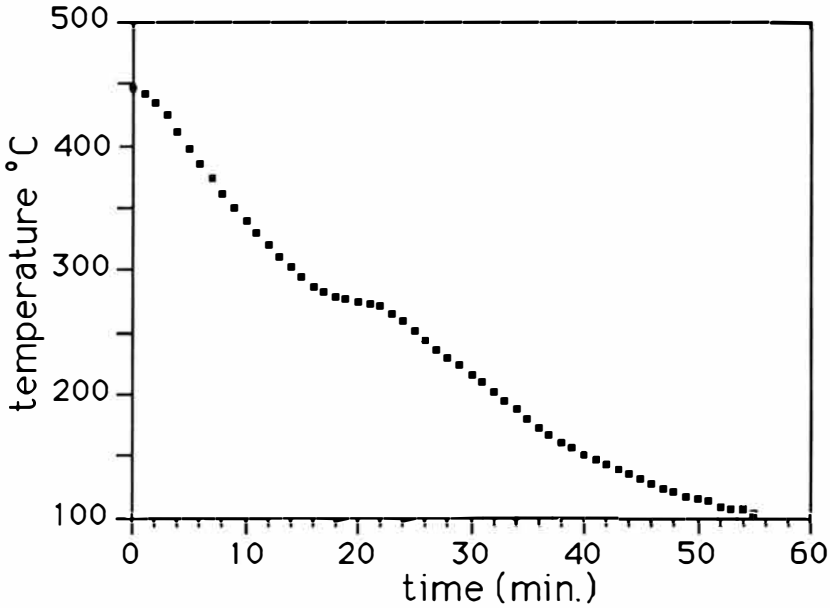

Fig.6 Typical temperature behaviour in the first hour of a run down as detected by the thermocouple TC2 in Fig. 5a). The phase transition around 280 °C is evident.

ACKNOWLEDGEMENTS

Particular thanks are due to the GINATTA TORINO TITANIUM SpA who supplied all the samples of high purity Ti.

REFERENCES

1) T. Bressani et al., published in Proc. 2nd Annual Conference on Cold Fusion (Como, 29 June-4 July 1991)

2) G.C. Bonazzola et al., in Proc. on "Understanding Cold Fusion Phenomena", Conf. Proc. Vol. 24 (ed. Ricci, E. Sindoni and F. De Marco), S.I.F., Bologna (1989), p.313

3) G.C. Bonazzola et al., Nucl. Instr. Meth. A299 (1990), 25

4) M. Agnello et al.,"Search for Neutron Emission in Titanium-Deuterium System", presented at the Workshop on "Anomalous Nuclear Effects in Deuterium/Solid Systems", Provo (Utah) 22-24 Oct. 1990

5) A.D. Mc Quillan and M.K. Mc Quillan "Titanium", Butterworths Scientific Publications, London (1956), p.211

Conference Proceedings Vol. 33
«The Science of Cold Fusion»
T. Bressani, E. Del Giudice and G. Preparata (Eds.)
SIF, Bologna 1991

A LARGE SOLID ANGLE MULTIPARAMETER NEUTRON DETECTOR

G. Ricco, M. Anghinolfi, P. Corvisiero, P. Prati and M.Taiuti
Dipartimento di Fisica and INFN,via Dodecaneso 33,16146, Genova, Italy

C. Boragno, R. Eggenhoffner, U. Valbusa
Dipartimento di Fisica and INFM,via Dodecaneso 33,16146, Genova, Italy

Abstracts

We present the results of recent measurements, performed in Genoa with a novel neutron detector, on some titanium-deuterium systems. In spite of the good detector sensitivity, better of the one claimed by Jones and co-workers, no neutron emission was found.

Introduction

After the first claims about the so called "cold fusion" phenomenum [1,2,3]a new, multiparameter, high efficiency neutron detector [4] was specifically designed in Genoa for cold fusion measurements and used in some typical experiments on titanium-deuterium gas systems. Our aim was to verify, with an improved neutron sensitivity, the results reported by Scaramuzzi and co-workers [3] and to investigate neutron emission during high deuterium adsorption in the titanium lattice.

Experimental Set-up

As shown in fig. 1 the detector is composed of three cylindrical co-axial scintillators shells, each shell being 20 cm long and about 5 cm thick [4]. The inner shell is filled with NE213 liquid scintillator and the outer two are plastic NE102A. Cadmium sheets 1 mm thick are interposed between the scintillators to capture neutrons thermalized inside the detector. An anticoincidence cosmic ray detector is placed over the neutron detector and the whole system is surrounded by a paraffin (20 cm) +copper (2 cm)+lead (10 cm) wall. A 30 cm^3

cylindrical sample can be inserted in the central hole. The NE213 light pulse has different decay times when produced by gamma rays or by neutrons: a pulse shape discriminator, operating on the inner scintillator pulses, efficiently separates gamma from neutron events. Due to the relatively large detector dimensions, a very high fraction of neutrons giving a signal in the liquid scintillator thermalizes and is captured by cadmium foils. Each neutron event in the liquid scintillator gives the START to a Time-to-Amplitude Converter that will wait 200 μs for the STOP from gammas rays produced by neutron capture on one cadmium sheet and detected by at least one of the three coaxial scintillators. A neutron event is identified by two consecutive trigger signals: the first corresponding to a neutron type pulse in the liquid scintillator and the second to the detection of capture gamma rays within the 200 μs time window. For each event the linear amplitude of the summed three scintillators pulses, proportional to the neutron energy, is recorded. The acquisition system, based on a CAMAC interface connected to a MICROVAX computer, allows off-line multiparameter analysis: as an example in fig. 2 is shown the pulse-shape and pulse-height correlation. The signals from the scintillators are stored on the computer each minute: in this way time trends can be monitored. The detection efficiency for 2.45 MeV monochromatic neutrons turned out (12.5 ± 0.5) %. For neutron energies below 2.45 MeV the background rate is 10^{-2} n/s and the detection sensitivity turns out to be $2.4 \cdot T^{-1/2}$ n/s, where T is the measure time.

The system used to load titanium with deuterium gas is sketched in fig. 3. Before admit D_2 gas in the cell, the system was evacuated up to 10^{-6} mbar by a turbomolecular pump. In a second step the gas was inserted in the dead volume (200 cc) flowing through a liquid nitrogen trap to promote impurities condensation. Finally, the gas was admitted in the cell through the valve V4. A manometer, with sensitivity 0.2 bar, was used to measure the pressure drop vs. time and then to estimate the

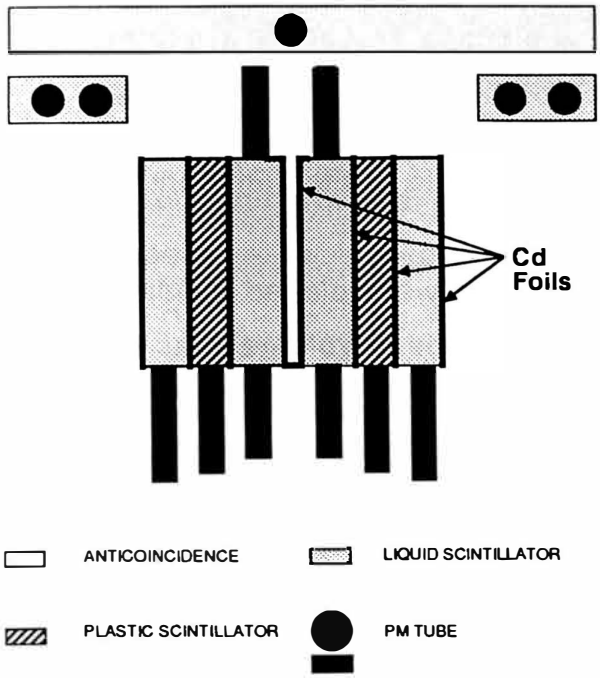

FIG. 1: detector composition and geometry (side view).

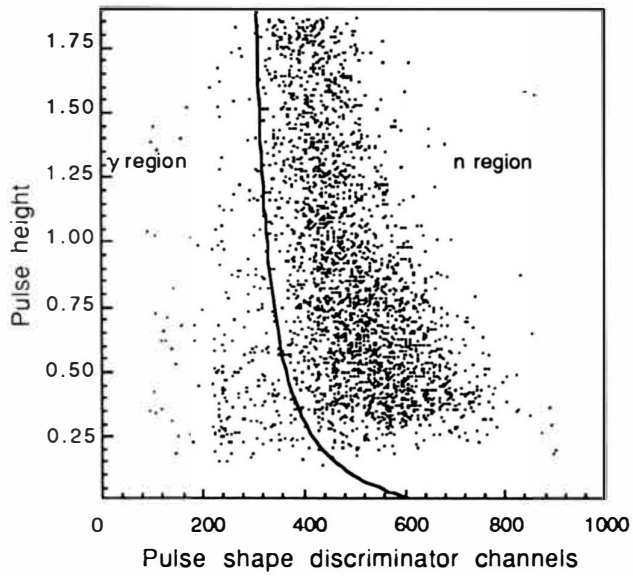

FIG. 2: Pulse height and pulse shape correlation for an Am-Be neutron source. Arbitrary units are used.

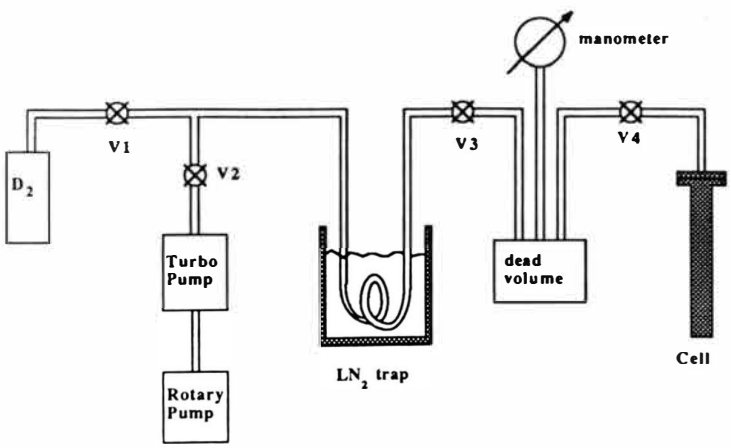

FIG. 3: Deuterium control system

adsorption rate of the titanium.

Measurements

We have performed measurements with two kinds of titanium samples: shavings and powders [5]:

a) Titanium shavings: 24 g of titanium shaving were placed inside the cell without any kind of thermal treatment. The dead volume was then filled, at room temperature, with deuterium gas at a 16.5 bar pressure and the valve connecting the dead volume with the cell was opened: neither pressure nor cell temperature variations were observed. In these conditions a 5 h measurement was performed and the neutron rate turned out compatible with the background level. After this first step the liquid nitrogen was admitted in the cryostat: the cell temperature went down to 77 K in about 10 minutes, then the liquid nitrogen was closed and the temperature went back to room temperature in about 4 hours. This thermal cycle was repeated consecutively 4 times. During all the cycles neither pressure variation nor neutron emission were observed. We assumed a deuterium absorption corresponding to the minimum pressure variation detectable with our system (0.2 bar): the parameter λ_{fus}, defined as the fusion rate per deuteron pair, turned out lower than 10^{-23} fus/D pair/s.

b) Titanium powder: 32 g of titanium powder were inserted in the cell and degassed by pumping and heating 2 h at 200 °C. Temperature was eventually raised up to 560 °C and the cell was maintained at this constant temperature in high vacuum conditions for approximately 7 h. The sample was then inserted in the detector and the dead volume was filled with 16 bar of deuterium gas. When the deuterium was admitted in the cell the pressure went down to zero bar in a few minutes and the cell temperature increased up to 600 C°. During this fast transient a neutron measurement was performed but no emission was detected.

Then, a longer measurement (15 hours) was performed holding the system in the same conditions, once again no neutrons emission was observed. After this first loading the dead volume was filled again with 10 bar of deuterium gas: when the deuterium was admitted in the cell the pressure in the dead volume went down to 8 bar and the cell temperature increased by 4 C°. We concluded that the sample was now loaded of deuterium at the maximum level and in these conditions we performed the following measurements:

- a 10 hours run with the titanium-deuterium system in stationary conditions
- two consecutively runs during thermal transients induced by filling the cryostat with liquid nitrogen.

During all the measurements no neutron emission was observed: since we evaluated, from the dead volume pressure variation, a deuterium to titanium ratio in the sample of about 0.65, the λ_{fus} parameter in these runs was lower than 10^{-25} fus/D pair/s.

Conclusions

Some measurements on deuterium-titanium systems were performed without observing any neutron signal above the background level also with a high deuterium absorption inside the titanium lattice. The experimental conditions was very similar, but not completely equivalent, to those of Scaramuzzi and co-workers [3]: in particular the thermal transients induced in the cell was slower and the multiparameter analysis performed on the detector signals had a dead time of 200 μs.

References

[1] S. E. Jones, E. P. Palmer, J. B. Czirr, D. L. Decker, G. L. Jensen, J. M. Thorne and S. F. Taylor: Nature, 338,737 (1989)
[2] M. Fleischmann, S. Pons and M. Hawkins: J. Electroanal. Chem., 261, 187, 301 (1989)

[3] A. De Ninno, A. Frattolillo, G. Lollobattista, L. Martinis, M. Martone, L. Mori, S. Podda and F. Scaramuzzi: Europhys. Lett., 9, 221 (1989)
[4] G. Ricco, M. Anghinolfi, P. Corvisiero, E. Durante, S. Maggiolo, P. Prati, A. Rottura and M. Taiuti: "A large solid angle multiparameter neutron detector", Nucl. Instr. and Meth., in press.
[5] P. Prati, G. Ricco, M. Taiuti, C. Boragno, R. Eggenhoffner and U. Valbusa: "Search for neutron emission from titanium-deuterium systems", to be published.

Conference Proceedings Vol. 33
«The Science of Cold Fusion»
T. Bressani, E. Del Giudice and G. Preparata (Eds.)
SIF, Bologna 1991

LIQUID SCINTILLATOR DETECTION AND MULTIPARAMETER DATA AQUISITION FOR NEUTRON DETECTION IN COLD FUSION EXPERIMENTS

K.A. Sjöland, P. Kristiansson and K.G.J. Westergård

Dept. of Nuclear Physics, Lund Institute of Technology, Box 118, S-221 00 Lund, Sweden

Abstract

We have designed a low level neutron detector for cold fusion experiments with titanium and deuterium gas. The basic principle of the system is to monitor as many relevant parameters as possible and store them event-by-event and analyze the data afterwards. The result of the experiment was that no significant excess of neutrons was observed. We also discuss the cosmic radiation that may influence low level measurements of neutrons.

Introduction

During the spring of 1989 two American research groups reported different signs of fusion at room temperaure in metal lattices by way of electrolysis.[1,2] Later experiments with titanium exposed to deuterium gas under pressure and cooled to the temperature of liquid nitrogen showed positive results as far as the detection of neutrons goes.[3,4] The work presented here is an attempt to confirm some initial positive results with the latter kind of experiment.

To detect the neutrons a neutron detection system based on a liquid scintillator and pulse shape analysis[5] was designed. Its basic principle is to monitor as many relevant parameters as possible and store them event-by-event and analyze the data afterwards. The system also takes into account the problem of cosmic radiation that may influence measurements of this kind.

The detector system

One of the signs of cold fusion would be the 2.45 MeV neutrons from the following reaction:

$$d + d \Rightarrow \begin{cases} {}^3He\ (0.82\ MeV) + n\ (2.45\ MeV) & (42\ \%) \\ p\ (3.02\ MeV) + t\ (1.01\ MeV) & (58\ \%). \end{cases} \qquad (1)$$

The detector system, shown in figure 1, is especially designed to detect neutrons above an energy of 1 MeV and separate them from the background gamma radiation. In the center the neutron detector is placed. It is a liquid scintillator, NE-213, which has the property to separate gamma rays from neutrons by pulse shape analysis. The experimental vessel, which contains the Ti/D_2-sample, is placed in a central well. The detector is shielded from background gamma radiation and, to some extent, background neutrons with lead and solid paraffin, which has advantages and disadvantages that we will come back to later.

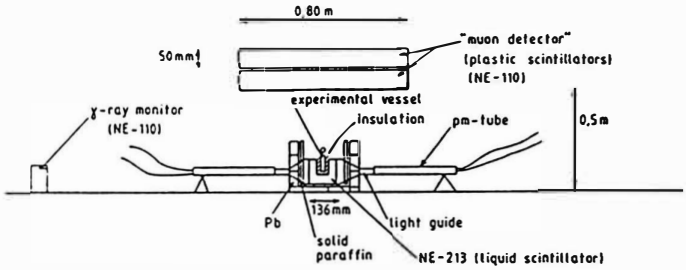

Figure 1. The experimental arrangement.

Above the neutron detector two layers of muon scintillation detectors (NE-110) are placed, which have about a 90 % geometri for cosmic muons. An additional plastic scintillator is placed a distance away in the same experimental room to monitor the variation in the overall gamma ray background.

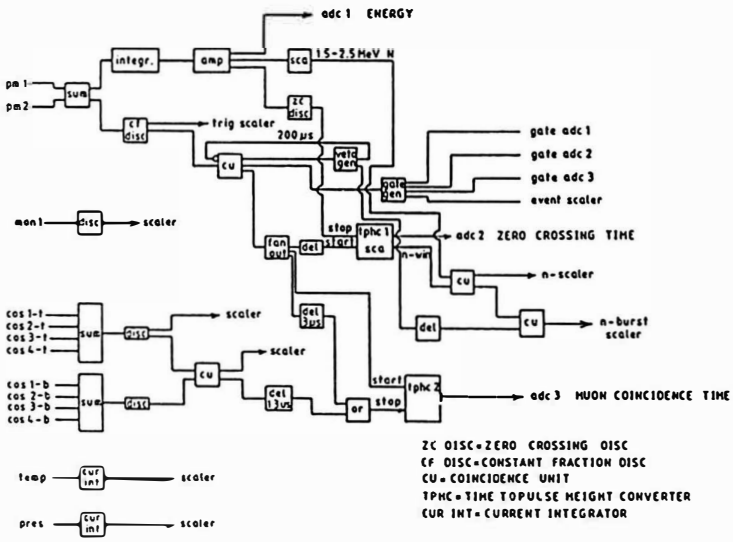

Figure 2. Block diagram of the detector system.

The block diagram of the electronics of the detector system is shown in figure 2. The two PM-tubes of the neutron detector are added and processed to give the energy to

ADC 1, the zero-crossing time to ADC 2 and the muon coincidence time, i.e. the time between an event in the muon detector and an event in the neutron detector, to ADC 3. For each trigger all three ADCs were read out consecutively and stored event-by-event.

The system also contains several scalers, e.g. the number of triggers, the number of accepted events, the number of hardware defined neutrons, the so called neutron burst watch (the number of neutron events during the dead time of the system (0.3 ms)), the gamma ray monitor and the digitalized values of the temperature and the pressure in the experimental vessel. The scalers were read out once every second and the values stored together with the ADC-data.

Energy calibration of the system was performed with gamma ray sources and pulse shape analysis calibration with a PuBe-source. To check the stability a pulser was put into the system before and after every run. Figure 3a shows a 2-dimensional diagram of the zero-crossing time, the energy and the intensity for a PuBe-calibration. The separation is good down to an energy of approximately 0.8 MeV neutrons. This type of PuBe-calibration was performed twice every day to check the stability of the system during the two weeks the experiments were in progress (figure 3d).

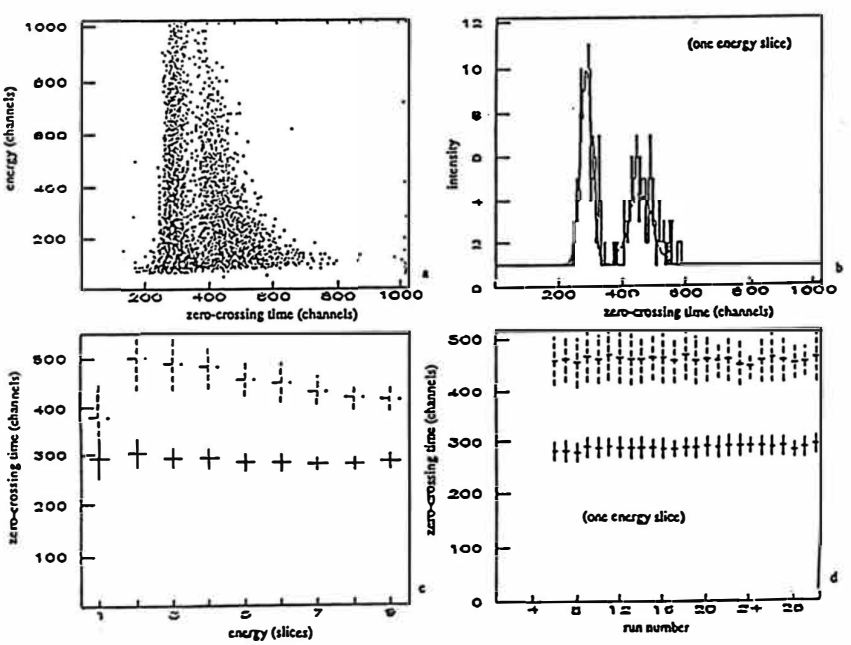

Figure 3. a) 2-dimensional diagram of energy vs zero-crossing time and intensity. b) Separation for one energy slice. A double gauss fit has been made. (For practical purposes unity has been added.) c) A parametrization of a). d) Zero-crossing stability for the experimental period (two weeks).

Experiment

The kind of experiment that the effort was concentrated on during this first running period was the so called gas experiment when titanium shavings under high D_2-pressure was

temperature cycled. The deuterium gas pressure varied between 35 and 65 bar, the cooling time between 5 and 10 minutes. The system was back to room temperature after approximately 90 minutes. The amount of Ti was between 10 and 50 g. We performed three to four cycles before changing the titanium.

We performed three types of experiments: 1) 99.8 % pure titanium in the shape of shavings (1 x 1 x 0.1 mm^3): 15 runs for totally 79 h. 2) The same titanium, but evacuated, heated to 300 °C, cooled, deuterium filled, reheated to 300 °C, recooled, refilled: 7 runs for totally 51 h. 3) The titanium alloy Ti-662 (92 % Ti, 6 % Fe, 2 % Zn) in the shape of threads: 3 runs for totally 12 h.

In addition to the runs described above we ran two types of background experiments between the D_2-experiments: a) As 1) above, but with hydrogen instead of deuterium: 3 runs for totally 20 h. b) Totally empty detector: 9 runs for totally 89 h.

Results

The analysis of the collected data was performed after finishing all data-taking. The PuBe-calibrations were used to establish where the neutrons are situated in the E-t-plot (figure 3c). Hence by using this parametrization we got a neutron energy spectrum for each run. Figure 4 shows the energy spectra for the sum of the three kinds of experiments subtracted by the corresponding background (normalized to time). Nothing significant is observed, and that goes for every single experiment as well.

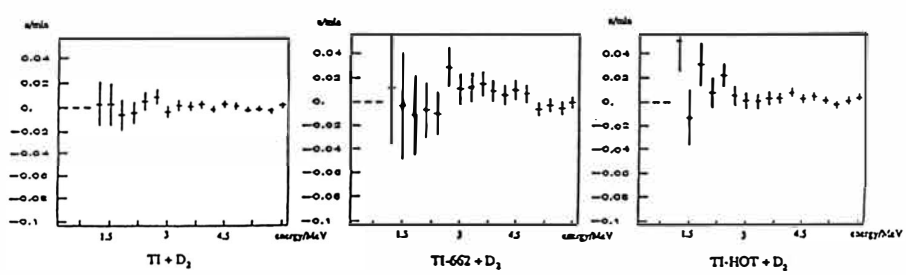

Figure 4. The energy spectra for the three kinds of experiment subtracted by corresponding background.

Cosmic radiation

In our experiments we could see that about 10 % of the observed neutrons are related to cosmic muons. They are produced in the shielding lead and other materials in the room when high energy muons collide with it, so called spalding. Lead is especially hard to deal with in this sense, because it has a very large neutron content.

Figure 5 shows the time between a muon is detected in the muon detectors and a gamma ray or neutron event in the neutron detector. Note that the gamma ray and the neutron time peaks have significantly different shapes. The tail of the neutron peak lasts for some 600 ns, which corresponds to a flight path for MeV neutrons of several meters.

This indicates that the neutrons can go around the room, maybe hitting the roof or the walls, and then go back into the neutron detector.

Nucleons also enter from the atmosphere. The rate of neutrons at the earth surface is dependent of temperature, wind, solar activity etc. But the the main factor is the air pressure. The fluctuation is 0.7 %/mbar from its avarage; i.e. quite large an effect as the air pressure can vary very much.[6]

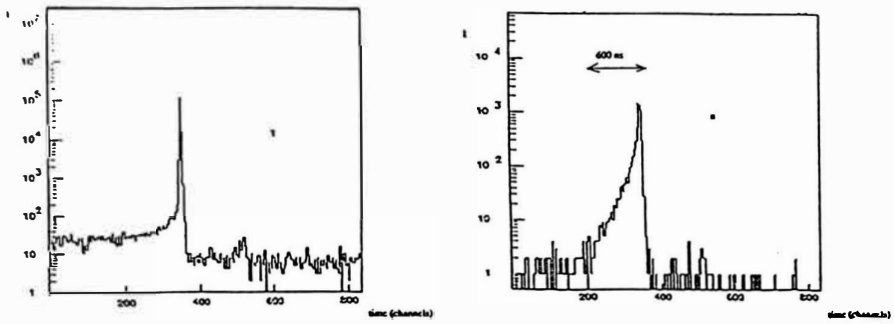

Figure 5. The time between a muon is detected in the muon detectors and a gamma ray (left) or a neutron (right) is detected in the neutron detector.

Conclusions

A low level neutron detector system has been constructed for cold fusion experiments. We conclude that:

1) It is possible to perform low level neutron measurements with this system in a reliable way.

2) No significant excess of neutrons was observed. The calculated detectable fusion rate was approximately 10^{-24} per deuteron pair and second.

3) The cosmic radiation should be paid attention to when performing low level neutron experiments. One way to deal with the problem is to have two similar systems in the experimental room to observe the neutron fluctuation.

References

1) Jones, S.E. et al: Observation of Cold Nuclear Fusion in Condensed Matter , Nature 338, 737-740 (1989)

2) Fleischmann, M. and Pons, S.:Electrochemically Induced Nuclear Fusion of Deuterium, J. Electroanal. Chem. 261, 301-308 (1989)

3) Menlove, H.O. et al: Measurement of Neutron Emission from Ti and Pd in Pressurized D_2 Gas and D_2O Electrolysis Cells, Los Alamos Nat. Lab., HOM28(J)7/27/89

4) Ninno, A. De, Scaramuzzi, F. et al: Evidence of Emission of Neutrons from a Titanium-Deuterium System, Europhys. Lett. 9 221-224 (1989)

5) Winyard, R.A. et al: Pulse Shape Discrimination in Inorganic and Organic Scintillators, Nucl. Instr. and Meth., 95 141-153 (1971)

6) Dorman, L I: Cosmic Rays - variations and space explorations, North-Holland Publ. Co., 1974.

Conference Proceedings Vol. 33
«The Science of Cold Fusion»
T. Bressani, E. Del Giudice and G. Preparata (Eds.)
SIF, Bologna 1991

CRACK-FUSION : A PLAUSIBLE EXPLANATION OF "COLD FUSION"

L.H. Bagnulo

ECOLINE ANTICORROSION Ltd.Co.- Muggiò (Milano) - Italy

Plausible dynamics are herein hypothesized on "cold fusion" in readily absorptive metals, such as Palladium or Titanium, for Hydrogen and its isotopes, the absorption at a high density level by these metals of mixtures of said isotopes (especially Deuterium and Tritium) and their successive liberation within internal cracks of the metal mass where pressures exceeding 10^{12} atm are expected to be created such that they generate fusion phenomena in accordance with the probable explosive sequence as follows: the formation of molecules, the increase in pressure, the formation of plasma, nuclear fusion.
Based on the formulated theory of "crack-fusion", a process is foreseen with relevant plants and devices for "controlled cold nuclear fusion" or "cold fusion" which envisages the absorption, at a high density level, of Deuterium atoms or their mixtures with Tritium or Helium by readily absorptive metals, such as Palladium or Titanium, for Hydrogen and its isotopes, and their successive liberation within quenching cracks, cracks due to plastic deformation, intercrystalline or transcrystalline micro-cracks or any micro-discontinuities present within and among crystals, created within the metal mass by metallurgical or mechanical means or in any other possible way. The strong influx into said cracks or micro-discontinuities of self-liberating Deuterium or Deuterium-Tritium atoms create such high pressures (practically between 10^{12} and 10^{24} atm) that their nuclei interfuse.
Deuterium and mixtures thereof with Tritium or Helium are brought into contact with the absorptive metal surfaces either by the cathodic polarization of said surfaces during the electrolysis of pure heavy water, or heavy water containing Tritium and Helium; or, alternatively, through physical contact with Deuterium or mixtures thereof with Tritium or Helium, both in a pressurized gaseous state.
It is foreseen: that this absorption occurs in the very same zone, as

that of the metal element, which contains micro-discontinuities and therefore where fusions among the liberated nuclei occur; or - on the assumption according to which nuclear fusion phenomena among Hydrogen isotopes generally take place only within micro-discontinuities in the metal masses- on the one hand, that the absorption occurs in an absorptive zone of the metal element devoid of cracks or any internal micro-discontinuities and, on the other hand, that the liberation occurs in another zone, contiguous to or distant from the former, which has to bear cracks or internal micro-discontinuities within its metal mass or pseudo-cracks between said metal element and another similar or dissimilar metal, endowed with a greater or lesser absorptive capacity, and which forcefully encompasses the former.
Furthermore, intervention with electric fields, electromagnetic fields, radiation, laser beams or particle accelerators is foreseen for the energizing of the absorbed nuclei so as to increase their flow-velocity within the metal element and the kinetic energy acquired by said nuclei during the liberation stage.
The process herein described also foresees, especially so whenever the absorption of Deuterium or mixtures thereof with Tritium and Helium is effected in gaseous phases, that the absorptive metal is subjected to temperature variations and that this absorption occurs when the metal is brought to a low or an extremely low temperature - approximately -200 °C; that is, under the conditions of contraction or maximum contraction of the metal so that the micro-cracks are compressed or extremely compressed as a consequence.
When the temperature is raised once more, the resultant expansion of the metal causes the dilation of the micro-cracks, micro-cavities and discontinuities within which the atoms of Deuterium of mixtures thereof with Tritium or Helium are drawn with the consequential occurrences of nuclear fusions.
Finally, it is foreseen that the liberation phase, in any case, occurs directly within the molten lithium.

Schemes A and B show two possible plant realizations, for the production of vapour and therefore electrical energy, which constitute the same practical applications of the plausible C R A C K FUSION dynamics.

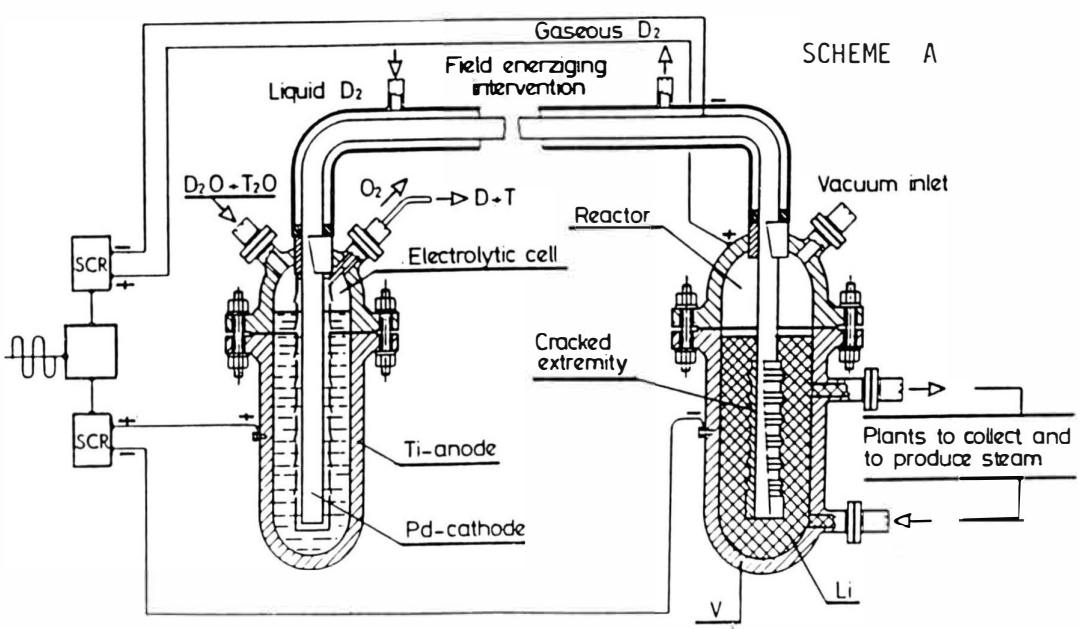

SCHEME B

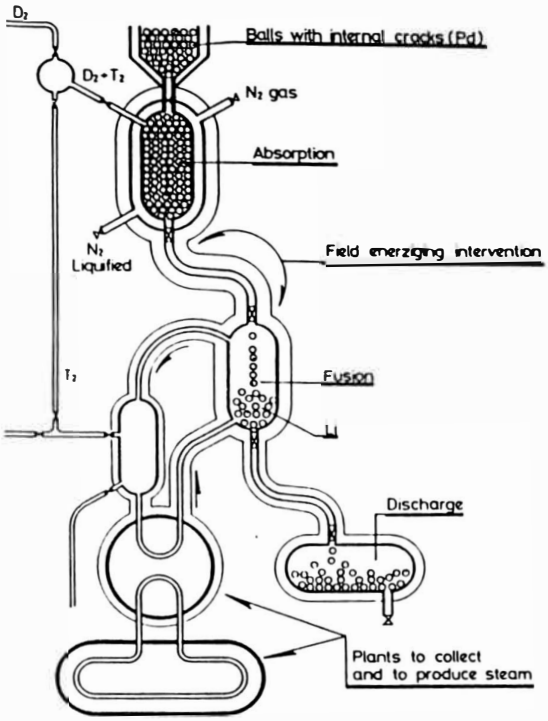

PHENOMENA KNOWN PRIOR TO "CRACK-FUSION"

Hydrogen, absorbed in an atomic state by steel during welding or electrochemical processes, is liberated within cracks, transformed into a molecular state thus creating pressures exceeding 10^7 atm which, in turn, give rise to "blistering" (Fig.1) and/or "internal cracking" (Fig.2). A particular case of "blistering" is the type (Fig. 3) between an enamel layer and a steel surface.

Analogous phenomena, occuring through the liberation of atomic Hydrogen from an electrolyte thus passing into a molecular state with an increase in volume, are those termed "Cathodic Disbonding" (Fig.4) i.e; the detachment of coatings from interred pipelines under cathodic protection; and that termed "Crevice Corrosion" (Fig.5) which occurs within external cracks of metal elements in the presence of an oxygenated electrolyte within the crack tip. Also extremely interesting is "Fracto-Emission" as described by certain authors; the emission of radio-frequency signals, photons and charged particles during the fracturing of deuterated Titanium.

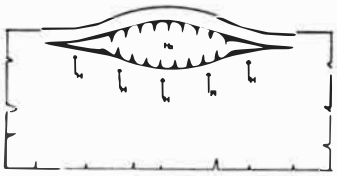

Fig.1

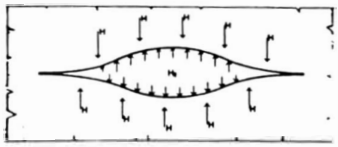

Fig.2

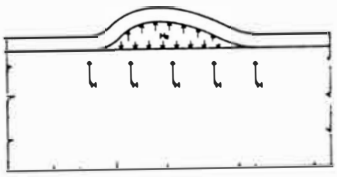

Fig.3

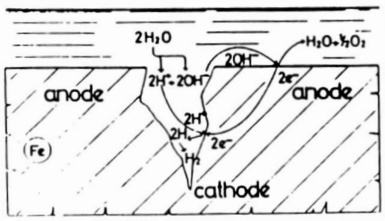

Fig.4

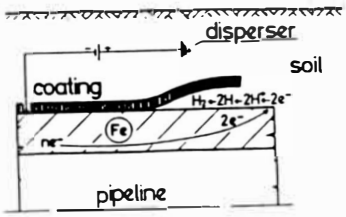

Fig.5

A POSTERIORI CLUES TOWARDS THE RELIABILITY OF "CRACK-FUSION"

GENERAL DIFFICULTIES WITH THE REPETITION OF "NUCLEAR FUSION".

Obtaining positive results with nuclear fusion seems to depend on having internal cracks within the Palladium or Titanium cathode or cracks created by plastic deformation after long charging.

THE DIFFICULTY WITH REPEATING FUSION ON THE SAME METAL UNDER THE SAME WORK CONDITIONS.
This difficulty is supposed to be caused by the entrapment of fusion products within the crack.
Sporadic repetitions experienced by certain researchers may be attributed to crack advancement and relative volume increase.

AN EXPERIMENT BY PROF. SCARAMUZZI
The Titanium shavings have most likely and largely favoured the positive outcome of the experiment since metal shavings naturally present numerous internal and external cracks. The repetition, at close frequency, of the fusion may be related to easier advancement and revitalizing of cracks within the shavings.

FRACTO-EMISSION
"FRACTO-EMISSION" has been hypothesized by certain researchers - see under (*) - prior to the event of "COLD FUSION".
Subsequently, in No. 1 dated January 1990 of the Materials Research Society an article appeared by the authors Dickinson, Jensen and others under the heading "Fracto-emission from Deuterated Titanium; Supporting Evidence for a Fracto-fusion Mechanism".
In this very interesting article the hypothesis we illustrate in Fig. 6 is postulated.
That is "that crack growth results in charge separation on the newly formed crack surfaces, which act like a miniature "linear accelerator"; i.e. D+ ions are accelerated in the electric field across the crack tip to kinetic energies of $10-10^4$ eV or more, sufficient to raise the D+D fusion probability".
We instead assume that also in the case of Deuterated Ti or Pd there is an occurrence of D + D fusion in accordance with the dynamics illustrated in Fig. 7 as hypothesized by us.
Here too it is a case of a fusion process resulting from the liberation of Deuterium atoms within the tip of an external crack.

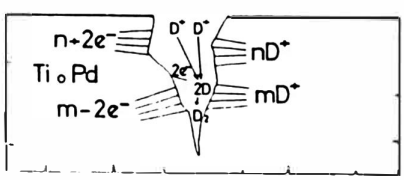

Fig.6

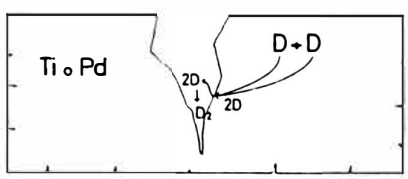

Fig.7

* J.T. Dickinson, E.E. Donaldson, and M.K. Park, "The Emission of Electrons and Positive Ions from Fracture of Materials" J. Mater Sci. 16, 2897-2908 (1981)
J.T. Dickinson L.C. Jensen, and A, Jahan-Latibari, "Fracto-Emission : The Role of Charge Separation", J.Vac.Sci.Technol. A2, 1112-1116 (1984)
J.T. Dickinson, W.D. Williams, and L.C. Jensen, "Fracto-Emission from Lead Zirconate-Titanate", J.Am. Ceram.Soc.68, 235-240 (1985).

Italian Patents of 14.06.1989 and 26.02.1990 extended to the European Community and thirteen other Extra-European States.

Conference Proceedings Vol. 33
«The Science of Cold Fusion»
T. Bressani, E. Del Giudice and G. Preparata (Eds.)
SIF, Bologna 1991

MEASUREMENT OF D-D AND D-6LI NUCLEAR REACTIONS AT VERY LOW ENERGIES

F.E. Cecil[a] and G.M. Hale[b]

[a]Colorado School of Mines, Golden CO 80401, USA
[b]Los Alamos National Laboratory, Los Alamos NM 87545, USA

ABSTRACT

The nuclear reactions of very low energy deuterons (down to center-of-mass energies of 2 keV) with deuterons and ^{6}Li have been measured. The measured D-D reactions are in good with agreement recent R-matrix calculations. The reaction ratios D(d,p)T/D(d,n)^{3}He and ^{6}Li(d,p)^{7}Li/^{6}Li(d,α)^{4}He in particular were examined for possible evidence of an Oppenheimer-Phillips type enhancement. No significant enhancement was found in either ratio or in the absolute yields of the reactions. The radiative capture reactions D(d,γ)^{4}He and ^{6}Li(d,γ)^{8}Be were likewise measured. The branching ratios of these radiative capture reactions to the nucleonic branches of the reactions appear roughly independent of energy. The role of these reactions in the production of heat in cold-fusion experiments is evaluated.

INTRODUCTION

The nuclear reactions between two deuterons and perhaps between a deuteron and a ^{6}Li nucleus are generally accepted as playing crucial roles in recently observed nuclear processes and significant heat production in condensed matter deuterium-metal systems. Independent measurements of the cross sections for these nuclear reactions at low energies will allow these assumed roles to be addressed. The ratio of the reactions D(d,n)^{3}He and D(d,p)T or the ratio of the reactions D(d,γ)^{4}He and D(d,p)T at very low energies will, for example, determine whether significant heat production is possible from D-D nuclear reactions in the absence of

enormous quantities of escaping and potentially hazardous radiation. Similarly, the ratio of the reactions $^{6}Li(d,p)^{7}Li$ and $^{6}Li(d,\alpha)^{4}He$ and the ratio of the reactions $^{6}Li(d,\gamma)^{8}Be$ and $^{6}Li(d,\alpha)^{4}He$ will allow the analogous determination for the D-^{6}Li reaction to be addressed. In this work, we report on our recent measurements of these reactions. While some of these reactions have been studied at relatively low energies[1-5], the present work extends our knowledge of these reactions to significantly lower energies. On the other hand, our measurement of the reaction $^{6}Li(d,\gamma)^{8}Be$ is the first reported observation of this reaction.

EXPERIMENTAL RESULTS

The D-D and D-^{6}Li reactions were studied using magnetically analyzed deuteron beams from the Colorado School of Mines low energy charged particle accelerator[6]. The targets consisted of pressed sheets of CD_2 and rolled foils of metallic Li, isotopically enriched to 94% ^{6}Li. The charged reaction products were detected with silicon surface barrier detectors placed at 150° from the beam direction and protected from the Rutherford backscatterd beam deuterons by a thin Al foil. The gamma rays were detected with a NaI(Tl) scintillation spectrometer surrounded by an active Compton scattered gamma ray and cosmic ray shield. This gamma ray detector system has been described elsewhere[7]. The techniques used in the gamma ray to charged particle branching ratio measurements have likewise been described in some of our earlier studies[8].

Charged particle spectra measured during the bombardment of the CD_2 and ^{6}Li targets are shown in Figure 1.

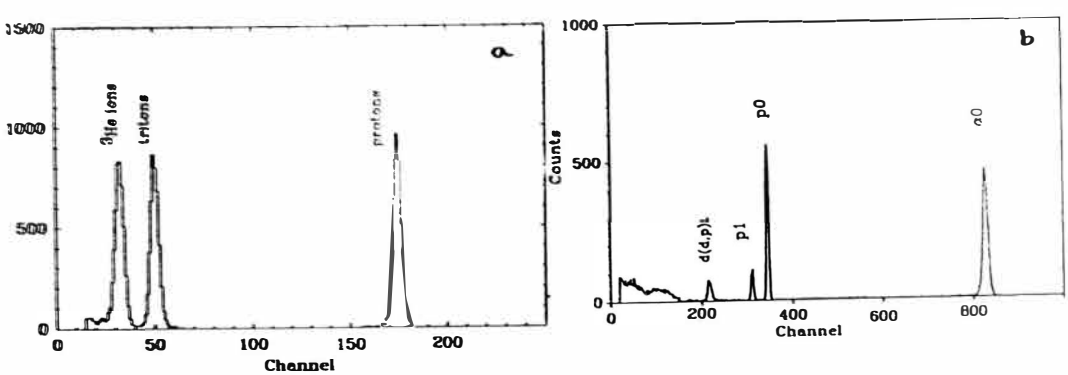

Figure 1. (a)Charged particle spectrum for D-D reaction at $E_{lab} = 10$ keV. (b) Charged particle spectrum for D-^{6}Li reaction at $E_{lab} = 150$ keV.

Since the angular distributions of the outgoing reaction products for the D-D and D-^{6}Li reactions have been shown to be nearly isotropic at low energies[1-3], the reaction ratios D(d,p)T/D(d,n)^{3}He and ^{6}Li(d,p)^{7}Li/^{6}Li(d,α)^{4}He are determined directly from the ratio of the yield of the peaks labelled "^{3}He ions" and "tritons" for the D-D reaction and "p0" and "α" for the D-^{6}Li reaction. The yield ratios so determined as a function of energy are given in Figure 2. The yield ratios for the D-D reaction presented in Figure 2 are compared to a recent R-matrix[9] calculation. Our measured yield ratios are consistent with the calculated ratio, indicating no enhancement of the (d,p) reaction as qualitatively suggested by Oppenheimer and Phillips[10]. While there have been no comparable calculations for the ratio of the reactions ^{6}Li(d,p)^{7}Li and ^{6}Li(d,α)^{4}He, Koonin[11] has calculated the (d,p)/(d,n) ratio for the D-^{6}Li reactions at low energies and has predicted no significant enhancement of the (d,p) reaction. Our results are consistent with these predictions since we would expect the (d,α) reaction to be unaffected by any Oppenheimer-Phillips type processes.

These spectra also allowed a determination of the absolute thick taget yield of the reactions. The measured yields are shown in Figure 3 and are compared, respectively, to yields based upon the R-matrix calculation noted above or calculated assuming a slowly varing astrophysical S-factor. There is good agreement between measured and calculated yields again indicating no anomolous behavior at very low energies.

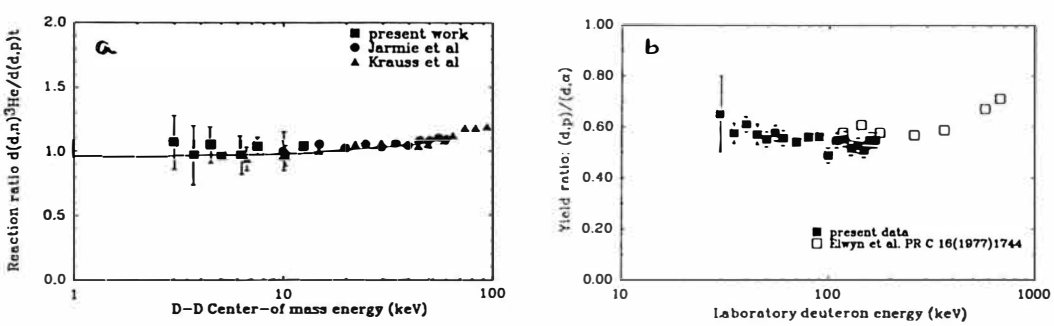

Figure 2. (a) Ratio of (d,p) to (d,n) branches for D-D reactions. (b) Ratio of (d,p) to (d,α) branches for D-^{6}Li reactions.

Gamma ray spectra were measured during the deuteron bombardment of the CD_2 and ^6Li targets between c.m. energies of 20 and 100 keV. The yield of the 23.8 MeV and 22.6 MeV gamma rays and the concurrent yield of the charged particles (see Figs 1) will determine the gamma ray to charged particle branching ratios for the D-D and D-^6Li reactions respectively after the yield ratios are corrected for the relative detector efficiencies. The branching ratios so determined are plotted in Figure 4. The D-D branching ratio is consistent at the higher energies with our earlier measurements. The fact that the measurements of the D-D gamma ray to charged particle branching ratio at c.m. energies of 20 and 40 keV are, to within errors, equal in value, suggest that the branching ratio is independent of energy. The energy dependence for the branching ratio for the D-^6Li reaction is somewhat inconclusive although energy independence is certainly not ruled out by virtue of the relatively large error bar on the lower energy data point for this reaction.

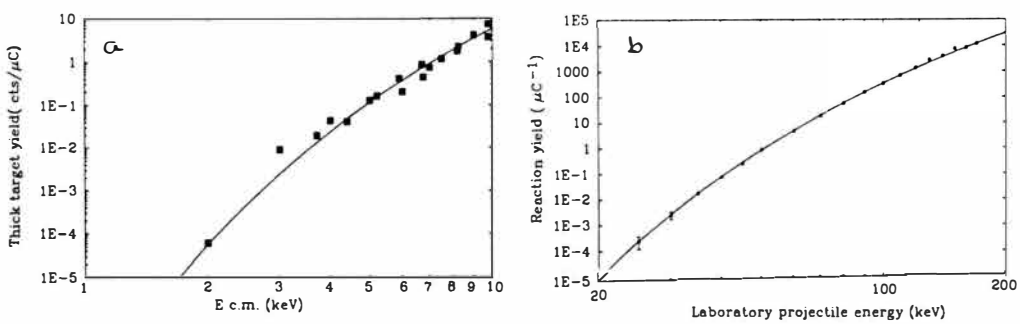

Figure 3. (a) Measured and calculated yields for D(d,p)T reaction. (b) Measured and calculated yields for $^6Li(d,\alpha)^4He$ reaction.

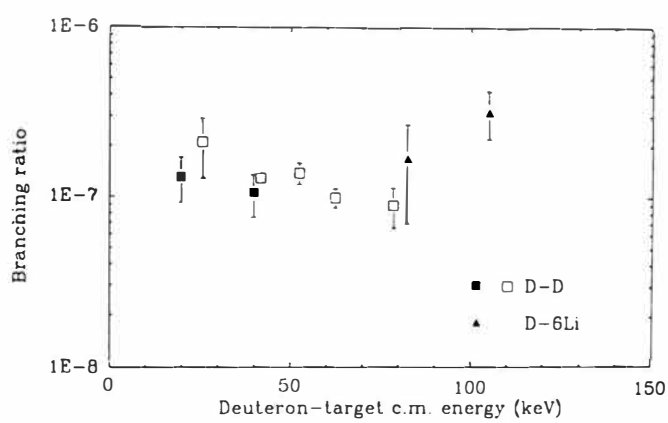

Figure 4. Gamma ray to charged particle branching ratios for the D-D and D-^6Li reactions. The open squares are from Ref. 4.

CONCLUSIONS

The results of our measurements have significant implications for any effort to associate the D-D or D-^{6}Li nuclear reactions with reports of heat production from cold fusion experiments. Specifically, if the particle-particle and gamma ray-particle branching ratios which we have measured at very low laboratory energies are characteristic of the branching ratios occuring in condensed matter fusion in deuterium-metal systems, then even low levels of heat production arising from these nuclear reactions will necessarily be associated with enormous quantities of escaping radiation. For example, based on the branching ratios given in Figures 2 and 4, if 1 Watt of power were produced by the D-D reaction, then there would be an accompanying production of about 10^{12} 2.5 MeV neutrons per second and about 10^5 24 MeV gamma rays per second. Comparable yields of neutrons and gamma rays will be associated will similar levels of power production by the D-^{6}Li reaction. If, therefore, the reported production of heat from condensed matter fusion in deuterium-metal systems is to be attributed to D-D or D-^{6}Li reactions, then the particle-particle and gamma ray-particle branching ratios at unmeasurably low energies must vary drastically from those measured at the low energies reported in this work.

This work is supported by the U.S. Department of Energy.

References

1. R. Brown and N. Jarmie, Phys. Rev. C41 (1990) 1391.
2. A. Krauss et al., Nucl. Phys. A465 (1987) 150.
3. A.J. Elwyn et al., Phys. Rev. C16 (1977) 1744.
4. F.J. Wilkinson and F.E. Cecil, Phys. Rev. C31 (1985) 2036.
5. C.A. Barnes et al., Phys. Lett. 197B (1987) 1922.
6. F.E. Cecil et al., NIM B40/41 (1989) 934.
7. F.E. Cecil et al., NIM A234 (1985) 479.
8. F.E. Cecil and F.J. Wilkinson, Phys. Rev. Letts. 53 (1984) 767.
9. G.M. Hale and D.C. Dodder, Proc. Int. Conf. on Nucl. Cross Sections for Technology. Knoxville (1979) J.C. Fowler, C.H. Johnson and C.D. Bowman editors. NBS Special Publication 594, p. 650.
10. J.R. Oppenheimer and M. Phillips, Phys. Rev. 48 (1935) 500.
11. S.E. Koonon and M. Mukerjee, Phys. Rev. C42 (1990) 1639.

Conference Proceedings Vol. 33
«The Science of Cold Fusion»
T. Bressani, E. Del Giudice and G. Preparata (Eds.)
SIF, Bologna 1991

MÖSSBAUER SPECTROSCOPIC CHARACTERIZATION OF SAMPLES FOR COLD FUSION EXPERIMENT

E. KUZMANN+, M. GÁL++ G. K. SÓLYMOS++ CS. SZELES+

+Department of Nuclear Chemistry, Eötvös University, Budapest, Hungary

++Department of General and Anorganic Chemistry, Eötvös University, Budapest, Hungary

Introduction

In this contribution we show a case in which we have applied the Mössbauer spectroscopy for characterization of samples which were expected to show anomalous nuclear effects upon to their deuterization.

The Mössbauer spectroscopy can provide information about the surrounding of a Mössbauer atom in deuterized samples by measuring the electrical monopole and quadrupole as well as magnetic dipole interactions. The introduction of deuterium (or hydrogen) into the vicinity of a resonance atom will influence the physical parameters which govern the Mössbauer spectrum, thus changes will be expected in the hyperfine interactions e.g. in isomer shift, quadrupole splitting, magnetic splitting (Fig. 1) and in other parameters. Consequently, the localization of deuterium can be sensitively studied.

The main question is : how can these investigations help us to understand more about the conditions of cold nuclear fusion?

In our previous works [1,2] Mössbauer spectroscopy (as well as neutron and gamma-spectroscopy) was used to study the possibility of cold nuclear fusion in Fe-Zr amorphous alloys deuterized electrolitically both in air and in nitrogen atmosphere.

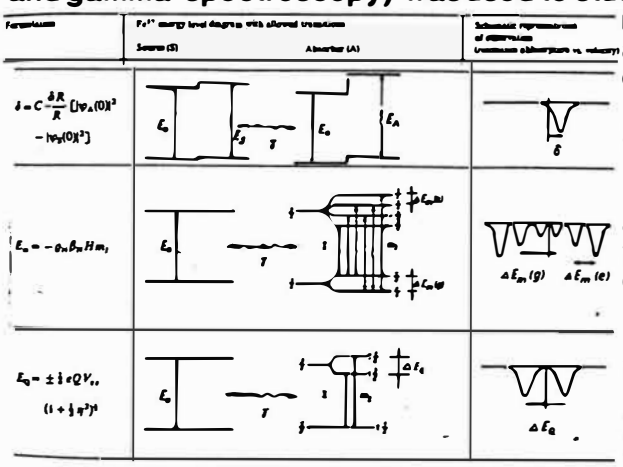

Fig. 1. Mössbauer isomer shift d magnetic splitting E_m, quadrupole splitting E_Q

Mössbauer spectroscopy can be especially advantageously applied to the study of the effect of electrolytical hydrogenation of Fe-Zr amorphous alloys because the considerable changes appearing in the spectra (due to the change in the deuterium concentration or due to small heat effects) allow us to detect any structural change caused by deuterization [3].

We have performed experiments on high temperature superconductors because Celani et al. [4] have shown anomalous nuclear effects due to deuterization in such a materials. Our earlier studies on high T_c superconductors [e.g. 5-7] showed that the different crystallographic sites can be sensitively investigated by Mössbauer spectroscopy.

Experimental

$EuBa_2(Cu_{0.99}{}^{57}Fe_{0.01})_3O_{7-d}$ high temperature superconductor samples were sintered from Eu_2O_3, CuO, $BaCO_3$ and $^{57}Fe_2O_3$ at 875°C for 120 min and heated at 430°C for 960 min in oxigen atmosphere.

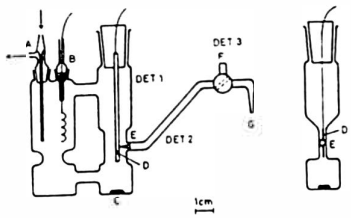

Fig. 2. Cell for deuterization

Hydrogenation and deuterization of samples were performed either by applying gas pressure (30 bar) in a bomb for 12 hours or by cathodic polarization of samples. The electrolysis was carried out in a cell (Fig. 2) using 0.1n NaOH or NaOD electrolyte for 60 min at 30 mA current and -1.7 mV potential relative to calomel electrode in nitrogen atmosphere. Effusing of hydrogen of gas loaded samples was performed in nitrogen atmosphere at 200°C.

^{151}Eu and ^{57}Fe Mössbauer spectra of nonhydrogenated and hydrogenated or deuterized samples were recorded in transmission geometry at 295 K and at 85 K by a conventional constant acceleration Mössbauer spectrometer. Isomer shifts are given relative to alpha-iron and EuF_3. The spectra were evaluated by conventional least-square fitting of lines.

Positron annihilation lifetime spectra of nonhydrogenated and gas loaded samples were measured at 295 K and at 55 K.

Results and discussion

Fig. 3. shows the structure of most intensively investigated high temperature superconductor of $YBa_2Cu_3O_{7-d}$. It has a threefold stacked orthorombic perovskite structure having two different Cu sites: the Cu(1) (chain site) and the Cu(2) (plain site) between the Y and Ba-O layers.

Typical ^{151}Eu and ^{57}Fe Mössbauer spectra of $EuBa_2(Cu_{0.99}{}^{57}Fe)_3O_{7d}$ sample are illustrated in Fig. 4. The broad singlet of Eu spectrum corresponds to a Eu^{3+} being in the rare earth site. The Fe spectrum can be decomposed into 3 doublets D1, D2 and D3. The Mössbauer parameters are shown in Table 1.

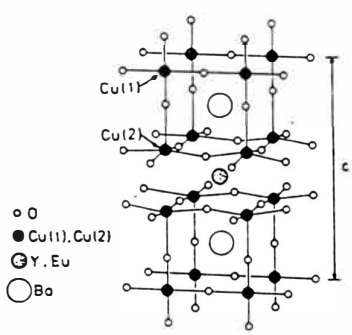

Fig. 3. Structure of 1-2-3 high T_c superconductor

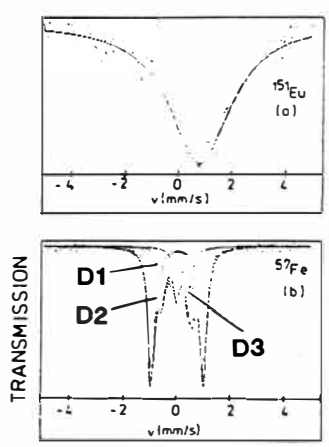

Fig. 4. ^{151}Eu (a) and ^{57}Fe (b) Mössbauer spectra of $EuBa_2(Cu_{0.99}{}^{57}Fe_{0.01})_3O_{7-d}$

Table 1.

MÖSSBAUER PARAMETERS OF $EuBa_2(Cu_{0.99}{}^{57}Fe_{0.01})_3O_{7-d}$ SUPERCONDUCTOR

^{57}Fe spectrum (T=85K)	IS (mm/s)	QS(mm/s)
D1	0.07+-0.01	1.99+-0.02
D2	-0.02+-0.01	1.35+-0.02
D3	0.39+-0.01	0.64+-0.02

^{151}Eu spectrum (T=295K)	IS(mm/s)	W (mm/s)
	0.95+-0.02	2.63+-0.03

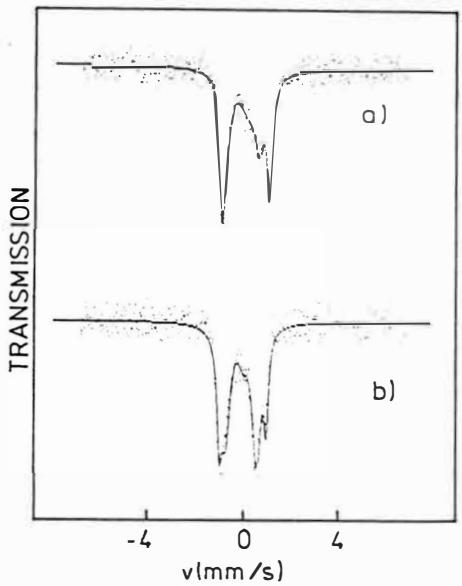

Fig. 5. ^{57}Fe Mössbauer spectra of non-hydrogenated (a) and gas-hydrogenated (b) sample

D1 doublet is associated with Fe in four coordinated Cu(1) site while D2 doublet is attributed to Fe in five coordinated Cu(1) site [6]. D3 doublet corresponds to Fe in Cu(2) site [6].

Fig. 5 and 6 shows the ^{57}Fe spectra of gas-hydrogenated and nonhydrogenated samples having lower and higher oxigen content. It can well be seen in Fig. 5-7 that the relative intensity of D2 doublet (representing iron atoms at Cu(1) site) in ^{57}Fe spectra increases due to gas deuterization.

The spectra of electrolytically hydrogenated (Fig. 8) and deuterized (Fig. 9) reflect how the relative intensity of the D3 doublet (representing iron atoms at Cu(2) site) in the ^{57}Fe spectra increases due to cathodic polarization.

No considerable changes appear in the ^{151}Eu spectra upon gas hydrogenation or deuterization as illustrated in Fig. 10 where Eu spectra of non-hydrogenated and gas deuterized sample are shown.

However, the isomer shift and the linewidth decrease in the ^{151}Eu spectra due to cathodic polarization, as shown in Fig. 11.

A lifetime positron annihilation spectrum of non-hydrogenated sample is shown in Fig. 12. No changes were observed in the spectrum after gas-hydrogenation or gas-deuterization.

The changes of the relative intensity of D2 can be associated with hydrogen or deuterium localized in the vicinity of Cu(1) site. The changes of the relative intensity of D3 doublet can be associated with hydrogen or deuterium in the vicinity of Cu(2) site. In the case of the cathodic polarization this change can partly be attributed to the appearing of some new Fe(3+) compound due to the decompositon of the sample.

The change of the hyperfine parameters (isomer shift, quadrupole splitting) of Eu spectra can be connected with the effect of hydrogen or deuterium in the neighbourhood of Eu.

The positron annihilation spectroscopy results are consistent with the site prefence of hydrogen and deuterium around the Cu(1) site in the gas loaded samples because this technique is more sensitive to the neighbourhood of Cu(2) site.

It could have some consequences that negative charged ion sites are supposed to be occupied by hydrogen or deuterium.

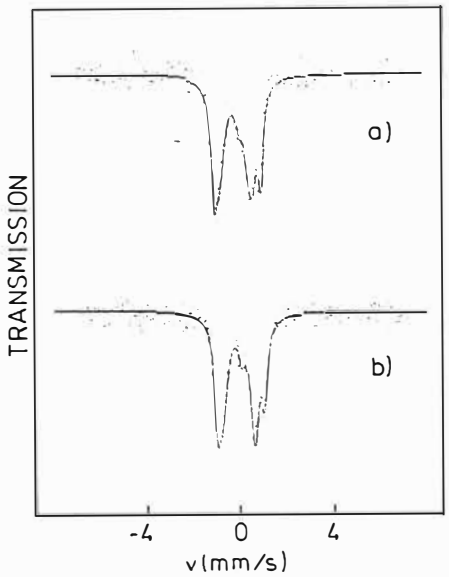

Fig. 6. ^{57}Fe Mössbauer spectra of non-hydrogenated (a) and gas-hydrogenated (b) sample

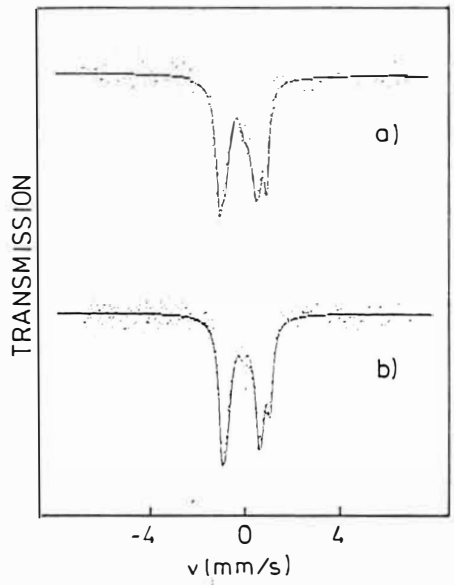

Fig. 7. ^{57}Fe Mössbauer spectra of non-hydrogenated (a) and gas-deuterized (b) sample

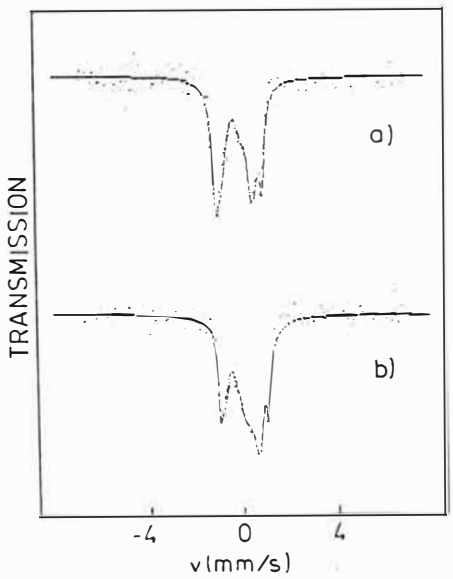

Fig. 8. ^{57}Fe Mössbauer spectra of non-hydrogenated (a) and electrolytically hydrogenated (b) sample

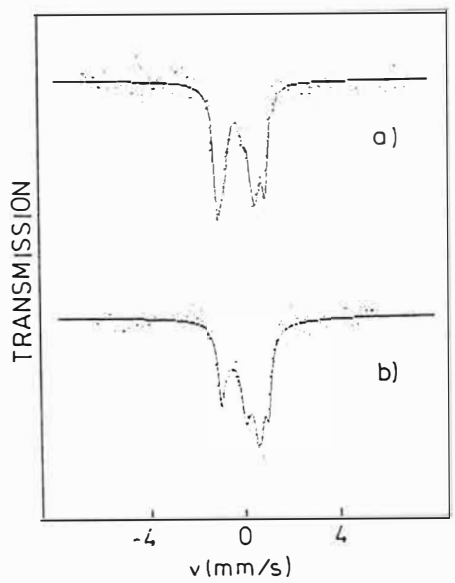

Fig. 9. ^{57}Fe Mössbauer spectra of non-hydrogenated (a) and electrolytically deuterized (b) sample

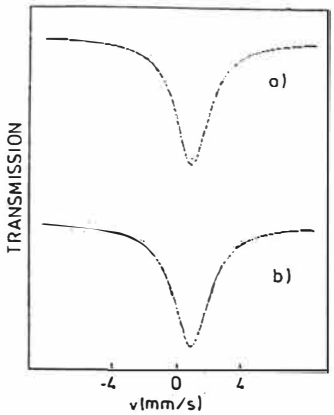

Fig. 10. ^{151}Eu Mössbauer spectra of non-hydrogenated (a) and gas-deuterized (b) sample

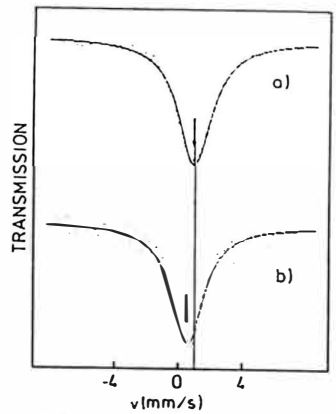

Fig. 11. ^{151}Eu Mössbauer spectra of non-hydrogenated (a) and electrolytically deuterized (b) sample

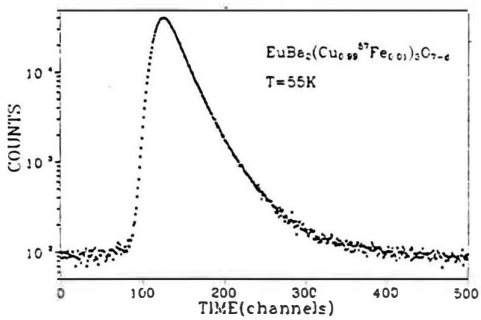

Fig. 12. Positron annihilation spectrum of a non-hydrogenated sample

The following conclusions can be drawn from the results:
(1) The hydrogen or deuterium is localized mainly around the Cu(1) site in these high temperature superconductors hydrogenated or deuterized by gas loading. (2) No differences can be detected between the localization of hydrogen and deuterium by gas loading. (3) The electrolytic hydrogenation and deuterization of these superconductors are accompanyed by partial decomposition of the material. Part of the hydrogen and deuterium tends to be localized around the Cu(2) sites.

References

[1] E. Kuzmann, M. Varsányi, L. Korecz, A. Vértes, T. Masumoto, F. Deák, Á. Kiss, L. Kiss, J. Radioanal. Nucl. Chem. Lett. 137, (1989) 243.
[2] E. Kuzmann, A. Vértes, M. Varsányi, L. Kiss, L. Korecz, F. Deák, Á. Kiss, T. Masumoto: Proc. Int. Conf. Anomalous Nuclear Effects in Deuterium/Solid Systems (Ed. S. Jones), APS, N.Y. (1991).
[3] E. Kuzmann, A. Vértes, Y. Ujihira, M. Fujinami, P. Kovacs, T. Ando, T. Masumoto, Hyperfine Int. 45, (1989), 279.
[4] F. Celani et al.: Proc. Int. Conf. on Anomalous Nuclear Effects in Deuterium Solid/Systems (Ed. S. Jones), APS, N.Y. (1991).
[5] E. Kuzmann, Z. Homonnay, A. Vértes, M. Gál, K. Torkos, B. Csákvári, G. K. Sólymos, G. Horváth, J. Bánkuti, I. Kirschner, L. Korecz, Phys. Rev. 39, (1989) 328.
[6] E. Kuzmann, Z. Homonnay, A. Vértes, I. Halász, J. Bánkuti, I. Kirschner, Hyp. Int. 55 (1990) 1337.
[7] E. Kuzmann, S. Nagy, Z. Homonnay, A. Vértes, I. Halász, M. Gál, B. Csákvári, K. Torkos, J. Bánkuti, I. Kirschner, Y. Wei, A. Nath, Struct Chem. 2 (1991) 267.

Conference Proceedings Vol. 33
«The Science of Cold Fusion»
T. Bressani, E. Del Giudice and G. Preparata (Eds.)
SIF, Bologna 1991

RECENT MODIFICATIONS TO THE MANITOBA DEUTERIUM IMPLANTATION ACCELERATOR AND A STUDY OF THE PROPERTIES OF THE ONLINE NEUTRON MONITOR DETECTOR†

M.S. Mathur, H.L. Johnston*, A. Mirzai*, J.S.C. McKee, G.R. Smith, J.J.G. Durocher, K. Furutani, J.K. Mayer, Y.H. Yeo, H. Hnatiuk, S. King and A. Hempel
University of Manitoba Accelerator Centre, Department of Physics, University of Manitoba, Winnipeg Canada R3T 2N2
and
K. S. Sharma and G. Williams
Department of Physics, University of Manitoba, Winnipeg Canada R3T 2N2

†Supported by the Natural Sciences and Engineering Research Council of Canada and Manitoba Hydro.
*Manitoba Hydro Fellow

ABSTRACT

Deuterium molecules have been implanted into Palladium, Titanium and Indium targets in recent experiments at Manitoba by means of the 60 keV, 100 μA D_2^+ 'Narodny' ion accelerator. Neutrons from D-D interactions involving beam particles with previously stopped D atoms were detected by a large plastic scintillator viewed by two Photomultiplier tubes. We describe recent modifications to the accelerator made to improve the quality of the implanting beam, and some of the properties of the neutron detector used.

INTRODUCTION

Interest in warm/cold fusion of deuterium nuclei was stimulated by the March 1989 announcement[1] of possible nuclear fusion at room temperature. The experiment involved electrolysis of heavy water using a platinum anode and a palladium cathode. The electrolysis sent deuterons to sites in the palladium generating, according to the scientists involved, several times more heat energy than the electrical energy consumed. Later results[2] from a similar experiment reported only minor amounts of heat generation but did produce some neutrons, typically 200 per hour, as a signature for nuclear processes being involved.

The University of Manitoba group attempted to simulate the electrolysis experiment in a similar but different non-equilibriumsituation without involving heavy water as an intermediate material. Assuming that the formation of a high concentration of deuterium nuclei in the surface region of the target material (palladium) was a prerequisite for the cold fusion phenomenon, we used the Narodny implanter to directly inject nuclei into the surface at concentrations far in excess of the earlier measurements.

In this experiment[3] a significant rise in neutron production was observed after nine hours of implantation with a 100 μA beam of 60 KeV D_2^+ ions (containing some D^+ and D^o contamination). Later, a further experiment was carried out in which similar results were obtained for titanium implantation and were confirmed for palladium. Little excess heat was observed. We now propose to repeat this work using an analyzed ion beam.

MAGNETIC DEFLECTION AND ANALYSIS SYSTEM

The deuterium ion beam accelerated in the Narodny accelerator, though largely molecular D_2^+, has a significant component of atomic D^+ and neutral deuterium whose precise concentration is unknown. To understand the nature of surfaces implanted with atomic and molecular ions - the composition of the beams must be known precisely. In order to solve this problem a 0.1 Tesla magnet was installed to bend the beam from the Narodny ion source into the horizontal plane. The separate beams of molecular and atomic D and ultimately the undeflected neutral beam can now be used to initiate surface changes according to species.

The magnet, a 178 mm diameter circular electromagnet, has been modified into a sector magnet with unity magnification i.e. the image and object distances are equal. To improve the magnetic field uniformity, the magnet poles were aligned to a precision better than 0.01 mm. and the homogeneity of the field after alignment was determined by field mapping for a coil current of 18.0 amperes and a 51 mm gap. Iron diaphragms were designed and appropriate shims were used to terminate the fringing field and complete the conversion to a sector magnet. The shims were positioned in such a way that the maximum possible area of the pole faces can be effectively utilized. The gap between iron diaphragms

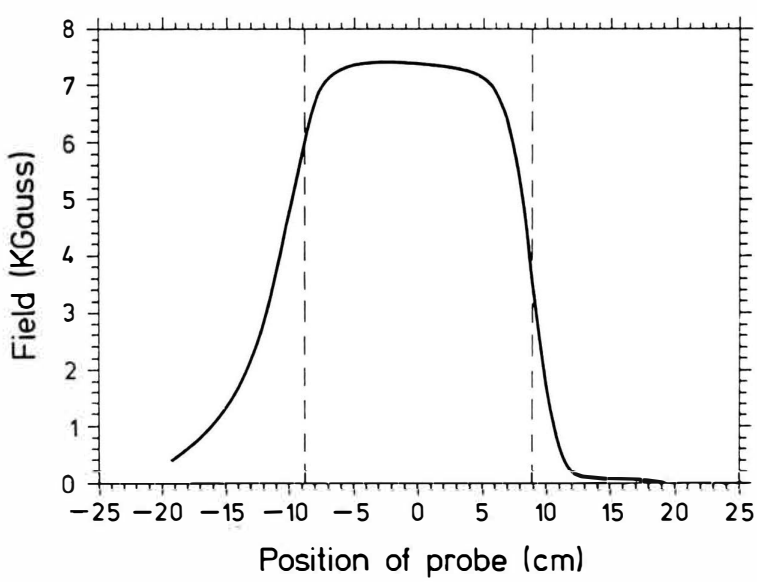

Figure 1. Field mapping of the magnet with shims and one of the iron diaphragms in place for the current and gap width described in the text.

and the shims was optimized to 10 mm. Fig. 1 illustrates the mapped field. The radius of curvature for the beam was selected to be 110 mm. A computer controlled power supply was designed and built for the analyzing magnet. The magnet is installed below the original target chamber on the linear accelerator. A 51 mm. diameter vacuum pipe carries the accelerated beam through the magnet to a new sample chamber where further experiments involving the implantation of gaseous ions in metals will be performed. The immediate concern is to study the separation of D^+ and D_2^+ species in the analysis system, which is underway.

THE ONLINE NEUTRON MONITOR

Experiments[3] conducted at the University of Manitoba on the implantation of heavy metals (Pd, Ti and In) with low energy deuterons led to the observation of neutrons from the $D(d,n)^3He$ interaction. As the concentration of deuterons in the heavy metal matrix increases, these deuterons form the target nuclei for bombardment by subsequent deuterons. Since some deuterons have energy exceeding the threshold energy of the reaction, neutron emission is expected. One searches the supply of generated neutrons for any anomalies in the production rate, or in the absolute number of neutrons produced during the experiment. Two strategies were adopted for the observation of these neutrons:

i. By placing a piece of In close to the target heavy metal, a meta-stable state, ^{115m}In, was formed by inelastic neutron scattering. After the implantation experiment had finished, the decay of the meta-stable state was observed in a low background environment. The total number of neutrons generated during the experiment was then estimated.

ii. A cylinder of NE-102 plastic scintillator was placed in the vicinity of the implantation chamber, and direct monitoring of neutron production observed. This device is called the On-line Neutron Monitor (ONM) and an investigation of the character of the neutron generation rate as a function of time in the experiment was made.

These methods can be checked against one another, since the record of the second experiment can be summed to yield an estimate of the total number of neutrons detected during the experimental run.

The ONM can operate as a proton recoil type neutron spectrometer and is designed to respond to fast neutrons in the energy range of about one to ten MeV. It consists of a cylindrical piece of NE-102 plastic scintillator viewed by two RCA 4522 photomultiplier tubes and provides a proton rich target for incoming neutrons[3]. Cosmic ray muons are continuously detected by the ONM. These signals have a definite spectrum and can be used to monitor the constancy of the overall gain of the detection system and help define the energy calibration of the detector. Environmental gamma rays are registered by the system and can contribute to the observed spectrum. Because of the high thermionic noise exhibited by the photomultiplier tubes, chance noise coincidences can be included in the data record. Finally, since both photomultiplier tubes view each other, light caused by afterpulses in the one tube

can be detected very efficiently by the other. All of these effects place practical limits on the range of energies to which the ONM is sensitive.

In the energy range up to 10 MeV, the neutron-proton(n-p) elastic scattering system produces neutrons isotropically in the centre of mass frame and thus all scattering geometries are equally probable. While the energy gained by the recoil proton may range from zero to the incident neutron energy on average, the proton receives half the incident neutron energy. In the energy range up to a few MeV, the light output of NE-102 is not a linear function of proton energy. The proton deposits much more energy per unit path length than can be converted into scintillation light[4]. As a result, the calibration of the spectrometer output in terms of proton energy is cumbersome. Since electrons in the same energy range deposit relatively little energy per unit path length, the light output of NE-102 increases linearly with electron energy. The ONM calibration is expressed in terms of equivalent electron energy, and the incident neutron (proton) energy is related to that electron energy.

Compton scattering of gamma rays of known energy is used to calibrate the ONM. A sodium iodide detector at a fixed scattering angle detects the scattered gamma ray and thus defines the energy of the Compton electron within the scintillator. The energy calibration of the ONM is shown in figure 2. Also included is a calibration point from cosmic ray muons.

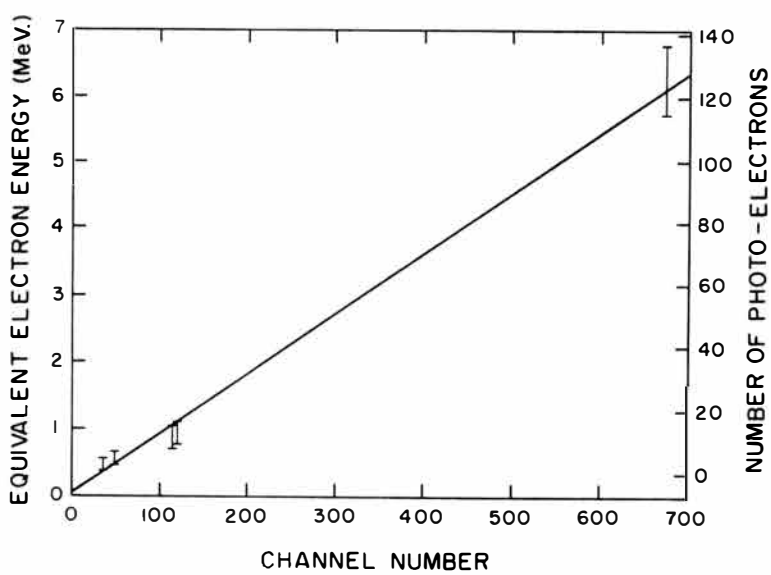

Figure 2. Calibration of the Online Neutron Monitor by compton scattered electrons from the gamma ray sources ^{22}Na and ^{137}Cs, and cosmic ray muons.

To estimate the light output and efficiency of the ONM, a prediction of the spectrum from neutrons of energies between one and ten MeV was made using a monte carlo simulation developed by Stanton[5].

The neutron is followed through the scintillator until it falls below a certain energy or it escapes from the detector, so that multiple scattering of the neutron within the scintillator can be included. Scattered protons are also monitored and if they escape from the scintillator a suitable light output is assigned. Only collisions between neutrons and protons that result in energy deposit in the scintillator within the integration time of the ADC (50 ns) after the first collision are included in the estimate. For neutrons in the energy range one to five MeV, n-p scattering dominates and neutron - Carbon (n-C) elastic scattering contributes little light because the highly ionizing, recoiling carbon nucleus quickly saturates the scintillator.

The results of the monte carlo simulation, coupled with the muon and Compton scattering calibration of the ONM demonstrate that the ONM is capable of detecting neutrons with energies of a few MeV. To confirm the calibration of the ONM, the detector was exposed to neutrons of known energy, using a technique developed by Filichenkov et al[6]. The Filichenkov method uses an alpha-beryllium neutron

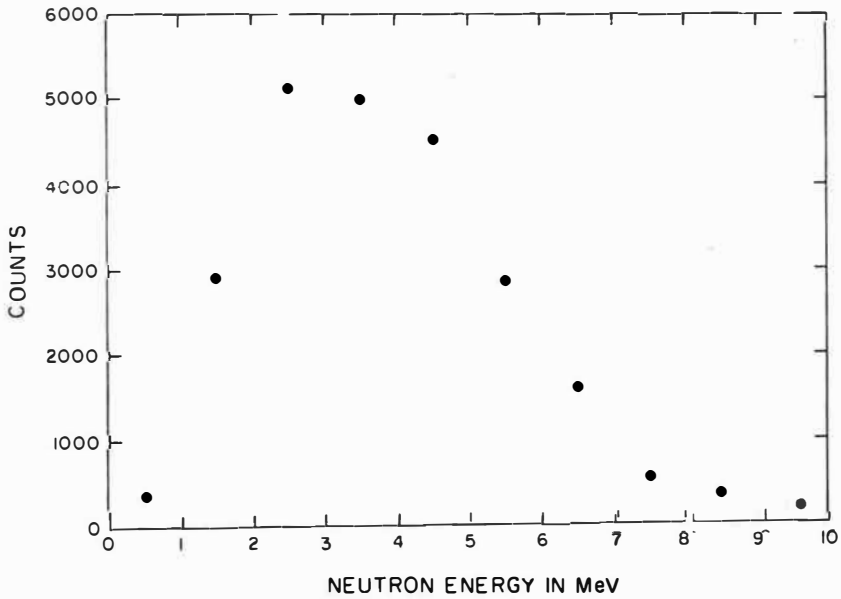

Figure 3. A neutron kinetic energy spectrum taken with the Online Neutron Monitor and a Am-Be neutron source. Energy axis values are determined by the neutron flight time.

source, in our case Am-Be. The neutrons are produced when an alpha particle and a ^{9}Be nucleus combine to make ^{13}C in an excited state, which quickly decays to ^{12}C by emitting a fast neutron. If the ^{12}C is created in its first excited state, that state decays immediately by emitting a 4.4 MeV gamma ray. The time interval between the detection of the 4.4 MeV gamma ray and the detection of an event in the ONM is measured by a time digitizer unit (TDC), yielding the energy of the neutron. A time-of-flight spectrum is shown in figure 3.

The goal of this exercise is to determine the energy calibration of one of the ONM energy spectra taken during one of the experimental runs. Figure 4 shows the energy spectrum detected during an implantation run where D was implanted into Pd[3]. Two features are prominent in the spectrum. The first, seen at the higher energy end of the spectrum, is the distribution due to the passage of cosmic ray muons and electrons. At somewhat lower energies, a broad peak is observed resulting from emissions due to the experiment. Clearly, the broad peak corresponds to neutron energies that are somewhat high if n-p elastic scattering is to explain its presence in the spectrum.This work is continuing.

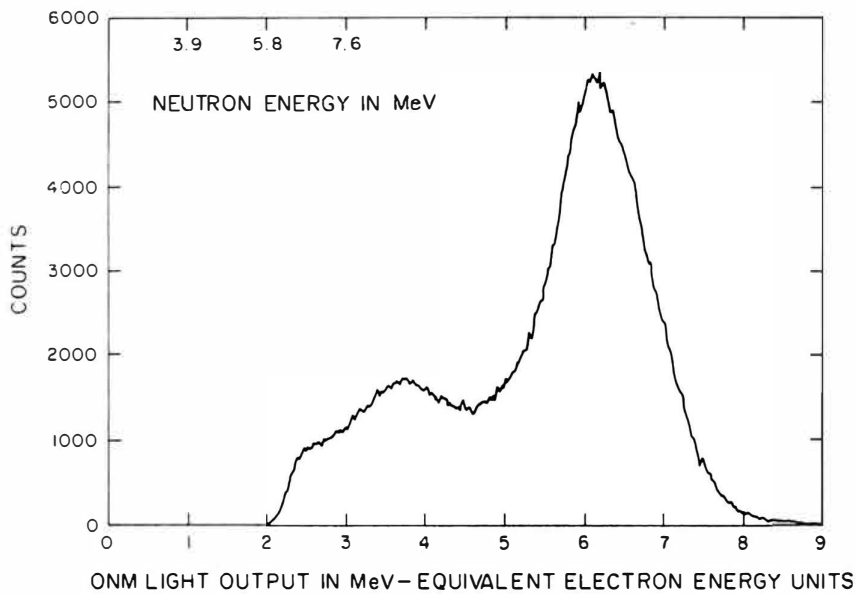

Figure 4. An energy spectrum of detected events taken during a D-Pd implantation run illustrating the cosmic ray and neutron like events. The horizontal axis is calibrated for equivalent electron and neutron energy values.

REFERENCES

1. M. Fleischmann and S. Pons, J. Electroanal. Chem. 261, 301 (1989).
2. S. E. Jones, E. P. Palmer, J. B. Czirr, D. L. Decker, G. L. Jensen, J. M. Thorne, S. F. Taylor, and J. Rafelski, Nature (London), 338, 737 (1989).
3. J. J. G. Durocher, D. M. Gallop, C. B. Kwok, M. S. Mathur, J. K. Mayer, J. S. C. McKee, A. Mirzai, G. R. Smith, Y. H. Yeo, K. S. Sharma, and G. Williams, "A Search for Evidence of Cold Fusion in the Direct Implantation of Palladium and Indium with Deuterium, Can. J. Phys. 67, 624 (1989).
4. J. B. Birks, Proc. Phys. Soc. A64, 874 (1951)
5. N. R. Stanton, Ohio State University Internal Report, COO-1545-92 (1971).
6. V. V. Filchenkov, A. D. Konin and A. I. Rudenko, Nucl. Instr. and Meth in Phys. Res., A294, 504 (1990).

«The Science of Cold Fusion»
T. Bressani, E. Del Giudice and G. Preparata (Eds.)
SIF, Bologna 1991

HIGH DEUTERIUM CONCENTRATION IN PALLADIUM FOR APPLICATION TO COLD FUSION

Han S. Uhm and W. M. Lee

Naval Surface Warfare Center
10903 New Hampshire Ave., White Oak
Silver Spring, Maryland 20903-5000, U. S. A.

Based on theoretical calculations, new schemes to increase deuterium density in palladium over its initial value is presented. High deuterium concentration in palladium is needed for application to the solid-state fusion. The first deuterium enrichment scheme makes use of the plasma ion implantation, which consists of a cylindrical palladium rod (target) preloaded with deuterium atoms, coated with diffusion-barrier material and immersed in a deuterium plasma. The second deuterium enrichment scheme makes use of the temperature gradient effects on the deuterium solubility in palladium. A heat source at temperature T_2 and a heat sink at temperature T_1 (where $T_2 > T_1$) are in contact with two different parts of a palladium sample, which has been presoaked with deuterium atoms and has been coated with diffusion-barrier material or securely locked in a metal case.

INTRODUCTION

When the atomic ratio γ of deuterium to palladium is considerably higher than unity, a substantial fraction of the palladium volume will be transformed into PdD_2 crystal, where the nearest-neighbor distance between deuterium atoms is d = 0.94 angstrom.[1] These deuterium atoms are located in a potential well created by the neighboring palladium atoms, executing oscillations with their fundamental oscillation amplitude λ = 0.1 angstrom. According to a recent calculation by Schwinger,[2] the D-D fusion cross section increases by a factor of 10^7 when the parameter d/λ changes from the natural value of d/λ = 9.4 to 7.52. Apparently, the fusion cross section depends

very sensitively on the vibration parameter d/λ of the oscillation. A slight decrease in the vibration parameter tremendously increases the fusion cross section, which is with a measurable range. In this regard, we propose two schemes to increase deuterium density inside a palladium rod by making use of plasma ion implantation[3,4] and temperature gradient effects.[4,5] Achieving a high concentration of deuterium atoms inside palladium is also an interesting subjects for basic electrochemical studies and for researches on hydrogen in metals.

PLASMA-ION IMPLANTATION SCHEME

Shown in Fig. 1 is a schematic presentation of a proposed experiment for deuterium enrichment inside palladium. A cylindrical palladium rod with radius a and coated with a diffusion-barrier material is immersed in a deuterium plasma which is contained by a grounded cylindrical chamber. The plasma with a density ranging from 10^9 cm^{-3} to 10^{12} cm^{-3} and with electron temperature ranging from 2 eV to 10 eV is generated by either RF or glow discharge or by thermionic filaments.[6] The palladium rod (target) is connected to a high-power modulator, which provides a series of 1 - 10 μs negative pulses with voltage V_0 ranging from 10 kV to 200 kV. The palladium rod may be initially soaked with deuterium atoms outside the chamber by a non-plasma method before coating with the diffusion-barrier material. The atomic ratio (γ = D/Pd) of deuterium to palladium in a deuterium soaked palladium rod can easily reach 0.6 without any pressurization.[7] During the application of negative pulses to the target, deuterium ions will penetrate the diffusion-barrier coating to be implanted inside the rod. A prolonged implantation of deuterium ions will increases the deuterium concentration inside the palladium over the initial atomic ratio γ = 0.6. The ion beam power deposited on the surface of the palladium rod is a tremendous heat source, which must be removed by a cooling system.

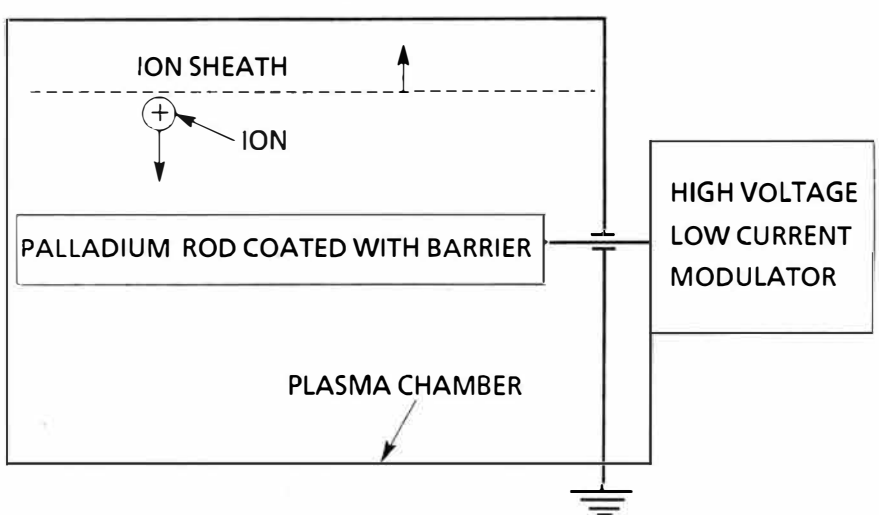

Fig. 1. Schematic presentation of the proposed plasma-ion implantation.

During this negative pulse, electrons are repelled from the target on the time scale of the electron plasma frequency, leaving behind an ion sheath. The ion sheath further expands in time as the negative-voltage pulse is sustained and the ions uncovered by the sheath bombard the target, penetrate through the diffusion-barrier coating and accumulate in palladium. The dynamics of the ion sheath has been studied extensively.[8] During the negative-voltage pulse, the ion sheath radius increases. The final radius R at the end of the negative-voltage pulse is determined in terms of the plasma density n_p, the pulse length τ and the applied voltage V_0. The ion current I_{peak} during the pulse is approximately expressed as

$$I_{peak} = \frac{\pi e n_p L}{\tau} R^2, \tag{1}$$

where L is the length of the palladium rod. The average ion current I is given by

$$I = I_{peak} \tau H, \tag{2}$$

where H represents the number of the negative-voltage pulses per second. It is shown that a good candidate for the barrier material is an alloy of 60 percent iron (Fe) and 40 percent nickel (Ni) in weight, whose diffusion constant and solubility are much less than those for palladium. There could be other materials which perform as a better diffusion barrier. A desirable thickness of the barrier coating should be less than 10^3 angstroms.

Prolonged implantation of deuterium ions will increase the deuterium concentration over the initial density $n_0 = 4 \times 10^{22} cm^{-3}$, which can be easily attainable even without pressurization. In a high-pressure environment of deuterium gas, the initial density can be higher than the above value. Increase of the deuterium density over its initial value is evaluated and is expressed in terms of diffusion coefficient and thickness of the barrier material. A deuterium density profile inside the palladium rod is also calculated, by making use of the rate equation and diffusion properties of deuterium atoms in palladium. Due to the small diffusion coefficient, the incoming ions do not diffuse quickly, thereby accumulating near the target surface. Assuming an applied voltage, $V_0 =$ 100 kV; plasma density, $n_p = 5 \times 10^9 cm^{-3}$, pulse duration, $\tau = 1$ μs, and pulse repetition rate, $H = 10^5 s^{-1}$, we found that the average ion current coming into the target is I = 0.4 ampere for a target size with radius a = 1 cm and length L = 10 cm. Assuming an iron-nickel alloy barrier with its thickness of 10^3 angstroms, the deuterium saturation density is calculated to be $\xi = 3 \times 10^{23} cm^{-3}$, which is five times higher than the palladium atomic number density. For a reasonable target size, the deuterium density in palladium can triple its original value within a few days of ion implantation time.

TEMPERATURE GRADIENT SCHEME

A heat source at temperature T_2 and a heat sink at temperature T_1 ($T_2 > T_1$) are in contact with two different parts of a palladium sample, which has been presoaked with deuterium atoms and coated with diffusion-barrier material, thereby creating a temperature gradient in the sample [Fig. 2]. Based on previous studies,[9] we assume that the solubility S(p,T) is an increasing function of the pressure p and a decreasing function of the temperature T, due to exothermicity associated with palladium-hydrogen bonding. That is, in general,

$$\frac{\partial}{\partial p} S(p,T) > 0, \qquad \frac{\partial}{\partial T} S(p,T) < 0. \tag{3}$$

Thus the deuterium atoms in the hot region are forced to migrate into the cold region due to the solubility difference between the regions. This migration results in a highly concentrated deuterium density in the cold region.

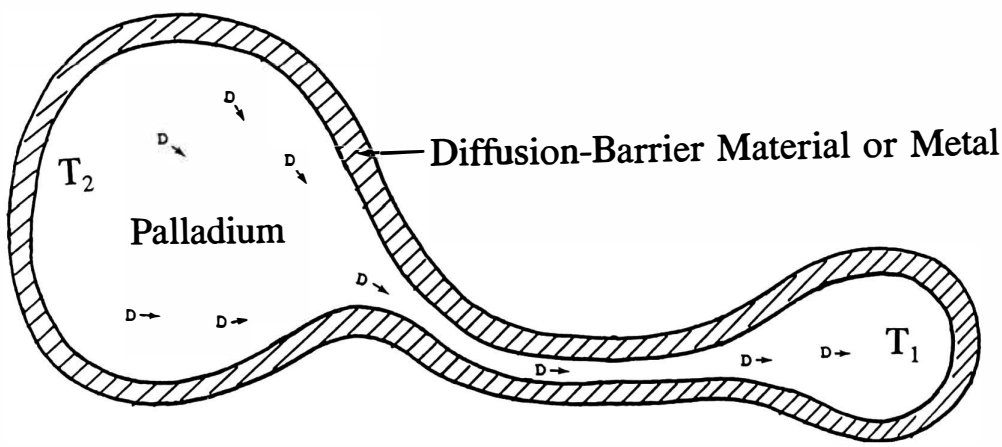

Fig. 2. Deuterium migration from a hot to cold region in palladium sample.

Since the total number of deuterium atoms in the rod is fixed during the migration, the local solubility S(n,T) must be a direct manifestation of the local deuterium density. The local solubility of deuterium in this situation is not yet fully understood. The detailed properties of the local solubility S(n,T) of deuterium, including the irreversible thermodynamic process, are currently under investigation by authors and will be presented elsewhere. The deuterium density in the steady-state condition is therefore expressed as

$$n(T) = \frac{S(n,T)}{S_0} n_0, \tag{4}$$

which must satisfy the conservation of the deuterium-atom number; i.e.,

$$[\frac{\partial}{\partial u} n(x,t)]_A = 0, \tag{5}$$

where $(\partial/\partial u)n$ represents the derivation of the density with respect to the direction perpendicular to surface A of the palladium rod. Note that the solubility S_0 and the density n_0 denote their values before the temperature gradient is established. Once the temperature gradient is established, the deuterium atoms start to migrate from the hot region to the cold region, and the density profile will eventually settle into the steady-state value. It was found that the deuterium density in the steady-state condition is described in terms of the ratio S_2/S_1 of the solubility in the hot region to that of the cold region. The deuterium density concentrated in the cold region can be a few times more than its initial value for a reasonably small value of the ratio S_2/S_1. This scheme is particularly advantageous over other methods for compressing deuterium density in a small region because of a wide range of temperature windows, that can be applied to the palladium sample.

Acknowledgement: This work was supported by the Independent Research Fund at the Naval Surface Warfare Center.

REFERENCES

1. Z. Sun and D. Tomanek, Phys. Rev. Lett. **63**, 59 (1989).
2. J. Schwinger, Z. Phys. D **15**, 221 (1990); J. Schwinger, **Proceedings of the First Annual Conference on Cold Fusion**, Salt Lake City, Utah, March 28 - 31, (1990) p. 130.
3. H. S. Uhm and W. M. Lee, **High Deuterium Concentration in Palladium from Plasma Ion Implantation**, Phys. Fluids, in press (1991).
4. H. S. Uhm and W. M. Lee, **High Concentration of Deuterium in Palladium**, submitted to an open journal publication (1991).
5. H. S. Uhm and W. M. Lee, **High Concentration of Deuterium in Palladium by Temperature Gradient Effects**, submitted to an open journal publication (1991).
6. H. S. Uhm, J. D. Miller, R. F. Schneider and D. J. Weidman, IEEE Transactions on Plasma Science **19**, 535 (1991).
7. F. A. Lewis, **The Palladium-Hydrogen System**, Academic Press, (London, 1967).
8. H. S. Uhm and W. M. Lee, J. Appl. Phys. **69**, 8056 (1991) and the references therein.
9. D. P. Smith, **Hydrogen in Metals**, The University of Chicago Press (Chicago, Ill. 1948), P 88.

INVITED PAPERS

Conference Proceedings Vol. 33
«The Science of Cold Fusion»
T. Bressani, E. Del Giudice and G. Preparata (Eds.)
SIF, Bologna 1991

COLD FUSION RESEARCHES IN JAPAN

Hideo Ikegami
National Institute for Fusion Science, Nagoya 464-01, Japan

ABSTRACT

Positive results as well as some negative results from cold fusion research in Japan are reviewed with some comments. Out of 11 research groups taken up in the present review, three groups are mainly working on excess heat calorimetry, and the rest of the eight groups are involved in the detection of nuclear fusion products.

INTRODUCTORY REVIEW

There are more than 100 scientists at present working on cold fusion in Japan, spanning more than 40 universities and institutions. They are organized into about 20 research groups which collaborate to carry out the experiments. Only three groups -- Yokohama National University, Tokyo University of Agriculture and Technology, and IMRA Japan, are working exclusively on excess heat, while the others mostly study fusion products (neutrons and charged particles such as tritium, proton, and helium-3).

A sort of steady-state, excess enthalpy output at 20 percent of the input power was observed only by IMRA Japan in a closed system, but the other two groups could not produce any definitive excess heat results in their closed cells. Large heat bursts of the kind observed by Fleischmann and Pons have never been observed, nor reported in Japan.

Successful neutron detection cases have, however, been quite abundant, although the events are not yet controllable. In order to clearly observe the neutron events in a multi-channnel analyzer in the scaler mode, the dwell time must be properly chosen/adjusted in relation to the efficiency of the neutron detector. Since the neutron emission in cold fusion is still a rare event under the present uncontrollable experimental situation,

if the dwell time is toolong, the neutron count rate will be observed to deviate only slightly from the background level. On the other hand, for a too short dwell time, what we would observe is rather frequent one-neutron, or two-neutron, events, unless under a condition of considerably, suppressed neutron background. However, if the dwell time is properly chosen, neutron signals can often be observed as "bursts", as shown by the Tokyo Institute of Technology group and also by the National Institute for Fusion Science.

Neutron energy spectra with a peak at 2.45 MeV are obtained with NE213 by three groups; Osaka University, Hokkaido University, and Tokyo Institute of Technology, which is a clear indication of the d-d fusion reaction.

As to the d-d fusion products other than neutrons, tritons are detected by three groups; Hokkaido University and Osaka University group, both of which claim an anomalous production rate (t/n) of 10^4-10^5, and NTT Basic Research Laboratories, which detects 1 MeV tritons, as well as concomitant 3 MeVprotons. Those protons are also detected by the Osaka City College group. Another group at Osaka University even claims its careful detection of helium-3, but no helium-4 has been detected.

These experimental results of verified d-d fusion products at their expected energies have now established the conclusion that cold fusion definitely exists, and that its fusion products are somewhat like those of the ordinary d-d fusion reactions, whatever the fusion mechanism may be. It must also be noted, however, that the amount of those fusion products are by orders of magnitude far too small to account for any detectable excess heat, or enthalpy.

Obviously the most important, key issue of cold fusion (the d-d fusion reaction and the excess enthalpy generation in/on deuterated metals) involves the base material itself, and the electrolysis, for example, would be no more than a means of charging deuterons onto the metal. In order to make it easier for researchers toexperiments and evaluate their results, in Japan, palladium rods and plates are supplied free of charge to those cold fusion groups by Tanaka Precious Metals Co. (Tanaka Kikinzoku Kogyo) according to the user's individual specifications. Most of the palladium and its alloy materials are strongly cold worked through various processes.

Some other works, which will not be presented in the present review are fracto-fusion experiments, carried out by crashing deuterated materials,

which has been done at both Chuo University and Kyoto University. Neither eventually could show any positive results to account for the cold fusion phenomena.

EXCESS HEAT CALORIMETRY

1. Yokohama National University (K. Ohta, et al)

Calorimetric studies with powerstat electrolysis detected no steady state, excess heat. Sometimes small bursts of excess heat were detected during the electrolysis of heavy water, but they were at the marginal error.

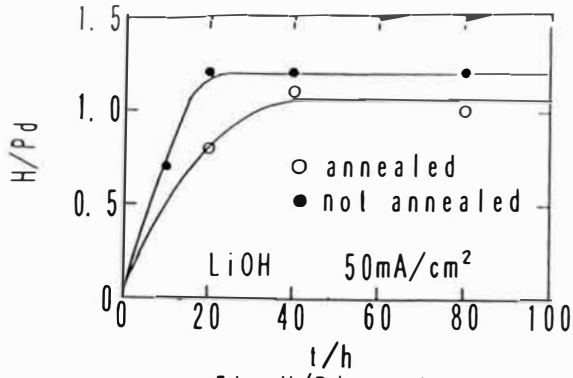

Fig. H/Pd ratio

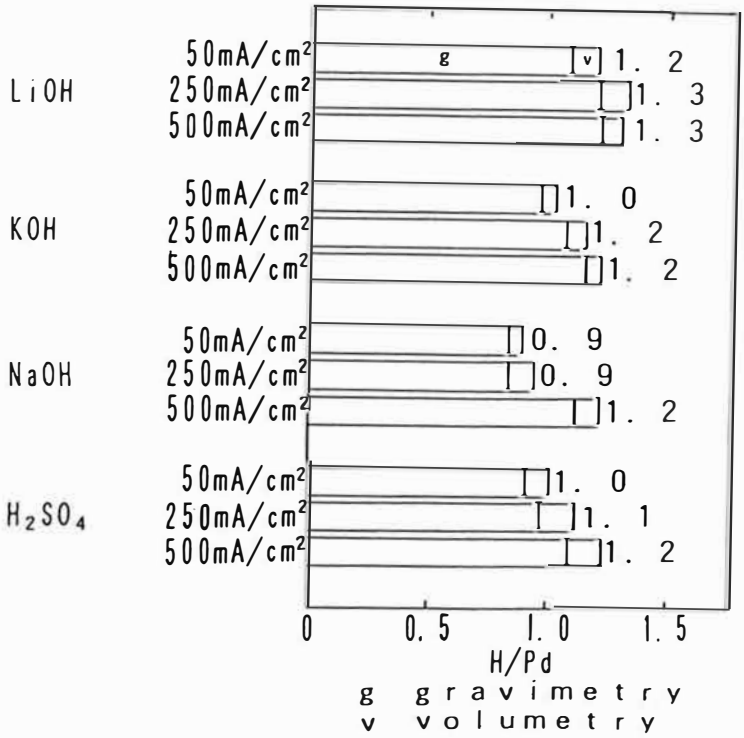

Fig. Total amount of hydrogen absorbed by Pd

Extensive studies are being made of the ratios of hydrogens to palladium atoms absorbed into a thin palladium plate (0.1x10x10 mm) It is shown in the figures above that without any special treatment, H/Pd = 1 can be attained irrespective of not only the electrolyte, but also of the current density, if it isabove 50mA/cm^2

2. Tokyo University of Agriculture and Technology (N. Oyama, et al)

An open cell system with constant current electrolysis is observed to generate excess heat up to 40 % of the input power, associated with neither neutrons, nor tritium detectable.

3. IMRA Japan (K. Kunimatsu, et al)

1. Electrolysis of 2.8 M -D_2SO_4 with a pair of rod palladium cathode (5o x 30 mm) and gas permeation anode can achieve D/Pd = 0.9 or above.

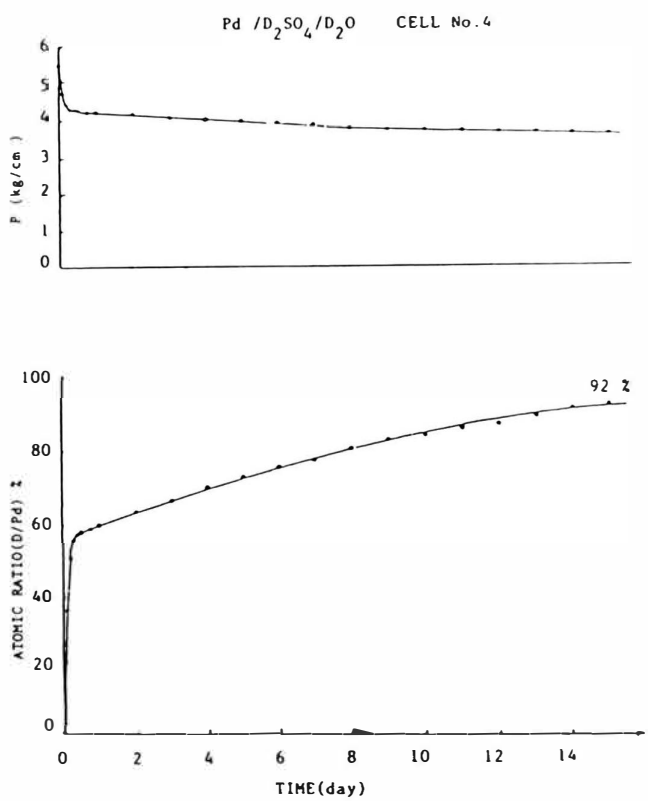

2. Steady excess heat of 5-20 % is observed to generate in a closed system above a certain current density.

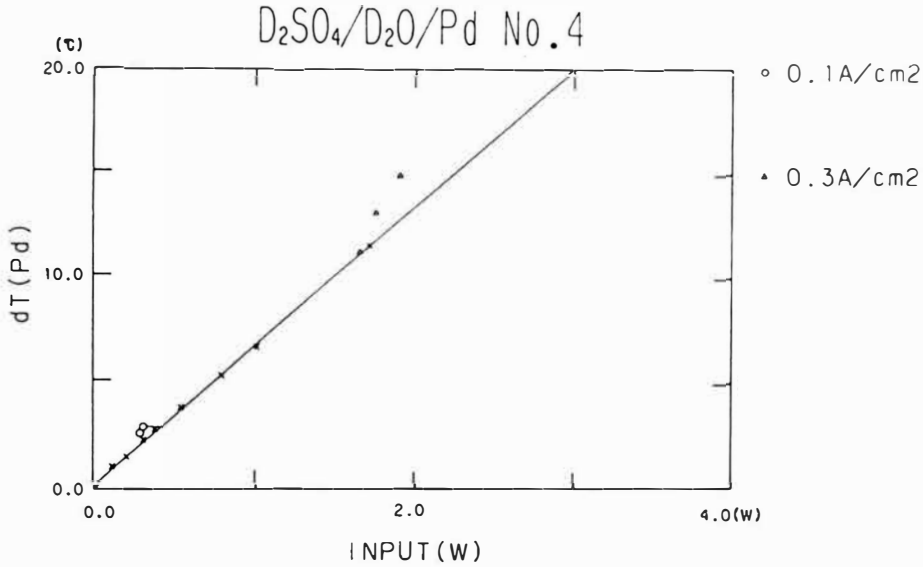

DETECTION OF FUSION PRODUCTS

4. Institute of Nuclear Study, University of Tokyo (T. Shibata, et al)

With a high sensitivity, low background, neutron detection system in the underground, no enhancement of neutron, nor tritium generation was observed. In the experiments, D/Pd ranges from 0.7 to 0.9, which is also significant.

Neutron counts per 10 min. tend to show a deviation from the Poisson distribution on the higher count rate side, which may indicate a very low rate of neutron bursts observable only if the dwell time is chosen properly in the MCS setting. It may be instructive to note that the cosmic ray induced neutrons, which determine the background level, are stronglyl influenced by the mass number of the surrounding construction elements as shown in the figure.

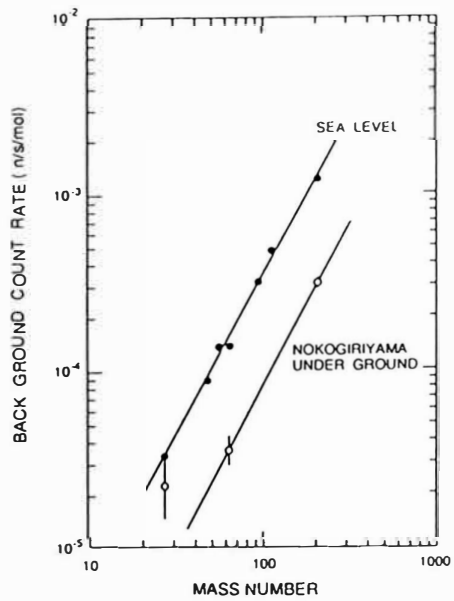

5. Tokyo Institute of Technology (M. Okamoto, et al)

Neutron bursts exceeding 3 are simutaneously detected by three counter channels each time approximately 5-6 hours after starting the electrolysis.

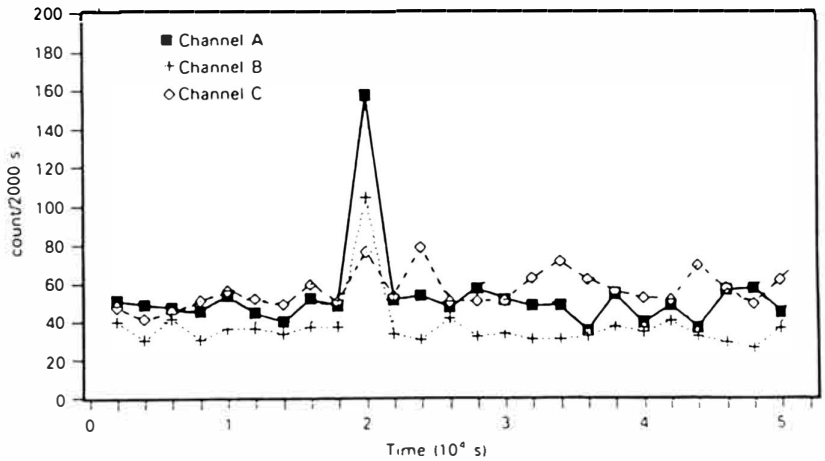

Fig. Neutron counts of each channel in run 2

6. Osaka University (G. Adati, et al)

Generation of helium-3 was observed in the process of deuterium absorption and desorption by La-Ni ingot. The detection reliability was ensured by comparing the ratio of helium-3 to helium-4 with blank cases rather than by measuring the absolute value of helium-3 generated. It is, however, hard to conclude that the detected helium-3 is due to d-d fusion activities as expected, since other possible fusion products are not studied.

Table Contents and isotopic ratios of He, Ne, Ar, Kr and Xe.

Sample	^3He ($\times10^8$)	^4He ($\times10^{14}$)	$^3He/^4He$ ($\times10^{-6}$)	^{20}Ne ($\times10^{14}$)	^{36}Ar ($\times10^{14}$)	^{84}Kr ($\times10^{12}$)
A	1.57(0.08)	1.45(0.07)	1.08(0.02)	2.38(0.12)	111(5)	15.1(0.7)
B	0.422(0.025)	0.561(0.027)	0.752(0.026)	0.336(0.017)	0.499(0.023)	0.479(0.023)
C	10.8(0.5)	7.08(0.34)	1.52(0.02)	10.7(0.5)	15.3(0.8)	7.21(0.34)
Air			1.399(0.013)[13]			

The noble gas contents are given in number of atoms existing in the reaction vessel.
Sample A was extracted from the $LaNi_5$ ingot by heating at 1123K.
Sample B was obtained from the applied D_2 gas.
Sample C was obtained from the D_2 gas absorbed in $LaNi_5$.
The measurement was performed twice for sample C.

7. National Institute for Fusion Science (H. Ikegami, et al)

Multiple neutron bursts displayed in MCS mode are shown in the figure. The signals are from two independent, helium-3 neutron counter systems (A and B), whose efficiency is 1 % and 0.5 %, respectively, with the dwell time setting of 100 seconds. Every large burst from the two independent system, accumulated in 100 seconds, shows remarkable time coincidence as shown in the figure, and its constituent pulse heights are checked to fall within a specified range of the helium-3 neutron detector. This observation eliminates any possibility of errorneous signals other than neutrons.

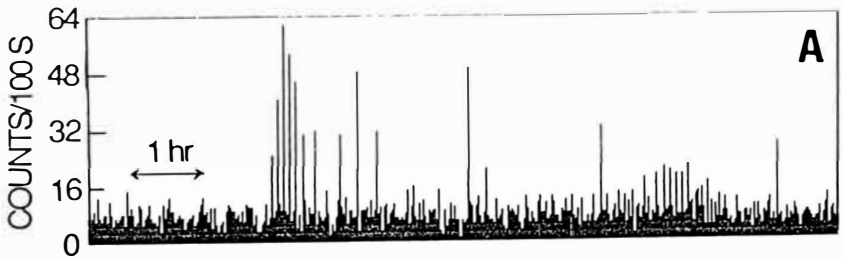

Fig. (a) Neutron Bursts of Exp.-I Measured with Sys.A(6-8 Spt. 1990).

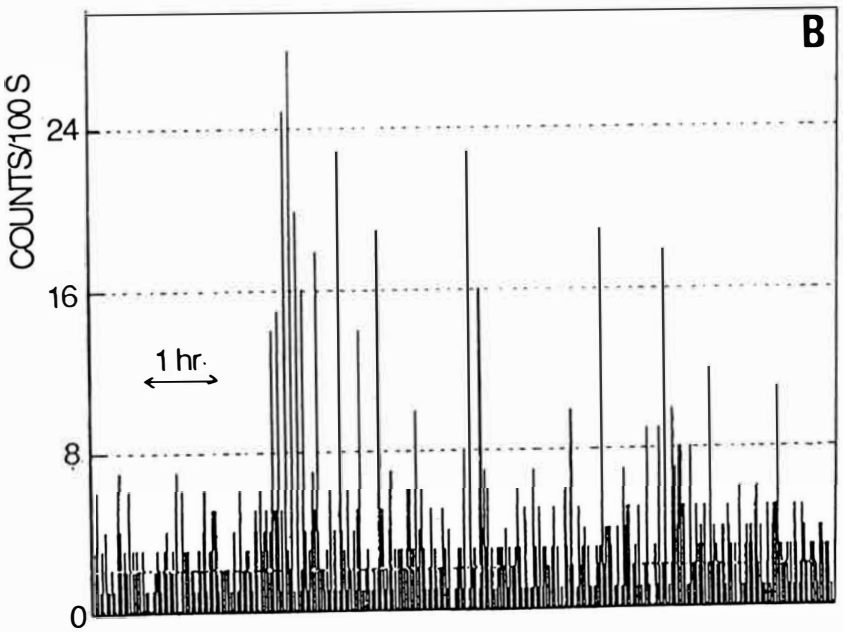

Fig. (b) Neutron Bursts of Exp.-I Measured with Sys.B(6-8 Spt. 1990).

When the bursts are seen with the dwell time, or accumulation time, of one second interval, each burst is observed to consist of frequent one-, or two-neutron events, so that those signals are due to random neutron emission rather than one big burst of neutrons in microseconds. On the other hand, if the dwell time is as long as several hours or so, it would be also difficult to see this sort of neutron emission clearly.

8. Hokkaido University (T. Mizuno, et al)

With the electrolysis of 0.5M LiOD with a large, palladium rod cathode (10ox100 mm), so-called typical cold fusion phenomena were observed and the experimental results/observation may be summarized as follows.

1) Neutron energy spectrum with 2.45 MeV peak was obtained.
2) Tritum anomaly such as t/n greater than 10^4 was observed.
3) Excess enthalpy detected was as much as 0.1 MJ/cm^3-Pd.

Density profiles of hydrogen and deuterium during zirconium cathodic discharging with 0.5M Na_2SO_4 were measured as shown in the figure below, which shows behavior of pre-absorbed hydrogens within the material.

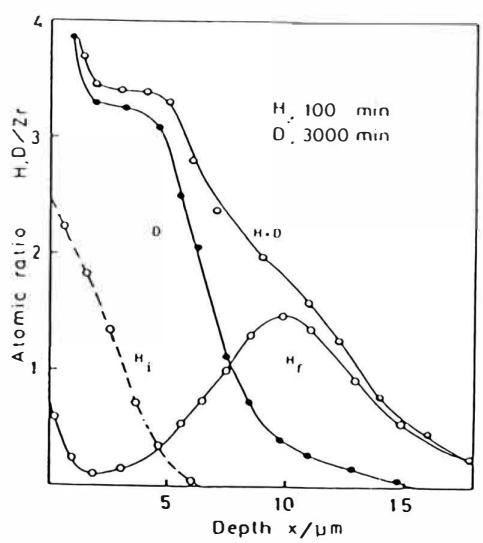

Fig. Change of a thin hydride layer profile after discharged in D_2O solution

9. Tokyo Institute of Technology (H. Numata, et al)

Neuton energy spectrum before unfolding was compared with that for the 2.45 MeV mono-energy neutrons (solid curve in the figure below). Clear indication of d-d fusion neutrons associated with the cold fusion is shown in the figure below.

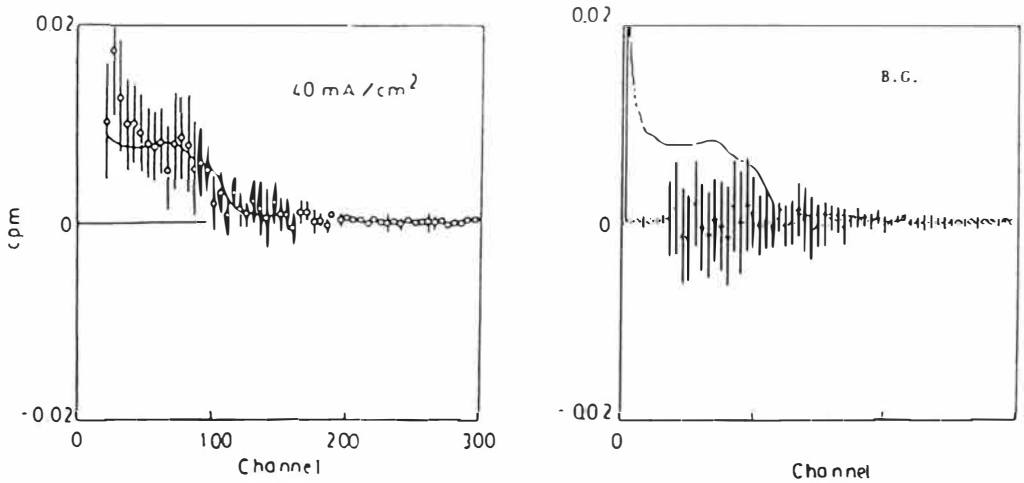

10. Osaka University (A. Takahashi, et al)

With the electrolysis of 0.3M LiOD with a large, palladium rod cathode (20ox30 mm), the cold fusion results/observation may be summarized as;

1) Neutron energy spectra with two components (2.45MeV and 3-7MeV),
2) Tritium anomaly, t/n = 10^5.

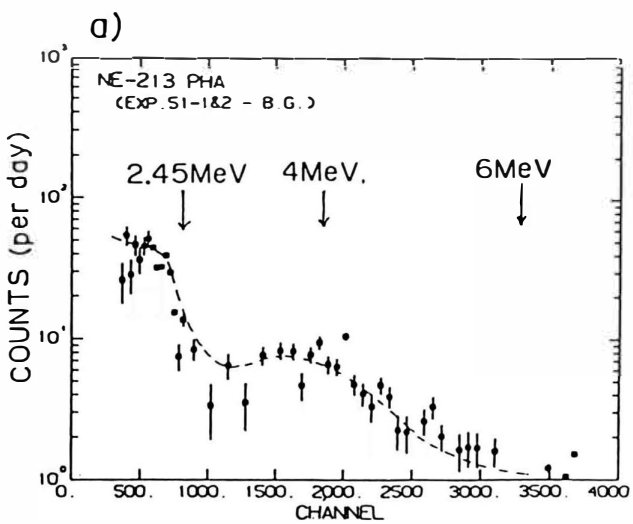

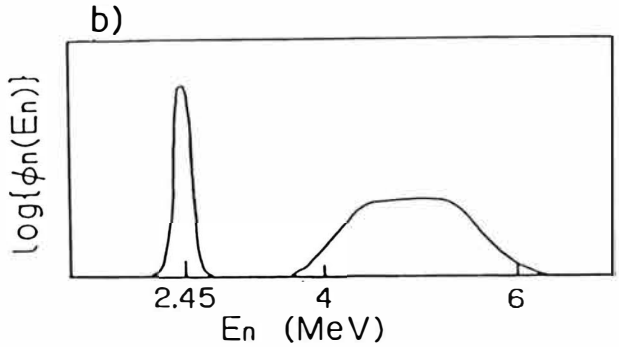

Fig. Fast neutron spectra obtained in Exp.51;
(a) pulse height spectrum of recoil protons for excess neutron counts
(b) approximate neutron spectrum which is obtained by differentiating smoothed curve (broken line in (a)) of pulse height spectrum.

11. NTT Basic Research Laboratories (E. Yamaguchi and T. Nishioka)

These are gas phase experiments with Oxides/Pd:D/Au thin, square plates (30 x 30 x 1 mm). After loading deuterim in the palladium plate, the cold fusion is triggered by a sudden creation of a vacuum in the chamber and by applying electrostatic potential of 2 volts or so across the plate surface, between the oxide layer (positive) and the gold plating (negative). The schematic diagram is as shown below, where TC refers thermocouple for temperature measurement and SSD means solid state detector for charged particle detection.

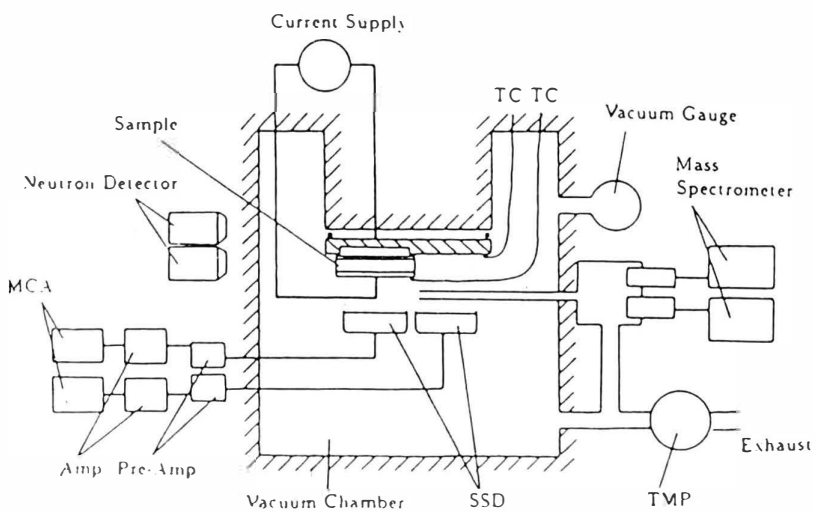

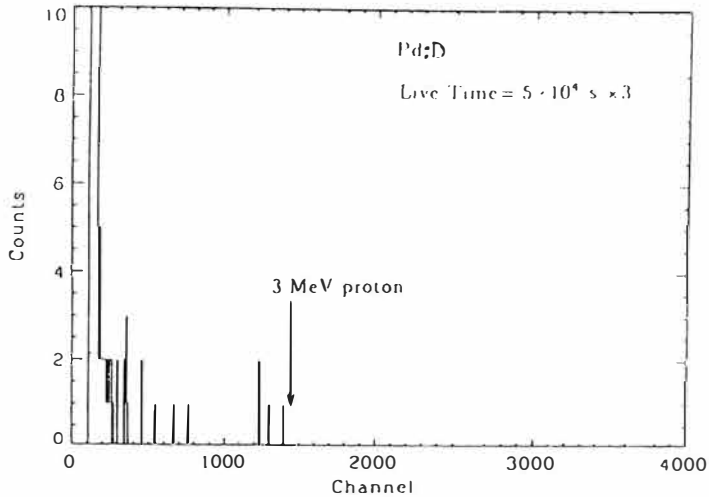

(Background)

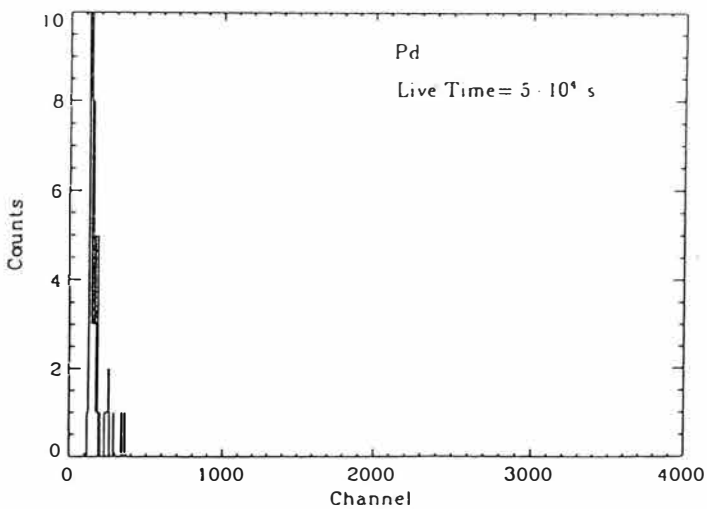

The major experimental results may be summarized as follows:

1) With deuteron implanted palladium plates, large neutron bursts (10^6n) are detected in association with a high heat flux (800℃).
2) By applying the voltage, medium heat flux (100-200℃) is observed to generate, however, it is irrespective of the use of hydrogen, or deuterium.
3) Concomitant with the events above, charged particles from d-d fusion, say 3 MeV protons and 1 MeV tritons, are detected, which is shown in the above figure.

Conference Proceedings Vol. 33
«The Science of Cold Fusion»
T. Bressani, E. Del Giudice and G. Preparata (Eds.)
SIF, Bologna 1991

CHINESE EFFORT IN UNDERSTANDING THE "COLD FUSION" PHENOMENA

Li, Xing Zhong

Tsinghua University, Beijing 100084, CHINA

ABSTRACT

Review on cold fusion research in China in the past two years is presented with the emphasis on the experiments after the first national symposium on cold fusion (May 10, 1990. Beijing). There were three phases: hot, quiet, and deep–going phases. Hot phase is characterized by failures in experiments in repetition and is restrained in thinking by the conventional ideas. Quiet phase started with different approaches and newly–designed experiments. Deep–going phase encourages the scientist to be respectful to the facts and creative in mind. Three anomalies in deuterium / solid system may exist.

INTRODUCTION

Under the auspices of the Natural Science Foundation of China and the Science and Technology Commission of China, cold fusion research persists in China. During the past two years, more than 28 research groups were working on this fascinating topics. Several hundred man power and about one million fund were engaged in this controversial research. Having experienced the hot, quiet, and deep–going phases, we are at the point to review the past and foresee the future.

HOT PHASE

March 1989 was an unforgettable month in the history of science. The aficionados of cold fusion set up quickly the equipments (whatever they had at that time) and strived to reproduce the "excess heat" [1] or "anomalous neutron emission". [2] So many research groups in China were involved that a complete list of them is almost impossible. Because of the difficulties in reproducing those sporadic phenomena, only a few groups published their results in the newspaper [3] and most groups stopped soon after the primary tests. Since the conventional fusion theory tells that if the "excess heat" was so large, the experimentalist should have been killed by neutron radiation already, people would rather believe the neutron emission than the "excess heat". Even the emission of neutron was attributed to anomaly or spurious signals, because none of existing fusion theory could explain the amount of neutron emission and its sporadic nature. Restrained by the conventional theory, people did miss some opportunities to have a new discovery. For example, the scientists at Southwestern Institute of Nuclear Physics and Chemistry discovered the anomalous neutron emission in the discharge tube early in April 19, 1989. [4] They did not realize that it was a new approach different from Utah's electrolysis approach or Frascati's gas–loading approach. They recorded 13250 neutron signals in 45 minutes. The energy of neutron is about 2.2 MeV. When the current of discharge increased, this signal increased also. When the current of discharge switched off, this signal decayed gradually to the back ground level. When palladium electrode was replaced by copper, or zirconium, this neutron signal disappeared. The voltage of D.C. discharge is only 4 kV, it is impossible to explain this neutron emission by beam–target interaction. Particularly, they saw a strange bluish glow around the tip of palladium cathode. It is unusual also, since the discharge glow in deuterium gas should be rose–like red. Maybe a trace of Helium made its unannounced debut in the bluish glow. Half a year later, Japanese scientists observed the anomalous neutron emission in an A.C. discharge tube also. [5] Now, more scientists in the US, USSR, Japan, India, China etc. are using various discharge technique to observe the anomalous nuclear effects. It seems that the discharge tube experiment has the highest probability in repetition, it gives the highest yield of neutron emission along with the

possible tritium production. Likely, it gives the signal of helium as well.

Another example was the neutron emission in an ion implantation experiment. [6] May–June, 1989, the fusion scientists at the Southwestern Institute of Physics observed the neutron emission from a titanium target immerged in the plasma of a mirror machine (an experimental device for thermonuclear fusion research). Neutron emission was observed more than four times from a negatively biased titanium target (−8kV to −11KV). The burst feature and the independence of bias voltage excluded the beam–target model for this neutron emission. Two counters, which were located at different distances from the titanium target, monitored the neutron emission and recorded the signals simultaneously. The counts in the closer counter is higher than that in the farther counter. Both of above–mentioned groups like most of other groups in China stopped their experiments unfortunately due to various reasons. The quiet period came soon after the Santa Fe workshop in Summer, 1989.

QUIET PHASE

'The heart would not stop beating until it reaches "Yellow River "'. This is an idiom in long history to describe the Chinese characteristics. While the unreproducibility of cold fusion phenomena became a prevailing trend in the world, and the hot phase turned into quiet phase; we asked ourselves a question: if the cold fusion phenomenon is true, what can we do to verify it. We thought of the detection of energetic charged particles in stead of the measurement of the "excess heat" or "neutron emission". The energetic charged particles are the necessary products of any nuclear reaction, since two charged nuclei must produce at least one charged particle after their reaction. On the other hand the neutron is not a necessary product of a nuclear reaction. However there was a good reason for selecting the neutron as an object of measurement, because it is easy for neutron to penetrate the electrolyte and the vessel. Besides, the chemical method, which was supposed to be used for tritium detection, is not as sensitive as nuclear method for neutron detection. It was a reasonable choice to detect the neutron for nuclear effects, although it requires a set of sophisticated instruments and advanced technology. However, based on the Frascati invention of gas–loading experiment, Tsinghua University team proposed to use CR–39 (plastic track detector) to detect the energetic charged

particles. CR–39 has high sensitivity and low background. CR–39 needs not any high voltage power supply; therefore, it has low electronic noise and is particularly suitable for Frascati type experiments in the high pressure vessel. CR–39 has no dead time and has high efficiency; hence, it is good for the measurement of bursts. By fortune, it turned out that the yield of tritium was much higher than that of neutron. Consequently, we had better chance in detection of any anomalous nuclear effects. [7] Fig.1 is a typical photo of the CR–39 detector exposed in a Frascati type experiment using the palladium foil imported from Russia in 1950's. In addition, we proposed the idea of "precursor of the cold fusion". [8] We believe that before the emission of nuclear products there must be some electromagnetic radiations due to the transition of the electrons from states to states. If we could find the correlation between these precursor (electromagnetic radiations) and the nuclear products, we might enhance the reliability of the measurement and improve the reproducibility. Thermoluminescence detector was proposed to detect those electromagnetic radiations. We did observe some positive results of this precursor.

In the same time, international collaboration was developed between Los Alamos Lab. in US and the Institute of Atomic Energy in China. Frascati type experiment was reproduced in China using US instruments and samples. The technique for treatment of sample was studied there also.

Professor Guo at Chengdu University of Science and Technology proposed a model for cold fusion phenomena and suggested to measure the "excess heat" and helium–4. Thermal couples, which were buried in the titanium or palladium electrode, were used to monitor the "excess heat". A series of anomalous jumps in the readings of thermal couple were recorded.

DEEP–GOING PHASE

The conferences in 1990 (I Annual Conference on Cold Fusion at Salt Lake City in March, The National Symposium on Cold Fusion at Beijing in May, The International Progress View on the Anomalous Nuclear Effect in Deuterium / Solid System at Provo in October) promoted the research forward continuously. After the DOE blue cover report [9] , more and more reproducible experimental results were published. Particularly, the detections of random neutron emission and the neutron bursts from the gas–loading

(Frascati type) titanium samples are getting better and better. In the coal mine, 600 m. deep underground, the team of Institute of Atomic Energy still detected the random neutron emission and neutron bursts using the same He–3 detectors as that at Los Alamos Lab. Having improved the treatment of Ti samples, they have obtained even higher repetition rate and higher intensity of burst. This eliminates the suspicion of cosmic–ray–induced bursts. In addition, they further studied the cooling effect on the helium–3 proportional counter. They found that cooling by liquid nitrogen might have caused some spurious signals like the neutron bursts,but it only happened under the condition that the cooling effect should have been so strong that it had been far beyond the range of interest. In positive side, they forged the Ti sample and obtained much higher burst intensity with even higher repetition rate; they measured the time–behavior of the neutrons in each burst in order to compare with the calculation using Fermi age theory of neutron diffusion in a slowing–down medium.

The team at Beijing Normal University, who first obtained a neutron spectrum from electrolytic cell early in 1989, continued their study in various methods (electrolyzing, gas–loading, A.C. gas discharging etc.). They have used CR–39 for detection of charged particles also. CR–39 plastic track detector becomes a very popular tool now in China. It is not only used by the above–mentioned team, but also by other teams at the University of Science and Technology of China, at the Beijing Institute of Physics, etc. The latter two teams used CR–39 in gas–discharge tube experiments. The team of the University of Science and Technology of China found reproducible emission of energetic charged particles near the palladium cathode rod. The team of the Beijing Institute of physics found the correlation between the bluish light and the anomalous nuclear radiation in the discharge tube.

Tsinghua University team is heading towards two goals: (1) using energetic charged particles as an object to study the anomalous nuclear effects; (2) using precursor to improve the reliability and reproducibility. Some progresses have been made in identifying the tracks of energetic charged particles in CR–39. Using standard alpha particle sources (Cf–252 and Am–241), we carefully calibrated the CR–39 in collaboration with the scientists at Institute of High Energy Physics. [10] The primary results indicate that the energy of the charged particles may be higher than 5 MeV, and the number of charge may be higher than or equal to 2. An international collaboration between the Tsinghua Uni-

versity team and the scientists from the National Cold Fusion Institute at Salt Lake City is being arranged for joint research on the identification of these tracks.

A new setup has been developed at the Institute of Nuclear Energy and Technology at Tsinghua University to search for precursor in real time. [11] A special gold–silicon surface barrier detector is used in gas–loading experiments (Frascati type) to detect both the electromagnetic radiations and charged particles. As expected, the low energy radiations appear as a burst in company with the emission of energetic charged particles. Surprisingly enough, the energy of these charged particles are mostly higher than 5MeV as well. The number of these charged particles are close to the number of tracks in CR–39 (several hundreds per cm^2 per day). There are two points revealed by this setup of experiment: (1) The energy of the charged particles becomes lower and distributes wider, when the temperature cycle runs once and once again. It implies that those charged particles may be emitted in the layer deeper and deeper under the palladium surface; (2) Twenty days after the experiment, the palladium foil keeps emitting the energetic charged particles even in the air. It might imply that the palladium be activated after the gas–loading experiment.

Tsinghua University team has used the CR–39 technique to scrutinize a variety of materials for cold fusion research [12]. Different materials such as palladium from USA, Russia, and from different sources in China; pure titanium (in porous state), titanium alloys (e.g. V6–Al6–Sn2 etc.); zirconium; nickel; lanthanum; and hydrogen–storage materials (e.g. $LaNi_5$) are tested using CR–39. Primary results show that: Among the various palladium foils Russian palladium foil imported in 1950's gives the highest yield of charged particles (greater than $10^3 / cm^2 \cdot$ day). The titanium alloy (Ti–662) is not as good as Russian palladium (about several hundred tracks per cm^2 per day), but it still has high repetition rate. The other materials give no evident signal distinct from background, which is less than 10 tracks per cm^2 per day. The yield becomes less and less after the first usage in the gas–loading experiment.

CONCLUDING REMARK

The detection of energetic charged particles has been proved to be a good approach in searching the anomalous nuclear effects. As long as we can identify

the existence of energetic charged particles, there will be no doubt about the nuclear effects. The experiments abroad [13] and inland have shown that certain deuterium / solid system does emit the energetic charged particles. This is the first anomaly—nuclear reaction at room temperature.

All these positive experiments showed that the energy of these charged particles may be greater than 5MeV, and some of their charge number is definitely greater than 1. This is the second anomaly—branch ratio is different from that of conventional D–D reaction.

It seems that the charge number of these charged particle might be greater than 2. This would radically change the whole picture of the reaction, since D–D reaction could not produce any charged particle with charge number greater than 2. This would be the third anomaly—palladium or titanium might be no longer a bystander but a participant of the reaction. In fact the experiment at Naval Research Lab. has indicated the anomalous enrichment of ^{106}Pd during electrolysis [14] is another evidence of this third anomaly.

If the above–mentioned three anomalies are true; then one may ask how the coulomb barrier of Pd is penetrated? It is reasonable to think of the neutral unknown particles. Professor Yang of the Hunan Normal University proposed the bi–neutron as a candidate for this unknown neutral particle. In fact other foreign scientists had made similar suggestions also early in 1990 [15] . I would like to draw the attention to a Chinese experiment, which indicated the existence of bineutron state. [16]

After two year struggle, now it is the time to be respectful to the new facts and to renew our mind. A window has been opened towards the back yard of the physics. A rose is there, although it is thorny.

ACKNOWLEDGEMENTS

Many thanks to my Chinese colleagues at different institutions for their advanced information. The work is supported by the Natural Science Foundation of China and the contingent research fund from the National Education Commission and Tsinghua University.

REFERENCES

〔1〕 M. Fleischmann, S. Pons and M. Hawkins, J. Electroanal. Chem. 261 (1989) 301.

〔2〕 S. E. Jones, et al. Nature 338 (1989) 737.

〔3〕 CHINA DAILY. April 24, 1989, P. 1.

〔4〕 R. H. Xiong, et al. "Experimental Studies on Cold Fusion Using Ionized Deuterium Gas ", Proceedings of National Symposium on Cold Fusion (May 10, 1990. Beijing)

〔5〕 N. Wada and K. Nishizawa, Japanese Journal of Applied Physics. 28 (1989), 2017.

〔6〕 S. Y. Duang, et al. " Cold Fusion Phenomena in a Mirror Confined Plasma", Proceedings of National Symposium on Cold Fusion (May 10, 1990, Beijing).

〔7〕 Tsinghua University team, " Search for Precursor of the Cold Fusion Phenomena", Ibid.

〔8〕 X. Z. Li, et al. " Precursor of the Cold Fusion Phenomena in Deuterium / Solid System" , Proceedings of the Progress View of the Anomalous Nuclear Effect in Deuterium / Solid System, October 21–24, 1990, Provo, USA.

〔9〕 DOE / S–0073, "Cold Fusion Research" , A report of the Energy Research Advisory Board to the United States Department of Energy, Nov., 1989.

〔10〕 S. C. Wang, et al, "Identification of the Energetic Charged Particles in Gas–Loading Experiment of 'Cold Fusion' Using CR–39 Plastic Track Detector". This Meeting.

〔11〕 D. W. Mo, et al, "Search for Precursor and Charged Particles in 'Cold Fusion'". This Meeting.

〔12〕 K. L. Wang, et al, "Search for the Better Material for 'Cold Fusion' Using CR–39". This Meeting.

〔13〕 S. E. Jones, Private Communication, Dec. 1990.

〔14〕 D. R. Rolison and W. E. O'Grady, Proc. NSF / EPRI Workshop (1989)

〔15〕 G. Andermann, "A New Theoretical Model (Nu–Q*) for Rationalizing Various Events of 'Cold Fusion' in Deuterium Loaded Palladium Cath-

odes" , Proceedings of the First Annual Conference on Cold Fusion, March 28–31, 1990, Salt Lake City, USA, P. 295.

〔16〕 Y. Q. Zhang, et al, "^{2}H (d, ^{2}He) 2n Reaction Induced by 15.7 MeV Deuteron" Scientia Sinica, A, (1987), 286.

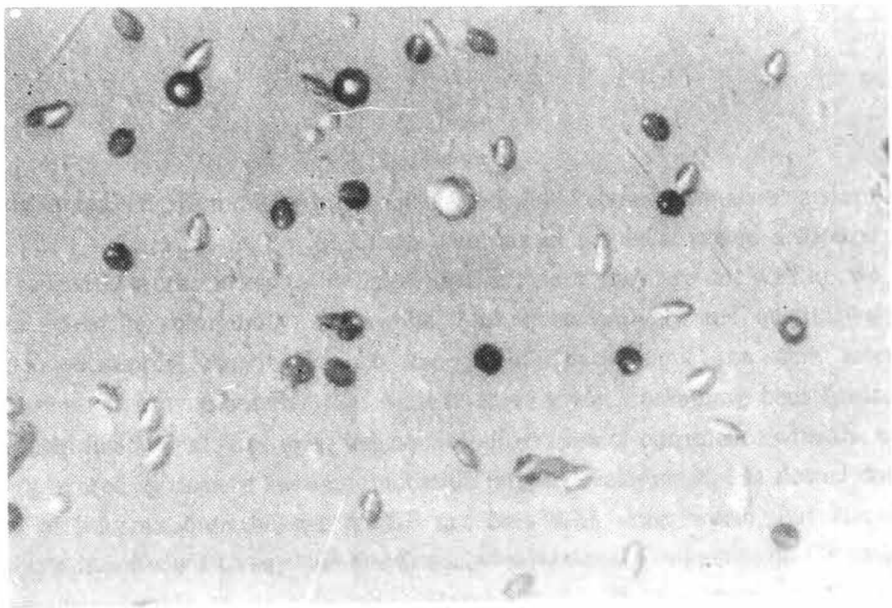

Fig.1 A typical picture for the signals of energetic charged particles in CR–39

Conference Proceedings Vol. 33
«The Science of Cold Fusion»
T. Bressani, E. Del Giudice and G. Preparata (Eds.)
SIF, Bologna 1991

COLD FUSION STUDIES IN THE USSR

V.A.Tsarev
P.N.Lebedev Physical Institute, Moscow, USSR

Introduction

The Organizing Committee kindly suggested that I should talk about a state of cold fusion (CF) studies in the Soviet Union. Offering of a special report dedicated to the soviet scientists works seems to be quite justified, since they are not well known to the western scientific community. Meanwhile, both quantitatively and qualitatively they bring a noticeable contribution to the world "data bank" on this interesting phenomenon. It is even possible that some of these soviet works have been "precursors" of the "cold fusion era". However, inadequate integration of our science with the western one, aggravated by scanty telecommunication media development, has slowed down the process of information exchange on CF not only with outer world, but also in our country. It is sufficient to say that the first Soviet National Conference on CF took place only recently in March of this year (March 22–26, Dubna–Moscow). Figuratively speaking up to now we have been working behind the scenes and watching the play. Now it is time to raise the curtain.

Fig.1 illustrates the "CF geography" in our country as it was presented at the Dubna Conference. These works are carried out by about 45 Institutes. The total number of laboratories which took part in CF experiments is no doubt more. However, many of them stopped or "freezed" their activities after the first unsuccessful attempts and under the pressure of wide–spread scepticism. The CF reputation in our country has suffered greatly from rush and inexact experiments of the initial period, widely boosted with a mass media.

The total number of soviet publications on CF certainly exceeds one hundred (more than 80 papers were submitted at the Dubna Conference). About half of them are devoted to CF experiments, about a quarter are connected with methodical and structural studies, and the rest – with theoretical models.

Until very recently there was no any large–scale program on CF in the Soviet Union, and all investigations were financed from budgets of institutes. Recently, thanks to academician N.A.Baraboshkin's initiative, the first All–Union Academical contest on CF was organized, which had quite a modest fund. At present a wider program is under discussion and preparation.

The lack of any long–term financial support resulted in the fact that a great

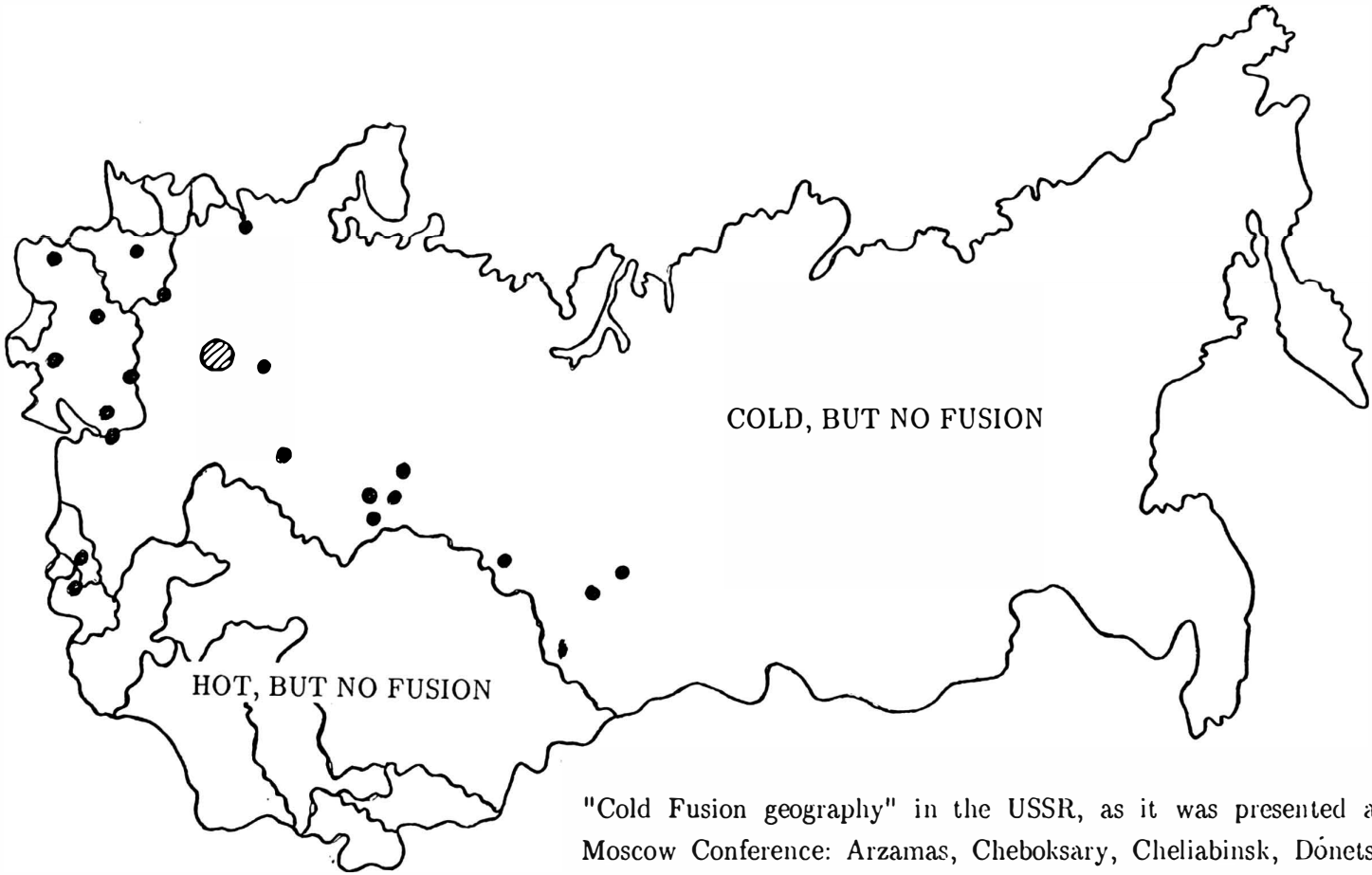

Fig.1. "Cold Fusion geography" in the USSR, as it was presented at Dubna–Moscow Conference: Arzamas, Cheboksary, Cheliabinsk, Dónetsk, Dubna, Erevan, Kaliningrad, Kharkov, Kiev, Krasnoyarsk, Leningrad, Lugansk, Moscow, Novosibirsk, Obninsk, Odessa, Omsk, Podolsk, Rostov, Sverdlovsk, Tbilisi, Tomsk.

majority of soviet works on CF are characterized both by small volume and duration. There are only few prolonged well equipped experiments with good statistics aimed to a high reproducibility. Calorimetric measurements were not widely spread and developed. At the same time a number of works based on new original ideas and techniques have been done, which might have interesting continuations. Below I'll concentrate mainly on such representative papers, where some new results have been obtained or new techniques have been used for the first time. Having in mind a specific character of the report, some historical excursus is justified in my opinion. Due to the lack of space, works of more "traditional" character in spite of their importance will be presented only in a tabulated form (Tables I–III). For the same reasons methodical and structural researches are excluded. At the end of the report some selected soviet theoretical works will be mentioned in short. More detailed information on the soviet papers may be found in reviews [54,62,71].

1. Nuclear mechanofusion

It seems to be reasonable to begin the presentation of soviet results with a so–called "nuclear mechanofusion" (NMF), which development has been started by the group from the Institute of Physical Chemistry of the USSR Academy of Science few years before the first publications on CF [46,47]. Now it is difficult to estimate the reliability of NMF experiments and their relation to CF. If it is confirmed and if NMF and CF mechanisms common nature is proved, these works may be considered as the first results on anomalous nuclear effects in deuterium–solid systems.

The experiments [9,17] performed in 1986 revealed an excess of about 2 times the background level (BG = 0.07±0.02 neutrons per shot) of neutron emission during mechanical fracture of heavy ice and LiD crystals. Taking into account the efficiency of the neutron detector ($\epsilon \simeq 1$–2 %) this leads to about 15–30 neutrons per fracturing act for D_2O–ice or LiD crystals. The detector consisted of 7 proportional counters, immersed into a tank with purified silicon oil, and was used by the group in all subsequent neutron measuring.

Three years later, after the first announcements on CF, the group returned to their investigations and performed the new series of neutron (and β–) measurings under mechanical impact on D–doped materials. The results of these experiments are shown in Table IV.

The authors interpreted their results in the terms of catalytic D_2O decomposition, formation and fracturing of hydrides.

The situation with NMF experiments is not clear at present. There are some confirmations in [48], but in [49,50] the effect is not confirmed within the limits of 15–20–fold decrease as compared to the results stated by the IPC group.

TABLE I: Summary of Neutron and γ–Measurements

Reference		Metal	Method	Detector	Efficiency %	Backgr. (c/s)	Results
Arzhannikov	[1]	Li	$LiD+D_2O$	CNM – 18×6	10	10^{-2}	(1.7±0.14)BG
Arzhannikov	[2]	Pd,Pt	redox reactions	CNM – 18×6	10	10^{-2}	(1.5–1.8)BG
Bashkirov	[3]	Pd,Ti	electrolysis	^{3}He plast. scintil.	10	0.06±0.01	2 BG
Bel'tyukov	[4]	Ti	electrolysis laser Heating				18 BG (n) 2 BG (γ)
Borovoj	[5]	Pd	electrolysis	LiI(Eu), $LiF(TiO_2)$ scintil.			10^1–10^2n/s
Bushuev	[6]	Pd	electrolysis	^{3}He6 CsI(Na)	10	0.3	Bursts 4×BG $N_\gamma \simeq$BG
Bystritskij	[7]	Ti Ti/Ni	electrolysis	BF_3(16+22)	26±1	$8\cdot10^{-2}$	Bursts $4.5\cdot10^5$BG I_b~1 n^{-1}
Bystritskij	[8]	Ti	D_2 gas	BF_3(16+22)	26±1	$8\cdot10^{-2}$	Bursts $4\cdot10^5$BG I_b~ 1 n^{-1}
Derjaguin	[9]	D_2O ice	destruction	^{3}He 7	1	0.15±0.06 per shot	3 BG
Golovkov	[10]	Ti	electrolysis				Bursts 100 BG
Golubnichij	[11]	Pd	electrolysis	^{3}He 10 plastic scintil.	10(SN) 30(FN)	0.005	Bursts 10-10^2 BG
Golubnichij	[12]	Pd	electrolysis	^{3}He 10	10	0.004	5 BG
Gorbachev	[13]	Pd	discharge	scintil.	1	$5\cdot10^{-3}$	Bursts 6–10 BG
Guzhovskij	[14]	Ti	electrolysis	^{3}He 12	20	0.014	20 BG
Guzhovskij	[15]	Pd	electrolysis self-heating	^{3}He 12	20	0.014	100 BG
Karabut	[16]	Pd	discharge	CNM – 18 scint.ZnS(Ag) stilben	5	10^{-1}–10^{-2}	10^8BG Bursts heat $E_n \lesssim 17$ MeV

Klyuev	[17]	LiD	desintegr.	^{3}He 7	1±0.5	0.16+0.06 /(short)	2.5 BG
Krizhanskij	[18]	Pd Ti	electrolysis	CH – 17 6	1	0.08	Burst s 10^3 BG
Kuz'min	[19]	Pd Ti	electrolysis	ZnS(Ag) scintil. ^{3}He	1	1.6	7.5 BG
Lipson	[20]	Ti	LiD, D_2Or PP(D_6) desintegr.	^{3}He 7	1±0.5	0.05	6 BG
Lipson	[21]	Ti	PE(D_4) friction	^{3}He 7	1±0.5	0.05	5 BG
Lipson	[22]	Ti	D_2O, mechanical activation	^{3}He 7	1±0.5	0.04	10 BG
Lipson	[24]	Ti	D_2O, cavitation	^{3}He 7	1±0.5	0.035± 0.005	1.5 BG
Novikov	[24]	Pd	electrolysis	^{3}He 6	10	0.17	10 BG
Polosukhin	[25]	Pd	0.4MPa, 70–5 7 OK	NaI, ^{3}He			$10^2 s^{-1}(\gamma)$
Rusov	[26]	Pd–Ag	electrolysis	MAND/p	10^{-4}tr/n	1–2Tr/cm^2	10 BG
Sannikov	[27]	Ti	steam, LiD	NaI(Tl) 2	7	0.2	8 BG
Yukhimchuk	[28]	V, Pd	50MPa,77–67OK 18MPa,77–69OK	^{3}He 15 st ilben	7	0.074	Burst s 700 BG
Zelenskij	[29]	Pd,Ti	ion implantation	BF_3	1	$2\cdot10^{-2}$	2 BG

Negative (non–conclusive) results

Anan'ev	[30]	Ti	ion implantation	CNM — 18 polymer	1 10^{-2}		posteffect
Bashko	[31]	Pd	electrolysis	SNM – 18×14	10	0.05	0
Brudanin	[32]	Pd	electrolysis D_2 gas	SNM - 14×2 Ge (Li)	0.32		$\Lambda_{dd}<6\cdot10^{-25}$
Brudanin	[33]	Ti	electrolysis 150 atm, 77K 150–600 atm, to 300K, 1atm 77–300 K	– " –	– " –		$\Lambda_{dd}<8.0\cdot10^{-25}$
Artyukhov	[34]	Ti,Zr	D_2 gas	BF_3 33	20	$8\cdot10^{-2}$	$\Lambda_{dd}<10^{-25}$
Grigor'ev	[35]	Pd,Ti	electrolysis	^{3}He 10	6		0

TABLE II: Charged Particles Registration

Reference		Metal	Method	Detector	Results
			Positive Results		
Borovoj	(36)	Pd	electrolysis	scintil.	$> 10^2 s^{-1}$
Golubnichij	(37)	Pd	electrolysis	CsI	$\Lambda_{dd} \sim 10^{-22} s^{-1}$
Karabut	(16)	Pd	discharge	semicond.	$E_{ch} \lesssim 20$ MeV
Zelenskij	(29)	Pd,Ti	ion implant. 100–800 K 100–78 K	semicond.	 $\Lambda_{dd}=5.5\cdot10^{-19}$(Pd) $\Lambda_{dd}=1.6\cdot10^{-19}$(Ti)
			Negative (non–conclusive) Results		
Anan'ev	(30)	Ti	ion implant.	semicond.	?
Bertsev	(38)	Ti,Nb	D_2,300–600 K	semicond.	$\Lambda_{dd}<2\cdot10^{-22}$
Brudanin	(39)	Pd	electrolysis	CR—39 (α) semicond.	$\Lambda_{dd}^{(\alpha)}<4\cdot10^{-27}$

TABLE III: Tritium Production

Reference		Results
		Positive
Bazhutov	(40)	Ti, D_2O electrolysis with current cycling, 5 BG
Golubnichij	(11)	TiD_x, thermodesorption, 10 BG
Grigor'ev	(35)	Pd, Ti, D_2O + KOD electrolysis, 10 BG
Guzhovskij	(14)	Ti, D_2O electrolysis (10–100) BG, $T/n \simeq 10^{8+1}$
Kosjachkov	(41)	The first paper with discharge, Ti, positive
Lipson	(42)	Ti + D_2O + PP(D_6), desintegration, 1.5 BG
Romadanov	(43)	Y, Er, Nb, Ta, discharge, 10^9 T/s
		Negative (non–conclusive)
Simonov	(44)	many metals and alloys, electrolysis, 100 experiments $\dot{N}_T < 2\cdot10^{-18} s^{-1}$
Vershinin	(45)	Pd, Pt, Mb, high–voltage, nanosecond discharge
Yukhimchuk	(28)	V, thermocycling, $N_T/N_n < 3\cdot10^7$

TABLE IV: Results on nuclear mechanofusion

Ref.	Materials	Impact	Results
[20] [42]	Ti + 10% D_2O + 4% PP(D_6)	agitation	n: 6 BG β: 1.5 BG
[21]	Ti + PE(D_4) + D_2O	friction	n: 5 BG
[22]	TiD_x; $LaNi_5$	mechanical activation (abrasive wheel)	n: 10 BG
[23]	Ti + D_2O	cavitation	n: 1.3 BG

2. Nuclear chemofusion

The first observations of neutron emission from chemical reactions have been reported by the group from Novosibirsk [1,2].

Two different chemical reactions were used:

a) $LiD + D_2O \rightarrow LiOD + D_2$. About 30 grammes of D_2O were placed into the test–tube and LiD crystals were put into it in small portions. The intensity of the neutron emission, accumulated in 30s intervals is shown in Fig.2a. During the chemical reaction neutron bursts with a duration of $\lesssim$ 5s were observed. The ratio R is:

$$R = \frac{\text{counts during the chemical reaction}}{\text{background counts}} = 1.70 \pm 0.14.$$

b) The oxidation–reduction reactions with $Pd(ND_3)_2Cl_2$, $(ND_4)_2(PtCl_6)$ and $Pd(NH_3)_2Cl_2$, $(NH_4)_2(PtCl_6)$ salts were compared. Results after six identical experiments are presented in Fig.2b.

The ratios R:

$$R(Pt,H) = 0.96 \pm 0.09;\ R(Pt,D) = 1.52 \pm 0.10$$
$$R(Pd,H) = 1.06 \pm 0.13;\ R(Pd,D) = 1.87 \pm 0.08$$

cannot be explained by the fluctuations, as it is seen from Fig.2c. Thus, a number of neutrons emitted in chemical reactions is a few dozens per gramme of deuterated material. The results were reproducible for about 100 runs.

3. Simultaneous direct registration of neutrons and charged products of dd–fusion

The work of the Khar'kov Physical Technical Institute group [29] (the first announcement appeared as early as in April 1989) is interesting from the point of view,

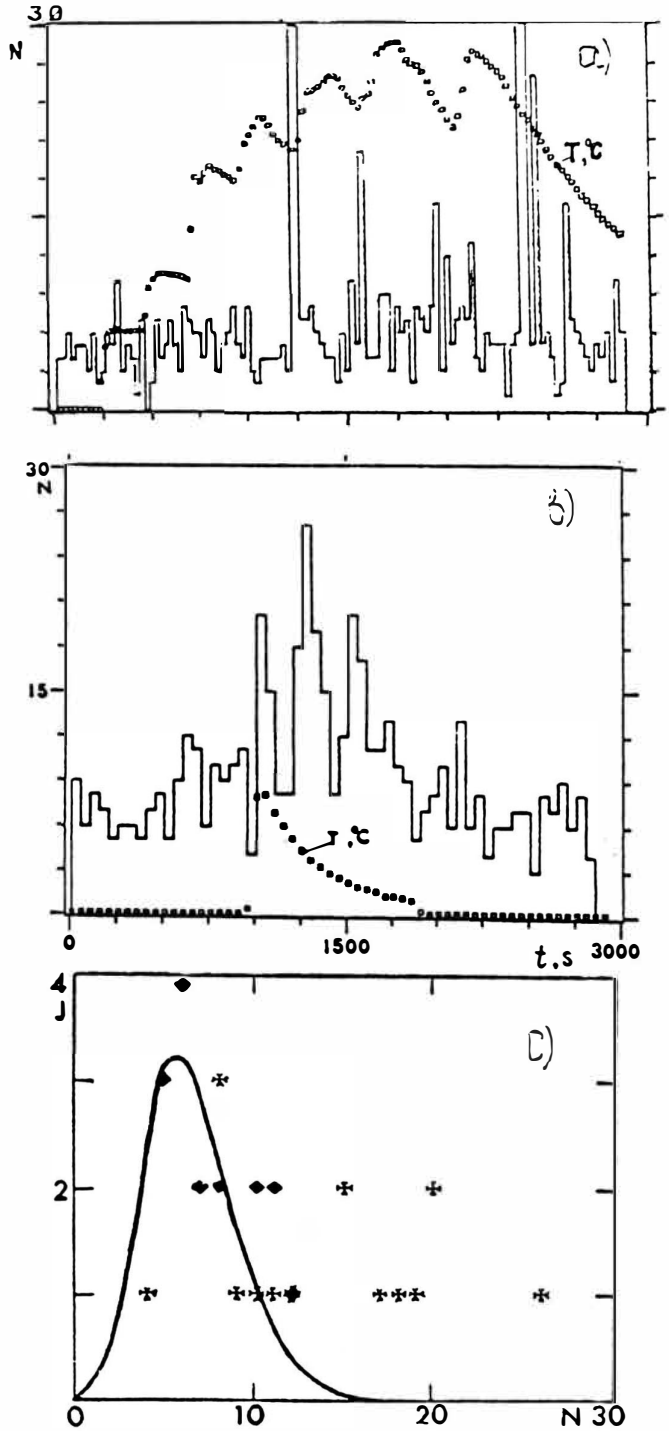

Fig.2.

The emission of neutrons a) in the LiD–D_2O experiment; b) in reaction between Pd salts and Zn; c) the number J of 50s intervals with selected number of counts N. Crosses–counts during the chemical reaction.

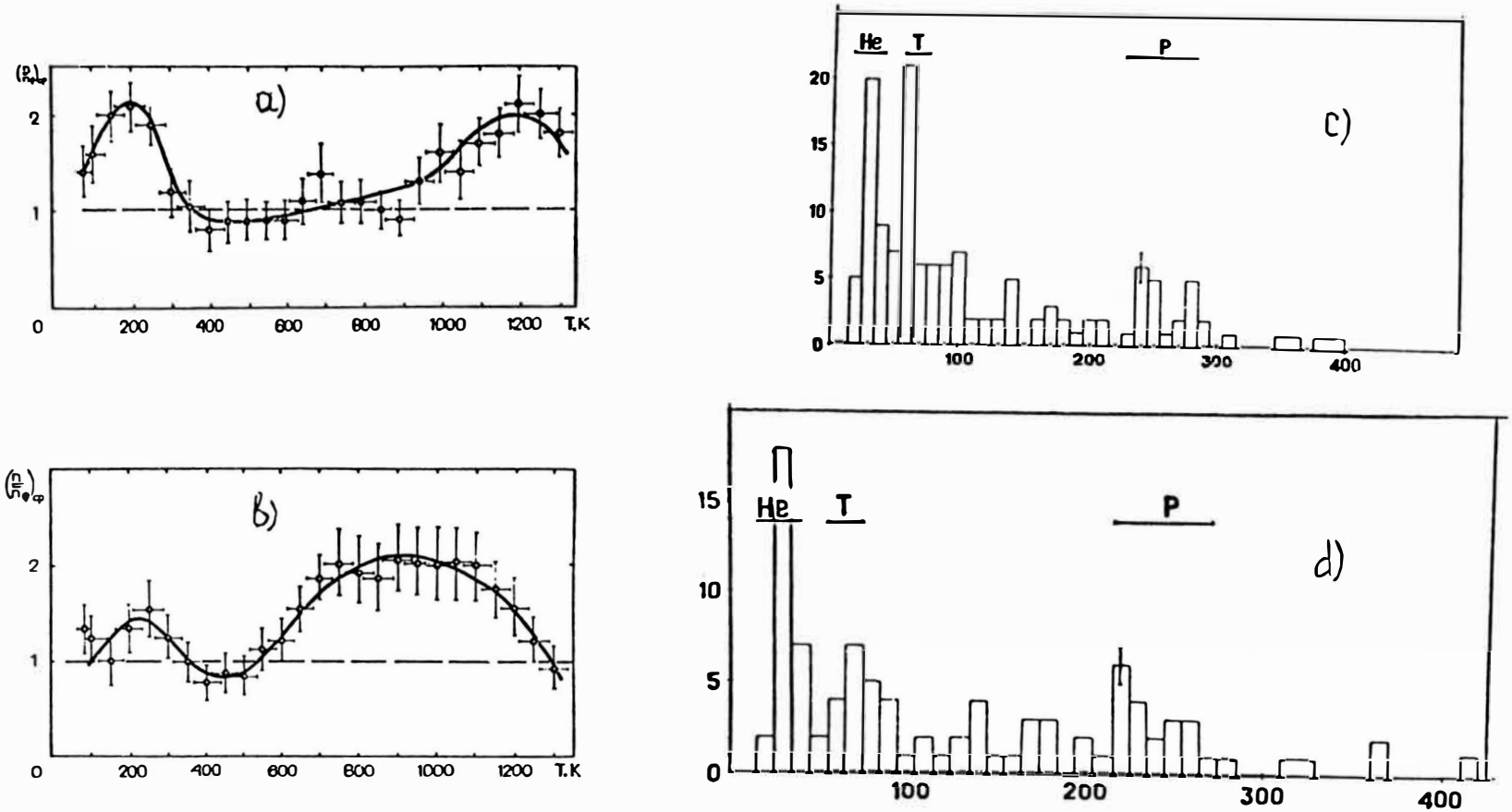

Fig.3. The neutron rate measured from a) Pd, b) Ti samples as a function of temperature: the ordinate is a ratio of detected neutrons to background. Energy spectra of charged particles from c) Pd and d) Ti targets. The position of the energies corresponding to ^{3}He, T and p are indicated.

that it was the first and may be up to date the unique experiment, where all the products of dd–fusion (except ^4He) were registered just in the same experiment. Besides, a clear temperature dependence of the CF rate (for 78–1300 K interval) was established for the first time. In the methodical sense it was the first CF experiment with successful application of ion implantation.

They used two kind of targets: thin Pd films (0.15–0.6 μm) precipitated on Ni layers (21 samples) and Ti foils (300 μm, 27 samples).

Loading was made using D_2^+–ion beam with E_D = 25 keV at T = 100 K. Saturation under irradiation controlled by the yield of ^3He, T and p was about D/Ti $\approx$ 5 and D/Pd $\sim$ 3 (Dose: $\sim 10^{19} D^+/cm^3$).

Results are shown in Figs.3a–3d.

a) Fig.3a,c displays the dependence of neutron counting rate on temperature for the temperature range of T = 78–1300 K, which has some correlation with D_2 thermo–desorption rate. The source estimate is $\dot{N} \simeq 10^2 n/s$. Some excess of $\dot{N}_n$ above the background was also observed during repeated Ti heating from 78 to 1300 K and cooling from 100 to 78 K. But $\dot{N}_n \simeq \dot{N}_{back}$ at T = 78–1300 K for samples implanted with H^+ ions.

b) Charged particles emission has been measured during cooling from 100 to 78 K and heating from 100 to 800 K. Fig.3c displays the spectra measured in 60 experiments with 10^3s duration for 9 samples, while Fig.3d shows the same for Ti (66 experiments). The excess above the background is clearly seen from the channels, which correspond to p, T and ^3He. Reaction constant is estimated as $\Lambda_{dd} = 5.5 \cdot 10^{-19} s^{-1} (dd)^{-1}$ for Pd and $\Lambda_{dd} = 1.65 \cdot 10^{-19} s^{-1} (dd)^{-1}$ for Ti.

4. Correlation measurements

In their early work ([51], April 1989) the group from Lebedev Physical Institute and Lugansk Machine–Building Institute suggested to measure the correlations between fusion products and acoustic (A) and electromagnetic (EM) emission. Thorough study of this phenomenon was conducted by this group through a series of experiments started in the middle of 1989. The first results of these experiments were presented at the Provo Conference [37,12] and might serve as a convincing arguments in a favor of "fractoacceleration model" (FAM) [51–55]. But strictly speaking it is possible that fracturing is only accompanied with CF, but not causes it. To clarify this problem the LPI–LMBI group continued their study of acoustic signal time–structure and space location of their sources [56]. Fast and slow neutrons were registered and acoustic signals from two sensors placed at the opposite ends of the sample were recorded. High statistics is collected on double correlations (hundreds events) between slow neutron counter

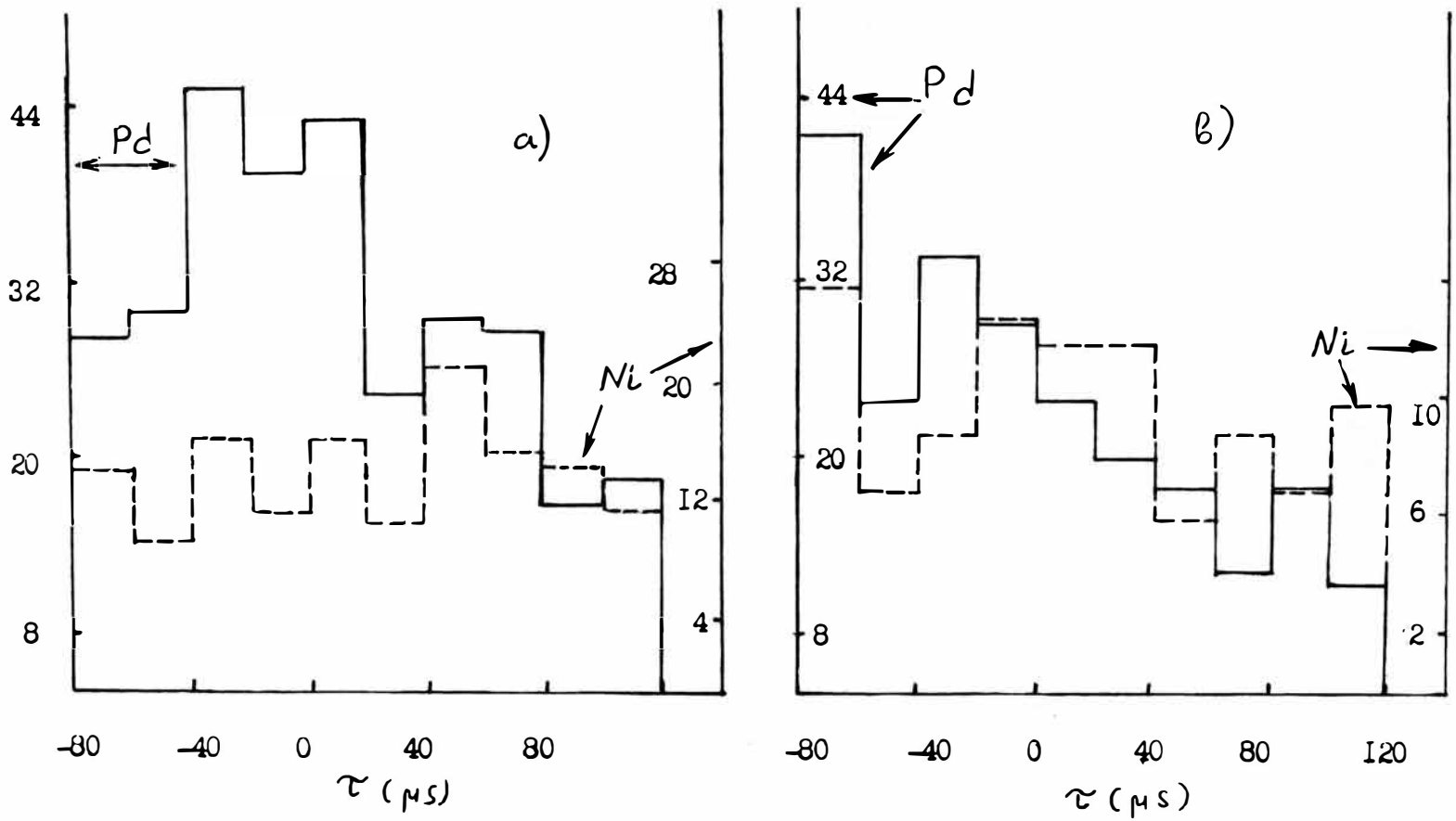

Fig.4. Correlations of slow neutrons with a) electromagnetic and b) acoustic signals for Pd and Ni (reference) cathodes.

(SNM, ^{3}He 12, $\epsilon \simeq 10\%$) and one of the acoustic detector signals; triple – from SNM plus both acoustic detectors; four–fold – from all four detectors. (Fast neutron detector presents a plastic scintillator with $\epsilon \simeq 20\%$ effectiveness). Some of these measuring results are shown in Fig.4. Positive results for Nb and steel were also obtained by this group.

5. Cold fusion observations in gas–discharge devices

The possibility of utilization of D–loading during a gas discharge in CF experiments was demonstrated for the first time in the early work [41] accomplished in April 1989 in the Institute of Metalophysics of the USSR Academy of Sciences. The standard titanium magnetic–discharge pump was used for the large Ti surface (0.5 m^2) treatment by deuterium ion beam with energies up to 9 keV. Mass spectrometry of the gas after a few hours of work revealed the presence of tritium produced in a course of device operation. However, the experiment was not quite determined quantitatively. Thereafter gas discharge experiments on CF were intensively carried out by two groups from NPO "Luch'" (Podol'sk).

a) V.A.Romadanov et al. results [43]. This group concentrated mainly on tritium search. For some cathode materials they registrated high rate of tritium production ~10^7–10^9 at/s (see Table V). Contact autoradiography of metal surface and its

TABLE V

Sample	Experim. duration (n)	Relative activity count/100s 2ml	Tritium content Bk/ml	Production rate at/s
D_2	–	238	131	$1.2 \cdot 10^5$
Yttrium	80	1238	287	$5.0 \cdot 10^5$
Erbium	38	2271	551	$4.2 \cdot 10^5$
Erbium	50	8010	1602	$1.1 \cdot 10^6$
Erbium	130	2890	526	$1.4 \cdot 10^5$
Erbium	140	2590	1253	$3.1 \cdot 10^5$
Niobium	162	$1.65 \cdot 10^5$	$4.7 \cdot 10^4$	10^7
Niobium	150	$7.75 \cdot 10^8$	$3 \cdot 10^6$	10^9
Tantalum	110	3148	3078	$9.6 \cdot 10^5$

β–activity measurements were conducted both with positive results. A slight excess of neutron emission above a background level was also observed ($\lesssim$ 2 BG).

b) A.V.Karabut et al. results [16]. Experiments of this group were carried out mainly with Pd with reproducibility of about 80%. The most important results are the following: 1) Neutron emission up to $\sim 10^7 s^{-1}$ was registrated. 2) Neutron spectrum was measured and the maximum observed neutron energy constituted $E_n^{max} = 17 \pm 1$ MeV; 3) 150% heat release excess over the electrical input is claimed which is about 3–5 kJ per 0.1g of cathode sample. The correlation between heat excess and neutron emission is observed. 4) The emission of charged particles with energies up to 20 MeV was registered. 5) Emission gamma–spectra were measured for various cathode materials. The majority of radioactive isotopes corresponded to the scheme (for palladium, as an example): ${}_{46}Pd^{110} \longrightarrow {}_{45}Rh^{110}$, i.e. the main reaction type were probably k–capture or (d,2p).

In order to check the Karabut group results [16] specialists from the Tomsk Nuclear Research Institute carried out experiments on gas discharge loading of palladium foils [13]. In the course of deuterium loading neutron bursts were observed within the time intervals of $\lesssim 10^2$s and with signal–to–background ratio of 5–10. However, after the current switching off the neutron emission disappeared. It might testify that the "overvoltage" effect, but not CF resulted in neutron emission both in this experiment and in the Karabut et al. works [16]. The results on charged particles were not confirmed as well: semiconductor surface–barrier detector didn't registered any excess of p and T emission.

6. 14.1 MeV neutrons registration from dt $\longrightarrow$ ^{4}He+n reaction [26]

This work completed in June 1989 is interesting from the viewpoint of the first evidence of CF proceeding via dt $\longrightarrow$ ^{4}He+n channel. In respect to methodics it is the first example of dielectric track detector application for CF studying, known to me. Electrolysis of the mixture of 50% D_2O and 50% dissolved tritium water has been carried out with the (72% Pd, 25% Ag and 3% Au) cathode. Two rare events were found in the CN–85 detector: three–ray "track stars", which arose due to carbon nuclei desintegration through $^{12}C(n,n')$ reaction and were considered as an unambiguous evidence of fast neutron existence with energies greater than 10 MeV. Later the dt–CF presence was confirmed by the Czechoslovak group electronic measurements [57].

7. Neutron burst during PdD self–heating

A curious phenomenon has been registered by a group from the Institute of Experimental Physics (Arzamas) in the course of electrolytic experiments with Pd [15]. After their D–loading Pd samples were taken out from electrolyte and placed into 4π–neutron detector together with a thermocouple. The self–heating occurred in some

cases due to the well–known physical–chemical reasons. In the experiments with 8.2 g Pd sample high counting rate was recorded in the sixth absorption–desorption cycle within two neighboring time intervals: 12337 counts/100s and 886 counts/100s. Integrated neutron yield is estimated as $7 \cdot 10^4$ neutrons.

8. Surface electron spectra measurements

The Moscow State University group performed the investigation on tritium content in Pd and Ti electrodes using the original method of electron spectra registration from a sample surface [19]. Some samples exhibited an extra–ordinary β–activity. The rough estimation of tritium amount gave approximately 10^8–10^9 atoms on the surface and about 10^{12}–10^{13} atoms in the electrode. The appearance of T in the electrode could not be explained by adsorption from the electrolyte (approximately 5 Bk/ml – initial D_2O activity).

9. Gamma quanta emission during electrolysis in the Ti–steam–gas–LiD system

In order to study CF in high temperature electrolytes a group from the Institute of Electrochemistry (Sverdlovsk) developed an original method [27]. Titanium sample was placed inside titanium or steel drum. The cell was heated up to 700–800°C in vacuum; 30 min later it was filled with D_2 gas ($P \simeq 1$ atm) and then cooled down. At 200–250°C D_2 gas was refilled. Then the cell was cooled and LiD added. Then the cell was heated again with simultaneous voltage application (500–1400 V) to Ti and drum electrodes. Gamma peaks at $E_\gamma \simeq 2.2$–2.5 MeV, approximately by an order of magnitude exceeding the background, were registrated.

10. Methods of CF stimulation

The possibility of CF stimulation with various "external effects" has been discussed in the early soviet paper [51], and later in [52]. Based on FAM the following methods have been suggested: mechanical deformation and desintegration in the course of D–loading, or after it, thermo– and cryoshocks, supersonic activation, current shocks (pulsing or stepwise current), ionizing radiation (both "external" and "internal" in a course of CF in stressed hydrides). Many of these methods were used in CF experiments (see [5,10,11,14,15,20,28,29,37,59,60] etc.) Some new CF stimulation methods have been reported by soviet groups at Dubna meeting: laser heating [4], nanosecond high–voltage discharge [45], X–ray irradiation [40].

11. Dubna group results

As an example of "traditional" approach let us consider the recent results of the

Dubna group [7,8]. They are worth to be mentioned for some reasons. This highly qualified group, which has experience in work on muon catalyzed fusion, started their CF experiments soon after the first announcement from Utah. They carried our very thorough study [32], but failed to find positive effect and presented very low limits on reaction constant (see Tables I, II). The group returned to the problem three times more [33,34,39], but again without any success. As for me, their results permanently clouded my belief in CF, and I was very glad, when just before this Conference Dr. V.M.Bystritskij informed me that in two latest experiments with some new procedure they at last managed to receive positive results. They changed both equipment and procedure and used amplitude and time information. The amplitude information essentially increased the degree of selection of "useful" events. The processing was of Menlove–type (two or more neutrons observed within 1 ms). These changes allowed a much lower background and a much higher reliability of identifying the effect.

Two types of experiments were performed: with electrolytic and D_2–gas loading. For electrolysis they used cathodes from pure Ti and Ti coated by 0.4 μm layer of nickel. For saturation with gaseous D_2 Ti chips send by Prof. S.Jones and H.Menlove from LANL were used.

The main results are the following:

a) In experiment with Ti cathode coated with Ni emission of neutrons in the form of separate bursts stochastically distributed in time was observed. (There was no effect for pure Ti).

b) Intensity of neutron in bursts is

$$I_n \simeq (3.6 \pm 0.9) \cdot 10^4 \ s^{-1}.$$

c) The burst frequency is $\langle \dot{N}_b \rangle \sim 1 \ h^{-1}$ and it decreases in time.

d) Burst duration is equal to

$$\tau \simeq 300 \ \mu s.$$

e) No correlations were observed between neutrons and acoustic signals. (However, it should be mentioned that they used too high threshold in the acoustic channel).

The gas experiment results are about the same ($I_n = (3.0 \pm 0.9) \cdot 10^4 s^{-1}$) and nicely confirmed the results of Menlove et al.

12. CF models

Due to the lack of space I can only mention some selected soviet theoretical works on CF, presented at the Dubna–Moscow Conferences.

a) Fracto–acceleration model (FAM). It was first suggested by IPC group for interpretation of their data on NMF [9,17] and later used by Lebedev–Lugansk group [51] for explanation of CF experiments [46,47] and presenting some predictions. (See also [52–55,61,62]).

b) Possible narrow resonances in DD–system. The idea of narrow Coulomb states for a system of two charged particles has been put forward in [63]. It is based on assumption of oscillating form of the potential at large distances [64] and predicts several resonances for DD–system in the kev energy region.

c) Catalysis by heavy stable particles. This model [66] combines the ideas of FAM and those of heavy particles catalysis [67], but with more sophisticated scheme of new catalytic particles ("erzions").

d) Barrierless fusion in crystal. Special conditions for D–atoms in cavities (cracks, defects) in crystal lattice suggested in [68], which may lead to higher fusion rate.

e) CF for geo– and astrophysics. A possible role of CF in the energy (and element) balance of the Earth, the Sun, the Jupiter and other planets is discussed in papers [69,70].

More information on soviet theoretical papers on CF can be traced from the review [71].

Acknowledgements

I benefited from discussions with many colleagues in the USSR and abroad and in particular with Drs. V.M.Bystritskij, P.I.Golubnichij, B.Ya.Guzhovskij, R.N.Kuz'min and D.H.Worledge, all of whom I wish to thank most warmly. I am also very indebted to the Organizing Committee of the ACCF 2 for hospitality and financial support.

References

1. A.V.Arzhannikov, G.Ya.Kezerashvili et al. Preprints Institute of Nucl. Phys., Novosibirsk 89–144, 1989; 90–36, 1990
2. A.V.Arzhannikov, G.Ya.Kezerashvili et al. ibid 89–152, 1989; 90–36, 1990
3. Yu.A.Bashkirov et al. Sov. JTF Letters, 1990, 16, 51
4. I.L.Beltyukov et al. DMWCA, Suppl. p.7
5. I.A.Borovoj et al. Preprints Institute of Monocrystals (Khar'kov) IMK–89–5; 89–9, 1989
6. V.S.Bushuev et al. KSF 1990, 5, 41, DMWCA p.11
7. V.M.Bystritskij et al. Contr. paper at this conference
8. V.M.Bystritskij et al. Contr. paper at this conference
9. B.V.Derjaguin et al. Colloid J., 1986, 48, 12
10. V.M.Golovkov et al. DMWCA p.8
11. P.I.Golubnichij et al. Sov. JTF Letters, 1990, 16, 46; Provo 1990, DMWCA p.14
12. P.I.Golubnichij et al. Sov. JTF Letters, 1990, 25, 46; Provo 1990, DMWCA p.18

13. A.F.Gorbachev et al. DMWCA p.9
14. B.Ya.Guzhovskij et al. DMWCA p.6
15. B.Ya.Guzhovskij et al. DMWCA p.3
16. A.B.Karabut et al. DMWCA p.13
17. V.A.Klyuev et al. Sov. JTF Letters 1986, 12, 1333
18. L.M.Krizhanskij et al. Talk at the DMWCA
19. R.N.Kuz'min et al. Preprint Institute for Nuclear Physics, Moscow State University, 90–58/204, 1990; DMWCA p.31
20. A.G.Lipson et al. Sov. JETP Letters 1989, 49, 588 DMWCA p.17
21. A.G.Lipson et al. Sov. JETP Letters 1989, 15, 26 DMWCA p.17
22. A.G.Lipson et al. Sov. JETP Letters 1989, 16, 54 DMWCA p.17
23. A.G.Lipson et al. Sov. JETP Letters 1989, 16, 89 DMWCA p.17
24. A.G.Novikov et al. DMWCA papers
25. B.G.Polosukhin et al. DMWCA p.19
26. V.D.Rusov et al. Sov. JTP Letters 1989, 15, 9 DMWCA, Suppl. p.11
27. V.I.Sannikov et al. DMWCA p.19
28. A.A.Yukhimchuk et al. DMWCA p.7
29. V.F.Zelenskij et al. Preprint Khar'kov Physical Technical Institute 89–61, 1989
30. S.P.Anan'ev et al. Preprint Kurchatov Institute of Atomic Energy 5273/7, 1990, DMWCA p.16
31. V.A.Bashko et al. Preprint Khar'kov Physical Technical Institute 90–39, 1990
32. V.B.Brudanin et al. Phys. Lett. A. 1990, 146, 347
33. V.B.Brudanin et al. Phys. Lett. A. 1990, 146, 351
34. V.M.Bystritskij et al. DMWCA paper, contr. paper at this conference
35. Yu.V.Grigor'ev et al. DMWCA paper
36. I.A.Borovoj et al. Preprint Institute of Monocrystals (Khar'kov) IMK–89–9, 1990
37. P.I.Golubnichij et al. KSF 1990, №8, 26, Provo 1990, DMWCA p.25
38. V.V.Bertsev et al. DMWCA Suppl. p.13
39. V.B.Brudanin et al. Preprint JINR D15–89–594, 1989
40. Yu.N.Bazhutov et al. DMWCA p.34
41. A.A.Kosjachkov et al. Sov. JETP Letters 1989, 49, 648
42. A.G.Lipson et al. Sov. JTP Letters 1989, 15, 88
43. V.A.Romodanov et al. DMWCA p.3
45. Yu.N.Vershinin et al. DMWCA p.33
46. M.Fleishmann, S.Pons, J. Elect. and Chem. 1989, 261, 301
47. S.E.Jones et al. Nature 1989, 338, 737
48. M.A.Yaroslavskij. DAN USSR 1989, 307. 369
49. P.B.Price. Nature 1990, 343, 542

50. L.G.Sobotha, P.Winter, Nature 1990, 343, 601
51. P.I.Golubnichij et al. Lebedev Physical Institute Preprint N°113 (April 1989), DAN 1989, 307, 99
52. P.I.Golubnichij et al. Lebedev Physical Inst. Preprint N°149 June 1989
53. V.A.Chechin et al. Paper submitted to Provo Conf. 1990
54. V.A.Tsarev. Uspekhi Fiz. Nauk 1990, 11, 1
55. P.I.Golubnichij et al. KSF, 1990, N°9, 15
56. P.I.Golubnichij et al. DMWCA p.22
57. P.Bem et al. Provo 1990
58. R.N.Kuz'min, B.N.Shvilkin "Cold Nuclear Fusion", Znanie, Moscow, 1989/10
59. F.Celani et al. Provo, 1990
60. P.I.Golubnichij et al. DMWCA p.23
61. S.S.Gerstein, L.I.Ponomarev. Talk at the Erice meeting, April 1989
62. V.A.Tsarev, D.H.Worledge. To be published in Fusion Technology, Nov. 1991
63. B.A.Arbuzov et al. Phys. Lett. B, 19990, 240, 477, Teor. Mat. Fiz. 1990 83, 175. Sov. JETP Letters 1989, 50, 236, IHEP preprint 90–124, Serpukhov, 1990, B.A.Arbuzov, Talk at the First Sakharov Conference, May 27–31, Moscow
64. J.von Neumann, E.Winger. Phys. Z. 1929, 30, 365
65. W.Zakowicz, J.Rafelski. Provo, 1990
66. Yu.N.Bazhutov, G.M.Vereshkov. Preprint TsNIIMash–1, 1990, DMWCA p.42
67. G.L.Shaw et al. Nuovo Cim. 1989, 102, 1441; J.Rafelski et al. Fusion Technology 1990, 18, 136
68. V.I.Vysotskij, R.N.Kuz'min. DMWCA p.50; Preprint Institute for Theor. Physics, Kiev, ITF–90–82R, 1990
69. P.I.Golubnichij, V.A.Tsarev. DMWCA p.40
70. Yu.N.Bazhutov, G.M.Vereshkov. DMWCA p.44
71. V.A.Tsarev, D.H.Worledge. To be published

Abbreviations used in the list of references:

1. DMWCA: Workshop "Nuclear Fusion Reactions in Condensed Matter" Dubna, JINR, March 22–24, 1991 and National Conference "Cold Nuclear Fusion" Moscow State University, March 25–26, 1991, Abstracts.
2. Provo: International Conference on Anomalous Nuclear Effects in Deuterated Solid Systems, Provo, Utah, October 22–25, 1990.
3. KSF: Kratkie Soobsheniya po Fizike (Lebedev Physical Institute).

Conference Proceedings Vol. 33
«The Science of Cold Fusion»
T. Bressani, E. Del Giudice and G. Preparata (Eds.)
SIF, Bologna 1991

THE MECHANISM OF DEUTERIUM EVOLUTION ON PALLADIUM: RELATION TO HEAT BURSTS PROVOKED BY FLUXING DEUTERIUM ACROSS THE INTERFACE

J. O'M. Bockris, D. Hodko and Z. Minevski
Department of Chemistry, Texas A&M University, College Station, Texas

INTRODUCTION

In spite of the electrochemical approach taken by Fleischmann and Pons, most of the research hitherto has concentrated upon manifesting nuclear effects (neutron emission, tritium formation) and there has been little [1,2] investigation of the situation of the surface chemistry of the palladium electrode, the mechanism by which molecular deuterium is formed or that by which adsorbed D diffuses inside the palladium, - and what its fugacity there would be. These factors may have a determinative influence on the triggering of the fusional effects, influencing not only the D/Pd ratio, but also internal cracking. Information on the relation between the surface characteristics and the fugacity may point to us conditions for the initiation of fusion.

In the present paper an interim report is given on the results of about one and one-half year's work of one sub-group at Texas A&M.

FUGACITY, MECHANISM OF DEUTERIUM EVOLUTION ON Pd

At extremely high density the properties of matter show that when the volume per atom becomes less than the usual size of the atom, the atoms lose their individuality and so the substance is transformed into higly compressed plasma of electrons and nuclei. It has been shown that at fugacities greater

than 10^{17} bar the increase in density leads to states where nuclear reactions consisting in the capture of electrons by nuclei (with emision of neutrinos) become thermodynamically favoured [3]. It is of fundamental importance to find out overpotentials for different mechanisms of deuterium evolution at which the fugacity exceeds above mentioned value. A given potential can give rise to fugacities differing by many orders of magnitude, depending on the path and rate-determining step in hydrogen evolution [see Table 3 of Ref 4]. For fast discharge-slow electrochemical desorption and for coupled discharge-combination mechanism a critical overpotentials are -0.5 V and -1.9 V, respectively.

The importance of the electrode kinetics programs reported here is to obtain independent evidence for the mechanism of deuterium evolution i.e., the sequence of reaction steps and the rate-determining step of the discharge of the deuterons on the surface, that the overpotential-dependent fugacity can be calculated [4].

The transient behavior at constant current is shown in Fig. 1.

It is usually possible from the study of such transients to obtain indications of the mechanism [5,6]. If a proton discharge mechanism is rate determining the rise time is expected to be: $\tau = 4\ C_{DL}R_{DL}$, where C_{DL} is the double layer capacitance and R_{DL} is the resistance of the interface. Taking the latter as RT/iF, (with $i = 10^{-3}$ A cm^{-2} and $C_{DL} = 50\ \mu$ F cm^{-2}, the calculated rise time is about 10^{-3} sec, whereas it is obvious from the diagram that it is about 100 sec.

So, this first test does not fit the mechanism derived earlier but it seems that the likely solution is that the reason for the delay in coming to a steady state is because the θ_D is coming to a slow equilibrium owing to the diffusion of the hydrogen inside or the deuterium inside.

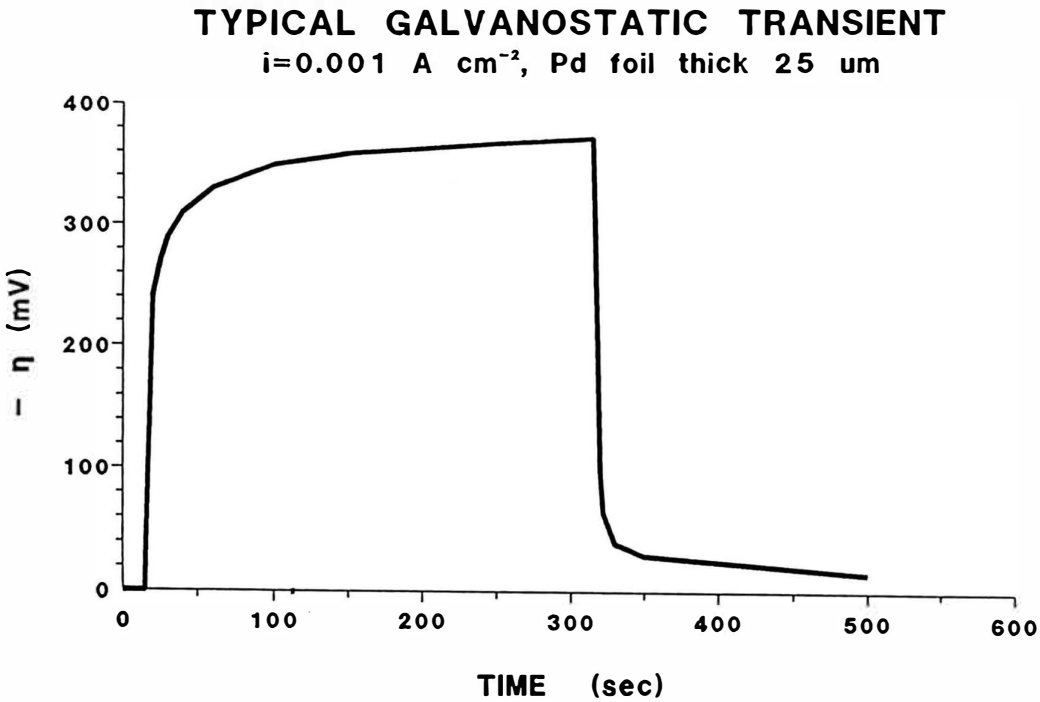
TYPICAL GALVANOSTATIC TRANSIENT
i=0.001 A cm⁻², Pd foil thick 25 um
400
300
200
100
0
- η (mV)
0
100
200
300
400
500
600
TIME (sec)

Fig. 1.

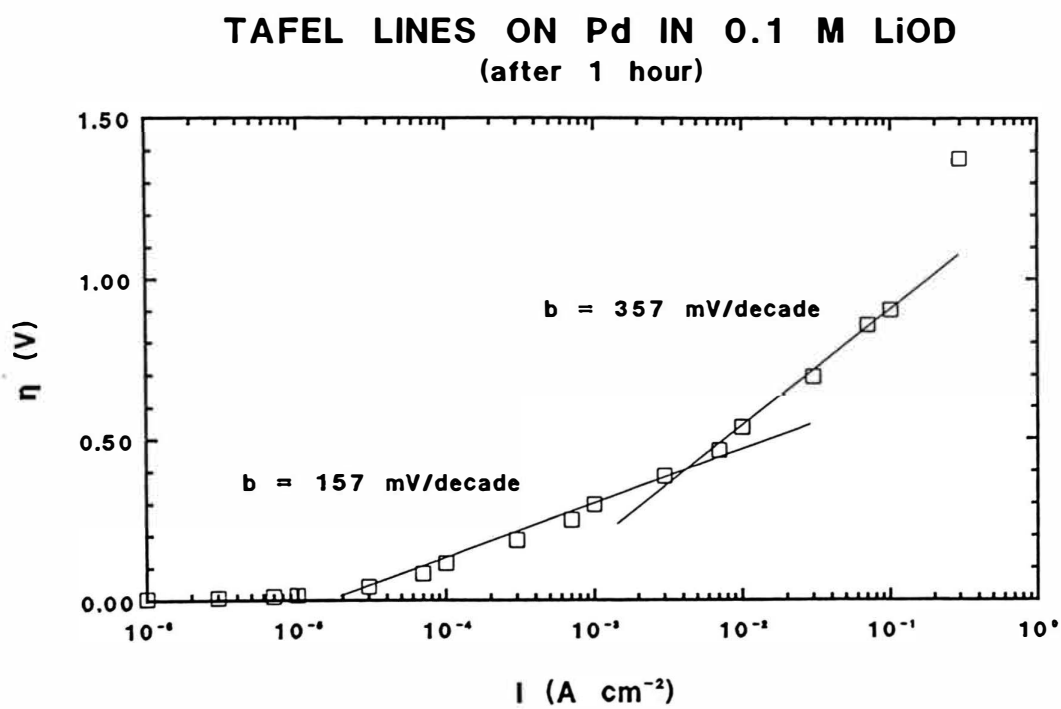
TAFEL LINES ON Pd IN 0.1 M LiOD
(after 1 hour)
1.50
1.00
0.50
0.00
η (V)
b = 357 mV/decade
b = 157 mV/decade
10⁻⁶
10⁻⁵
10⁻⁴
10⁻³
10⁻²
10⁻¹
10⁰
I (A cm⁻²)

Fig. 2.

To test this let us take the thickness of the membrane which is 25 μm so that we have that from: $\Delta^2 = 2D\tau$ and with $\Delta = 25\ 10^{-4}$ cm, and $D = 10^{-7}$ cm^2 sec^{-1}, one finds τ 60 seconds which is about the right time.

In looking at the Tafel lines (Fig. 2.) there are two separate gradients. The first one has a slope of 0.157 volts per decade which compared with the theoretical value of 2.303 . 2RT/F which would come to 0.120 V/decade. Hence the slope is somewhat high but the formal slope of 2RT/F is calculated with a transfer coefficient of 0.5 and the slope we need corresponds to a transfer coefficient of about 0.34, which is quite within the bounds of acceptability [7].

Hence this first gradient which takes us from an overpotential of 0 to about -0.4 V is reasonably in agreement with a coupled discharge and recombination mechanism. As we go up to the second slope, we come into a region of the Tafel coefficient b for which there is no mechanism known and so we need a special explanation. Let it be supposed that there is a film on the surface of the electrode, - it may be a blocking film or it may be a film of adsorbed material, e.g., other atoms which form a dipole with the palladium or etc., on the surface. Suppose that the potential which is normally measured is then changed by the potential due to a dipole layer on the surface. Then it is possible to show that the new gradient should be

$$b = 2.303 \frac{RT}{T} \left(\frac{2}{3} \beta + \frac{2}{3} \frac{\Delta\mu}{\delta e_0} \right)$$

Here the δ is the thickness of the layer concerned and e_0 is the electronic charge where $\Delta\mu$ is the dipole moment of the layer. To obtain the slope concerned (357 mV/decade corresponds to a dipole of about 2.5 Debye and this is an eminently possible dipole moment, for example, were at a water layer it would be about 2.2. So that although we cannot identify what this layer is it would seem that it offers, at least for the time being, a reasonable rationalization of the results obtained.

In Fig. 3. are shown the results of an EDS analysis of an electrode (Pd, Hoover and Strong) which had had no annealing and no electrochemical treatment. The second diagram shows the situation after annealing at 800°C and cooling in an Argon atmosphere with no electrochemical treatment. The surface becomes carburized. The third diagram shows the situation after one hour electrolysis at 0.5 A cm^{-2}. The carburized section has broken off. This is visible in the cell and the darker looking surface is then replaced by a bright shiny surface, the composition of which at the beginning is about 96% palladium (original Pd, > 99.9). It seems probable that the carbon arises from oil in the vacuum pump used in the system for annealing.

EDS analysis showed 10% platinum in a 1 micron layer on the surface after three weeks electrolysis (Fig. 4.). It is easy to calculate that about $1 \cdot 10^{-6}$ M of platinum have deposited in three weeks (0.10 of $5\ 10^{-5}$ cm^3). From Faraday's Law of electrolysis follows that to deposit platinum observed would need a partial current for platinum deposition of $1 \cdot 10^{-5}$ A, and this can be regarded as the limiting current density and must be related to a certain concentration. Assuming $i_L = 0.02$ nc, where c is the concentration in M per liter it follows that the concentration of platinum in the solution is around $2\ 10^{-4}$ M. Taking exchange current density of oxygen evolution on platinum around 10^{-8} A cm^{-2} and from the reversible potential solution Pt of 1.2 V (NHE) one calculates the overpotential for the dissolution of Pt of approx. 0.18 V. With the assumption of Pt dissolution current of 10^{-9} A cm^{-2} maximum dissolution velocity would be about 0.1 μA cm^{-2} whereas the required value is about 10^{-4} A cm^{-2}, a discrepancy too great to be explained by the

TREATMENT:

- not annealed
- no electrochemical treatment

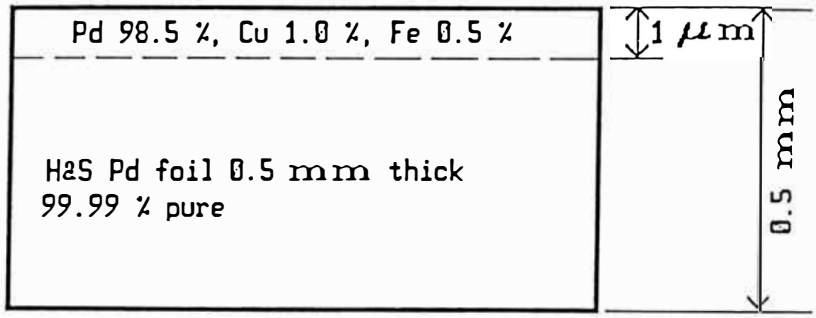

TREATMENT:

- annealed at 800 °C, and cooled in Ar atmosphere
- no electrochemical treatment

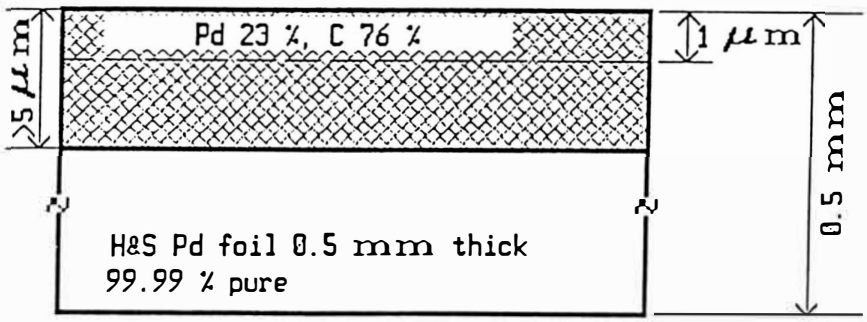

TREATMENT:

- annealed at 800 °C, and cooled in Ar atmosphere
- after 1 hour of electrolysis at 0.5 A cm^{-2}

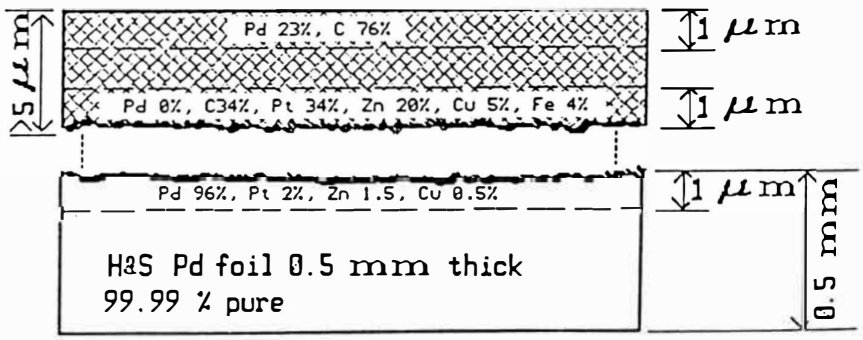

Fig.3.

EDS ANALYSIS OF Pd ELECTRODES AFTER DIFFERENT TIMES OF ELECTROLYSIS

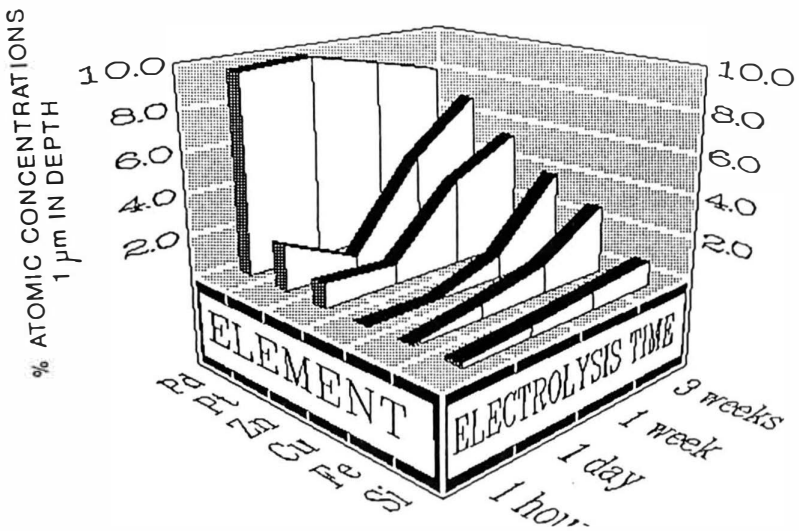

• Pd CONCENTRATIONS ARE SHOWN 10 TIMES DIMINISHED

Fig. 4.

XPS ANALYSIS OF Pd ELECTRODES AFTER DIFFERENT TIMES OF ELECTROLYSIS

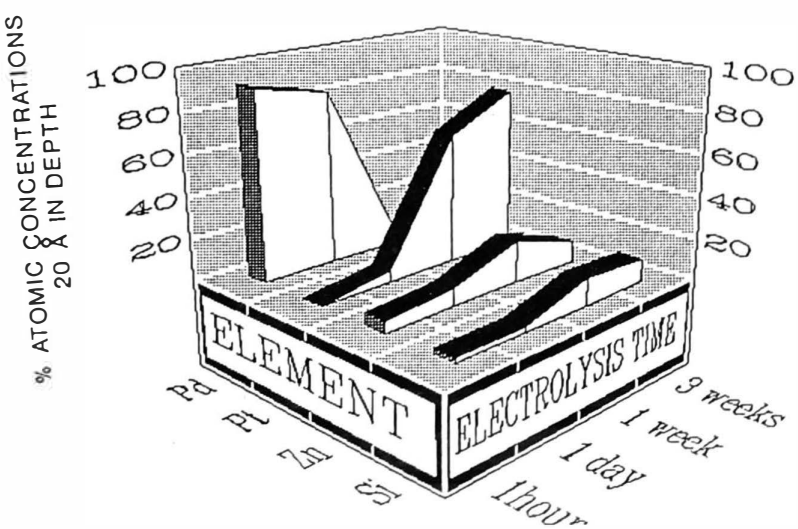

Fig. 5.

approximations of the calculation. We wish to make here a suggestion that it dissolves chemically due to a breaking up of the oxide on the surface.

In Fig. 5 is shown the XPS analysis of a region near the surface over three weeks time. The platinum is the most remarkable constituent: after three weeks it covers about 80% of the surface. A conclusion from our surface analysis is that the surfaces upon which we are conducting our experiments are first of all lithium - palladium alloys and the alloy concentration is around $LiPt_3$ with liberal amounts of platinum covering the whole surface after three weeks and small amounts of silicon, zinc and copper and other materials. There is some evidence for dendritic growth forms.

Solution analysis

Solutions were carefully analyzed after different times of electrolysis by ulilizing Inductively Coupled Plasma Spectrosopy. The results confirmed gradual increase in concentration of impurities, mainly Pt, Si and Zn, in solution during the three weeks electrolysis time.

THE HEAT BURSTS

Charging of the cells is performed typically starting with 50 mA cm^{-2} and changes in resistiviy were monitored. When D/Pd ratio attained the constant value (usually after 2-4 days at these low currents charging) the current was increased to 0.5 A cm^{-2}. Almost in all cells this caused an enhancement in charging and thus increase in D/Pd ratio. After that a current was increased normally to 1 A cm^{-2}. No additional increase in D/Pd was observed by such treatment of the electrodes. The electrodes were than pulsed by applying different pulsing regims.

Pulsing regimes were carried out by the use of pulses which could take the cell cathodically up to 2 A from the open circuit condition and

XPS DEPTH PROFILES AT DIFFERENT ELECTROLYSIS TIMES

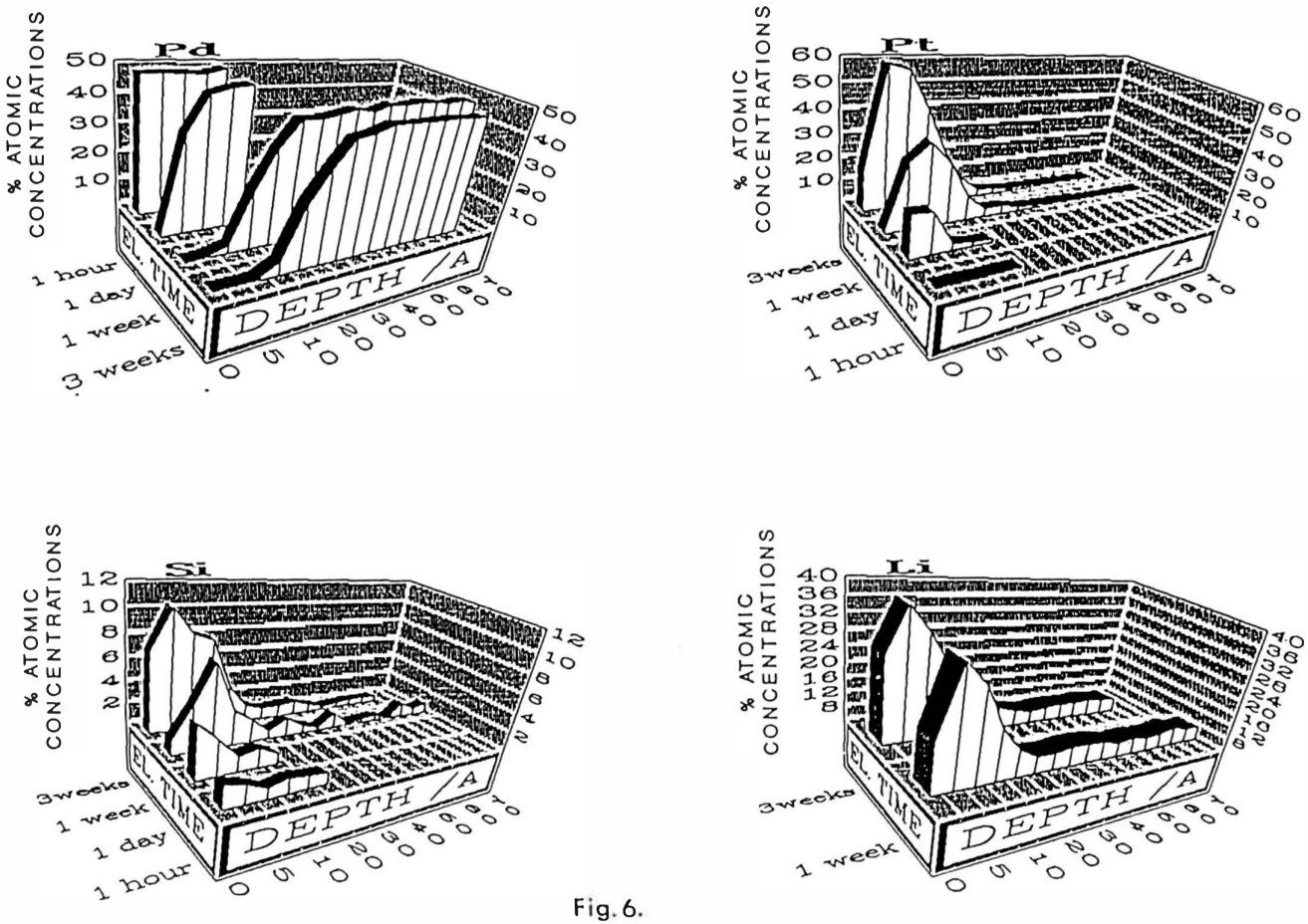

Fig. 6.

EXCESS HEAT ON CELL 16-P

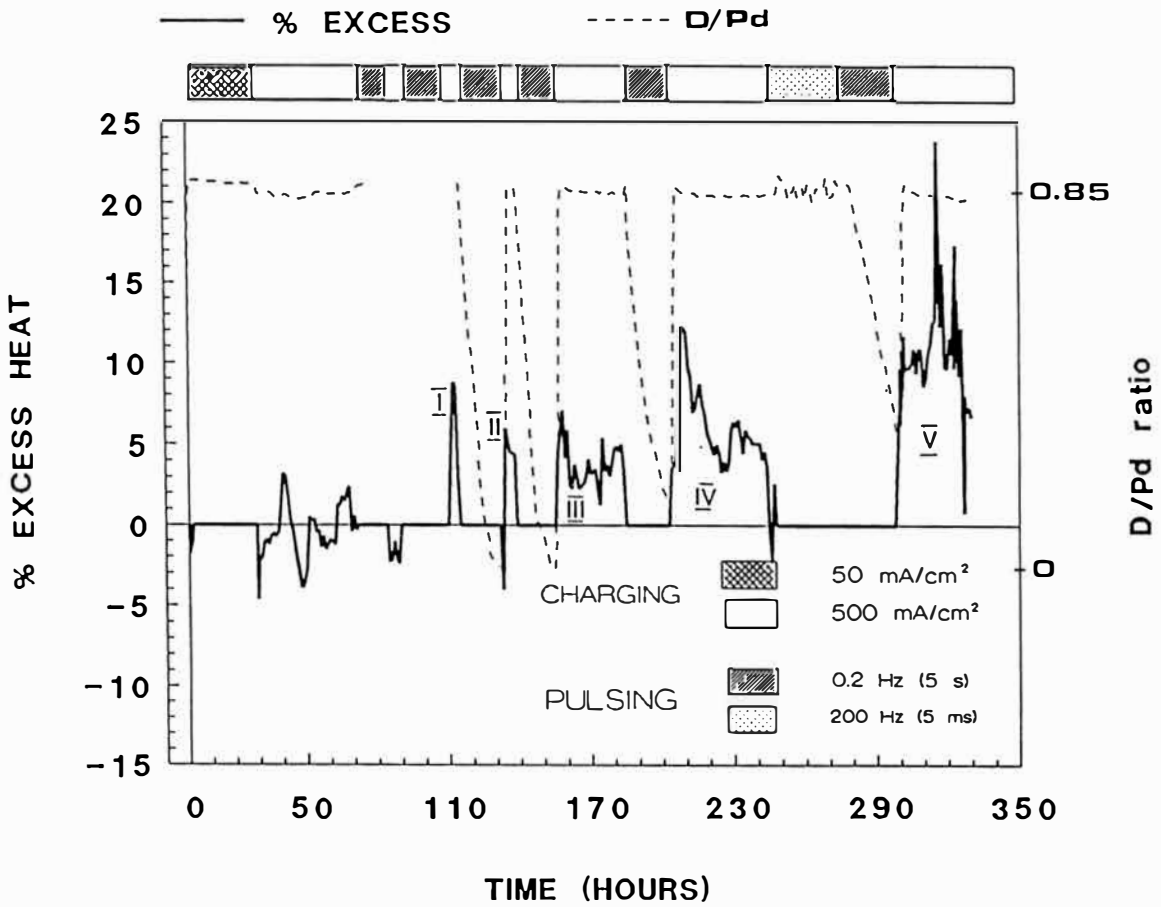

Fig.7.

anodically to 0.1 A for the discharge. The measurement of heat cycles in cells began on the 2. April, 1991 with one cell and the cells were run up to two month. Fig. 7 shows five consecutive heat bursts occuring after successive application of pulsing regime (cathodically 5s for 1 A cm^{-2}, and anodically 5s for 0.1 A cm^{-2}). It is interesting to note that cells pulsed with 5 ms pulses did not show any excess heat. A total energy output exceeds 35 MJ/mol. A critical observation was made in respect to the effect of the pulsing upon the concentration of hydrogen in the cell. In some cases the pulsing led to a reduction of the amount of deuterium in the electrode and under these cases heat was observed (Fig. 7.). However, in most cases the pulsing did not lead to fluxing and in such cases no heat bursts were observed. In respect to charging, the incoming charge has to compete with the combination on the surface. When the surface is saturated only a small number of atoms, less than 20% at the beginning, and in the end less than 1%, actually go into the cell to diffuse in. Most recombine. On the other hand, during the anodic cycle there is no competing process and all processes lead to hydrogen dissolving anodically out of the cell. Hence, for the passage of the same number of coulombs in each direction, the anodic processes are more efficient than the cathodic: OH comes out easier than it goes in. Thus, what was found to be successful was pulsing which causes a flux inside the cell, and "cleans it out". This may apply literally to dislocation. Thus Gittus and Bockris [8] suggested that the critical point with the available of dislocation of pile ups and points of triaxial stress to be available for incoming deuterium. These materials would certainly be covered mostly with poisons, particularly with H. If, however, a flux of anodic deuterium is put in it is likely that they are cleaned out, the hydrogen dissolves away from them and when the deuterium comes in in an increasing fraction deuterium is able to get onto the dislocations and, as shown by Bockris and Supramaniam, these are the places where the internal stress is highest. Points of triaxiel

stress and other high stress areas are those where the greatest congregation of internal deuterium lies. These internal atoms must be deuterium atoms and not hydrogen. The washing out would contribute to this.

The reason some cells do not wash out may be because of films on surface. When there is too much lithium, zinc, sodium, and platinum on the surface the recombination is so high that little hydrogen goes in and when an attempt is made to bring the hydrogen out the exits are blocked.

A major conclusion of this work therefore is that a critical element is pulsing, the object of this pulsing is to flush out impurities from the inside of the electrode and that this pulsing only happens if the electrode surface is sufficiently clean.

Another observation was that the length of the heat bursts is in the region of 30 to 40 hours which corresponds to those of other workers. It is possible that, after a certain time, even the dislocations poison up again, thus, there is always some hydrogen coming in and left long enough the hydrogen will displace the deuterium on the surface. This is a point in favor of utilizing very pure D_2O.

REFERENCES

1. J. McBreen, J. electroanal. Chem., 187 (1990)279.
2. M. Ulmann et. at., J. Electroanal. Chem., 286(1990)1989.
3. E.M. Lifshitz and L.P. Pitewsky, Properies of matter at very high density in Statistical Physics, Part I, 3rd edition, Vol 5, Pergamon Press, 1963, Chapter 11, page 317.
4. J. O'M. Bockris and P. K. Subramanyan, Electrochim. Acta., 16(1971)2169.
5. N. Pentland, J. O'M. Bockris and E. Seldon, J. Electrochem., Soc., 104(1957)182.
6. T. Maoka and M. Enyo, Aelectrochim. Acta.,26(1981)615.
7. A. Despic and Bockris, J. Chem. Physics, 32(1960)389.
8. M. Gittus and J. O'M. Bockris, Nature, May 11, 1989.

Conference Proceedings Vol. 33
«The Science of Cold Fusion»
T. Bressani, E. Del Giudice and G. Preparata (Eds.)
SIF, Bologna 1991

THE CALORIMETRY OF ELECTRODE REACTIONS AND MEASUREMENTS OF EXCESS ENTHALPY GENERATION IN THE ELECTROLYSIS OF D_2O USING Pd-BASED CATHODES.

Stanley Pons* and Martin Fleischmann**

*,**University of Utah, Salt Lake City, Utah, USA,
**University of Southampton, Southampton, UK

Introduction

In the period since March 1989, there has been much comment and doubt expressed concerning the accuracy of the calorimetric techniques that we adopted to demonstrate the presence of excess enthalpy generation during the electrolysis of D_2O solutions at palladium-based electrodes.[1-6] As it is only the end of the second year of research in this area, it seems appropriate at this point in time to summarize what we have actually done and to comment on the work in progress.

We point out at the start that such calorimetric measurements are not trivially simple since there are many variables and details of the calorimeter design that have to be considered. Many of these variables and design details do not play a significant role in the determination of the thermal outputs of the calorimeters, while a few of the factors are critically important. This was well-known before the publication of our preliminary note[1,2] but in view of the often repeated criticisms it became necessary to establish this conclusion by further extensive investigations of the effects of all the pertinent variables on the behavior of our calorimetric systems. While it is certainly true that these investigations influenced the development of the calorimeter design and methods of data analysis, the conclusions which we reached in March 1989 have not been markedly affected.

One factor which was of key importance to our choice of calorimeter design was the variability of the magnitudes of the rates of excess

enthalpy generation and the sensitivity of these rates to a wide range of system variables so that a large number of experiments were required (and this need continues!). In consequence it has been necessary to use low-cost calorimeters. Most importantly, it has always been evident that each experiment be carried out for very long times: the minimum time for a single experiment has been three months.

In this paper we outline first of all the general considerations which influenced our choice of calorimeter and then describe the evolution of the design since October 1989. We go on to discuss the methodology which we have adopted to obtain accurate thermal balances for the cells. In this discussion we pay particular attention to a number of issues which have been raised repeatedly and which are important to the understanding of the limits of accuracy as well as the sensitivity of the measurements with such calorimeter designs; some of these issues have not yet been adequately described in the literature but are of crucial importance to measurements of excess enthalpy generation at very low enthalpy inputs. These measurements are part of our ongoing program, this part being aimed at the understanding of the reality or otherwise of a "threshold" for the onset of excess enthalpy generation. In the final section we give an outline of some of our recent measurements at the opposite extreme of intermediate to high current densities. The excess enthalpy generated under such conditions is so high that precise characterization of the calorimeters proves to be unnecessary since, in the limit, heat transfer from the cells is dominated by evaporation of the solvent.

Factors Influencing the Design of Electrochemical Dewar Calorimeters: Early Designs.

In the experiments reported to date, we have been concerned mainly with the electrode reactions

$$2\,D_2O + 2e \rightleftarrows D_2 + 2OD^- \qquad \text{(i)}$$

$$4OD^- \rightleftarrows O_2 + 2D_2O + 2e \qquad \text{(ii)}$$

in which O_2 gas is continuously evolved at the anode surface while D_2 gas is evolved at the cathode following the charging of the lattice with deuterons. The possible sources of heat generation in the cell will then be due to reactions (i) and (ii), any catalytic recombination of deuterium and oxygen in the cell, any other chemical reactions occurring in the solution or at the electrode surfaces (or at the surfaces of any

other cell components), Joule heating of the electrolyte solution and any excess enthalpy generation in the metal lattice.

The total enthalpy generation in the cell will be coupled to heat flow into and out of the calorimeter through the radiant surfaces and through the thermally conductive components of the cell at the top of the calorimeter. The sources of heat generation are localized and the temperature fluctuations due to these localized sources are dissipated by the decay of eddies; we have pointed out that the simplest method of efficiently reducing these non-uniformities at low cost is to build calorimeters that are in the shape of long cylinders, and the first generation calorimeter was of the type shown in Fig. 1. In such calorimeters, enthalpy generation at or in the electrodes is uniform in the axial (z) direction. The gas evolution reactions (i) and (ii) ensure that the thermal equilibration of temperature in the cell will then be due to convective stirring by the eddies developed in the electrode boundary layers and their subsequent relaxation into the bulk of the solution. We have demonstrated that this occurs rapidly, and that the rate of radial mixing is about one order of magnitude faster than total mixing in the axial direction. We have reported that for intermediate to high rates of electrolysis of H_2O or D_2O (current densities in the range of about 50-2000mA cm^{-2}; cell currents 200-1600mA) the gas evolution gives rise to radial mixing on a time scale on the order of ~3s and axial mixing on a scale of about ~20s. Axial gradients in temperature therefore are never established, and the thermal relaxation times ($\tau \sim M_0/4k'_R\theta^3_{bath}$) of these calorimeters are known to be ~1 hour; the calorimeters behave as well-stirred tanks (uniform temperature).

We have drawn a number of conclusions regarding the design criteria of these calorimeters from consideration of the likely sizes of the diffusing thermal eddies and their rate of relaxation into the solution. In summary, we have concluded that it is necessary to decrease the diameter of the cells with respect to the length and to minimize the total volume as far as possible. Furthermore, it is necessary to scale the radiant surface area of the calorimeter so that sufficiently large values of the differences in temperature between the cell contents and the bath are established so as to allow sufficiently accurate measurements to be made. In this way we can also minimize the effects of the fluctuations and achieve an adequate signal/noise for the measurement of the sought effects. The likely maximum values of the errors

encountered in the enthalpy generation in this type of calorimeters have been reported elsewhere[4].

In our estimation many other workers have not given careful consideration to these factors and conclusions have been reached based on experimental results that therefore are subject to excessive sources of systematic and random errors. This is true especially of conclusions regarding the accuracy of such measurements which, needless to say, are strongly affected by the scaling of the electrodes and Dewar cells (other factors are discussed below).

The evolution of our own calorimeter design has followed an iterative program so as to establish that measurements of the excess enthalpy generation are large compared to the systematic and random errors and this program of work is still in train. The measurements made with the generation of calorimeters used in the collection of data up to the report contained in the first full paper[4] Fig.1, were shown to be primarily dependent on four independent parameters: (1) the heat transfer coefficient of the cell (at a chosen time of the experiment), (2) the water (heavy water) mass equivalent of the cell, (3) a parameter to allow for the time dependency of the contents of the cell, and therefore the time dependency of the heat transfer coefficient, and (4) the magnitude of any excess enthalpy generation. The understanding and application of the parameter (3) has, in most instances, been ignored or misused, eg[7,8] (see further below) and, as a result, the natural evolution of calorimetric studies of the electrochemical reactions has been severely impeded.

Further Evolution of the Calorimeter Design.

In late 1989 we adopted a new type of calorimeter for some sets of experiments. The change in design was adopted so as to remove most of the effects of changes in the cell contents on the measurements (parameter (3)). A schematic of this cell is shown in Fig. 2. The design is closely similar to that of the earlier cells, Fig. 1, except for one important change: the silvering of the top portion ensures that heat transfer to the surrounding water bath is dominated by radiation through the lower unsilvered portion. In this way we can ensure that the heat transfer coefficient remains substantially constant during a given measurement cycle providing the fall of the level of electrolyte in the cell due to the combined effects of electrolysis and evaporation is

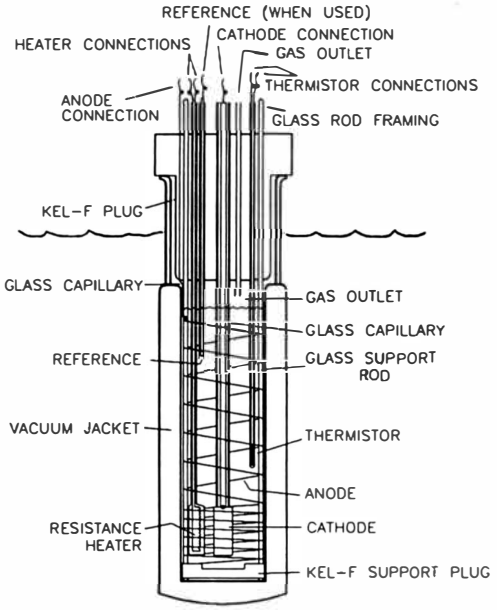

Fig. 1. Original Dewar calorimeter.

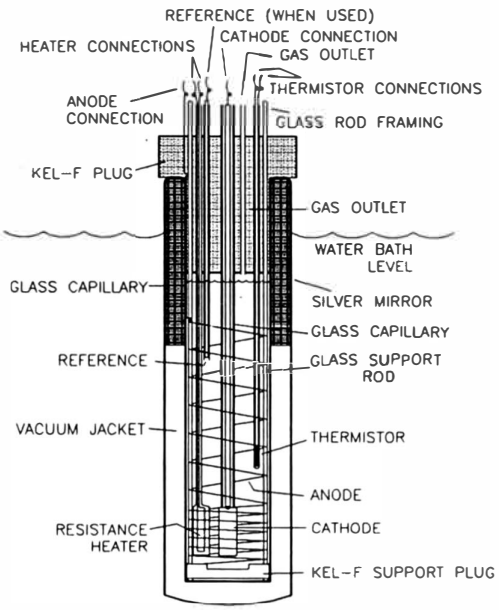

Fig. 2. Silvered Dewar calorimeter.

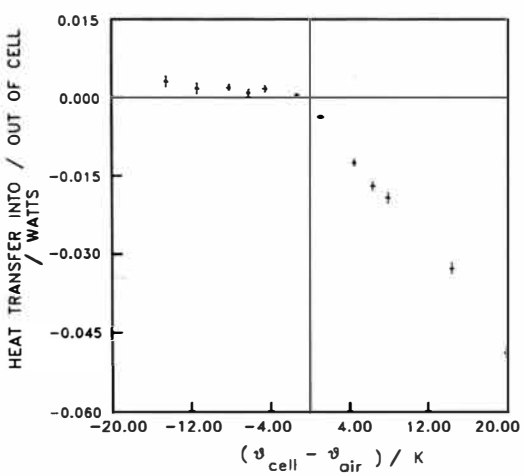

Fig. 3 Plot of rate of heat transfer vs. difference in cell and ambient temperatures.

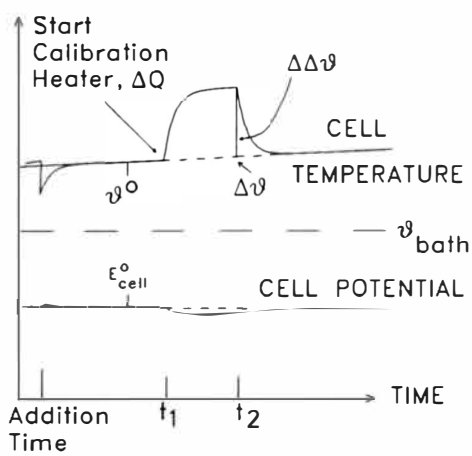

Fig 4. Schematic of methodology used in calibrating the various calorimeters.

confined to the upper silvered section of the Dewar. The slope of the temperature-time base-line is thereby markedly reduced.

The heat transfer coefficients determined for these new cells is close to the values calculated from the Stefan-Boltzmann coefficient and the radiant surface area. The larger values determined for the cells used in our earlier work[1-6] were due to conduction across the "vacuum gap" due to imperfect evacuation of the cells ie, the conduction path was in parallel to the radiative path not to the air through the top of the cell (see further below).

Further simple changes in the cell design are being investigated at the present time. The objective of these changes is to ensure a more complete sealing of the cell contents and a restriction of air circulation within the closure of the top of the Dewar.

Other Experimental Considerations.

Numerous experimental variables must be controlled so as to reduce the systematic and random errors which can affect the open-cell calorimetric experiments. Some of these variables are self-evident such as the accurate calibration of thermistors and of heater powers used to derive heat transfer coefficients. The effects of other variables is less obvious. Thus, for example, it is not well understood that it is necessary to control the ambient room temperature (and, to a lesser extent humidity) in order to achieve close control of the temperatures of the water baths. In our own work we achieve ± 0.003 degree although the experiments are scaled so as to never require better than ± 0.01 degree.

One statement which has been frequently made about the precision of our measurements is that this is markedly reduced by lack of control of heat transfer by conduction through the top of the cell. That this statement is erroneous is shown by the data in Fig. 3 (note also that we control the room temperature to ± 1°). Thus Fig. 3 relates the heat flow out of or into the cell to the difference between the cell and air temperature (according to whether this is negative or positive). The direction of heat flow in these measurements was controlled by changes in the temperature of the water bath (it should be noted that the cell temperature is close to that of the bath in these experiments). The reason for the change in magnitude of the heat transfer coefficient is almost certainly due to increased air circulation in the glass tubes passing through the Kel F plug. However, the effects of these conductive

contributions are in any event quite minor for appreciable differences between the cell and bath temperatures. If necessary, the effect of conduction through the top of the cell can be eliminated by adjusting the cell to the room temperature (using auxiliary cooling of the water bath) but the contribution can also be calculated to better than 0.1mW. We have shown elsewhere that the effects of conduction can in any event be taken into account by defining a modified radiative heat transfer coefficient which is derived from appropriate calibrations of the cell using a resistive heater. This procedure leads to an underestimate of the heat transfer from the cell.: we have always followed procedures which lead to such systematic underestimates but these effects can be corrected for if this is required.

Consideration of Various Methods for the Determination of Heat Transfer

The determination of the heat transfer coefficients and subsequently the rate of the rates of enthalpy generation in these open electrochemical systems is complicated, as mentioned above, by the fact that the contents of the cell change with time; this is true particularly for the results taken completely with unsilvered Dewars[1-6]. In such a situation, it is clear that a true steady state cannot be attained inside the cell. This would require that $E_{cell}(t)$ = constant as well as $\theta(t)$ = constant, and this is never observed. The values of the heat transfer coefficients, therefore, determined from the experimental data depend on the nature of the assumptions underlying the evaluations. Some of our colleagues and associates have argued that it is possible to assume a quasi-steady state and to set $\frac{d\Delta\theta}{dt}=0$ in the non-linear inhomogeneous differential equations which describe the appropriate "black-box" models of the calorimeter. This risky assumption of course is motivated by the fact that the evaluation of k_R' and $(E_{cell}(t) - E_{thermoneutral,bath})I + Q_f$ is considerably simplified since one can then ignore the water/heavy water mass equivalent M^0 of the cell (the total amount of material in the cell) If we also assume the value of the excess enthalpy $Q_f(t)$ (if this term is present) to be independent of the experimental conditions and further neglect the rate of change in the evaporation of the solvent one determines a value of the heat transfer coefficient which we denote by

$$(k_R')_1 = \frac{\Delta Q - \left\{[E_{cell}(t)]_1 - [E_{cell}(t)]_2 I\right\}}{\left[(\theta_{bath} + \Delta\theta_2)^4 - (\theta_{bath} + \Delta\theta_1)^4\right]} \qquad (1)$$

where the definitions of the terms are given in Fig. 6. If we treat the change in the evaporation term in the same way as the change in the cell potential, we obtain by analogy to (1) the heat transfer coefficient

$$(k_R')_2 = \frac{\Delta Q - \left\{[E_{cell}(t)]_1 - [E_{cell}(t)]_2 I\right\} - \frac{3I}{4F}\left\{\left(\frac{P_2}{P^*-P_2}\right)\left[(C_{P,H_2O,v} - C_{P,H_2O,\ell})\Delta\theta_2 + L\right] - \left(\frac{P_1}{P^*-P_1}\right)\left[(C_{P,H_2O,v} - C_{P,H_2O,\ell})\,\Delta\theta_1 + L\right]\right\}}{\left[(\theta_{bath} + \Delta\theta_2)^4 - (\theta_{bath} + \Delta\theta_1)^4\right]} \tag{2}$$

where P_1, P_2, and P^* are the vapor pressures at the two temperatures and under standard conditions, respectively, and L is the latent heat of evaporation. We regard these two estimates of the heat transfer coefficients to be lower limits.

We have argued that the change in the electrode potential due to the heater pulse ΔQ should not be included in estimating the heat transfer coefficient since the value of k_R' derived by excluding this change is then used to estimate $E_{cell}(t) - E_{thermoneutral,bath}\}I + Q_f$. We obtain the heat transfer coefficient

$$(k_R')_3 = \frac{\Delta Q}{\left[(\theta_{bath} + \Delta\theta_2)^4 - (\theta_{bath} + \Delta\theta_1)^4\right]} \tag{3}$$

In deriving this heat transfer coefficient we have also already included any change of the term $\frac{3I}{4F}\left\{\left(\frac{P}{P^*-P}\right)\left[(C_{P,H_2O,v} - C_{P,H_2O,\ell})\,\Delta\theta + L\right]\right.$ with any change in $\Delta\theta$ caused by the application of a calibration pulse ΔQ. If we were to split off the change in this quantity with $\Delta\theta$ from the variation of $E_{cell}(t)$ with $\Delta\theta$, then by analogy with equations (1) and (2) we would define a heat transfer coefficient

$$(k_R')_4 = \frac{\Delta Q - \frac{3I}{4F}\left\{\left(\frac{P_2}{P^*-P_2}\right)\left[(C_{P,H_2O,v} - C_{P,H_2O,\ell})\,\Delta\theta + L\right] - \left(\frac{P_1}{P^*-P_1}\right)\left[(C_{P,H_2O,v} - C_{P,H_2O,\ell})\,\Delta\theta_1 + L\right]\right\}}{\left[(\theta_{bath} + \Delta\theta_2)^4 - (\theta_{bath} + \Delta\theta_1)^4\right]} \tag{4}$$

We have regarded $(k_R')_3$ as an upper limit.

Finally, we have estimated another $(k_R')_5$ based on the application of

non-linear regression fitting of the appropriate "black-box" model of the calorimeters to experimental data derived using these calorimeters. This regression fitting procedure naturally also yields estimates of M^0 and Q_f as well as the error limits for all parameters.

The most straightforward way of testing the applicability of the various heat transfer coefficients is the simulation of θ-t curves using the various models, the known values of the various parameters, values of $E_{cell}(t)$ determined directly from the operating cells and choosing values of M^0 and $\left(k_R'\right)_5$ derived by the application of the non-linear regression fitting procedure. We then in turn use equations (1)-(4) to estimate the heat transfer coefficients which are based on the various approximations and we can reapply the non-linear regression procedure to the data simulated with these coefficients, Fig. 5. The divergence between the various heat transfer coefficients is also brought out clearly by Fig. 6 which is based on simulated data alone and includes the effects of the heater calibration pulse. It can be seen that the values $\left(k_R'\right)_1$ and $\left(k_R'\right)_2$ are incorrect. The main cause in the invalidity of the steady state approximation is that the relevant differential equation must be integrated across the whole of the time region to give a correct account of the shape (and especially the amplitude) of the θ-t profile due to the heater calibration pulse.

The results confirm our belief that $(k_R')_1$ and $(k_R')_2$ are lower limits while $(k_R')_3$ is an upper bound. $(k_R')_4$ may be an overestimate or underestimate depending on the conditions but we have not pursued this question further since any of the values $(k_R')_1$-$(k_R')_4$ can be used as starting points for the non-linear regression fitting; the question of why the use of $(k_R')_1$-$(k_R')_4$ is subject to "double subtraction errors" is in our view not worthwhile pursuing since an exact method of data evaluation is in any event available. The fact that this procedure recovers the "exact" values of the heat transfer coefficient should not be surprising. It is well known, for example, in the field of chemical kinetics that it is necessary to fit the integrated rate equations to the experimental data rather than to carry out mass balances at a given point. This argument applies especially to the differential equation which includes the heater calibration pulse which is clearly more non-linear as well as more inhomogeneous than the differential equation that does not contain the heater calibration pulse.

We have found also that determination of a heat transfer coefficient

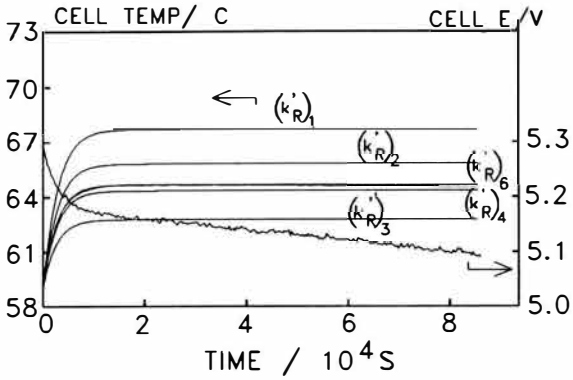

Fig. 5. Simulations of the cell response using the various heat transfer coefficients for a three parameter model.

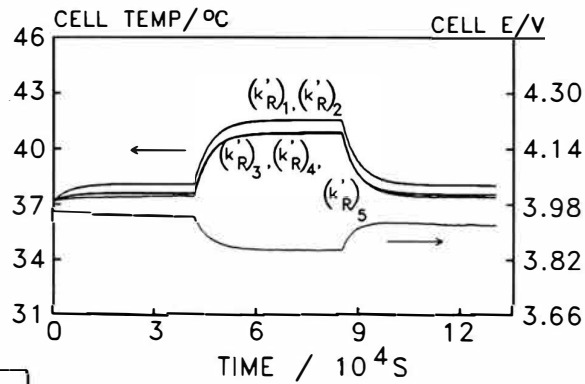

Fig. 6. Simulations of the cell response for a four parameter model.

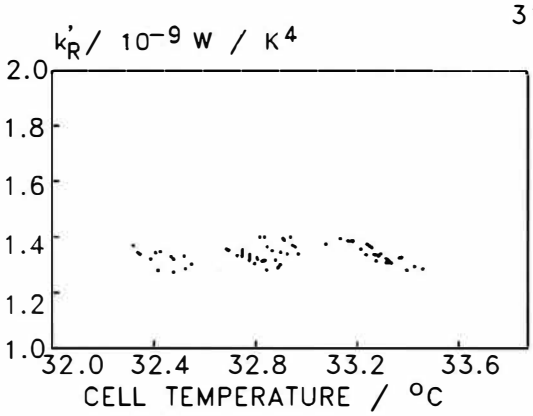

Fig. 7. Plot of the heat transfer coefficients as a function of the cell temperature.

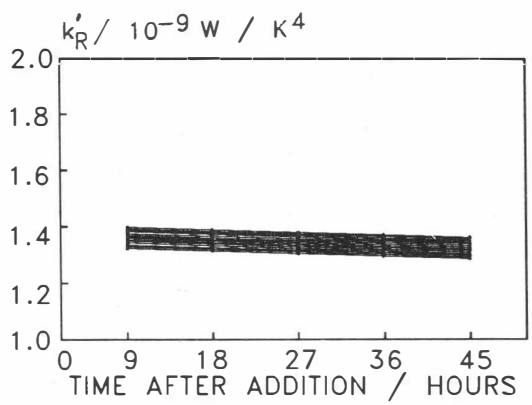

Fig. 8. As Fig. 7 except plotted as a function of the time of determination after cell filled.

$(k_R')_6$, based on the application of the non-linear regression procedure to θ-t profiles in the absence of the calibration pulse, ΔQ, ie where the only perturbation of the system is due to the addition of the solvent gives values that are close to $(k_R')_5$; this is to be expected. For instance, it is well known in the field of relaxation techniques that any perturbation of the system is sufficient for the determination of kinetic data. It follows that it is advantageous in this form of calorimetry to allow the cell contents to change with time as the θ perturbation due to the make-up of the cell suffices for the determination of all the required parameters.

We note here also that the heat transfer coefficients $(k_R')_1$-$(k_R')_6$ are apparent values in that any contribution due to conduction through the top of the cell is included in the radiation term (see above). The use of such apparent radiative heat transfer coefficients leads to an underestimate of the heat output from the cell.[4] Coefficients derived according to the procedures embodied in equations (1)-(4) invariably show considerable scatter eg Fig. 7. This scatter is entirely due to systematic errors induced by uncertainty in the level of filling of the cells since sequences of measurements fall on parallel straight lines, Fig. 8. Indeed superposition of the results at the center point shows that the residual error is given by 0.155%. However, in view of the uncertainty of the values of M_0 at any given time, the heat balances can only be derived following a calibration of the cell and, as has been noted above, a non-linear regression procedure should be used to evaluate the three or four parameters governing the behavior of the "black box" model. Since up to 1000 measurement points are used in each evaluation, a very high level of accuracy can be achieved, this accuracy being set mainly by the precision of our measurement of the power inputs to the resistive heaters.

Moving on Towards Clearer Demonstrations of Excess Enthalpy Generation

The careful analyses of the behavior of the calorimeters described have provided us with a reliable, accurate testing system for determination of enthalpy generation and heat flows for electrochemical experiments. We have been interested more recently in systems that lead to conditions which deviate markedly from the relatively low levels of excess enthalpy generation such as that shown in Figs. 9 and 10. In these systems, the cell contents are driven to boiling under conditions

where the excess enthalpy generation is far greater than the total enthalpy input. Under these conditions, it is found that the heat transfer is almost totally dominated by evaporation of the cell contents through the vents in the top of the cell, and the need to determine a heat transfer coefficient due to conduction or radiation becomes somewhat academic.

Application of our models to sections of the data of cells containing blank electrode/electrolyte combinations (D_2O solutions with Pt cathodes or H_2O solutions with Pd cathodes) gives $Q_f \approx 0$ indicating the adequacy of the modelling procedures that we have adopted as well as the applicability of this type of calorimetry to the study of electrode reactions. It is of interest that, as expected, the use of $(k_R')_1$ and $(k_R')_2$ in the analysis of these blank cells indicates endothermic operation (which is clearly impossible) whereas the use of $(k_R')_3$ indicates exothermic operation (which is highly unlikely). Only the use of $(k_R')_5$ or $(k_R')_6$ indicates thermal balance. It is also of interest that this thermal balance is maintained even when the cell current is raised so as to drive the cell towards the boiling point. A more demanding test of the calorimetry is based on the cumulative production of excess enthalpy: no cumulative excess enthalpy is predicted during the entire course of the experiment. The exact balance using the best estimate of k_R' indicates the adequacy of the modelling and evaluation procedures. We note also that we can obtain an exact material balance by accounting for electrolysis and evaporation even when the cell is driven to high temperatures.

Application of the same procedures to cells containing palladium based cathodes in D_2O electrolytes, however, show excess enthalpy generation for all cells tested when analyzed by the same procedures. Of more interest is the fact that the cell contents themselves are evaporated from the cell at a rate that cannot be explained by consideration of the values of the total enthalpy input, even if the heat transfer coefficient is considered to be zero. It is clear that near the boiling point, as mentioned above, the heat flow is totally dominated by evaporation from the cell and that it is impossible to explain the evaporation of the entire contents of the cell in the time scales observed by Joule heating. Fig. 11 shows one example of such behavior (the rate of excess energy generation required to explain the evaporation is ≈50 watts corresponding to specific excess of ≈1200 watts cm^{-3}).

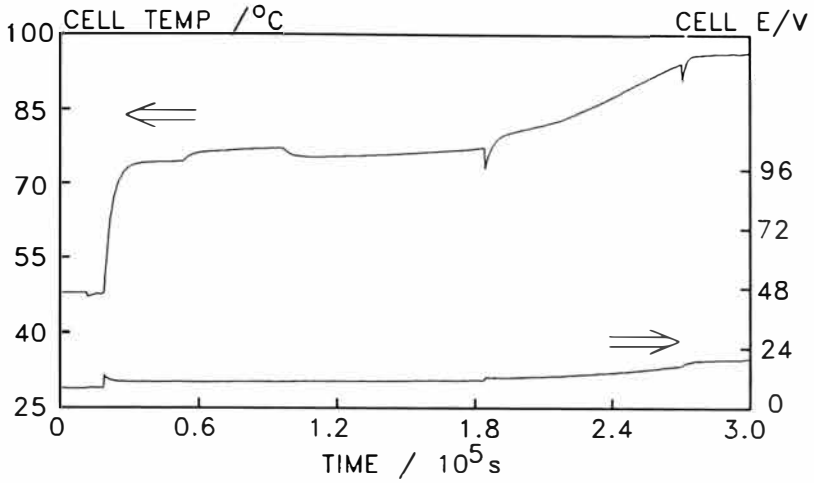

Fig. 9. Typical cell response for a cell which drives itself to boiling.

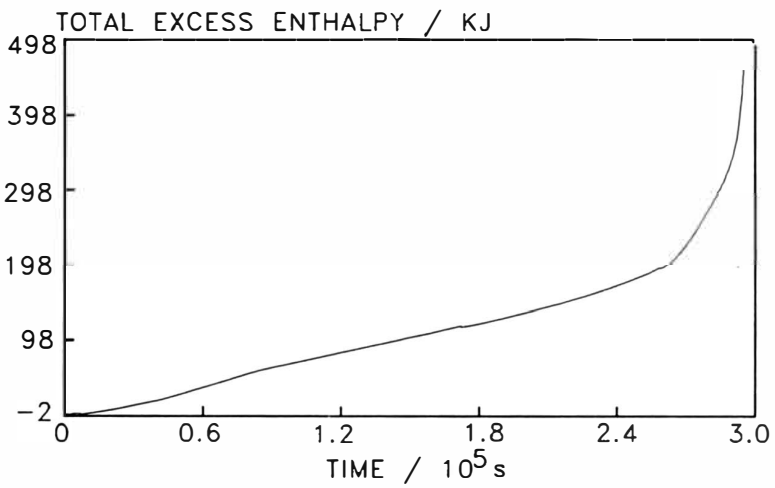

Fig. 10. Plot of the accumulated excess enthalpy for the cell in Fig.9.

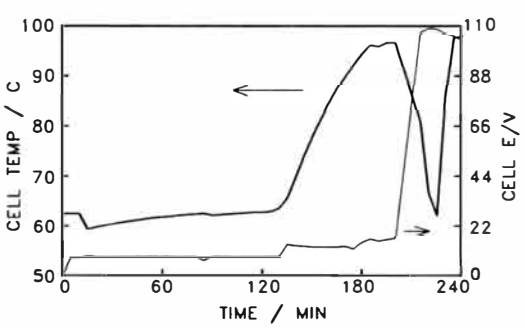

Fig. 11. Cell response for a system which boils out the total cell contents in a short period of time.

While these systems are intriguing, we note here that under such conditions, these calorimeters are very energy inefficient sources of heat, and the next generation of calorimeters must be designed to take this fact into consideration.

Finally, our most recent work is directed toward the design of new sealed calorimeter systems which are not complicated by the factors introduced by applying external power input. Such devices are based entirely on attaining the necessary critical operating conditions in the cathode lattice using new types of enhancement. These conditions are the same that we have previously described, except that these new devices are, in essence, "self-driven" to the extent that the observed excess enthalpy generation is continuous and initiated completely within the device. The observed excess enthalpies are at least 5 orders of magnitude larger than the magnitude of any possible driving forces inside the device. Thermal measurements are then reduced to the trivial measurement of absolute temperatures of operating and blank cells.

REFERENCES

1. M. Fleischmann, S. Pons, and M. Hawkins, J. Electroanal Chem. 261 (1989) 301-308, and errata, ibid 263 (1989) 187-188.
2. M. Fleischmann, S. Pons, , M. W. Anderson, L. J. Li, and and M. Hawkins, J. Electroanal Chem.287 (1990) 293-348.
3. S. Pons and M. Fleischmann, J. Fusion Technology 17(1990) 669-679.
4. S. Pons and M. Fleischmann, Proceedings 1st Annual Cold Fusion Conference, Salt Lake City, Utah, March (1990) 1.
5. M. Fleischmann, ibid, March (1990) 334.
6. S. Pons and M. Fleischmann, N.S.F.-E.P.R.I Meeting, October, 1989.
7. N. S. Lewis, C. A. Barnes, M. J. Heben, A. Kumar, S. R. Lunt, G. E. McManis, G. M. Miskelly, R. M. Penner, M. J. Sailor, P. G. Santangelo, G. A. Shreve, B. J. Tufts, M. G. Youngquist, R. W. Kavanaugh, S. E. Kellog, R. G. Vogelaar, T. R. Wang, R. Kondrat, and R. New, Nature 340 (1989) 525-530.
8. D. E. Williams, D. J. S. Findlay, D. W. Craston, M. R. Sene, M. Bailey, S. Croft, B. W. Hooten, C. P. Jones, A. R. J. Kucernak, J. A. Mason, and R. I. Taylor, Nature 342 (1989) 375-384.

Conference Proceedings Vol. 33
«The Science of Cold Fusion»
T. Bressani, E. Del Giudice and G. Preparata (Eds.)
SIF, Bologna 1991

HEAT AND HELIUM PRODUCTION IN COLD FUSION EXPERIMENTS

M. H. Miles, B. F. Bush*, G. S. Ostrom, and J. J. Lagowski*
Chemistry Division, Research Department
Naval Weapons Center, China Lake, CA 93555

*Department of Chemistry
University of Texas, Austin, TX 78712

ABSTRACT

A critical issue in determining whether or not the cold fusion process exists is the measurement of nuclear products in amounts sufficient to match the excess heat effects. Calorimetric evidence of excess heat up to 27% was measured during the electrolysis of heavy water using palladium cathodes. Effluent gas samples collected during episodes of excess heat production and sent to the University of Texas for analysis by mass spectrometry showed the presence of ^4He. Furthermore, the amount of helium detected correlated approximately with the amount of excess heat and was within an order of magnitude of the theoretical estimate of helium production based upon fusion of deuterium to form ^4He. Control experiments performed exactly the same but using H_2O + LiOH in place of D_2O + LiOD gave no evidence for helium.

INTRODUCTION

It is now known that the observation of cold fusion effects in electrochemical cells [1, 2] requires special attention to many details such as cell geometry, electrode arrangements, current density, deuterium loading, and control of impurities as well as considerable patience [3]. Our initial efforts, representing five months of research, did not produce any measurable excess heat effects [4]. In retrospect, it is not surprising that many research groups were unsuccessful in their few weeks of frenetic cold fusion activities [5]. The low intensity of neutrons has prompted proposals of cold fusion processes that yield only heat and helium as products [6-9]. We report here the results of electrochemical calorimetric experiments designed to detect helium in the effluent gases while rigorously excluding possible helium contamination from other sources.

EXPERIMENTAL

The electrolysis cell initially contained 18 g of 0.2 M LiOD + D_2O (99.9%, Cambridge Isotope Laboratories). The palladium rod cathode (Johnson Matthey, 99.96%, d = 0.63 cm, l = 1.1 cm) was spot-welded to a nickel lead. A tightly-wound coil of Pt-20% Rh (5.35 g, d = 0.1 cm) served as the counter electrode and was symmetrically positioned about 0.3 cm from the cathode. Both the anode and cathode leads were covered with heat shrinkable Teflon tubing to prevent exposure of the bare metal to the gases in the headspace. Two identical isoperibolic calorimetric cells were always run in series (cells A and B) in a constant temperature bath set at 27.50 °C. Details of the calorimetric cell design and determinations of the calorimetric constants (K_i) are given elsewhere [10]. Previously determined mean values of these constants [10] were used in this study (K_1 = 0.138 W/°C, K_2 = 0.143 W/°C and $K_4 = K_5$ = 0.135 W/°C for the two thermistors in each cell). The constants were determined in four separate experiments over a one-year period and showed no significant change with time.

Strenuous efforts were made to avoid contamination of the effluent gas from atmospheric helium. The system was always under positive pressure since the effluent gas was evolved through an oil bubbler. Details of the gas collection system are given elsewhere [11]. The entire system was thoroughly flushed with boil-off nitrogen that contained no detectable helium [11]. Furthermore, the system was self-flushing due to the steady evolution of D_2 and O_2 gases. The gas evolution rate was calculated to be 6.73 mL min^{-1} at 528 mA (200mA/cm^2) at 297 K and 700 Torr assuming ideal gas behavior. Actual measurements of the gas evolution rate by the displacement of water yielded 6.75 ± 0.25 mL min^{-1} for cell A and 6.69 ± 0.15 mL min^{-1} for cell B. This data adds to the substantial evidence that excess enthalpy effects are not explainable by the recombination of D_2 and O_2 gases within the cell [10, 12].

The effluent gas samples collected at the Naval Weapons Center in 500 mL flasks were sent to the University of Texas for analysis by mass spectrometry. A cryofiltration system was employed to remove all gases except helium [11]. Nevertheless, mass spectral measurements had sufficient resolution to baseline separate D_2 and ^4He. Based on air samples collected in the Chemistry Laboratory at the University of Texas and assuming a normal helium concentration of 5.22 ppm by volume [13], the detection limit for helium in our measurements is approximately 8 x 10^{11} atoms of ^4He in 500 mL of gas sample [11].

RESULTS

A portion of the calorimetric studies using palladium rod cathodes in 0.2 M LiOD + D_2O are presented in Fig. 1. The equation

$$X = \frac{\text{Heat out}}{\text{Joule heat in}} = \frac{K\Delta T}{(E - E_H^o)I} \qquad (1)$$

was used where K is the calorimetric cell constant, E is the cell voltage, E_H^o is the thermal neutral potential, and ΔT is the temperature difference [10]. Excess enthalpy is present when X>1.00 where X is the daily mean value of the heat ratio. Gas sample collection dates for helium analysis are given for cells A and B, thus the highest excess enthalpy (27%) was observed on 10/21/90 in cell B. This value may actually be somewhat higher since the week-end room temperature (21.5°C) was cooler than normal. The first 12 days are not shown in Fig. 1 due to several shut-downs of the electrolysis to correct leaks in the gas collection system. No significant excess enthalpy effects were observed in the first 10 days. These calorimetric measurements continued until the two cells were turned off on December 25. Calorimetric results around the 12/17/90 time period are questionable due to unusual increases in cell voltages with time as the D_2O solution level dropped below the electrode level.

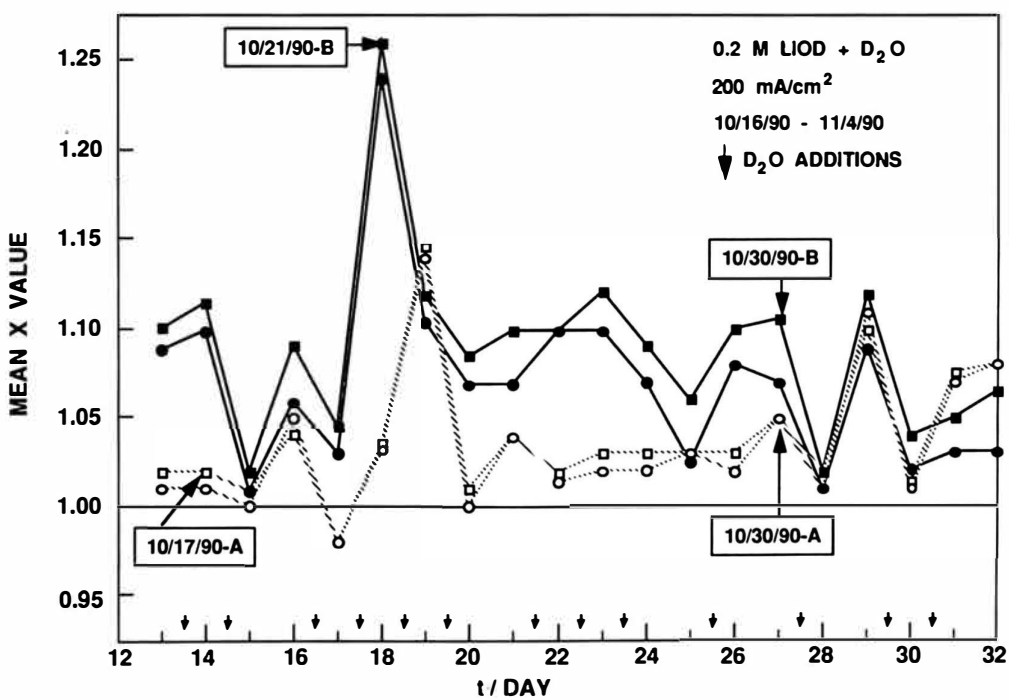

Fig. 1. Sample of calorimetric measurements and effluent gas collection dates in D_2O + LiOD.

The helium analysis results in Table 1 show that the effluent gases contained ^4He when the electrolysis of D_2O produced significant excess heat and power. No ^3He was detected [11]. Small peaks near the detection limit of the mass spectrometer are assigned a value of 10^{12} atoms of ^4He per 500 mL of effluent gases. Medium peaks were roughly an order of magnitude greater while large peaks were about two orders of magnitude above

Table. 1. Helium Production During D_2O Electrolysis.

Sample	P_{EX} (W)	X	^4He Atoms/500 mL
12/14/90-A	0.52[a]	1.20[a]	10^{14} (large peak)
10/21/90-B	0.46	1.27	10^{14} (large peak)
11/25/90-B	0.36	1.15	10^{14} (large peak)
11/20/90-A	0.24	1.10	10^{13} (medium peak)
11/27/90-A	0.22	1.09	10^{14} (large peak)
10/30/90-B	0.17	1.12	10^{12} (small peak)
10/30/90-A	0.14	1.08	10^{12} (small peak)
10/17/90-A	0.07	1.03	$<10^{12}$ (no peak)
12/17/90-A	0.40[b]	1.19[b]	10^{13} (medium peak)
12/17/90-B	0.29[b]	1.11[b]	$<10^{12}$ (no peak)

[a] $i = 250\ mA/cm^2$. All other experiments used $i = 200\ mA/cm^2$.
[b] Possible calorimetric errors due to low D_2O solution levels. No ^3H was detected. Mass spectrometer always at highest sensitivity.

the detection limit. The values reported for the excess power (P_{EX}) and heat (X>1.00) are those measured within 1-2 hours of removing the gas collection flask in order to obtain the best time correlation. The excess heat and power measurements were always quite steady during this time period. The samples are arranged in order of decreasing power except for the 12/17/90 samples where the low D_2O levels likely created calorimetric errors. Nevertheless, these samples also show more helium in the cell that produced more excess heat. The only sample not listed in Table 1 is 12/14/90-B that broke during shipment. The input power for each measurement is given by $P_{EX}/X-1.00$, hence the input power is 2.60 W for the 12/14/90-A sample.

Results of dental film experiments are shown in Fig. 2. The film that was wrapped around the outside of the electrolysis cell A and hence closest to the palladium showed the greatest exposure. Clear regions are due to a peeling away of the emulsion rather than non-exposure. The film in cell B was further away from the palladium and deeper in the secondary compartment, hence the bottom half was somewhat shielded by the Teflon pedestal used to hold the palladium in position [10]. This film showed partial exposure for the top portion and less exposure near the bottom portion where any direct radiation would

have to pass through the Teflon pedestal. These films were in distilled water contained in the secondary (gap) compartment [10]. The control film was immersed in distilled water for the same time period and showed only scattered exposure due to background radiation. Samples of fresh films with no exposure and total exposure are also shown for comparisons. Cell A was producing the larger excess heat effect when the film was first inserted, but cell B produced the larger effect in the seven days that followed.

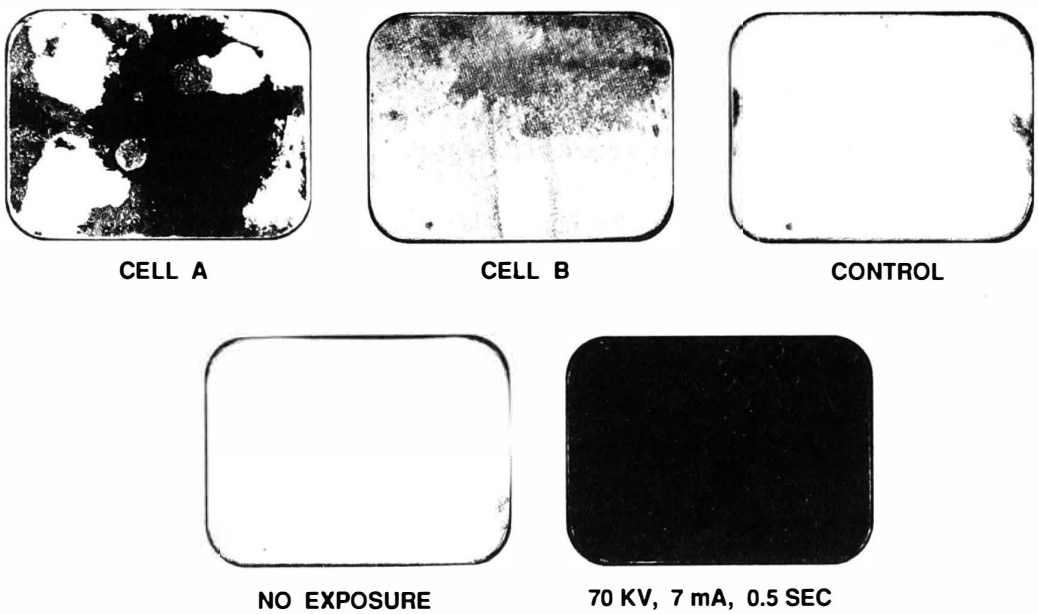

Fig. 2. Results of dental film experiments.

In a following control experiment of major importance in proving helium production, H_2O + LiOH was used in place of D_2O + LiOD, yet the same cells, electrodes, gas lines, and collection flasks were employed exactly as with D_2O. Results of the H_2O-control experiments are shown in Table 2. No helium was observed in any experiment. The H_2O + LiOH electrolysis, conducted in an identical manner to the D_2O + LiOD electrolysis, is the best indication of our ability to exclude ^4He contamination from the air. The H_2O + LiOH experiments did not produce any significant excess heat or exposure of dental film. The mean calorimetric values for 15 days of electrolysis are $\overline{X}_1 = 1.025 \pm 0.02$, $\overline{X}_2 = 1.035 \pm 0.03$ for cell A and $\overline{X}_4 = 1.01 \pm 0.02$, $\overline{X}_5 = 1.00 \pm 0.03$ for cell B at the 99% confidence interval ($\pm 2.58\ \sigma/\sqrt{n}$, n = 15). Earlier reports of unexplained excess heat effects in H_2O + LiOH [11] were due to the dental film studies. The secondary compartments containing the films were not tightly sealed, hence loss of water by evaporation or possibly by a wicking action created a calorimetric error. We reported previously that there is a 2% increase in X per mL of H_2O lost from the gap [10].

Table 2. Results of H_2O + LiOH Control Experiments.

Sample[a]	Results[b]
1/16/91-A	No ^4He or ^3He observed
1/16/91-AA	No ^4He or ^3He observed
1/16/91-B	No ^4He or ^3He observed
1/17/91-A	No ^4He or ^3He observed
1/17/91-B	No ^4He or ^3He observed

[a] Used same cells, electrodes, gas lines, and collection flasks as in D_2O experiments. i = 200 mA/cm^2.

[b] Mass spectrometer always at highest sensitivity. Any gas passing through the cryofilter was allowed time to accumulate and then surged into the mass spectrometer.

Previous calculations suggest that neutron activation of indium or gold foils should occur for flux levels of 10^4 s^{-1} if the foils are placed at the outer glass surface of our electrochemical cell [14]. No activation of indium or gold foils was detected in this study, hence the average neutron flux was less than 10^5 s^{-1} during the time period that these foils were in the cells. The detection of neutron flux levels as low as 10^3 s^{-1} is possible for gold foils, however the foils used in our experiments were lost for about a week despite express shipment to E. G. and G. Rocky Flats Inc., Golden, Colorado, for activation analysis.

DISCUSSION

The amount of helium (^4He) observed in the gaseous products maintained an approximate correspondence to the amount of excess power or heat observed in electrochemical calorimetric cells (Table 1). This indicates that ^4He is produced at or near the surface of the palladium electrode rather than deeper in the bulk metal and that the preponderance of the helium escapes from the electrode and resides in the effluent gas. Several theories have predicted this behavior [9, 15].

Although the exact nature of the fusion reaction(s) producing the excess heat effect is not known, the process

$$^2D + {}^2D \longrightarrow {}^4He + 23.8 \text{ MeV (lattice)} \qquad (2)$$

can be used as a basis for an estimate of helium production. For this fusion process, 1 W corresponds to a rate of 2.62 x 10^{11} ^4He s^{-1}. The highest excess power observed at 528 mA (0.46 W, 10/21/90-B, Table 1) would therefore produce 5.4 x 10^{14} atoms of ^4He in the time period required to fill the 500 mL collection flask with D_2 and O_2 gases (4440 s).

About 10^{14} atoms of ^4He were detected which is within experimental error of the theoretical amount.

Despite the approximate correlation of excess heat and helium, possible error sources proposed by cold fusion critics include air contamination, helium diffusion into the glass flask, and the escape of helium contained in the palladium rod. Ignoring the helium/heat relationship (Table 1), the simple yes or no detection of helium in 7/7 experiments producing excess heat and the absence of helium in 6/6 experiments not producing excess heat (1 in D_2O, 5 in H_2O) implies a chance probability of $(1/2)^{13} = 1/8192$ or 0.0122%.

The diffusion of helium through glass is a valid concern and can be expressed by

$$q = \frac{KP}{d} \tag{3}$$

where q is the diffusion rate, K is the permeability, P is the partial pressure of helium, and d is the glass thickness [16]. The value of K varies greatly with the type of glass, its treatment, and temperature [16]. For the Pyrex glass flasks used in this study, theoretical calculations yield $q = 1.5 \times 10^{10}$ He cm^{-2} day^{-1} or 4.7×10^{12} He day^{-1} ($A = 314$ cm^2). Experimentally, however, there is no measurable evidence for any effect due to helium diffusion through glass. The amount of helium observed versus the time interval that the effluent gas sample resided in the glass is shown in Fig. 3. For D_2O-LiOD experiments, high and low helium levels occur at both short and long time intervals that ranged from 14 to 61 days. In fact, the least square line shows a negative correlation if any exists at all. For H_2O-LiOH experiments, no helium was detected for gas resident periods up to 20 days. The N_2-filled flasks were often shipped by air and had shorter time intervals for helium diffusion.

A possible explanation for the lack of measurable helium diffusing through the glass is the opposing flow of deuterium or hydrogen out of the glass. Since D_2 makes up 2/3 of the gas within the flask, its rate of diffusion outward is about 3 orders of magnitude greater than the diffusion of atmosphere helium into the flask. Helium and hydrogen (deuterium) diffuse through glass by similar mechanisms and sites [16] and show similar kinetic parameters [17]. Furthermore, hydrogen removes helium from glass [18]. Although no specific literature study could be located that investigated the effect of hydrogen on the diffusion of helium through glass, Paneth and Peters [19] reported that after 15 days less than 3×10^9 He atoms had diffused into a 3 liter flask ($A = 1300$ cm^2) containing 10 Torr of hydrogen gas.

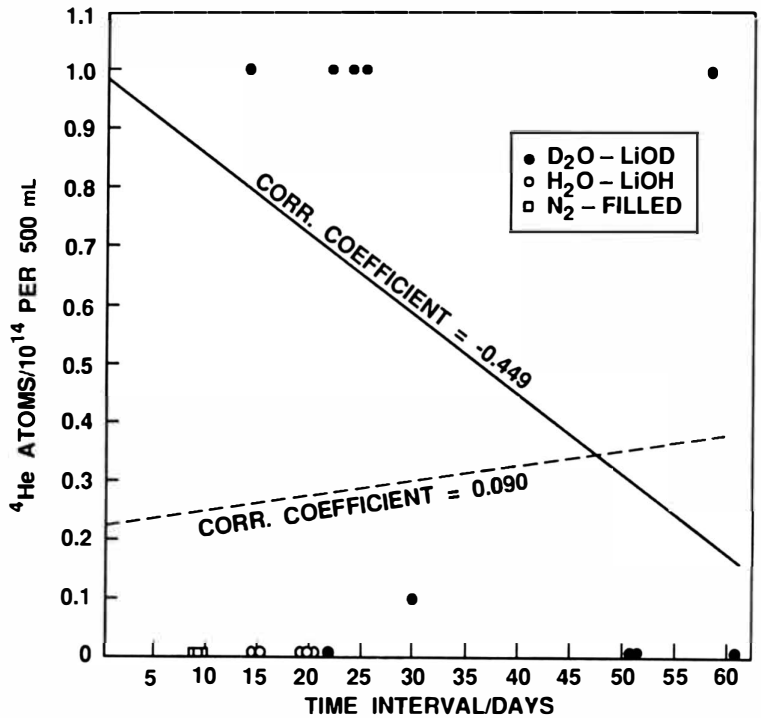

Fig. 3. Experimental effect of atmospheric helium diffusing into the Pyrex glass flasks. Solid line is for D_2O-LiOD experiments while dashed line is for all experiments.

Samples of our unused palladium were analyzed for helium by Rockwell International. No ^{3}He or ^{4}He was observed in any of our palladium samples. In terms of helium concentrations, the uncertainties correspond to less than 10^8 atoms/mg for ^{3}He and ^{4}He. This indicates that our palladium cathodes originally contained less than 5 x 10^{11} He atoms, hence any helium originally present in the palladium electrode is not sufficient to explain our helium measurements. Furthermore, the same palladium electrodes were used in prior experiments [10]. A sample of the palladium electrode used in these D_2O + LiOD and H_2O + LiOH experiments also failed to show any significant level of ^{3}He or ^{4}He. This result, however, is somewhat inconclusive since the palladium electrodes were polished after the D_2O study that produced excess heat and helium and then were used in the H_2O + LiOH study (Table 2).

The reproducibility of our excess heat and helium results was recently demonstrated by using a modification of the Szpak co-deposition method [20]. Palladium and deuterium were simultaneously deposited onto our Pd rods using 0.3 M LiCl to produce the excess enthalpy effect. Effluent gas samples sent to a commercial laboratory yielded 7.0 ± 2 ppb ^{4}He or 8.5 x 10^{13} ^{4}He/500 mL for a cell producing 0.14 W of excess power (X = 1.12) at 528 mA. This sample was within a factor of two of the theoretical ^{4}He based on Eqn. 2.

A second gas sample gave 7.5 ± 2 ppb ^4He or 9.2 x 10^{13} ^4He/500 mL for a cell producing 0.54 W of excess power (X = 1.25) at 874 mA. Some recombination of D_2 and O_2 was observed in this cell, hence the measured excess heat and power is too high. Nevertheless, the amount of ^4He was within a factor of four of the theoretical. It should be stressed that these recent experiments involved a different electrolysis method, employed a different person collecting the gas samples, and had a different laboratory doing the helium analysis, yet the results gave ^4He amounts even closer to the theoretical.

The major errors in our calorimetric measurements are likely fluctuations in the room temperature and fluctuations in the cell voltage due to gas bubble effects. These error sources limit our accuracy to about ±0.04 W or about ±2%. Nevertheless, the major error source in correlating the amount of helium with the excess enthalpy is in the helium analysis. Improved measurements of helium and excess enthalpy could precisely identify the energy of the dominant fusion reaction. Experiments to do this are in progress.

CONCLUSIONS

Our cold fusion experiments show a direct correlation between the time of generation of excess heat and power and the production of ^4He, established in the absence of outside contamination. This correlation in the palladium/D_2O system provides strong evidence that nuclear processes are occurring in these electrolytic experiments and that helium is produced at or near the surface of the palladium rather than deeper in the bulk metal. The major gaseous fusion product in D_2O + LiOD is ^4He rather than ^3He. No helium products are found in H_2O + LiOH experiments.

ACKNOWLEDGMENTS

We thank Dr. Brian M. Oliver (Rockwell International) for measurement of helium levels in our palladium rods, Dr. Robert E. Miles (E. G. and G. Rocky Flats, Inc.) for analysis of gold foils, and Drs. Joseph M. Nunez and John F. Martino for assistance in the dental film experiments. We also thank Dr. Richard A. Hollins for encouragement, helpful discussions and assistance in calorimetric measurements. One of us (G.S.O.) expresses appreciation for an ONT/ASEE postdoctoral fellowship. We would also like to thank the staff of the Analytical Services Laboratory at The University of Texas for technical discussions that made it possible for us to perform the helium analysis. Finally, we gratefully acknowledge the financial support of the Naval Weapons Center (Independent Research Funds) and the Robert A. Welch Foundation.

REFERENCES

1. M. Fleischmann, S. Pons and M. Hawkins, *J. Electroanal. Chem.*, *261* (1989) 301; err. 263 (1989) 187.
2. M. Fleischmann, S. Pons, M. W. Anderson, L. J. Li and M. Hawkins, *J. Electroanal. Chem.*, *287* (1990) 293.
3. E. Pennisi, *Science News*, *139* (1991) 392.
4. D. E. Stilwell, K. H. Park and M. H. Miles, *J. Fusion Energy*, *9* (1990) 333.
5. E. F. Mallove, "Fire From Ice," John Wiley and Sons, Inc., New York (1991).
6. C. Walling and J. Simons, *J. Phys. Chem.*, *93* (1989) 4693.
7. J. Schwinger, *Z. Naturforsch.*, *45a* (1990) 756.
8. J. Schwinger, *Z. Phys. D*, *15* (1990) 221.
9. G. Preparata in "The First Annual Conference on Cold Fusion, Conference Proceedings," Salt Lake City, UT (1990) pp. 91-98.
10. M. H. Miles, K. H. Park and D. E. Stilwell, *J. Electroanal. Chem.*, *296* (1990) 241.
11. B. F. Bush, J. J. Lagowski, M. H. Miles and G. S. Ostrom, *J. Electroanal. Chem.*, *304* (1991) 271.
12. N. Oyama, T. Ohsaka, O. Hatozaki, Y. Kurasawa, N. Yamamoto, S. Kasahara, N. Ohta, Y. Imai, Y. Oyama, T. Nakamura, T. Shibata, M. Imamura, Y. Uwamino and S. Shibata, *Bull. Chem. Soc. Jpn.*, *63* (1990) 2659.
13. B. M. Oliver, J. G. Bradley and H. Farrar IV, *Geochimica et Cosmochimica Acta*, *48* (1984) 1759.
14. M. H. Miles and R. E. Miles, *J. Electroanal. Chem.*, *295* (1990) 409.
15. T. A. Chubb and S. R. Chubb, *Fusion Technol.*, *20* (1991) 93.
16. S. Dushman and J. M. Lafferty, "Scientific Foundations of Vacuum Technique," *2nd ed.*, John Wiley and Sons, Inc., New York (1962), pp. 491-500.
17. S. Glasstone, K. J. Laidler and H. Eyring, "The Theory of Rate Processes," McGraw-Hill, New York (1941), pp. 537-544.
18. F. Paneth, *Nature*, *119* (1927) 706.
19. F. Paneth and K. Peters, *Z. Physikal. Chem. B*, *1* (1928) 17.
20. S. Szpak, P. A. Mosier-Boss and J. J. Smith, *J. Electroanal. Chem.*, *302* (1991) 255.

Conference Proceedings Vol. 33
«The Science of Cold Fusion»
T. Bressani, E. Del Giudice and G. Preparata (Eds.)
SIF, Bologna 1991

STUDIES OF ELECTROLYTIC AND GAS PHASE LOADING OF PALLADIUM WITH DEUTERIUM

F.G. Will, K. Cedzynska, M-C Yang, J.R. Peterson, H.E Bergeson, S.C. Barrowes, W.J. West and D.C. Linton

National Cold Fusion Institute, University of Utah
390 Wakara Way, Salt Lake City, Utah 84108

Highlights are presented of recent results obtained on deuterium and hydrogen loading of palladium both in electrolytes and in the gas phase. Reproducible tritium generation has been found on palladium cathodes with deuterium loadings approaching one deuterium atom per palladium atom. Tritium generation has been observed on four out of four such highly loaded cathodes. No tritium has been observed in four light water control cells operating simultaneously. Total tritium analysis was performed on all hermetically sealed cells before and after each experiment. Tentative evidence is presented for neutron generation and a single anomalous heat excursion. A novel high-pressure electrochemical cell is also described which employs a fuel cell approach, thereby avoiding oxygen evolution. Two anomalous heat excursions have been observed in this cell with excess power values up to 30%. Gas phase experiments of the Wada-type have been performed on palladium, using electrical discharges to activate the palladium. Neutron bursts up to 280 neutrons in 128 microseconds and tritium enhancements in the palladium of up to 25X background have been observed in the palladium. In both electrolytic and gas phase experiments, the tritium distribution in the palladium wires was found to be non-uniform.

INTRODUCTION

Since Fleischmann and Pons first reported on cold nuclear fusion in cells containing palladium cathodes and heavy water electrolyte [1], many groups have confirmed the occurrence of nuclear reactions in deuterium-loaded metals by identifying some of the nuclear by-products formed. In particular, a large number of groups has reported evidence for neutrons [2-5] and tritium [6-9]. While neutrons have generally been detected at only very low levels, tritium generation has been reported at 10^7 to 10^9 higher levels. Unfortunately, these findings are not generally reproducible or predictable, which has made

systematic research of cold fusion phenomena most difficult. The present study reports on the reproducible generation of significant levels of tritium on Pd cathodes in acid electrolytes. Reproducibility of tritium generation has been achieved by developing a method to reproducibly attain deuterium to palladium loading ratios near and sometimes slightly higher than unity. This study also reports on tritium and neutron findings in palladium, loaded with deuterium in the gas phase.

EXPERIMENTAL

In contrast to cell designs generally used in cold fusion studies, the cell used in most of our electrolytic experiments, Fig. 1, employs a fritted (porous) glass cylinder to separate the Pd cathode from the Pt anode, thus avoiding O_2 gas evolved on the anode to come into contact with the Pd. Furthermore the cell is hermetically sealed, employs a catalyst to recombine D_2 and O_2, and has provisions to continuously measure the D:Pd loading ratio. A simple water-filled manometer, comprised of two burets which are connected at their lower ends with flexible tubing, serves to determine volume changes in the gas volume above the electrolyte. The volumetric technique, developed earlier by NCFI Engineering [10], allows reliable measurement of the D:Pd loading ratio during electrolysis. A key feature of the technique involves evacuation of the cells and refilling with deuterium or hydrogen gas prior to conducting electrolysis. Before and after each experiment, which generally lasted for about one week, the electrolyte, Pd electrode and gas were analyzed for tritium. Since the cell is sealed during the experiment, any increase in tritium level can only result from tritium generation in the experiment itself. Considerations regarding deuterium-tritium partitioning between gas, electrolyte and Pd are therefore eliminated. A light water control cell was always run in electrical series with each heavy water cell.

In other electrolytic experiments, we employed the cell design #2 shown in cross-section in Fig. 2. A Pd wire of 2mm diameter is wrapped with battery separator material, followed by a cylindrical fuel cell anode and another layer of separator material. The porous battery separator is pre-wetted with D_2SO_4 (or H_2SO_4) and reaches into a glass cup filled with electrolyte. The cell is contained in a pressure vessel which is evacuated prior to an experiment and then refilled with deuterium or hydrogen of typically 3 atm pressure. When loading the Pd with D by making it the cathode, D^+ ions are reduced to D atoms which may enter the Pd or form D_2 gas. On the Pt anode, D_2 gas is oxidized to D^+ ions and no O_2 gas is evolved if the cell voltage is kept below approximately 1.2V. The D_2 pressure in the pressure vessel decreases during Pd loading and affords continuous measurement of the deuterium loading ratio.

In both cells, experiments were carried out on 99.9% pure 2mm Pd wires (Hoover & Strong) in 0.5M H_2SO_4 control cells and 0.5M D_2SO_4 for the heavy water cells. The heavy water had a typical tritium content of 36ppm/ml. The acid solutions were prepared

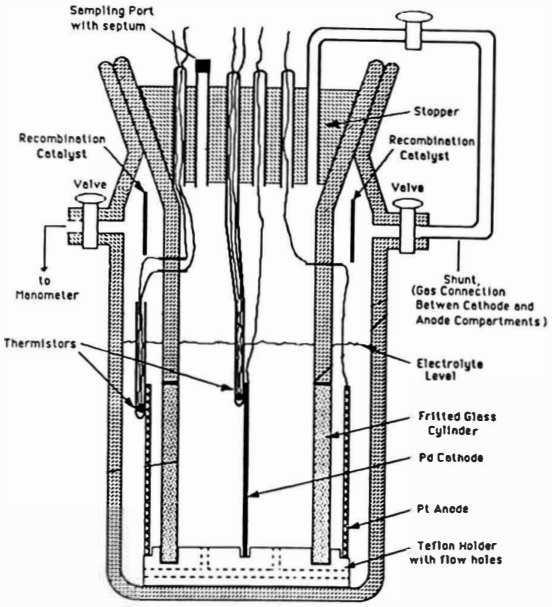

Figure 1. Electrolytic Cell #1

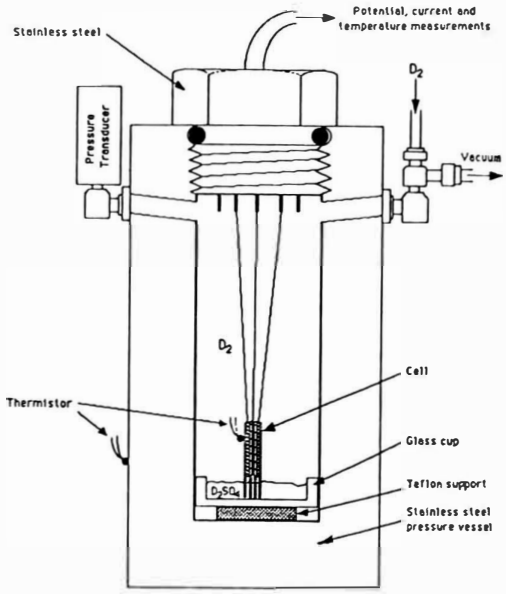

Figure 2. Electrolytic Cell #2. Cross-Section and Pressure Vessel.

from reagent-grade chemicals. D_2 gas was electrolytic grade and contained 0.13 to 0.14 nCi/liter tritium according to our own analysis. Temperatures were measured with Thermometrics thermistors to ±0.2°C. Pd wires were palladized and pre-loaded in D_2 gas; the Pt anodes in cell #1 were platinized and Pt fuel cell anodes for cell #2 were purchased from Giner, Inc.

In the gas phase experiments described here, a simple cyclindrical glass cell was employed that could be evacuated to 10^{-3} torr pressure and refilled with D_2 to 3 atm. Coiled Pd wires (Hoover & Strong) of 1m length and 0.5mm diameter were used as electrodes and pre-etched with aqua regia. The Pd was "activated" by applying a 1.2kV a.c. discharge between two Pd coil electrodes in vacuum, followed by a second discharge at ~0.1 atm of D_2 gas. After cooling in vacuum, the Pd was loaded with D at an initial pressure of ~2 atm. The decrease in pressure during loading allowed continuous measurement of the loading ratio.

Tritium analysis was performed by employing a closed-system analytical procedure described elsewhere [11]. Neutrons were measured with a ^{3}He detection system. In the electrolytic experiments, two ^{3}He were employed for each cell. The counting efficiency was approximately 2% and the time gate 8μsec. In the gas phase experiment described here, a system with 34% efficiency and a 120μsec time gas was used [2].

RESULTS AND DISCUSSION

Electrolytic Cell Employing Volumetric Technique.

Typical results of our loading ratio measurements as a function of time are presented in Figs. 3a and 3b for D and H, respectively. Similar results were obtained in three other

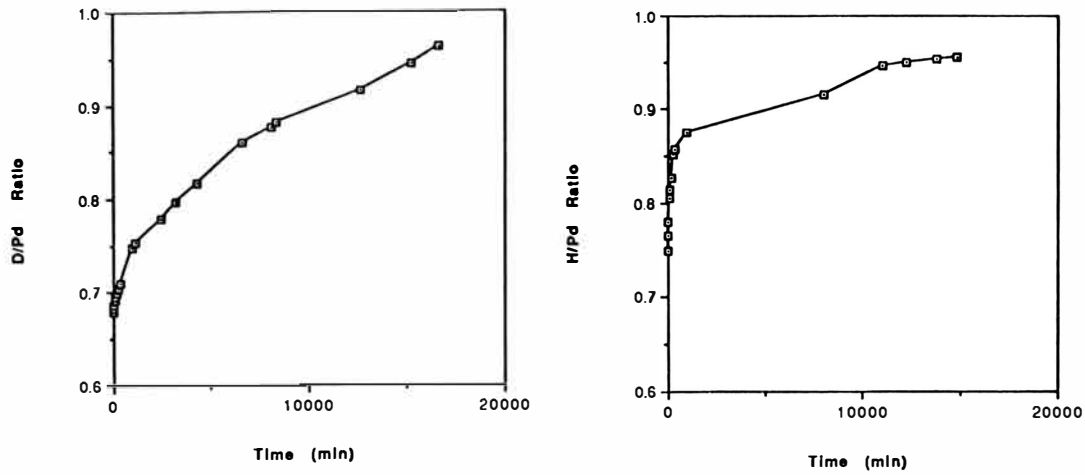

Figures 3a and 3b. D/PD and H/Pd loading ratio as a function of time for 2mm Pd wires of experiment #2. Only fraction of data points shown. Details omitted.

experiments. The electrolytic deuterium loading experiment was performed for 12 days employing current densities of generally 10 and 20mAcm^2. At the start of applying an electrolytic current, the loading ratio already had a finite value which for the deuterium cell was 0.68 and for the hydrogen cell 0.75. The figures show only a small fraction of the large number of data points taken. Both curves show a continuous rise in the loading ratio to values of about 0.95. The loading ratio in the deuterium cell appears to continue increasing, whereas the H/Pd appears to be saturating. Actually it is the tendency to saturate that is observed in most cases.

The electrolyte, palladium and gas above the electrolyte in each D_2 cell were analyzed for their tritium content before and after each experiment. In the H_2 cells, only electrolyte and Pd were analyzed. Table 1 summarizes the tritium analysis results for all four experiments. We have found in experiments to be reported elsewhere, that tritium is generated predominantly at loading ratios in excess of 0.85. Table 1 lists the times at which this loading ratio is attained. The table also gives the maximum loading ratios that were achieved in the four D_2 cells and four H_2 cells. It is noted that the loading ratios lie between 0.95 and 1.15, with an experimental uncertainty of ±0.05. Tritium was not detected in any of the four H_2 control cells. On the other hand, significant tritium enhancements are found in all four D_2 cells, in particular, in the electrolyte and in the palladium. The total amount of tritium contained in the gas phase is relatively small. The palladium cathode area in all four cells was approximately 2cm^2 and the number of T atoms generated in the four cells is in a relatively tight band, from 4.3 x 10^{10} to 1.1 x 10^{11} T atoms/cm^2. These values are in

Table 1

Tritium Analysis of Electrolyte, Pd and Gas

Exper. #		1		2		3		4	
Time at LR > 0.85 [h]		163.8		169.7		144.4		161.3	
Electrolyte		D_2SO_4 +Li_2SO_4	H_2SO_4 +Li_2SO_4	D_2SO_4	H_2SO_4	D_2SO_4	H_2SO_4	D_2SO_4	H_2SO_4
Loading Ratio Atom Fraction		0.99	1.030	0.96	0.95	1.02	1.07	1.15	1.01
#T atoms Electrol.	Before	3.8×10^9	ND	2.9×10^9	ND	* 1.0×10^{11}	ND	2.4×10^9	ND
	After	1.9×10^{11}	ND	8.0×10^{10}	ND	1.4×10^{11}	ND	8.7×10^{10}	ND
#T atoms in Pd	Before	ND	ND	ND	ND	ND	ND	ND	ND
	After	1.7×10^{10}	ND	1.6×10^{10}	ND	2.1×10^{10}	ND	4.7×10^{10}	ND
#T atoms Gas	Before	1.8×10^8	NM	1.8×10^8	NM	1.8×10^8	NM	1.8×10^8	NM
	After	1.8×10^8	NM	8.3×10^8	NM	6.2×10^9	NM	NM	NM
#T atoms Total	Before	4.0×10^9	ND	3.1×10^9	ND	1.0×10^{11}	ND	2.6×10^9	ND
	After	2.1×10^{11}	ND	9.7×10^{10}	ND	1.7×10^{11}	ND	1.3×10^{11}	ND
T Generated [# atoms]		2.1×10^{11}	ND	9.4×10^{10}	ND	7.0×10^{10}	ND	1.3×10^{11}	ND
Enhancement Factor		52.5	ND	31.2	ND	1.7	ND	50.0	ND
T Generated [# atoms/cm^2]		1.1×10^{11}	ND	4.5×10^{10}	ND	4.3×10^{10}	ND	6.5×10^{10}	ND
T Generate Rate [# atoms/cm^2/S]		2.0×10^5	ND	7.4×10^4	ND	8.3×10^4	ND	5.8×10^4	ND

* = Batch of D_2O with high T content

ND = Not Detected

NM = Not Measured

LR = D/Pd or H/Pd Loading Ratio

good agreement with those obtained by several research groups at the Bhabha Atomic Research Center in Bombay, India [7]. Their values run from a low of 5×10^9 to a high value of 1.7×10^{14} T atoms/cm^2. Predominantly, however, their values are in the range from 10^{10} to 10^{11} T atoms/cm^2. These experiments were run for comparable lengths of time as our experiments. The average tritium generation rate in our experiments varies

from 5.8 x 10^4 to 2.0 x 10^5 T atoms/cm^2/sec and the tritium enhancement factor (tritium after to tritium before the experiment) attained values of up to 52.

The tritium analysis of the palladium cathodes was carried out by analyzing several small pieces cut from the entire electrode. The tritium distributions in the four Pd cathodes are shown in Fig. 4

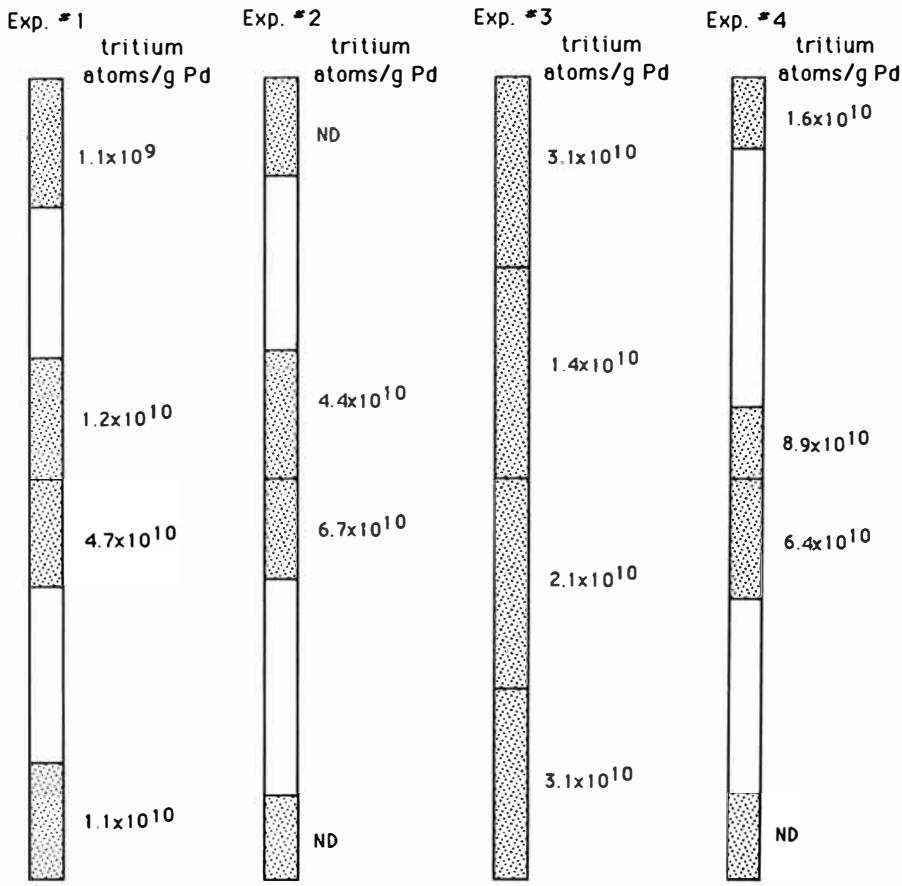

Figure 4. Tritium distribution in Pd cathodes after D_2O electrolysis. ND = not detected; detection limit is 5 x 10^8 tritium atoms/g.

Comparatively much less tritium is found in the ends of the wires as compared to the center. The 8 pieces near the center of the 4 electrodes show a surprisingly tight band of values, namely, from 1.2 x 10^{10} to 8.9 x 10^{10} T atoms/g Pd. It appears that the ends of the Pd wires either did not charge as efficiently as the center regions or that tritium escaped from the ends more readily. Since the detection limit of our analytical procedure is 5 x 10^8 T atoms/g Pd, the tritium levels are up to 180 times larger than the maximum possible contamination level before electrolysis.

The results of our neutron measurements are presented in Table 2. It is seen that the

number of triples monitored in three of the four D_2 cells is consistently between a factor of 2.0 and 2.6 higher than in the H_2 cells. In the entire two month period of observation, the total number of triples is 40 for the four D_2 cells and 18 for the four H_2 cells.

Table 2

Triple and Quadruple Neutron Counts in D_2SO_4 (D) and H_2SO_4 (H) Cells

Experiment#	1		2		3		4	
	D	H	D	H	D	H	D	H
# Doubles/24h	77	36	61	32	62	34	44	39
# Triples	13	5	14	7	13	5	0	1
# Quadruples	1	0	0	0	1	0	0	0

The total number of neutron events and the difference in numbers for D_2 and H_2 cells are small. Further, the role of one Pb brick each, used as a weight in the vicinity of both cells in all four experiments, needs to be explored. Reassuringly, removal of the bricks in a fifth experiment, lasting 22 days, resulted in 11 triples in the D_2 and only 5 triples in the H_2 cell.

Figures 5a and b show the electrical input power into the cell and the temperature of the Pd cathode and Pt anode as a function of time for the D_2 cell in Fig. 2 for the time interval from 15,430 to 16,030 minutes. The electrical input power to the cell increases steadily with time. Whereas the temperature of the platinum anode stays constant at 26.84°C during the entire time period of 700 minutes, the temperature of the Pd cathode shows a relatively constant values of 26.7°C only in the first 370 minutes of the time period shown. The relatively sudden temperature excursion of the Pd cathode from 26.7°C to 27.7°C followed by less elevated temperatures in the subsequent 70 minutes represents an increase in temperature which cannot be explained on the basis of the smoothly rising electrical input power. On the basis of a temperature-power input calibration performed on the cell, the temperature excursion in Fig. 5b corresponds to an excess power excursion with a peak value in excess of 10W, representing a 187 times increase over the electrical input power. The excess energy produced during this power excursion amounts to approximately 5 x 10^4 Joules. Operation of the thermistor was verified as correct after the conclusion of the experiment. However, the cell is not set up to do precise calorimetry and these results should be regarded as tentative.

In the high-pressure cells employing fuel cell anodes (Fig. 2), D:Pd loading ratios were consistently lower than in cells of type 1, minor tritium was found only in one of three experiments with 2mm Pd wires, and no neutrons were detected. However, two excess

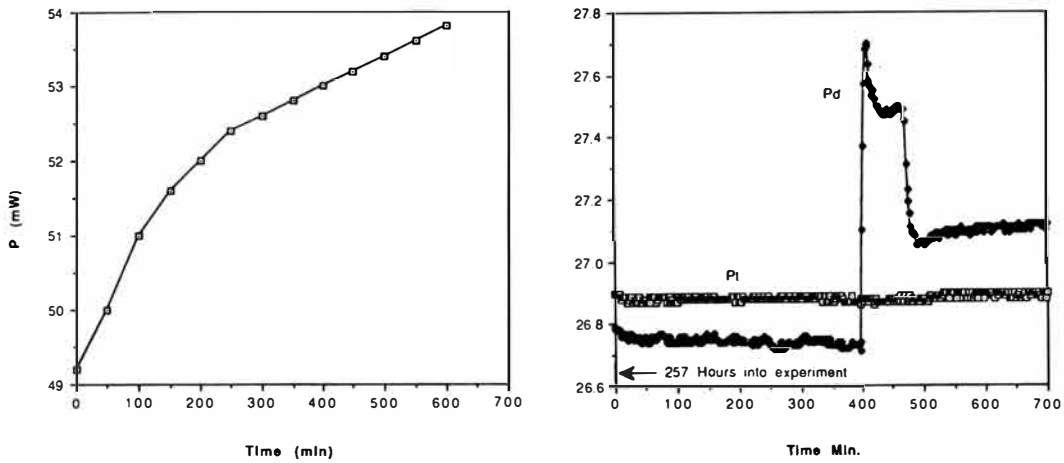

Figure 5. (a) Electrical power input of D_2SO_4 cell in experiment #2.
(b) Observed temperature - time curve of Pd Cathode and Pt anode.

heat events occurred during a 12-day experiment employing 2mm Pd. These two events are shown in Fig. 6 in the time interval 8000 to 17,000 minutes. The cell had been calibrated, yielding a temperature change of 0.035°C/mW/cm^2. The power output exceeds the power input in two events, from 10,500 to 12,775 minutes and from 14,200 to 16,939 minutes. The apparent excess power excursions go to highest values of 13mW as compared to an electrical power input of 10mW, thus amounting to excess power values of up to 30%. The apparent energy generated in the two time intervals amounts to approximately 300 Joules. It should be emphasized that (1) these are the results of a single experiment at this time, (2) the temperature excursions are very small, (3) there was only one thermistor measuring the temperature and (4) light observed temperature and power excursions as tentative observations that require considerable verification.

In gas phase loading experiments of Pd wires with D, employing the Wada technique, we have found evidence for neutron and tritium generation. The most successful experiment was performed in collaboration with S.E. Jones at Bringham-Young University. After Pd activation and D_2 gas loading, four neutron bursts were observed in a time period of 100 hours. These corresponded to bursts of 20, 20, 30 and 280 source neutrons (detection efficiency 34%) in a 128μsec time gate. This is shown in Fig. 7.

The tritium distribution in Pd electrodes used in our Wada-type of gas loading experiments was usually highly non-uniform. Figure 8 shows the results of our tritium analysis on the Pd wires used in the experiment of Fig. 7. In "hot spots", we observed tritium levels of up to 10^{10} atoms/g Pd. Before the experiment, the Pd did not contain tritium within the detection limit of the analysis, that is, ~4 x 10^8 atoms/g Pd.

Of twenty "valid" (equipment debugged, procedures developed) experiments with Pd, nine or ten exhibited elevated levels of neutrons and/or tritium, representing a success rate of 45 to 50%.

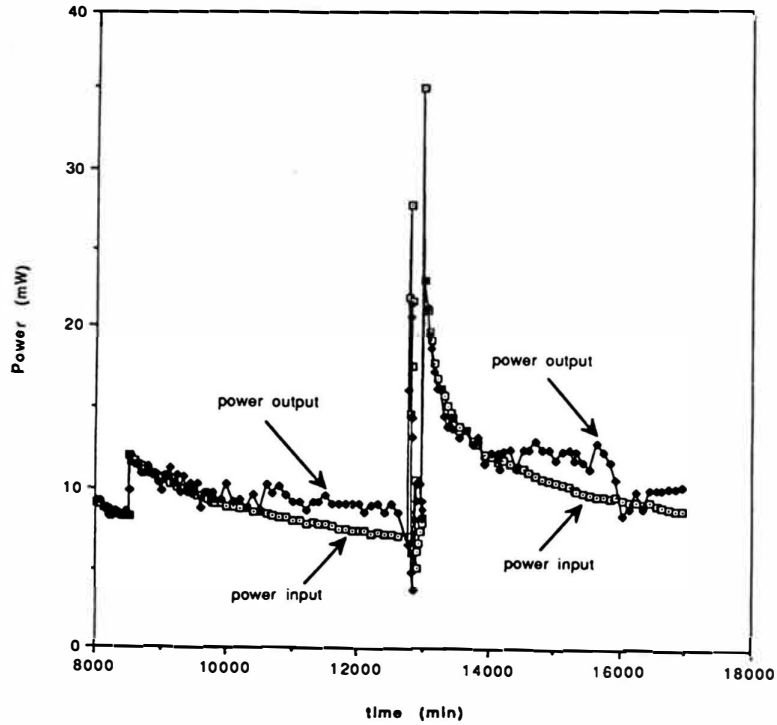

Figure 6. Measured electrical power input and calculated power output (from measured cell temperature) when deuterium loading 2mm Pd wire.

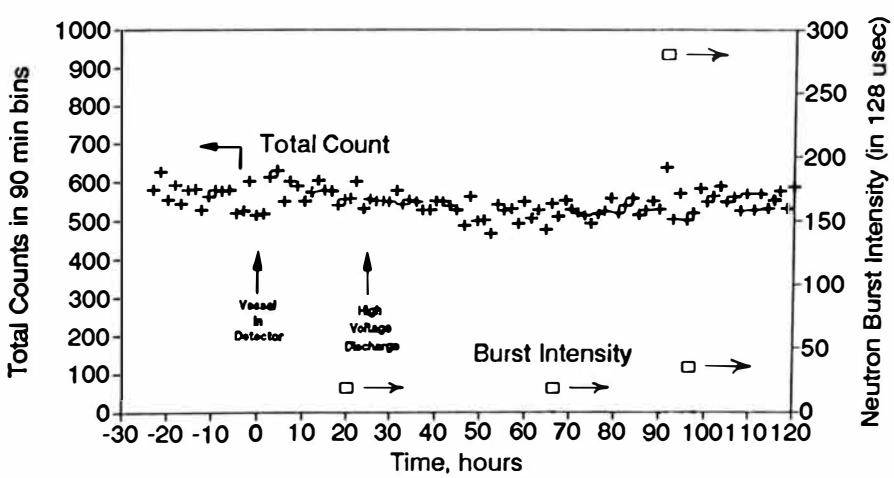

Figure 7. 90-minute total neutron count averages and neutron bursts (in source neutrons) on Pd wires in Wada-type D_2 gas loading experiment.

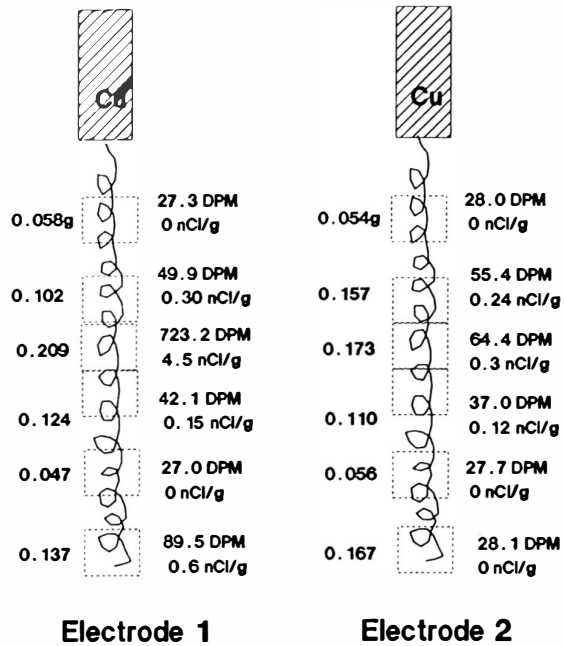

Figure 8. Tritium distribution in Pd wires used in Wada-type experiment of Fig. 7.

CONCLUSIONS

Employing a hermetically sealed electrolytic cell and a volumetric measurement technique for the D:Pd ratio, we have developed a procedure to attain loading ratios close to unity. With such high loading ratios, tritium generation has been observed reproducibly in four out of four heavy water cells whereas none of the four light water controls showed tritium generation. Tritium enhancements up to a factor 52 were observed. As we performed total tritium analysis on electrolyte, electrode and gas before and after each experiment, and as the cells are hermetically sealed, we conclude that the tritium can only have been generated by nuclear phenomena in the deuterium-loaded palladium during the experiment. Neutron generation has also been observed in these heavy water cells, but at very small levels. Excess heat generation has tentatively been observed in three cases: A 70-minute event with 10W excess power and $4 \cdot 10^4$ Joules energy on one of the four heavy water cells and two 38- and 46h events with up to 30% excess power and 300 Joules in one of our high-pressure electrolytic cells. In 45 to 50% of our "countable" Wada-type D_2 gas loading experiments on Pd wires, we have observed neutron and/or tritium generation. The most intense burst consisted of 280 source neutrons in a time gate of 128μsec. The largest amount of tritium was found near the center of one of the electrodes which had produced the 280-neutron burst. A tritium concentration equivalent to 4.5nCi/gPd or 10^{10} tritium atoms/g Pd was found. This compares to a maximum possible tritium contamination level in the Pd of 4×10^8 atoms/g Pd.

ACKNOWLEDGEMENTS

We would like to acknowledge the help of X. Du, J. Yuan and B. Nikamsi in the tritium analysis, the design of the high-pressure vessel by Robert Boehm and Mark Case and the glass blowing expertise of Hans Morrow. We also would like to thank M.W. Wadsworth and the Metallurgy Group for their assistance in metallurgical questions, S.E. Jones at Brigham Young University for his cooperation in neutron measurements and C.A. Markowski for the preparation of this paper. This work was made possible through the financial support from the State of Utah.

REFERENCES

[1] M. Fleischmann, S. Pons, and M. Hawkins, J. Electroanal. Chem. **261**, 301 (1989).

[2] S.E. Jones, E.P. Palmer, J.B. Czirr, D.L. Decker, G.L. Jensin, J.M. Thorne, S.F. Taylor, and J. Rafelski, Nature **338**, 737 (1989).

[3] A. DeNinno, A. Frattolillo, G. Lollobattista, L. Martinis, M. Martone, L. Mori, S. Podda, and F. Scaramuzzi, Il Nuovo Cimento **101A**, 841 (1989).

[4] H.O. Menlove, M.A. Paciotti, T.N. Claytor, H.R. Maltrud, O.M. Rivera, D.G. Tuggle, and S.E. Jones, Proc. Conf. Anomalous Nuclear Effects in Deuterium/ Solid Systems, Provo, Utah, October 22-24, 1990.

[5] A. Takahashi, T. Takeuchi, T. Iida and M. Watanabe, J. Nucl. Science and Technol. **27**, 663 (1990).

[6] E. Storms and C. Talcott, Fusion Technology **17**, 680 (1990).

[7] P.K. Iyengar and M. Srinivasan, Proc. 1st Annual Conf. Cold Fusion, Salt Lake City, Utah, March 28-31, 1990, p. 62.

[8] T.S. Murthy, T.S. Iyengar, B.K. Sen, and T.B. Joseph, Fusion Technology **18**, 71 1990).

[9] J. O'M. Bockris, G.H. Lin, and N.J.C. Packham, Fusion Technology **18**, 11 (1990).

[10] A.M. Riley, J.D. Seader, D.W. Pershing, A. Linton, and S. Shimuzu, NCFI Final Report (1991); submitted to J. Electrochem. Soc.

[11] K. Cedzynska and F.G. Will, Final Report, National Cold Fusion Institute, Vol. 1, Technical Inform. Series PB91175885, June 1991; accepted by Fusion Technology.

Conference Proceedings Vol. 33
«The Science of Cold Fusion»
T. Bressani, E. Del Giudice and G. Preparata (Eds.)
SIF, Bologna 1991

LOW-BACKGROUND MEASUREMENTS OF NEUTRON EMISSION FROM Ti METAL IN PRESSURIZED DEUTERIUM GAS*

H. O. Menlove, M. A. Paciotti,
T. N. Claytor, and D. G. Tuggle

Los Alamos National Laboratory
Los Alamos, New Mexico 87545 USA

ABSTRACT

A wide variety of neutron detector systems have been used at various research facilities to search for anomalous neutron emission from deuterated metals. Some of these detector systems are summarized here together with possible sources of spurious signals from electronic noise. During the past two years, we have performed experiments to measure neutron emission from pressurized D_2 gas mixed with various forms of titanium metal chips and sponge. Details concerning the neutron detectors, experimental procedures, and results have been reported previously. Our recent experiments have focused on increasing the low-level neutron emission and finding a way to trigger the emission. To improve our detection sensitivity, we have increased the shielding in our counting laboratory, changed to low-background ^{3}He tubes, and set up additional detector systems in deep underground counting stations. This report is an update on this experimental work.

INTRODUCTION

During the past two years, a considerable amount of work has taken place in an attempt to detect neutron emission from deuterided metal systems. The proposed nuclear reaction is $d + d \rightarrow {}^3He + n$ (2.45 MeV). This reaction competes with the fusion reactions yielding tritium (T) and protons (P) or ^{4}He. In general, neutrons have the desirable property that they readily penetrate the sample, container, and the experimental apparatus.

*This work is partially supported by the US Department of Energy, Office of Safeguards and Security.

High-efficiency neutron detectors have been designed to measure the neutron production rate in bulk samples that include the entire experimental sample. For low-background underground experiments, the detectors are sensitive enough to detect a few d,d fusion events per hour from the samples.[1]

For neutron detection, the detector parameters of interest include the efficiency, neutron energy resolution, pulse time information, sensitivity to gamma-ray and cosmic-ray backgrounds, and noise susceptibility. These characteristics, together with shielding, will determine the sensitivity of the system to measure low-level neutron signals.

This paper describes some typical neutron detectors that have been used for "cold fusion" type experiments, and it gives some of the sources of false signals and some techniques to protect against them. Also included is an update on the recent neutron measurements that we have performed at Los Alamos.

NEUTRON DETECTORS

A wide variety of neutron detectors have been used for the investigation of neutron emission from deuterated metallic-lattice experiments. A summary of the publications corresponding to these experiments can be found elsewhere.[2,3] Table I lists the detector types that have been used in the experiments. The total neutron detection efficiencies range from 10^{-5} to 0.44 with the ^{3}He systems generally giving the higher efficiencies. Note that for neutron coincidence or time-correlation counting, two or more neutrons from a single event must be counted and the coincidence counting efficiency varies as the square of the singles efficiency. Thus, low-efficiency detectors are not well suited to measure neutron coincidence burst events.

There is a basic difference between the thermal-neutron detectors and the fast-neutron detectors listed in Table I. The advantages of the thermal-neutron detectors include

1. higher efficiency,
2. simpler operation,
3. very low gamma-ray sensitivity, and
4. burst detection capability by moderator thermalization time.

The advantages of the fast-neutron detectors include

1. neutron energy spectra,
2. fast time information, and
3. lower neutron backgrounds.

The experiments that use a combination of detector types are especially good for noise rejection because the detectors are usually vulnerable to different types of problems.

Some possible sources of noise that give false neutron signals are listed in Table II. Most of the noise events are electrical but some are nuclear in that cosmic-ray events and radioactive decay might be misinterpreted.

Table III lists some of the techniques that can be used to protect an experiment from noise events and/or to flag noise events in the data analysis. In general, experiments that have been performed during the past year have incorporated more of the noise protection techniques than the experiments during the previous year. As long as the neutron emission results remain intermittent and irreproducible, a great amount of attention must be paid to the noise vulnerability question.

TABLE I. Neutron Detectors Used for Cold Fusion Experiments

Type	Neutron Energy	Reaction	Typical efficiency (%)	γ-sensitive
^{3}He tubes	Thermal	^{3}He (n,p)	1-44	No
BF_3 tubes	Thermal	^{10}B (n,α)	0.5-20	No
H_2O + NaI/Ge	Thermal	H (n, γ)	<0.1	No
Activation foils	Thermal	(n, γ) or (n,F)	0.1-5	No
Li glass	Thermal	^{6}Li (n,α)	1-20	No
Liquid scintillator	Fast	n,p recoil	1-25	Yes
Plastic scintillator	Fast	n,p recoil	1-20	Yes
Plastic combination	Fast/Thermal	(n,p) + (n,α)	10-25	Yes/No
Cerenkov	Thermal	(n, γ) + e	15-20	High energy

TABLE II. Potential Sources of False Signals

	Electrical Noise
1.	Tube high-voltage leakage (moisture seal)
2.	EMI* noise pickup (EMI seal)
3.	Power line noise (filters, veto counters, etc.)
4.	Microphonics
	Cosmic-ray Background
1.	Total counts (cosmic-ray interactions in the shielding)
2.	Coincidence counts (spallation in the detector and shielding)
3.	D_2 target reactions
	Area Background Neutrons
1.	Accelerators and reactors
2.	Radioactive sources (manmade)
3.	Natural radioactivity (uranium, radon)

*EMI corresponds to electromagnetic interference.

TABLE III. Protection Against False Signals
1. EMI* shielded signal lines and high voltage
2. Hermetically sealed and dried high-voltage components
3. Power-line noise filters
4. Multiple independent counter segments
5. Two (or more) different detectors
6. Neutron spectral energy
7. Pulse time of arrival (slowing down)
8. External veto detectors
9. Variable distance detectors
10. Pulse shape analysis
11. Cosmic-ray shielding (underground)
12. Rigorous control runs
*EMI corresponds to electromagnetic interference.

To gain better sensitivity in the experiments, it is necessary to reduce the cosmic-ray background signal by electronic means or shielding or both. The true neutron background has a random component from the decay of radioactive elements and a time-correlated component from cosmic-ray spallation reactions in the sample or detector body. The time-correlated background can be greatly reduced by performing the experiment underground. For example, the coincidence background decreases by a factor of 10^3 in the 70-m-deep tunnel at Los Alamos and by a factor of 10^5 at the deep-mine locations at Leadville, Colorado, and Kamioka, Japan[1] (1000 m). The coincidence neutron background rate is only ~0.1 counts/d for a 32% efficient ^{3}He detector in the Leadville tunnel.

HIGH-VOLTAGE-LEAKAGE NOISE TESTS

In response to an observation[4] that electronic noise bursts can be caused by moisture condensation in the high-voltage (hv) section of the detector during liquid nitrogen (LN) temperature cycles, we performed a series of experiments to look for this problem. A low-temperature cycle of the sample in the detector can reduce the detector temperature so that moisture condensation might cause hv leakage on the signal line. This problem normally is prevented by the presence of desiccant in the hermetically sealed hv box. However, if there is an air leak into the box, the interior condensation can occur under humid air conditions.

For the tests, we directly applied steel pieces (~2 kg) that had been cooled by LN to the hv junction box and the detector body. The counts from the detector were collected for 8 to 12 hours as the system returned to room temperature. The cooling-warmup cycle was repeated about 10 times for the three ^{3}He-detector systems 1, 3, and 4 listed in Table IV.[5] Detectors 1 and 4 demonstrated no vulnerability to the noise tests. However, detector 3 gave intermittent noise bursts during the warm-up period, but the noise occurred only on humid days (rainy days). To enhance the problem, we placed detector system 3 in a plastic bag containing water to increase the relative humidity to ~100%.

TABLE IV. Neutron Detector Characteristics

Identification	Shape[a]	Size	No. of ^{3}He Tubes	^{3}He Pressure (atm)	Cavity Size (cm)	Total Efficiency[b] (%)	Singles Bkgd (s^{-1})	Coincidence Bkgd (h^{-1})
System 1	Rectangular	25 x 35 x 35 cm^3 channel	18	4	12 x 23 x 35	21	0.19	0.1
System 2	Cylindrical	23 cm ϕ x 37 cm cavity	6	4	5(diam) x 20	26	0.07	0.5
System 3	Cylindrical	22 cm ϕ x 35 cm cavity	16	6	9(diam) x 28	34	0.16	1.6
System 4	Cylindrical	22 cm ϕ x 35 cm cavity (inside ring)	16	4	9(diam) x 28	31	0.39	1.8
		(outside ring)	8	4	same	5	0.22	0.1

All of the noise events had a time-correlation count greater than 50, and the noise bursts did not satisfy the correlation timing relationship between the totals count and the coincidence gate count. This relationship is $R = N(N - 1)/2$, where R is the coincidence count and N is the totals count that occurs within the 128-μs coincidence gate. The cosmic-ray background rate for coincidence counts was 1-2 counts/h and no excess of small correlation events above background was observed in any of the detector systems during the tests.

We conclude from these tests that the ^{3}He systems can be vulnerable to hv noise from moisture condensation under temperature cycling in humid conditions. Detector systems that have effective air seals and drying agents such as desiccant are not subject to the problem.

Our newer detector configurations have the signal lines segmented to give independent readouts of ^{3}He detector banks and the ratio of the segments easily identifies hv-leakage noise events. However, some of our previous results[5] using detector system 3 were subject to this noise problem.

SAMPLE CHARACTERISTICS

In October 1990, we reported[6] neutron emission results using a consistent sample preparation procedure involving clean samples and high-purity gas preparation. Under these conditions, the titanium (Ti) samples would readily absorb deuterium gas after the oxide layer was breached. For the results included in this paper, we have tried a wider range of sample preparations and experimental procedures in an attempt to trigger the neutron emission by inducing sample disequilibrium with deuterium gas absorption or temperature change. We have attempted to duplicate the reported productive procedures of others as well as our previous[5] positive results. Most of the samples consisted of lathe chips of pure Ti metal; Ti alloyed with 6% aluminum, 6% vanadium, and 2% tin; or Ti alloyed with 6% aluminum and 4% vanadium. Some electrolysis residue samples were used. The cleaning procedure normally included multiple washes with methylene chloride, methanol, and water. For about one-third of the samples, the fill temperature was raised to 400-500°C to activate the Ti for deuterium absorption. For pure gas and clean sample conditions, the samples all absorbed deuterium gas after multiple LN temperature cycles. Nineteen samples containing Ti metal and deuterium gas were prepared during the period between November 1990 and March 1991 for the measurements at Los Alamos.

RESULTS

Of the 19 samples prepared during the current set of experiments, only two gave excess neutron emission above the background levels. Many procedural variations were tried including deuterium gas loading at high temperature (400 to 500°C), gas loading at low temperature (-100° to 23°C), and temperature cycling from -197°C to 400°C inside the counting chamber. We gave a typical sample 10 to 20 LN temperature cycles before we stopped the measurements.

Sample DD-17. We measured the highest neutron emission from sample DD-17. This sample contained 304 g of Ti (6,6,2) contained in a 1-ℓ stainless steel (SS) sample bottle. The sample was degassed at a maximum of 230°C using helium to flush out the remaining air and cleaning agents.

During the neutron measurements, LN temperature cycles were performed with a small amount (1 to 4 ℓ) of D_2 gas being absorbed during the warmup from LN temperature. On the seventh LN cycle, 17 ℓ of D_2 were accidentally added to the sample while at LN temperature. About 1 h into the warmup, a portion of the Ti chips went into a hot exothermic reaction excursion when all of the gas was absorbed in about 15 s. A localized spot on one side of the SS bottle was hot; the rest of the bottle was still covered with frost. The bottle was immediately dunked into LN for 10 min and then removed from the LN and allowed to warm up in the detector.

During the first 2 h after the hot absorption, the sample emitted three bursts of neutrons as shown in Fig. 1. Detector system 4 has both inner and outer rings of ^{3}He detectors as shown in Fig. 2. The 16 inner tubes have a counting efficiency of 31% and the 8 outer tubes have an efficiency of 5%. The ratio for the inner/outer detector efficiency is 6.22 as measured with a ^{252}Cf source (2.3 MeV). The detectors have independent electronics. The collection time bins for the inner detector were 200 s long and the outer time bins were 10 000 s. The ratio of the excess neutron counts in inner/outer rings was 6.2 ± 2.1 that compares well with the calibration ratio of 6.22 for ^{252}Cf neutrons. Based on Monte Carlo calculations,[7] this ratio would be ~2.6 for 14-MeV source neutrons.

After three additional LN temperature cycles with little or no neutron emission above background, sample DD-17 was moved to the ^{3}He detector (system 1) that was located in the underground tunnel (70 m deep) at Los Alamos to obtain a higher counting sensitivity. The first LN cycle in detector 1 consisted of multiple short cycles where the sample was recooled in LN a total of five times during the 6-h warmup period. The cold sample at -197°C was filled with 8 ℓ of D_2 gas and the temperature and pressure were monitored during warmup. The observable gas absorption process began when the temperature reached ~-100°C and the absorption rate increased with temperature. After about 1.5 ℓ of gas were absorbed and the temperature reached -30 to -10°C, the sample bottle was dunked into LN for ~1 min to cool the sample below -100°C and stop the absorption process. This process was repeated five times, after which the sample was left in the detector for ~5 d of counting.

Figure 3 shows the neutron coincidence counts collected in detector system 1 where the first large burst came after the first short cycle. Two bursts were observed during the multiple LN cycles and the excess activity continued for ~50 h with 15 bursts as shown in Fig. 3. In addition to the large bursts, there was an excess of small time-correlated events in which only two neutrons were detected. The average control cell background rate in this detector is ~2 counts/d and during the excess activity period the doublet rate was three times higher than normal. Sample DD-17 was temperature cycled eight more times over a 30-d period with no further neutron emission above background levels.

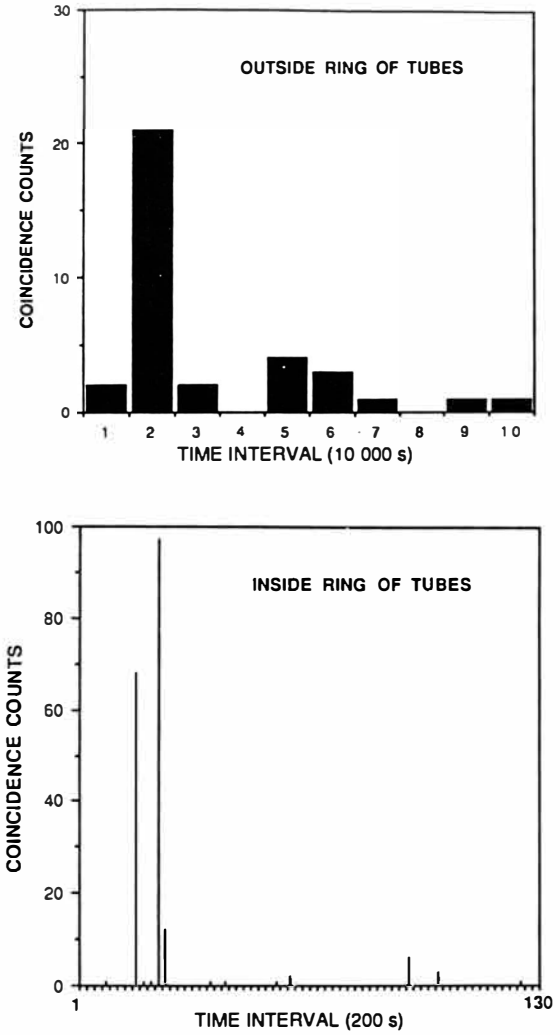

Fig. 1. Neutron coincidence results for sample DD-17 in detector system 4 where the counting intervals are 200 s for the inside ring of tubes (lower graph) and 10 000 s for the outside ring of tubes (upper graph).

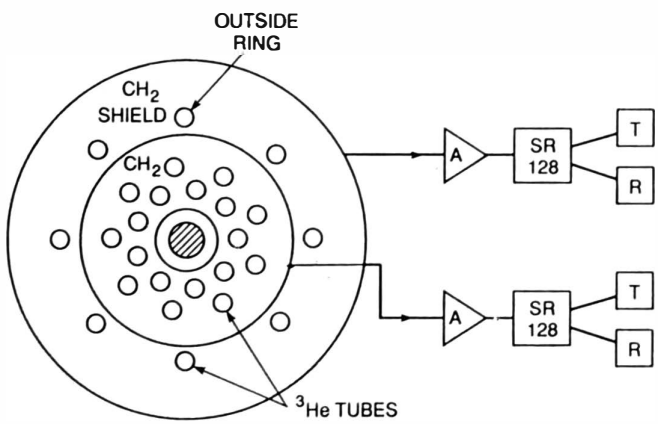

Fig. 2. Schematic diagram of detector system 4 showing the ^3He tubes and the signal processing electronics including the amplifiers (A), shift registers (SR), total scaler (T), and coincidence scaler (R). The inside and outside rings of ^3He tubes have independent electronics and the inside/outside count ratio is used as a consistency check.

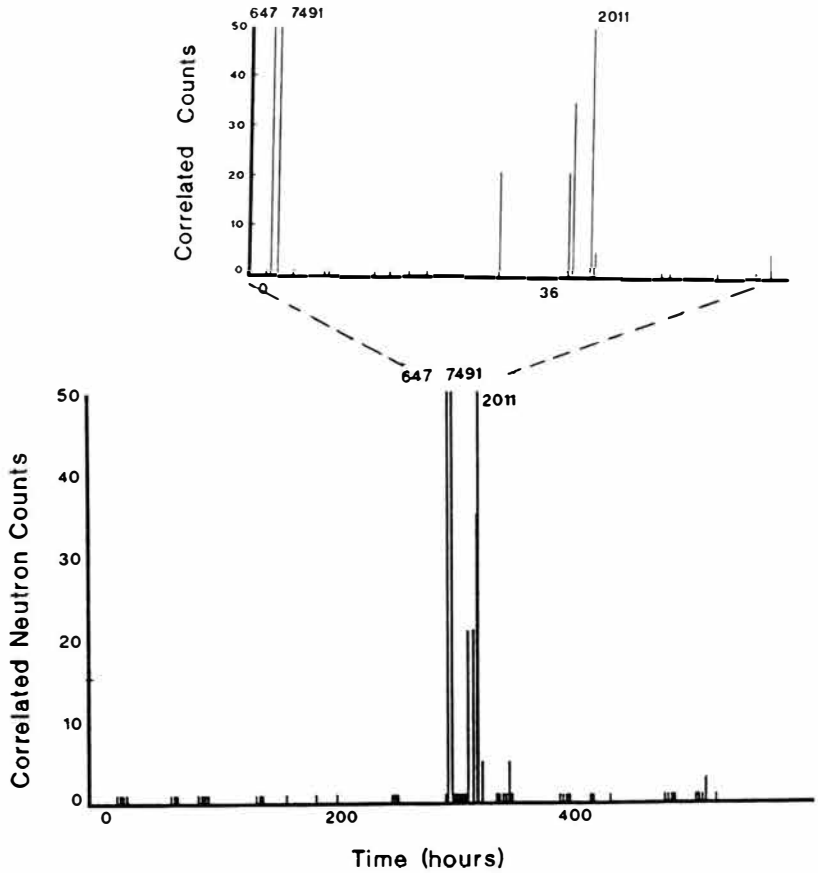

Fig. 3. Neutron coincidence results for sample DD-17 in detector system 1 where the counting intervals are 100 s. The top graph shows a time expansion of the active period. The 280 h of data prior to the active period correspond to the control sample or alternatively an inactive sample (DH-13) in the detector including LN temperature cycles.

Sample Ti-48. Excess neutron emission was observed from sample Ti-48 that contained 56 g of Ti metal and sponge in a 250-mℓ SS bottle. The Ti used in Ti-48 had previously been exposed to deuterium through D_2O electrolysis experiments. The Ti consisted of 35 g of sponge, 11 g of metal pieces, and 10 g of 1.5-mm-thick Ti plate with a thin layer of palladium deposited on one side. The sample was evacuated at 220°C and filled with 53 atm of deuterium gas. The gas pressure slowly decreased to 43 atm during the 90-d measurement period.

The measurements of sample Ti-48 were performed in detector 2 (see Table IV). Figure 4 shows the control runs for system 2 over a six-month period. Each data interval in Fig. 4 corresponds to the average of approximately 24 h of data collection. The control sample was a 300-mℓ SS bottle containing 100 g of Ti chips in air. Previous experiments[5] had demonstrated that control runs with air or H_2 gas gave the same results.

Figure 5 shows the data from sample Ti-48 in detector 2 where each data interval corresponds to the average coincidence rate for ~24 h of data collection. The control runs are shown interspersed between the sample runs. There are several days with excess neutron emission from sample Ti-48 with the highest day having an average yield of 1.12 counts/h

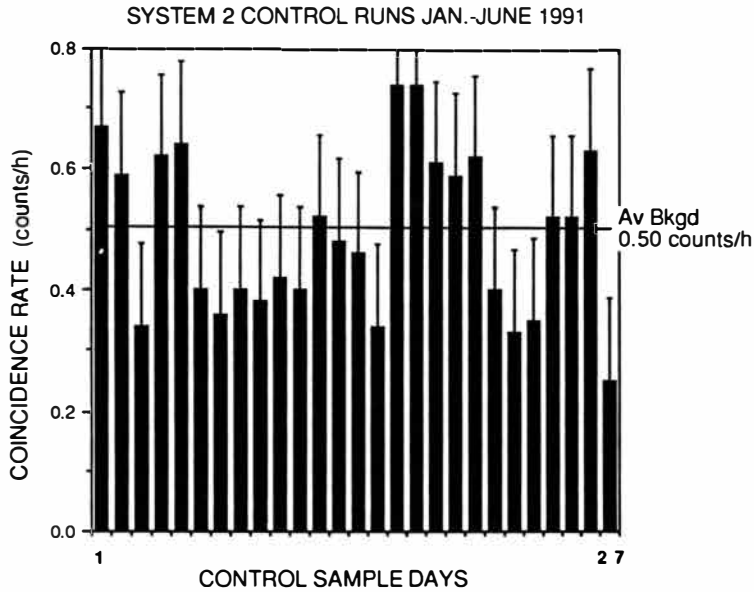

Fig. 4. Neutron coincidence background (control sample) rate in detector system 2. Each data interval corresponds to the average rate for ~24 h of counting. An LN cycle normally began the data interval.

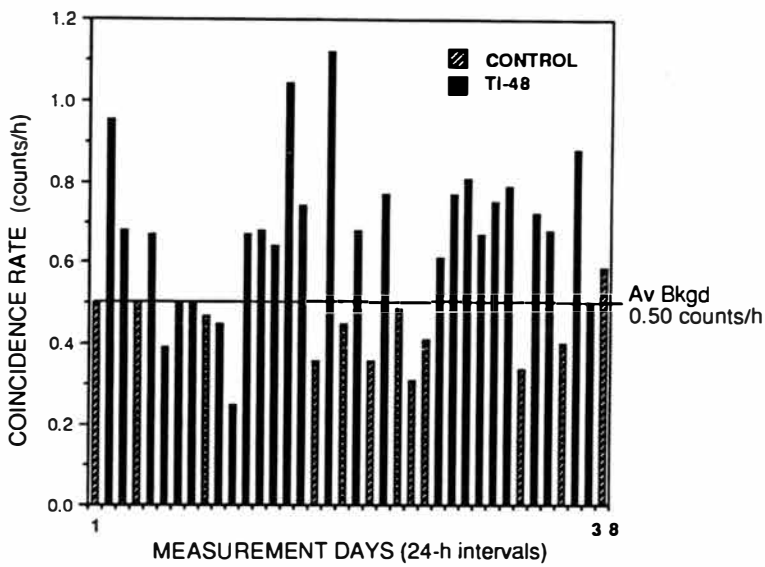

Fig. 5. Neutron coincidence results for sample Ti-48 in detector system 2. Each data interval corresponds to the average rate for ~24 h of counting. Most of the time intervals were initiated with an LN temperature cycle.

and a statistical significance of 3 σ. If we take the average of all the Ti-48 sample days and compare it to the control sample backgrounds, we obtain a 4-σ significance level.

SUMMARY

During the past two years, we have performed experiments to measure neutron emission from pressurized D_2 gas mixed with various forms of Ti metal chips and sponge. Our recent experiments have focused on increasing the anomalous low-level neutron emission. Thus far we have been unsuccessful in finding a way to trigger the emissions, although we have measured several samples that yielded excess neutrons above background. To improve our detection sensitivity, we have increased the shielding in our counting laboratory and we have located additional detector systems in deep underground counting stations.

Our overall detector efficiencies range from 20% to 44% for the four separate detector systems that are operating in parallel experiments. Two of the detector systems are segmented to provide separate signal outputs for a consistency check on the origin of the signals. Our coincidence background depends on the detector and shielding location and ranges from 2 counts/h to less than 0.5 counts/wk in the deep mine locations.

Only two of the 19 samples emitted excess neutrons during the current series of experiments; however, the excess yields were observed in three independent detector systems (detectors 1, 2, and 4). The neutron yield from sample DD-17 in detector 1 was several orders of magnitude above the control-run background levels, and the yield was the largest that we have observed during two years of experiments. This result was obtained in the low-background underground laboratory at Los Alamos.

Our search for a trigger mechanism for the neutron emission has been unsuccessful and our sample success rate is less now than it was one year ago. We think that part of the reason for the low success rate is that we have tried a large variation in sample types and experimental procedures. The number of experimental variables far exceeds our capacity to investigate the parameters.

ACKNOWLEDGMENTS

The authors thank S. Jones for his advice and help in the experiments. The assistance of J. Baca and O. M. Rivera was essential for the sample preparation.

REFERENCES

1. S. E. Jones, et al., "In Quest of a Trigger Mechanism for Neutron Emissions from Deuterium/Solid Systems," *Proceedings of Anomalous Nuclear Effects in Deuterium/Solid Systems* (American Institute of Physics, 1991), pp. 206-235.
2. E. Storms, "Review of Experimental Observations About the Cold Fusion Effect," to be published in *Fusion Technology* (1991).
3. L. Anderson, et al., "Investigation of Cold Fusion Phenomena in Deuterated Metals," Final Report, Vol. I, Technical Information Series PB91175885, National Cold Fusion Institute, University of Utah, Salt Lake City, Utah (June 1991).
4. Rongbao Zhu, Peoples Republic of China, private communication (October 1990).
5. H. O. Menlove, M. M. Fowler, E. Garcia, M. C. Miller, M. A. Paciotti, R. R. Ryan, and S. E. Jones, "Measurements of Neutron Emission from Ti and Pd in Pressurized D_2 Gas and D_2O Electrolysis Cells," *Journal of Fusion Energy* **9**(4), 495-506 (1990).
6. H. O. Menlove, M. A. Paciotti, T. N. Claytor, H. R. Maltrud, O. M. Rivera, D. G. Tuggle, and S. E. Jones, "Reproducible Neutron Emission Measurements from Ti Metal in Pressurized D_2 Gas," *Proceedings of Anomalous Nuclear Effects in Deuterium/Solid Systems* (American Institute of Physics, 1991), pp. 287-301.
7. H. O. Menlove and M. C. Miller, "Neutron Burst Detectors for Cold Fusion Experiments," *Nuclear Instruments and Methods in Physics Research* **A299**, 10-16 (1990).

Conference Proceedings Vol. 33
«The Science of Cold Fusion»
T. Bressani, E. Del Giudice and G. Preparata (Eds.)
SIF, Bologna 1991

TRITIUM GENERATION AND NEUTRON MEASUREMENTS IN Pd-Si UNDER HIGH DEUTERIUM GAS PRESSURE

T. N. Claytor, D. G. Tuggle, and H. O. Menlove

Los Alamos National Laboratory, Los Alamos, NM 87545

INTRODUCTION

This paper summarizes some of the methods applicable for low level tritium detection needed in the search for anomalous fusion in metal hydrides. It is also intended to further detail our tritium and neutron results that have been obtained with the Pd-Si-D system, originally presented at earlier workshops [1,2]. A measure of reproducibility that was not evident in our previous work has been achieved partially due to the better detection sensitivity afforded by the use of low tritium deuterium and partially from the fact that the foil-wafer cells can be made with nearly identical electrical characteristics. This reproducibility has allowed us to narrow the optimum conditions for the experiment. While this experiment is rather different from the "standard" electrolytic cell[3,4,5] or the Ti gas hydride experiment[6], similarities exist in that non equilibrium conditions are sought and the tritium generation levels are low and neutron emission is extremely weak. In contrast to many electrochemical cell experiments, the system used in these experiments is completely sealed during operation and uses no electrolyte.

The major improvements to the experiment have been the use of very low tritium deuterium for the hydriding and the replacement of the aluminum neutron counter tubes with ones of stainless steel. These changes have resulted in pronounced improvements to the detection systems since the background tritium level in the gas has been reduced by a factor of 300 and the neutron background has been decreased by a factor of 14.

MATERIALS

The detailed analysis of our materials has been described previously. The Y12 deuterium gas had tritium levels of 110 to 17 $\mu Ci/m^3$ and was 99.3% pure. Major impurities found in the D_2 are H_2 (0.6%), H_2O, O_2, CO, CO_2 and N_2 (< 0.1%). The new deuterium from Cryogenic Rare Gases has a tritium level less than 0.15 $\mu Ci/m^3$ and is said to be 99.995% pure in aluminum cylinders. To assess the tritium level in the high purity gas it was necessary to combine the deuterium with

oxygen on a palladium catalyst, collect the water and count the colorless fluid in a Packard scintillation counter as described later.

The palladium powder was obtained from Englehard and formed by precipitation from an aqueous solution of $Pd(NH_3)_4Cl_2$ using reagent quality chemicals. This process results in an powder composed of small (0.3 to 0.5 μm) spheres that form chains or agglomerates up to 30 μm in dia. The raw material was said to be virgin sponge obtained from a South African mine. The major impurities in the palladium are oxygen (980 ppm) Chlorine (80 ppm), Nitrogen (65 ppm) and Carbon (47 ppm), all other major impurities are (each) under 35 ppm by weight. A total of 512.7 g of palladium powder has been used in the experiments described in this paper, of that amount, 87.3 g was used in various control experiments to test for tritium contamination. Palladium powder was not reused in experiments once it had been removed from a cell. A total of 43.2 g of palladium foil from Johnson and Matthey was used in the foil cells; 0.44 g of this foil was checked for tritium contamination by dissolution[7] . The 220 micron thick foils were laser cut and then annealed at 850 C for 2 hours at 10^{-6} torr. After the dehydride, the foil was reannealed at 850 C and reused. These foils have been hydrided, dehydrided and annealed seven times and show neither a monotonic decrease or increase in tritium production.

Tritium contamination in the palladium was tested by three independent methods: dissolution and scintillation counting, hydriding and dehydriding and suspension in a scintillation gel. By these means we can assign an upper limit on tritium contamination of 0.02 nCi/g (ie. no tritium detectable within experimental error). In addition, because the powder was obtained from a large bottle by pouring, one would expect that if the bottle was contaminated we would find that the tritium production would be dependent on the amount of palladium used in the experiment. In fact, the two cells with the largest palladium loads are among the cells with the smallest excess tritium.

The silicon powder size distribution and morphology has been discussed previously[1], however, we are now using a monosized, sieved, intrinsic silicon with a particle size of 10 to 20 μm. Added to the silicon powder was 3% (wt) of either PVA or Dow XUS 40303 binder. These binders and ethanol solvents were tested for tritium contamination by dissolving 132 to 460 mg of binder and solvent in water and placing the resultant mixture in a scintillation cocktail. No tritium could be detected over background by this method. Also, no counts over background could be detected when the silicon powder (44 mg) was suspended in a scintillation gel and counted.

In some cells, Sb doped silicon wafers (0.01 ohm-cm in resistivity by 0.5 mm thick disks, 3.07 cm dia.) obtained from Monsanto were used. Between the silicon wafers would be placed the 220 μm thick palladium foil. Because of surface roughness, the plates would only touch over a small fraction of their surface area.

Four types of cells have been made: those with palladium powder and silicon powder, those with palladium foil and silicon powder, those with palladium foil and silicon wafers and one with palladium foil and silicon powder. A typical cell, made with powders, might contain 12 to 21 grams of palladium in eight layers (one to two grams per layer) and 6 to 8 grams of silicon distributed between seven layers. Silicon layers are typically 0.76 to 2.15 mm thick by 3.17 cm in dia. while the palladium

layers vary from 1.16 to 0.48 mm thick by 3.05 cm in dia. for different type cells. The palladium powder was pressed (11.2 MPa, 2000 psi) into disk form and then oxidized, in air, at 350 C for 2 hours (weight gain of 0.37%). Layers of alternating palladium disks and silicon powder were then pressed into a ceramic form at a pressure of 11.2 MPa resulting in densities of 26% and 68% of theoretical density for the palladium and silicon respectively.

TRITIUM MEASUREMENT TECHNIQUES

Various techniques exist to detect tritium in the environment and in samples with a very high sensitivity. These techniques have been condensed and adapted from reference 8 and are compared and summarized in Figures 1 and 2. Because the morphologies for liquids and solids vary widely, the data in the Figures 1 and two are only approximate.

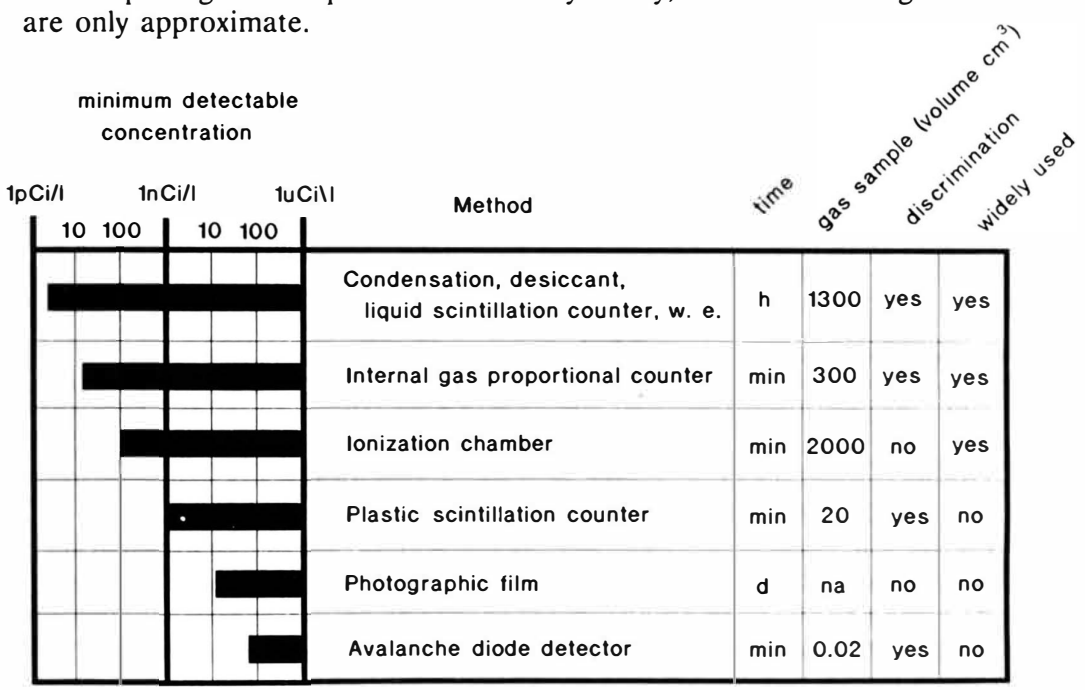

Figure 1. Comparison of tritium detection methods for tritium in gases.

Tritium detection in gases is easily accomplished by the oxidation of the hydrogen and collection of the tritiated water vapor for counting in a scintillation counter. The gas proportional counter is almost as sensitive as the scintillation gauge but involves more effort and chance for contamination than the ionization gauge. The advantages of the ionization gauge over the proportional counter and the scintillation counter are that it is fast, uses no counting gas (which can introduce ^{14}C and ^{85}Kr isotopes to the chamber), and samples do not need to be handled as in the case of the scintillation counter. Scintillation counting, if done carefully, can take days from the time of sample collection. The other techniques listed in Figure I are too insensitive for consideration.

To detect tritium in liquids one typically uses a scintillation counter (such as the Packard CA 1600)[9] and if additional sensitivity is required for water enrichment by electrolysis at 10 °C will result in enhancements of up to 70 times the original

concentration. The most sensitive method relies on the buildup of ^3He over a period of months and the subsequent detection of the He by a mass spectrometer. For rapid sample turnaround this method is obviously impractical. No other methods than the scintillation counter need be considered for liquids.

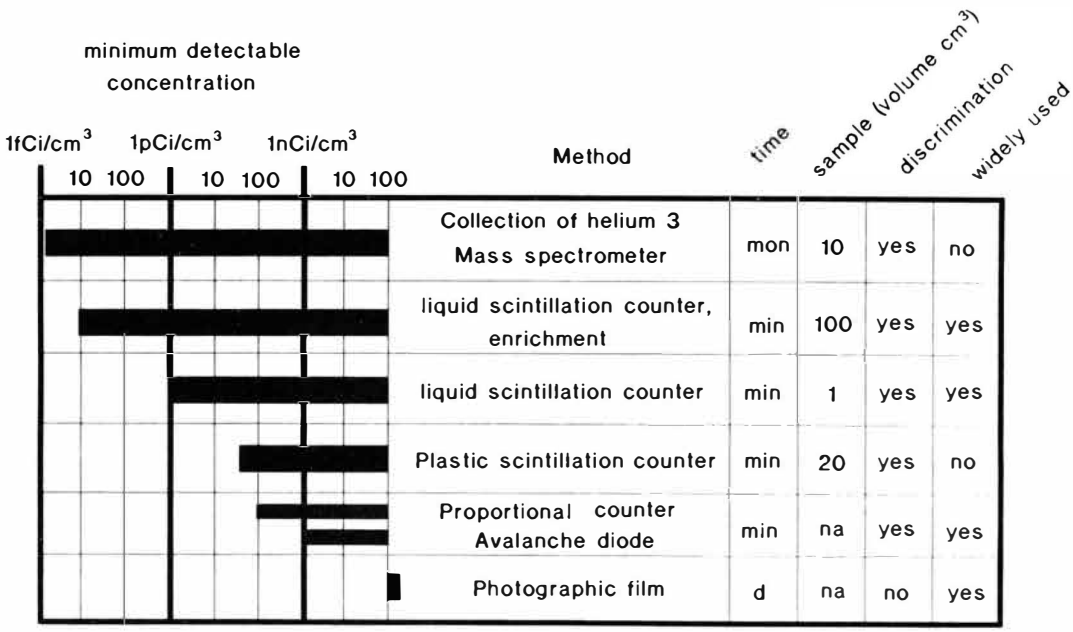

Figure 2. Comparison of tritium detection methods for tritium in liquids.

To detect tritium in solids, a variety of techniques may be applied depending on sensitivity and sample size and sample condition desired at the end of the experiment. If the sample is a powder, suspension of the dilute powder in a scintillation gel will give good results although for very opaque specimens misleading results. For opaque specimens an increase in sensitivity can be achieved by the use of scintillating inserts in the vial which effectively increase the surface area measured. Gas flow proportional counters[10] are the most sensitive method for measurement of small samples if the samples are to be tested non destructively. Semiconductor avalanche detectors[11], photographic film[12], and the measurement of beta stimulated X rays are less sensitive methods.

APPARATUS

The primary tritium measurement device used in this study was a two liter ionization gauge in a stainless steel recirculating gas loop containing a 310.9 cc calibration volume. Gas ionization gauges are used extensively in the detection of tritium and have been shown to be stable, reliable and sensitive[13]. The instrument rejects pulse type radioactive events which effectively discriminate against radon and cosmic ray ionization. The instrument showed good stability in measuring the tritium background in the deuterium gas in over a year of operation with several different bottles of deuterium (maximum deviation during a year of ± 2.5%). Shown in Figure 3 is the tritium measurement time history for all background tritium measurements made with the Overhoff ionization gauge. The tritium level varies from 4 to 66 $\mu Ci/m^3$ and is relatively constant for a bottle unless the system is

cleaned. Because of tritium adsorbed on the analysis system walls, the minimum background for the Overhoff is effectively 3-4 $\mu Ci/m^3$. This memory effect is commonly found for instruments that have been exposed to tritium containing gases for long periods.

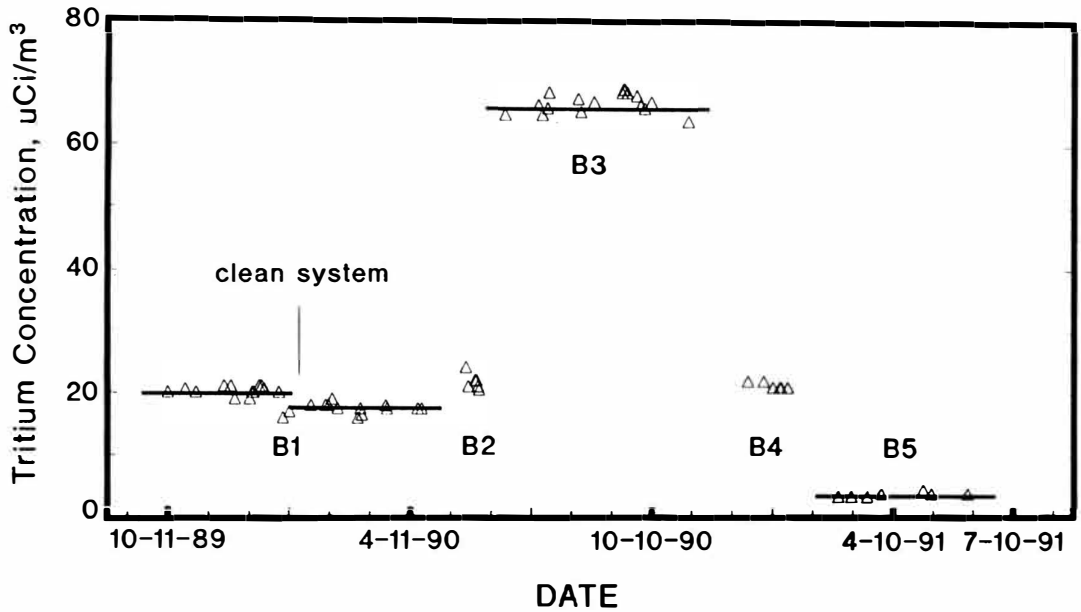

Figure 3. Stability of background tritium measurements for various bottles of deuterium gas.

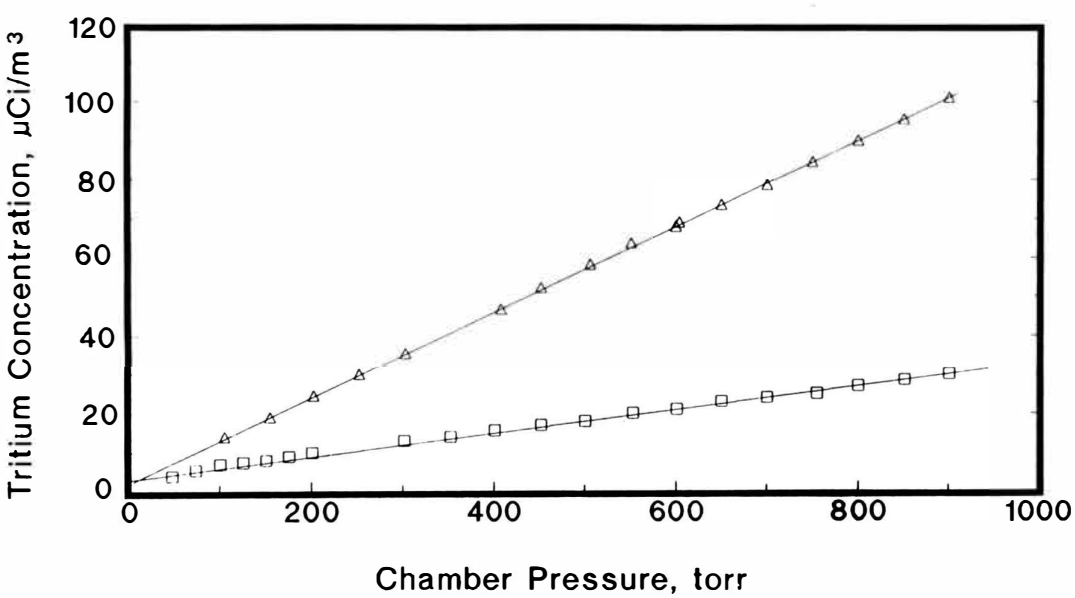

Figure 4. Linearity of Overhoff tritium ionization gauge to trace amounts of tritium in deuterium over a wide pressure range.

Figure 4 shows the linearity of the instrument to two concentrations of tritium in deuterium as a function of chamber pressure. Offsets near zero pressure

correspond to ionization currents caused by small amounts of adsorbed tritium on the chamber walls. Absolute calibration was accomplished by inserting the chamber into a circulating loop containing a standard, calibrated ionization gauge while circulating various concentrations of tritium enriched deuterium. Calibration was performed at twelve points from 498 $\mu Ci/m^3$ to 114 $\mu Ci/m^3$. Sensitivity to air contamination was checked by comparing the response of the meter with deuterium and with deuterium mixed with small amounts of air, no difference was found within experimental error. The response of the gauge to a deuterium water vapor mixture was also measured showing negligible effect at low water concentrations (<38 torr).

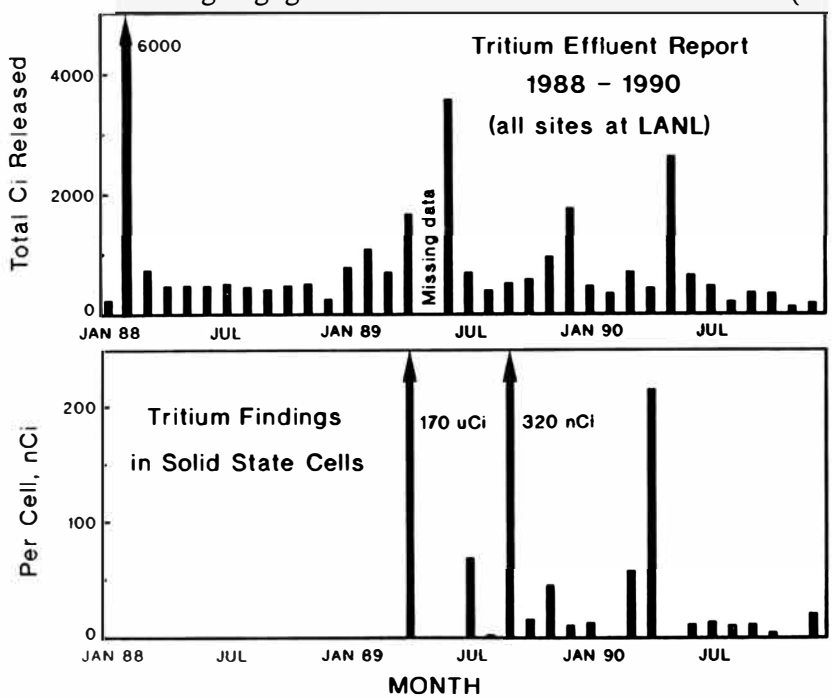

Figure 5. Controlled and accidental tritium releases at Los Alamos and tritium measurements from solid state cells.

As previously discussed, precautions were taken to mitigate the possibility of tritium contamination of our materials. The major precaution was to prepare the samples in a tritium free laboratory, seal the cell and then move it to the filling area which is in a tritium handling area. The cell would be attached to a vacuum system and then opened to a vacuum. Therefore, the inside of the cell was never exposed to the atmosphere in the tritium laboratory. In any case, the atmosphere in the laboratory was not a factor since it was always much less than the background found in the deuterium. In addition, we have compiled the tritium release data for Los Alamos, these data are shown in Figure 5 where it is seen that there is no correlation with the three large releases, which are all accidental and hence unpredictable, with our tritium findings. The fabrication area is also located 3.7 km from the nearest tritium handling facility. All materials handling and assembly work was done with disposable latex gloves and paper bench liners.

The neutron detection equipment is similar to that used by Menlove and has been thoroughly described elsewhere[14,15]. The main feature of the counter and

electronics is that they provide data on neutron totals (total counts accumulated in a specified time) and a number designated as reals, which are correlated neutron counts in a 128 μs gate. The reals counts are indicative of a neutron burst. The counters and tube enclosures are environmentally hardened and have shown excellent totals stability in the underground environment in over a year of operation. Two significant modifications to the counter have been made in the past year. First the aluminum counter tubes have been replaced by low background stainless tubes and the counter has been segmented with the addition of a second set of coincidence electronics.

To illustrate the magnitude of underground backgrounds, in Menlove's underground laboratory[15], the average background totals rate and correlated count rate was 870 ±6 c/h (24 hr) and 3.6 c/h (for correlated counts) while at the environmentally controlled underground tunnel (1) (15 m deep), we found 701 ±6 c/h and 0.6 c/h while for the still deeper tunnel (2) (70 m, overburden density ≈1.9 g/cc) the rates were 637 ±6 c/h and 0.15 c/h. When the stainless tubes were installed the background totals dropped to 44 ± 2 c/h and 0.14 c/h for tunnel 2 as shown in Figure 6.

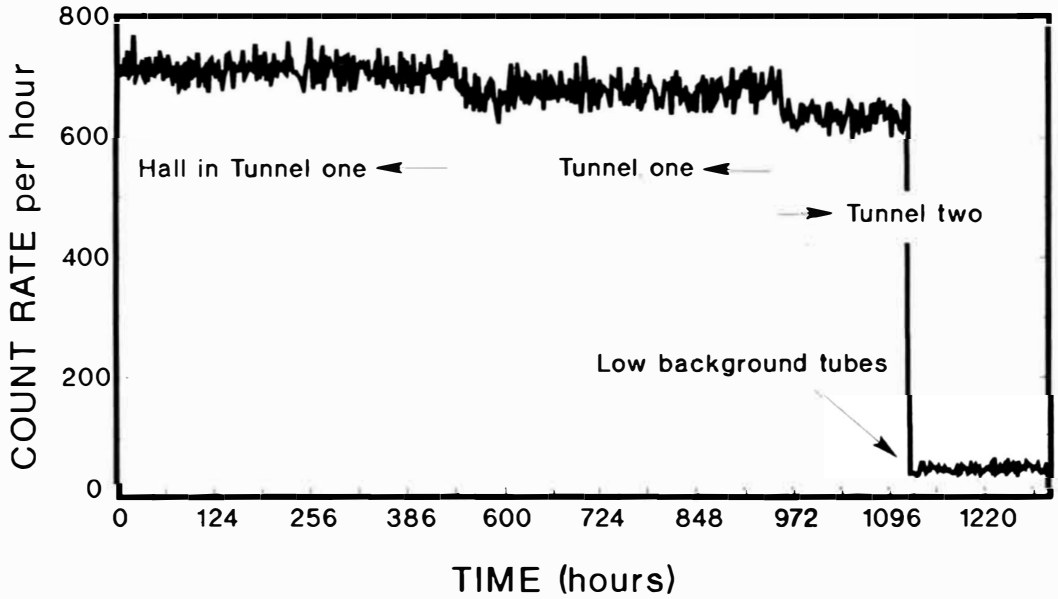

Figure 6. Neutron background summary for two tunnel locations and effect of low background tubes.

The channel counter was calibrated with a ^{252}Cf source (average energy ≈ 2.3 MeV) both in a cell body and in the open counter. The efficiency was 18.5% for the bare source and 20.0% with the source in the stainless body, which has large flanges that reflected the neutrons, subsequently increasing the efficiency.

PROCEDURE

The procedure for hydriding a cell was to first measure the background tritium concentration in the deuterium fill gas. Then the loop and cell were evacuated and the tritium analysis loop was filled with fresh deuterium gas at a

known pressure less than 1000 torr. The tritium level could therefore be measured in this gas again. The cell was then opened and allowed to absorb the gas. Because the pressure in the analysis system and the volume of the system is known, an accurate measure of the gas absorbed by the cell could be made. Subsequent filling with higher pressures allows a determination of the amount of deuterium gas contained in the cell. A comparison of the predicted amount of gas that should be contained in the cell based on the free volume and the amount of palladium and pct curves agrees within 10 percent. The error is thought to be due to the imprecision of the pct curves at pressures greater than 7 x 10^5 Pa (100 psi)[16]. An additional advantage of this filling technique is that after the gas had been let into the cell, the remaining gas could be checked for tritium enrichment or deficit. In all cases that were checked, we found that the deuterium remaining in the analysis system had the same tritium concentration as the original fill gas in the analysis bottle to within experimental error ± 3%. After the cell was completely hydrided and removed from the loop, another check of the tritium background of the deuterium gas was made.

After the cell had been filled, it was placed in the neutron counter and a voltage of 200 to 2500 V generated by a Velonex model 360 pulse generator was applied to the cell. In typical operation, a unipolar, square pulse with a width of at least 150 μs at a repetition rate of 100 pulses per second was used at voltages as high as possible before breakdown occurred, typically 1200 to 2500 V. Currents of up to 5 A were used in some experiments. A minimum of 100 hours of pulsing was used; however, in some cases the experiment was terminated earlier than 100 hours because of sudden electrical breakdown of the cell.

The gas analysis after the electrical pulsing was the reverse of filling. Background checks were made before and after the dehydride, and care was taken to measure the volume of gas evolved from the cell. The cells initially were opened to the evacuated analysis system at room temperature, but near the end of the dehydride the cells had to be heated to at least 125 C and then opened to the vacuum of the analysis system to release the remaining deuterium.

The procedure for the tritium detection by oxidation and subsequent scintillation counting was to first oxidize hydrogen from an uncontaminated cylinder and collect two, separate, 2-ml samples of water for use as background samples. Then the deuterium was oxidized from each of the D_2 bottles and again 2-ml samples were collected in two separate vials. Hydrogen was again oxidized in two more 2-ml samples to test for tritium holdup and then sample 36 was dehydrided.

One ml of each of the samples was then placed in 19 ml of Ultima Gold scintillation cocktail. These samples as well as standards (two uncontaminated H_2O samples, two tritium standards, and two straight cocktails) were counted for 100 minutes on three separate days. The data agree to within ± 2 sigma in all cases except the tritium standard which varied by 2.5 sigma. These results are shown in Figure 7 in order of analysis. No tritium was detected above instrument background for the standard water or hydrogen samples combined before or after combining the deuterium gas. We also show dehydride results for cell 36 (filled from the Liquid Carbonics cylinder), but because only 40% of the deuterium was recovered from the cell, we cannot draw a conclusive case for excess tritium in this cell even though the level was elevated over that of the fill gas by four sigma.

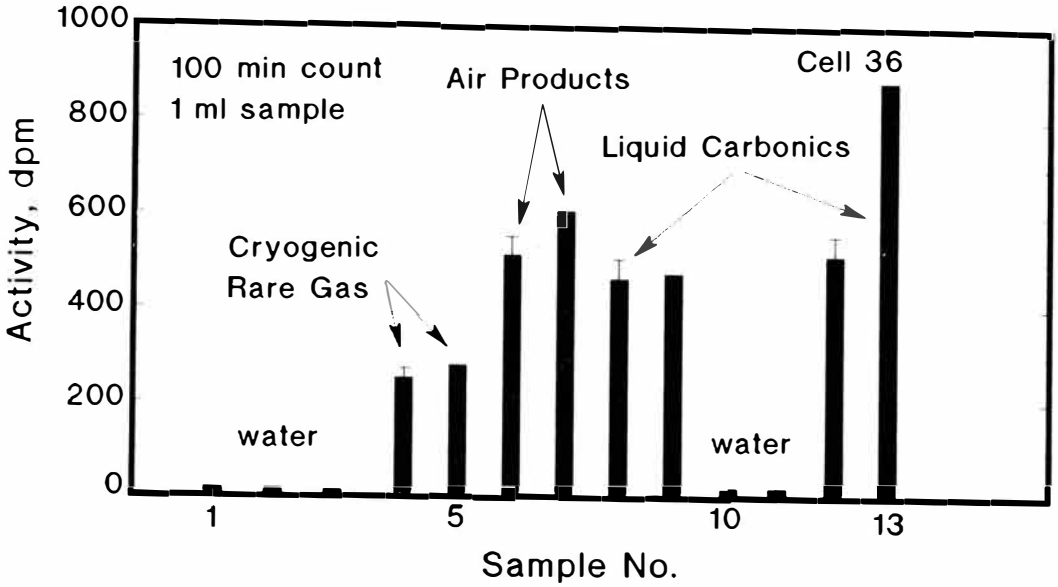

Figure 7. Tritium analysis of several bottles of low tritium deuterium and one solid state cell (36).

RESULTS

Tritium Measurements

Shown in Figure 8 is a summary of all the tritium results obtained after the cell designs had become stable and after the background tritium measurement technique had become standard. It is clear that the cells fall into definite categories with some exceptions. We find that the tritium output depends on current and that various types of cells have different efficiencies. A point worth noting is that the current density axis in Figure 8 is really current through the cell divided by the cell area (8 cm^2). In all cases, the actual area of contact between the silicon and palladium is a fraction of the 8 cm^2. Regardless of this, the contact for a particular type cell should be relatively constant within that cell type.

Our most reproducible cells have been the foil-wafer cells, which can have nearly identical electrical characteristics from cell to cell. As can be seen in Figure 8, these cells show the least scatter of any cell type. Unfortunately, these also give the least amount of tritium generation.

Several cells showed current instability, which was later determined to be arcing. When those cells were disassembled surface regions of the powder had been melted and pitted over as much as 50% of the surface of the palladium pellets. Arcing did not seem to be beneficial to higher tritium production. Cells that gave the most tritium did not show any obvious degradation due to the current flow.

A significant point to note is that the highest amount of excess tritium found for the foil-wafer cells was obtained with the low tritium deuterium and was obtained after the foils had been dehydrided and annealed 6 times. Incomplete dehydrides and separation effects would have given higher values with the deuterium containing larger amounts of tritium. Any tritium containing impurity would probably have been exhausted or depleted by exchange during the numerous anneals and hydridings.

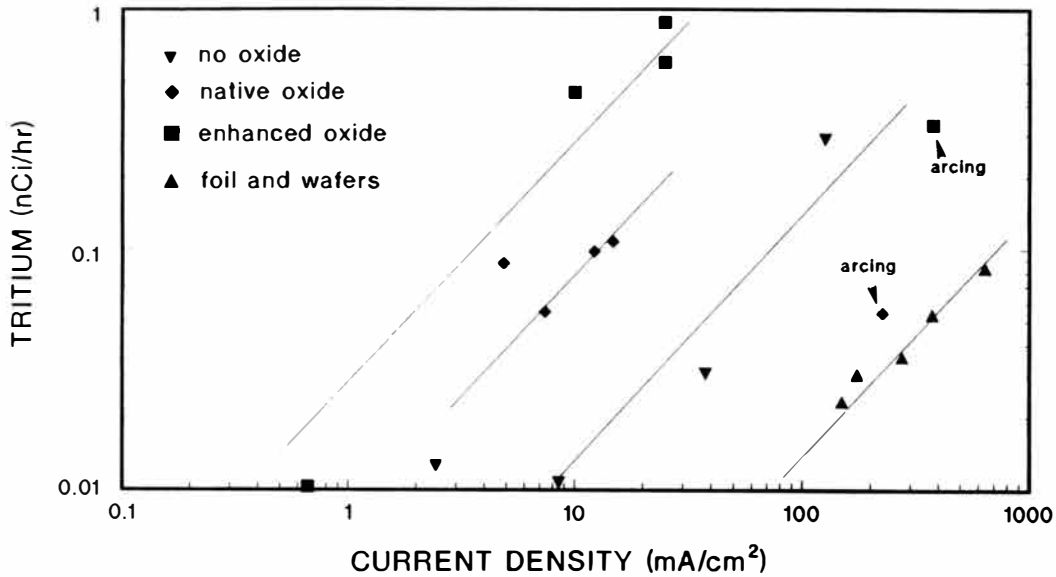

Figure 8. Tritium production of cells correlated with current density and cell type.

Greatest tritium generation rates have been achieved with powder-powder cells with oxidized Pd powder and voltages greater than 800 V at 0.1 A. Originally, it was thought that the binder used in these powder-powder cells had an effect, but it was shown that the only effect of the binder was to increase silicon uniformity and hence raise the breakdown voltage. In addition, the foil-wafer cells had no binder or oxidized palladium and yet produced measureable amounts of excess tritium.

Four hydrogen control cells have been made by either the usual method with layers between silicon or by simply pressing 12 to 30 g of virgin palladium powder into the ceramic form and then hydriding with hydrogen and subsequently dehydriding to test for contamination intrinsic to the palladium. All of these tests give a positive excess tritium result from 6 to 12 nCi total. This can be attributed to the effect of water and hydrogen gas in displacing small amounts of TDO from the ionization chamber and system walls. This TDO finds it's way to the ionization chamber and sticks in the chamber until the system is evacuated. Therefore, this "excess" cannot be readsorbed by the palladium bed as is the case with the tritium in the deuterium gas. These control cells also do not show the same dehydriding signature characteristic for the deuterided material. When palladium is deuterided and then dehydrided after a short period of time as seen for those cells that have shorted out (16, 23, 31), one finds either a very small excess tritium or none at all within experimental error.

Three cells 28, 33 and 35 have been run at low currents or high voltages for greater than 60 hours and then dehydrided. Small amounts of excess tritium or none within experimental error was found. These cells were then rehydrided and operated at higher currents for periods of up ot 300 hours with the result that up to 7 times more excess tritium was found after the longer runs at higher current.

An analysis of the dehydriding behavior of the cells reveals that in all cases the excess tritium is evolved when the palladium is dehydrided. If the tritium was slowly diffusing out of the container walls or ceramic insulator sleeve or other

materials, we would expect to find more tritium than we do in the gas overpressure. If the ionization species was not tritium gas but some other isotope (or even TDO,THO), we would not be able to reabsorb the tritium back onto the palladium bed reversibly as we are able to do with the deuterium containing samples.

While in the majority of cases the amount of excess tritium is small, in cell 20 the excess amount of tritium was 540 times the maximum amount found by the dissolution checks and it was 2.2 times the total amount of tritium contained in all of the deuterium gas used to hydride this cell. Figure 8 indicates that there is a wide range in tritium production rates. It is reasonable to assume that future improvements in the maximum rate will be possible. The greatest rate, achieved reproducibly, equates to a generation of 3.4×10^6 tritium atoms per second. Obviously if neutrons were generated at parity with tritium one would expect to easily detect neutrons.

Neutron Detection

Our previous experiments[1,2] have indicated that there is an anomalously low value for neutrons detected to tritium produced ($\leq 4 \times 10^{-9}$). Because we have attained a reproducible but small tritium generation rate, we have been striving to make the neutron sensitivity equivalent to that of the tritium detection apparatus. We anticipate that our improved neutron sensitivity illustrated in Figure 6 will make it possible to detect a neutron signal that is unambiguously above zero.

Shown in Table 1 is a summary of all of the neutron data that have been collected since the counter was moved to the tunnels. Three locations are shown, with slightly different backgrounds. The first entry in Table 1 compares all tritium producing cells (in the group 17 through 24.5) with the current applied to the background which was composed of non tritium producing cells, hydrogen control cells and time when no current was applied to the cells. There is seen to be a slight excess of counts with this comparison. This can be compared to the other foreground background measurements of 24.5-29 and 30-35 where there is practically no difference between the foreground and the background, and the tritium production is quite low compared to that of cells 17-24.5.

The column listed as reals/hr and total reals/hr differ in that the reals/hr only counts singles events (two neutrons detected). The total reals/hr includes all singles and higher multiplicity events. It appears that excess neutrons occur primarily as single neutron events (totals) and rarely as bursts (reals/hr). No bursts to rival the hundreds of neutrons detected from the titanium cells have ever been seen from these palladium experiments even though this particular neutron counter has been used for some of the titanium measurements that have detected large bursts.

The set of cells 24.5 through 29 was compared to two different backgrounds, one background was indicative of the neutron background with a deuterium containing cell in the counter but with the current off. The other background was obtained by including data from dummy (palladium, steel) cells. This background varies by more from the previous background than the variation in the foreground to the initial background. However, the total variation over some 2400 hours is, at most, only 0.4% indicating the excellent long term stability of these counters.

Cell No's	Location	Conditions	Excess Tritium	Hours	Totals/hr	Reals/hr (Singles)	Total Reals/hr
17-24.5	Center	Foreground (current applied)	374±20	810.6	707.9	0.441	0.635
	Tunnel 1	tritium producing cells only					
		Background (no current) and		829.3	700.3	0.434	0.604
		non tritium producing cells					
24.5-29	Hall	Foreground(current applied)	39 ±10	837.5	713.9	0.607	0.99
	Tunnel 1						
		Background (no current)		958.8	712.9	0.541	0.735
		Background (no current) and		1560	710.8	0.576	0.799
		dummy cells					
30-35	Center	Foreground (current applied)	65 ±16	878.8	638.1	0.084	0.109
	Tunnel 2						
		Background and dummy		343	637.2	0.122	0.146
		cells					

Table 1. Summary of neutron data for three tunnel locations and a comparison of tritium generation rates with the neutron output.

Care should be taken in the interpretation of these data (especially that of the reals) because the counters could be subject to drift over these long periods and a few very high correlated counts can skew the results significantly. Regardless of these caveats, these data are self consistent and consistent with our other measurements.

If the neutron to tritium partition ratio is $\approx 4 \times 10^{-9}$, this implies that we should be able to see a neutron totals of 5 sigma over background in 24 hours at a tritium production of 0.5 nCi/h with our new neutron background. From Figure 8 it can be seen that a tritium production rate of 0.5 nCi/h has been achieved several times. However, since these tubes were installed only a few months ago, we have been able to run one cell with the new tubes, and that cell showed no excess neutron output and gave a tritium output of less than 0.01 nCi/h. Thus, at this point, the results from the new tubes are consistent with the neutron output.

CONCLUSIONS

A reproducible method of tritium generation has been demonstrated. The tritium output scales with the current applied to various configurations of the cells. The tritium yield is found to depend strongly on the type of palladium metal used (powder or foil) and it may be expected that other parameters that have not been investigated thoroughly will have similar effects. Various tests for tritium contamination confirm that there is little chance of initial tritium contamination in the powder, foil, or other materials used in this study. The tritium and neutron results are self consistent, and consistent with other reports. However, more sensitive neutron measurements are required to give a definitive neutron emission result.

ACKNOWLEDGEMENTS

Special thanks to Dr's. J. Thompson and M. Fowler for an analysis of tritium in the virgin powder and cell 36 and Dr K. Cedzynska for the tritium analysis of the metal and powder specimens by dissolution. Also, this work would not have been possible without the special abilities of our technical staff of K. Greichen, W. Ely, J. Ortega and our student aides, Lisa Catapano and Royce Taylor.

REFERENCES

1. T. N. Claytor, D. G. Tuggle, H. O. Menlove, P. A. Seeger, W. R. Doty and R.K.Rohwer, "Tritium and Neutron Measurements From Deuterated Pd-Si", AIP Conference Proceedings 228, Anomalous Nuclear Effects in Deuterium/Solid Systems, Ed. S. Jones, F. Scaramuzzi and D. Worledge, Provo Ut. 1990.

2. T. N. Claytor, P. A. Seeger, R. K. Rohwer, D. G. Tuggle and W. R. Doty, "Tritium and Neutron Measurements from a Solid-State Cell", LA-UR-89-3946, October 1989, Presented at the NSF-EPRI workshop.

3. S.E. Jones, E.P. Palmer, J.B. Czirr, D.L. Decker, G.L. Jensen, J.M. Thorne, S.F. Taylor and J. Rafelski, "Observation of Cold Nuclear Fusion in Condensed Matter", Nature, 338, 737-740, (1989).

4. M. Fleischmann and S. Pons, "Electrochemically Induced Nuclear Fusion of Deuterium", J. Electroanal. Chem., 261, 301-308, (1989).

5. E. K. Storms, "Review of Experimental Observations About the Cold Fusion Effect", to be published in Fusion Technology 1991.

6. A. De Ninno, A. Frattolillo, G. Lollobattista, L. Martinis, M. Martone, L. Mori, S. Podda, and F. Scaramuzzi, "Emission of Neutrons as a Consequence of Titanium-Deuterium Interaction", Il Nuovo Cimento, 101A, 5, 841, 1989.

7. Dr. Krystyna Cedzynska, private communication, December 1990. See also these proceedings.

8. W. C. Reinig, et. al., "Tritium Measurement Techniques", NCRP Report No. 47, NCRP Publications, Washington DC. 20014, 1976.

9. Packard CA 1600, Packard Instrument Co., 1 State St., Meriden CT 06450.

10. Berthold LB110, EG&G Instruments, Nuclear Products Group, 100 Midland Road Oak Ridge TN. 37831.

11. SP10R, Radiation Monitoring Devices Inc., 44 Hunt St. Watertown MA. 02172.

12. LKB Ultrofilm, LKB-Produkter AB, Box 305, S-161 26 Bromma, Sweden.

13. Overhoff & Associates, Inc., "Technical Manual for the Tritium Monitor Betatec", Milford Ohio. also Femtotech Inc., PO. Box 8257, Carlisle OH. 45005.

14. H. O. Menlove and J.E. Swanson, "A High-Performance Neutron Time-Correlation Counter", Nucl. Technol. 71, 497-505, (1985).

15. H. O. Menlove, M. M. Fowler, E. Garcia, M. C. Miller, M. A. Paciotti, R. R. Ryan and S. E. Jones, "Measurements of Neutron Emission from Ti and Pd in Pressurized D_2 Gas and D_2O Electrolysis Cells," Joun. of Fusion Energy, 9 (4) (1990).

16. R. Lasser and K. H. Klatt "Solubility of Hydrogen Isotopes in Palladium", Phys. Rev. B, 28, 748 (1983) and also Dr. Ivar Lindstrom, Private Communication, November 1990.

Conference Proceedings Vol. 33
«The Science of Cold Fusion»
T. Bressani, E. Del Giudice and G. Preparata (Eds.)
SIF, Bologna 1991

HYDROGEN AND ITS ISOTOPES IN AND ON METALS

LOUIS SCHLAPBACH

Solid State Physics Research Group, University of Fribourg, CH-1700 Fribourg, Switzerland

Abstract

A summary description is given of phenomena related to the surface adsorption and bulk absorption of hydrogen and of its isotopes by a metallic host. Thermodynamic and surface properties, electronic and crystal structure and diffusion are illustrated for the examples of the hydride formation of Pd and of $LaNi_5$ as typical examples of hydride forming elemental metals and intermetallic compounds.

Introduction

"Hydrogen (deuterium) in and on metals" as a topic attracts metallurgists, solid state scientists, mechanical and chemical engineers, energy technology specialists and nowadays also those scientists who try to clarify the cold fusion phenomena.

Let us consider a metal-hydrogen system. It consists of a metal, of hydrogen in a gaseous or condensed phase and of an interface inbetween. We then ask how hydrogen reacts at the interface with the metal, whether and how hydrogen diffuses into the metal and forms a solid solution, a metal hydride or other types of "hydrogen-metal-alloys". As a metal hydride we define a single phase compound between a host metal and hydrogen, e.g. $PdH_{0.6}$, MgH_2, $LaNi_5H_{6.5}$. Then we would like to know the properties of these hydrogen-metal alloys and whether isotope effects appear. Deuterium, tritium and also the positive muon μ^+ are considered as hydrogen isotopes. Finally we have to

ask whether situations may exist in which two hydrogen (deuterium) atoms come closer than 0.35 Å to raise the fusion rate.

For further reading we recommend [1-5].

Structural and thermodynamic properties

A simplified and frequently used (one-dimensional) model to describe H_2 gas and a hydrogen dissolving metal is shown in Fig. 1. A hydrogen molecule approaching the metal can be dissociated at the interface, adsorbed at appropriate surface and near surface sites and dissolved at interstitial sites of the host metal. If the local hydrogen concentration exceeds a certain limit, a hydride phase precipitates. Upon electrochemical charging an electron transfer reaction converts adsorbed H_2O into adsorbed H and OH^-.

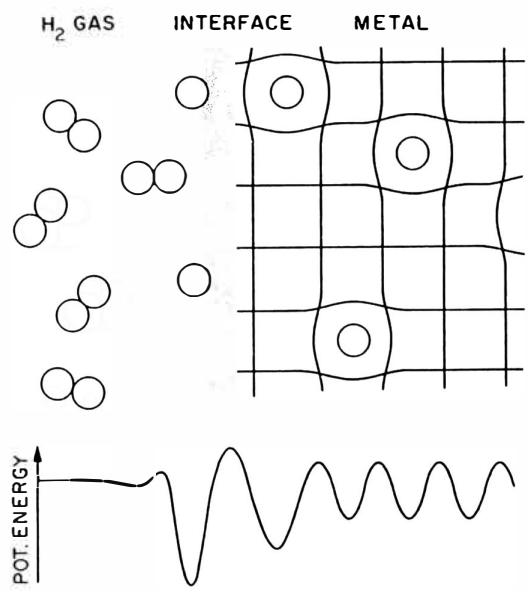

Fig. 1. Simplified model of the dissociation of molecular hydrogen at an interface and of the solution of hydrogen atoms in the bulk, on interstitial sites

The thermodynamic aspects of hydride formation (gaseous hydrogen) can be described by pressure-composition isotherms (pcT curves, Fig. 2). The host metal dissolves some hydrogen as a solid solution (α-phase). As the H_2 pressure, and herewith the concentration C_H of dissolved H, is increased, the H-H interaction becomes locally important and nucleation and growth of the hydride phase (β) start.

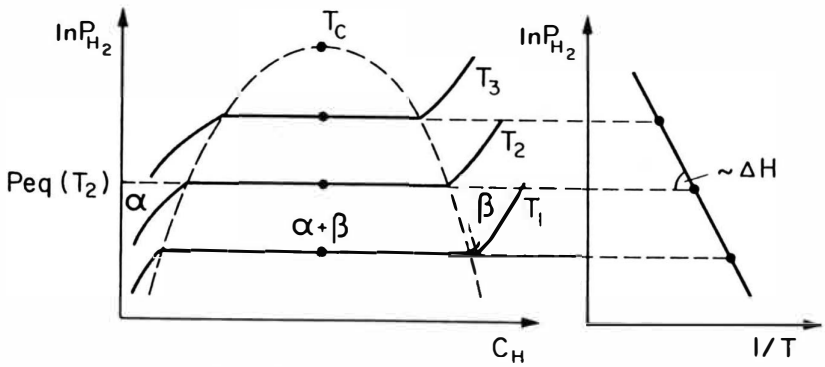

Fig. 2. Pressure-composition isotherms for the solid solution of hydrogen (α-phase) and hydride formation (β-phase). The region of coexistence of the two phases is characterized by the flat plateau at the equilibrium pressure p_{eq} (T) and ends at the critical temperature T_c. The enthalpy of hydride formation ΔH is obtained from the variation of the equilibrium pressure (on a logarithmic scale !) with temperature in a van't Hoft plot [4].

At the electrochemical interface the electrochemical potential replaces ln p(H_2) in Fig. 2 according to the Nernst equation. While the two phases α and β coexist, the isotherms show a plateau, the length of which determines how much H_2 can be stored reversibly with small pressure variations. In the pure β-phase the H_2 pressure raises steeply with the concentration. At higher H_2 pressure further plateaux and further hydride phases may be formed. The two-phase region ends in a critical point T_c. The plateau pressure p_{eq}(T) strongly depends on temperature. From the slope of a so-called van't Hoff plot of the plateau pressure (on a logarithmic scale) versus T^{-1}, the enthalpy of hydride formation ΔH can be evaluated. At room temperature p_{eq} amounts to and 1.6 bar for Pd and $LaNi_5$, respectively.

Most host metal lattices expand upon the absorption of hydrogen; the crystal structure changes mostly with a reduction of symmetry, a H-sublattice is formed, order-disorder transitions of the H-sublattice occur, lattice defects are formed, strain fields grow, and even non crystalline and probably quasi-crystalline materials can be formed.
The equilibrium pressure p_{eq}(T) for deuterium or tritium absorption is for many metals higher than for hydrogen absorption, the so called normal isotope effect.

The equilibrium position of hydrogen and of its isotopes on interstitial sites is determined experimentally by neutron diffraction. All diffraction pattern measured so far are in agreement with the occupation of interstitial sites by one or zero hydrogen atoms. There is no experimental evidence for "hydrogen clusters" in the same interstitial hole. Upon increasing the pressure additional hydrogen goes into different sites. The

H-H or D-D- separation was never found to be smaller than 2.1 Å in metallic hydrides and 1.87 Å in complex hydrides such as K_2ReHg [6].

In the two phase region the expanded hydride phase β and the host metal phase α coexist. In ductile metals like Pd the $\alpha \rightarrow \beta$ transition across the two phase region introduces lattice defects; brittle materials like many intermetallics disintegrate into a powder, a special type of hydrogen embrittlement. $LaNi_5$ disintegrates into powder of $\approx 10\mu m$ grain size and $\approx 0.3\ m^2/g$ specific surface area.

Non equilibrium phenomena may be related with that crack formation and propagation upon hydrogen absorption. Among others strong local electric fields where mentioned [7].

Electronic Properties

The dissolution of hydrogen in a metal lattice and the formation of a metal hydride perturbs considerably the electrons and phonons of the host metal. Four different effects are in general relevant for understanding the changes in the electronic structure:

1) the generally observed expansion of the lattice often accompanied by a change in the crystal structure results in a modification of the symmetry of the states and in a reduction of the band width.

2) The attractive potential of the proton affects those metal wavefunctions which have a finite density at the H site and leads to the so-called metal-hydrogen bonding band below the metal d-band.

3) The additional electrons brought by the H atoms into the unit cell result in an upward shift of the Fermi level.

4) H-H interaction leads to new features in the lower portion of the electron density of states.

Effect 2), the lowering of host metal states to form the bonding band, corresponds to an exothermic contribution to the enthalpy of hydride formation whereas effect 3), the

upward shift of E_F represents an endothermic contribution. In a first approximation the balance of 2) and 3) decides on the stability of the hydride [8]. The effects are clearly visible in the calculated density of electronic states of Pd and PdH_x (Fig. 3a) and in the measured x-ray photoelectron spectra of the valence band of $ZrMn_2$, $ZrCr_2$, ZrV_2 and their hydrides (Fig. 3b).

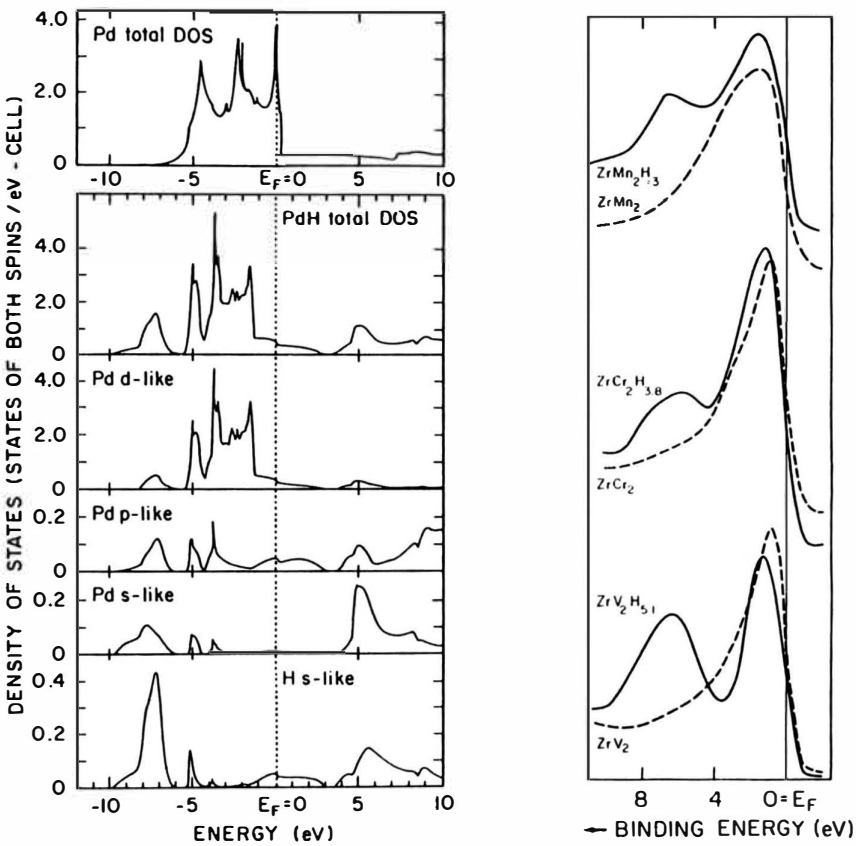

Fig. 3a (left): Calculated total density of electronic states (DOS) of Pd metal (top) and stoichiometric PdH as well as partial DOS of PdH. [8 and ref. cited therein].

Fig. 3b (right): X-ray photoelectron spectra of the valence bands of $ZrMn_2$, $ZrCr_2$, ZrV_2 and their hydrides [8 and ref. cited therein].

Dynamics and diffusion of hydrogen

Hydrogen atoms dissolved in a metallic host lattice may perform motional processes on very different time scales: They vibrate on interstitial sites at frequencies much higher than the neighbour metal atoms and amplitudes of ≈ 0.1 - 02. Å. After many

oscillations on one site a H atom may jump into another site. Subsequent jumps may lead either to local motions over spacially restricted areas or to long range diffusion.

Diffusion of interstitial H in transition metals and transition metal alloys has been known for a long time to be very fast; the diffusion coefficient D reaches values up to 10^{-4} cm^2/s around room temperature (Fig. 4),

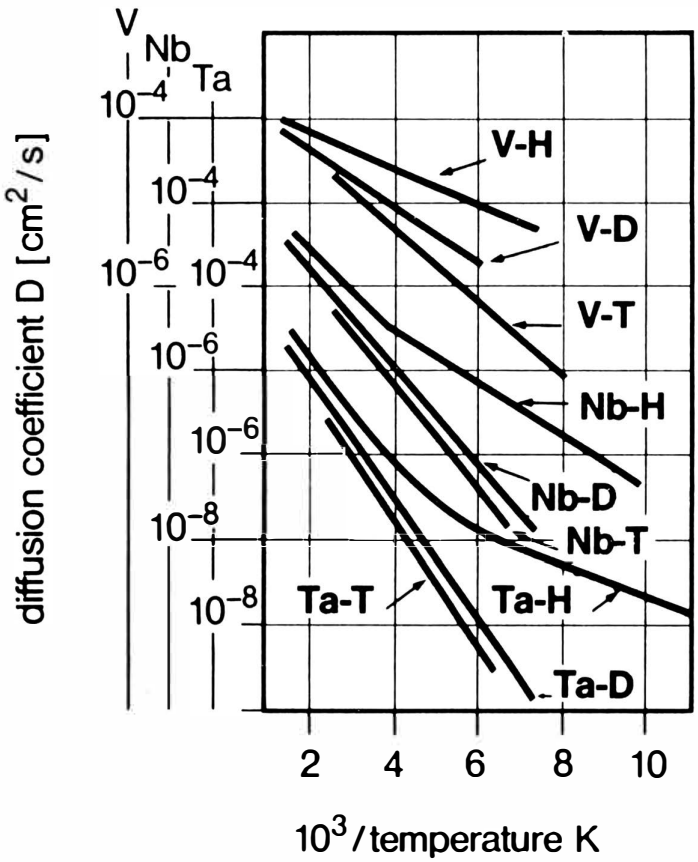

Fig. 4: Diffusion constant of hydrogen, deuterium and tritium in bcc metals as a function of inverse temperature [9].

i.e. values 10 to 15 orders of magnitude higher than for nitrogen or oxygen. In terms of an Arrhenius law $D = D_0 \exp(-E_a/kT)$ the activation energies E_a are very low, of the order of 100-200 meV and account for the high values of the diffusion constants.
The isotope effect observed for D_0 and E_a does not exhibit the behaviour expected for classical jump diffusion. Quantum effects play a significant role. For H diffusion the quantum effects dominate low temperature diffusion; for the diffusion of the light isotope μ^+ they are more pronounced already at higher temperatures.

A discrepancy between measured jump length and distances between interstitial sites lead to the assumption of time correlated jumps according to the following model: the distortion field around an interstitial H atom lowers its potential energy by 0.1 eV relative to that on neighbouring unoccupied sites. If the residence time is much shorter than the lattice relaxation time jumping from an interstitial site into the nearest interstitial site and again into the next nearest interstitial sites may be favorable [9].

The D atom vibrations are not expected to bring D atoms on adjacent interstitial sites significantly closer together.

Surface Properties

The first step in the formation of metal hydrides and solid solutions from molecular hydrogen gas or by electrochemical charging occurs on the surface of the host metals. The interaction with H_2 can consist e.g. of sticking, dissociative chemisorption, surface diffusion and solution in the near surface or bulk region. The H-metal bonding is of electronic nature at the surface as in the bulk.

In order to minimize the free energy of a crystal the equilibrium position of surface atoms is different from that given by the lattice periodicity of the bulk. This surface relaxation often amounts to a 5-10% contraction between the first and second layer without noticeable change in the lateral symmetry. In few cases clean metal surfaces are reconstructed, i.e. the lateral symmetry of the top layers differs from that of the bulk. Upon increasing coverage adsorbed H atoms form disordered or ordered surface phases. The adsorption itself can induce relaxation or reconstruction of the substrate surface or even cancel the relaxation or reconstruction of the clean substrate surface. There is experimental and theoretical evidence that chemisorbed H does not necessarily occupy sites on top of the first metal atom layer, but also sites between and underneath top surface metal atoms. Subsurface H was observed together with a strong surface reconstruction (surface hydride formation). The H-H (and D-D) equilibrium distances are comparable to those between bulk interstitial sites, i.e. ≥ 2 Å. The distance between planes of surface D and subsurface D e.g. on Pd (111) can be shorter, however, it is unlikely that a surface D sits on top of a subsurface D in thermal equilibrium distribution [10].

Whenever dynamical processes dominate the interaction, isotope effects can occur. They have been reported for the H binding energy, the dynamics of trapping and sticking as well as for surface diffusion. None of them point to extraordinarily short D-D- distances so as to be required to raise the D-D fusion rate.

In studies of the interaction of Pd(100), Pd(110), and Pd (111) with H and D at low temperature (≈ 115 K) an up to 10 times slower rate of filling of α states (bulk H sites) was observed when using D instead of H [11]. These results were obtained on the reconstructed surfaces, i.e. after saturation coverage of the chemisorption sites. That isotope effect is normal in the sense that the higher equilibrium pressure of the D_2-Pd bulk-isotherms cause a higher driving force for D_2 at equal H_2 and D_2 pressure. The size of the effect, however, is larger than expected and might point to strong quantum phenomena.

The influence of a high electric field on the photon stimulated desorption of hydrogen and deuterium from Rh and Ni surfaces yield H^+, D^+, H_2^+ and D_2^+ as desorbing species and apparently no isotope exchange [12].

Electrode surface contamination by heavy metals

We analyzed the surface of several Pd electrodes after electrochemical charging in D_2O (LiOD) and H_2O (LiOH) at different current densities during some hours up to several weeks. X-ray photoelectron spectroscopy (XPS), which probes the top 20 to 30 Å, was used. Surprisingly, strong Pb contamination of more than one atomic monolayer together with weak Hg and Bi contamination was observed (Fig. 5).

On the Pd electrode of the cold fusion experiment done at PSI (Villigen, Switzerland) we found Zn as major contamination in amounts of several monolayers and some Pb and Hg.

Additional test experiments proofed that the heavy metal impurities originated from D_2O. They were electrochemically deposited on the Pd electrode. It is evident that monolayers of heavy metal impurities change the surface/interface properties of electrodes considerably. Experienced electrochemists may be aware of that problem and clean their electrolytes prior to the experiments.

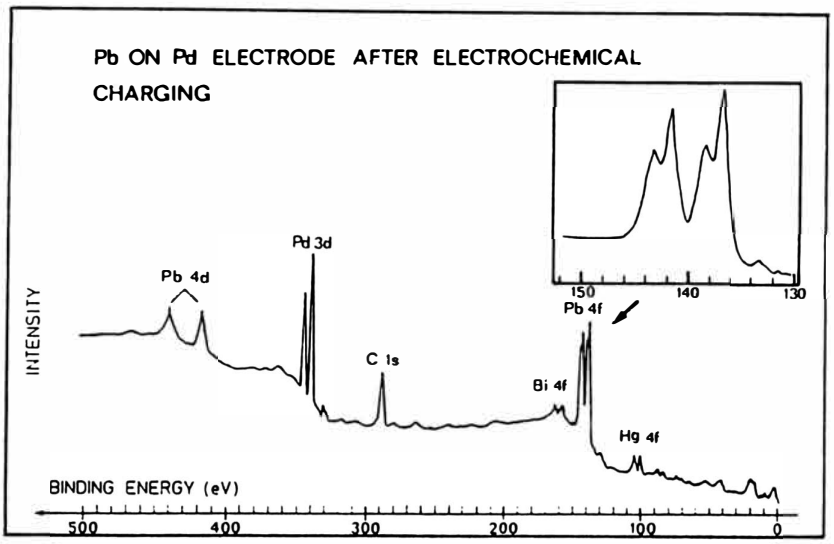

Fig.5. Photoelectron spectrum of a palladium electrode taken after an electrochemical cold fusion experiment in D_2O (LiOD) showing unexpected lead contamination of the order of an atomic monolayer and minor mercury and bismuth contamination as well as the usual carbon contamination. The splitting of the Pb $4f_{7/2}$ emission into peaks at 136.8 eV and 138.4 eV indicates a mixture of metallic Pb and Pb oxide, resp. [13].

That detection led us to the development of a new extremely sensitive method to detect heavy metal impurities in liquids by electrodeposition and subsequent analysis by XPS [13,14]. The sensitivity is better than 1 ppt.

Acknowledgment: Collaboration with Thomas Greber and Alban Fischer and financial support by NEFF (National Energy Research Foundation) are gratefully acknowledged.

References

1) W.M.Müller, J.P. Blackledge, G.G.Libowitz: Metal Hydrides (Academic Press, New York 1968).

2) G.Alefeld, J.Völkl: Hydrogen in Metals, Vols. I and II, Topics in Applied Physics Vols. 28 and 29, Springer-Verlag Berlin, 1978.

3) G.Bambakidis, R.C.Bowmann: Hydrogen in Disordered and Amorphous Solids, NATO ASI, Series B: Physics Vol. **136** (Plenum Press, New York 1986).

4) L.Schlapbach: Hydrogen in Intermetallic Compounds, Vols. I and II, Springer Topics in Applied Physics, **63** (1988) and **67** (in press), Springer-Verlag Berlin.

5) J.J.Reilly, G.D.Sandrock: Sci. Am. **242**, 118 (1980).

6) K.Yvon, P.Fischer: Crystal and Magnetic Structures of Ternary Metal Hydrides, chap. 4 in ref. 4, Vol. I

7) J.S. Cohen, J.D.Davies: Nature **342**, 487 (1989); S.E.Segre, S.Atzeni, S.Briguglio, F.Romanelli: Europhys. Lett. **11**, 201 (1990) and Conf. Proc. "Understanding Cold Fusion Phenomena", R.A.Ricci et al., eds., Soc. Italiana di Fisica, 1990, p. 147.

8) M.Gupta, L.Schlapbach: Electronic Properties, chap. 5 in ref. 4, Vol. I.

9) D.Richter, R.Hempelmann, R.Bowmann: "Dynamics of hydrogen in intermetallic hydrides", chapt. 3 in ref. 4, Vol. II; R. Hempelmann, D.Richter, T.Springer: IFF-Bulletin 35/1989, KFA, D-5170 Jülich; R.Hempelmann, D.Richter: Europhys. News **22**, 110 (1991).

10) L.Schlapbach: "Surface properties and activation", chap. 2 in ref. 4, Vol. II.

11) R.J.Behm, V.Penka, M.G.Cattania, K.Christman, G.Ertl: Chem. Phys. **78**, 7486 (1986); G.E.Godowski, R.H.Stulen, T.E.Felter: J. Vac. Sci. Technol. **A5**, 1103 (1987).

12) S.Jaenicke, J.Dösselmann, A.Ciszewski, W.Drachsel, J.H.Block, D.Menzel: Surf. Science **211/212**, 804 (1989)

13) T.Greber, A.Fischer, C.Rhême, S.Drissi, J.Osterwalder, J.Kern, L.Schlapbach: Conf. Proc. "Understanding Cold Fusion Phenomena", R.A.Ricci et al., eds., Soc. Italiana di Fisica, 1990, p. 219.

14) A.Fischer, T.Greber, L.Schlapbach: Swiss Patent CH 678 662 A5 (1991).

Conference Proceedings Vol. 33
«The Science of Cold Fusion»
T. Bressani, E. Del Giudice and G. Preparata (Eds.)
SIF, Bologna 1991

ISOTHERMAL FLOW CALORIMETRIC INVESTIGATIONS OF THE D/Pd SYSTEM

By:

Michael C. H. McKubre, Romeu Rocha-Filho
Stuart I. Smedley, Francis L. Tanzella
SRI International

and

Steven Crouch-Baker, Thomas O. Passell, Joseph Santucci
Electric Power Research Institute

INTRODUCTION

An experimental program was undertaken to explore the central idea proposed by Fleischmann *et al.*[1] that heat, and possibly nuclear products, could be created in palladium lattices under electrolytic conditions.

Three types of experiments were performed to determine the factors that control the extent of D loading in the Pd lattice, and to search for unusual calorimetric and nuclear effects. It is the purpose of this communication to discuss observations of heat output observed calorimetrically in excess of known sources of input heat.

The central postulate guiding the experimental program was that anomalous effects previously unobserved or presently unexplained in the deuterium-palladium system occur at a very high atomic ratio D/Pd. Emphasis was placed on studying phenomena that provide a fundamental understanding of the mechanism by which D gains access to the Pd lattice, and how very high loadings (near, at, or perhaps, beyond unity) can be achieved and maintained.

Measurements of the interfacial impedance and of the Pd cathode voltage with respect to a thermodynamic reference electrode were made in order to characterize the electrochemical kinetic and thermodynamic processes that control the absorption of D into Pd.

Measurements of the Pd solid phase resistivity were used to monitor on-line, the degree of loading atomic ratios, specifically D/Pd, H/Pd and H/D. Calibration of the resistance ratio - atomic ratio functionality has been made by reference primarily to the works of Baranowski[2-4] and Smith[5,6], but also by volumetric observation of the displacement of gas during loading in a closed system at constant pressure and temperature.

The overall conclusions of this study are that, by careful control of the electrode pretreatment, the electrolyte composition and the current density, it is possible to load Pd to an atomic ratio D/Pd $\gtrsim$ 1, and to sustain this loading for periods of weeks.

Calorimetric experiments were performed in palladium rods, highly loaded with D and/or H, and electrolyzed at substantial current densities (typically 300-600 mA cm^{-2}, but up to 6400 mA cm^{-2}) for considerable periods of time (typically 1000-2000 hours). The application of knowledge gained from the independent loading studies was essential in achieving these conditions.

Our calorimeters were designed with the philosophy that in precise calorimetry, and in the search for unusual reaction products, it is desirable to have a closed system, and a knowledge at all times of the composition of the reacting system. All experiments were performed with closed and sealed electrochemical cells operating from 40 to 10,000 psi above atmospheric pressure. Axial resistance measurements were made to monitor the D/Pd or H/Pd ratio.

Approximately 30 experiments have been performed with flow calorimeters operating at constant power input. The calorimeters were designed and constructed with the following features:

- Conceptually simple system based on the first law of thermodynamics.
- Maintenance of complete control of operating parameters (including cell temperature).
- A large dynamic range of heat input and output (0.1 - 100 W).
- On-line monitoring of all important variables.
- Multiple redundancy of measurement of critical variables *e.g.* temperature.
- High accuracy and precision (the greater of 10 mW or 0.1%).
- Known sources of potential error yield conservative estimates of output heat.
- Steady state operation leading to simple analysis.

EXPERIMENTAL METHODS

Two systems of flow calorimeters were designed in accordance with the principles outlined above. One system accommodated up to four large electrochemical cells (working volume up to 200 cm^3 and power input ≥ 100W). The other accommodated three "small" cells (working volume 50 cm^3 and power input up to ~ 30 W).

These two systems had several features in common. In both, a sealed electrochemical cell was fitted with a helically wound compensation (and calibration) heater and sheathed with axially oriented heat exchanging fins. This unit was immersed directly in the calorimeter heat transfer fluid inside an isothermal and insulating boundary (the calorimeter). The isothermal boundary was itself immersed in a well regulated (± .003°C) bath of the same fluid. In early experiments this fluid was silicone oil, chosen for its low

heat capacity, low corrosivity, and its good electrical insulation properties. In recent experiments the calorimeter fluid was water for which the heat capacity is better known and exhibits smaller dependence on temperature.

The heat transfer fluid was pumped from the bath, past the cell inside the calorimeter volume, using FMI (QV-OSSY) constant displacement pumps. The mass flow rate was determined by pumping the flow to an auto siphon device placed on a digital balance. The control/measurement computer polled the balance periodically to determine the average mass flow rate as $\delta m/\delta t$.

All experiments were performed with thermodynamically closed electrochemical cells at D_2 partial pressures between ambient and ~10,000 psi. In high pressure cells the charging current was sustained by the anodic reaction of $1/2\ D_2 + OD^- \rightarrow D_2O + e^-$ (in base). At higher anodic current densities or low D_2 partial pressures, O_2 was evolved at the anode. A large area catalyst was provided in the head space of the cells to recombine evolved O_2 and D_2 so that the net reaction in all cells after the Pd rod is loaded is $D_2O \rightarrow D_2O$, for which the thermoneutral voltage is zero.

Constant current or slowly ramped current conditions were used in all cases. Commonly, experiments were performed electrically in series in order to test the effects of different variables *e.g.* D_2O versus H_2O. Under current control, the cathode voltage and cell voltage frequently were observed to fluctuate significantly, particularly at high current densities in low pressure cells where the presence of large D_2 and O_2 bubbles disrupted the electrolyte continuity. Three electrode potentiostatic control, or two terminal voltage control of a series string, in the presence of a fluctuating load (cell resistance) will cause a fluctuation in both the cell voltage and current and make an unmeasured contribution to the input power (that may be interpreted incorrectly as excess heat) unless the *rms* levels are monitored. On the other hand, if the cell current is provided from a source that is sensibly immune to noise and level fluctuations, then the current would operate on the cell voltage (or resistance) as a scalar. As long as the voltage noise or resistance fluctuations are random, no unmeasured *rms* heating can result under constant current control.

The power input to the calorimeter by the electrochemical current was considered to be the product of that current and the voltage at the isothermal boundary. Under experimental conditions this input power changed due to voltage or resistance variations in the cell, or at times when the current was ramped. This had two undesirable consequences. A change in input power changed the cell temperature so that the electrochemical conditions were no longer under control. A change in the temperature also moved the calorimeter from its steady state as the calorimeter contents took up or released heat. To minimize these effects, a compensation heater was used to correct for changes in electrochemical power so that the sum of the heater and electrochemical power input to the calorimeter was held constant. A computer controlled, power supply was used to drive the compensation heater element operated in galvanostatic mode in order to avoid possible unmeasured *rms* heat input. This heater also was used for calorimeter calibration, where the input power was measured as the product of the heater current and voltage at the isothermal boundary.

Figures 1 and 2 show schematic detail of the small and large calorimeter vessels. Different strategies were employed in these two designs to minimize the conductive heat loss through the many wires which enter the vessel for electrical sensing and current control. A simple labyrinth design was used in the small calorimeter in which the electrical leads are taken from the cell by a tortuous path to the outside, and are forced to give up heat in a counterflow of incoming fluid. For the mass flow rates typically used in our experiments (1-2 g s^{-1}), the conductive power loss was of the order of 1-2% of the total input power calculated as above.

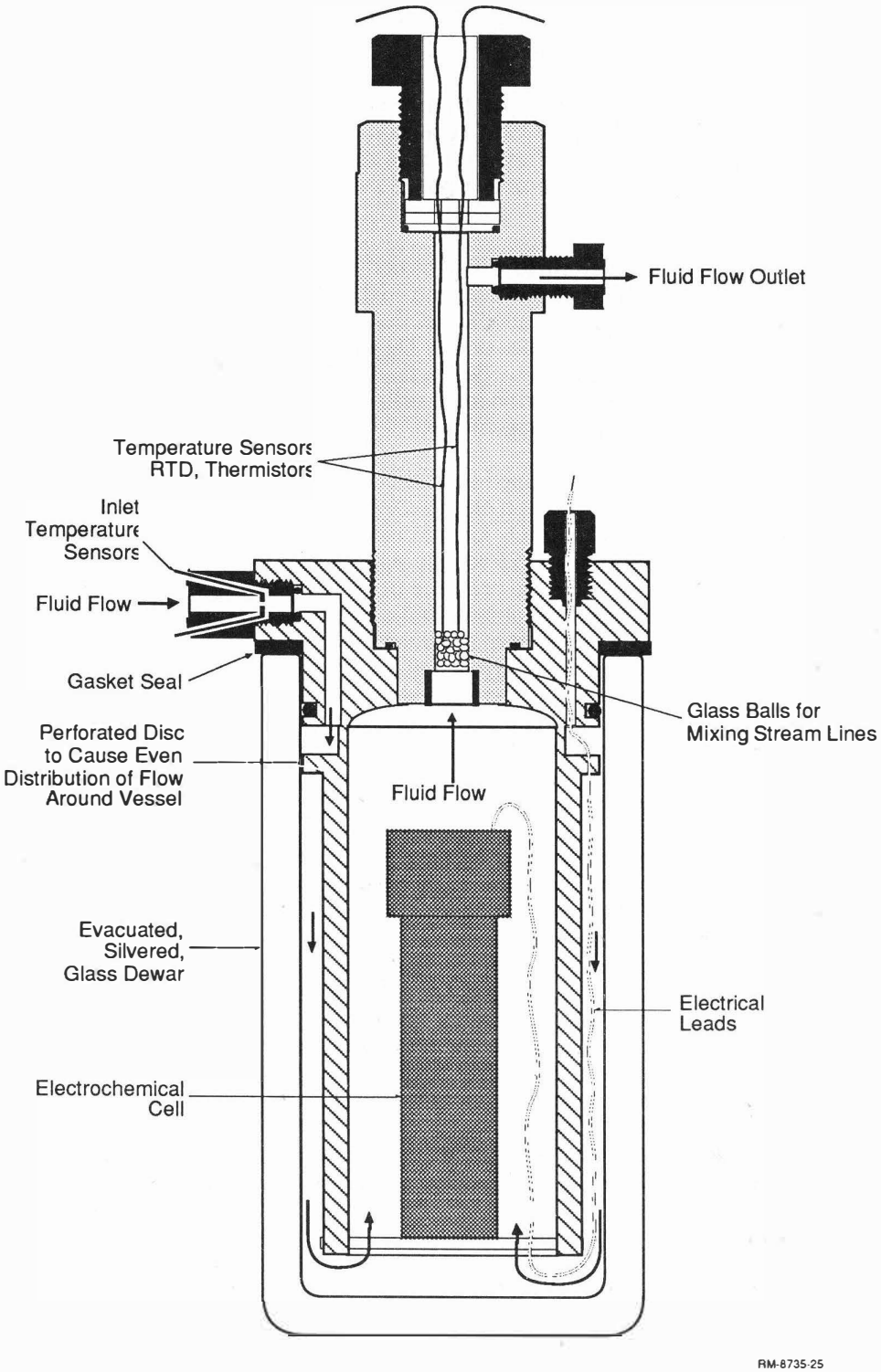

Figure 1. Small flow calorimeter, detail.

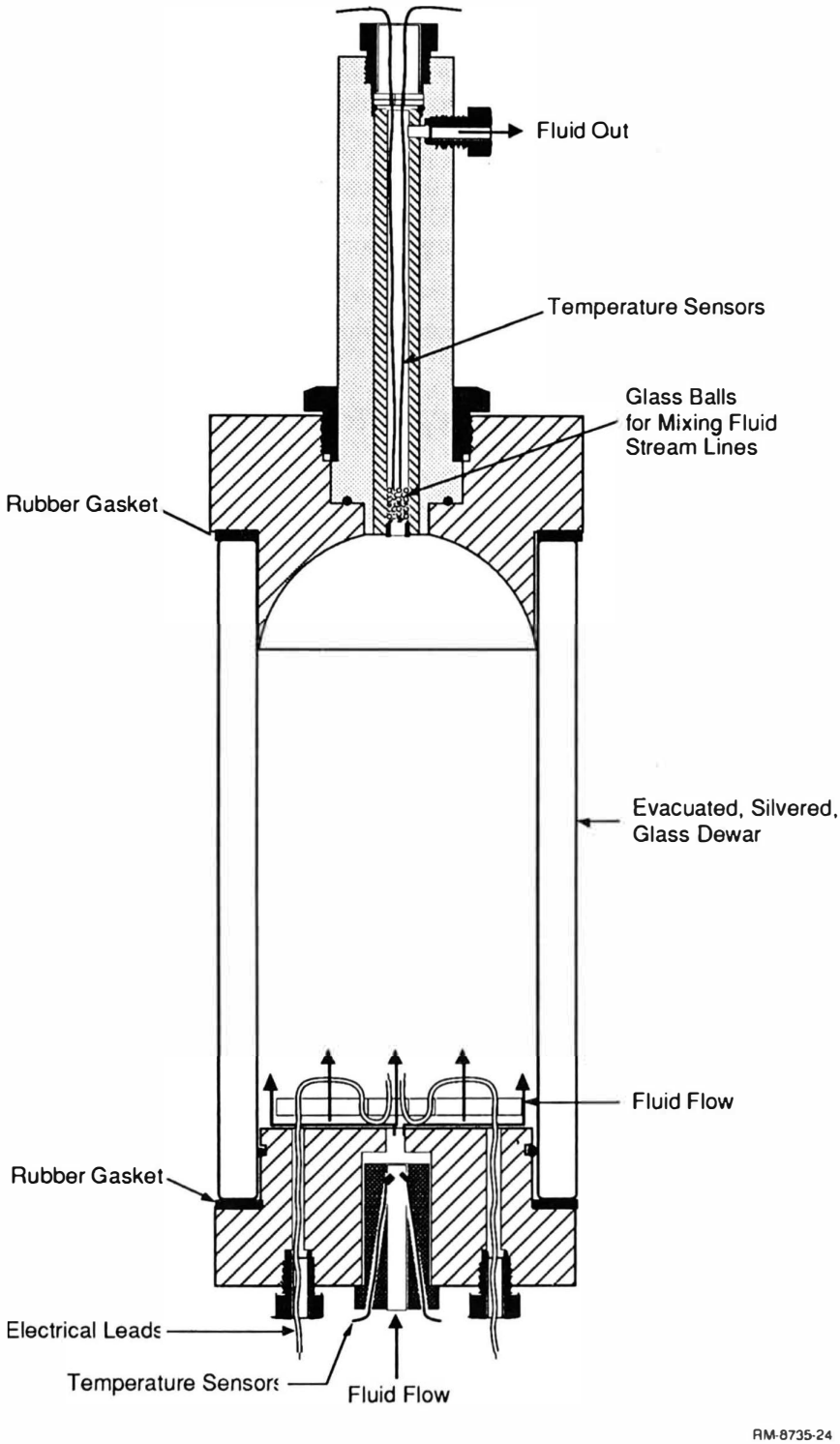

Figure 2. Large flow calorimeter, improved design.

Advantage was taken in the large calorimeters of the fact that the incoming fluid was at the same temperature as the bath, and that predominant heat transport was upward. All electrical leads were taken through the bottom insulating boundary across which ΔT (and therefore conductive loss) was a minimum. An additional feature of the large calorimeters was the pressure pipe which extended from the cell to a pressure transducer above the bath. The pressure pipe also contained a PTFE catheter that was used to insert chemical species into operating cells. For practical reasons the pressure pipe emerged through the top insulating boundary and contributed an additional conductive loss term. For the mass flow rates used, conductive power loss in the large calorimeters represented typically 3-5% of the total input power.

The steady state equation of heat output from the calorimeter can be given as

$$P_{output} = (C_p\, \delta m/\delta t + k')\,(T_{out} - T_{in}) \qquad [1]$$

where C_p is the average value of the heat capacity of the calorimeter fluid in its transit through the calorimeter, $\delta m/\delta t$ is the fluid mass flow rate, k' is the effective conductive loss term, T_{in} is the inlet (or bath) temperature and T_{out} is the average temperature of the emerging fluid.

Similarly, for the power input to the calorimeter,

$$P_{input} = |I_c\, V_c| + |I_h\, V_h| + P_u \qquad [2]$$

where I is current, V is voltage measured at the calorimeter boundary, and subscripts c and h refer to the electrochemical cell and compensation heater. The additional term, P_u, is any unaccounted power source, and may be positive, negative or zero.

Currents were measured as a voltage dropped across a calibrated, series resistor;

$$I_c = V_{cr}/R_c;\ I_h = V_{hr}/R_h \qquad [3]$$

and the primary temperature measurements were made with platinum resistance temperature devices (RTD's), so that

$$T = T^\circ + (R - R^\circ)/\alpha R^\circ \qquad [4]$$

where T° is the temperature at which the device resistance is R°, and α is the temperature coefficient of resistance of platinum.

In examining potential sources of error, it is useful to express P_u in terms of the directly measured variables. Combining equations we obtain:

$$P_u = P_{output} - P_{input} = \left[C_p \frac{\delta m}{\delta t} + k'\right]\left[\frac{R_{out}}{R^\circ_{out}} - \frac{R_{in}}{R^\circ_{in}}\right][1/\alpha] - \frac{V_h V_{hr}}{R_h} - \frac{V_c V_{cr}}{R_c} \quad [5]$$

This equation has three different classes of variables and constants, with different potential sources of error.

Measured variables: $\delta m/\delta t$, R_{out}, R_{in}, V_h, V_{hr}, V_c, V_{cr}

Predetermined constants: C_p, α, R°_{out}, R°_{in}, R_h, R_c

Calibration constant: k'

Efforts were made to maintain the accuracy of each parameter at better than 0.1%, and also to ensure that potential sources of error result in an underestimate, not an overestimate, of P_u.

Errors in temperature measurement may be attributed to errors in the ratio's R/R° or to α. Resistance measurements were made in a four terminal mode where all RTD's were multiplexed sequentially to a single multimeter calibrated against NIST traceable standards. Since temperature was measured from a resistance ratio, absolute calibration was not of primary importance, although multimeter drift must be avoided Two RTD's were used to sense the inlet and outlet temperatures; the temperature difference was then calculated from the two independent pairs. The inlet sensors were held at the bath temperature, and the bath was held constant with respect to a calibrated thermistor. The inlet RTD's can thus be regarded as secondary resistance standards, referenced to the temperature set by the control thermistor. In this way any trend in resistance due to change in multimeter calibration could be observed.

In some experiments the outlet temperature was sensed with an additional two thermistors to guard further against range-specific resistance calibration drift.

The temperature coefficient of resistance, α, is easily calculated from the Calendar - Van-Dusen equation, the constants of which for platinum are well known. While not independent of temperature, α is effectively constant within a small temperature range. This value was considered unlikely to change with time. Inlet and outlet temperatures each were measured with an accuracy of $\pm$ 0.001K.

Outlet power was determined primarily by the temperature difference and the product $C_p\ \delta m/\delta t$. In all experiments reported here, high purity, air saturated H_2C was used as the calorimeter fluid, for which the thermal capacity was taken to be 4.188 ± 0.004 J g^{-1} K^{-1} in the interval $30 \leq T \leq 40°C$.

Mass flow rates were measured using a Setra model 5000L digital balance with an accuracy of better than 0.01% ($200 \pm .01$g / $240 \pm .01$ seconds). This accuracy reflects the determination of the mass delivered to the balance. Precautions were taken to ensure that fluid was not lost following its transit through the cell before flow rate determination. This was checked, and assured, by employing a 1/4" line with Swagelok® fittings from

calorimeter to pump, and pump to mass balance. The calorimeter vessel was placed on the negative pressure side of the constant displacement pump so that potential leaks from the bath into the calorimeter would be of fluid conveyed past the outlet temperature sensors. Beyond this point leaks would have allowed air into the system; this would not have produced errors in flow rate determination (although this may influence the flow rate).

A schematic diagram of the placement of the large calorimeters in their constant temperature bath is shown from a top view and in profile in Figures 3 and 4; Figure 5 shows the hydraulic flow system for two cells in the large bath. The cells were placed on legs to be above the bottom of the bath and in the well-mixed water. The water supplied to the bath was purified first by ion exchange and then by reverse osmosis. The rate of supply was approximately twice that withdrawn by the calorimeter pumps so that level of the bath was maintained by overflow.

In the large bath, electrochemical cells were connected electrically in series, but the calorimeter systems were hydraulically in parallel. Separate pumps were provided for each calorimeter and the flows were multiplexed for two cells to a single mass-balance. Mass flow rates were measured for one cell during the filling of the auto-siphon vessel (capacity ~ 3500 cc). When the computer sensed that the auto-siphon was operating ($\delta m/\delta t < 0$) the output of both pumps was sent to waste. After a predetermined time, flow from the previously unmeasured cell was sent to the vessel and the cycle repeated. The constant displacement pumps used were relatively immune to a flow rate variation with small changes in head. Nevertheless, care was taken to ensure that the flow rate during the measurement period was the same as that during the eclipse when flow was sent directly to waste. This was done by ensuring that the hydraulic resistance and static heads from the pump to the point at which the flow emerges to the siphon vessel were the same as those from pump to waste. In a number of experiments the flow rate was continuously monitored volumetrically using a rotameter for each cell, to further insure against errors.

Input power was determined for both the cell and the heater as the product of two measured voltages normalized by a precalibrated resistance. Voltages were measured using a Keithley 195A 5-1/2 digit digital multimeter with 0.01% dc volt accuracy and 0.015% resistance accuracy. Resolution was 1 ppm (Ω) and 10 ppm (dcV). Each 5-1/2 digit measurement was averaged 32 times before being recorded. Resistance standards were calibrated periodically against NIST traceable standards using NIST traceable calibration-instruments yielding an accuracy of ~ 0.1%

It is important to note that experiments typically were run with a single controlled current passing through two or more electrochemical cells in series. All measurements were multiplexed to a single multimeter that was periodically interchanged with another precalibrated meter. In this way, a series cell effectively acted as a standard for the others; if P_u was observed not to be zero in one cell while zero in another, then its origin was unlikely to be an artifact of voltmeter miscalibration. Monotonic calibration drift was monitored by multimeter interchange. The current was monitored independently in each of the cells in series so that R_c for each cell acted as a standard for other series cells. The resistors were interchanged, replaced, and removed and recalibrated during periods of excess power production ($P_u > 0$), reducing the likelihood that errors were associated with the measurement of current.

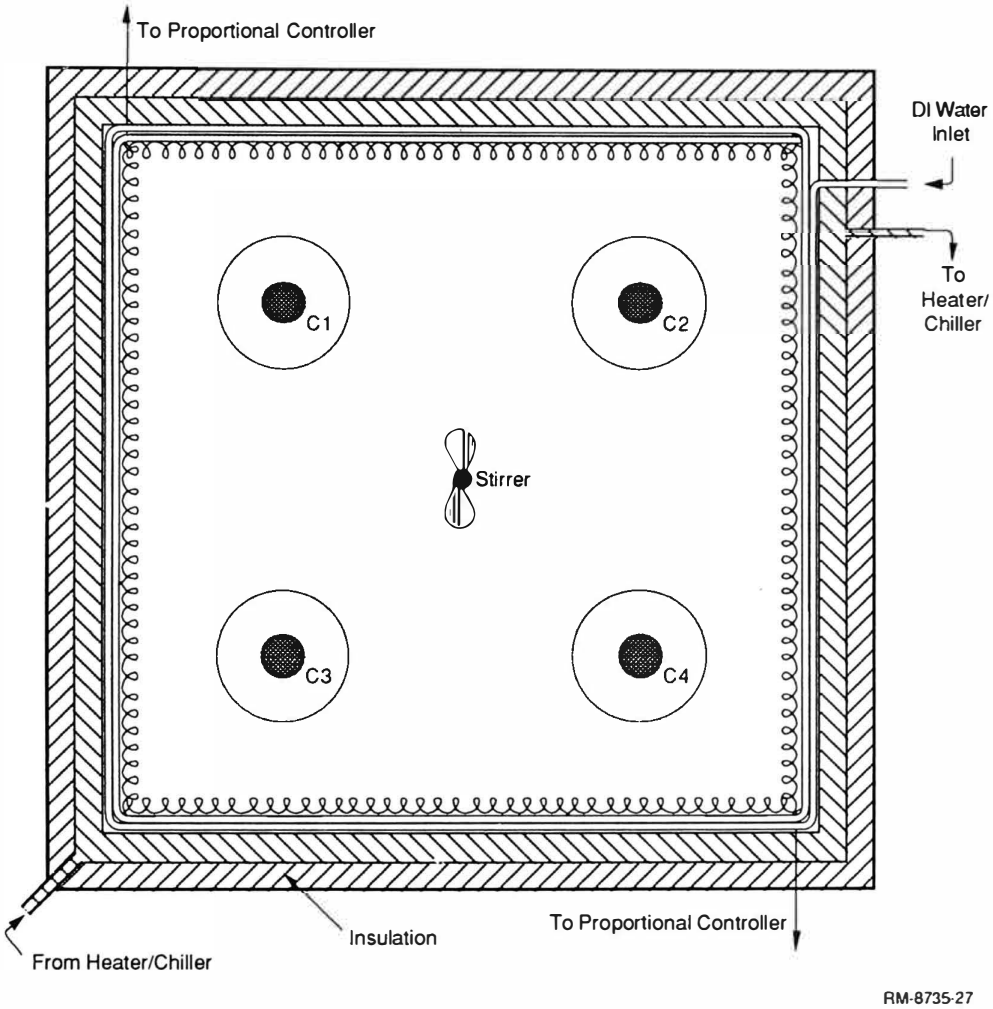

Figure 3. Large bath for calorimetric experiments, top view.

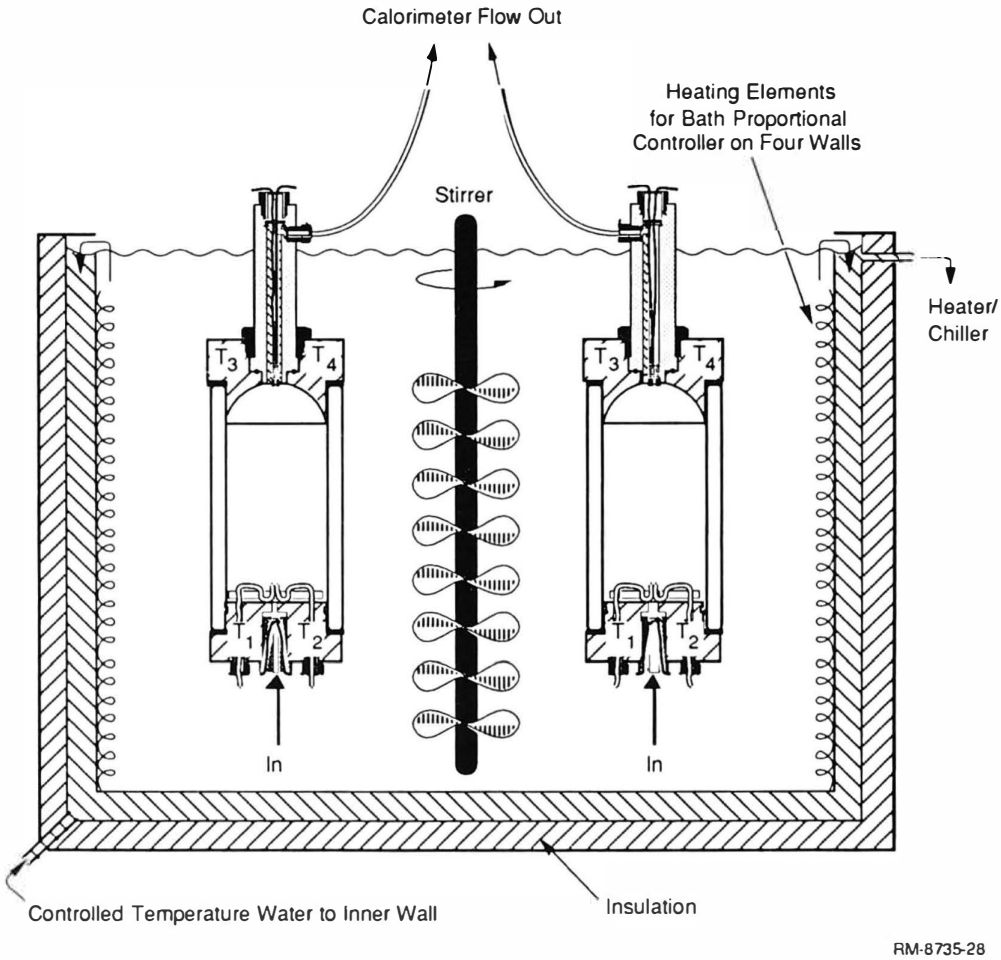

Figure 4. Large bath for calorimetric experiments, side view.

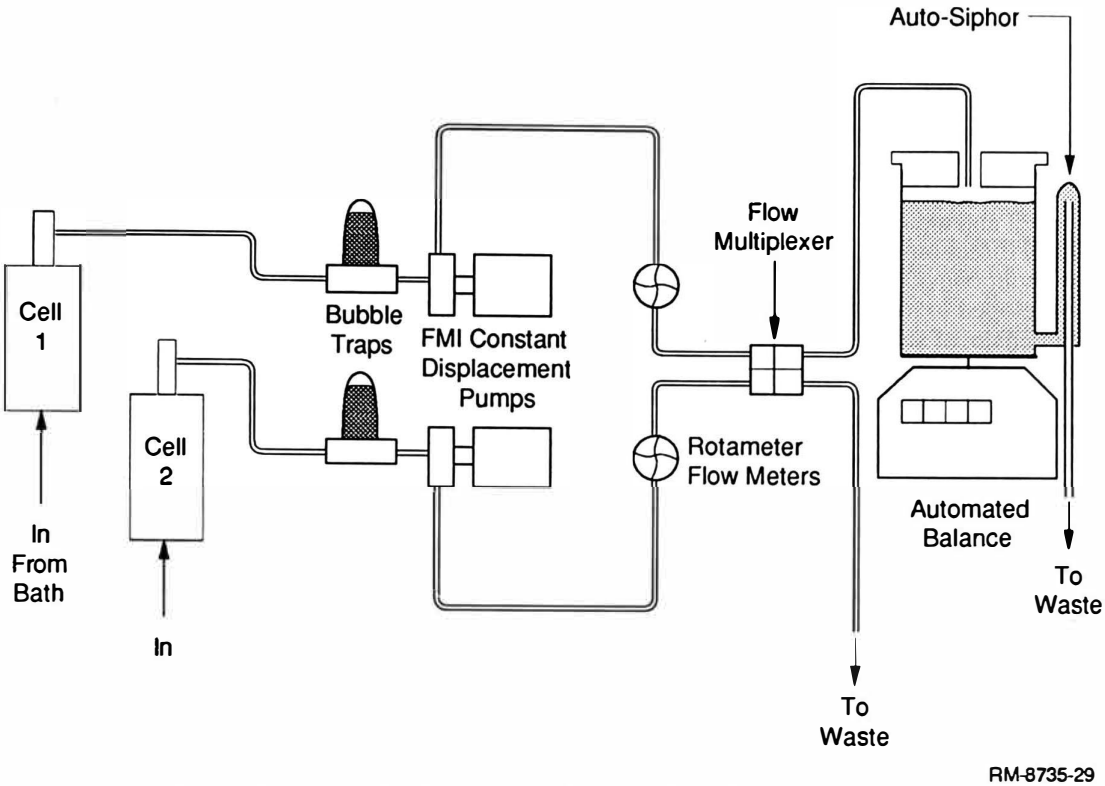

Figure 5. Hydraulic flow system for calorimetric experiments.

The remaining term in equation [5] for discussion, is the "effective" conductive loss term, k'. This term is special, and has been the subject of considerable analysis that is not reported here. Conductive heat transport occurred because the electrochemical cell, its contents, and the contents of the insulating, isothermal boundary of the calorimeter vessel, were at a temperature different from that of their surroundings. By submerging the calorimeter vessels in a well-mixed, well-controlled and constant temperature bath, the environment of primary significance was that of the fluid bath . This fluid entered the vessel; in the small cell by a convolved path, in the large cell at the bottom, on the cylindrical axis. Once the flow approached the cell or the conductors contacting the cell it was heated. A conductive loss therefore occurred with respect to the bath.

An added complexity with the large calorimeter was heat transported through the pressure pipe that emerged through the top insulating boundary. This pipe contacted the bath fluid but terminated in the air above the bath. Depending on the ambient and cell temperatures, heat could have been conducted in or out of the calorimeter.

A number of distributed heat conduction paths were therefore present which we have analyzed at three levels of complexity. In a lumped parameter model the cell and heater inside the enclosing metal boundary were treated as a point source that was represented by the average properties: mass, heat capacity and temperature. This point source was considered to give up heat to the flowing fluid and exchange heat conductively with the environment through the pressure pipe, and with the bath through the conductive cables. The emerging fluid may exchange heat with the bath through the walls and top of the calorimeter vessel.

In a distributed parameter model, we have determined the heat balance with sources and sinks distributed in one dimension along the axis of the calorimeter. We considered separately the inlet plenum (elements of flow after the inlet sensor and before the cell), along the length of the cell, and in the outlet plenum (up to the outlet sensors at the calorimeter boundary).

These two approaches made use of the metallic boundary provided by the pressure vessel and axial heat fins to approximate a heat source that was isothermal in the radial and axial directions, (lumped parameter) or just the radial dimension (distributed parameter), without consideration to the distribution of sources inside. A finite element model is being developed to more accurately represent the various distributed heat sources: the two dimensional sources at the anode and cathode interfaces, the three dimensional source of the electrolyte volume, the three dimensional source of the recombiner at the top of the cell, the approximately two dimensional source of the helical compensation heater, and the roughly linear sources of current flowing to the cell in the conductive cables inside the calorimeter boundary.

The lumped parameter model has been analyzed for both the steady state and transient response of the calorimeter. The distributed parameter model has been developed to obtain a steady state solution, while no results have yet been obtained from the finite element model.

On the basis of the modeling, thus far, we are able to draw a number of useful conclusions:

- It is meaningful to define an effective loss term, k', composed of several different heat flows from distributed sources.
- The value of k' is negligibly influenced by the distribution of the heat source within the pressure vessel.
- Within the variations of bath and room temperature experienced and expected, k' may be considered to be constant within the limits of experimental error.
- Within the range of mass flow rates used, the calorimeter response could be represented by a single exponential response, with time constant varying approximately inversely with mass flow rate. Using water as the calorimeter fluid at 1 g s^{-1} the time constant was approximately 16 minutes.

The data that we present here are based on a simple lumped parameter model with k' taken to be a constant determined by calibration. In the results presented, no correction was made for departures from the steady state condition. However, failure to consider deviations from steady state would yield transient errors in P_u, but no error in its average value or in excess energy.

There was one further point of concern in the determination of ΔT and hence k' and P_{out}. It is important that the temperatures measured accurately represent the average values at the inlet and outlet. This was of little concern for the inlet temperatures since the fluid issues from a well-mixed tank. Significant errors could result in the determination of ΔT, however, if the outlet sensors were not placed in a region where the fluid flow was well

mixed. Several solutions to this problem were employed: porous plugs and packed beds to promote turbulence, fluidized beds of glass spheres, and imposition of turbulent flow through a Venturi orifice.

Calibration was performed first by determining the values of R° *in-situ*, under flow conditions at known bath temperature and zero or low input power. The total input power was then stepped to successively higher values using the heater (in the presence of low electrochemical power), allowing at least 20 time constants (~ 6 hours) to reach a steady state. The quantities $\delta m/\delta t$, R_{out}, R_{in}, V_h, V_{hr}, V_c, V_{cr} were measured on line and the steady state values were fitted to equation [5], assuming $P_u = 0$, to determined k'. It should be noted that this method of calibration determines k' in terms of the other externally calibrated constants: C_p, R_{out} and R_{in}, α, R_h and R_c, and the voltage calibration of the multimeter. In this way the cumulative inaccuracy of the determination of k' was greatly reduced. From this time on, only changes in calibrated values would have given rise to error.

As stated above, the calorimeter was run under conditions of constant power. This was achieved in a stepwise fashion. First, a maximum desired input power was established. Then the heater was allowed to slowly turn off by ramping the electrochemical power while maintaining the total power constant. In many experiments, and in all experiments for which the D/Pd ratio was less than ~ 0.9 or the duration of electrolysis was ≤ 300 hours, the substitution of electrochemical power for heater power yielded no excess power. That is, $P_u = 0 \pm 50$ mW for $P_{total} \leq 18$ W.

Apple Macintosh computers equipped with an IO-tech IEEE-488 interface, Keithley 706 scanner, Keithley 195A DMM, Tecrad DMO-350 micro-ohmeter, Setra 5000L balance, black box COS/4 serial port multiplexer were used to record the parameters of the experiment. The Macintosh interface controlled a Kepco BOP 20-20M power supply to apply cell current and a Kepco BOP 50-2M power supply to control compensation heater power. The power supplies were controlled using internal IEEE-488 interfaces. In addition to the parameters necessary for calorimetric determinations, a number of variables are measured to monitor the physical and electrochemical conditions of the experiments. A list of parameters follows:

Parameters Measured

Voltages:	Cell at calorimeter boundary
	Heater at calorimeter boundary
	Reference electrode
Currents:	Cell
	Heater
Temperatures:	Bath (RTD)
	Inlet (2 RTD)
	Outlet (2 RTD+ 2 thermistor)
	Room ((RTD)
Transducers:	Cell pressure
	Volumetric flow (rotameter)
	Gravimetric flow (multiplexed)
Palladium resistance	(multiplexed to Tecrad DMO-350)

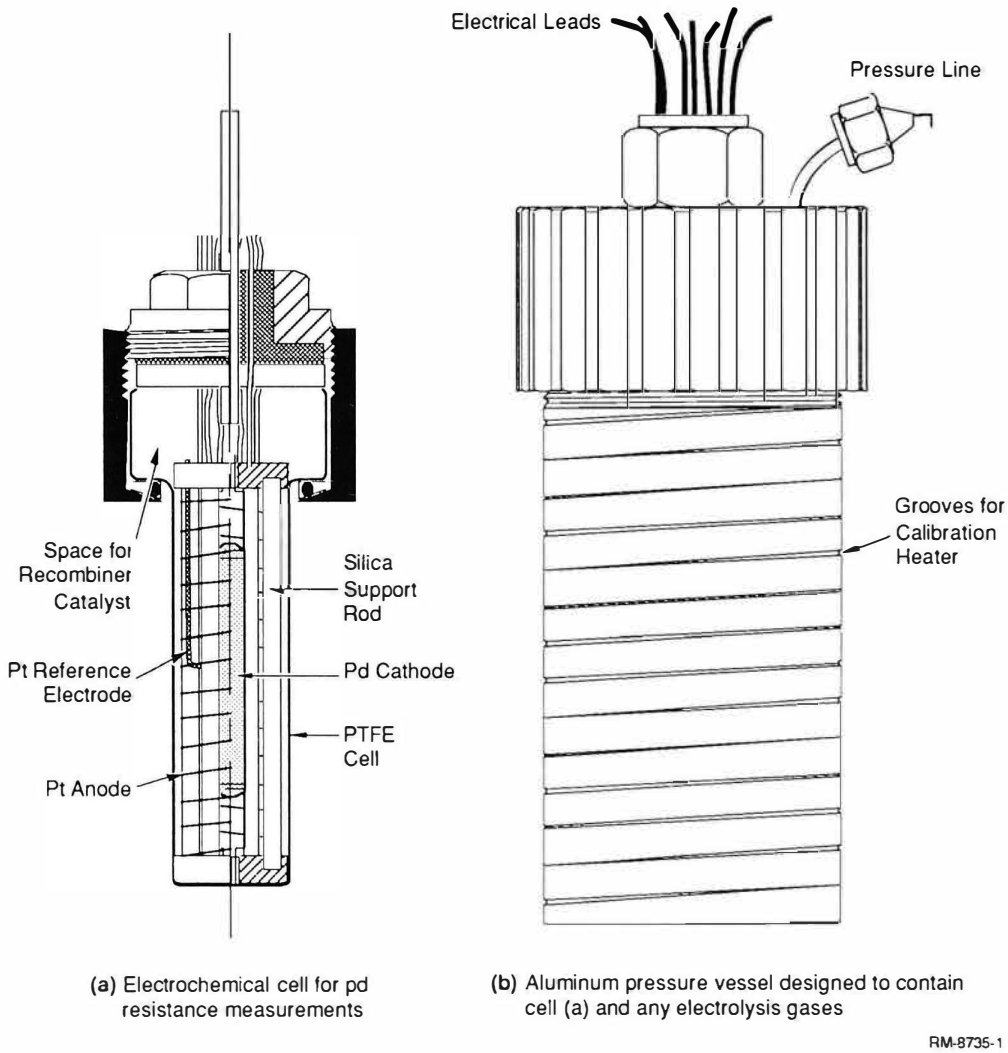

Figure 6. Electrochemical cell and pressure vessel for electrochemical experiments.

A Tecrad model DMO-350 micro-ohmeter was employed in a multiplexed mode to monitor the axial resistance of Pd cathodes and thus determine the D/Pd loading. A Solartron model 1250, 1254 or 1260 Frequency Response Analyzer, interfaced to an Apple Macintosh microcomputer was used periodically during experiments to determine the Pd/electrolyte interfacial impedance and thus assess the electrochemical condition of the interface.

Results are presented here from a series of five experiments performed in sequence, designated P12-P16. This series of near-ambient temperature experiments was chosen to demonstrate the features of internal consistency and experiment-to-experiment repeatability, the necessity for high loadings and long times, the need for D_2O and the use of H_2O controls, and the effect of current density on loading and excess heat production.

All experiments were performed using 0.3 cm diameter x 5 cm length Engelhard Pd cathodes of 99.9% purity. Anodes were coaxial helices of Engelhard CP Platinum STD Grade Pt thermocouple wire formed from 100 cm of 0.5mm diameter wire wound on 6 quartz rods. In all cases the electrolyte was 1.0 molar in Li, formed by the reaction of 99.8% purity (natural isotopic ratio) Aesar Li with H_2Oor D_2O.

To perform an experiment, cathodes first were machined to the correct diameter with grooves to receive the four 0.5 mm Pt wire contacts for current contact and axial resistance measurement. Electrodes were then degreased and cleaned and the four wires mechanically wrapped then spot welded into place. This assembly was annealed for 2 hours at 850°C in vacuo allowed to cool in argon, rinsed in "heavy" or "light" aqua regia (for D_2O or H_2O experiments), rinsed repeatedly in the appropriate water, dried, and carefully
mounted inside the pre-prepared anode cage avoiding contaminant contact. The assembled structure was placed inside the sheathed pressure vessel, freshly prepared electrolyte added, and the vessel sealed (and pressurized with D_2). The pressure vessel was then installed in the calorimeter, charging current applied and monitoring begun.

For the experiments described here, the large calorimeters were used; initial charging and calibration were performed contemporaneously, as described in the previous section.

Experiment P12, which was the prototype for the sequence of experiments described here, was performed alone in the large calorimeter bath. P12 was a heavy water experiment, and exhibited output power in apparant excess of the known sources of input power. P13 was prepared as a light water blank of P12, and replaced P12 in the calorimeter. P13 was run, initially alone, using the same electronics as had been used for P12. After a period of ~ 600 hours, P14, a heavy water replicate of P12 was run electrically in series with P13, multiplexed to the same electronics.

Experiments P15 and P16 were started simultaneously, electrically in series, following the termination of P13 and P14. P15 and P16 both were heavy water cells. The cathodes in experiments P12, P14 and P16 were implanted with helium following the 850°C annealing step, and instead of the aqua regia etch, as an alternative electrode pretreatment. Typically 5×10^{16} atoms of helium were implanted to a depth of approximately 3 μm; ^4He was used in P12 and P14, ^3He was used in P16. The act of implantation also resulted in a layer of metallurgical damage or restructuring at the surface, < 1 μm thick.

RESULTS

In the space available it is not possible to present the data for the complete duration of the experiments reported, or even of all the parameters measured in a single time interval. What is presented here primarily are results of excess power, being the difference between the output and known sources of input power, determined from equation [5].

A single episode of excess power is presented each for P12, P14 and P15; these are intended to exemplify particular features of the apparent excess power production. In these examples, P13 and P16 function as blanks, concurrent with P14 and P15, and sequential to P12.

For each of the cells P12 through P16, there were occasions when, for nominally identical current ramps, similar average D/Pd ratios were obtained but with no manifestation of excess power within the sensitivity of the calorimeter. For the full duration of the P13 experiment, the calorimeter was observed in the steady state to be within ± 50 mW of thermal balance.

Figure 7 shows the electrochemical parameters together with the measured axial resistance ratio and the calculated excess power for P12. Zero time on this plot represents a total time of charging of 1300 hours. The results presented allow examination of the dynamic response of the cathode voltage (measured with respect to a Pt pseudo-reference electrode), the resistance ratio, the excess heat and the cathodic current density.

From 0 to ~280 hours, the calorimeter was operated at a constant input power of 10 W. During this time the cell current was held constant at 0.1A (~20 mA cm^{-2}) and 2.0A (~400 mA cm^{-2}) and ramped and stepped between these limits. The reference voltage and the Pd resistance ratio exhibit a response to the current density. At the initial current density, the resistance ratio attained a value of ~1.75, decreasing (corresponding to loading) slightly with time as the reference voltages slowly increased, while the calorimeter maintains a thermal balance. As the current increased, the reference voltage rose in part due to IR and kinetic effects, but the resistance ratio fell to ~1.67 at ~100 mA cm^{-2} indicating that the electrode was absorbing deuterium.

The increase in current density and absorption of deuterium was accompanied in this case by an apparent evolution of excess power. The top curves in Figure 7 show raw data taken from the two independent pairs of temperature sensors converted to excess power using equation [5]. Departures from steady state can be seen at times when the current was abruptly stepped at 60, 80, 90, 110 and 310 hours. Apart from this effect, the excess power responded essentially monotonically with the current density, above a certain threshold value. At each instance of a step in the current density, the excess power responded with a time constant indistinguishable from that of the calorimeter. That is, the phenomenon that gave rise to this effect itself had a time constant of a few tens of minutes or less.

It should be noted, however, that the resistance ratio did not decrease monotonically with increasing current density; a maximum in loading apparently being achieved in this experiment at current densities as low as ~200 mA cm^{-2}. At higher current density the loading appears to decrease, while the excess power increases.

- CELL P12 -

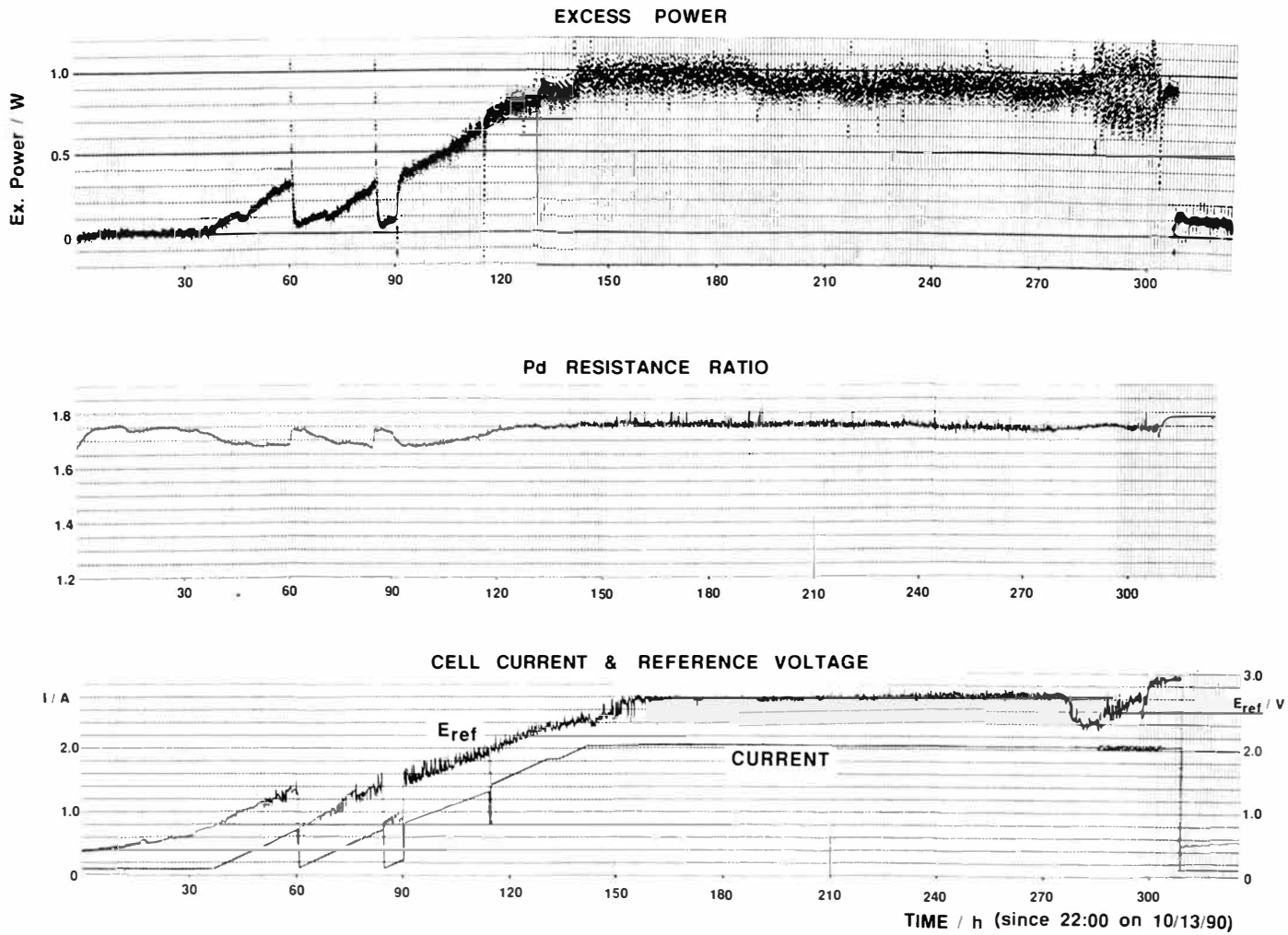

RA-8735-31

Figure 7. Experiment P12; cell current, reference voltage, resistance ratio and excess power.

During the sustained hold at 2A from ~160 to 280 h, the cell voltage slowly increased due to loss of conductive species from the liquid phase in the cell. At ~ 280 h the product $I_c * V_c$ exceeded 10 W so that the system departed further from its steady state, and the quality of data was reduced. At ~303 h the total power was raised to 12 W, and at ~309 h the current was reduced to 0.1 A. At this point it was clear from the resistance ratio that the electrode had de-loaded. In subsequent experiments it was found not to be possible to re-load the electrode with deuterium, or to observe excess heat. Following termination of P12, P13 was placed in the calorimeter using the same hardware, electronics and flow system. This experiment was intended as a blank, and an attempt was made to achieve nearly identical conditions to those of P12, excepting only that the electrolyte was prepared from H_2O and the cathode was not implanted with helium. This experiment was operated for a total of 815 h and exercised over the same range of current densities and loadings as P12, during which time the steady state response of the calorimeter maintained a thermal balance, and within ± 50 mW no excess power was observed.

P13 was operated alone in the calorimeter (as had been P12) for ~290 h at which time a heavy water replicate of P12 was placed electrically in series, and hydraulically in parallel, in the calorimeter. The current was ramped through the two cells in series, twice, with no observation of excess heat in P13 or P14, despite the fact that both cells had apparently achieved loadings H/Pd and D/Pd, respectively, of > 0.95.
Figure 8 shows the results of the third occasion on which P13 and P14 were jointly subjected to current ramps. The quality of the calorimetric data was reduced because the two experiments were held under constant power control only for periods within the time interval shown. At other times the total power was permitted to change as the current and cell voltages changed. Total power for P13 varied over the time interval shown from 8 to 15W; for P14 the range was 8 to 12.5W. Because of the reduced quality of the raw data, the data shown in Figure 8 represent an approximately 1h average of data for both independent pairs of temperature sensors. In each case, within the scatter of the data the two sensor pairs reported identical steady state responses.

Although the observed excess power was small, in absolute, percentage and integral (energy) terms, there was nevertheless a quantitative difference between the response of the heavy water cell, P14, and the light water blank, to the current density stimulus. For both electrodes there was a "high frequency" fluctuation of the excess power with periods of ~0.1 - 1h which correlated with cell pressure variations, characteristic of partially intermittent operation of the catalytic recombiner. Eliminating this feature, the excess power observed for P13 was essentially flat and zero while that for P14 departed significantly from zero at current densities above ~200 mA cm^{-2}, and generally increased with increased current density.

The current was sourced from the same device, and the electrical and calorimetric parameters were measured with the same devices multiplexed between the two experiments, making it less likely that the difference in results can be accounted for in terms of an instrumental artifact.

Experiments P13 and P14 were replaced in the large calorimeter with P15 and P16, both heavy water cells, nominally identical, and varying only in the electrode final treatment. The cathode in P15 was subjected to annealing followed by heavy aqua regia rinse, while the P16 cathode was implanted with ^3He as described above.

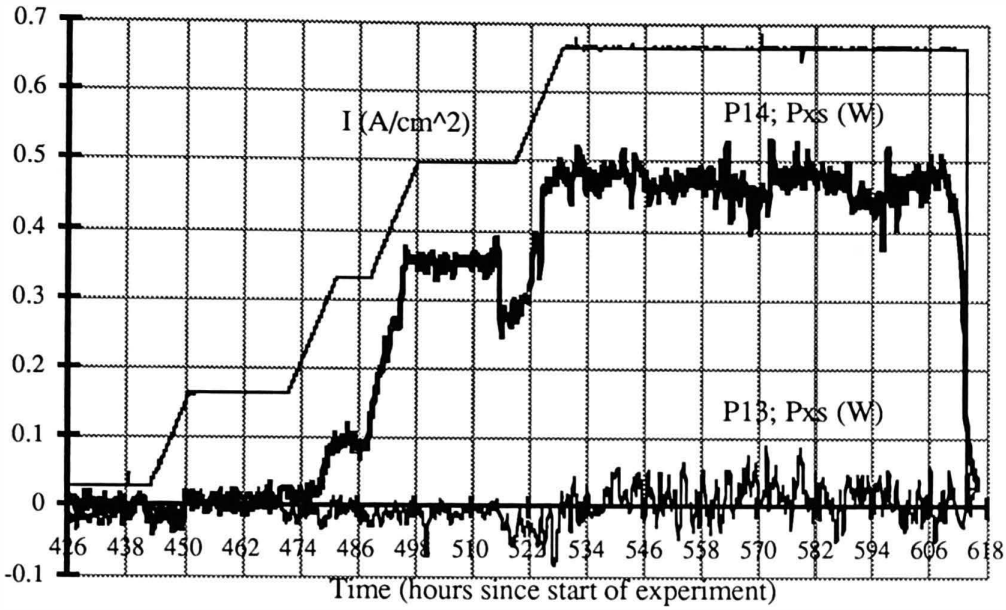

Figure 8. Current density and excess power for experiments P13 and P14.

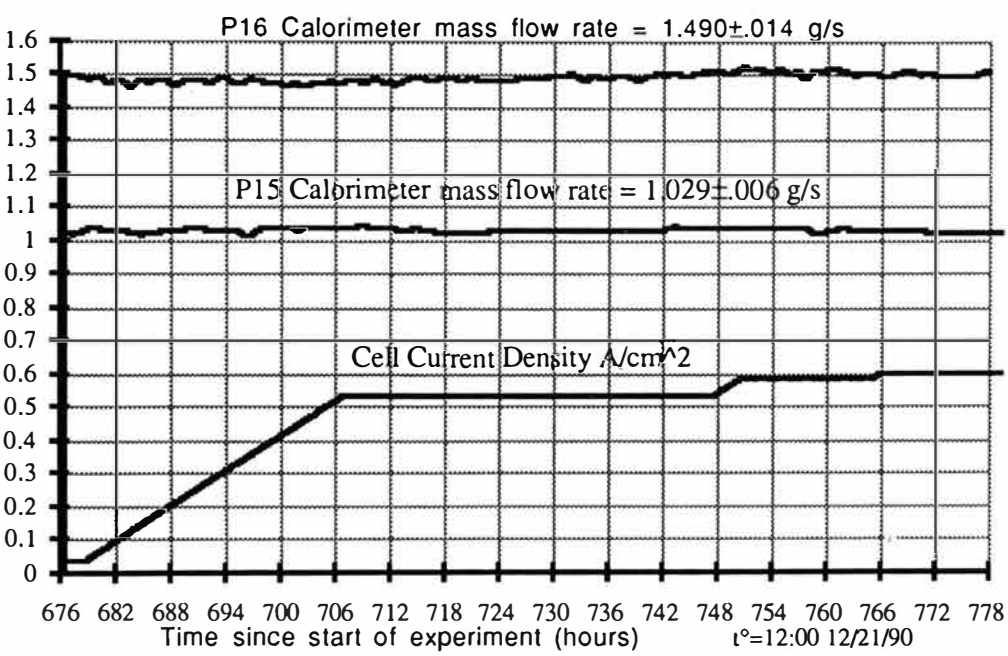

Figure 9. Current density and mass flow rate for experiments P15 and P16.

Figure 9 shows the profile of current density for P15 and P16, for an interval of time in this joint experiment that lasted at a total 1104 hours. Also shown in Figure 9 is the gravimetrically determined calorimeter fluid mass flow rate for both cells.

In part because of the different electrode pretreatments the response of the loading of the two cathodes to the ramped current density differs. Figure 10 shows the resistance ratio calculated for P15 (heavy line) and P16 (light line); the dashed line interpolates a region where data were not available for P16. It is clear that both electrodes absorbed deuterium in response to the current ramp. For P16 the resistance ratio decreased from ~1.77 (D/Pd ≈ 0.9) at i = 33 mA cm^{-2} to a minimum of ~1.6 (maximum loading D/Pd ≈ 0.97) at a current density i ≈ 500 mA cm^{-2}. For P15 the resistance ratio was always lower and decreased in resistance ratio from ~1.69 (D/Pd ≈ 0.94) to a minimum of ~ .555 (maximum loading D/Pd ≈ 0.99) sustained at higher currents and for longer times than P16. Because the temperature of the Pd cathode was unknown, it was not possible to completely interpret the measured resistance ratio of P15 in terms of the loading. Excess power would increase the temperature and hence the resistance of the Pd cathode, and cause an underestimate of the loading. It is important to note that both electrodes initially were rather well loaded, and became better loaded with increasing current during the current ramp.

Figure 11 shows the temperatures registered by the inlet sensors of P15. Figure 12 shows the total measured input power, initially controlled at 10 W and then stepped to 12 W as the cell voltage rose at constant current. Also shown is the power in the heater used to compensate for changes in the electrochemical input power due to the current ramps or temporal drift.Because the temperature of the Pd cathode was unknown, it was not possible to completely interpret the measured resistance ratio of P15 in terms of the loading. Excess power would increase the temperature and hence the resistance of the Pd cathode, and cause an underestimate of the loading. It is important to note that both electrodes initially were rather well loaded, and became better loaded with increasing current during the current ramp. It is clear from Figures 9, 11 and 12 that, within the interval of time shown, the mass flow rate, the inlet temperature and the inlet power for P15 all are sensibly constant. From inspection of equations [1] - [5] it is clear that, provided that P_u is zero, the outlet temperatures also must be constant.

Figure 13 shows the measured profile of temperature for the two platinum resistance sensors in the outlet plenum of the P15 calorimeter. Two thermistors also were present in the outlet flow stream. All four sensors record essentially the same profile of temperatures, and these were not constant, varying by as much as 0.6°C with a measurement accuracy of ± 0.001°C (reduced for the thermistors) and sensitivity of 0.0001°C. The thermistors had a better precision but lower accuracy than the RTD's.

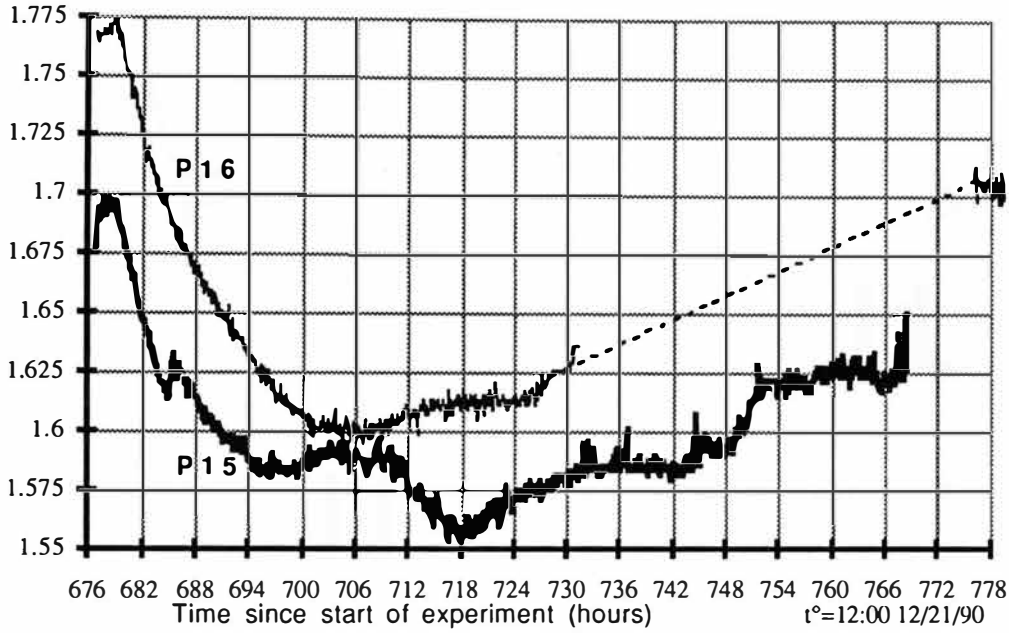

Figure 10. Resistance ratio for experiments P15 and P16.

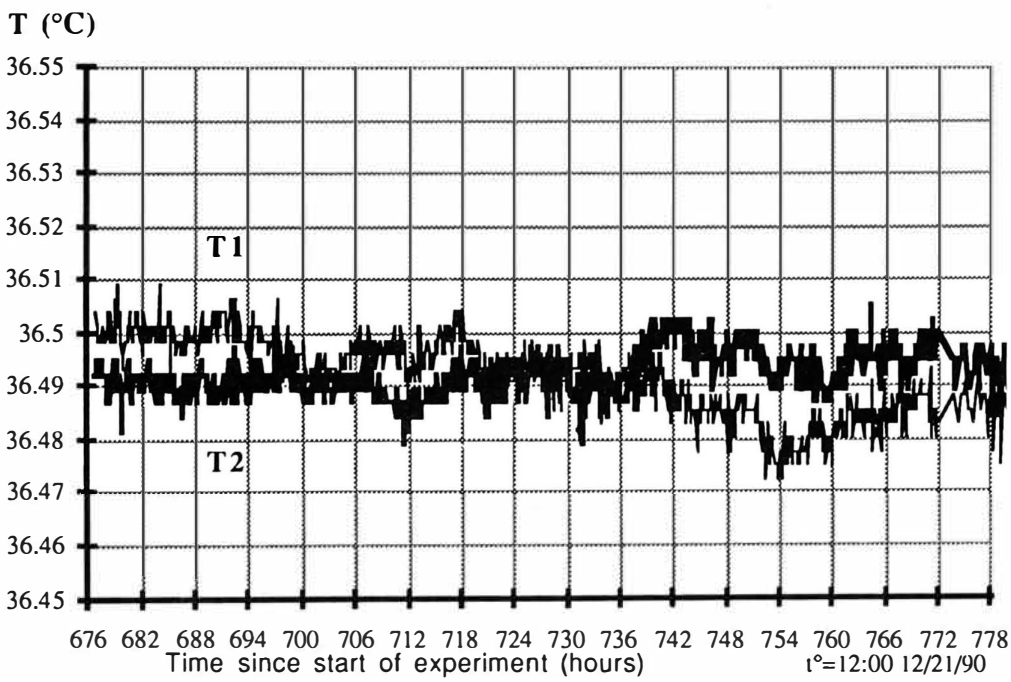

Figure 11. Temperatures in the inlet plenum for experiment P15.

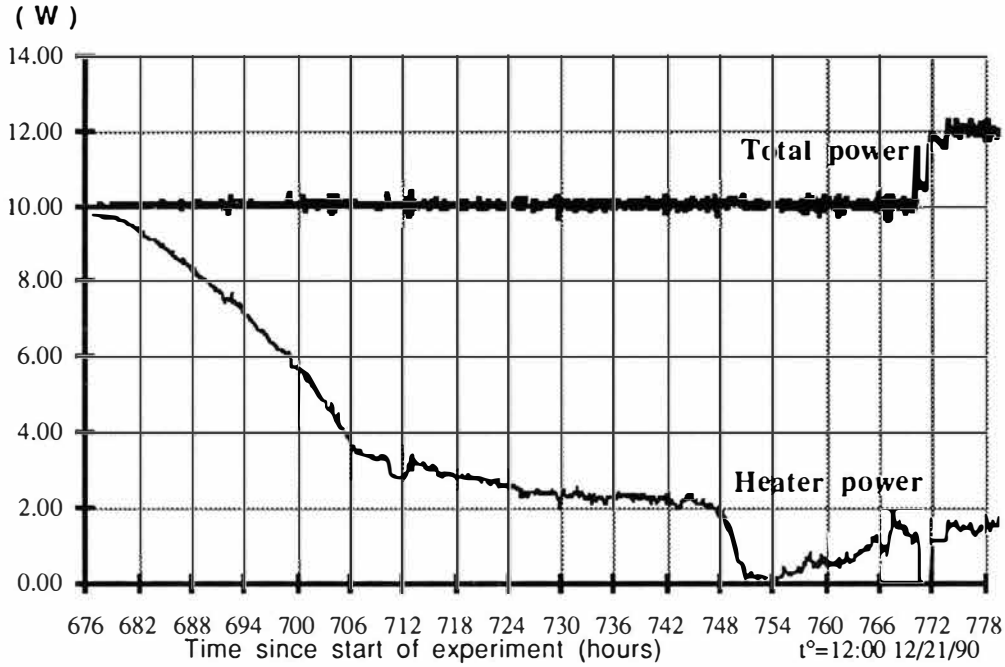

Figure 12. Total power and compensation heater power for experiment P15.

Figure 13. Temperatures in the outlet plenum for experiment P15.

One interpretation of the observed temperature variation is that there is an unknown power source within the calorimeter of an amount that we can quantify using equation [5]. Figure 14 shows the "excess power" normalized with respect to the measured electrochemical input power ($I_c * V_c$) and the controlled total power ($I_c * V_c + I_h * V_h$). A very irregular profile of excess power is seen with a threshold at ~ 200 mA cm^{-2}. The high frequency fluctuations of period 0.1 - 1 h are present due to inconstant recombiner operation. Superimposed on the ramped response to current also are apparently spontaneous fluctuations with substantially greater amplitude and period (~ 3-6 h) that were not correlated to variations in pressure or any other of the measured parameters of the system. It is worth noting that during this time interval, and subjected to the same current, P16 exhibited no departure from the thermal balance that was detected with the same instruments as for P15.

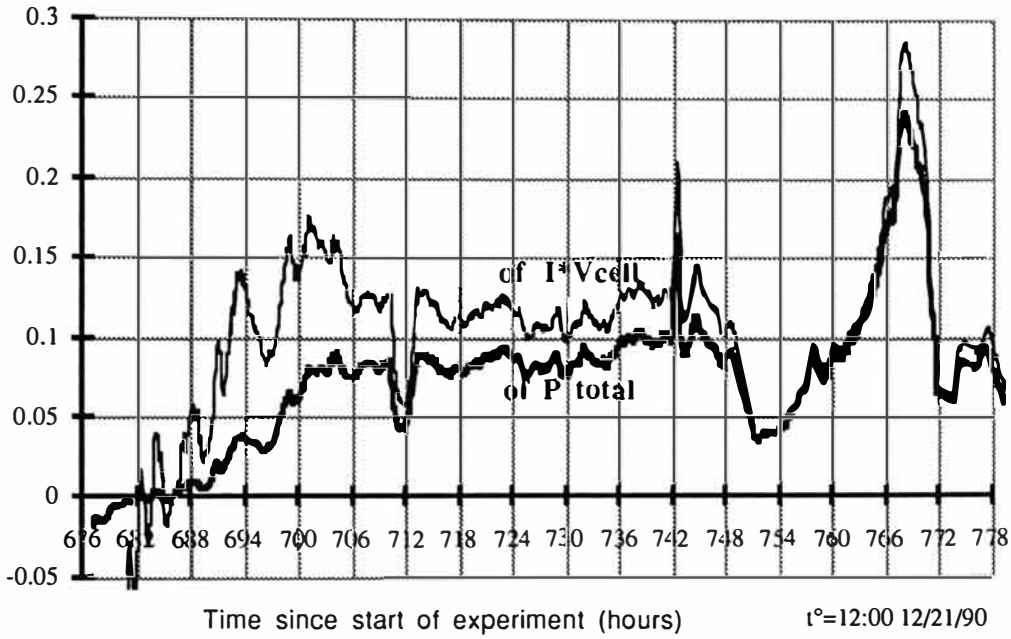

Figure 14. Excess power for experiment P15, expressed as a fraction of the electrochemical and total power input .

DISCUSSION AND CONCLUSIONS

In this paper we have described a calorimetric tool for use in observing the characteristics of unexplained thermal processes in the D/Pd system. Representative examples of results have been given from which a number of observations and conclusions may be made.

We have observed unexplained excess heat in palladium cathodes when a minimum of three criteria were met: an average loading (D/Pd) approaching or exceeding unity; this

high loading was maintained for considerable periods of time (100's of hours for 3 mm diameter cathodes); the interfacial current density exceeded a certain critical value.

With appropriate control of the interfacial conditions it has been shown to be possible to load both H and D into Pd to molar ratios of approximately unity. Electrode preconditioning apparently plays a significant role in the ability to attain and maintain high loading under electrochemical conditions, and the appearance of unaccounted heat in deuterium loaded systems. Helium implantation provides a suitable means of surface activation to facilitate loading; the presence of helium is not obviously implicated in the generation of excess power.

For the thermodynamically closed and intentionally isothermal systems described here, output power was observed to be as much as 28% in excess of the electrochemical input power or 24% above the known total input power. When excess power was present, it was more typically in the range 5-10%, in a calorimeter that was accurate to $\pm$ 0.1%.

In the examples given the largest observation of excess energy corresponded to 1.08 MJ, or 45.1 MJ/mole or ~450 eV/atom normalized to the Pd lattice or to the deuterium in the palladium at a presumed loading of ~1.

The experiments reportted here demonstrate that internal repeatability is possible when the three criteria above are achieved. Apparent excess heat was observed under these conditions when the current density reached a critical value, and excess heat was not observed when the current density was reduced below the critical value. Furthermore, the threshold current density appeared to decrease with time, up to the point that, due to interfacial or external effects, high values of loading could no longer be attained or maintained.

There appeared also to be some degree of experimental reproducibility between cells. Experiments P13-P16 were attempts to replicate P12 with only minor variations in electrode and electrolyte treatment. All the heavy water experiments (P14, P15, P16) produced excess heat, reproducing in general form the observation in P12 (excess heat data for P16 are not shown here). It is worth noting, however, that excess power in these four experiments was <u>not</u> produced in exactly the same amounts, or at exactly the same times, in response to the same stimuli. However, we could not reproduce exactly the electrochemical conditions of cathodic overvoltage, the loading (resistance ratio), and the interfacial impedance. Clearly there are issues of interfacial contamination which arise in experiments with sustained high current electrolysis, that await resolution.

Except for times when the calorimeter was caused to depart significantly from its steady state condition, and during periodic fluctuations introduced by nonconstant recombiner operation, "negative excess" was never observed. In terms of equation [5], P_u was observed always to be positive or zero. Always, where significant quantities of H_2O were used in the electrolyte, P_u was zero. Also, no excess was observed before a critical "initiation time", even in cells that subsequently yielded values of $P_u > 0$.

As demonstrated in the P13/P14 and P15/P16 twin, series experiments, excess power was observed asynchronously in series cells. That is, cells subjected to the same current from the same source and monitored in a multiplexed manner to the same electronics were observed to yield in one cell $P_u \approx 0$ while in the other $P_u > 0$. It is very difficult to attribute such an observation to an artifact of the common instrumentation .

The association of apparent excess power with a set of necessary conditions for the D/Pd system implies a degree of reproducibility. These conditions are not easy to attain, a

fact which may explain the irreproducibility of the phenomenon of excess heat. Examined separately the three criteria may be taken as normal conditions of reacting systems (chemical or nuclear). The criterion of loading is of a thermodynamic driving force; a measure of the activity or chemical potential of a possible reactant species. The need to maintain loading for considerable periods of time before the onset of excess heat suggests a mass transport constraint, possibly involving nucleation and growth of an active region within the volume of the bulk Pd lattice. The final requirement of large interfacial current density suggests a kinetic criterion. Because of the intimate coupling between electron flux and the creation of adsorbed D, and a very facile equilibrium between D_{ads} and D_{abs}, current density can be viewed as the means by which absorbed D are given the energy to undergo reaction.

As a final note, we are unable to account for the observed excess temperature by any artifact known to us and are forced to conclude, tentatively, that the source of the excess power is a property of the D/Pd system. Further, we cannot account for the measured excess heat by any chemical or mechanical process with which we are familiar.

ACKNOWLEDGEMENT

We gratefully acknowledge the financial support and considerable technical assistance of the Electric Power Research Institute.

REFERENCES

1. M. Fleischmann, S. Pons and M. Hawkins, "Electrochemically Induced Nuclear Fusion of Deuterium", J. Electroanal. Chem., **261** (1989) p. 301 and *errata*, **203** (1989), p. 87.

2. B. Baranowski and R. Wisniewski, Phys. Stat. Sol. 35, 593 (1969).

3. B. Baranowski, S. M. Filipek, M. Szustakowski, J. Farny and W. Woryna, J. Less-Common Metals, **158**, 347 (1990).

4. A. W. Szafranski and B. Baranowski, Phys. Stat. Sol. (a) **9**, 435 (1972).

5. G. Bambakidis, R. J. Smith and D. A. Otterson, Phys. Rev. **177**, 1044 (1969).

6. R. J. Smith and D. A. Otterson, J. Phys. Chem. Solids **31**, 187 (1970).

«The Science of Cold Fusion»
T. Bressani, E. Del Giudice and G. Preparata (Eds.)
SIF, Bologna 1991

SURVEY OF GAS LOADING EXPERIMENTS

F. Scaramuzzi
ENEA, Area Innovazione, Dipartimento Tecnologie di Punta,
C.P. 65 - 00044 Frascati, Italy

WHY GAS LOADING ?

In March 1989 the results of two experiments (1,2), claiming for nuclear reactions taking place, at room temperature, in metal lattices (Pd and Ti) charged with deuterium, were presented. In both cases the technique chosen for charging the metals with deuterium consisted in using an electrolytic cell, containing heavy water, in which the cathodes were made out of Pd or Ti.

Soon later, in April, the Group led by the writer addressed a very straightforward question: if nuclear reactions take place in a metal lattice because of the interaction between the deuterium nuclei and the lattice, is electrolysis the only route to be followed, in order to produce them? Wouldn't it be possible to perform experiments, having the same purpose, by letting the lattice to interact with deuterium in the gaseous phase? The question seemed quite appealing, mostly for one reason: the physical system consisting in an electrolytic cell is a very complicated one, and has to take into account a great number of parameters, while the system consisting in a metal and a gas looks much simpler. The latter would permit much cleaner experimental conditions, and thus it would be possible to analyze more clearly the experiments; it would also favour a higher reproducibility, and would enable testing the proposed theories. Experiments were performed at the Frascati Laboratory of ENEA following this alternative route, using titanium: furthermore, it was decided that, in order to favour nuclear reactions, temperature cycles should be performed on the system (from 77 K to room temperature). Positive results were obtained, consisting in the detection of neutron bursts, and were soon published (3).

Since then, many laboratories have used this technique, called "gas loading", with various success, detecting the emission of neutrons and charged particles and the accumulation of tritium in the metal. The basic idea is that the unknown

mechanism that produces nuclear reactions in the system is connected to the thermodynamic transformations taking place in it, while the temperature of the sample, the pressure of the gas, and the related parameters, such as deuterium absorption, are changing.

This is presently one of the most used techniques in Cold Fusion research. Many results have been reported also in this Conference, and will be reviewed in the following. But, at two and half years from the starting of this experimental technique, it is worth to address a question, in the light of the lack of reproducibility that still characterizes its results: is the system under study really a simple system, as it appeared to be at the beginning?

The answer to this question is not easy: in a first approximation, it can be stated that the system is simple in principle, but that most of the particular solutions chosen up to now to study it, including the Frascati experiment of April 1989, show a very high complexity, that tends to cancel the advantage of this "theoretically simple" system. In order to enlighten this concept, I will examine in detail the intrinsic complexity of a typical "gas loading" experiment, then I will survey the experiments pertaining to this class presented in this Conference, and finally I will try to suggest, also in the light of the papers presented here, new possible routes, that could help reducing the complexity of the studied system, taking thus advantage of the real intrinsic simplicity of the metal-gas system.

INTRINSIC COMPLEXITY OF A GAS LOADING EXPERIMENT

I will try to list here (being aware that the list is not exhaustive) the many operations on the sample, while performing a gas loading experiment, and the relative parameters: in the hypothesis that the studied phenomena are connected with thermodynamic transformations (in particular phase transformations) taking place within the sample, each of them can influence the outcome of the experiment. I choose to refer to the experiment of the Frascati Group at the Gran Sasso Laboratory of INFN, presented at this Conference. The list is reported in Table 1: on the left I described briefly the procedure or the parameter, on the right I reported the solution chosen for this experiment. It must be clear that in many cases the choice of the procedure or of the particular value for a parameter did not follow from a thorough knowledge of the role played by that parameter or that procedure in the experiment: it is often suggested only by practice, mostly acquired in preceding measurements. Thus, changing that procedure or the value

Table 1. Complexity in gas loading experiments. The data refer to the paper by De Ninno on these Proceedings.

PROCEDURE/PARAMETER	FRASCATI CHOICE
A. Choice of the sample	
1. substance	Ti-662
2. purity	99.6%
3. impurities	?
B. Shape and amount of sample	
4. shape	shavings
5. size	section: 0.05 x 1.00 mm^2
6. amount	$\approx$ 120 g
C. Preparing the sample	
7. machine used	lathe
8. cutting tool	sharpened at beginning of machining
9. cooling while cutting	flow of pure ^4He gas
10. after cooling	sample exposed to air
D. Cleaning the sample	
11. acid etching	no
12. organic solvent	no
E. Pretreatment of the sample	
13. cell used	stainless steel
14. vacuum on sample	turbomolecular pump, p $\approx$ 10^{-6} torr
15. degassing the sample	pumping at 100°C, 2 hrs
F. Charging D_2 gas (at Gran Sasso Laboratory)	
16. time from step 15	$\approx$18 hrs
17. charging circuit	uses a zeolite trap in LN_2 in order to clean the gas
18. charging pressure	20 bars
19. time at room temperature before heating	2 hrs
G. Heating sample to favour absorption	
20. temperature vs. time	up to $\approx$ 300°C in 1 hr
21. control of absorption	see Fig.1
22 restored pressure	P = 30 bars
H. Thermal cycle (repeatable)	
22. time to return to room temperature	$\approx$1 hr
23. cooling procedure	immersion of the cell in LN_2; 3-5 min to reach 77 K
24. warm-up procedure	cell immersed in a dewar full of LN_2, in the well of the detector; $\approx$24 hrs to warm up to room temperature

of that parameter would be a proper way to learn about its role: the multiplicity of them, however, renders this task quite difficult.

It is clear, looking at Table 1, that this experiment has quite a number of undefined features. Let me try to point out those that seem to be more relevant:

- Temperature is measured with a thermocouple, within the cell, touching the upper part of the tangled mass of shavings. Due to the poor heat conductivity of titanium, the deuterium gas gives a better contribution than the titanium itself to a uniform distribution of temperature. In spite of this, since non-equilibrium conditions are purposely searched in the experiment, temperature gradients and time variations of temperature and of temperature gradients are likely to be created.
- Other parameters that are presumably relevant to the experiment are the D/Ti concentration, its gradient and the time evolution of both, which depend on the absorption procedure. Tests made on samples used in this type of experiment have shown the presence of high concentration TiD_x, while the average concentration is usually in the order of a few percent D atoms per Ti atom.
- The treatment of the Ti shavings before putting them in contact with deuterium is also most probably relevant, including the thermal treatment produced when making them on the lathe, the successive chemical cleaning, the degassing, and so on.

To control all these parameters in this kind of experiment is extremely difficult. Most probably, during one run a great number of different experiments, in which each of the relevant parameters has a different value, unknown to us, are performed in different sites of the sample. This feature probably increases the probability of positive results, but puts a severe limit to the reproducibility of the experiment.

In order to improve reproducibility, a more rational approach to the problem is paramount. On one side one should try to better understand the processes that take place in a metal (in particular titanium and palladium) when interacting with deuterium. The literature is rich, and we had in this Conference a very interesting lecture by Professor Schlapbach on this subject. Nevertheless, the information available, in particular for titanium, seems to require more investigation, in order to gather information useful for cold fusion experiments. An extremely inspiring paper has been presented at this Conference by Professor Sanchez, in which he showed us a correct route to follow in order to better understand the systems on which we are working.

Another possible approach consists in the search for much better characterized systems on which to perform experiments. Many interesting

suggestions in this direction have come out in this Conference: I will address this subject in the last part of this paper.

GAS LOADING EXPERIMENTS PRESENTED AT THIS CONFERENCE

It would be difficult, and at the same time pointless, to review here in detail all the papers referring to gas loading experiments presented at this Conference: they are published in these Proceedings. I tried to list them, in Table 2, reporting a few descriptive data, and I will propose some comments.

The first feature that appears is the large number of experiments belonging to this general area; at the same time, it has to be noted that there is a great variety of particular features, that, with a few exceptions, renders every experiment different from the other. The high quality and accuracy of some of them has also to be pointed out: in particular, the neutrons' energy measurement of Bressani, the time resolution in neutron detection of Menlove and of De Ninno, the neutron measurements at Dubna, the tritium measurements of Lanza.

As far as neutron detection is concerned, it has to be pointed out the "dilemma" about whether or not to measure the energy of the emitted neutrons. The measurement of the energy, beyond giving an important information on the physics of the problem, has the advantage of guaranteeing a better identification of the neutron, but requires the accumulation of many data, i.e., long times. The choice of privileging the analysis of the time structure of the emission (the "bursts"), on the other side, requires the use of a moderator, in order to enable the detector to see also neutrons emitted within a very short time interval (μs, ns ?), and to increase the overall efficiency of the system; thus, all information about the energy of the detected neutrons is lost. The latter, at the same time, has the advantage of correlating in real time the neutron emission with the evolution of the thermodynamic parameters of the system. Both approaches are important and should be followed. It seems to me, to summarize the issue, that the second type of approach could be more helpful in the search for a better reproducibility; but there is no doubt that, as soon as a more reproducible experiment will be at hand, it will be paramount to measure the energy of the emitted neutrons.

Going back to the problem described in the first part of this paper, the complexity shared by most experiments, it has to be noted that, among the papers presented at this Conference, many show possible routes to follow in order to reduce it. I will try to list them in the following, looking for systems and procedures that are likely to be used in gas loading experiments, aiming to a

Table 2 - Gas Loading experiments presented at this Conference.

Author	Metal	Part.	Temp.	Notes
Bressani	Ti	n	T_a-540	energy = 2.5 MeV
Cecil 1	Ti	cp	77-T_a	bursts; high DC current in sample (400 mA)
Cecil 2	Ti	cp	T_a	glow discharge
Celani	YBCO	n	77-T_a	superconductive transition, stimulation by n
Claytor	Pd-Si	t,n	T_a	pulsed electric current
De Ninno	Ti	n,t	77-T_a	low background lab, bursts
Duan	Ti	n	T_a	implantation
Ikegami 1 (Hitachi)	Ti	n	77-T_a	bursts
Ikegami 2 (NIFS)	Pd	n	T_a	electric discharge
Ikegami 3 (NTT)	Pd	n	T_a	oxide/Pd:D/Au interface,electric current
Lanza	Ti,Zr, Hf,T_a	t	77-T_a	careful control of deuteration
Li 1 (Tsinghua)	Pd	cp	77-T_a	CR-39 used,search of precursors, E > 5 MeV
Li 2 (At.En.)	Ti	n	77-T_a	bursts,low background laboratory
Li 3 (various)	Pd	cp	T_a	CR-39 used,gas discharge
Menlove	Ti	n	77-T_a	low background lab, bursts
Miley	Ti,Pd Th,Fe	-	T_a	proposal:thin films, implantation
Seeliger 1	Ti	n	77-T_a	correlations,p,dp/dt
Seeliger 2	Pd	n	Ta-650	electrolysis-charged
Tsarev 1 (Dubna)	Ti	n	77-T_a	bursts

Legend:
PART = type of particles detected; n = neutron; cp = charged particles; t = tritium; T_a = ambient temperature, Temperatures are expressed in K

Note. In the column entitled "author" one of the authors, in most cases the speaker, is quoted, and the same name is used in the text when commenting the Table. In the whole paper the references to the presentations appearing in these Proceedings will not be reported: the reader will easily find out the corresponding paper in the Proceedings by looking at the alphabetic index.

Table 2 - Gas Loading experiments presented at this Conference.

Author	Metal	Part.	Temp.	Notes
Tsarev 2 (Kharkov)	Pd,Ti	n,cp	77-1300	D_2 implanted at low T then rapid heating
Tsarev 3 (various labs)				various techniques, including mechanical treatment, discharge
Wang	Pd,T	cp	77-T_a	CR-39 used
Will	Pd	t	T_a	electric discharge

Legend:
PART = type of particles detected; n = neutron; cp = charged particles; t = tritium; T_a = ambient temperature; Temperatures are expressed in K

Note. In the column entitled "author" one of the authors, in most cases the speaker, is quoted, and the same name is used in the text when commenting the Table. In the whole paper the references to the presentations appearing in these Proceedings will not be reported: the reader will easily find out the corresponding paper in the Proceedings by looking at the alphabetic index.

better reproducibility of the measurements. In particular, the issues at stake are a better characterization of the sample, and a better definition of the procedure to follow in order to obtain the non-equilibrium conditions necessary for the phenomenon to take place.

- A procedure that looks very promising is the D and D_2 ion implantation on metals, in order to achieve high values for the D-concentration, which can be definitely higher than those obtained both with electrolysis and gas loading. The damage produced by the implanted ions in the lattice, however, has to be taken into account. Also the use of "plasma focus" plants belongs to this category. (Tsarev/Kharkov, Srinivasan/BARC ((4),not presented in this Conference), Duan, Miley (proposal), De Ninno (proposal))

- The experiment of the Los Alamos Group (Claytor) with Pd and Si stacks pulsed with high electric current represents an interesting compromise between electrolysis and gas loading, still keeping the "intrinsic simplicity" of a gas-solid system, but at the same time realizing a much simpler system than the traditional one described here (Table 1).

- The experiment on Pd films coated with "barrier layers" (Ikegami/NTT) shows as well a very interesting route to follow, in order to have a well characterized system, and investigates one of the possible mechanisms for the nuclear reactions to take place.

- Also the use of gas discharge, being careful not to produce "hot fusion" events, is an interesting possibility for cold fusion investigation. (Cecil, Li, Will)

- Finally, referring to the issue of producing well characterized samples, it would be interesting to realize particular structures, like superlattices (Miles), or growing a film on a support, by evaporating or sputtering deuterium and the chosen metal at the same time in the wanted proportion (5).

I would like to remember here the suggestion of Prof. Li to give more attention to the detection of charged particles, in particular with integrating detectors, such as C-39, which are simple to use and not expensive. The detection of tritium should also be pushed forward. Gas loading experiments are well suited for the detection of all these particles.

References

1. M. Fleischmann, S. Pons, M. Hawkins, Journal of Electroanal. Chem., **261**, 301 (1989)

2. S.E. Jones, E.P. Palmer, J.B. Czirr, D.L. Decker, G.L. Jensen, J.M. Thorne, S.F. Taylor, J. Rafelski, Nature, **338**, 737 (1989)

3. A. De Ninno, A. Frattolillo, G. Lollobattista, L. Martinis, M. Martone, L. Mori, S. Podda, F. Scaramuzzi, Europhys. Letts, **9**, 221 (1989)

4. P.K. Iyengar, M. Srinivasan, Proceedings of the First Annual Conference on Cold Fusion, Salt Lake City, March 28-31, 1990, edited by the National Cold Fusion Institute, pag.62 (1990)

5. S. Scaglione, P. Zeppa, private communication

«The Science of Cold Fusion»
T. Bressani, E. Del Giudice and G. Preparata (Eds.)
SIF, Bologna 1991

COLD FUSION: WHAT DO THE LAWS OF NATURE ALLOW AND FORBID?

Giuliano Preparata
Dipartimento di Fisica - Università di Milano
INFN - Sezione di Milano
and
INFN - Laboratori Nazionali di Frascati

1. INTRODUCTION

This talk will not be a summary of the theoretical contributions to this Conference: I think that the individual papers that this book collects can give a much better representation of the work that is now going on in the field than I can possibly attempt to give in a short talk. As a partial excuse I may quote a recent review article of mine[1], where I try to discuss the most significant theories of cold fusion, and the fact that nothing much new has happened in the last few months. Nor will I discuss cold fusion in the non-equilibrium conditions prevailing in Titanium[2], fracto-emission[3] and 'lukewarm' fusion[4].

I shall rather try to examine first the strange facts of hydrogen incorporation into Palladium, and then I shall discuss the phenomena of cold fusion in relation to those facts. In the light of the known experimental data I will then discuss the general features of what we might call 'possible' and 'impossible' theories of cold fusion, somehow drawing a demarcation line between which theoretical ideas can and cannot explain those observations, given the well established and accepted general laws of condensed matter (Quantum Electro Dynamics, QED) and nuclear physics (Quantum Chromo Dynamics, QCD).

My discussion will follow quite closely a paper recently completed in collaboration with M. Fleischmann and S. Pons[5].

2. FACTS

As Martin Fleischmann and Stanley Pons have explained us time and again they were induced to undertake a work «... that was initiated on the strength of a calculation that no moderately intelligent graduate student, let alone experienced electrochemists, ought to take seriously... »[6] by their being puzzled by the odd behaviour of Hydrogen - and its isotopes - when inserted in a host metal lattice, like Palladium. Let me try to briefly list and describe the strange facts that captured the imagination of our friends.

– High concentration of Hydrogen in Pd

When a piece of Pd is put in an atmosphere of gaseous Hydrogen at normal pressure it soakes a large quantity of the gas spontaneously and exothermally up to a ratio

$$x = \frac{H}{Pd} \simeq 0.6 .$$

In order to get much higher x one needs very large pressures; in any case with accessible pressures one cannot reach from gaseous Hydrogen the apparently relevant 'threshold' x=1 (see later)[7].

– High Hydrogen mobility

The anomalously high mobility of Hydrogen in Pd, in particular its being accelerated by electric fields shows that Hydrogen and its isotopes (D and T) in Pd exist in their nuclear (not atomic) state, immersed in a very dense plasma of d-electrons[8]. And the natural question is: why highly compressed Hydrogen does not form?

– High H/D separation factor at equilibrium

In equilibrium conditions H and D exhibit a high separation factor, completely consistent with a statistical mechanics model based on delocalized classical oscillators showing high affinity for Pd.

In order to appreciate the latter statement let us consider two possible Born-Haber cycles (Fig. 1) for molecular Hydrogen to penetrate into Pd.

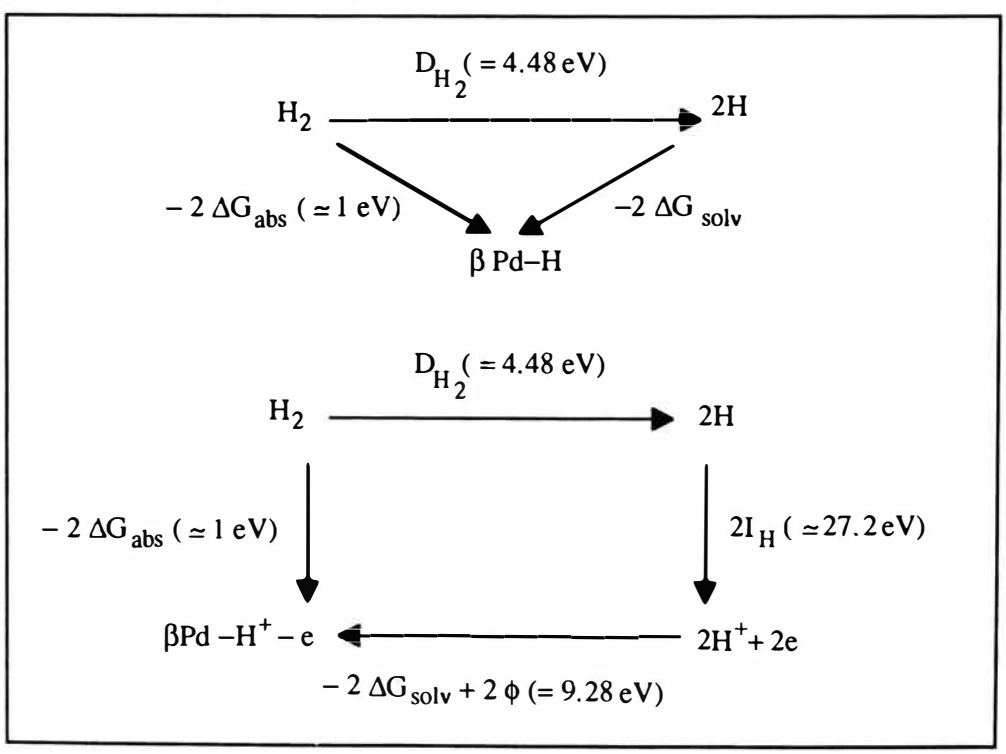

FIG. 1 - Two possible Born-Haber cycles for β Pd-H.

One sees that one obtains solvation potentials of Hydrogen in Pd of the order of several eV's, a most noteworthy physical phenomenon.

– Large diffusion coefficients - Inverse isotope effect

Transport measurements show that the diffusion coefficients D of Hydrogen in Palladium are of the order of 10^{-7} cm^2 sec^{-1} - a very large value - and are ordered as[9]

$$D_D > D_H > D_T . \qquad (1)$$

The inversion of the diffusion coefficients of D and T, that runs contrary to what one would have expected from their masses, is a kind of 'inverse isotope effect', which is also observed for the critical temperatures of the superconducting Pd - hydrides ($T_D > T_H$)[10].

– High chemical potential of dissolved Hydrogen

All these facts can be assembled to build the 'Scenario' reported in Table I.

TABLE I - Scenario from the facts of Hydrogen in Palladium.

FACTS	DEDUCTIONS
High concentration - Ionized species	Large electrostatic fields to 'undo' molecular and atomic H; 'deep' electrostatic potential holes
High affinity - high separation factors	Highly delocalized wave-functions, 'shallow' potential holes
Large diffusion coefficients	'Shallow' holes
Inverse isotope effect	Bosons (D) have a configuration space different from fermions (H,T)
High chemical potentials	Formation of large proton clusters

Let us now turn our attention to the facts of Cold Fusion (CF) as we have learned them in the last two years.

• Sporadicity, variability, metallurgical factors

The phenomenology that has accumulated so far shows that the 'irreproducibility' of the CF phenomena is most likely tied to the large number of relevant parameters and even to path-dependences in the space of parameters.

• Low T-levels, $n/_T \ll 1$, absence of γ-rays and secondary n's

The nuclear physics of CF has been since the beginning[11] (March 1989) a tremendous puzzle, why the outgoing channels are not $^3T + {}^1H$ and ^3He + in 1 : 1 proportion, like it happens in the vacuum? Indeed this dramatic discrepancy has convinced the majority of physicists that CF phenomena must be a bogus.

- **Bursts in T, n production**

  Are they due to non-equilibrium conditions?[12]

- **High energy T, n and protons**[13]

  Unconventional nuclear physics?

- **Soft X-rays**

  As shown by Szpak's [14] and Miles' [15] dental films.

- **^{4}He unaccompanied by high energy γ rays**

  As shown by the beautiful experiments of Melvin Miles and collaborators[15].

- **Excess enthalpy production far above that corresponding to T + n production**

  In particular the new results of Fleischmann and Pons[16], that have been corroborated by Wilford Hansen's independent analysis[17], indicate powers of kW/cm^3.

The scenario that originates from assembling these facts together is reported in Table II.

TABLE II - Scenario from the facts of CF phenomena in Pd.

FACTS	DEDUCTIONS
Sporadicity, Variability, Path-dependence	Delicate conditions, thresholds
Low T-levels, $^n/_T \ll 1$, no γ's	Asymptotic Freedom (AF)badly violated inside lattice
Bursts in T, n production	Strange non-equilibrium conditions - Special domains
High energy T, n and p	AF is violated - DDD fusion?
^{4}He and no γ's	AF is violated - e.m. coupling to electron plasmas
Excess enthalpy	AF is violated

3. - POSSIBLE AND IMPOSSIBLE THEORIES

We shall now try to bring the 'facts' and the scenarios of the preceding Section to bear upon the key question of this talk, namely which of the the proposed theories are possible, and which among them, on the other hand, are impossible. But before going into the specifics, it is important to set down a clear demarcation between possible and impossible theories, which might run as follows:

Any 'possible' theory must explain the new phenomena (facts) without 'unexplaining' the old.

To this we may add the corollary: the old theory (ies) which does not explain the new phenomena cannot be used against the new theory in the realm where the old theory 'worked'.

Or, said differently, the 'successes' of the old theory cannot be taken as evidence that there is no need of different explanations of those successes.

3a - Hydrogen and its Isotopes in Pd

According to the scenario of Table I inside and at the surface of Pd there must exist very strong electrostatic fields. We realize at once that these fields must be able to polarize the Hydrogen molecule so strongly as to break it into its elementary components - p, d, T and electrons -, thus piercing through an energy barrier which is as high as $\simeq$ 30 eV. The 'deep potential holes' that are created by such fields, however, cannot have gradients that exceed ~ 70eV / 0.5 Å, for otherwise ^{4}He would also exist in the form of an α-particle, and this is contradicted by observations. This fact nicely disposes of the arguments, embodied in the Baym-Leggett Theorem[18], that were made against CF. Indeed, in the Pd lattice the observed behaviour of ^{4}He is completely different from that of pairs of D's, contrary to the 'reasonable' assumptions of Ref. [18].

From the very existence of the β-phase the number of 'deep holes' (with electric fields 30 eV / Å < $|\vec{E}|$ <140 eV / Å) must exceed $x_\beta = 0.6$, and the well known difficulty of charging the Pd electrodes above $x \simeq 1$ makes it plausible that the number of such holes equals just the number of Pd-nuclei. Here, however, a severe difficulty shows up: how can we reconcile the existence of such 'deep holes' with the fact that Hydrogen is delocalized? The oddity of this fact puts all the generally accepted theories, based on two-body electrostatic forces between matter constituents, in the category of IMPOSSIBLE THEORIES.

Also the magnitudes and the inverted ordering ($D_D+ > D_H + > D_T+$) of diffusion constants speak against the usual theories, for they appear to require the existence of collective bosonic/fermionic states for the Hydrogen 'plasma'.

We may thus draw a fundamental demarcation between POSSIBLE AND IMPOSSIBLE THEORIES of Hydrogen in Pd in their allowance for collective many-body phenomena.

In models invoking explicity the existence of collective phenomena[1,19] the 'deep holes' that must form in roughly 1 : 1 proportion originate from coherent plasma oscillations of d-electrons. The difficult problem of 'delocalization' can be solved by imagining that the collective dynamics makes the Hydrogen state deep in the potential wells unstable. This can only happen if there are interactions other than electrostatic which provide the necessary negative interaction energy that allows the Hydrogen to occupy highly excited (delocalized) states in the potential well.

The only theoretical proposal, known to me, that achieves just that is the simplified model of plasma that is discussed in Ref. [20]. According to this model, as long as the charged particle of a plasma moves in a harmonic potential, its coupling to the e.m. quantum modes with the frequency $\omega = \omega_p$ (ω_p is the plasma frequency) will lift it up indefinitely, its excitation stopping when strong non-harmonicities appear.

This means that the Hydrogen nuclei will go to band states of the deep (~ 100 eV) potential that are highly delocalized, and in such circumstances all other properties discussed in the preceding Section appear to find a natural explanation.

3b - Nuclear Fusion Processes in Pd

As discussed in Ref. [1] the difficult problems that must be dealt with by any theory of these phenomena are two:

(i) How can the Coulomb barrier be penetrated at such large rates?
(ii) How can the process avoid the restrictions posed by 'Asymptotic Freedom' (AF)?

As for problem (i), all simple evaluations of 'tunnelling' probabilities lead to estimates that are 50-60 orders of magnitude much too small! Regarding problem (ii) one must notice that, even if the former severe difficulty could be resolved, there remains the even more severe difficulty that fusion in the lattice does not proceed experimentally in the same way as in hot-fusion processes.

In particular, the discoveries of high excess enthalpy uncorrelated to T-production and of the large T/n ratio imply that the lattice must play a fundamental role and, consequently, AF, with its implications of independence of nuclear processes from lattice dynamics, must be violated in a fundamental way. Besides a deep reason for the violation of AF, a good theory should also give some explanation of variability, dependence on x, bursts in T and n and generation of high energy n, p and T.

Getting now to the proposed theories of the penetration of the Coulomb barrier, I note that a simple application of the Gamow-formula (which contains essentially all the 'juice' of the problem of the penetration of the Coulomb barrier) requires the existence of a screening potential of about 100 eV, just in order to enhance the naive estimates of fusion rates by the 50 orders of magnitude necessary to account for the relatively rare neutron emission processes.

All POSSIBLE theories must thus include at least a semiquantitative explanation and estimate of screening potentials of such size. IMPOSSIBLE are those theories which do not consider explicitly this problem[22].

Among IMPOSSIBLE theories, I note those which try to avoid the barrier either by having 'off-shell' neutrons to initiate the fusion process[1], or 'on-shell' neutrons that originate from an incoherent exchange of energy with the lattice[23]. Equally IMPOSSIBLE is to have tight De bound states up to 300 F (Hydrons)[24], which appear in clear conflict with known phenomenology.

On the other hand the superradiant plasmas considered in Ref. [20] do provide for such screening in a natural way[25].

The necessary violation of AF puts all theories based on the usual, electrostatic view of condensed matter interactions among the IMPOSSIBLE theories. For in a lattice governed by short-range forces no room for such striking phenomenon can be found: indeed, with such forces there is absolutely no way in which the space-times of a lattice (10^{-8} cm and 10^{-15} sec) can influence the space-times of a fusion process (10^{-12} cm, 10^{-21} sec). I note in passing that similar mismatches occur in the physics of the Mössbauer effect, putting this well known phenomenon in the category of natural mysteries - at least within the conventioned picture of condensed matter[26]. POSSIBLE theories of CF must take due account of these odd collective phenomena, which the theory of superradiant plasmas explains naturally.

Recall, in fact, that the theoretical analysis based on superradiant behaviour[19] explicitly violates AF and provides estimates of the rates of ^{4}He (plus excess heat), T and n-production in reasonable agreement with known phenomenology. In particular, the production of ^{4}He unaccompanied by γ-rays demands a very fast ($\sim 10^{-21}$ sec) energy transfer to the lattice electrons (which then will release it away in various ways: heat, ultraviolet light, x-rays...). Without a macroscopic quantum behaviour the impossibility of any theoretical description is clearly seen by computing the velocity υ of such transfer from the site of fusion (somewhere inside the lattice) to the nearest atom ($\sim$ 3 Å away), one has

$$\upsilon = \frac{3\text{Å}}{10^{-21}\ \text{sec}} \simeq 10^3\ c\ !$$

Remember the EPR paradox? Something like it seems to be occurring here[27].

Getting now to the sporadicity of some CF phenomena I would like to note that the theory which invokes the existence of heavy charged particle showering the earth from outer space[28], though a logical possibility, appears rather unlikely. On the other hand the existence of a threshold at $x \simeq 1$, as discussed in Ref. [29], seems a more likely explanation. Furthermore lattice defects, dislocations etc. interfering with the basic electron cooling mechanism responsible for the production of γ-less ^{4}He[1,19], might naturally explain T-production. It is clear, however, that along these lines a lot of work needs to be done.

4 - CONCLUSIONS AND OUTLOOK

I would like to end this talk with a few 'lapidary' statements, that try to capture the essence of my analysis.

- CF exists, its phenomenology is diverse but coherent, and reproduced by many different groups in different conditions.
- No previously known law of nature (QED and QCD) appear to be violated by CF phenomena.
- Deductions from these laws of nature, based on the generally accepted notion of AF, belong to the class of IMPOSSIBLE THEORIES.
- The key ingredient to construct POSSIBLE THEORIES is

  MACROSCOPIC QUANTUM MECHANICS (Macro QM)

  which originates from Quantum Field Theory (QFT) as applied to complex systems.

Let me note that a demarcation is seen to be emerging between simple (micro QM) and complex (Macro QM) systems and of their theoretical description. It appears that a powerful, detailed, correct theory of CF must be constructed along the lines of a macroscopic Quantum Mechanics, induced by long-range electromagnetic (radiative) interactions[20], i.e. according to QFT of Superradiance.

I hope that the next few years will see a lot of work along these lines. CF will then be looked upon not only as a magnificent gift to energy-hungry mankind, but as an essential window to the deep and subtle behaviours of condensed matter, which have remained hidden for such a long time.

REFERENCES AND FOOTNOTES

[1] G. Preparata, Some theories of Cold Fusion: A review, Fusion Tech. 20 (1991) 82.

[2] A De Ninno et al., Europhys. Lett. 9, (1989) 221; H.O. Menlove et al., J. Fusion Energy 9, (1990) 495; for a nice review see M. Srinivasan, 'Current Science' (1991).

[3] V.A. Kluyev et al., Sov. Tech. Phys. Lett. 12 (1986) 551.

[4] R. J. Buehler et al., Phys. Rev. Lett. 63 (1989) 1292.

[5] M. Fleischmann, S. Pons and G. Preparata, Possible and impossible theories of Cold Fusion, preprint MITH 91/23 (1991).

[6] B. Pippard, Nature 350 (1991) 29.

[7] For a recent discussion of the many aspects of Hydrogen in Pd see L. Schlapbach (ed.) 'Hydrogen in Intermetallic Compounds' Vol. 1 in 'Topics in Applied Physics Vol 63' Springer Verlag, Berlin Heidelberg (1988).

[8] The best evidence for this behaviour comes from the Hall effect, see A. H. Verbraggen, R. Griessen and J. H. Rector, Phys. Rev. Lett. 52 (1986) 1625.

[9] See for instance J. Völkl and G. Alefeld, in Hydrogen in Metals I, eds. G. Alefeld and J. Völkl; Springer: Topics Appl. Phys. 28, 1978 Berlin, p. 321.

[10] T. Soskiewicz, Phys. Status Solidi All (1972) k123; B. Stritzker and W. Buckl, Z. Phys. 257 (1972) 1.

[11] M. Fleischmann, S. Pons and M. Hawkins, J. Electroanal. Chem 261 (1989) 301; for some corrections ibid 263 (1989) 187.

[12] J. O'M. Bockris, G. H. Liu and N. J. Packham, Fusion Tech. 18 (1990) 11.

[13] T. N. Claytor et al., Proc. Anomalous Nucl. Effects in Deuterium Systems, Provo, Utah, October 1990; A. Takahashi et al., Fusion Tech., 19 (1991).

[14] S. Szpak et al. J. Electroanal. Chem., 302 (1991) 255; and S. Szpak's contribution in these Proceedings.

[15] B. F. Bush et al., J. Electroanal. Chem., 304 (1991) 271; and M. Miles' contribution in these Proceedings.

[16] S. Pons, these Proceedings.

[17] W. Hansen, these Proceedings.

[18] A. J. Leggett and G. Baym, Nature 340 (1989) 45.

[19] T. Bressani, E. Del Giudice and G. Preparata, Nuovo Cimento 101A (1989) 845; G. Preparata, First Annual Conference on Cold Fusion, Conference Proceedings National Cold Fusion Institute, Salt Lake City (USA), 1990, p. 91.

[20] G. Preparata, Quantum Field Theory of Superradiance, in Problem of Foundamental Modern Physics, Ed. by R. Cherubini, P. Dal Piaz and B. Minetti (World Scientific, Singapore) 1990.

[21] J. Schwinger, First Annual Conference on Cold Fusion, Conference Proceedings, National Cold Fusion Institute, Salt Lake City (USA); 1990, p. 130.

[22] A discussion of typical theories of this sort can be found in Ref. 1, see also Ref. [21].

[23] P. Hagelstein, these Proceedings.
[24] F. Meyer, these Proceedings.
[25] M. Baldo in these Proceedings appears to be thinking along these lines.
[26] T. Bressani, E. Del Giudice and G. Preparata, What makes a crystal stiff enough for the Mössbauer effect? Preprint MITH 90/6 (to be published).
[27] Nevertheless, notes are being circulated by S.E. Jones who on the basis of such 'paradox' pretends to prove that excess enthalphy generation à la Fleischmann Pons is impossible, hence wrong.
[28] J. Rafelski et al., Fusion Tech. 18 (1990) 136.
[29] M. Mc. Kubre, these Proceedings.

SUMMARIES

«The Science of Cold Fusion»
T. Bressani, E. Del Giudice and G. Preparata (Eds.)
SIF, Bologna 1991

IS COLD FUSION A REALITY? THE IMPRESSIONS OF A CRITICAL OBSERVER

Heinz Gerischer

Fritz-Haber-Institut der Max-Planck-Gesellschaft,
Faradayweg 4 - 6, D-W-1000 Berlin 33, F. R. G.

Having received, at short notice, the invitation to attend the second international conference on cold fusion as a sceptical observer, I began to study some of the papers which have appeared since the fall of 1989 after which I had stopped following the publications in this area. Being sceptical from the beginning, the many negative reports from renowned laboratories seemed to confirm that the disputed claims of cold fusion occurring in a solid were, unfortunately, based on the erroneous interpretation of ill-defined experiments. I now realize that in the meantime many new positive results have been published which can not be pushed aside quite so easily. Two reviews, currently in the course of publication, were very helpful and yielded much information on the present situation. These are the reviews of M. Srinivasan [1] and E. Storms [2]*. Together with my reading and the lectures given on the first days of the conference, I eventually felt able to present my impressions in a lecture on the last day of the conference, as the organizers had requested. I am aware that all the arguments pro and contra the reality of cold fusion have been pointed out by others before. The first part of my contribution to the report of this conference is therefore mainly a reminder of the problems. In the second part I raise some questions seen with the eyes of a physical chemist being specially experienced in electrochemistry.

* I am indebted to J.O'M. Bockris for sending me preprints of these reviews.

Arguments pro and contra

1. *Anomalous phenomena*

Pro: Anomalous phenomena have been observed in several laboratories (excess neutrons, excess tritium, excess heat) during the electrolytic reduction of D_2O at Pd or Ti electrodes or after loading of the metals with D_2 at high pressure. No comparable effects have been found with H_2O or H_2.

Contra: Many laboratories could not reproduce these results. Even groups publishing positive findings concede that they cannot reproduce these effects at will. Checks with H_2O for comparison are often missing in reports.

2. *Neutron generation*

Pro: Neutrons have been found during electrolysis of D_2O at Pd and during heating of Ti loaded with D_2 at low temperatures. They appear in bursts.

Contra: The measured neutron level is often hardly above background. In many experiments no effects at all were found. The intensity bears no relation to the claims of excess heat production.

3. *Tritium generation*

Pro: An increase in T concentration was found in the electrolyte during electrolysis with D_2O and Pd cathodes at several places. Such events are unpredictable and occur sporadically, but the increase is far above the well-known separation factor in electrolysis.

Contra: Irreproducibility of the T production. Contamination with T_2O suspected from the D_2O which has to be added continuously in order to compensate the loss by electrolytic decomposition of the water in open cells. Instead of the 1 : 1 relation between neutron and tritium genera-

tion found in hot or myon catalyzed cold fusion and in accordance with the theory of D + D fusion reactions, a relation n : T of $1 : 10^6 - 10^9$ has been reported.

4. *Excess heat generation*

Pro: Several groups have reported excess heat generation for hours between 10 - 600 % of the electric energy input during electrolysis of D_2O at Pd electrodes. Calorimetry has been improved since the first announcement and was applied in some cases to closed systems where no gas can escape and carry off energy.

Contra: Besides the unpredictability of the effect, many attempts to reproduce the heat effect have failed. The products of nuclear reactions which could produce such amounts of heat have not yet been found. The tritium generation rate is by far too small. ^4He production has been suggested as the source of the heat and has recently been found by one group in the D_2 gas produced by electrolysis [3], but has not yet been confirmed by independent measurements. From well-established theory and experiments of fusion in hot plasmas, the process $D + D \rightarrow {}^4He + \gamma$ (23.5 MeV) is the least probable one. The accompanying γ radiation has not been observed.

Open questions from an electrochemical point of view

It appears that the most pronounced anomalous effects have been reported in the electrolytic experiments, particularly the generation of excess heat, of tritium and maybe of ^4He. The reason might be that the concentration of deuterium in the solid during electrolysis is much higher than it can be obtained under equilibrium conditions from the gas phase. This can be related to the kinetics of the cathodic reduction of water.

Reaction kinetics

This process occurs in two steps with the intermediate formation of adsorbed deuterium atoms on the metal surface. The following equations describe the electrolytic D_2 generation from a basic solution where the primary reagent is D_2O.

I	D_2O	+	e^-		$\rightarrow$	D_{ad}	+	OD^-	V_I
IIa	D_{ad}	+	D_{ad}		$\rightarrow$	D_2			V_{IIa}
IIb	D_{ad}	+	D_2O	+ e^-	$\rightarrow$	D_2	+	OD^-	V_{IIb}
IIc	D_{ad}				$\rightleftarrows$	D_{bulk}			V_{IIc}

Reactions I, IIa and IIb can be considered as irreversible at high current densities. V_i are the rates of the individual reactions which depend on the following parameters:

$$(1) \qquad V_I \sim F_1(1-\vartheta) \cdot \exp\left(-\beta_1 \frac{e_0 \eta}{kT}\right)$$

$$(2) \qquad V_{IIa} \sim G(\vartheta^2)$$

$$(3) \qquad V_{IIb} \sim F_2(\vartheta) \cdot \exp\left(-\beta_2 \frac{e_0 \eta}{kT}\right)$$

$$(4) \qquad V_{IIc} \sim S(\vartheta) - B(X_D)$$

In these equations the parameter ϑ represents the coverage of the metal surface with adsorbed D atoms. The activity of the vacant surface sites which are available for reaction I varies with $(1-\vartheta)$ in a way which depends on the local structure and on the chemical composition of the surface. This is represented by the function $F(1-\vartheta)$ which can hardly be predicted, particularly not on a polycrystalline surface.

For the formation of D_2 molecules there exist two competing reactions, IIa and IIb. The rate of both depends on ϑ, again in a complex way which is represented by the functions $G(\vartheta^2)$ and $F_2(\vartheta)$. The term ϑ^2 in the function G shall indicate that this step is a bimolecular reaction in which two adsorbed D atoms

take part. All these functions will be non-linear in ϑ but G will increase much steeper with ϑ than F_2. Only reactions I and IIb are influenced by the electric bias applied to the electrodes. The bias is here expressed by the overvoltage η for the water reduction which is negative. η is the voltage difference $\Delta\phi_H$ in the Helmholtz double layer at the interface between equilibrium for the overall reaction, $2\ D_2O + 2\ e^- \rightleftarrows D_2 + 2\ OD^-$ with $\Delta\phi_H = \Delta\phi_0$ and the voltage at a given current density, i, $\Delta\phi_H$ (i): $\eta = \Delta\phi_H\ (i) - \Delta\phi_0 < 0$. β_1 and β_2 are the so-called charge transfer coefficients. They are usually in the range of 0.4 - 0.6.

The rate of diffusion of D atoms into the bulk will equally depend on the activity of adsorbed D atoms which is expressed by the function $S(\vartheta)$. Here, however, the reverse process depending on the activity of the deuterium in the lattice, represented by the relation $x = D/Pd$ in the solid, will eventually compensate the rate of D uptake that $V_{IIc} \rightarrow 0$ in the steady state. One can only conclude that the higher ϑ and with it $S(\vartheta)$, the higher will be the D content x in the steady state.

All experiments where anomalous effects have been observed are performed after saturation of the bulk with deuterium or at least under conditions where V_{IIc} became very small because the diffusion into the depth of the bulk had slowed down further uptake. It is therefore sufficient to discuss the steady state situations. In this state:

$$(5) \qquad 2\ V_I = V_{IIa} + 2\ V_{IIb} \text{ and } V_{IIc} = 0$$

The current voltage curves for hydrogen evolution at palladium indicate that at low current densities the recombination IIa is rate determining. This should result in a slope of the current voltage curve of $d\eta/d \log i = -kT/2\ e_0 = -0.029$ V, if the metal surface were uniform in adsorption sites for deuterium. The real slope on inhomogeneous surfaces will be larger.

At higher current densities where the coverage of the surface with deuterium atoms becomes high, the rate determining step changes. Because the rate of the electrochemical desorption, reaction IIb, increases with the bias, this process will become faster than reaction IIa. This is seen in a decrease of the slope of the current voltage curve which should approach $d\eta / d \log i = - kT / \beta_2 e_0$ for a surface with uniform adsorption sites for deuterium. Again, for inhomogeneous surfaces the slope will be larger than the ideal slope of - 0.12 V, if $\beta_2 = 0.5$.

The most important consequence for the present discussion is that, if the reaction II_b becomes rate determining, the surface activity of adsorbed D atoms can only increase slowly. In this situation

$$(6) \qquad 2\, V_{IIb} \gg V_{IIa} \quad \text{and} \quad V_I \approx V_{IIb} \quad \text{, therefore,}$$

$$(7) \qquad \frac{F_2(\vartheta)}{F_1(1-\vartheta)} \approx \exp\left((\beta_1 - \beta_2) \frac{e_0 \eta}{kT} \right)$$

If $\beta_2 = \beta_1$, this relationship will remain constant. For $\beta_1 > \beta_2$, $F_2(\vartheta)$ can still increase with increasing bias (negative η), this being more pronounced for larger $(\beta_1 - \beta_2)$. However, F_1 will also grow with ϑ, and therefore the increase of the activity of adsorbed D atoms can only be small in the range of these current densities. The opposite could occur if $\beta_1 < \beta_2$. This is in sharp contrast to the region of low overvoltages where the activity of adsorbed D atoms would on a uniform surface increase quadratically with the current density as long as reaction IIa was rate determining.

Reproducibility

The relative rates of all three reactions I, IIa and IIb will depend very critically on the surface properties of the solid and can be affected by all substances which may be adsorbed on the surface or electrolytically deposited. This is par-

ticularly critical in experiments of very long duration in which even minute amounts of impurities can be collected at the electrode. They can also influence the structural changes of the Pd electrodes when they are transformed from the α- to the β-phase of the deuteride which occurs during the heavy loading with deuterium. Such factors will limit the reproducibility if they are not strictly controlled.

An instructive example can be found in a recent publication of M. Ulmann et al. [4] where current voltage curves for Pd cathodes in $LiOD/D_2O$ solution are represented. One sees a change in the slope of $d\eta/d \log i$ from very low values (not exactly given in the paper) to values of 0.18 V and more, above current densities of 3 mA cm^{-2}. The overvoltage is substantially higher if the electrolyte has not been pre-electrolyzed for removal of impurities prior to the use in the experiment. Surface composition analysis by XPS after electrolysis has shown how much foreign metals were deposited on the surface in these experiments after long periods of electrolysis. Even in pre-electrolyzed electrolytes large amounts of platinum were found on the palladium surface. The source was obviously the Pt counter electrode which corroded somewhat during anodic oxygen evolution. This has also been reported by Bockris [5].

Bulk or surface reaction

There are different opinions as to whether the anomalous effects occur in the bulk or at the interface. The first is frequently assumed when the excess heat generation measured with small electrodes is extrapolated to heat per unit volume. On the other hand, there are several arguments for a process occurring on or very close to the surface. The tritium is found in open cells in the electrolyte where it is present as DTO or OT^-. Any tritium generated by the process: $D + D \rightarrow T + H$ can only enter the solution by an exchange reaction from the adsorbed state on the surface:

$$\text{III} \quad T_{ad} + D_2O \rightleftarrows D_{ad} + TDO$$

If T would be generated in the bulk it has to reach the surface by diffusion prior to this exchange reaction. This could hardly result in the rather fast concentration increase in the solution during short periods as reported by several authors [6,7,8].

^{4}He has also been found in the gas phase, not in the palladium bulk, if the reported experiments are correct [3]. This would support the latter conclusion since He is immobile in Pd at room temperature.

If the anomalous effects require a high oversaturation of the lattice with deuterium, a composition of $x > 0.8$ [9], one would expect that this first occurs near the surface. The diffusion coefficient of D in Pd decreases at large x values [10]. If the activity of D_{ad} should suddenly increase by some reason, this would quickly let x increase next to the surface, but extend only slowly into the bulk. These arguments support the assumption that the processes in question should primarily occur close to or on the surface.

Role of lithium

Li^+ ions in the electrolyte seem to be essential for the occurrence of the anomalous effects [11]. It is striking that in the current voltage curves of M. Ulmann et al. [4], mentioned previously, the slope $d\eta/d\log i$ increases dramatically to 0.5 - 1.0 V at current densities above 100 mA cm^{-2}. This cannot be explained by any normal mechanism of the reactions I, IIa and IIb. Li can be alloying Pd [12]. This large slope indicates that an additional charge transfer resistance is created on the Pd surface in this current density region. One is reminded of the phenomenon of "undervoltage deposition" [13]. In the case of Li deposition from non-aqueous electrolytes containing some water, the formation of lithium hydride was observed as the result of underpotential

deposition [14]. A similar process could occur in aqueous electrolytes at high current densities and drastically modify the D_2 evolution kinetics.

Can it become a source of energy?

If excess heat generation requires electrolysis, this heat does not only have to compensate the energy input but also the energy conversion losses in the electric power station. If the conversion efficiency there would be 40 %, the excess heat should be 150 % of the electric energy input, in order to reach the break-even point. As a practical source of energy a much higher excess would be required. As a development to a source of free energy (electric power) the Carnot restriction has to be taken into account. More valuable would be a system generating excess heat at elevated temperatures. However, if heat generation requires a high concentration of D in palladium, then the decrease of the equilibrium capacity for hydrogen of all metallic hydrides [10] plus the increase in the rate of all electrochemical reactions with temperature (corresponding to a decrease in overvoltage) makes it very questionable that such conditions can be reached at elevated temperatures.

Conclusions

The primary goal in the present situation should be to demonstrate that fusion reactions occur in metal deuterides. A convincing proof would be finding the reaction products which can generate the excess heat in the corresponding amount. The search for T and ^4He should be performed in closed cells where no products can escape. Parallel test runs with normal water are mandatory for any proof.

With regard to reproducibility, the electrochemical parameters have to be investigated much more carefully than have been to date. Excess heat should always be reported in relation to the energy input per surface area; the extrapolation to unit volume is misleading. The analysis of the kinetics indi-

cates that one should try to find conditions where the rate constants for the recombination steps IIa and IIb are as low as possible in relation to the rate constant for step I. Any impurity deposition which catalyzes recombination like platinum, should be prevented.

The question of economic applications can be postponed until a definite proof is available and the decisive parameters have been clarified. The publicity of this research area and of unjustified claims for practical applications have not been helpful towards finding the truth. Only systematic and critically analyzed experiments will pave the way to a true understanding of the phenomena and to consensus in the scientific community.

References

1. M. Srinivasan, Current Science **60** (1991), 417.
2. E. Storms, Fusion Techn., submitted.
3. B.F. Bush, J.J. Lagowski, M.H. Miles and G.S. Ostrom, J. Electroanal. Chem. **304** (1991), 271.
4. M. Ulmann, J. Liu, J. Augustynski, F. Meli and L. Schlapbach, J. Electroanal. Chem. **286** (1990), 257.
5. J.O'M. Bockris, lecture on this conference.
6. N. Packham, K.L. Wolf, J.C. Wass, R.C. Kainthla and J.O'M. Bockris, J. Electroanal. Chem. **270** (1989), 451.
7. E. Storms and C. Talcott, Fusion Techn. **17** (1990), 680.
8. P.K. Iyengar, M. Srinivasan et al., Fusion Techn. **18** (1990), 32.
9. F. Will, lecture on this conference.
10. B. Baranowski, in *Topics in Applied Physics* (eds. G. Alefeld and J. Völkl), Vol. 29, pp. 157. Springer, Berlin 1978.
11. A.J. Appleby, Y.J. Kim, O.J. Murphy and M. Srinivasan, Proc. 1st Ann. Conf. Cold Fusion, Salt Lake City 1990, p. 32.
12. Landolt-Börnstein, *Numerical Data and Functional Relations in Science and Technology*, New Series, Group III, Vol. 19, p. 285. Springer, Berlin 1988.
13. E.g. D. M. Kolb, in *Advances in Electrochemistry and Electrochemical Engineering* (eds. H. Gerischer and Ch.W. Tobias), Vol. 11, pp. 125. Wiley, New York 1978.
14. H. Gerischer and D. Wagner, Ber. Bunsenges. Phys. Chem. **92** (1988), 1325.

Conference Proceedings Vol. 33
«The Science of Cold Fusion»
T. Bressani, E. Del Giudice and G. Preparata (Eds.)
SIF, Bologna 1991

THE PRESENT STATUS OF RESEARCH IN COLD FUSION

Martin Fleischmann

Department of Chemistry, The University, Southampton
Hants. SO9 (Great Britain)

EDITORIAL NOTE:

Martin Fleischmann has recently been asked by the Royal Society of Chemistry to give an account of the II Annual Conference on Cold Fusion for the Newsletter of the Electrochemistry Group of the Society. The editors thought it would be a very useful addition to the Conference Proceedings. We thank Martin Fleischmann and the Royal Society of Chemistry for having agreed to publish this text in these Proceedings.

In the development of any new area of research (and especially in one likely to arouse controversy!) it is desirable to achieve first of all a qualitative demonstration of the phenomena invoked in the explanation of the observations. It is the qualitative demonstrations which are unambiguous: the quantitative analyses of the experimental results can be the subject of debate but, if these quantitative analyses stand in opposition to the qualitative demonstration, then these methods of analysis must be judged to be incorrect[1].

Research in the area of Cold Fusion affords an excellent illustration of this principle. Contrary to popular belief it is relatively easy to show qualitatively that Pd cathodes polarized in LiOD solutions in D_2O generate excess enthalpy over and above that of the enthalpy input to the electrochemical cell. All that is required is that a sufficient number of electrodes of sufficiently well-controlled properties be polarized for a sufficiently long time in D_2O having a sufficiently low content of H_2O and using calorimeters of sufficient sensitivity (signal:noise) in a sufficiently well-controlled environment[2]. It will then be found that a proportion of the experiments will show temperature-time and cell potential-time plots of the form illustrated in Fig. 1. We also make the following observations about this particular type of experiment:

(i) the current efficiency for the electrolysis of D_2O is virtually 100%: there is no additional chemical source of enthalpy in the system;

(ii) heat transfer from the cell to a surrounding thermostat is controlled by radiation and the heat transfer coefficient for the particular cell is virtually independent of time;

(iii) our experiments in H_2O do not show these effects.

---

[1] This principle, which should be self-evident, is usually overlooked in the unseemly haste to develop research. It may come to be known as Pons' and Fleischmann's first principle (designed to irritate the scientific public in general and nuclear physicists in particular). We have some even more irritating principles but will save these for a later discourse.

[2] The explanation of the term "sufficient" in each of these contexts is beyond the scope of this article; these points can be taken up by correspondence.

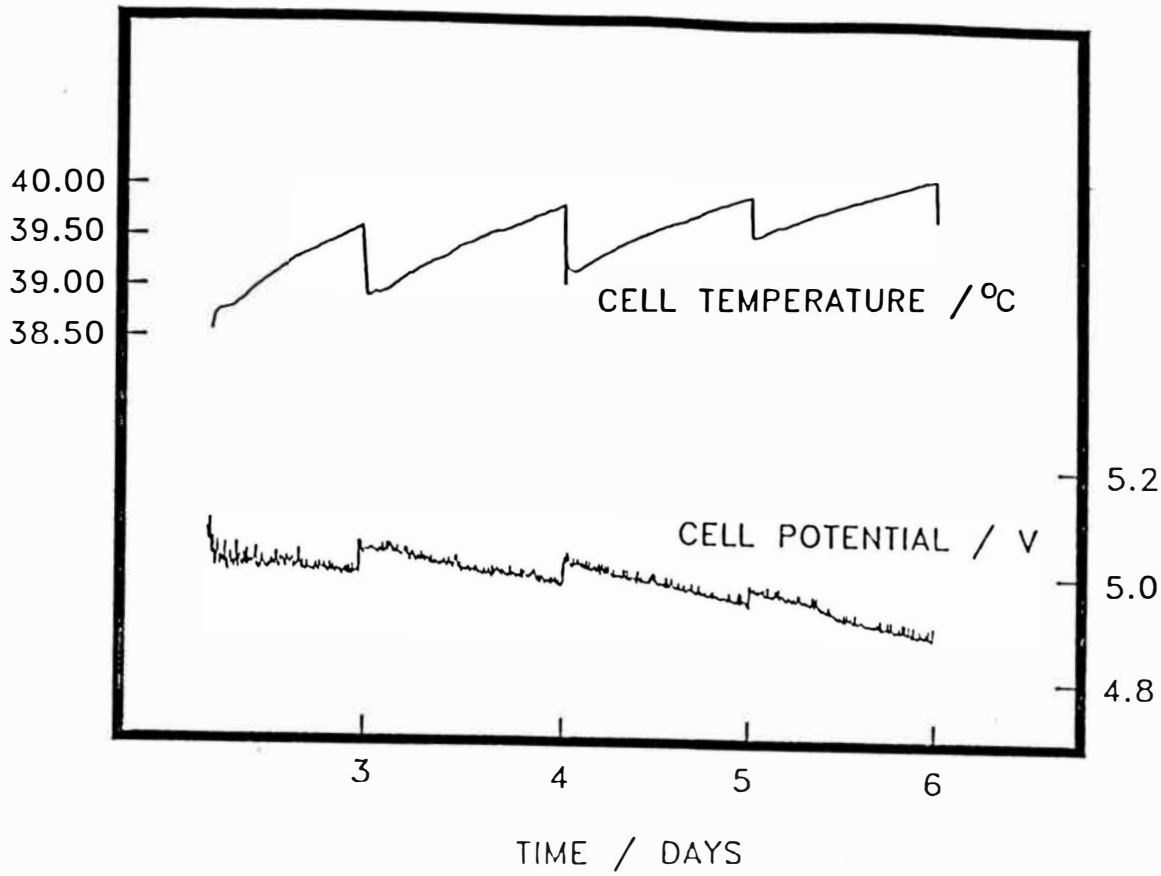

FIG. 1. Cell temperature (upper) and cell potential (lower) vs. time since cell was started for the electrolysis of D_2O in 0.6M Li_2SO_4 solution at pH 10 at a palladium rod cathode (0.4 x 1.25 cm). The cell current was 400mA, the water bath temperature was 30.00°C, and the room temperature was 21°C. The rate of excess enthalpy generation at the end of each day was 0.045W (day 3), 0.066W (day 4), 0.086W (day 5), and 0.115W (day 6). The accumulation of excess enthalpy for this period was on the order of 26KJ.

How then are we to explain an increasing thermal output of the cell coupled to a decreasing thermal input? The first law of thermodynamics requires that there be a source of enthalpy in the system and the strength of this source increases with time during the period illustrated. Such observations were valid in 1989 (they were valid

before then!), they were valid in 1990 and they are valid now.

The next step naturally is to seek a quantitative interpretation of such data. The last two years have seen the development of something akin to a cottage industry whose objective appears to be to explain away the reality of the phenomena by a combination of using incorrect (or inappropriate) methods of data analysis and invalid methods of overestimating the errors of the calorimetry (10% is the target figure). There is in truth scope for the former because the experiment is complex; the latter will come as a surprise to chemists who have hitherto relied on calorimetric methods as the main plank of thermodynamics. In judging the validity of such methods of calculation and of such estimates it is important to bear in mind the qualitative information conveyed by the experiments: any quantitative evaluation which removes or obscures the qualitative information must be judged to be invalid. Equally, failure to observe comparable qualitative effects when using other calorimetric methods must be judged to be due to inadequacies of the experimental methods[3] or, possibly, erroneous interpretation of the results.

Our own interpretation of the data in Fig. 1 gives the values of the rates of excess enthalpy generation and of the total excess enthalpy also shown on the Figure. Over the period shown the specific excess enthalpy amounts to 172 kJ cm^{-3} corresponding to 1.52 MJ (g mole Pd)$^{-1}$. It is our view that enthalpies of this magnitude can only be attributed to the operation of nuclear processes. The most rudimentary measurements of the generation of tritium and of the neutron flux (or rather the lack of it!) show that the nuclear reaction paths

$$^{2}D + {}^{2}D \rightarrow {}^{3}He(0.81\ MeV) + n(2.45\ MeV) \qquad (i)$$

$$^{2}D + {}^{2}D \rightarrow {}^{3}T\ (1.01\ MeV) + {}^{1}H(3.02\ MeV) \qquad (ii)$$

---

[3] These include: failure to control the H_2O content of the electrolyte, inadequate experiment times and other factors such as cracking of the electrodes (repeated use of the cathodes?) or lack of symmetry of the disposition of the anodes around the cathodes leading to low D/Pd ratios; excessive sophistication of the instrumentation (which obscures the significance of the results) and incorrect choices of the experimental protocols.

which are dominant in high energy fusion (and which have roughly equal cross-sections under those conditions) contribute to only a very small extent to the observed phenomena.

We reach the conclusions:

(i) the lattice has an important influence on the nuclear processes;

(ii) the observed processes are substantially aneutronic;

(iii) the generation of excess enthalpy is the main signature of these new nuclear processes.

These conclusions were valid in 1989, they were valid in 1990 and they are valid now. As chemists we are naturally interested in the main signature of the processes-side reactions can give important information but, in the end, one always has to investigate the major reaction route. Research in Chemistry teaches one that an understanding of the major processes normally leads also to an understanding of the side reactions[4]. This dictum has not been followed in most of the research carried out during the last two years.

Some Comments on Research since 1989: the Second Annual Conference on Cold Fusion. Como, Italy. 29th June - 4th July 1991

The holding of the Second Annual Conference on Cold Fusion prompts a reassessment of the work carried out since March 1989. The papers presented at the conference will be published by the Italian Physical Society later this year. Summaries of earlier work can be found in the following reviews:

J. O'M. Bockris, Guang H. Lin and N.J.C. Packam (Texas A&M University) "A Review of the Investigations of the Fleischmann-Pons Phenomena", Fusion Tech., 18 (1990) 11.

J. O'M. Bockris and D. Hodko (Texas A&M University) "Is there Evidence for Cold Fusion?", Chemistry and Industry 21 (1990) 688.

[4] This principle is so well understood by Chemists that it doesn't qualify for Pons' and Fleischmann's second principle of research in Chemistry; it could, however, qualify as the second principle of research in Nuclear Physics. As the saying goes: Chemists are interested in making Chemicals but Physicists are not interested in making Physicals.

before then!), they were valid in 1990 and they are valid now.

The next step naturally is to seek a quantitative interpretation of such data. The last two years have seen the development of something akin to a cottage industry whose objective appears to be to explain away the reality of the phenomena by a combination of using incorrect (or inappropriate) methods of data analysis and invalid methods of overestimating the errors of the calorimetry (10% is the target figure). There is in truth scope for the former because the experiment is complex; the latter will come as a surprise to chemists who have hitherto relied on calorimetric methods as the main plank of thermodynamics. In judging the validity of such methods of calculation and of such estimates it is important to bear in mind the qualitative information conveyed by the experiments: any quantitative evaluation which removes or obscures the qualitative information must be judged to be invalid. Equally, failure to observe comparable qualitative effects when using other calorimetric methods must be judged to be due to inadequacies of the experimental methods[3] or, possibly, erroneous interpretation of the results.

Our own interpretation of the data in Fig. 1 gives the values of the rates of excess enthalpy generation and of the total excess enthalpy also shown on the Figure. Over the period shown the specific excess enthalpy amounts to 172 kJ cm^{-3} corresponding to 1.52 MJ (g mole Pd)$^{-1}$. It is our view that enthalpies of this magnitude can only be attributed to the operation of nuclear processes. The most rudimentary measurements of the generation of tritium and of the neutron flux (or rather the lack of it!) show that the nuclear reaction paths

$$^{2}D + {}^{2}D \rightarrow {}^{3}He(0.81\ MeV) + n(2.45\ MeV) \qquad (i)$$

$$^{2}D + {}^{2}D \rightarrow {}^{3}T\ (1.01\ MeV) + {}^{1}H(3.02\ MeV) \qquad (ii)$$

---

[3] These include: failure to control the H_2O content of the electrolyte, inadequate experiment times and other factors such as cracking of the electrodes (repeated use of the cathodes?) or lack of symmetry of the disposition of the anodes around the cathodes leading to low D/Pd ratios; excessive sophistication of the instrumentation (which obscures the significance of the results) and incorrect choices of the experimental protocols.

which are dominant in high energy fusion (and which have roughly equal cross-sections under those conditions) contribute to only a very small extent to the observed phenomena.

We reach the conclusions:

(i) the lattice has an important influence on the nuclear processes;

(ii) the observed processes are substantially aneutronic;

(iii) the generation of excess enthalpy is the main signature of these new nuclear processes.

These conclusions were valid in 1989, they were valid in 1990 and they are valid now. As chemists we are naturally interested in the main signature of the processes-side reactions can give important information but, in the end, one always has to investigate the major reaction route. Research in Chemistry teaches one that an understanding of the major processes normally leads also to an understanding of the side reactions[4]. This dictum has not been followed in most of the research carried out during the last two years.

Some Comments on Research since 1989: the Second Annual Conference on Cold Fusion. Como, Italy. 29th June - 4th July 1991

The holding of the Second Annual Conference on Cold Fusion prompts a reassessment of the work carried out since March 1989. The papers presented at the conference will be published by the Italian Physical Society later this year. Summaries of earlier work can be found in the following reviews:

J. O'M. Bockris, Guang H. Lin and N.J.C. Packam (Texas A&M University) "A Review of the Investigations of the Fleischmann-Pons Phenomena", Fusion Tech., 18 (1990) 11.

J. O'M. Bockris and D. Hodko (Texas A&M University) "Is there Evidence for Cold Fusion?", Chemistry and Industry 21 (1990) 688.

[4] This principle is so well understood by Chemists that it doesn't qualify for Pons' and Fleischmann's second principle of research in Chemistry; it could, however, qualify as the second principle of research in Nuclear Physics. As the saying goes: Chemists are interested in making Chemicals but Physicists are not interested in making Physicals.

M. Srinivasan (Bhabha Atomic Research Centre) "Nuclear Fusion in a Lattice: an Update on the International Status of Cold Fusion Research", Current Science, April 1991.

E. Storms (Los Alamos National Laboratory) "Review of Experimental Observations about the Cold Fusion Effect" to appear in Fusion Tech (1991).

There are other excellent reviews but these are not so readily accessible.

In what follows, comments about work done prior to the Como meeting will be indented in the text. The results will be described under several headings.

Tritium Generation

New results on tritium generation in closed electrochemical systems were presented notably by the collaborative groups between CNR, Padua, and the Department of Physics, University of Padua (G. Mengoli, C. Manduchi et al.) and by the group at the National Cold Fusion Institute, Salt Lake City (F. Will et al.). Conditions have been achieved by these and other groups which lead to an increase in the T-content of the closed systems by factors of 25-40 over that of the initial inventory.

Details of an interesting new variant of the electrochemical method were reported by the collaborative group between the Naval Ocean Systems Laboratory, San Diego and the D.O.E., Washington (S. Szpak). In these experiments palladium and D are codeposited at high negative potentials which appears to lead to an immediate generation of tritium and the detection of autoradiographic images in the immediate vicinity of the cathodes (presumably due to the emission of soft x-rays); it also leads to an immediate generation of excess enthalpy.

Further results on the generation of tritium (and neutrons) in solid state cells consisting of alternating layers of Pd powder or foil and of Si powder or wafers were reported by the group at Los Alamos National Laboratory (T.N. Claytor). Increases in the tritium levels up to 150 times of the initial inventory have been achieved under pulsed current conditions.

References to earlier work will be found in the reviews. These earlier investigations (notably those at the Bhabha Atomic Research

Centre) include spectacular examples of the autoradiography of Ti loaded with D and subjected to temperature cycles, the detailed characterisation of the tritium β-ray emission spectra and of x-ray emission from the Ti samples (presumably due to Coulomb excitation induced by the β-decay). There are also reports by the groups in India and at Texas A&M University of the generation of very high levels of tritium in and at palladium cathodes.

The generation of high energy tritons is referred to below under the heading "Miscellaneous Observations".

Neutrons

A survey of neutron detection experiments was presented by H. Menlove (Los Alamos National Laboratory) and this was also a major component of the surveys of gas loading experiments by F. Scaramuzzi (Frascati), of research in Japan by H. Ikegami (National Institute for Fusion Science, Nagoya), in the Soviet Union by V. Tsarev (Lebedev Institute, Moscow) and in China by Xing Z. Li (Tsinghua University, Beijing). A major new result is the detection of neutrons from experiments on Pd cathodes conducted in the Kamiokande mine by H. Menlove and S. Jones (Brigham Young University). These measurements rely on the detection of highly energetic γ-rays from the (n,γ) reaction on ^{35}Cl (present as 20% NaCl in the surrounding water bath). It appears that the results obtained are at a higher level of statistical significance than that of the neutrinos detected in the Kamiokande mine from the 1987 supernova.

The improvement in the methods of characterising individual neutrons continues apace such as in the time-of-flight spectroscopy reported by T. Bressani (I.N.F.N., Sezione di Torino). An improvement in the statistical significance of the data has been a general feature of the results such as in the time-correlated detection of bursts of neutrons from gas loaded samples of Pd reported by T. Tazima (National Institute for Fusion Science, Nagoya).

Earlier work has shown that both gas loaded samples and Pd cathodes show two types of signal, a very low level background count which is difficult to detect at high levels of significance (and which may be Poisson distributed) and bursts in the neutron production.

The results now available show that these bursts in the neutron production cannot be attributed to spallation induced by cosmic rays.

The results presented at the meeting confirmed yet again that the

branching ratio for reactions (ii) and (i) differs markedly from unity (factors as high as 10^7-10^9 have been reported). Such changes in the branching ratio from the value ~1 for "hot" fusion show that the nuclear processes in the lattice cannot in any sense be discussed by analogy to fusion in high temperature plasmas. This is also shown by the observation of high energy neutrons (a broad peak in the range 3-6 MeV in addition to the 2.45 MeV peak due to reaction (i)) which was again reported at the meeting by A. Takahashi (Osaka University - Matsushita Electric Company group).

Excess Enthalpy Generation

The rapid generation of excess enthalpy in thin films of Pd (either sputtered or electroplated onto Ag substrates) was reported by R. Bush (California State Polytechnic University); rapid generation in Pd-D codeposited at very negative potentials was also reported by S. Szpak (Naval Ocean Systems Laboratory). M. McKubre (EPRI-Stanford S.R.I.) gave results of excess enthalpy measurements on Pd cathodes using sealed flow calorimeters while S. Pons described measurements on alloy electrodes which lead to very high releases of excess enthalpy (> 1kW cm^{-3}) so much so that the main cause of heat transfer becomes the boiling of the electrolyte[5]. An independent analysis of some of our calorimetric data was presented by W. Hansen (Utah State University, Logan) using other methods than those employed by us. This analysis has given results closely similar to those which we have obtained although our estimates of the excess enthalpy appear to be conservative (which we have already anticipated because this is a feature of our methodology).

J. O'M. Bockris (Texas A&M University) reported that Pd cathodes subjected to pulse conditions give high levels of excess enthalpy but only when the D/Pd ratio approaches ~1.

Miscellaneous Observations

The sub-title unfortunately gives the wrong connotation because some of the most interesting results are included under this heading.

The correlation of ^4He measurements in the gas phase with the

---

[5] Arguments about the magnitude of the heat transfer coefficients, the characterisation of the calorimeters etc. then become meaningless. A watch, to time the boiling to dryness and one's finger will do (if one doesn't mind getting scalded).

levels of excess enthalpy generation in Pd cathodes was reported by M. Miles (Naval Weapons Research Centre, China Lake - University of Texas, Austin collaboration).

The detection of charged particles from thin Ti foils loaded with D from the gas phase, temperature cycled to -180°C and then subjected to moderately high current densities was reported by F. Cecil (Colorado School of Mines - Solar Energy Research Institute collaboration). It is possible to make very sensitive measurements on such systems using Si surface barrier detectors and such measurements are relatively unambiguous.

There are earlier reports of such measurements from the Soviet Union and especially from the Naval Research Laboratory, Washington, D.C. (G. Chambers). In this particular study of Ti foils ion implanted with deuterons ~5 MeV particles of mass 3 were detected (probably tritons). Such particles cannot arise in simple D-D reactions and this result should be compared with the observation of energetic neutrons in the 3-6 MeV range.

The fact that excess enthalpy generation is observed on electrodes having a D/Pd ratio ~1 was brought up several times at the meeting. By contrast, tritium generation appears to be favoured by lower charging ratios and/or non-equilibrium conditions (equally true of gas loaded samples subjected to temperature cycles). Neutron generation also appears to require non-equilibrium conditions (e.g. pulsed electrolysis).

The detection of neutrons from essentially aneutronic processes naturally poses difficulties and an unfortunate feature of much of the work to date has been the mismatch of the effort and information devoted to the instrumentation on one hand and the experiment design on the other[6]. At the final round table discussion we appealed that, as far

---

[6] We do not decry the effort devoted to the instrumentation but note that the experiment design is usually rather crude in comparison. However, we also note that several groups (ours included) have information that the neutron generation rate lies in the range 5-50 neutrons s^{-1} $Watt^{-1}$ (if excess enthalpy generation is observed). There appears to be some coyness about reporting such facts. It might well prove to be more useful therefore to increase the scale of the experiments rather than to improve the instrumentation to find next to nothing at all.

as electrochemical experiments are concerned, research workers should at the very least report the light water content of the electrolyte used, the D/Pd charging ratio and the number of times an electrode has been used as well as the position of any particular measurement cycle in the experiment sequence.

Theory

A number of ideas about the possible mechanism of "Cold Fusion" were presented at the meeting. The subject was reviewed by G. Preparata (University of Milan). Our speculation (in the last section) about the possible explanations of the phenomena are based on a paper which will appear as part of the conference proceedings[7,8].

What about the explanations?

We have to look for answers to the following questions:

(a) Why is it so much easier for deuterons to overcome the Coulomb barrier to fusion when the deuterons are in a lattice than when they are, say, in a high temperature plasma?

(b) Why is the outcome of fusion in a lattice so different to that of fusion "in a vacuum"?

(c) How does it come about that the lattice can affect processes which take place at very short space-times, say 10^{-21}s and 10 F?

---

[7] Summary of the present position. Contrary to the views which were expressed in 1989 that the phenomenon of "Cold Fusion" would "go away" with improved experiments and instrumentation, the evidence has become stronger and the statistical level of significance of the various measurements has increased.

[8] Readers will find that there is only a passing resemblance between this report and Douglas Morrison's Cold Fusion Update No. 5 (which must be about his 27th message about the subject). The difference is that we have reported what people actually said not what we feel they ought to have said (or wished they would have said). It is for this reason that we have separated our own thoughts about this section into the footnotes 5-8.
In the context of the reportage of this field we would add that it is not helpful to classify those workers who obtain positive results as "Believers" and those who obtain zero effects as "Skeptics" nor to give off the cuff comments about the validity of particular results. A judgement as to the latter frequently involves almost as much effort as the original investigation and science normally does not progress via such back-biting. We trust that Heinz Gerischer will publish his observations on the meeting which were an object lesson on how to avoid such nonsense.

Not surprisingly, simple models based on the collisions of two deuterons (with the possible screening by single electrons) cannot provide an explanation of (a) (the ingoing channel): the overlap amplitude

$$\eta - \exp\left\{ - \int_{r_N}^{r_o} \left[2\mu\left(V(r)-E\right)\right] dr \right\}$$

is simply too small. Here r_N is a typical nuclear distance (a few Fermis), r_o is the classical turning point, μ is the reduced mass, V(r) ($=\alpha/r$) is the Coulomb potential and E the kinetic energy of the colliding nuclei. Based on such arguments one would conclude that there can be no fusion in a lattice - it must all be a delusion, mistake, fraud or something to that effect.

It is important to realise, however, that whereas much of plasma physics has been based on ideas drawn from the solid state the transfer of concepts in the reverse direction cannot be achieved in a simple way[9]. An important key to the understanding of the system is given by the strange properties of D (and of H and T) in such lattices. We must ask: how can it be that D can exist at a ~100 molar concentration and high supersaturations without forming D_2 in the lattice? How can it be that D diffuses so rapidly through the lattice (diffusion coefficient $> 10^{-7}$ cm^2 s^{-1} greater than that of either H or T!) whereas He is practically immobile? The answer to the last question is, of course, that deuterium is present as the deuteron whereas ^4He does not form α-particles. These observations alone set interesting limits on the intense fields experienced by D as it moves through the lattice (say $>30eV\ (A)^{-1}$ and $<70eV\ (A)^{-1}$). The deuterons sit in deep energy wells and yet behave as though they are almost unbound (they behave as classical oscillators). This fact in itself shows that the deuterons must be part of a macroscopic quantum system so that they can experience such marked anharmonic excitations.

---

[9] A proper consideration of such condensed systems has to be based on the Quantum ElectroDynamics (Q.E.D.) of superradiating plasmas. Those interested in this topic should consult the papers of G. Preparata.As far as the present system is concerned one concludes that the deuterons form an ordered array (D/Pd =1!) in a coherence domain described by a macroscopic wave function; the deuteron plasma interacts with the coherent oscillations of the electron plasma.

These observations in turn give an explanation of the increase in the overlap amplitude, for hot fusion is based on the increase of E by increasing the temperature (say to 100 eV at 10^8K) while "cold" fusion depends on the lowering of V. The increase in η due to this is sufficient to explain the very low rates of neutron production which have now been extensively reported. Summation over all the "fusion paths" of the coherence domain gives the further increase in η demanded by the high rates of enthalpy generation.

The second important set of questions is why the outcome of fusion in a lattice should be so different to that in a plasma? The simple view is that processes at short space-times cannot be affected by the much slower lattice vibrations[10,11]. It is thought by many that the outgoing channels must therefore follow (i) and (ii). By the same token processes such as

$$^2D + {}^2D \text{ -----}\rightarrow {}^4He + \gamma \text{ (23.9 MeV)} \qquad \text{(iii)}$$

are not expected to contribute significantly (the cross-section of (iii) is about 10^{-6} that of (i) and (ii) under "hot" fusion conditions). However, in plasma fusion the dipole coupling for (iii) is to the vacuum whereas in the lattice this coupling is to the macroscopic wave-function of the coherent electron plasma. It would therefore be expected that most of the energy flow will be to the electron plasma which will

---

10 In Quantum ChromoDynamics (Q.C.D.) this separation of a process at short space-times from those at much longer space-times is referred to as "asymptotic freedom". However, in the presence of coherent interactions, this principle is generally inapplicable, as shown by Preparata.

11 This view is widely held notwithstanding the fact that lattices do affect nuclear processes as is shown, for example, by Moessbauer spectroscopy. You may wish to ask yourself whether the short space-time scale of γ-ray emission could ever be affected by phonon interactions? Why should the lattices be so stiff on such short time scales? The answer to this conundrum lies once again in the Q.E.D. of the superradiant plasmas as has been shown by Preparata. As electrochemists are imaginative people you might then ask yourself what other consequences this might have for Chemistry, Nuclear Physics, Cosmology or anything else that comes to mind.

rapidly thermalise the system[12, 13]. On this view the formation of T and n is due to incoherent cooling of the compound nuclei the H-T configuration then being favoured because of the large electromagnetic current due to the rapid motion of the proton (in the n-^{3}He configuration it is the neutron which is rapidly moving).

Conclusions

This short account has been based on only a small part of the information available. It is probably too soon, for example, to attempt a comprehensive explanation of the formation of high energy tritons (~5MeV) and neutrons (3-6 MeV) except to say that they certainly cannot arise in simple two-body collisions. We also note that other explanations of the phenomena have been put forward: we have simply chosen the one which at this time is most free from objections and which also has the essential advantage that it leads to predictions for the outcome of novel experiments. Future surveys will have to cover the much wider range of observations already to hand and may well have to include the strange patterns of behaviour of compressed deuteron plasmas which are being reported in related fields of research such as in the application of Plasma Focus devices.

It is our view that the scientific interest of the subject has now been amply established; the scope for technological applications remains to be evaluated. However, to date, it has certainly been true that all aspects of electrochemistry, no matter how esoteric, eventually find some practical use.

---

12 The information about the system is in the macroscopic wave-functions. Neglect of this fact leads to paradoxes of the Einstein-Rosen-Podolsky type.

13 This argument should not come as a surprise to electrochemists since there is some analogy between the deuteron-electron plasma coupling and the dipole fluctuation induced activation of outer sphere redox reactions. Indeed, it is our view that the latter processes would best be described by the relevant macroscopic wave functions of that superradiant system.

APPENDIX

Conference Proceedings Vol. 33
«The Science of Cold Fusion»
T. Bressani, E. Del Giudice and G. Preparata (Eds.)
SIF, Bologna 1991

APPENDIX

REPORT TO THE UTAH STATE FUSION/ENERGY COUNCIL ON THE ANALYSIS OF SELECTED PONS FLEISCHMANN CALORIMETRIC DATA

Wilford N.Hansen

Physics Department Utah State University
Logan, UT 84322-4415

Editorial Note

One of the highlights of the Conference has been the independent analysis of Fleischmann's and Pons' data, collected at the National Cold Fusion Institute, by Wilford Hansen.
In this Appendix we integrally reproduce Hansen's Report to the Utah State Fusion/Energy Council.

INTRODUCTION

Here is reported my analysis of a series of electrochemical experiments run by Pons and Fleischmann, P/F. This series produced some remarkable results which were revealed only through a careful analysis.

When I was asked last January by the Fusion/Energy Council of the state of Utah to head a committee to investigate unpublished and unreleased data of Pons and Fleischmann, I knew it would be a difficult and interesting assignment. Still there were many surprises, and it took longer and was more difficult than expected. I received help and good advice from colleagues, including some who were pro and some who were con. While others have helped, I take the full responsibility for this report. I am sorry to say that we have not conducted any actual experiments. In spite of good intentions, the Pons lab has not been used so far in our work. But we have received sets of data and have analyzed some of them in depth. Our strategy has been to obtain and closely

examine the most significant data available. We believe that has been done. The data discussed in this report lay no claim to being typical. They are chosen because they illustrate some remarkable results we found to have been obtained by the P/F group.

In approaching this analysis there are many attitudes one could take. Let me illustrate by mentioning three. First consider what I will call "scientific chauvinism". I have used it myself on occasion. When the University asks me to check out an invention of someone and I find that it is another perpetual motion machine, I just discount it completely and try to get the guy out of the office as smoothly as possible. Some seem to regard the P/F effect in a similar light. After examining P/F data, one "official" reviewer said to me, "They may have something interesting going on, but it certainly has nothing to do with nuclear physics." A second attitude is one of extreme skepticism. Because of the importance and unprecedented nature of the claimed discovery, and the lack of quick confirmation by most in a worldwide effort, many aren't going to believe until it is proven beyond doubt. A problem then arises because nothing can be proven "absolutely". Still something of such profound importance must be given careful scrutiny. A third attitude is that taken by the typical reviewer of articles for, say, Physical Review. He looks for quality in the research, for internal consistency, and for clear results. He doesn't usually ask to inspect the author's laboratory, nor does he doubt the word of a scientist with a good reputation. On the other hand even the best of scientists can make mistakes, so careful review is needed, and is usually desired by all.

So what is my attitude in the present case? Well, I have some sympathy for all three cases above. They may all be honest and legitimate attitudes. I avoid the first two because in the present case they would be fruitless. I choose the last, but with more skepticism than usual. The raw data are assumed to be real as given. It would be pointless to do otherwise. But I want to be extra careful on this one because of its great importance. I came into this assignment neither for nor against. Halfway through I was still neutral. I must admit to having become somewhat pro recently, but am trying to remain objective.

OVERALL REMARKS ON THE P/F CALORIMETRY

Neither time on this analysis nor detailed experience with the P/F project are sufficient to allow me to give an exhaustive appraisal.

However critical issues will be faced and evaluated. The most important ones are discussed below.

Adequacy of the experimental setup

The P/F calorimetry has been the subject of a great deal of discussion since March 1989, much of which I have heard. To some extent it's a matter of picking your experts. I make several observations:

1. Improvements have gradually been made to perfect the P/F calorimeters, and the ones used in this series are of the advanced silvered type. This improves constancy of heat transfer and makes analysis easier. It also reduces the heat loss rate by conduction at the top, making the cell contents more uniform in temperature.

2. The assumption of isothermal cell interior has been checked by P/F and collaborators and has been found to be adequate. This has been discussed with P/F and with others who have made independent evaluations. Only one temperature measuring unit was present within a cell in a typical run, however, so consistency of temperature was not continuously monitored. Details of the water bath and other cell environment factors have been reviewed and personally observed and are considered adequate.

3. Loss of electrolyte due to open cell evaporation: according to P/F this has repeatedly been checked with the following conclusions. There is no recombination of electrolysis products inside the cell and the loss rate is approximately as predicted by the mathematical model. Keep in mind that the cells are filled to the mark periodically, typically once a day. A record is kept of how much solvent this takes. Unfortunately these detailed data were usually not available to us. We assume that the cell was full at the beginning after each refill. Observations on blankcells and heatcells tend to show in general that recombination was not a factor. Others who are doing P/F type calorimetry state that with care in covering metal parts above the electrolyte, there is no recombination.

4. It is generally assumed that the voltage, galvanostat, temperature and other instrumental readings had negligible error so far as the instrument itself is concerned, since this is reasonably easy to assure.

Adequacy of the model of the cell calorimetry

This is a subject of active investigation at present and has been the subject of talks and publications in the past. We use the latest P/F model, unabridged, which is well known and will not be given here. There

are experts who still say that the P/F model is wrong in certain important respects. This debate will have to run its course as the subject has many subtleties. In the current analysis a competitive model was also used. It made little difference, and made essentially no difference in the crucial aspects of the analysis. It was also observed that the P/F model worked well on the blank cells, even up to high temperatures.

OUR OVERALL APPROACH TO DATA ANALYSIS

Modern fast computers permit the luxury of using the full model equations without approximation. For this reason it is called the "exact" approach. Of course it isn't really exact. No model of a physical system is exact. But insofar as the model is correct, curve fittings, inversions, and other numerical manipulations can be done in an optimal fashion not limited by trying to make the algebra convenient with the use of approximations. The full blown model equations for open cell calorimetry are rather complicated, and there is little hope of finding simple algebraic solutions. Actually, the latest computers make the use of open cell calorimetry much more attractive. In our approach we avoid many of the arguments about how to reduce the data with approximate methods. In fact much of the criticism of the P/F methods still revolves around how approximations should be made. In our approach, this conflict disappears. For a blankcell, with excess heat known to be zero, it is easy to get the heat transfer coefficients at all times and temperatures within limits which can be determined by digital data analysis. Direct calculations using linear or nonlinear regression analysis can be used to determine both heat transfer coefficient and excess heat in the case of heatcells. Even the effective heat capacity of the cell can be determined at the same time. When heat pulses of known wattage are added to the cell the analysis is particularly straightforward. These can also be used to check the internal self consistency of the data and model. Our data analysis is accomplished entirely with this computer approach.

ANALYSIS OF PONS/FLEISCHMANN CALORIMETRIC DATA

Part One

The cells discussed here are all of the "silvered" type where the vacuum jacket extends out of the water to the top of the cell and the top section is silvered down to a point under the water level of the bath. This makes the heat loss more radiative and smaller. It also makes the change in rate of heat transfer as the water level within the cell goes down during electrolysis less.

The raw data for all cells were received in the form of columns of time and corresponding temperature (celsius) and cell voltage. The cells were always run in galvanostatic mode, with the constant current given. The voltage and temperatures were recorded every 5 minutes. Auxiliary data for cells 1-5 and cell 8 are given in table 1. The detailed history of the cells was not made available to us, and sometimes there were extraneous data attached before and/or after the run of interest. Nor was the serial number of the flask used given. Because the cells were not all alike, it may prove very useful to have these and other data in the future, and they may be available from notebooks.

First we will discuss the "blankcells", i.e., cells deliberately designed to be like the "heatcells" but produce zero "excess heat". For these, $Q_f = 0$, except for small amounts due to loading at the beginning. In this set there are two, cells 8 and 3. Cell 8 is blank because a platinum electrode (three 1 mm dia. x 1.25cm Pt wires bound together) was used instead of palladium. Otherwise the cell contents were the same as those used in the "heatcells", i.e. those intended for possible heat production. Cell 3 used the same type of cathode as cell 8. In addition light water was used. Cell 1 is claimed to be the same flask, but is a "heatcell", with heavy water and palladium cathode. There may be other small differences, here and among the cells in general. For example the heat capacities of the various cathodes are probably somewhat different. Also the cells may not all have had the resistance heating well and resistors in place, since heat calibration pulses were not used in cell 8 nor in cell 1 in the main run. Early on it was thought that cell 3 was a blank for cell 7, but that proved not to be the case. From the information we have, cells 1, 3, and 8 are the same flask and all others are different individual flasks with none in common. Cell 3 used a platinum cathode (three 1mm dia. x 1.25 cm Pt wires bound together).

TABLE 1

Auxiliary Data for Cell Runs

RUN	CATHODE	Electrolyte	Heat Pulses	Current
Blankcell	Pt wire	D_2O + LiOD	none	800mA
Cell 8*	3-1mm x 1.25 cm bound together	0.1M		
Blankcell	Pt wire	H_2O + LiOH	two	800mA
Cell 3*	3-1mm dia x 1.25 cm	0.1M	0.270 watts	
Heatcell	Pd alloy	D_2O + LiOD	one	800mA
Cell1*	4 mm dia x 10 cm	0.1M		
Heatcell	Pd alloy	D_2O + LiOD	one	200mA
Cell 2	1mm dia x 1.25 cm	0.1M	0.270 watts	400mA
Heatcell	Pd alloy	D_2O + LiOD	one	400mA
Cell 4	4mm dia x 1.25 cm	0.1M	0.270 watts	800mA
Heatcell	Pd alloy	D_2O + LiOD	one	400mA
Cell 5	2mm dia x 1.25 cm	0.1M	0.270 watts	800mA

*Cells 1,3 and 8 are same flask, other cells all have different flasks.

Using hindsight, the fact that most of the cells had no blank is of course unfortunate. It would be nice to have blankcells for all heatcells, and to have in addition heat calibration pulses for every cell, including all blankcells. The most important change in this set of similar cells from an analysis point of view, is that the heat transfer coefficients vary from cell to cell.

EVALUATION OF BLANKCELLS

Now concentrate on cell 8. The raw data are plotted in figure 1. Further data include: the cathode comprised three platinum wires 1 mm in diameter by 1.25 cm long, wrapped together, the electrolyte was 0.1 M LiOD, and the current was 800 mA throughout. Data for the fillings with D_2O were typically 8.0 ml per day for a cell using 800 mA. The detailed filling data for cell 8 are not given, but the behavior of the raw data indicates that they were regular and uniform. We will now present an analysis scenario that reveals a number of characteristics of this cell, and indicates some general things about this type of cell. We use a real-time Kalman filter and run through the data from left to right (increasing time). This gives us a relatively noise free data line for Q_f as a function of time throughout the whole set of data. The model used to calculate Q_f is that of Pons/Fleischmann, (P/F hereafter). Since the model does not hold for the short time of water refreshment, a spike in the filtered Q_f output results. In addition, the Kalman filter takes a few points to settle down after the spike, so there is a period of time after each refill where the filter output points are first false and then doubtful. These periods are obvious from the graph, figure 2. In running the filter, a fixed radiative heat transfer coefficient, K_r, for the cell is given and Q_f calculated. Actually, of course, Q_f should be zero everywhere if small chemical changes in the platinum electrode are neglected, which appears reasonable. This requires a K_r that changes as the day progresses. The small changes involved seem transparent at this point and will not be plotted here. (We will, however, confirm our results by another approach later.) We take the data for a given day as a batch, use a curve fit to, say, $Q_f=0$, using an appropriate modelling equation, and see what the average K_r is. K_r may also be taken linear with time or quadratic with time. At this point it should be noted that the heat transfer is not pure radiative but has a conductive component which is given by $K_c(T_{cell} - T_{bath})$ while the radiative heat loss is given by $K_r(T_{cell}^4 - T_{bath}^4)$. Using the current type cell it is nearly

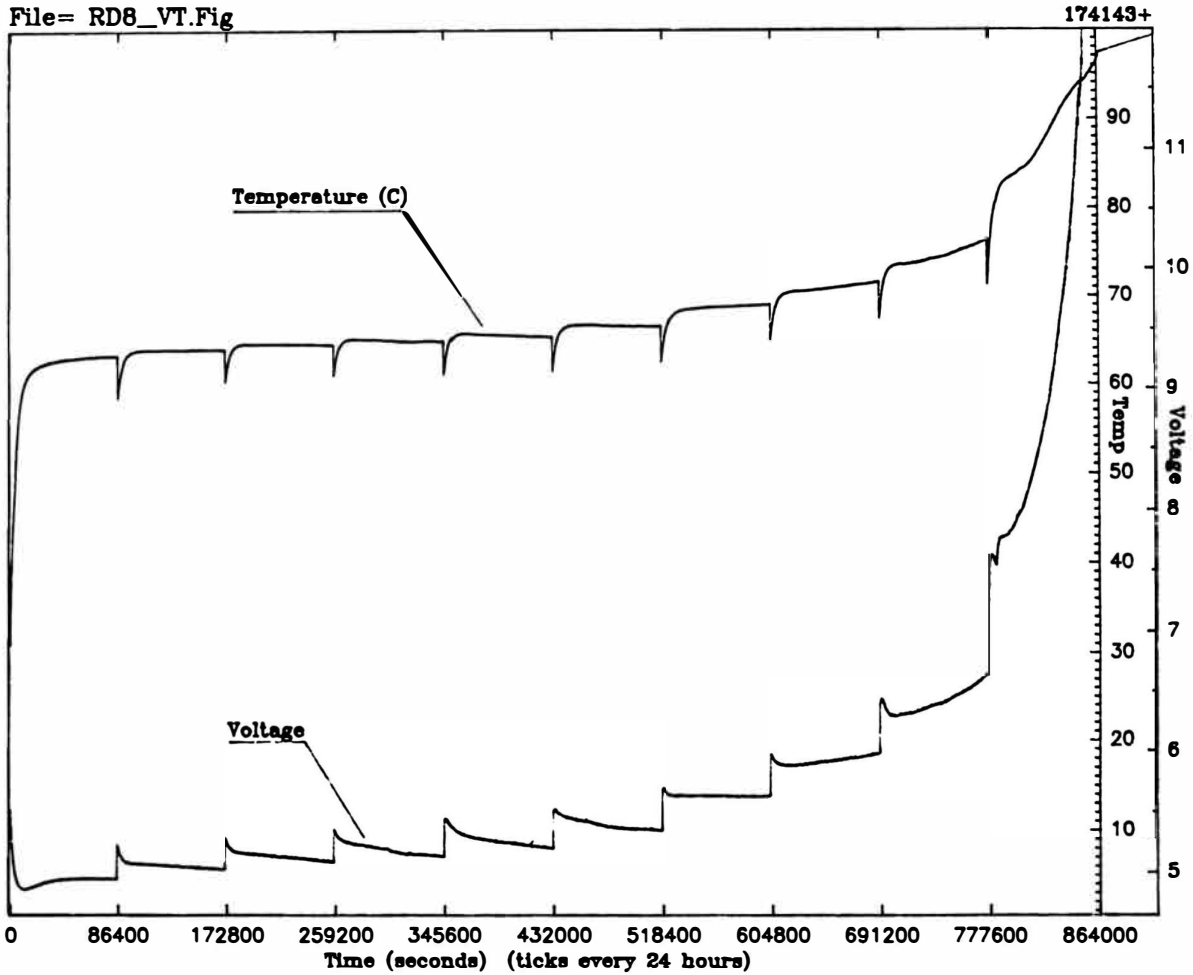

Figure 1. Plot of raw data for blankcell 8 experiment. Electrolyte is 0.1 F Li OD in D_2O. Cathode is Pt.

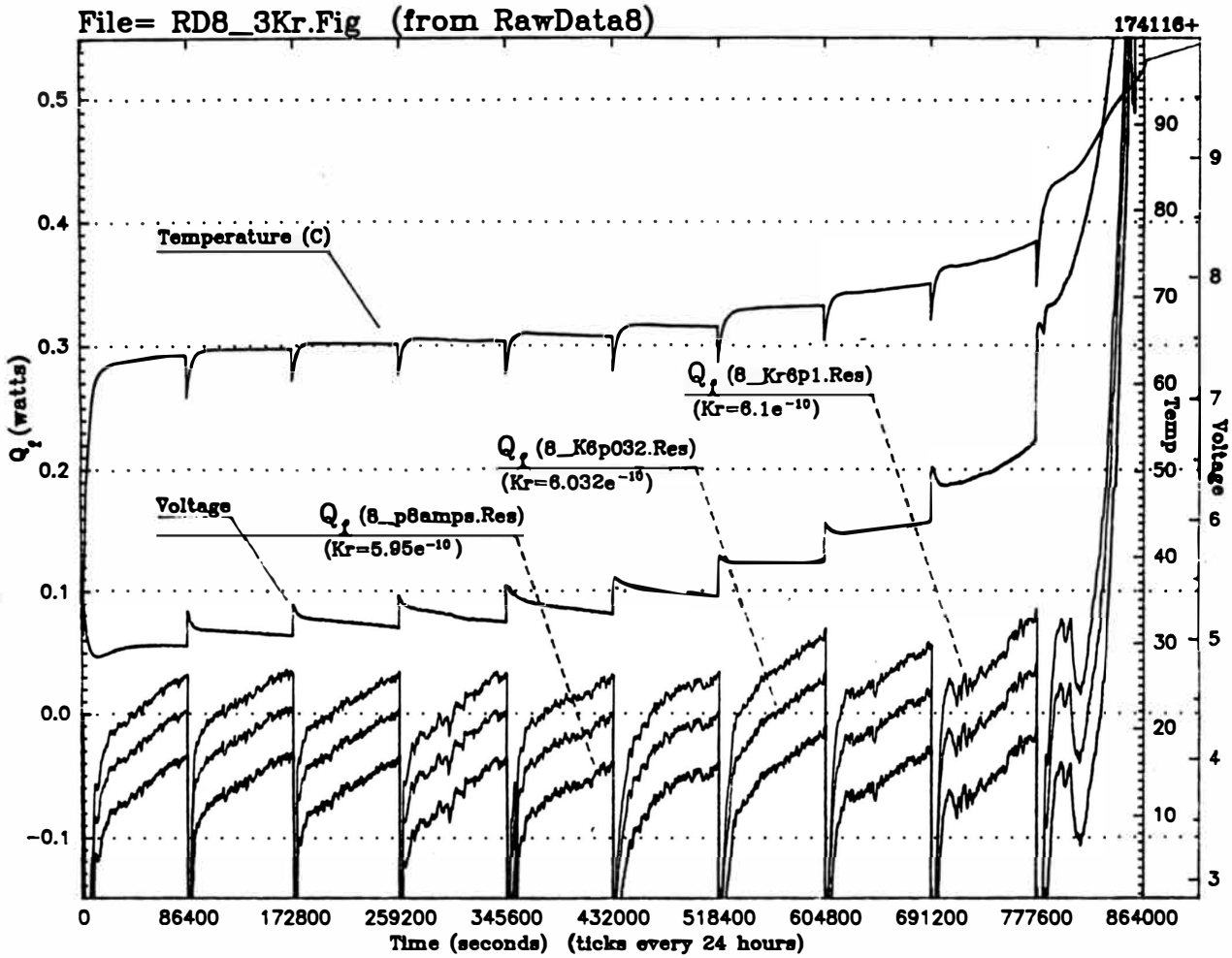

Figure 2. Cell 8 experiment. Kalman filter calculation of Q_f to show what K_r must be for this blankcell.

correct to use the pure radiative heat loss mode, at least for cells with a coefficient of, say, 6.1 10^{-10} or less. It should be noted that by using pure K_r and no K_c, Q_f is underestimated and not vice versa. By using both modes and two heat loss coefficients, the blank cell heat loss could be fit at the first and last days without changing the K_r value. The change probably occurs because at high temperatures the use of the power four terms overstates the heat loss a bit. However, the change in K_r is so small in the present case that the use of a pure radiative term is a good approximation. We will return to this point later. At this point let's see what K_r is required to fit cell 8 to about 90°C.

Because the cell is open and the contents change throughout the day, the actual K_r of the cell changes a little also. The strategy used here is to find the K_r that gives Q_f = 0 at the middle of the day. It will be seen from the graph that K_r = 6.1 10^{-10} accomplishes this quite well at the beginning of the run. At the end of the run, after the last filling, up to where the temperature approaches 90°C, K_r=6.032 10^{-10} does the job. This is a change of 1.1%, and within the precision we have come to expect in this analysis. The use of K_r=5.95 10^{-10} clearly gives results too low everywhere. We will present other analyses below and look into things in more detail, but we can see right now that the model fits what is happening to +/- 2% or so throughout the entire cell history up to 90°C or so (keeping in mind that the regions associated with the steep spikes downward don't count). All this is very important, for this cell covers the high temperature range where it was thought by some to be too difficult to model the cell properly and take data accurately. The low temperature region is indeed easier to model, especially if it is rather constant in temperature. This is true for two reasons. First the heat balance equation becomes very simple and, second, the K_r remains nearly constant with time. Another point needs to be made here. If a heatcell produces no heat, it is impossible to distinguish it from a blankcell. From the analysis of cell 8 we know what to expect in general from other cells of similar design. We also know some behavioral patterns even of heatcells. For one thing, the model works up to about 90 deg C if temperature and voltage don't change too fast.

Cell 3 will not be discussed in detail at this time. The two heat pulses of this cell were not steady for some reason. It does appear that

parts of the heat pulses were proper and assuming that these sections represent the 0.27 watts intended, the K_r value obtained by fitting these sections does indeed give a Q_f of zero, showing internal consistency.

ANALYSIS OF A HEATCELL

Now consider a heatcell set up in the same flask. The only change is that the cathode is now palladium and a little larger which increases the heat capacity a little. (But as we shall see this size is of little importance in the analysis). The raw data are plotted in figure 3 for this run. Note that there is an instrument problem that gives a spurious hump in temperature the last day. Evidently these points can be simply ignored, which we have done, including the short Kalman filter glitch evident in figure 4 where we include the filter output for K_r=6.1 10^{-10} and for 6.032 10^{-10}. The former is for the lower temperatures and the latter for the higher, as indicated by the analysis of cell 8. Of course the cell constant could have changed during runs, but there are no data to point to such a change, and the change might just as probably have given a larger K_r rather than the smaller K_r required here to give a zero Q_f, i.e., make it look like a blankcell. If the K_r remained constant from run to run we could already be certain that there was a modest amount of excess heat produced, increasing with time and temperature, the maximum being about 0.38 watts.

Now let us use a different analysis approach on these two runs in the same cell. Here we will use nonlinear curve fitting, also called nonlinear regression analysis. It is based on minimization of the mean-square error as explained in a handy book by S.M. Bozic pp 92 ff [1], see also refs [2] and [3]. To accomplish this the Marquardt-Levenberg algorithm is used. At first we will simply assume that K_r is a constant for a day, take the day's data points as a batch and find the best K_r that fits the day. We could just as well let K_r vary linearly or even quadratically through the day. The convergence of the iterative process works very well. It is just more cumbersome to discuss, and the single K_r per day is well within a 2% accuracy. Along with the computed values we will be giving data that indicate expected errors in those values and other statistical data.

In a typical day there is only a point or two that cannot be fit by the model. The model does not work for the few minutes it takes to add D_2O to refresh the cell. However uniform temperature should return

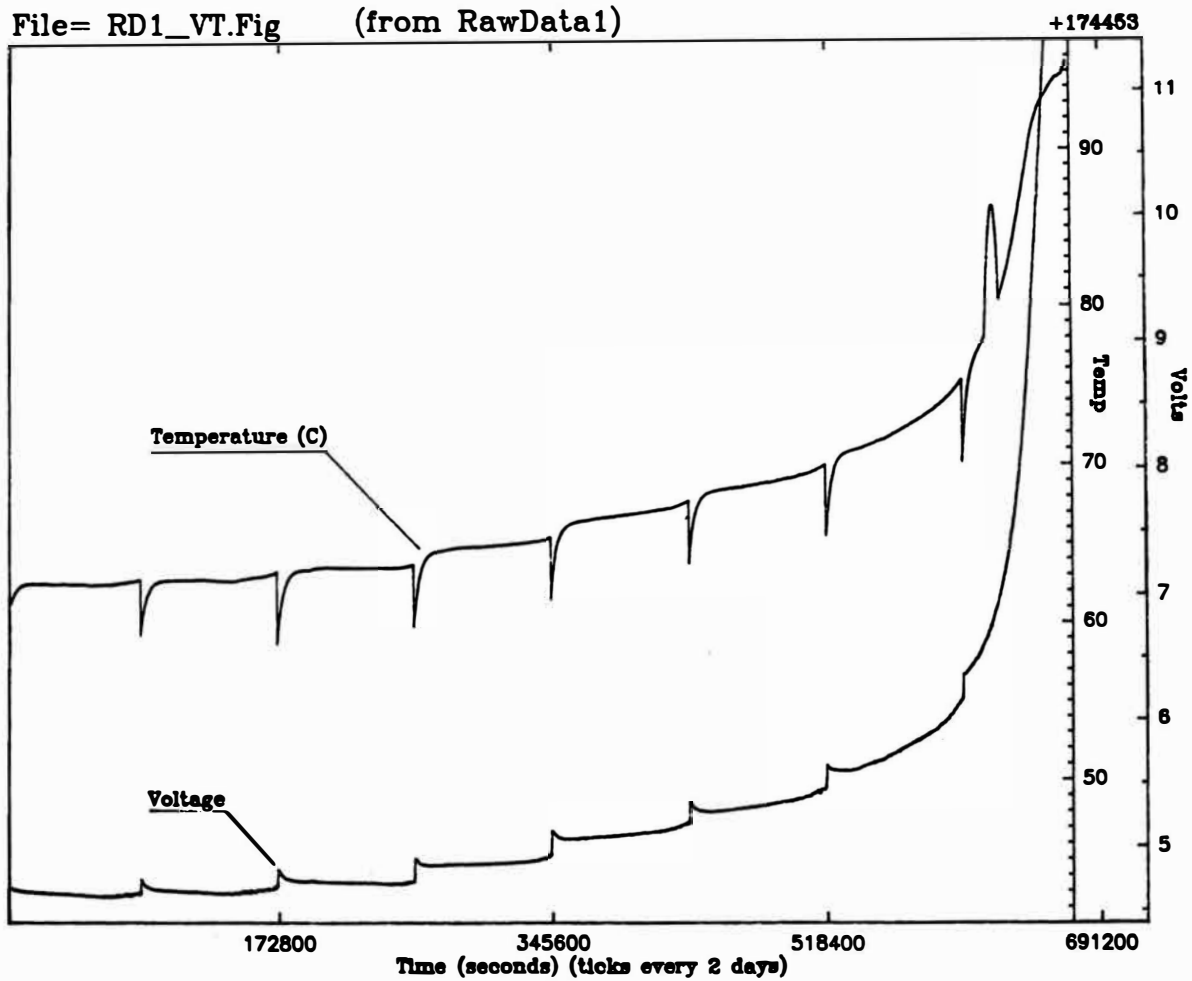

Figure 3. Plot of raw data for heatcell 1 experiment. Electrolyte is 0.1 F LiOD in D_2O. Cathode is Pd.

within the cell within a few minutes, and only a point or two need be lost (Data are taken every five minutes). Avoiding these points, the rest of the day's points are useable. In the case of the blankcell they are taken as a batch and used to fit the equation $Q_f=0$. There are differences in the P/F and Walling formulas. These are small at low temperatures. The P/F formulas use more detail which may become important at the high temperatures. We have used both. We have modified the Walling formula to use the full $K_r(T^4-T_b^4)$, and call it MWF.

Heatcell 1 is first analyzed by running a Kalman filter for Q_f over the entire run with K_r set at the values indicated by the blankcell run, i.e., $K_r=6.032\ 10^{-10}$ and $K_r=6.1\ 10^{-10}$. The results are presented in figure 4. A modest excess heat is shown. (Remember that even a small deviation from the blankcell is significant in the sense that it demands an explanation.) Perhaps the excess heat in the present case is just some chemical reaction with the electrode. Perhaps it is simply due to the K_r of the cell changing since the cell was used as cell 8. This isn't expected, but if K_r were smaller during the heatcell run, and the larger expected values were used in the calculation, erroneous excess heat would show. From this point of view it would be nice to know the history of the cell. We don't. Just to show what value of K_r would be required for $Q_f=0$, we have made the necessary Kalman filter calculation and show it in figure 5. Note that even at this low K_r of $5.63\ 10^{-10}$, there is still excess heat. This is a forced fit, but it shows how important it is to know the cell histories and relationships. Perhaps some mistake has been made in identifying cells, or possibly the cell constant has changed. At the moment we have no way of knowing for sure. We need a better calibration procedure, which we demonstrate below.

ANALYSIS USING HEAT PULSES

Actually P/F have designed at least some of their cells with a resistor placed in a tube near the bottom of the cell, in about the position taken by a small cathode. The idea is that at any time desired they can superimpose a known amount of extra power into the cell. They have done this by putting a fixed and known current through the constant resistance. Occasionally they measure the voltage also to confirm the wattage. This then gives a heat pulse that should give exactly the same results as a transient Q_f of the same shape. If the heat pulse is known, the response of the cell to Q_f is indicated. The heat pulse can be turned on at any time and temperature. These calibrations occur right in

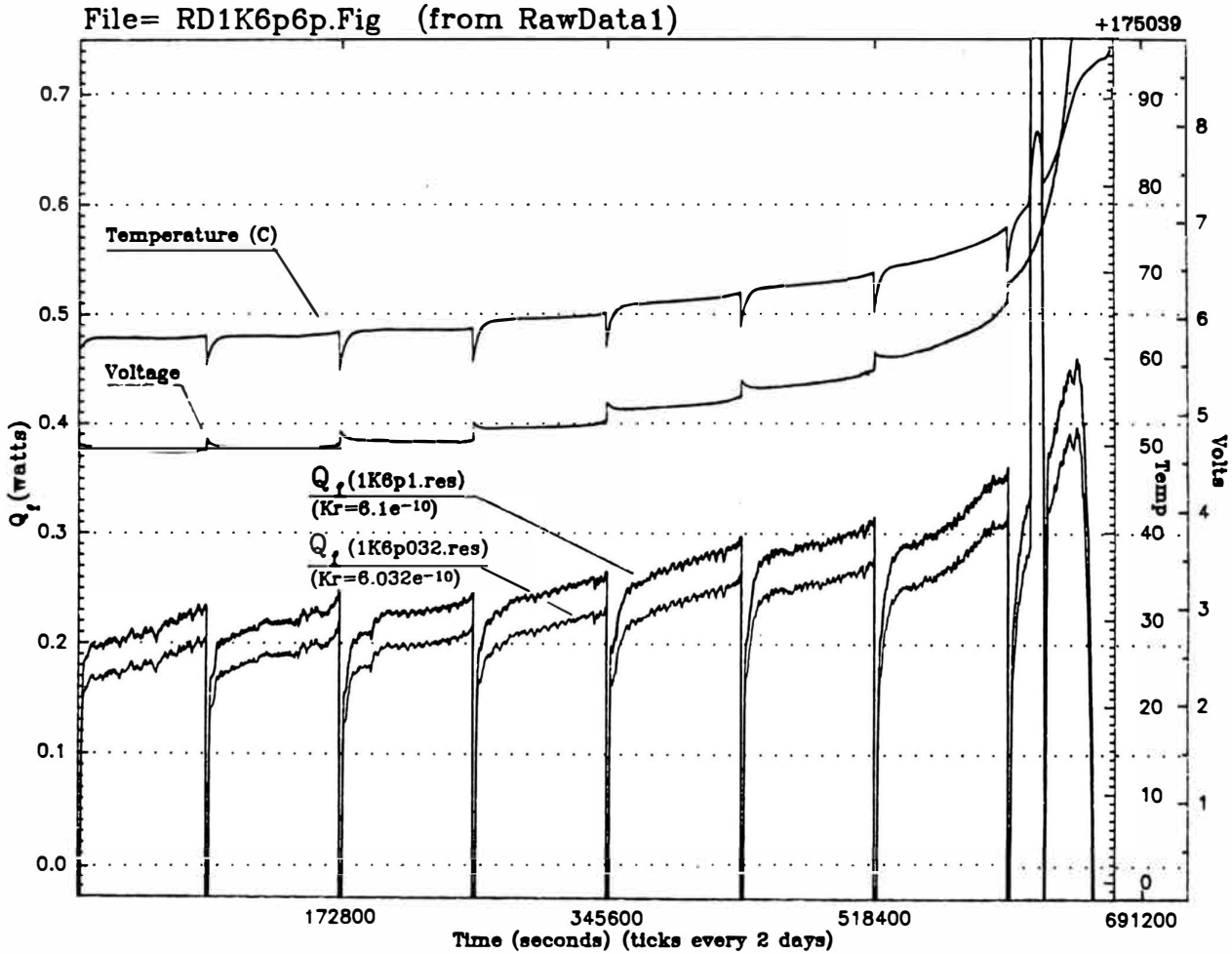

Figure 4. Cell 1 experiment. Kalman filter calculation of excess heat, Q_f, assuming heat transfer coefficients of cell 8, the same flask.

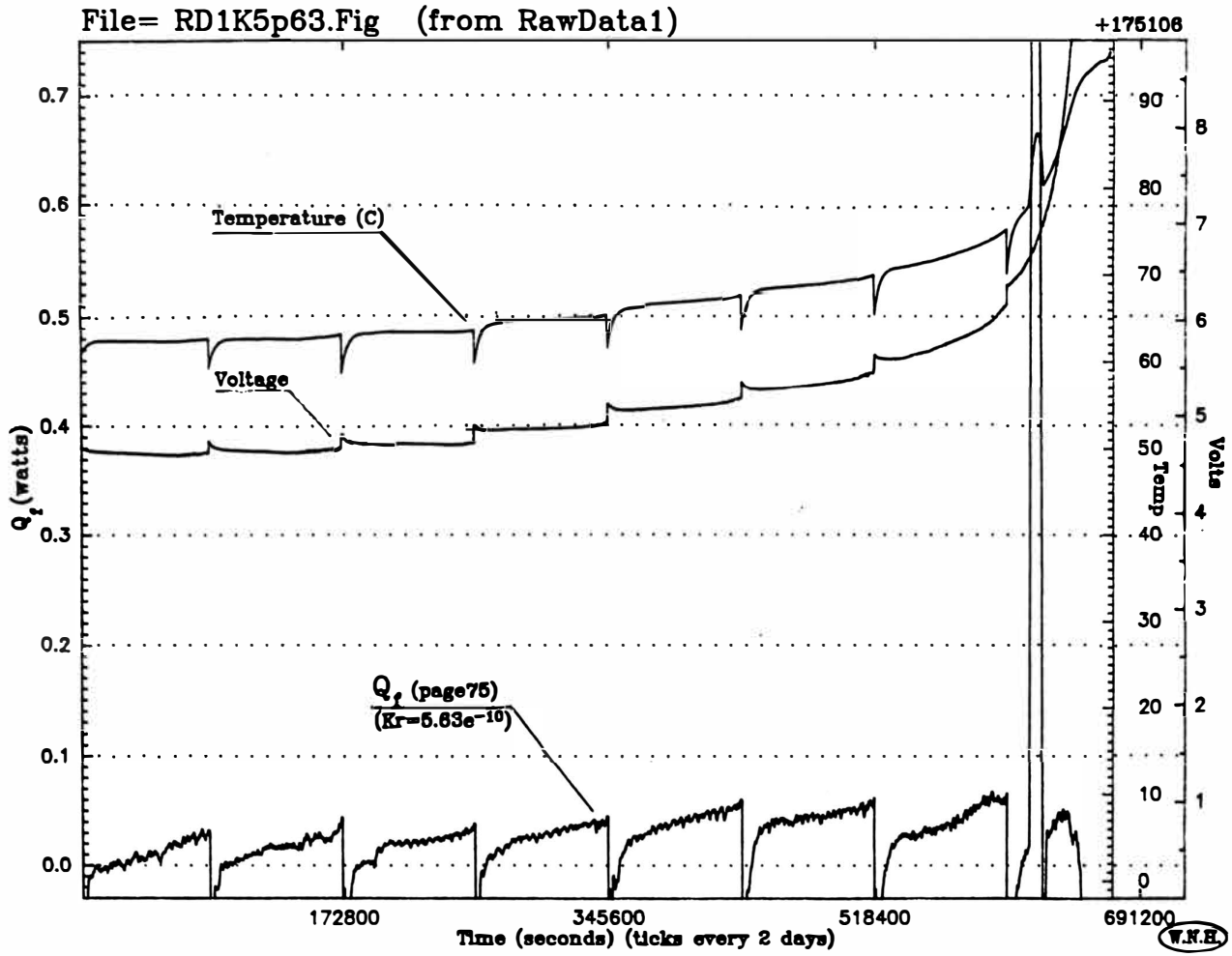

Figure 5. Cell 1 experiment, showing the K_r required for blankcell status and the resulting Kalman filter calculated Q_f.

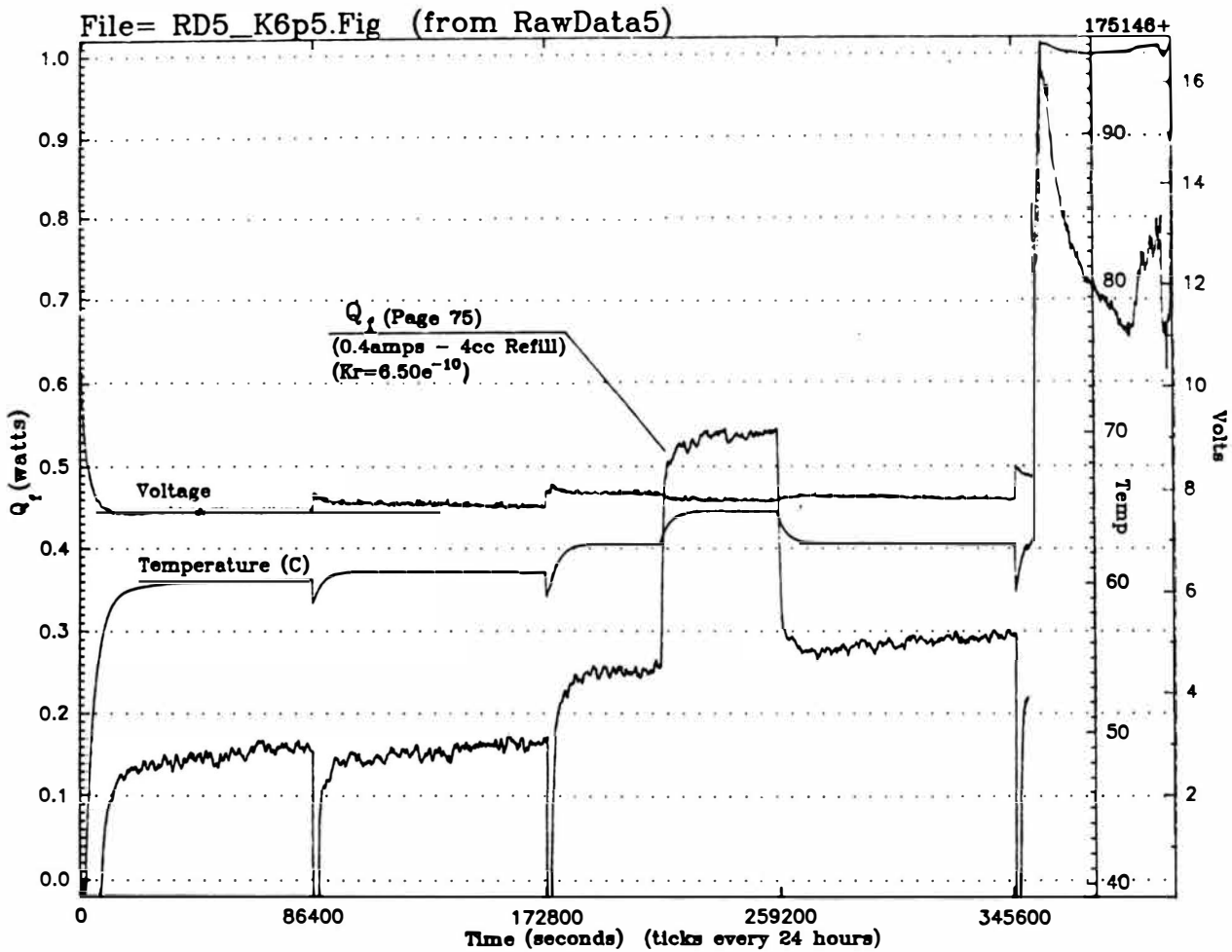

Figure 6. Raw data and Kalman filter output of cell 5 with heat pulse of 0.270 watts. The K_r used is required to make the heat pulse equal to 0.270 watts. Note the sudden increase in Q_f near 172800 seconds, not characteristic of a blankcell. Also note the very rapid temperature rise to boiling at the end.

the midst of the cell run at just the time the data are needed. In our opinion they are the answer to cell evaluation and they should be used extensively, on blankcells as well as heatcells.

Before we discuss how we use the heat pulses to analyze cell behavior we mention that they have been the subject of no small controversy. It seems to us that the source of this controversy is the fact that the cell voltage changes during the pulse due to the change in the conductivity of the electrolyte as the temperature changes. This in turn is probably due mainly to the increased mobility of the ions with temperature. There can be no argument if the data are handled by one of the regression methods we discuss below. The results of calculations using the pulses are unambiguous and very accurate. Of course we are thinking of numerical accuracy. The calculations cannot be accurate if the power of the pulse is not known accurately.

We have used the heat pulses in several effective ways. All are in perfect agreement with each other. The method of choice depends on what is wanted. One method is to simply run the Kalman filter for Q_f using a K_r that gives the known correct pulse height. This is easily estimated after viewing the results of a close guess. The height of the pulse can readily be determined by sight, a straight edge and a set of vernier calipers, after the Kalman results have been plotted in large profile. Notice that the Kalman filter treatment reduces the pulse to a step function. It is not necessary to measure the pulse height by hand, however. The full power of batch processing and statistical treatment of data are available in curve fitting. The heater pulse wattage, HP, is known as a function of time, as are other variables. We can solve the needed equation for HP = "..." and fit "..." to the known value of HP. In doing so we allow K_r and Q_f to seek their values, using a nonlinear fit algorithm (actually the algorithm can be a general linear fit, since "linear" refers only to the coefficients allowed to vary). The convergence of the iterations is fast and the answer is sure. In fact C_p can also be allowed to seek its own value, typically with little effect on K_r or Q_f if T isn't changing very fast. In fact at places where the temperature is changing rapidly (but still in equilibrium within the cell), Q_f, K_p and C_p can sometimes be found without a heat pulse present, but with less accuracy. Typically data are treated a day at a time in this curve fitting process. On occasion, however, we have treated multiple days in one session.

As an example of the nonlinear regression analysis consider heatcell 5. The raw data along with a Kalman filter calculation of Q_f are shown in figure 6. Note that K_r is chosen to give a heat pulse of 0.27 watts, the value of HP for this cell. (The value of HP is 0.27 watts for all of the pulses used in this set of cells.) When the data are fit to HP throughout the two day period, K_r=6.5 10^{-10} is obtained with statistics as given in table 2. It is seen that the fit is good and there is no doubt about the excess heat calculation from the data. This of course depends on the data being accurate. A point to mention here is that even if the K_r is obtained by letting the Q_f at the beginning of the run, day 1, be zero (the most conservative situation possible) and ignoring the heat pulse data, there is still excess heat as shown in figure 7.

Cell 5 is claimed by P/F to give a great deal of excess heat at the end. The data and reasoning are as follows. All but a small amount, say 5 cc, of the electrolyte was smoothly boiled away at the last after the current was raised to 0.8 amps, within a period of 42 minutes. The raw temperatures and voltage of this period and beyond are given in figure 8, as well as a marked off 45 min period. The higher current starts at the left of the 45 min period. The liquid was down to the position of the small electrode in the cell within 45 min. Let us perform a quick simple calculation to see what this implies. There was about 3.3 moles of D_2O boiled away in say 45 min. The heat of vaporization at 101.4°C is 496.5 cal/gm or 41550 joules/mole. Take this as the value to use here. This translates to ca. 114 kJ excess heat in 45 min (assuming 9 watt input), or 470% excess heat. The electrode has only 1/226 of a mole of Pd. This gives 267 eV/Pd atom for the excess energy. It also corresponds to about 1 kilowatt per cc of Pd electrode. It only takes about 5 eV per Pd atom to heat Pd to 4000°C and vaporize it. Cell 4 behaved almost exactly like cell 5 throughout a similar run, and the data show that it also boiled off in a similar fashion in the same time period, with the same results. The electrode was four times larger, so the effects per Pd atom are about four times less. This analysis depends on the accuracy of the data given. In the case of the boiloffs the data are somewhat subjective. One would think they could hardly be off by more than, say, 50%, however. If the data are anything like that reported, they are spectacular! Of course we can discount them completely. That is a separate issue. This analysis is conducted as though the data are

TABLE 2

Fitting of Cell 5 Data

Fit	Range	Value	% Random error Estimate	Comments
1	entire 2-day period with heat pulse	K_r=6.479 10^{-10}	1.0	C_{po} fixed at 434 modified
		Q_f=0.248	11.5	Walling formula (MWF)
2	entire 2-day period with heat pulse	K_r=6.571 10^{-10}	1.0	C_{po} also allowed to fit
		Q_f=0.288	10.2	MWF
		C_{po}= 472	17.7	

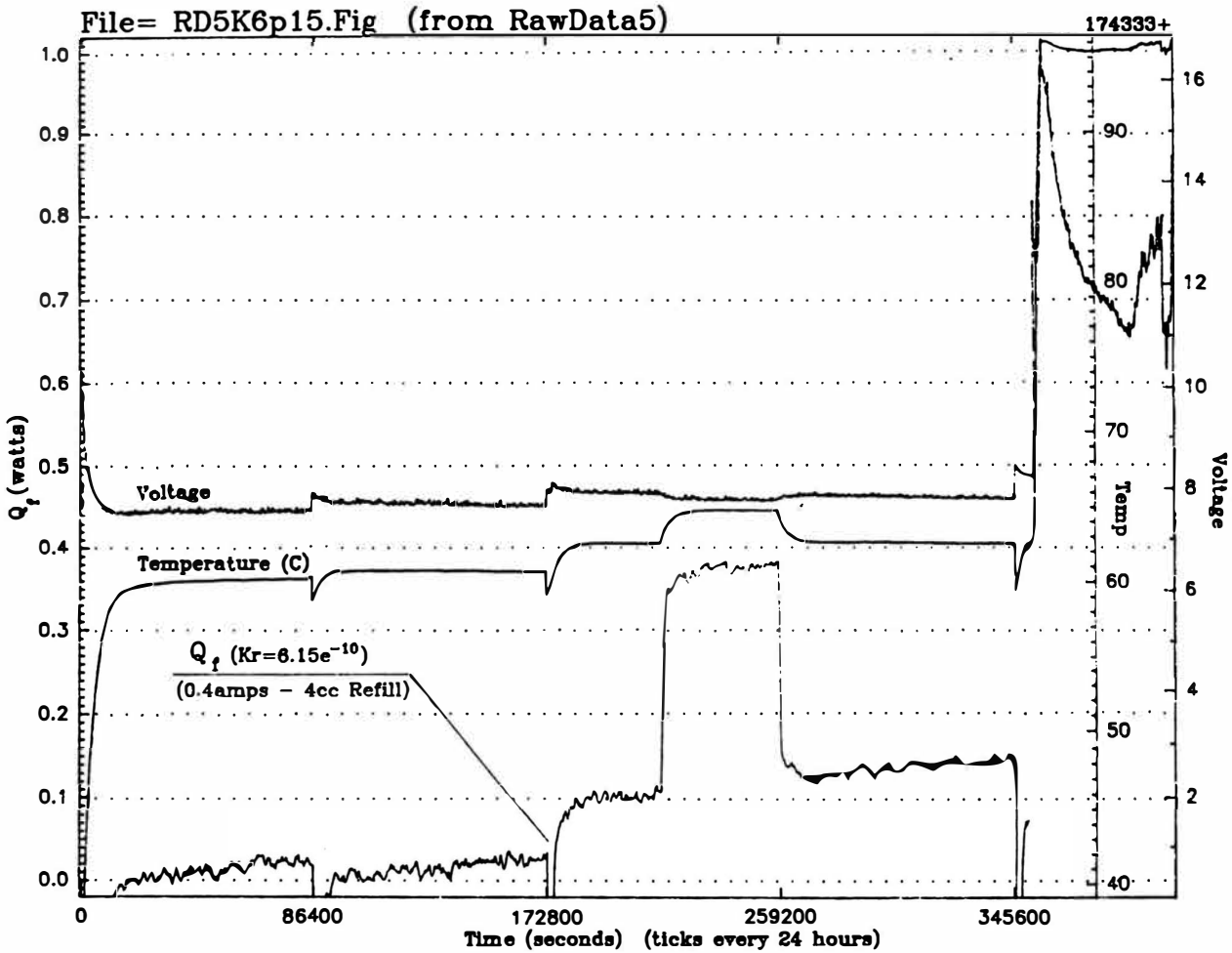

Figure 7. Kalman filter output for cell 5 experiment using a K_r that gives Q_f=0 at the beginning. This gives a lower bound on Q_f for this heatcell, ignoring the heat pulse,and shows that Q_f is still significant at the end of the 0.4 amps period.

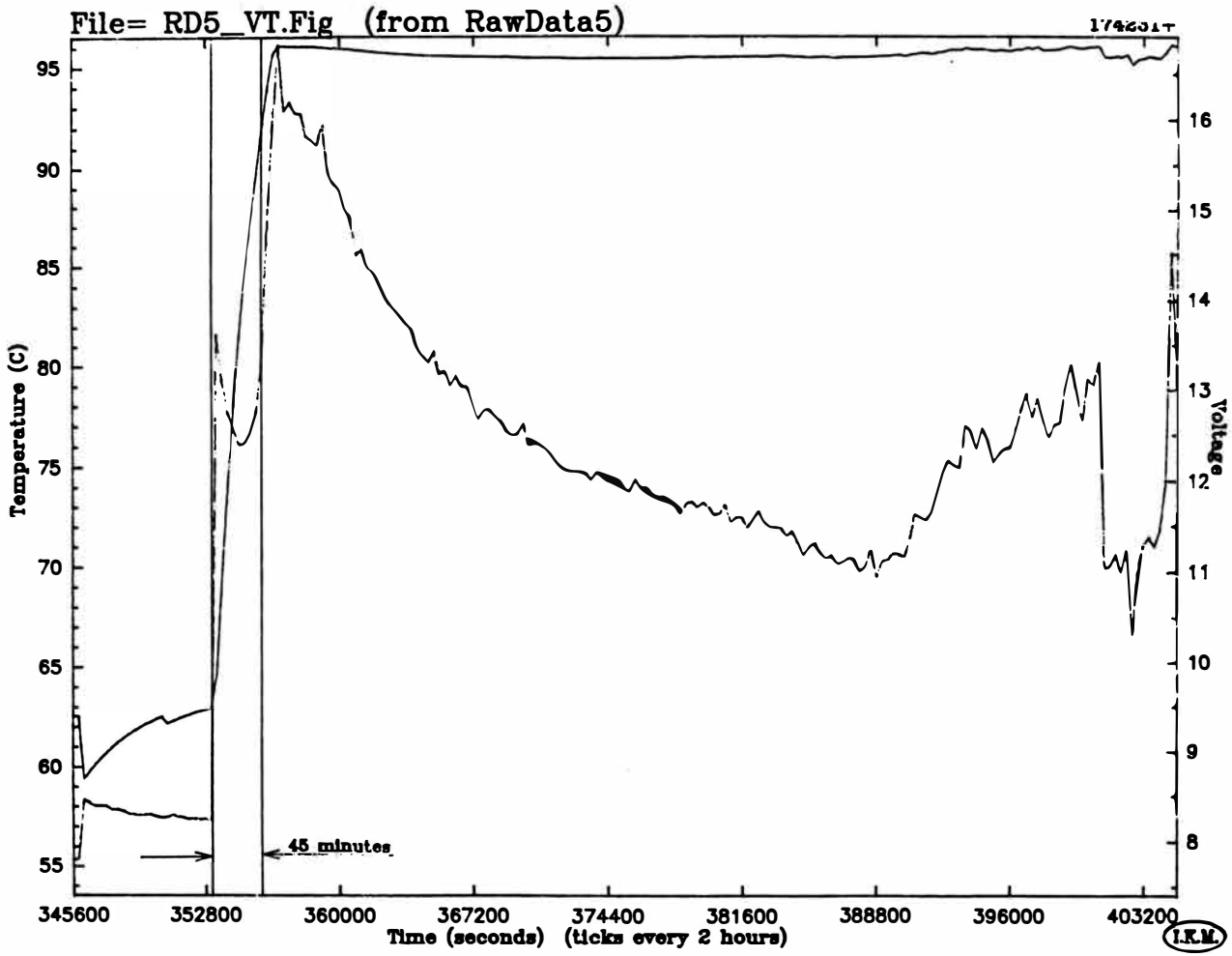

Figure 8. An expanded view of events at the end of the cell 5 run. About 3.3 moles of D_2O were vaporized in about 45 minutes.

reasonably reliable. These last data on the spectacular heat production at the last of the run were reproduced on a second cell, for example, which should decrease the chance for misunderstanding or outright mistake. The idea that the fluid was expelled like a geyser was considered, but smooth boiling can be expected from a cell with a constant source of nucleated bubbles at the electrode surface. In addition it was reported by Pons that the boil off was only liquid free vapor.

Let's look at cell 5 from yet another point of view. The behavior of the cell is ideal in the 0.4 amps region. The model is expected to fit very well indeed. Suppose we don't even use the heat pulse for calibration. We simply use the fact that Q_f isn't expected to be negative in order to get a lower bound on later Q_f. Set $Q_f = 0$ at the beginning of the run. We now have a very good lower bound. Consider the plot of Q_f again in figure 7. During days 3 and 4, Q_f cannot be less than 0.1 watts or so--say 0.11 watts. Just for the two days this corresponds to 45 eV per Pd atom. This is already an order of magnitude larger than the energy to vaporize the entire Pd electrode. We have thought of no other self consistent explanation than that the excess heat is real and very significant. Also notice that the smallest K_r that can be given this cell is $6.15\ 10^{-10}$.

In figure 9 are shown results for cell 4, almost identical to those for cell 5. It will be noticed that here the K_r dictated by the heat pulse is $6.43\ 10^{-10}$, while the value that puts $Q_f = 0$ at the left end is $5.95\ 10^{-10}$. Statements about excess heat are essentially the same as for cell 5 except that in cell 4 there is four times the Pd. Also note the rapid boiloff just as in cell 5, with similar implications with regard to excess heat.

ANALYSIS OF HEATCELL 2

This cell was run at 0.2 amps for a short while, and then increased to 0.4 amps. It took about three days at 0.4 amps to reach 95°C. The first two day period at 0.4 amps contained a heat pulse of the usual 0.27 watts. Solving the model equation for heat pulse power, HP, and then fitting the equation to the known HP as a function of time gives the excess heat, Q_f, and the cell heat constant K_r. Once again, assuming the data are correct as given, there is little room for doubt as to the required values of K_r and Q_f. The statistics for the data are given in table 3. This fitting process is done by the batch method, where the

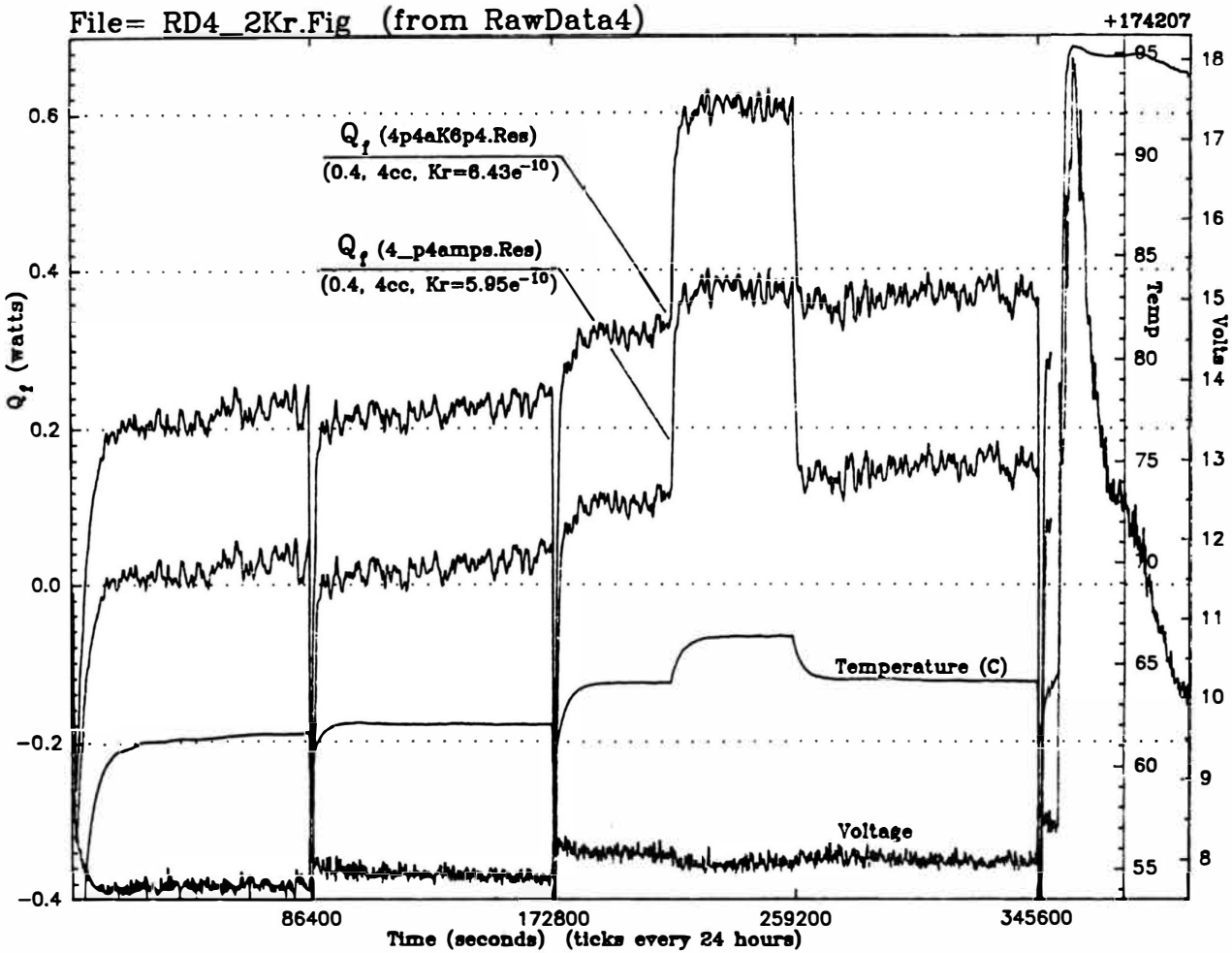

Figure 9. Heatcell 4 run.These results are nearly a duplicate of those from cell 5 except that the data are noisier because of noisier voltage. The upper Kalman filter curve for Q_f is the one demanded by the heat pulse data, 0.270 watts. The lower one is a lower bound, demanded by the fact that Q_f cannot be negative.Note that these data confirm the data of cell 5, including the boil off at the end.

TABLE 3

Fitting Cell 2 Data

Fit	Range	Value	% Random Error Estimated	Comments
1.	pts 27-200 from first	K_r=6.52 10^{-10}	2.7	P/F formula
	of 0.4 amps region	Q_r=0.56	19.7	fit M at beginning
	to middle of pulse	M=5.763	2.3	of region
2.	pts 27-350 from first	K_r=6.47 10^{-10}	1.9	P/F formula over heat
	of 0.4 amps reg., past	Q_r=0.536	15.	pulse fit M at beginning
	pulse	M=5.78 moles	2.0	of region
3.	pts 27-350 over pulse	K_r=6.535 10^{-10}	0.65	Modified Walling formula
		Q_f=0.547	4.8	(MWP) M=5.78, i.c.
				C_{po}=434
4.	pts 574-836 or to	K_r=6.512 10^{-10}	2.8	$Q_f=Q_{fo}(1+L)\ t$
	T=93°C	Q_{fo}=537	22.	M=5.78, i.c.
	No Pulse	L=7.37 10^{-6}	6.7	C_{po}=434
				MWP
5.	pts 574-792 up to 90°	K_r=6.446 10^{-10}	2.8	$Q_r=Q_{fo}+at+bt^2$
		Q_{fo}=0.526	23.	C_{po}=434
	No pulse	a=4.467 10^{-7}	151.	MWP
		b=5.379 10^{-11}	12.	
6.	pts 574-836 or to	K_r=6.758 10^{-10}	3.0	$Q_f=Q_{fo}+at+bt^2$
	T=93°C	Q_{fo}=0.712	20.	C_{po}=434
		a=3.85 10^{-6}	17.	MWP
	No pulse	b=1.25 10^{-11}	44.	
7.	pts 574-859	K_r=6.711 10^{-10}	3.8	$Q_f=Q_{fo}+at+bt^2$
	entire region	Q_{fo}=0.658	26.	C_{po}=434
		a=5.918 10^{-6}	12.	MWP
	No pulse	b=-2.15 10^{-11}	27.	

batch of points is taken over a time period where Q_f and K_r change very little. The average values of Q_f and K_r are found. An advantage of the Kalman filter calculation of Q_f is that it gives the dynamic Q_f as a function of time. It does, however, have a several point time constant, say six or eight 300 sec periods. (Points are taken every 300 sec.) Figure 10 shows the raw data of cell 2 plus a Kalman filter calculation of Q_f assuming $K_r = 6.57\ 10^{-10}$, which is required to fit the heat pulse to 0.270 watts. Also included is the calculation of Q_f using the P/F formulas, using the same K_r. This is also about the same K_r as found by the regression approach (see table 3) in the heat pulse region.

Using the data of day 3 it is very interesting that regression analysis can be used to obtain K_r and Q_f without a heat pulse. This has been done in a number of ways. First of all, using points 27-350 of the pulse containing period and allowing the "moles equivalent", M, of the cell to be fit, we obtain a value of 5.78 moles. This is close to the value we obtain for these cells time and again. Now using this M we fit the data of the next period after D_2O addition. Here we fit for both Q_f and a K_r that is allowed to very with the first and second powers of time, i.e., $K_r = K_{ro} + a\ t + b\ t^2$, where t is the time after the beginning of this period. As shown in table 3, the agreement with K_r determined by the heat pulse is very good. In fact the values determined by taking data only to 90 deg C are in agreement with those taken to 93 deg, and even those taken to the end of this period, which is close to boiling. All this tends to verify the validity of fitting at these high temperatures in the present case. This cell may be especially well behaved. Notice that the voltage is smooth throughout this period. Most of all, the finding of a solution for K_r in this region which is the same as that given by the heat pulse is strong evidence for internal consistency and the validity of the heat pulse value given. With the heat pulse value correct as given, there must be excess heat as given. Note that the use of data at the highest temperatures isn't necessary to show the excess heat, but it certainly strengthens the evidence and helps rule out error in the heat pulse data. The same thing can be said of the data below 90 deg in the third 24 hr period.

Taking $Kr = 6.5\ 10^{-10}$ and using data of day 3 up to 90°C, and at this value of Q_f to the end of the day, we can say the following about the results: Q_f(max) is about 1.2 watts or about 20% of the radiative output at 90°C. Near the beginning of the 0.4 amps run Q_f is 0.54 watts

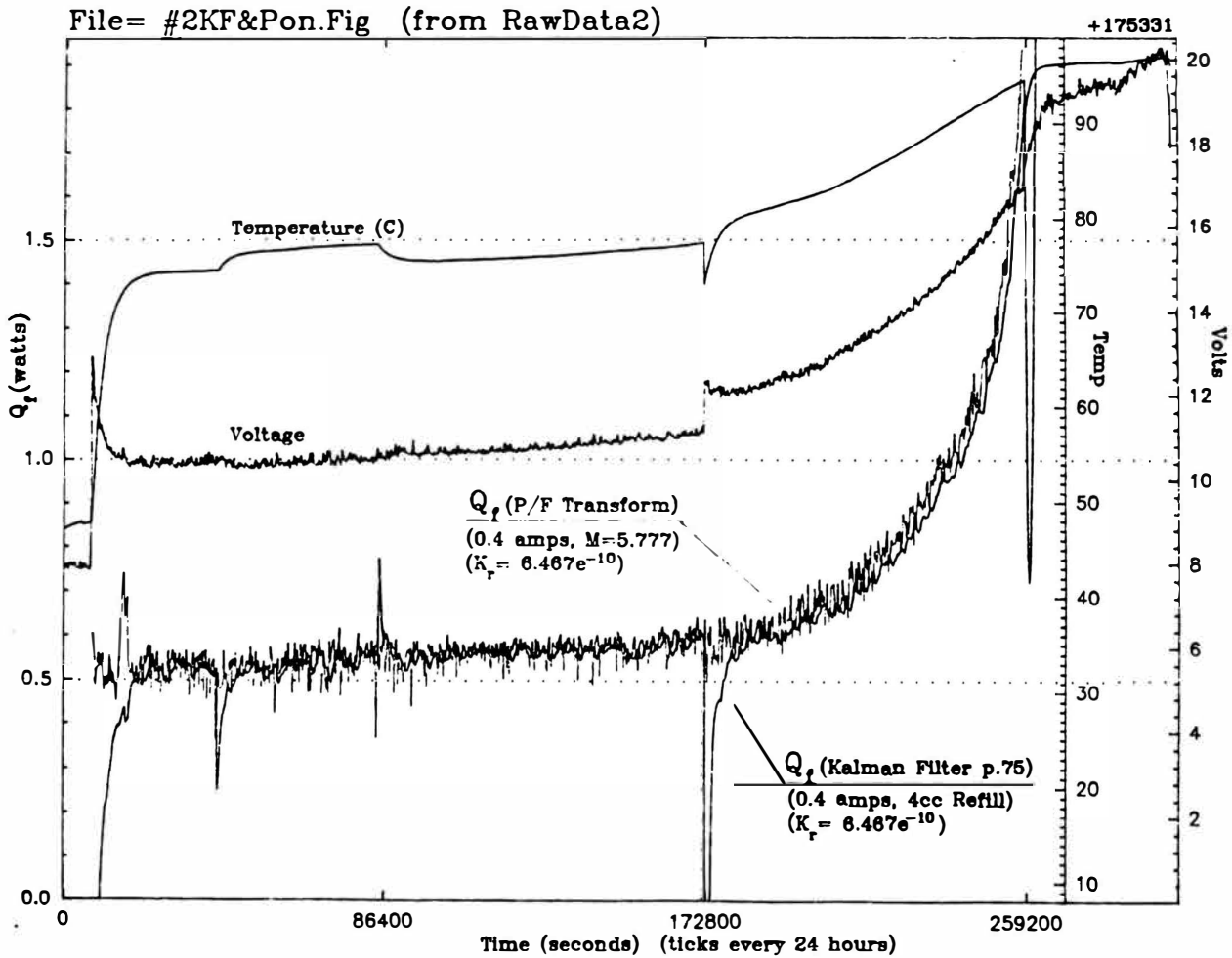

Figure 10. Raw data and calculated Q_f for heatcell 2. Superimposed on the Kalman filter output for Q_f is the Q_f calculated by the full P/F equation for the model. Note how the Kalman calculation is a real-time low pass filter, and cannot follow rapid changes in temperature.

TABLE 4

K_r Values Required for Q_r to Be Zero

Cell 2

Point	Time	Temp	K_r (to force $Q_f = 0$)
576	173387	74.763°C	$5.69\ 10^{-10}$
600	180587	79.760	$5.618\ 10^{-10}$
650	195587	81.689	$5.609\ 10^{-10}$
700	210587	83.844	$5.579\ 10^{-10}$
750	225587	87.014	$5.497\ 10^{-10}$
792	238187	90.026	$5.322\ 10^{-10}$
(792,793,794)	average		$5.322\ 10^{-10}$
(790,791,792)	average		$5.352\ 10^{-10}$
800	240587	90.578	$5.352\ 10^{-10}$
859	258287	94.434	$4.498\ 10^{-10}$
(2-23)P/F formula		47.109 to 47.704	$5.725\ 10^{-10}$
(2-23) M W formula		47.109 to 47.704	$5.746\ 10^{-10}$

or about 14% of the radiative output. The integrated excess heat is about 170 megajoules per mole of palladium or about 1700 eV per Pd atom. This is about 400 times the vaporization energy of Pd for the electrode of cell 2!

Now suppose for some reason we don't want to accept the given heat pulse value for cell 2, i.e., the 0.27 watts value. What can we say about the results without this datum? For one thing we can expect the excess heat to remain above zero. Suppose we again take an approach that gives us a lower bound on Q_f throughout the run by letting Q_f be zero in the 0.2 amps region at the begining. A Kalman filter calculation is made throughout the run, and K_r is adjusted to set $Q_f = 0$ in the 0.2 amps region. This requires a K_r of $5.95\ 10^{-10}$. Throughout the 0.4 amps range Q_f still averages about 0.25 watts for three days. The shape of things just isn't that of a blankcell. In table 4 are shown the values of K_r required at various points to make Q_f equal to zero. Not only is a great range required, atypical of a blankcell, but the shape of Q_f with fixed K_r is unreasonable for a blankcell. Therefore cell 2 appears to be producing large amounts of excess heat, with the amount increasing with temperature.

REFERENCES

1. S.M. Bozic, "Digital and Kalman Filtering", John Wiley and Sons, New York, 1980.
2. P.R. Bevington, "Data Reduction and Error Analysis for the Physical Sciences", McGraw-Hill Book Co., New York, 1969.
3. W.H. Press, B.P. Flannery, S.A. Teukolsky, and W.T. Vetterling, "Numerical Recipes (Fortran Version)", Cambridge University Press, Cambridge, 1989.

ANALYSIS OF PONS/FLEISCHMANN CALORIMETRIC DATA

Part Two

In part two we continue to discuss members of the set of silvered cells which we have analyzed. Most of the space will be allotted to the cell 6 experiment because of its great significance in the whole study. We will also include a short discussion of cell 7. Both are heatcells with 0.1 F LiOD in D_2O as electrolyte and Pd electrodes.

ANALYSIS OF HEATCELL 7

There is no blank for this run, and there are no heat pulses applied during the run. Also we have found no good places during the run to solve for K_r, Q_f, and C_p all together. Figure 1 shows what we get for Q_f using a Kalman filter with K_r taken as a conservative $5.95\ 10^{-10}$. (That is the K_r for cell 3, a blankcell, the lowest we have found in this set of cells.) A modest excess heat is indicated, but we have found no compelling proof of it.

ANALYSIS OF HEATCELL 6

In figure 2 are shown the raw data for cell 6. Notice the two current ranges. In the 0.2 amps period the temperature is low and unusually steady. The voltage is noisy (probably because of bubbling) but very useable. In the 0.4 amps range the temperature rises smoothly to boiling. A unique feature of this run is the presence of four heat pulses. Once again the power of the pulses is 0.27 watts (actually 0.272 watts in the present case). There is even a pulse of the same wattage in the high temperature region. This gives us a chance to compare output pulse heights in the two temperature regions, examine internal consistency, and further test the validity of the model.

In figure 3 is shown the Kalman filter output of Q_f as a function of time. Here a value of $8.0\ 10^{-10}$ is used for K_r. It is clearly the value demanded by the heat pulses. This can be seen by inversion of data through the region of any heat pulse or by insisting that the Kalman filter output be a square pulse of height 0.272 watts. While this large heat coefficient is easily understood as caused by a little gas spoiling the vacuum of the cell dewar vessel, the fact that it happens in the largest heat producing cell is puzzling. We will speak more of this later. It should be understood here that there is no mistake concerning what Pons gives as the heat pulse wattage. In yet third discussion of this subject, on May 21, 1991 Pons told me personally, and another who

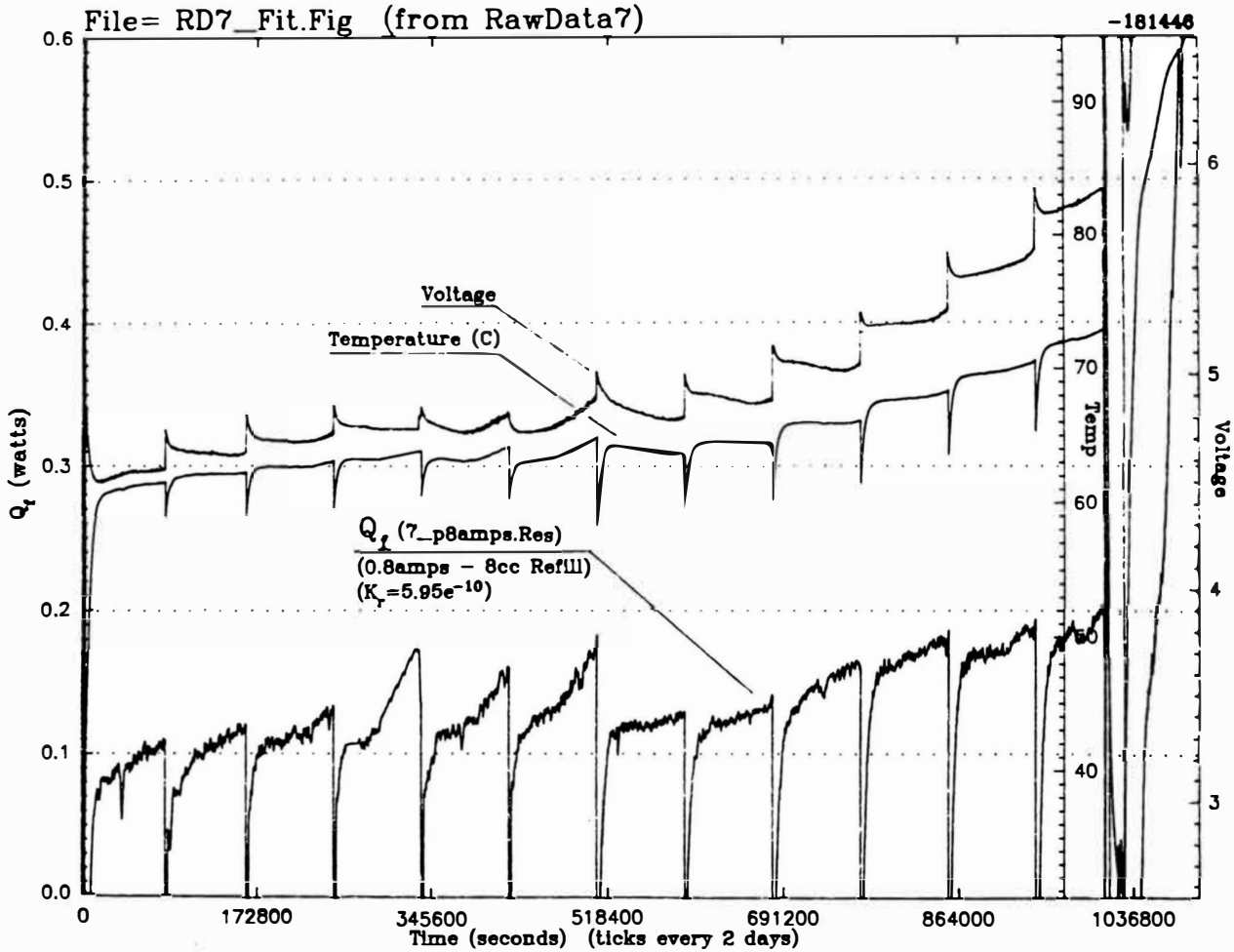

Figure 1 of Part Two. Raw data and Kalman filter calculation of Q_f for Cell 7.

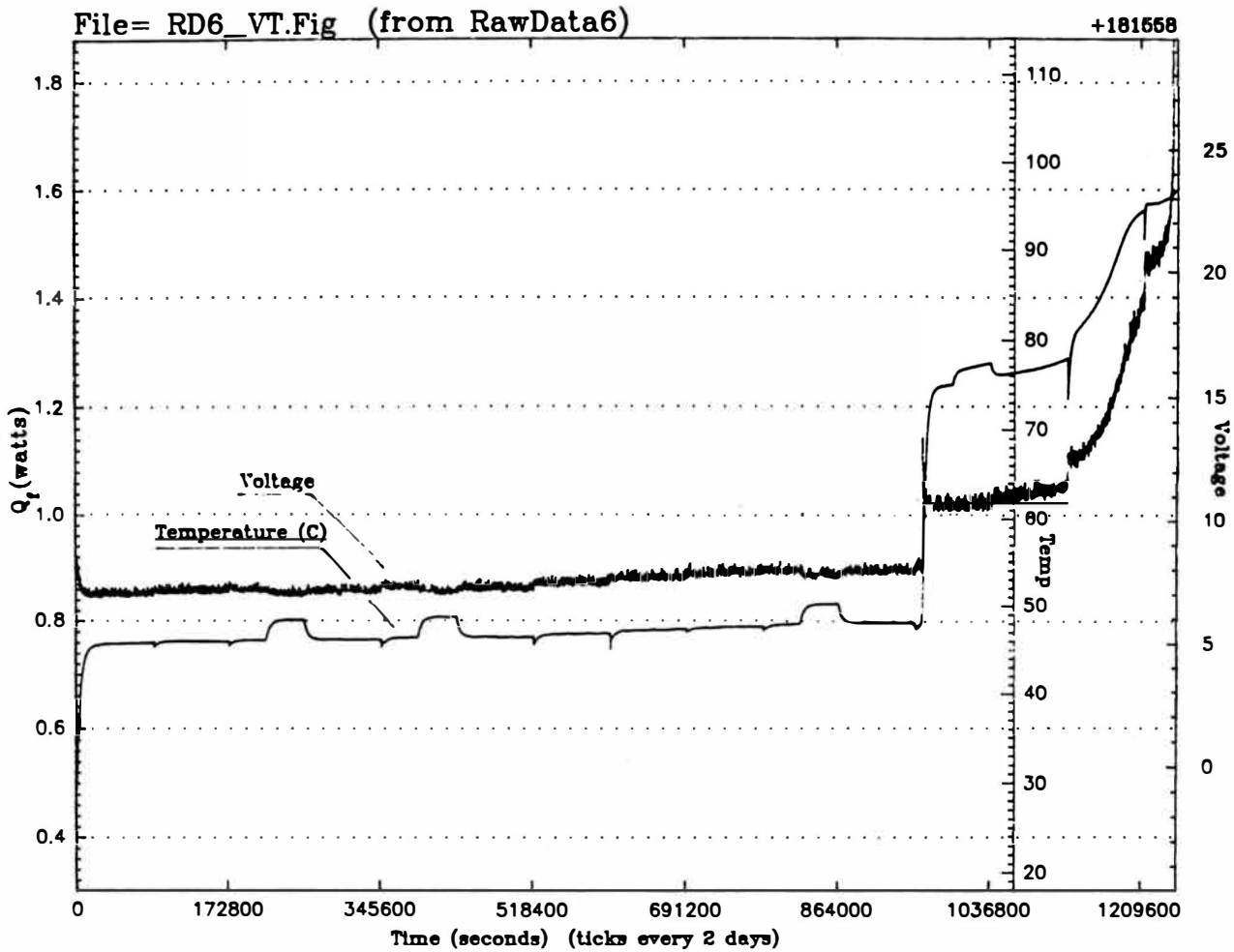

Figure 2 of Part Two. Raw data of Cell 6 experiment. Current is 0.2 amps for 11 days, then switched to 0.4 amps

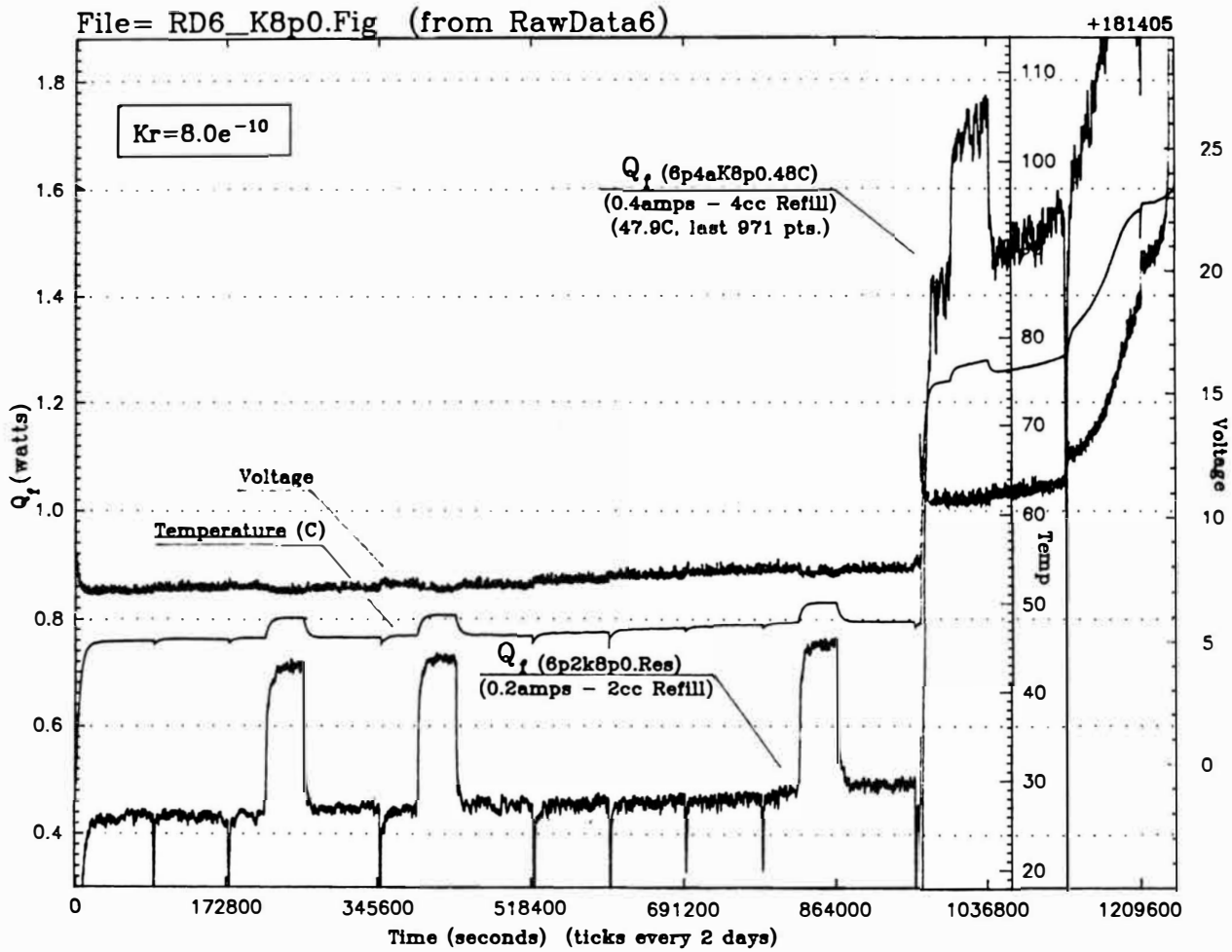

Figure 3 of Part Two. The Kalman filter output of Cell 6 using a K_r necessary to make the pulse height equal to 0.27 watts

had helped run the experiments verified, that they had always used 0.27 watts in the heat pulses of this set, a constant current of 50 milliamps through a precision, temperature insensitive resistor string. This gave a measured voltage drop of 5.44 volts in the case of cell 6, or 0.272 watts.

In figure 4 is shown the total excess heat input, Q_f + HP, calculated in three different ways, by Kalman filter, by P/F model formula, and by MWF. They all agree well except in the highest temperature region, i.e. in the region beyond the last heat pulse. Here the MWF calculation deviates. This is to be expected because the P/F formulation was used in the Kalman filter and the MWF approach doesn't account for vapor evolution in such a detailed way. It should be noted that even though the non-filtered calculations look very noisy, especially in the high temperature region, all of the information is there, and a statistical analysis of the data yields well defined values of Q_f and of the heat pulses, HP.

It would be a nice confirmation of the large K_r dictated by the heat pulses if an analysis of data in a no heat pulse period gave a similar result. The most likely place to look is day 13 outside the heat pulse period and day 14. We have done this, and do indeed get by regression analysis a value of K_r similar to that obtained by using the heat pulses. We have gotten similar results using the P/F formulas and the MWF approach. By allowing Q_f to vary quadratically in time, and solving for K_r and Q_f using points from T < 90 deg C, we get K_r = 7.74 10^{-10} and Q_f at 1.126 mega seconds of 1.46 watts, going up quadratically from there. We also get a solution using the MWF formula. Here K_r = 7.810^{-10} and Q_f = 1.49 watts. Other periods might also be present in the data which give solutions. We have not exhausted the possibilities.

If this analysis holds, and we see no way around it at the present time, the excess power of cell 6 is impressive indeed. The excess power is about 1.5 watts for the first two days of the 0.4 amps region. The electrode is small, 1mm dia by 1.25 cm long. Counting the 0.4 amps period and the 0.2 amps period, there is about 6000 eV per Pd atom excess energy, or over a thousand times the energy required to vaporize the electrode. Putting it this way it is easy to see that we are not dealing with known chemistry or metallurgy. At issue is a profound energy source. It is of utmost importance that these results be

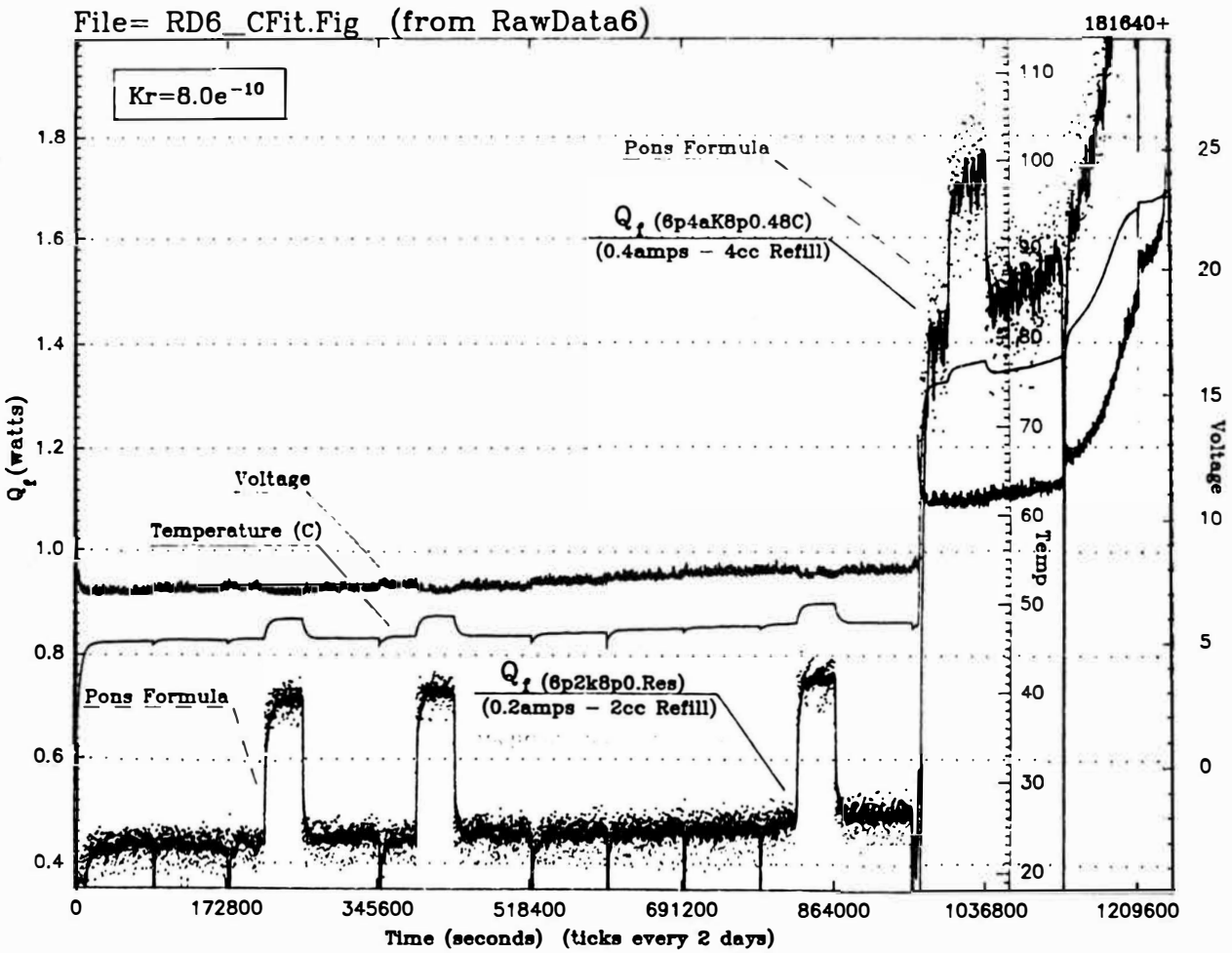

Figure 4 of Part Two. Raw data and calculated data for Cell 6.

reproduced.

SPECIAL POINTS

In this section we will discuss a number of special points that have come up during the analysis. This analysis has been far from exhaustive even though we have spent some months on it. We have gone further than reported here in a number of ways, but some things have not yet been formalized in report form. For example, we have redone much of the regression analysis using both a radiative heat transfer coefficient, K_r, and a conductive coefficient, K_c, in parallel. We now believe this is the correct way to do it. However, the use of K_c tends to increase Q_f, so the use of K_r alone was a conservative approach.

The use of heat pulses as a calibration of cells easily can be shown to be completely valid as far as the mathematics is concerned. Let us discuss the physics. The heaters are placed inside the cell in a position approximating that of an electrode. The response of the cell to heat from the resistors would be the same as the response to Q_f generated in the electrode. The heat pulse can be applied any time. When the analysis is carried out "exactly" as we have done, the pulse can be of any time duration, so long as good numerical derivatives are possible. In the data we have addressed the pulse was maintained at a constant power long enough to reach a new steady state, presumably to facilitate analysis. We encourage the frequent use of heat pulses in the future in this type of work. For example, if blankcells had frequent and carefully placed heat pulses, not only could the K_r be determined, but the K_r, K_c, and C_p of the cell could be determined, and at various temperatures. Also the degree to which the cell analysis is valid could be checked in detail. For example, if the heat pulses get reproduced correctly by the analysis at 93 deg C then the analysis is valid at this temperature. After all, the end purpose of the analysis is to determine unknown heat production, Q_f.

On the matter of heat transfer out of the cell, we believe that it should be represented by $K_r(T^4-T_b^4) + Kc(T-T_b)$, where K_r and K_c are the radiative and conductive heat transfer constants, and T and T_b are Kelvin temperatures of cell and bath. These act in parallel. The K_r can be expected to remain constant because it depends mainly on geometry. It can be approximated by blackbody theory, but glass surfaces are not blackbodies because of the 5% or so specular reflection and because they are semi-transparent in the near infrared. Water and heavy water are

also semi-transparent in the near infrared, but D_2O has a different spectrum than H_2O in the near infrared and in the mid infrared. The main radiation flux involved is in these spectral regions, and the wavelength in the infrared at which the electrolyte becomes opaque is shifted a great deal by the mass of the deuteron being twice that of the proton. Therefore, the emissivity of a cell probably varies with the electrolyte. In any case, the K_r is surely less than that calculated by blackbody theory. It should be constant, however, from run to run and even from cell to cell. The conductive part, however, easily changes by a little outgassing into the vacuum jacket. K_c can be expected to vary from cell to cell and perhaps even with temperature and time. One technique, then, is to fix K_r at some reasonable value, say, $5.0\ 10^{-10}$ or $5.5\ 10^{-10}$ and fit K_c by the data instead of fitting K_r. One advantage of this procedure is that detailed fit math now works with T instead of T^4, and less precision is required. Also the model is closer to reality.

When looking at the overall results of this study it will be noticed that there is a correlation between excess heat and the size of K_r. One would expect none. Some have suggested that this correlation is unacceptable and that the data must be wrong. Of course anybody's data "could" be wrong. It is also often the case that correlations show up when they aren't expected. In the present case we can think of at least one possible reason for a correlation. It has recently been reported by researchers that He is produced by cells generating excess heat. It turns out that He readily diffuses through pyrex glass. Perhaps excess heat is accompanied by He which spoils the vacuum a bit increasing Kc enough to give the high heat transfers found. A quick calculation indicates that there might be enough He to do it. Of course there also might be simpler explanations.

In this study we use the mathematical models of Pons and Fleischmann and C. Walling. The P/F models are discussed in references [1-5]. The Walling formula was in an unpublished work given to me by Walling. We modified it to use $(T^4-T_b^4)$ instead of $(T-T_b)$, and further to use both K_r and K_c.

REFERENCES

1. S. Pons and M. Fleischmann, "Calorimetric Measurements of the Palladium/Deuterium System: Fact and Fiction", Fusion Technology 17, 669 (1990).
2. S. Pons and M. Fleischmann, "Calorimetry of the Palladium-Deuterium System", p. 1, Proc. First Annual Conference on Cold Fusion, Salt Lake City, March 28-31, 1990.
3. M. Fleischmann, S. Pons, M.W. Anderson, L.J. Li, and M. Hawkins, "Calorimetry of the Palladium-Deuterium-Heavy Water System", J. Electroanal. Chem. 287, 293 (1990)
4. M. Fleischmann, S. Pons and M. Hawkins, "Electrochemically Induced Nuclear Fusion of Deuterium", J. Electroanal. Chem. 261, 301 (1989).
5. M. Fleischmann, S. Pons, and M. Hawkins, Errata, J. Electroanal. Chem. 263, 187 (1989).

Finito di stampare
nel dicembre 1991
Tipografia Compositori - Bologna